

THE UNIVERSITY *of* EDINBURGH

This thesis has been submitted in fulfilment of the requirements for a postgraduate degree (e.g. PhD, MPhil, DClinPsychol) at the University of Edinburgh. Please note the following terms and conditions of use:

- This work is protected by copyright and other intellectual property rights, which are retained by the thesis author, unless otherwise stated.
- A copy can be downloaded for personal non-commercial research or study, without prior permission or charge.
- This thesis cannot be reproduced or quoted extensively from without first obtaining permission in writing from the author.
- The content must not be changed in any way or sold commercially in any format or medium without the formal permission of the author.
- When referring to this work, full bibliographic details including the author, title, awarding institution and date of the thesis must be given.

Methyl Halide and Biogenic Volatile Organic Compound Fluxes from Perennial Bioenergy Crops and Annual Arable Crops



Eilidh Christina Morrison

A thesis submitted in fulfilment of the requirements
for the degree of Doctor of Philosophy
to the
University of Edinburgh

2013

The Wishing Tree

by
Kathleen Jamie

I stand neither in the wilderness
nor fairyland

but in the fold
of a green hill

the tilt from one parish
into another.

To look at me
through a smirr of rain

is to taste the iron
in your own blood

because I hoard
the common currency

of longing: each wish
each secret assignation.

My limbs lift, scabbed
with greenish coins

I draw into my slow wood
fleur-de-lys, the enthroned Brittania.

Behind me, the land
reaches toward the Atlantic.

And though I'm poisoned
choking on the small change

of human hope,
daily beaten into me

look: I am still alive–
in fact, in bud.

Abstract

The depletion of fossil fuel resources, pollution concerns and the challenge of energy security are driving the search for renewable energy sources. The use of lignocellulosic plant biomass as an energy source is increasing in the United Kingdom and worldwide. In the UK, up to 0.35 MHa (6% of total arable land) may be planted with perennial bioenergy crops by 2020 in order to meet renewable energy and CO_2 reduction targets. Several plant species that produce high biomass from low inputs have been identified. The most promising for the UK climate are the genus *Miscanthus*, a perennial rhizomatous grass which can grow up to 3.5 m in a year, and short rotation coppice (SRC) willow (*Salix* spp.), plantations of which can remain viable for up to 30 years.

Although bioenergy crops are perceived as "carbon neutral", changes in land use can have a wider impact on atmospheric composition than through CO_2 alone. This study compares vegetation fluxes of methyl halides (CH_3Br and CH_3Cl) and biogenic volatile organic compounds (BVOCs) from perennial bioenergy crops and annual arable crops at three sites in the UK. Methyl halides are the most abundant natural vectors of bromine and chlorine into the stratosphere and play an important role in stratospheric ozone destruction. BVOCs affect atmospheric oxidising capacity and are a major precursor to the formation of ozone and secondary organic aerosols in the troposphere. Although terrestrial vegetation is an important source of these trace gases there are very few previous measurements of these reactive gases from bioenergy crops. This study describes measurements conducted at two SRC willow sites in Scotland, and one site in England planted with adjacent perennial bioenergy crops and annual arable crops, to quantify and characterise natural methyl halide and BVOC fluxes from vegetation.

Measurements were conducted with branch chambers, using static enclosure techniques to measure methyl halide fluxes and dynamic enclosures to measure BVOCs such as isoprene and α-pinene. Fluxes were calculated from the concentration difference between background/inlet samples and after enclosure/outlet samples. Methyl halide concentrations were determined by sampling gas from static enclosures followed by analysis using an oxygen-doped GC-ECD with a custom-built pre-concentration unit. Samples for BVOC analysis were collected onto

adsorbent tubes and a thermal desorption GC-MS was used to determine BVOC concentrations. Potentially influential environmental variables such as photosynthetically active radiation (PAR), total solar radiation, air temperature, soil temperature, internal chamber temperature and soil moisture were recorded in parallel to the enclosures to determine their potential relationships to fluxes. Long-term environmental data was also available from on-site or nearby weather stations.

Long-term measurements were carried out for 2 $\frac{1}{2}$ years at a site in Lincolnshire, England where adjacent fields are planted with *Miscanthus*, SRC willow and annual arable crops (wheat and oilseed rape crop rotation). Vegetation measurements were made almost every month throughout the period, with more intensive measurements such as full diurnal cycle carried out during the summer. Ten sampling points are sampled in each field and semi-diurnal measurements are taken regularly. Long-term measurements were also carried out at two sites in Scotland planted with SRC willow, one in Arnot, Perth & Kinross which was sampled for a year and one in East Grange, Fife which was sampled for half a year. Up to 30 sampling points were employed in Arnot and another 10 in East Grange.

The bioenergy crops and wheat emitted low fluxes of methyl halides in comparison to the oilseed rape. Mean annual net fluxes of CH_3Br and CH_3Cl from *Miscanthus* were 1.8 ng g (dry weight)$^{-1}$ h^{-1} and 11 ng g^{-1} h^{-1}, respectively. At the three willow sites, mean annual net fluxes of CH_3Br and CH_3Cl ranged between 0.6 - 1.7 ng g^{-1} h^{-1}, and 1.7 - 12 ng g^{-1} h^{-1}, respectively. Negligible fluxes of methyl halides were measured from wheat but oilseed rape was found to emit large fluxes of methyl halides with mean annual net fluxes of CH_3Br and CH_3Cl of 20 ng g^{-1} h^{-1}and 144 ng g^{-1} h^{-1}, respectively.

The largest BVOC fluxes were measured from SRC willow at the Brattleby site, with high mean annual net fluxes of isoprene (77 µg g^{-1} h^{-1}), α-pinene (46 µg g^{-1} h^{-1}), β-pinene (5.5 µg g^{-1} h^{-1}), limonene (3.7 µg g^{-1} h^{-1}) and δ-3-carene (11 µg g^{-1} h^{-1}). However, mean annual net BVOC fluxes measured at Arnot and East Grange were much lower. High fluxes of α-pinene were measured from *Miscanthus* in 2010 (giving a mean annual net flux of 65 µg g^{-1} h^{-1}) but no other significant BVOC fluxes were distinguished. Negligible fluxes of isoprene were measured from wheat but fluxes of monoterpenes were high with mean annual net fluxes of 65 µg g^{-1} h^{-1} and 25 µg g^{-1} h^{-1} for α-pinene and limonene, respectively. No significant fluxes of BVOCs were measured from the oilseed rape.

All fluxes demonstrated a strong seasonal trend with higher emissions during the summer growing season and low to zero emissions over winter. The high spatial variability was captured by sampling from many points in each field. Some diurnal measurements exhibited a clear pattern of higher emissions during the day and low to zero emissions at night. Some positive correlations between fluxes and environmental variables such as PAR and air temperature were

observed. An experiment carried out on willow cuttings in the greenhouse found no clear increase or decrease in fluxes of BVOCs in response to N fertiliser treatment, instead fluxes were found to vary significantly with some of the observed environmental variables.

UK estimates were derived by extrapolating measured fluxes using the current respective land cover areas for *Miscanthus* and SRC willow. Estimated UK annual fluxes of CH_3Br and CH_3Cl from *Miscanthus* were $0.01\,\mathrm{Mg\,y^{-1}}$ and $0.05\,\mathrm{Mg\,y^{-1}}$, respectively and from SRC willow were $0.06\,\mathrm{Mg\,y^{-1}}$ and $0.4\,\mathrm{Mg\,y^{-1}}$, respectively, accounting for a very small percentage of total global annual turnover of CH_3Br and CH_3Cl. Estimated UK annual fluxes of the BVOCs isoprene and α-pinene from *Miscanthus* were $0.01\,\mathrm{Mg\,y^{-1}}$ and $0.4\,\mathrm{Mg\,y^{-1}}$, respectively and from SRC willow were $3\,\mathrm{Mg\,y^{-1}}$ and $1\,\mathrm{Mg\,y^{-1}}$, respectively. Future planting of SRC willow to meet the UKs energy needs could lead to a potential annual isoprene flux of $150\,\mathrm{Mg\,Mg\,y^{-1}}$.

Declaration

I do hereby declare that this thesis was composed by myself and that the work described within is my own, except where explicitly stated otherwise.

Eilidh Morrison

May 2013

Acknowledgements

During the course of this project I have had the pleasure of meeting and working with many different people. I would like to thank my supervisor Mat Heal for his patience in reading and correcting my work and for his invaluable advice. My supervisor Julia Drewer provided much needed practical advice as well as making fieldwork and the long drives to fieldsites more enjoyable with her banter and (usually) good taste in music.

Emanuel Blei and Catherine Hardacre both took time out of their thesis writing to answer my many questions on methyl halides and the inner workings of "the beast". The extra strong coffee available in the museum fuelled some interesting and not always chemistry related conversations with the PhysChem group and the other students and staff at UoE. Fika Fridays were a highlight, with cakes not just from Asda but from all over the world. I greatly enjoyed working with UoE final year students Alice Meehan and Jocelyn Timperley, who assisted me in the field and sometimes even fetched the dry ice. Thanks to Mark Hammonds for bringing a sense of calm to the office but no thanks for initiating discussions about climbing.

Sue Owen and Neil Cape at CEH Edinburgh had many helpful suggestions and also succeeded in rescuing the GC-MS so vital to my project. Thanks to Nick Hewitt and Brian Davison at Lancaster University who also helped in this endeavour. I am also grateful to the rest of the staff and students at CEH Edinburgh for providing an endless supply of useful advice and equipment.

I would like to thank the University of Edinburgh and the Centre for Ecology and Hydrology for funding this work. Thanks to the National Centre for Atmospheric Science for funding my attendance at their Atmospheric Summer Measurement school on the beautiful island of Arran. I am still in contact with many of the people I met there. Thanks to the Royal Meteorological Society and the James Rennie Bequest for their support in attending BIOGEOMON in the equally beautiful setting of Maine. The Royal Society of Chemistry also supported my attendance at their events around the UK.

Viv and Rob Bogusz at Robindale B & B whom I stayed with on the majority of my trips to Brattleby were so welcoming and made an otherwise solitary trip feel like visiting friends. I

am grateful to Jonathon Wright, the landowner, for allowing me access to the Brattleby site and to stick pink flags around the fields. Thanks to Malcolm Steel at Greenhead of Arnot for allowing me access to his land and taking an interest in my work. Thanks also to the Forestry Commission for allowing me to tag along and work at their site in East Grange.

To my long-suffering family and friends I would like to express my gratitude for their support. To my partner Fraser, many thanks for helping me lug field equipment around and buying me a beer after a long shift in the lab. Special thanks to Nichola Copeland for being such a good friend, not to mention helping and advising on so many parts of my project.



Contents

Abstract i

Declaration iv

Acknowledgements v

Contents vii

1 Introduction 1
- 1.1 Bioenergy . . . 1
  - 1.1.1 Perennial bioenergy crops . . . 3
- 1.2 Trace Gases . . . 10
- 1.3 Methyl Halides . . . 11
  - 1.3.1 Unidentified or misestimated methyl halide sources . . . 15
  - 1.3.2 The mechanism of CH_3X production . . . 16
  - 1.3.3 Trends and environmental drivers . . . 17
  - 1.3.4 Analysis of methyl halides . . . 18
- 1.4 Biogenic Volatile Organic Compounds . . . 20
  - 1.4.1 Qualifying and quantifying BVOCs . . . 21
  - 1.4.2 Production of BVOCs . . . 22
  - 1.4.3 Trends and environmental drivers . . . 23
  - 1.4.4 Sampling and analysis of BVOCs . . . 25
- 1.5 Overall aims . . . 26
- 1.6 Thesis layout . . . 26

2 General Methodology 29
- 2.1 Vegetation enclosures . . . 29
- 2.2 Methyl halides . . . 31
  - 2.2.1 Flux measurements . . . 31
  - 2.2.2 Enclosure time . . . 32
  - 2.2.3 Gross and net methyl halide fluxes . . . 33
  - 2.2.4 GC-ECD analysis system . . . 33
  - 2.2.5 Standard make up and calibration curves . . . 34
  - 2.2.6 Linear regression . . . 35
  - 2.2.7 Intercalibration . . . 36
  - 2.2.8 Stability of CH_3Br and CH_3Cl in Tedlar and Flex Foil Bags . . . 37

2.3 Biogenic Volatile Organic Compounds (BVOCs) . . . 38
2.3.1 Flux measurements . . . 38
2.3.2 Enclosure time . . . 39
2.3.3 Gross and net BVOC fluxes . . . 40
2.3.4 GC-MS analysis system . . . 40
2.3.5 Standard make up and calibration curves . . . 41
2.3.6 Quantification . . . 43
2.3.7 Stability of BVOCs on adsorbent packed tubes . . . 43
2.4 Environmental monitoring . . . 44
2.5 Other general methods . . . 44
2.5.1 Soils . . . 44
2.5.2 Plant material . . . 46
2.6 Data analysis, statistics and quality control . . . 46
2.6.1 Estimation of Errors and Uncertainties in CH_3X and BVOC Fluxes . . . 46
2.6.2 Statistical methods . . . 51
2.7 Sampling sites and characterisation . . . 51
2.7.1 Brattleby, Lincolnshire . . . 52
2.7.2 Greenhead of Arnot, Perthshire . . . 55
2.7.3 East Grange, Fife . . . 57

3 Long term flux measurements in *Miscanthus* 61
3.1 Introduction . . . 61
3.2 Description of *Miscanthus* site and sampling points . . . 63
3.3 Outline of CH_3X flux measurements . . . 64
3.3.1 CH_3X flux trends . . . 64
3.3.2 Statistical analysis of seasonal fluxes and potential drivers . . . 84
3.3.3 Diurnal and sub-diurnal trends . . . 86
3.4 Outline of BVOC flux measurements in *Miscanthus* . . . 95
3.4.1 BVOC flux trends . . . 95
3.4.2 Sub-diurnal trends . . . 110
3.5 Summary . . . 112
3.6 Discussion . . . 113

4 Long term measurements in willow 115
4.1 Introduction . . . 115
4.2 Brattleby . . . 120
4.2.1 Site description . . . 120
4.2.2 Outline of CH_3X flux measurements . . . 121
4.2.3 CH_3X flux trends . . . 121
4.2.4 Statistical analysis of seasonal fluxes and potential drivers . . . 140
4.2.5 Sub-diurnal trends . . . 142
4.2.6 Outline of BVOC flux measurements . . . 146
4.2.7 BVOC flux trends . . . 146
4.2.8 Statistical analysis of seasonal fluxes and potential drivers . . . 189
4.2.9 Sub-diurnal trends in isoprene . . . 192
4.3 Arnot . . . 194

4.3.1 Site description . . . 194
4.3.2 Outline of CH_3X flux measurements . . . 194
4.3.3 Statistical analysis of seasonal fluxes and potential drivers . . . 231
4.3.4 Outline of BVOC flux measurements . . . 233
4.3.5 Statistical analysis of seasonal fluxes and potential drivers . . . 276
4.4 East Grange . . . 278
4.4.1 Site description . . . 278
4.4.2 Outline of CH_3X flux measurements . . . 278
4.4.3 Outline of BVOC flux measurements . . . 283
4.5 Summary . . . 286
4.6 Discussion . . . 288

5 Annual arable crops 291
5.1 Introduction . . . 291
5.2 Description of annual arable crop site and sampling points . . . 293
5.3 Outline of CH_3X and BVOC flux measurements in wheat . . . 294
5.3.1 CH_3X flux trends in wheat . . . 294
5.3.2 BVOC flux trends in wheat . . . 294
5.3.3 Statistical analysis of seasonal fluxes and potential drivers of BVOC fluxes from wheat . . . 309
5.4 Outline of CH_3X and BVOC flux measurements in oilseed rape . . . 311
5.4.1 CH_3X flux trends in oilseed rape . . . 311
5.4.2 Statistical analysis of seasonal fluxes and potential drivers of CH_3X fluxes from oilseed rape . . . 326
5.4.3 Sub-diurnal trends CH_3X fluxes in oilseed rape . . . 327
5.4.4 BVOC flux trends in oilseed rape . . . 331
5.5 Summary . . . 331
5.6 Discussion . . . 333

6 Comparison of perennial bioenergy crops and annual arable crops 335
6.1 Comparison of CH_3X fluxes in perennial bioenergy and annual arable crops . . . 336
6.1.1 Comparison of CH_3X fluxes to other studies . . . 336
6.1.2 Annual CH_3X flux trends . . . 337
6.1.3 Diurnal CH_3X flux trends . . . 337
6.1.4 Behaviour of CH_3Br and CH_3Cl fluxes . . . 338
6.1.5 Influence of environmental variables on CH_3X fluxes . . . 338
6.2 Comparison of BVOC fluxes in perennial bioenergy and annual arable crops . . . 339
6.2.1 Comparison of BVOC fluxes to other studies . . . 339
6.2.2 Annual BVOC flux trends . . . 340
6.2.3 Diurnal BVOC flux trends . . . 342
6.2.4 Behaviour of various BVOC fluxes . . . 342
6.2.5 Influence of environmental variables on BVOC fluxes . . . 342
6.3 Summary . . . 343

7 Controlled experiment 345
7.1 Introduction . . . 345

7.2 Experimental design . . . 346
7.2.1 Vegetation enclosure design . . . 347
7.2.2 Sample collection . . . 348
7.3 Results . . . 349
7.3.1 Arnot . . . 349
7.3.2 Brattleby . . . 353
7.3.3 Statistical Analysis . . . 356
7.4 Summary . . . 357

8 Scale up of CH_3X and BVOC fluxes **359**
8.1 Introduction . . . 359
8.2 Method . . . 361
8.3 Results . . . 364
8.3.1 CH_3X emission estimates . . . 364
8.3.2 Implications for CH_3X budgets . . . 365
8.3.3 BVOC emission estimates . . . 366
8.3.4 Implications for BVOC budgets . . . 367
8.4 Conclusion . . . 369

9 Final conclusions **371**

Bibliography **375**

Chapter 1

Introduction

The amount of energy consumed globally has increased more than 10-fold during the 20th century (Boyle, 2004). The demands of our energy hungry world are expected to be increasingly met by energy derived from bioenergy crops. All terrestrial plants are a potentially important source of trace gases known as methyl halides (CH_3Br and CH_3Cl), which impact on levels of stratospheric ozone, and another subset of trace gases known as biogenic volatile organic compounds (BVOCs), which affect atmospheric oxidising capacity and the formation of tropospheric ozone and aerosols. The compounds emitted and the rate of emissions are specific to each plant and are difficult to estimate. Therefore it is important to characterise emissions from these plant species and to investigate whether extensive planting of bioenergy crops is likely to contribute significantly to budgets of these trace gases. The annual arable crop oilseed rape is thought to be a relatively large emitter of CH_3Br and therefore any increase or decrease in planting of this crop has the potential to influence atmospheric chemistry locally and globally. This thesis assesses the potential contribution of both bioenergy crops and annual arable crops to the budgets of these trace gases. The measurements described here were made in the UK, but this research also has wider implications for Europe and the rest of the world.

1.1 Bioenergy

Non-renewable fossil fuels are currently our main energy source but these resources are finite and will eventually become too costly to harvest. Renewable sources of energy are being sought in order to combat the rising costs and severe environmental impacts of fossil fuels.

In the UK, agriculture occupies 77% of the total land area and is the largest emitter of the greenhouse gases (GHGs) methane (CH_4) and nitrous oxide (N_2O), which are 25 and 298 times, respectively, more potent contributors to global warming than the more infamous carbon dioxide (100-year GWP (IPCC, 2007)). There is potential to reduce the current GHG emissions from agricultural land and also to use it indirectly to aid GHG mitigation. Bioenergy crops are usually grown under a kinder management regime than annual arable crops, i.e. reduced or zero fertiliser

inputs and no annual ploughing, and this is hypothesised to lead to comparatively lower GHG emissions (Crutzen et al., 2007). Bioenergy crops are also considered to act as a sink for carbon and nitrogen via sequestration in the soil (Grogan and Matthews, 2002; Kahle et al., 2001; Lemus and Lal, 2005; SEERAD, 2006).

Government policy in the UK and in many other countries promotes the use of biomass energy. In the UK, the Non-Fossil Fuel/Renewables Obligation (RO) (www.dti.gov.uk) obliges electricity suppliers to source some of their energy from renewable sources. Co-firing is the preferred option, in heat or combined heat and power plants, with 15 of the 18 UK electricity plants co-firing (Woods et al., 2006).

Currently more than 70% of the biomass used for energy production in the UK is derived from municipal waste or forest residues rather than dedicated energy crops (Aylott et al., 2008). However, planting of bioenergy crops is increasing at a rapid rate and as much as 6% of the UK's 18.5 Mha of arable land in the UK may be planted with bioenergy crops by 2020 (DEFRA, 2007).

In Europe, it has been estimated that 20-30% of all agricultural land could be used for energy crop production by 2030 (EEA, 2006). However, estimations of future land requirements are fairly speculative due to the limited information on the anticipated supply and spatial yield data of these crops and how this will develop in the future (Aylott et al., 2008). What is certain is that they are likely to play an important role in the long-term climate change mitigation strategy in Europe as they are the only biomass fuel that can be increased sufficiently to significantly shift the pattern of European energy supply (EEA, 2006).

Biomass currently makes up almost two-thirds of the total renewable energy in Europe, including 18% of renewable electricity (Don et al., 2011). However, only 3% of this energy comes from dedicated bioenergy crops (Edenhofer et al., 2011). Worldwide, bioenergy accounted for around 7% of total energy production in 2000 (Fernandes et al., 2007).

The main drivers for biomass use are to provide energy security and to mitigate climate change (McKay, 2006). Energy security is achieved by reducing reliance on fuel imports and providing a stable supply of biomass. The attraction of bioenergy crops in terms of climate change mitigation is the perception that they are "carbon neutral" i.e. the carbon released using the bioenergy crop is balanced by the carbon absorbed in the growing feedstock (Lemus and Lal, 2005; SEERAD, 2006). The UK Energy White Paper sets a target of reducing CO_2 emissions to 60% of current levels by 2050 and it is believed that increased use of biomass will contribute to meeting this target (DTI, 2007).

However, there is heated debate over the benefits of bioenergy in many published articles and in the media in general. The public perception of energy from biomass combustion in the UK is often negative as it is seen as no better than waste incineration or other "dirty" sources of energy

that it is replacing (Upreti, 2004). Jean Ziegler, United Nations special rapporteur on the right to food, has claimed that large-scale deployment of bioenergy crops will lead to famine and drought and destroy biodiversity and soil quality (Maier, 2009). Increased bioenergy production has also been cited as one of the causes of dramatic increases in food prices in recent years (Tirado et al., 2010).

The benefits in terms of climate change mitigation are also unclear. The potential GHG savings vary widely depending on the crop, how it is planted and harvested, how it is utilised (power, heat, combined heat and power (CHP) and the fossil fuel it is replacing, or ethanol and biodiesel for transport), the management regime i.e. whether fertiliser is used (Crutzen et al., 2007) (including fossil fuel input to manufacture chemicals) and the land use that the crop is replacing.

A recent review of the potential environmental impacts of large-scale bioenergy crop planting in the UK found that, when compared to conventional arable crops, bioenergy crops will have positive effects on GHG mitigation as well as on soil properties, biodiversity, energy balance, carbon footprint and will have a minimal visual impact (Rowe et al., 2009). However, these benefits are minimal or non-existent when bioenergy crops replace land other than arable land (Don et al., 2011; Heller et al., 2003; Hillier et al., 2009).

The two main aspects of climate change mitigation are the replacement of fossil fuels and changed agricultural practices which result in carbon sequestration in soils (Boman and Turnbull, 1997). Decreased GHG emissions in comparison to fossil fuels (Adler et al., 2007; Crutzen et al., 2007; Don et al., 2011; Drewer et al., 2011) and short-term increases in soil carbon under perennial bioenergy crops have been reported (Hansen et al., 2004; Heller et al., 2003; Matthews, 2001; Tolbert et al., 2002). However, sequestration of carbon in the soil is neither permanent nor constant and the long-term significance of these changes remain uncertain.

Although there have been numerous studies into the potential economic and environmental impacts of wide-scale cultivation of crops for energy generation rather than food production, measurements of trace gas emissions from bioenergy crops are few and far between. The short-term and long-term effects on the budgets of trace gases are largely unknown, and must be investigated if we are to fully understand the impact of continued expansion of bioenergy crops on atmospheric chemistry.

1.1.1 Perennial bioenergy crops

Bioenergy crops include first generation crops such as the oil crops oilseed rape, linseed and sunflower, starch crops such as potato, cereals such as barley, wheat and oats as well as second generation dedicated lignocellulosic crops such as the tall grass *Miscanthus* and short rotation coppice (SRC) willow and poplar. SRC willow (*Salix spp.*) and *Miscanthus* (*Miscanthus x*



(a) *Miscanthus* at full height **(b)** *Miscanthus* after harvesting

Figure 1.1: *Miscanthus* before and after harvesting.

giganteus) are thought to be the most suitable bioenergy crops for the UK. Currently, the biomass they produce is used to co-fire combined heat and power plants.

Both SRC willow and *Miscanthus* are physiologically different to annual arable crops; they are perennial with economic lifespans of up to twenty years and they are deep rooted (around 2 m) with a generally greater root biomass (Liebig et al., 2005) which confers high water-use efficiency. They also have much taller canopies (over 3 m high) and are adapted to more acidic conditions so they do not require liming. Unlike other high N demanding energy crops such as oilseed rape and maize, *Miscanthus* and SRC willow do not require high N fertilisation and can grow well on poor soils.

Miscanthus

Miscanthus (Figure 1.1a), also known as Elephant Grass, is a genus of perennial grasses of the same taxonomic group as crops such as sugarcane, sorghum and maize (Naidu et al., 2003). It is native to subtropical and tropical regions of Africa and southern Asia but is also resilient to lower temperatures, making it well-suited for growth in the UK. *Miscanthus x giganteus* is a sterile hybrid that has been trialled as a biofuel in Europe since the early 1980s. It can grow to heights of more than 3.5 m in one growth season and its dry weight annual yield can reach 25 t ha^{-1} (Rowe et al., 2009). It is harvested annually, usually between January and March (Figure 1.1b).

The main growth stages for *Miscanthus* are shown in Figure 1.2. The crop is harvested in March and the emergence of new shoots from the rhizomes occurs in May when average temperatures at the site are between 3 and 6 °C. Leaf growth occurs in June, usually at temperatures of

between 5 and 10 °C (Clifton-Brown and Jones, 1997; Hastings et al., 2009). Biomass is then rapidly accumulated throughout the summer and is thought to peak around September (Heaton et al., 2010). Senescence occurs in November and the crop is then harvested again in March after dry down over the winter period.

Miscanthus is attractive as a bioenergy crop due to its favourable ratio of energy output to energy input (fertilizer, biomass processing, biomass transport, propagation and harvest), reported to be around 14:1 (Lewandowski et al., 1995). *Miscanthus* biomass also has high combustion quality due to its low water concentration as well as its low Cl, K, N, S and ash concentrations compared to other lignocellulose plants (Lewandowski and Kicherer, 1997).

In recent years there have been several studies of growth and yield of *Miscanthus* in the UK (Bauen et al., 2010; Hillier et al., 2009; Smith and Slater, 2010) and Europe (Christian et al., 2008; Clifton-Brown et al., 2004; Danalatos et al., 2007; Glowacka, 2011; Himken et al., 1997; Lewandowski and Kicherer, 1997; Price et al., 2004). It is a sterile crop requiring propagation, making it costly to establish. In order to recover the establishment costs the crop must therefore remain productive for several years. It is believed that *Miscanthus* remains productive for 15-20 years (Lewandowski et al., 2000). However only one experiment has monitored long-term productivity (15 years) (Clifton-Brown et al., 2007).

Field trials in Europe during the last 15 years have shown that this genotype can, from its second to third year following establishment, produce annual harvestable yields from 10 to 40 t dry matter $\mathrm{ha}^{-1}\,\mathrm{y}^{-1}$ (Lewandowski et al., 2000). Reports of plant losses of this hybrid during winter in some climates have led to field trials to test other hybrid *Miscanthus* genotypes. However, where no over-wintering problems have occurred, *Miscanthus x giganteus* has proven to be among the most productive of all genotypes tested to date (Clifton-Brown et al., 2004).

There have also been numerous investigations into the potential of *Miscanthus* to contribute to GHG mitigation (Beale and Long, 1997; Brandão et al., 2011; Davis et al., 2010; Don et al., 2011; Dondini et al., 2009; Drewer et al., 2011; Rowe et al., 2009). Root derived carbon flow in *Miscanthus* is thought to be moderated by the rhizome so there is potential to store carbon and nitrogen below ground. *Miscanthus* has the potential to sequester up to 0.6 Mg soil C $\mathrm{ha}^{-1}\,\mathrm{y}^{-1}$ (Don et al., 2011). Furthermore, decomposition is likely to be slower than in conventional annual crops due to the absence of disturbance through cultivation.

Miscanthus has shown a significant increase in soil organic carbon (SOC) compared to adjacent grassland areas, but the effect depends on the soil texture (Kahle et al., 2001). Another study used carbon isotopes to determine that carbon from *Miscanthus* made up a significant proportion of the SOC pool, accounting for 13% and 31%, respectively, of the SOC of a 9-year-old and 16-year-old *Miscanthus* plantation (Hansen et al., 2004). The turnover time of the organic matter increases with time under *Miscanthus* cultivation (Foereid et al., 2004).



Figure 1.2: The main growth stages of *Miscanthus* illustrated using photos taken at the Brattleby fieldsite.

Generally, it is agreed that using *Miscanthus* plantations as a renewable energy source will have a beneficial impact on reducing GHG emissions, with one study suggesting that *Miscanthus* could provide around 10 000 kg CO_2 ha^{-1} y^{-1} of avoided CO_2 emissions (Brandão et al., 2011). A study by Drewer et al. (2011) attributed lower N_2O emissions from *Miscanthus* than from annual arable crops wheat and oilseed rape to the difference in management regime, with regular fertilizer application and tillage in the annual arable cropping systems but not the bioenergy crop.

The environmental benefits are only felt if agricultural land is used (King et al., 2004) and management regime is less harsh (Drewer et al., 2011). In order to determine the effects of nitrogen fertiliser on the GHG budget of *Miscanthus* (the other main bioenergy crop grown in the UK), ^{15}N-labelled fertiliser was applied to *Miscanthus* during an experiment at the Brattleby fieldsite (Drewer et al., 2011). Application of $^{14}NH_4{}^{15}NO_3$ at a rate equivalent to 50 kg N ha^{-1} resulted in a fertiliser-induced increase in N_2O emission. Before the application of fertiliser, *Miscanthus* N_2O emissions were around zero but N_2O emissions increased within a day. A maximum N_2O emission of 320 μg m^{-2} h^{-1} was measured 36 hours after fertiliser application. Emissions decreased steadily and dropped to zero after 3 days.

Application of N has a limited effect on the yield of *Miscanthus* (Danalatos et al., 2007). *Miscanthus* is unusual in that it can use the C_4 synthetic pathway at a significantly lower temperature than most C_4 plants (Naidu et al., 2003). The use of nutrients and water is very efficient and perennial energy yields for *Miscanthus* in Northern Europe match or exceed those reported for SRC willow (Davis et al., 2010).

Miscanthus had the highest nitrogen, energy and land use efficiencies at all N fertilizer and energy input levels compared to two other bioenergy crops, reed canary grass and triticale (Lewandowski and Schmidt, 2006). The main reasons cited for this were that *Miscanthus* is perennial and that it uses a C_4 photosynthetic pathway for carbon fixation which uses water and nitrogen more efficiently than the common C_3 pathway (Sage and Monson, 1998). Perennial crops internally recycle N, translocating it from the above ground biomass to the rhizomes during the autumn and then translocating it to emerging shoots in spring (Lewandowski and Schmidt, 2006).

C_4 plants fare better than C_3 plants under conditions of drought, high temperatures, and nitrogen or CO_2 limitation (Sage and Monson, 1998). At 30 °C, C_3 grasses lose approximately 833 molecules of water per CO_2 molecule that is fixed, whereas C_4 grasses lose only 277 water molecules per CO_2 molecule fixed (Sage and Monson, 1998). This increased water use efficiency of C_4 grasses means that soil moisture is conserved, allowing them to grow for longer in arid environments.

In the UK, the most recent available land use data stated that there were 12 700 ha of

Miscanthus at the end of 2009 (DEFRA, 2009). In Europe in 2009/2010, the land cover area for *Miscanthus* was around 25 756 ha (Don et al., 2011). Cultivation of *Miscanthus* is likely to continue to increase in the coming years, although reaching a realistic estimate of exactly how much *Miscanthus* may be planted is challenging due to the lack of information on the potential land available and the spatial yield.

Short rotation coppice (SRC) willow

Short rotation coppice (SRC) willow consists of densely planted, high-yielding varieties willow (*Salix spp.*), (Figure 1.3a) harvested on a 2 to 5 year cycle, commonly every 3 years. Osier (*Salix viminalis*), a shrub willow, is parental stock to the majority of willow varieties planted for use as an energy crop (DEFRA, 2004). After coppicing (cutting back to ground level to encourage the growth of multiple stems), the rootstock or stools remain in the ground with new shoots emerging the following spring (Figure 1.3b). Plantations remain viable for 15 to 30 years. SRC willow is planted in the spring and grows rapidly in the first year, reaching up to 6 m in height.



(a) Willow



(b) Willow after coppicing

Figure 1.3: SRC willow trees before and after coppicing.

The main growth stages of SRC willow are shown in Figure 1.4. The SRC willow was coppiced in winter 2010. After coppicing, branches begin to develop in April followed by bud break and leaf development in May. These stages occur slightly earlier if the willow has not been recently coppiced, with bud break occurring in early March and full leaf development by the start of April. Willow reaches full biomass in August/September. Senescence begins in October followed by loss of foliage during November and dormancy over winter.

SRC willow has an extremely high ratio of energy output to energy input at 30:1 (Cannell, 2003), which makes it a promising bioenergy crop. The willow species employed in bioenergy crop plantations have an impressive growth rate and their dry weight annual yield can reach 15 t ha^{-1} y^{-1} (Andersen et al., 2005).

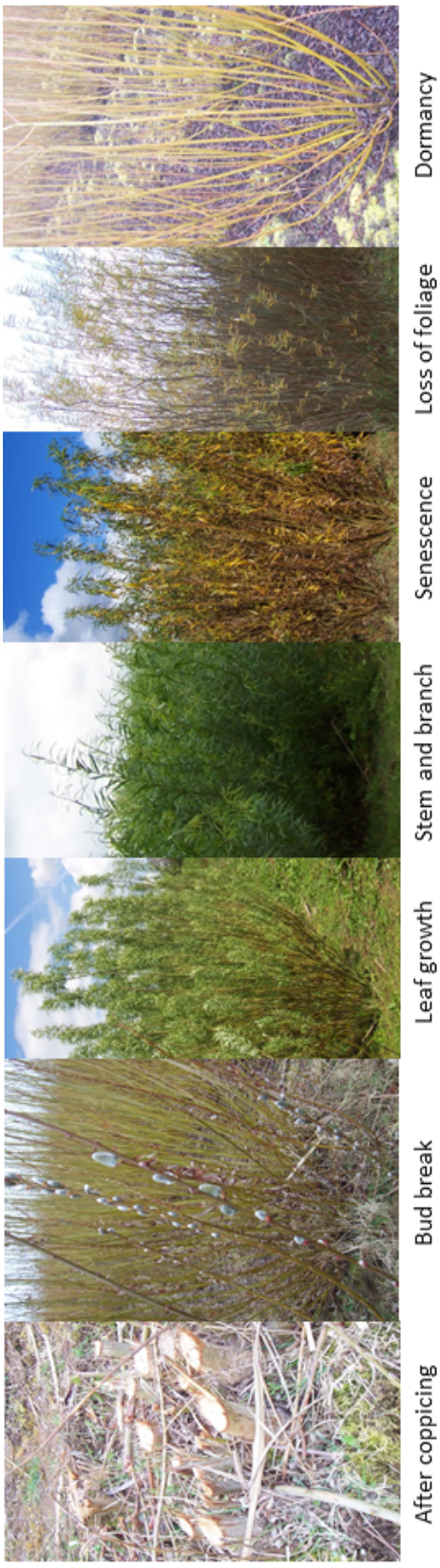


Figure 1.4: The main growth stages of SRC willow illustrated using photos taken at the Brattleby fieldsite.

Several studies have found that SRC willow contributes to CO_2 mitigation by replacing fossil fuels (Heller et al., 2003; Hillier et al., 2009; Matthews, 2001; Rowe et al., 2009). SRC willow has the potential to sequester up to 0.44 Mg soil C ha^{-1} y^{-1} (Don et al., 2011). A recent modelling study suggested that increases in SOC under SRC could contribute 5% of the carbon mitigation benefits of SRC willow (Grogan and Matthews, 2002). However, another study reported a loss of 15% of original SOC at a site on former grassland, suggesting that initial SOC levels are an important consideration when locating SRC plantations (Jug et al., 1999). SRC willow also provides other environmental benefits such as the protection of ground water quality in intensively farmed areas (Jørgensen et al., 2005).

Biomass yields can be increased further using fertiliser (Quaye et al., 2011). However, this offsets some of the environmental benefits of the bioenergy crop. Nitrogen fertilizer input into SRC willow production systems in the USA has been estimated to account for 37% of the non-renewable fossil energy input to these systems (Heller et al., 2003). Drewer et al. (2011) attribute the lower N_2O emissions from SRC willow in comparison to annual arable crops wheat and oilseed rape to the difference in management regime, with regular fertilizer application and tillage in the annual arable cropping systems but not the bioenergy crop.

At the end of 2009, there were 6 400 ha of willow in the UK (DEFRA, 2009) and around 24 185 ha in Europe (Don et al., 2011). Planting is projected to continue increasing, although by how much is still under debate, with some estimates suggesting that up to 72 Mha in Europe may be planted with willow and *Miscanthus* in the future (Ashworth et al., 2013). However as *Miscanthus* does not grow well in Scotland and parts of northern Europe due to the cold climate, SRC willow has the potential to contribute enormously to Scotland's renewable energy needs (Andersen et al., 2005) as well as those of the UK as a whole (Aylott et al., 2008).

1.2 Trace Gases

Although trace gases constitute less than 1% of the composition of the atmosphere, they regulate the Earth's greenhouse effect, the balance of stratospheric ozone and most of the chemical reactions in the atmosphere (Monson and Holland, 2001). Any changes to the cycles of carbon, nitrogen, sulphur and the halogens chlorine, bromine and iodine between the atmosphere, the lithosphere and the hydrosphere can have direct effects on plants, animals and ecosystems (Shallcross et al., 2003). For example, the rise in levels of CO_2 in the atmosphere is expected to lead to warming of the Earth's surface, the extent and consequences of which are of considerable debate.

For some trace gases their sources and sinks are clearly defined. However for others the global budgets are out of balance. Numerous studies have examined trace gas fluxes from a variety of

ecosystems. There is great spatial and temporal variability in fluxes which hinders the estimation of current and future global budgets.

The majority of the trace gases found in the atmosphere are from biogenic sources and are emitted to the troposphere from the land surface (Matson and Harris, 1995). As changes occur in the landscape due to human activities, changes occur to the composition of the troposphere over a range of scales. These changes include increased acid deposition, local and regional ozone loss and potential climate change (Monson, 2002). Growing awareness of the importance of understanding these changes and our attempts to manage them drives the continued investigation and discovery of the origins and abundance of trace gases.

1.3 Methyl Halides

Methyl bromide (CH_3Br) and methyl chloride (CH_3Cl), together with methyl iodide (CH_3I), are known as methyl halides (CH_3X). CH_3Br and CH_3Cl play a significant role in stratospheric ozone depletion; however CH_3I is considered not to (WMO, 2006) and is not discussed further here. Although their average tropospheric mixing ratios are low, 7.9 pptv (parts per trillion by volume) CH_3Br and 550 pptv CH_3Cl, a large amount of bromine and chlorine atoms are transported into the stratosphere due to their long atmospheric lifetimes of 0.8 years and 1 year respectively (WMO, 2011).

Once in the stratosphere, CH_3X contribute to the destruction of the ozone layer which protects the Earth from harmful UV radiation coming from the sun. CH_3X also contribute to the depletion of ozone in the polar regions of the Earth which results in holes in the ozone layer in these areas. After the discovery of the ozone holes, man-made substances such as CFCs with significant ozone depleting potentials (greater than 0.2) were gradually phased out. The ozone depletion potential (ODP) of a chemical compound is the relative amount of degradation to the ozone layer it can cause, with trichlorofluoromethane (R-11 or CFC-11) being fixed at an ODP of 1.0. CH_3Br has a relatively high ODP of 0.51 and is a controlled substance being phased out under the Montreal Protocol. CH_3Cl has a lower ODP of 0.02 and is not subject to any legislation. However, the majority of CH_3Br and CH_3Cl emissions are from natural sources.

CH_3Br and CH_3Cl photolyse in the stratosphere upon exposure to shortwave radiation of 185 to 210 nm. The Br and Cl radicals released catalytically destroy stratospheric ozone by a series of reaction cycles (Figure 1.5). It is estimated that one Cl atom destroys of the order of 100 000 ozone molecules before it is removed. Br is around 150 times less abundant in the atmosphere but is around 60 times more destructive to stratospheric ozone than Cl so is actually more destructive on a molecule by molecule basis. This is because the termination reaction i.e. the formation of HBr, is endothermic and therefore extremely slow. Secondly, the reservoir species

$BrONO_2$ is photolytically unstable and lasts just 10 minutes in the lower stratosphere compared with 6 h for the equivalent Cl reservoir species $ClONO_2$ (Seinfeld and Spyros, 2006).

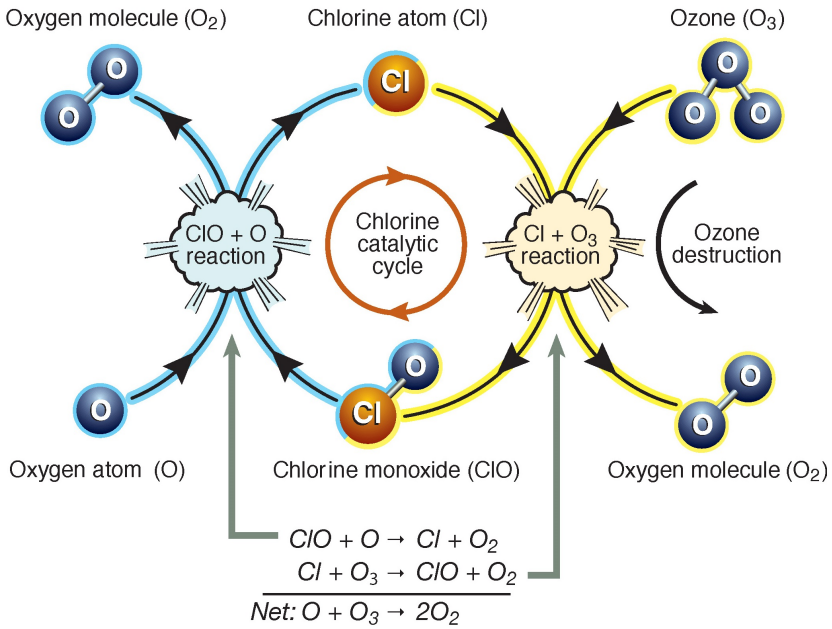


Figure 1.5: The destruction of ozone in the stratosphere at tropical and middle latitudes, where ultraviolet sunlight is most intense, involves two separate chemical reactions. Source: Fahey (2007).

CH_3Br

The most recent estimates of CH_3Br sinks and sources globally are shown in Table 1.1. The ranges described show that there is a high degree of uncertainty in estimation of CH_3Br budgets. The introduction of an almost comprehensive ban on production and use of CH_3Br has caused a decline in the atmospheric burden of CH_3Br in recent years. Until recently, CH_3Br was widely used in agriculture as a pesticide for the control of insects, nematodes, weeds, pathogens and rodents. Under the Montreal Protocol on Substances that Deplete the Ozone Layer, production and use of methyl bromide was to be completely phased out by 2005 with some exemptions.

A recent post-Montreal Protocol analysis using global model simulations and comparable measurements from the National Oceanic and Atmospheric Administration (NOAA) flask network found that that there may be a large missing source in the global budget. The best estimate of the annual global budget imbalance in 2008 was around 36 Gg y^{-1} in sources (Table 1.1). Other studies employing flask networks found that the initial decline of CH_3Br was around twice as large as expected (Montzka et al., 2003; Yokouchi et al., 2002). This huge decline was partly explained by the underestimation of anthropogenic CH_3Br emissions (around 20%).

Table 1.1: Summary of the estimated source and sink strengths (Gg y^{-1}) of CH_3Br for the periods 1996-1998 and 2008. All asterisked items were estimated from measurements of net fluxes and may be influenced by sinks within them, thus they represent minimum gross fluxes. n.q. = not quantified. Source: WMO (2011).

		1996–1998	Range	2008	Range	Reference
SOURCES	Fumigation-dispersive (soils)	41.5	(28.1 to 55.6)	6.7	(4.6 to 9.0)	1, 2
	Fumigation-quarantine/pre-shipment	7.9	(7.4 to 8.5)	7.6	(7.1 to 8.1)	1, 2
	Ocean	42	(34 to 39)	42	(34 to 49)	3, 4
	Biomass burning	29	(10 to 40)	29	(10 to 40)	5, 6
	Leaded gasoline	5.7	(4.0 to 7.4)	< 5.7		7
	Temperate peatlands	0.6	(-0.1 to 1.3)	0.6	(-0.1 to 1.3)	8, 9, 10
	Rice paddies*	0.7	(0.1 to 1.7)	0.7	(0.1 to 1.7)	11, 12
	Coastal salt marshes*	7	(0.6 to 14)	7	(0.6 to 14)	13,14,15,16
	based on Californian saltmarshes	14	(7 to 29)	14	(7 to 29)	13, 14
	based on Scottish saltmarshes	1	(0.5 to 3.0)	1	(0.5 to 3.0)	15
	based on Tasmanian saltmarshes	0.6	(0.2 to 1.0)	0.6	(0.2 to 1.0)	16
	Mangroves	1.3	(1.2 to 1.3)	1.3	(1.2 to 1.3)	17
	Shrublands*	0.2	(0 to 1)	0.2	(0 to 1)	18
	Rapeseed	4.9	(3.8 to 5.8)	5.1	(4.0 to 6.1)	19
	Fungus (litter decay)	1.7	(0.5 to 5.2)	1.7	(0.5 to 5.2)	20
	Fungus (leaf-cutter ants)	0.5		0.5		21
	Other potential terrestrial sources					
	Tropical trees	n.q.		n.q.		22, 23
	Temperate woodlands	n.q.		n.q.		24, 25
	Tropical ferns	n.q.		n.q.		26
	Abiotic decomposition	n.q.		n.q.		27
	Subtotal (Sources)	**143**		**111.5**		
SINKS	Ocean	56	(49 to 64)	49	(45 to 52)	3
	OH and photolysis	77		63.6		3
	Soils	40	(23 to 56)	32	(19 to 44)	28,29,30,31,32,33
	Subtotal (Sinks)	**177**		**147.6**		
	Total (SOURCES - SINKS)	**-34**		**-36.1**		

References: 1. UNEP/TEAP (2010). 2. UNEP (2007). 3. Yvon-Lewis et al. (2009). 4. King et al. (2002). 5. WMO (2006). 6. Andreae and Merlet (2001). 7. Thomas et al. (1997). 8. Varner et al. (1999a). 9. White et al. (2005). 10. Dimmer et al. (2001). 11. Redeker and Cicerone (2004). 12. Lee-Taylor and Redeker (2005). 13. Rhew et al. (2000). 14. Manley et al. (2006). 15. Drewer et al. (2006). 16. Cox et al. (2004). 17. Manley et al. (2007). 18. Rhew et al. (2001). 19. Mead et al. (2008a). 20. Lee-Taylor and Holland (2000). 21. Mead et al. (2008b). 22. Blei et al. (2010a). 23. Gebhardt et al. (2008). 24. Drewer et al. (2008). 25. Rhew et al. (2010). 26. Saito and Yokouchi (2006). 27. Wishkerman et al. (2008). 28. Shorter et al. (1995). 29. Varner et al. (1999b). 30. Rhew et al. (2007). 31. Hardacre et al. (2009). 32. Rhew and Abel (2007). 33. Teh et al. (2008).

CH_3Cl

CH_3Cl is thought to be responsible for about 13% of the destruction of the stratospheric ozone layer (Butler, 2000). CH_3Cl is the most abundant halocarbon in the atmosphere (average concentration of CH_3Cl in the atmosphere is 540 pptv (Khalil and Rasmussen, 1999)) and the

estimated annual flux required in order to balance loss through reaction with hydroxyl radicals is 3.5 Tg (Yokouchi et al., 2000). This gives CH_3Cl an atmospheric lifetime of 1 year (WMO, 2006). Although it is not a controlled substance, CH_3Cl has several natural sources and sinks in common with CH_3Br, which is a controlled substance.

The most recent estimates of CH_3Cl sinks and sources globally are shown in Table 1.2. The three biggest sources of CH_3Cl are oceanic production, biomass burning (Keene et al., 1999) and tropical plants and their leaf litter. Other terrestrial sources include biosynthesis and emissions from wood-rot fungi (Harper, 1985) and from other plants and soils (Rhew et al., 2002; Yokouchi et al., 2000).

The main global sink for CH_3Cl is thought to be the reaction with tropospheric and stratospheric hydroxyl radicals. However, soils may also be a potentially significant sink for CH_3Cl (Khalil and Rasmussen, 1999). CH_3Cl can be co-metabolised by bacteria, both by oxidation and hydrolysis. In addition, several methylotrophic bacteria can use CH_3Cl as a growth substrate (McAnulla et al., 2001).

Table 1.2: Summary of the estimated source and sink strengths (Gg y^{-1}) of methyl chloride (CH_3Cl) for 2006 taken from WMO (2006).

Source or sink type	Source or sink estimate (Gg y^{-1})	Reference	3D model studies	
			Lee-Taylor 2001	Yoshida 2004
SOURCES				
Tropical and subtropical plants	820-8200	1,2	2380	2900
Tropical senescent or dead leaves	30-2500	2,3		
Biomass burning	325-1125	1,4	733	611
Oceans	380-500	5,6	477	508
Salt marshes	65-440	1,2	170	170
Fungi	43-470	1	128	-
Wetlands	48	7	48	48
Rice paddies	2.4-4.9	8	-	-
Fossil fuel burning	5-205	1		
Waste incineration	15-75	1	162	162
Industrial processes	10	9		
Subtotal	(1743-13578)		4098	4399
SINKS				
OH-reaction	3800-4100	6,8	3850	3994
Loss to stratosphere	100-300	1		
Cl reaction	180-550	1	-	-
Soil	100-1600	1	256	256
Loss to cold waters (polar oceans)	93-145	5	-	149
Subtotal	(4273-6695)		4106	4399
Total (SOURCES - SINKS)	**(-4952-9305)**		**-8**	**0**

References: 1. WMO (2003). 2 Blei et al. (2010a). 3. Hamilton et al. (2003). 4. Andreae and Merlet (2001). 5. Moore (2000). 6. Yoshida et al. (2004). 7. Varner et al. (1999a). 8. Lee-Taylor and Redeker (2005).

However, the estimates of sources and sinks are highly uncertain. A large imbalance in the

budget of CH_3Cl is most likely due to the likelihood of unidentified sources as well as the uncertainty associated with current best estimates of known sources and sinks.

1.3.1 Unidentified or misestimated methyl halide sources

Despite the importance of CH_3Br and CH_3Cl both environmentally and economically, the estimates of sources and sinks are highly uncertain and remain poorly understood and quantified. The importance of constraining CH_3X budgets was first brought to the attention of the scientific community in an article by Butler (2000), appearing in Nature in 2000 and prompting further investigation. Known natural sources are estimated to significantly outweigh anthropogenic sources. Estimating natural sources and sinks of these methyl halides is inherently difficult because of the heterogeneous nature of natural systems. Achieving representative data across and within natural systems is difficult but if sufficient individual measurements can be taken then the scaling up or modelling of this data is possible. As such, anthropogenic sources can be reasonably estimated but the current estimates of natural source strengths are highly uncertain. A better understanding of the natural budget is required for understanding any potential effects of environmental and land-use change on global methyl halide concentrations.

Currently, the estimated known anthropogenic and natural sources (such as oceanic production and emissions from biomass burning) are substantially outweighed by the estimated sinks (which include removal via oxidation by hydroxyl radicals, uptake and degradation by the oceans and consumption by soils). A lack of understanding about sources and sinks and their strengths is more likely to have caused this large imbalance than any radical change to the atmosphere (Yokouchi et al., 2002).

Previous oceanic measurements of CH_3Br and CH_3Cl show that the imbalance cannot be corrected by emission or uptake by the oceans (Moore et al., 1996; Groszko and Moore, 1998). It is generally anticipated that missing sources are related to emissions from terrestrial vegetation and are not likely to be the result of overestimated sinks (Yvon-Lewis et al., 2009). Nearly all natural terrestrial systems investigated have been found to contribute to methyl halide fluxes to some extent. Therefore, recent study has focussed on the terrestrial biosphere to identify other natural sources of these compounds.

Several studies have contributed to an increased understanding of the contribution of terrestrial systems to methyl halide budgets in the atmosphere. Previous studies have looked at the fluxes of both methyl bromide and methyl chloride from various locations including salt marshes in Scotland (Blei et al., 2010a; Drewer et al., 2006) and Southern California (Rhew et al., 2002), temperate woodland ecosystems (Drewer et al., 2008), tropical vegetation and leaf litter (Blei et al., 2010a), and sub-arctic wetland in Sweden (Hardacre et al., 2009). These studies indicate that there are previously unidentified sources of methyl halides present in natural systems. They

also show that previous global estimates of certain sources may be incorrect due to lack of detailed data from different regions and seasons.

1.3.2 The mechanism of CH_3X production

The reason that plants synthesize and emit methyl halides is still unknown. The emission of these gases may be a means for plants to remove excess halide ions (Ni and Hager, 1999) or simply a "metabolic" accident that has no physiological function (Manley, 2002). However, salt tolerant species that might be expected to remove a large amount of excess halide ions have relatively low methyl transferase activities (Saini et al., 1995) and the amount of CH_3X emitted represents a only a fraction of the halide content in plants (Manley, 2002; Redeker et al., 2004).

The cellular-level production of CH_3X in plants appears to be related to the activity of the predominant methyl donor S-adenosyl methionine (SAM) (Manley, 2002; Saini et al., 1995) (Figure 1.6). However, the methylation of halide ions appears to be due to their ubiquitous occurrence in cell tissue rather than a particular affinity for halide ions of the enzymes responsible. Methyltransferase catalyzes a nucleophilic attack on the electrophilic carbon atom next to the sulfonium centre of SAM. Methyl transferase activity is known to be particularly high in Brassica species, from which high CH_3X emissions have been measured (Gan et al., 1998; Rhew et al., 2003b; Saini et al., 1995).

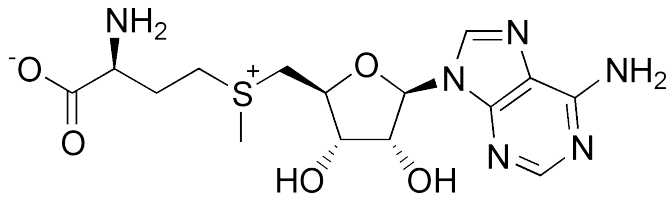


Figure 1.6: The chemical structure of S-adenosyl methionine (SAM). The transferable methyl group is bound to the nucleophilic sulfonium ion in the centre of the structure. Picture taken from: `http://en.wikipedia.org/wiki/S-Adenosyl_methionine`

The formation of CH_3Cl using this enzymatic mechanism has been reported for higher plants (Attieh et al., 1995; Saini et al., 1995; Wuosmaa and Hager, 1990), marine algae (Wuosmaa and Hager, 1990), and fungi (Watling and Harper, 1998; Wuosmaa and Hager, 1990). CH_3Cl appears to be accidentally emitted from fungi due to an imbalance in production and consumption of CH_3Cl at certain growth stages. The coupled pathways of CH_3Cl synthesis and utilisation are:

$$\mathrm{SAM} + \mathrm{Cl}^- \xrightarrow{\text{methyl transferase}} \mathrm{SAH} + \mathrm{CH_3Cl}$$

$$\mathrm{CH_3Cl} + \mathrm{RCOOH} \longrightarrow \mathrm{RC(O)OCH_3} + \mathrm{HCl}$$

where SAH is S-adenosylhomocysteine. In some species the pathways are tightly coupled and

CH_3Cl emissions are small (Harper et al., 1990) and in other species the imbalance is large, releasing large amounts of CH_3Cl to the atmosphere (Harper et al., 1989). The limiting factor for CH_3Cl release is therefore the imbalance in production and consumption rather than the speed of production.

CH_3Br was not considered to be a significant product of fungal growth due to the generally low bromine concentrations in terrestrial ecosystems and is not well described. However, several studies on both plants and fungi have come to the conclusion that preferential methylation of bromine over chlorine may explain the relatively greater CH_3Br emission despite the lower natural abundance of bromine (Attieh et al., 1995; Blei et al., 2010a,b; Hardacre and Heal, 2013; Manley, 2002; Redeker et al., 2004; Saini et al., 1995; Watling and Harper, 1998).

1.3.3 Trends and environmental drivers

Many long-term investigations have discovered an underlying annual cycle in CH_3X fluxes from several different ecosystems, including saltmarshes (Blei et al., 2010b; Drewer et al., 2006; Manley et al., 2006), peatlands (White et al., 2005), wetlands (Hardacre et al., 2009; Hardacre and Heal, 2013), rice paddies (Redeker and Cicerone, 2004) and temperate woodland leaf litter systems (Blei and Heal, 2011; Drewer, 2007). Fluxes were found to broadly correspond to seasonal trends in plant growth cycles, air temperature and light intensity with the highest emission rates observed during the growing season. Interestingly, some small emissions were also observed from a Scottish saltmarsh site during the non-growing season (Drewer et al., 2006). However, seasonal trends in CH_3X fluxes were not apparent in all long-term investigations (Manley et al., 2006; Rhew et al., 2002), possibly due to the comparatively mild winter climate conditions.

Diurnal variation in CH_3X fluxes has been observed at Scottish saltmarshes (Blei et al., 2010b; Drewer et al., 2006), some temperate woodland leaf litter sampling points (Drewer, 2007), Californian saltmarshes (Rhew et al., 2002), and from some tropical plant species (Blei et al., 2010a; Saito and Yokouchi, 2006). The observed diurnal cycles generally found that peak emissions corresponded to the warmest and lightest part of the day. Notably, where CH_3X emissions were observed, they generally continued into the night, albeit at a lower rate than in the daytime.

One exception to the normal CH_3X diurnal emission pattern was found in the tropical fern *Cyathea lepifera*, where the emission rates were lowest around midday and then peaked during the night (Saito and Yokouchi, 2006). There was no clear reason for the reversal in diurnal pattern for this particular species.

1.3.4 Analysis of methyl halides

Many analyses of methyl halides are carried out using a Gas Chromatograph (GC) which can separate and analyse compounds that can be vaporised without decomposition. The GC is usually coupled to either an electron capture detector (ECD) or a mass spectrometer (MS), although coupling to a less sensitive flame ionisation detector (FID) has been known (Saito et al., 2008). The analysis of halogenated hydrocarbons was revolutionised with the invention in 1957 of the ECD by Lovelock (1958), a detector capable of measuring small quantities of electronegative compounds such as CFCs. This design is still in use today. However, this system was not widely used until the 1970s when measurements were made of background CFC concentrations over the North Atlantic (Lovelock, 1971; Lovelock et al., 1973). These data, combined with other studies, were used to propose a global ban on CFCs for which Mario J. Molina, Paul J. Crutzen and F. Sherwood Rowland won a Nobel Prize in 1995.

An ECD cell (Figure 1.7) contains a radioactive source, usually ^{63} Ni, which emits β particles. The β particles repeatedly collide with carrier gas molecules producing secondary electrons which are further reduced in energy by further collisions. The low energy electrons can then be captured by suitable sample molecules, for example those containing a halogen atom(s), and the total electron population within the cell is reduced. In a pulse-modulated constant-current ECD any un-captured electrons are removed from the cell by applying short voltage pulses to the cell electrodes. The cell current that is created is maintained at a constant level relative to a reference current so that I_{cell} - I_{ref} = 0, by adjusting the pulse interval. When an electron capturing molecule passes through the cell the pulse rate increases and is measured as a voltage.

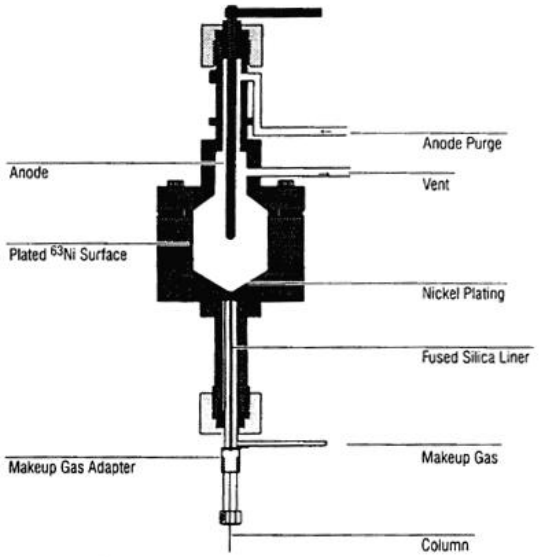


Figure 1.7: Schematic diagram for an ECD.

A GC-ECD is an appropriate method of analysing halide-containing compounds. However, it is not sensitive enough for analysis of low pptv CH_3Cl samples. One of the methods used to increase sensitivity is to dope the ECD with a very low flow of oxygen (O_2) (Zlatkis and Poole, 1981). O_2 doping is a common method of increasing ECD sensitivity and is achieved by adding a small amount of O_2 to the ECD make-up gas. Without O_2 doping there is direct electron capture by the sample molecule.

$$\text{radiation}\,(\beta) \longrightarrow P^+ + e^-$$

$$e^- + A \longrightarrow A^- + \text{neutrals}$$

If the sample molecule does not have a high electron affinity direct electron capture is too slow. Oxygen doping introduces an ion-molecule reaction between O_2^- and the sample molecule (CH_3Cl) which is faster than the direct electron capture by CH_3Cl:

$$\text{radiation}\,(\beta) \longrightarrow P^+ + e^-$$

$$e^- + O_2 \longrightarrow O_2^-$$

$$O_2^- + A \longrightarrow A^- + \text{neutrals}$$

Oxygen doping can be used in conjunction with a cryogenic trap to pre-concentrate the sample before analysis (Kerwin et al., 1996). Some studies have used only cryogenic pre-concentration (Redeker et al., 2000; Rhew et al., 2000) and others have used it in combination with adsorbent pre-concentration (Serça et al., 1998). One method of O_2 doping is to diffuse O_2 into the N_2 carrier gas flow across a sealed Teflon tube (Kerwin et al., 1996).

Cryogenic traps are the most commonly used pre-concentration units. Their main purpose is to reduce the sample volumes to less than a mL. They also allow the rapid injection of the pre-concentrated sample onto the column using flash heating, reducing the probability of peak broadening in the chromatogram. The materials commonly used are steel tubes packed with solid adsorbents such as Tenax or Carbotrap or glass beads (Blei, 2010; Drewer, 2007; Hardacre, 2010; Redeker et al., 2003; Rhew and Abel, 2007; Rhew et al., 2007; Saito and Yokouchi, 2006; Saito et al., 2008).

In order to cool the traps, either cryogenic materials such as dry ice (Redeker and Cicerone, 2004), solid CO_2 (Huang et al., 2000) or liquid N_2 (Redeker et al., 2003; Rhew et al., 2001; Rhew and Abel, 2007; Rhew et al., 2007; Saito and Yokouchi, 2006), Peltier cells (Prinn et al., 2000; Worton et al., 2008) or even Stirling motors (Saito et al., 2008) are used. The flash heating required for column injection is achieved by resistive heating either of the trap itself (Prinn et al., 2000) or of heating wires wrapped around it (Saito et al., 2008) or by reversing

the Peltier-cooling (Worton et al., 2008). Further detail on the GC-ECD chromatogram and pre-concentration system for methyl halide determination is given in Section 2.2.4.

1.4 Biogenic Volatile Organic Compounds

Estimates of emissions of biogenic volatile organic compounds (BVOCs) exceed emissions of anthropogenic VOCs by a factor of around ten worldwide, around $1150\,\mathrm{Tg\,C\,y^{-1}}$ from biogenic sources (Guenther et al., 1995) compared to $150\,\mathrm{Tg\,C\,y^{-1}}$ from anthropogenic sources (Müller, 1992). The importance of BVOCs was first recognised over 50 years ago with the discovery that the blue haze seen over forests was due to terpene emissions (Went, 1955).

BVOCs are important trace gases as they directly and indirectly control the distribution of air pollutants and GHGs and their lifetimes in the atmosphere. BVOCs react with atmospheric oxidants to generate tropospheric ozone, which acts as a pollutant in the troposphere (Fehsenfeld et al., 1992; Pierce et al., 1998). Recently, several studies have emphasised the role of BVOCs in the production of secondary organic aerosols (SOA) (Bonn and Moortgat, 2003; Bonn et al., 2004; Claeys et al., 2004; Lim et al., 2005; Singh et al., 1995; VanReken et al., 2006; Volkamer et al., 2006) which affect the Earth's radiative balance and cause air pollution episodes such as smog which may have health effects.

At the end of the 19th century, chemists struggled to define the structures of monoterpenes without the chromatographic and spectroscopic techniques now available. Otto Wallach won the Nobel Prize in Chemistry in 1910 for his concept of joining together isoprene units (C_5H_8) to produce terpenoid compounds, known as the "isoprene rule". Leopold Ruzicka also won a Nobel Prize in Chemistry in 1939 for his refinement of this mechanism, which he called the "biogenetic isoprene rule". He hypothesized the involvement of electrophilic reactions that generated carbocationic intermediates, which underwent subsequent C_5 addition, cyclization, and in some cases skeletal rearrangement before elimination of a proton or capture by a nucleophile to yield the observed terpenoid products (Monks, 2003).

Isoprene (Figure 1.8) and monoterpenes (Figure 1.9) are isoprenoids (or terpenoids), whose carbon skeletons are composed of characteristic C_5 units (McGarvey and Croteau, 1995). According to the number of C_5 units, they are subdivided into hemiterpenes (C_5 e.g. isoprene), monoterpenes (C_{10} e.g. α-pinene), sesquiterpenes (C_{15} e.g. β-caryophyllene) and other subgroups. Isoprene is the most dominant BVOC and is estimated to account for around $500\,\mathrm{Tg\,C\,y^{-1}}$ (43%) (Guenther et al., 2006). Monoterpenes also play an important role in atmospheric chemistry as well as being of economic significance, providing essential oils, carotenoid pigments and natural rubber. Sesquiterpenes are thought to be less important in terms of impact on atmospheric chemistry although some studies have reported emission rates on a

scale similar to monoterpenes (Schuh et al., 1997; Winer et al., 1992).

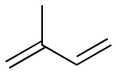


Figure 1.8: Isoprene.

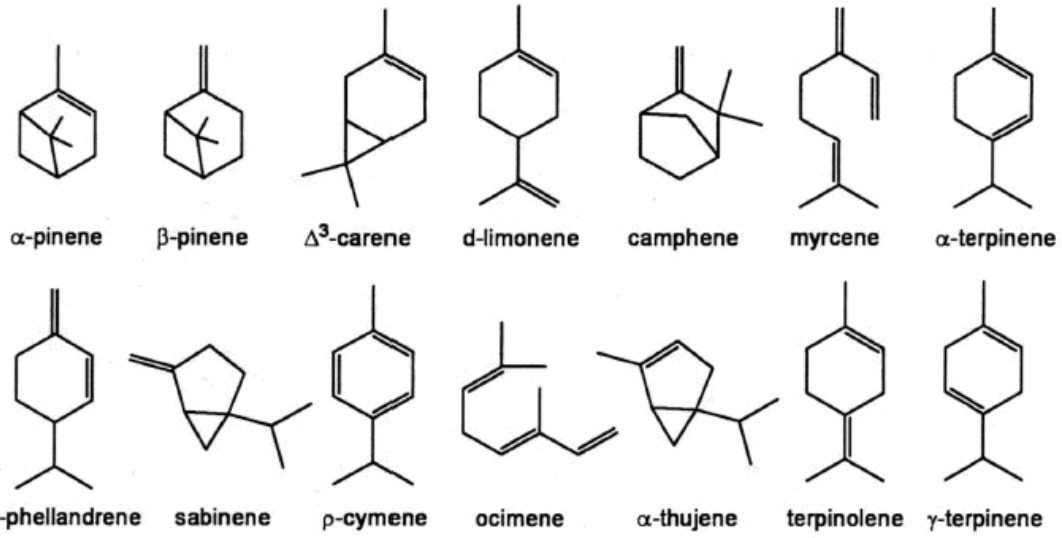


Figure 1.9: Some of the main monoterpene compounds including α-pinene, the most ubiquitous monoterpene.

As their name suggests, BVOCs are reactive under atmospheric conditions and many have a residence time of only a few hours (Table 1.3). Typical concentrations are in the pptv region although in forests concentrations of up to 15 ppbv can be reached (Finlayson-Pitts and Pitts, 2000).

1.4.1 Qualifying and quantifying BVOCs

Atmospheric composition and air quality are highly sensitive to BVOC emissions, in particular to isoprene (Pierce et al., 1998; Roselle, 1994). Despite the abundance and importance of BVOCs, considerable uncertainty persists because accurate emission estimates remain elusive for even the most highly emitted and well-studied BVOCs, namely isoprene and monoterpenes. The lack of experimental biomass densities and emission data on BVOC, in particular for agricultural plants, currently limits the set-up of a highly accurate plant-specific emission inventory (Karl et al., 2009).

The rate and composition of BVOC emissions varies widely between and within plant species so it is important to make measurements to build up an inventory of all terrestrial sources. The emission rates of isoprene and monoterpenes from many plants are quite well documented,

Table 1.3: Comparison of BVOC categories, lifetimes are estimated in relation to $[NO_3] = 10$ ppt, $[O_3] = 20$ ppb for night; and to $[OH] = 10^6$ molecules cm^3, $[O_3] = 20$ ppb for daylight conditions (Goldan et al., 1993; Guenther et al., 1995; Neeb et al., 1997; Singh et al., 1994). Source: Kesselmeier and Staudt (1999)

.

Name	Chemical lifetimes		Example	Atmospheric concentrations
	Day	Night		
Isoprene	3 h	1.5 h	isoprene	ppt to several ppb
Monoterpenes	2-3 h	5-30 min	α-pinene, β-pinene, sabinene	
	40-80 min	5-20 min	limonene, myrcene, t-β-ocimene	
	15-20 min	<1 min	terpinolene, α-phellandrene	
	<5 min	<2 min	α-terpinene	
Sesquiterpenes	<4 min	<2 min	α-caryophyllene	not detectable due to high reactivity
Other VOCs	>1 day		methanol, acetone	2-30 ppb

however there are a limited number of continuous and long-term flux measurements and there is still considerable uncertainty regarding the magnitude and seasonality of fluxes from different environments. Compounds emitted and emission rates vary widely between plant species and even within species. For example, standard emission rates (described in Section 4.1) of between 12 and 115 μg $g^{-1}_{dryweight}$ h^{-1} have been reported for different species of willow (Copeland et al., 2012; Evans et al., 1982; Hakola et al., 1998; Isebrands et al., 1999; Karl et al., 2009; Niinemets et al., 2010; Olofsson et al., 2005; Owen and Hewitt, 2000; Owen et al., 2003; Pio et al., 1993; Winer et al., 1992; Zimmerman, 1979) with a standard emission rate of between 18 and 41 μg $g^{-1}_{dryweight}$ h^{-1} reported for just one species of willow (*Salix alba*) (Karl et al., 2009; Niinemets et al., 2010; Pio et al., 1993).

It is also important to provide measurements to validate modeling of atmospheric BVOCs. With potentially dramatic future changes in land use and in climate it is important to understand not only the current BVOC budget but what might happen in the future. Modeled scenarios such as European afforestation and biofuel plantations in western USA and the Amazon calculated greatly increased emissions of isoprene, leading to increase groundlevel ozone concentrations and SOA (Ashworth et al., 2013; Lathiere et al., 2006; Wiedinmyer et al., 2006). Due to the importance of BVOC abundance in determining tropospheric O_3 and OH, systematic measurements and analyses of their sources is important in understanding the regional and global atmospheric chemistry.

1.4.2 Production of BVOCs

The reason that plants produce VOCs remains somewhat mysterious. Isoprene has no clear function (Fall, 1999), though it is thought it may have a role in protecting plants from thermal damage (Loreto and Velikova, 2001). The function of monoterpenes is also largely unknown, however they are thought to have a general ecological role, providing functions as diverse

as attracting pollinators, competitive phytotoxicity, and defending against herbivores (Monks, 2003).

Isoprene is synthesized directly from DMAPP (dimethylallyl diphosphate) by diphosphate elimination. This is catalyzed by the enzyme isoprene synthase (ISPS) which requires Mg^{2+} or Mn^{2+} to catalyze the elimination of inorganic pyrophosphate (OPP) from DMAPP to yield isoprene and OPP (Fall and Wildermuth, 1998) (Figure 1.10).

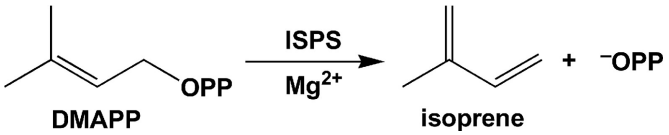


Figure 1.10: The synthesis of isoprene from DMAPP.

DMAPP exists in equilibrium with IPP (isopentenyl pyrophosphate). The electrophilic double bond isomerization catalyzed by IPP isomerase is a highly reversible reaction, with an equilibrium IPP:DMAPP ratio of about 6:1. In the next step of isoprenoid biosynthesis, the two five-carbon isomers condense to form a 10-carbon isoprenoid product called geranyl diphosphate (GPP). Monoterpenes are generated from DMAPP/IPP, via GPP (geranyl pyrophosphate) (McGarvey and Croteau, 1995). The simplest monoterpene synthase reaction is catalyzed by limonene synthase, a useful model for all terpenoid cyclizations (Hyatt et al., 2007) (Figure 1.11). An interesting feature of the monoterpene synthases is the ability of these enzymes to produce more than one product; for example, pinene synthase from several plant sources produces both α- and β-pinene.

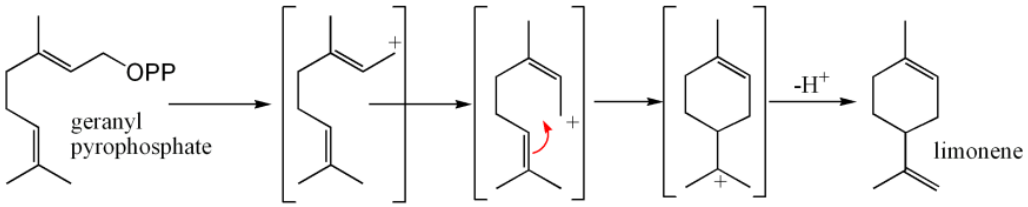


Figure 1.11: Limonene is formed from GPP (geranyl pyrophosphate) via cyclisation and deprotonation of a carbocation intermediate. Picture taken from: `http://en.wikipedia.org/wiki/File:LimoneneBiosynthesis`

1.4.3 Trends and environmental drivers

The compounds emitted and the emission patterns of different plant species are incredibly wide ranging so it is challenging to determine the effect of individual environmental factors. Any

environmental factor in a plant habitat may affect BVOC emission in the short-term or the long-term. Long-term influences alter the amount and composition of BVOC emissions slowly over days, months and years and are superimposed on short term influences. However, it is generally accepted that light and temperature greatly influence BVOC emissions.

There are few long-term studies on BVOC emissions, with the exception of Pressley et al. (2005), where growing season emissions were measured for several consecutive years. In this study, isoprene emissions were found to follow a strong diurnal cycle, increasing throughout the day with increasing temperature and light levels, peaking at mid-afternoon, and decreasing rapidly at night-fall. BVOC emission rates also follow a seasonal trends, with higher emission rates in warmer and lighter conditions (Monson et al., 1995).

Isoprene emission rates are controlled by both the capacity of the leaf to emit isoprene and the prevailing environmental conditions (Geron et al., 2000; Monson et al., 1994). Most plants do not emit isoprene immediately after bud-break but only reach their full potential emission rates after further leaf development and expansion (Monson et al., 1994). Monoterpene emission rates are dependent on the availability of monoterpenes from storage pools within the plant (Lerdau et al., 1995; Monson et al., 1995) and are also subject to environmental controls (Guenther et al., 1991; Yokouchi and Ambe, 1984).

The effect of variation in light and/or temperature were simulated for several plant species by Guenther et al. (1993) using a measured base emission rate and modelled light and temperature dependencies. Isoprene emissions were shown to exhibit behaviour similar to that of CO_2 i.e. emissions continue to increase with higher temperatures until a maximum emission rate is reached at about 40 °C, after which emissions rapidly decline (Guenther et al., 1993). This temperature dependence of isoprene emission is related to the enzymatic production of isoprene which is denatured at high temperature (Monson et al., 1992). Isoprene emissions were also found to increase with photosynthetically active radiation (PAR) up to a saturation point at 700-900 μ mol m^{-2} s^{-1} (Guenther et al., 1993). Monoterpene emission rates are highly dependent on temperature, although rates also vary depending on the type of monoterpene, the plant species, and other factors (Guenther et al., 1993).

Mechanical stress and injury can affect the emissions of BVOCs by plants. Several studies on known monoterpene emitters have reported emission bursts after slight mechanical stress such as mounting of vegetation in plant enclosure systems (Kesselmeier and Staudt, 1999). This is only observed for plants that store monoterpenes in secretory organs and represents a potential source of error when studying emissions in plant enclosure systems. Isoprene emissions appear to be unaffected.

Induced BVOC emissions are typically caused by insect attack (Gatehouse, 2002). For example, the release of BVOCs by corn seedlings as a reponse to caterpillar feeding was demonstrated

to attract wasps which attack and drive off the caterpillars (Turlings et al., 1995). In another study, herbivore-induced BVOC from tobacco plants were shown to repel ovipositing female moths and discourage larval feeding which damages the plant (De Moraes et al., 2001). Typical molecules used in plant defense systems are methanol, short-chain aldehydes, linalool, cis- and trans-β-ocimene and SQTs, such as β-caryophyllene and α-farnesene (Loreto et al., 2006).

Given the light dependency of isoprene and several monoterpenes and the correlation to photosynthetic activity, BVOC emissions would also be expected to to be sensitive to CO_2 concentration. Studies of this CO_2 dependency are scarce and limited to isoprene, investigating both the short- and long-term responses of isoprene emissions to CO_2 concentration. The magnitude of the response to changing CO_2 appears to vary according to plant species and other conditions (Arneth et al., 2007; Rosenstiel et al., 2004; Sharkey and Yeh, 2001).

1.4.4 Sampling and analysis of BVOCs

Field techniques

Conditioned stainless steel tubes packed with a mixture of adsorbents allows different BVOCs to be sampled simultaneously. Adsorbent techniques are a convenient way for BVOC sampling since adsorbent cartridges are usually small and robust enough for outside sampling. In these techniques, air is drawn through a tube filled with one or more solid adsorbents. As the air moves through, hydrocarbons stick onto the surface of the adsorbent. As different materials adsorb different compounds, the right adsorbent for target compounds has to be selected. Two or more adsorbents can also be used together so that air flows through the weaker adsorbent that adsorbs the larger molecules, and through the stronger one, adsorbing smaller molecules.

There are a wide variety of adsorbent materials, each with their own advantages and disadvantages. Tenax TA is a porous polymeric resin which can be used to collect monoterpenes and other hydrocarbons larger than C_6. Carbotrap is a carbon-based adsorbent, which can be used to collect C_3-C_{12} hydrocarbons. The compounds are desorbed for analysis from the adsorbent by heating up the adsorbent tube to around 300 °C.

Laboratory techniques

Gas Chromatography - Mass Spectrometry (GC-MS) is used to separate a gas mixture of compounds and is ideal for identification and quantification of BVOCs due to the complex mixture of compounds. Gas chromatography (GC) separates individual components according to their vapour pressures and solubility inside the GC column material as described in Section 1.3.4. In a mass spectrometer, chemical compounds are ionised to generate charged molecules

or molecule fragments which can then be measured as a mass-to-charge ratio. MS instruments consist of three modules: an ion source, which can convert gas phase sample molecules into ions; a mass analyzer, which sorts the ions by their masses by applying electromagnetic fields; and a detector, which measures the value of an indicator quantity and thus provides data for calculating the abundances of each ion present. Further detail on GC-MS chromatogram and mass spectra for BVOC determination is given in Section 2.3.4.

1.5 Overall aims

The principal aim of this study was to characterise the fluxes of methyl halides and BVOCs from both bioenergy crops and annual arable crops in order to compare them. To fully characterise the CH_3X and BVOC fluxes it was important to achieve good spatial and temporal coverage, and to monitor external environmental parameters. To achieve this, observational studies were carried out over a period of two and a half years at a site in England and for a year and half a year at two sites in Scotland.

The characterisation of fluxes was made in order to predict the possible future impact on atmospheric budgets caused by continued expansion of bioenergy crops. The fluxes of CH_3X and BVOCs from perennial bioenergy crops are not well understood and there is a paucity of data. This study provides long-term datasets which help to address this gap in the knowledge.

1.6 Thesis layout

The collection of air samples for analysis of CH_3X and BVOCs using gas chromatography techniques is described in Chapter 2 along with vegetation enclosure design. The calculations of CH_3X and BVOC fluxes from a gas concentration value are presented, together with a discussion of the uncertainties associated with these calculations. The characteristics of the three fieldsites are also described.

The CH_3X and BVOC datasets from the *Miscanthus* bioenergy crops are presented in Chapter 3. Seasonal, diurnal and inter-annual trends are discussed as are trends in fluxes in relation to the measured external environmental parameters (PAR, ambient air temperature, enclosure air temperature, soil temperature and soil water content).

Chapter 4 discusses the CH_3X and BVOC fluxes measured from SRC willow bioenergy crops, their trends and the relation to environmental observations.

The fluxes measured from the annual arable crops wheat and oilseed rape are described in Chapter 5. The trends and the relationships with environmental observations are also discussed.

Chapter 6 compares the CH_3X and BVOC fluxes measured from the bioenergy and annual arable crops.

Chapter 7 presents results from a controlled experiment using N fertiliser on *Miscanthus* in the greenhouse.

Chapter 8 offers a tentative scale-up of fluxes using the net fluxes measured at the three fieldsites.

Final conclusions are then presented in Chapter 9.

Chapter 2

General Methodology

In this chapter the general methods that were used throughout the project are described. The vegetation enclosures employed are detailed first, followed by the sample collection methods and the analysis techniques for methyl halides and BVOCs. Also illustrated are the calculation of fluxes and their associated uncertainties. The fieldsites are then described in depth. Methods that are only relevant to particular parts of the project are discussed in the relevant chapters.

2.1 Vegetation enclosures

The fundamental objective of this work was to obtain methyl halide and BVOC flux measurements from vegetation at various bioenergy crop sites. The main considerations for the enclosure system were to mimic natural conditions as closely as possible and for the system to be mobile and robust. It was also important to achieve reproducible conditions and allow monitoring of the conditions inside.

Vegetation enclosures were deemed to be the most appropriate approach to measuring fluxes. Previous enclosure systems employed in the study of CH_3X and BVOCs have been both static (no purge flow) and dynamic (flow-through). In a static system, compound concentrations increase with time following enclosure. A flux is calculated by dividing the change in concentration (emitted from the enclosed foliage) by the length of time that the vegetation is enclosed, and by the mass of the leaves.

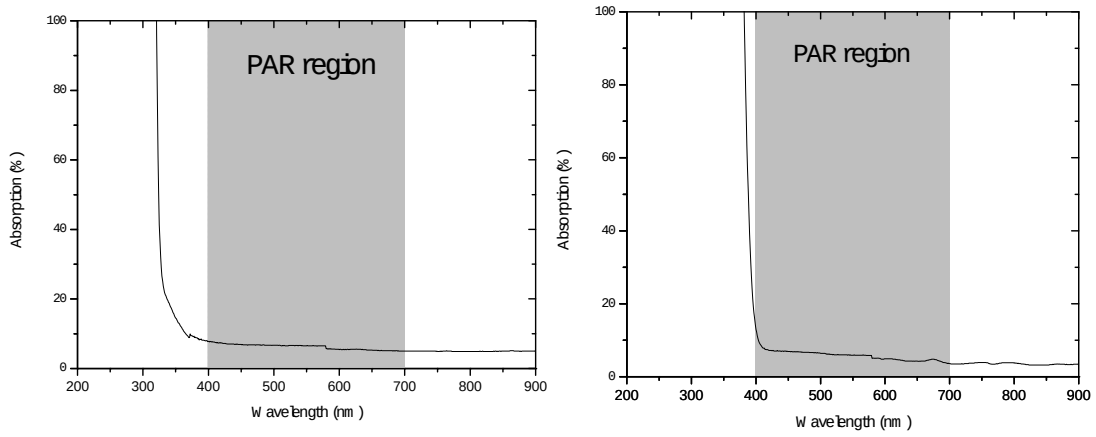
The advantage of static enclosures is the rapid concentration build up or depletion of any gases produced. Measuring a flux simply involves taking a before and after enclosure sample. This system is useful for measuring small fluxes. However, static enclosures can encounter problems of overheating and increased relative humidity due to the transpiration of the plant. There is also a concern that these strong concentration changes may alter the behaviour of the enclosed vegetation. These potential problems can be minimised by the use of shorter enclosure times and also by dynamic enclosures. However, one of the main disadvantages of dynamic enclosures is that the concentration differences between the samples at the start and the end of the enclosure

period are much smaller than for a static enclosure and therefore the measurement of small fluxes is more challenging.

CH_3X fluxes were measured using a static enclosure system because, despite the limitations listed, a build up of concentration of CH_3X was required in order to achieve measurable concentrations. A dynamic enclosure system was employed for BVOC measurements. This allowed the system to mimic natural conditions closely and reduce problems of overheating and increased relative humidity.

Materials such as Tedlar (polyvinyl fluoride), Teflon (fluorinated ethylene propylene, FEP), polycarbonate and polyethylene terephthalate (PET) are often used for vegetation enclosures. They are chosen for their flexibility in terms of size and shape, their chemical inertness, and their transparency to photosynthetically active radiation (PAR). This is important as CH_3X and BVOC fluxes can be influenced by PAR (Rhew et al., 2002). They are also durable and lightweight for use in the field.

Two enclosure chambers were used, one of polycarbonate of 1 mm thickness (26 L) and one of polyethylene terephthalate - cyclohexane dimethanol copolyester (PETG) of 1 mm thickness (66 L). Both materials are highly transparent to light in the photosynthetically active range (400-700 nm wavelengths), with very similar absorption spectra as shown in Figure 2.1.



(a) PETG **(b)** Polycarbonate

Figure 2.1: Absorption of radiation in the UV-Vis range by (a) PETG and (b) polycarbonate. The analysis was carried out on a small piece of sheet material which was placed in a UV-Vis spectrometer (ATI Unicam UV2-100).

The enclosures were constructed by bending the material into a cylindrical shape and then fixing in place using several opaque plastic rings slipped around the cylinder. The joining ends of the sheet were screwed together to form an air tight seal and one end of the cylinder was closed using a circular sheet of the same material. The open end of the cylinder was then lined with two rings of door-and-window-seal P-profile on the outside to allow a bag to be attached for use

in fitting the enclosure to a branch. Chambers were also fitted with a socket for mounting the chamber on a camera tripod.

Diameter and length of the enclosures were 32.5 cm diameter and 80 cm length for the bigger enclosure (66.36 L) and 25 cm diameter and 52.5 cm length for the smaller enclosure (25.77 L) (Figure 2.2). Both enclosures also featured two separate openings that were used to draw gas samples and to monitor inside air-temperature via a data-logger. The sampling port consisted of an 8 mm diameter hole, that was lined with an 8 mm grommet through which a 1 ml disposable syringe was fitted. The plunger of the outwards facing syringe had been removed and the the tip was connected with a silicone tube to a three-way tap (Discofix - 2, Braun, Melsungen, Germany).



Figure 2.2: Branch chamber design used for long-term field measurements. The enclosure here has length 52.5 cm and diameter 25 cm.

2.2 Methyl halides

2.2.1 Flux measurements

A static enclosure system was used for CH_3X flux measurements. After mounting the chamber on the tripod, several branches were enclosed within the vegetation chamber, with disturbance of the vegetation kept to a minimum. After enclosure for a defined period of time, an air sample of around 0.85 L was then extracted using a 1 L acrylic gas syringe (1000MAR-LL-GT, SGE Analytical Science Ltd, VIC, Australia) with three way tap and stored in 1 L air sample bags. These bags were Tedlar (polyvinyl fluoride) with polypropylene valves (232-01, SKC Inc., PA,

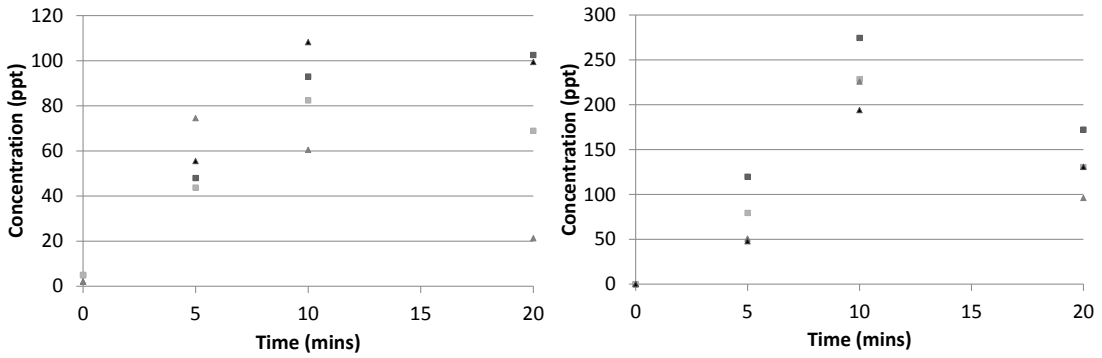
USA). Background samples of ambient air were collected and stored in the same way. Once filled the sample bags were stored at room temperature in darkness until analysis.

2.2.2 Enclosure time

The effect of enclosure time on the sampled CH_3X concentration was investigated in the field. CH_3X fluxes in $ng\,g^{-1}\,h^{-1}$ can be calculated more accurately from a longer enclosure time, but previous studies have shown that CH_3X fluxes can decrease during a longer enclosure (Dimmer et al., 2001).

In order to investigate the effect of various enclosure times on flux measurements, experiments were carried out at the fieldsite in Brattleby (described later in this chapter). Two sampling points in the *Miscanthus* and two in the SRC willow were sampled. The vegetation was enclosed and air samples were withdrawn at 3, 5, 10 and 20 minutes after the initial enclosure.

As shown in Figure 2.3, the CH_3Br and CH_3Cl concentrations increased after 3 minutes and again after 10 minutes (with one exception). However, the general trend was for emission to decrease after 10 minutes with lower fluxes at 20 minutes. This may be because plant activity was reduced due to stress during the enclosure, or because the gas concentration in the chamber was sufficiently high that it could no longer diffuse out of the plant stomata.



(a) Enclosure time series of CH_3Br

(b) Enclosure time series of CH_3Cl

Figure 2.3: Enclosure time series of CH_3Br and CH_3Cl concentrations conducted at Brattleby on the 13th July 2011: In *Miscanthus* (■) and (■) and in willow (▲) and (▲).

A 10 minute enclosure time was chosen as a compromise for continuity across all sampling sites. The enclosure time had to be sufficiently long for CH_3X to accumulate to detectable levels in the chamber at low activity sites, but short enough that fluxes were not under-estimated. Several other studies have utilised a 10 minute enclosure time (Blei, 2010; Drewer, 2007; Hardacre, 2010). A more accurate calculation of CH_3X fluxes could have been obtained by taking samples at three time points, e.g. 3, 5 and 10 minutes so that the CH_3X flux could be extrapolated back

to $t = 0$. However, this would have generated too many samples to analyse on a regular basis as one sample takes around 30 minutes to analyse.

2.2.3 Gross and net methyl halide fluxes

Using the best-fit line from the calibration curve, in the form $y = a + bx$, the mixing ratio of CH_3X (in pptv) in an unknown air sample was determined. The net CH_3X flux in an enclosure was derived from the difference between the mixing ratio of CH_3X in parallel enclosure and ambient air samples. From this mixing ratio the number of moles of CH_3X was calculated by rearranging the ideal gas law (pV = nRT) to give Equation 2.2.1, and the flux in the enclosure then calculated in $\mathrm{ng\,m^{-2}\,h^{-1}}$ using Equation 2.2.2.

$$n = \left(\frac{p \times V}{R \times T}\right) \times \mathrm{CH_3X\ mixing\ ratio\ in\ pptv} \times 10^{-12} \tag{2.2.1}$$

where p is the air pressure (assumed to be the standard atmospheric pressure of 101325 Pa), V is the volume of the chamber in $\mathrm{m^3}$, R is the gas constant of $8.314\,\mathrm{J\,K^{-1}\,mol^{-1}}$ and T is the air temperature during sampling in K.

The general formula for calculating methyl halide fluxes from static enclosures is:

$$\mathrm{flux} = \left(\frac{n \times M_R}{m_{dry} \times t}\right) \times 1 \times 10^9 \tag{2.2.2}$$

where M_R is the molar mass of CH_3Br ($95.94\,\mathrm{g\,mol^{-1}}$) or CH_3Cl ($50.54\,\mathrm{g\,mol^{-1}}$), t is the enclosure time in hours and m_{dry} is the dry mass of leaves enclosed by the chamber in grams.

2.2.4 GC-ECD analysis system

CH_3Br and CH_3Cl analysis in this study was carried out using an HP5890 gas chromatograph equipped with oxygen-doped electron capture detection and a ZB642 capillary column (Phenomenex Inc., Torrence, CA, USA) 30 m in length, i.d. 0.32 mm and 1.8 μm film thickness. A custom built, two-stage preconcentration unit was used prior to GC separation. This was controlled using a Labview program.

The first trap was a $\frac{1}{4}$ inch diameter by 100 mm long stainless steel tube filled with Tenax TA 60/80 mesh (Supelco, Bellefont, PA, USA). This was cooled to -30 °C before sample loading using dual two-stage Peltier cells (Melcor, Trenton, NJ, USA) so that all gases with boiling points lower than the trap temperature were flushed out with the carrier gas stream.

The second trap was a $\frac{1}{8}$ inch diameter by 200 mm long stainless steel tube filled with fine glass beads and cooled to -80 °C using dry ice. Again all gases which were not retained were flushed out of the vent, further concentrating the analyte. A 100 mL sample aliquot was loaded onto the first trap and the trapped analytes subsequently transferred to the second trap by heating to 150 °C and using switching valves (VICI, Houston, TX, USA). After 5 min the second trap was flash heated to 180 °C to transfer the analytes into the GC and onto the capillary column. The temperature programme inside the GC over was 5 min at 40 °C, ramping for 5 min at 40 °C min^{-1} and hold for 5 min at 240 °C, to remove any remaining compounds to avoid contaminating the next analysis.

The carrier gas was an argon methane mixture (90% argon, 10% methane) with a flow rate through the capillary column of ∼1.3 mL min^{-1}. When the sample reached the ECD it was made up with a 4% O_2/N_2 gas mixture with a flow rate of 15 mL min^{-1}, and a separate N_2 gas stream with a flow rate of ∼15 mL min^{-1} to give a total of 31.3 mL min^{-1}.

The combined modifications of cryogenic trapping and O_2 doping of the ECD allowed CH_3Cl to be analysed in combination with CH_3Br. The resulting chromatogram was recorded by a PC using TurboChrom software (Perkin Elmer) and the peak areas for the methyl halide peaks were integrated manually on the computer (see Figure 2.4). The retention times for CH_3Cl and CH_3Br were around 3.8 minutes and 4.8 minutes respectively.

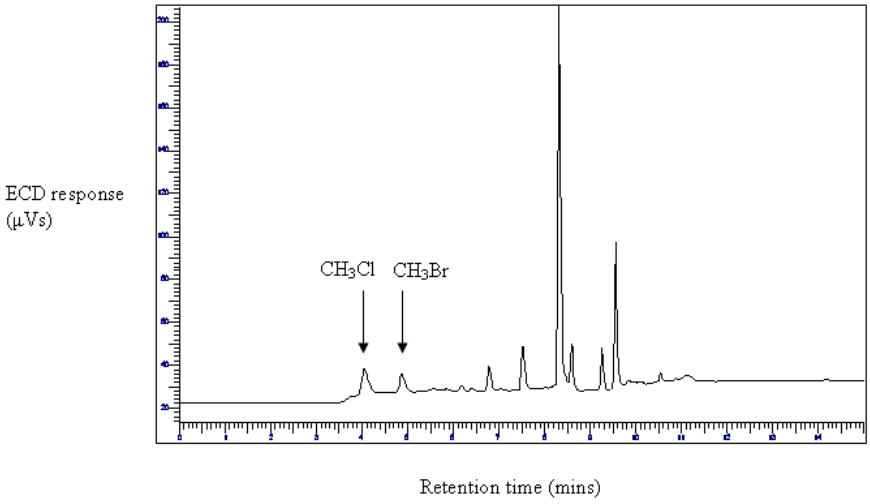


Figure 2.4: An example chromatogram for a 250 pptv CH_3Br/7900 pptv CH_3Cl standard. The x-axis is the retention time in minutes and the y-axis is the ECD response in μVs.

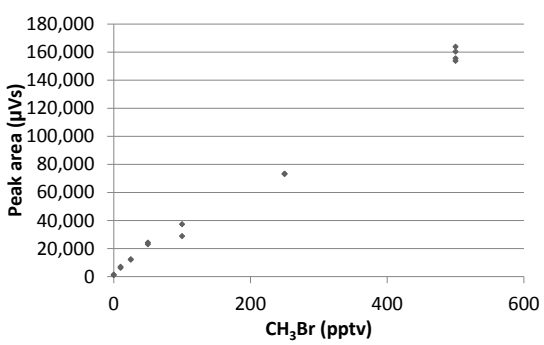
2.2.5 Standard make up and calibration curves

Calibration curves for CH_3Br and CH_3Cl were prepared weekly using dilutions of certified standards: 500±10 ppbv CH_3Br in nitrogen (Air Products Inc.) and 15.8±0.5 ppmv CH_3Cl in

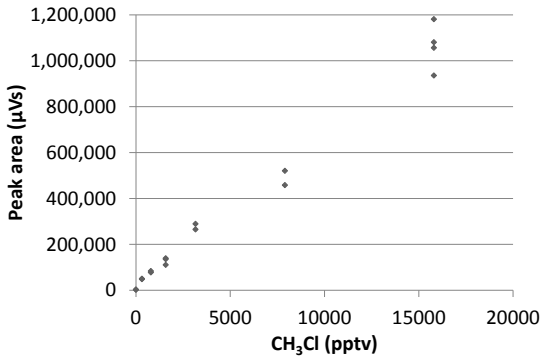
nitrogen (Air Liquide). A 5 L Tedlar bag was filled with 50 mL each of the the primary standards (500±10 ppbv CH_3Br and 15.8±0.5 ppmv CH_3Cl) and then made up to exactly 5 L with research grade nitrogen. This secondary standard was then further diluted in 5 L Tedlar bags to make up the final calibration standards (see Table 2.1). Example calibration curves are show in Figure 2.5.

Table 2.1: Calibration standards for CH_3X

CH_3Br (pptv)	CH_3Cl (pptv)
0	0
10	316
25	790
50	1580
100	3160
250	7900
500	15 800



(a) Calibration curve for CH_3Br



(b) Calibration curve for CH_3Cl

Figure 2.5: Calibration curves for CH_3X analysis by GC-ECD.

2.2.6 Linear regression

Assuming that the detector response is linear over the range of the calibration curve (which was checked visually for all calibration curves) linear regression can be used to describe the calibration curve. The slope b of the regression line is calculated as:

$$b = \frac{\sum_i \{(x_i - \bar{x})(y_i - \bar{y})\}}{\sum_i (x_i - \bar{x})^2} \tag{2.2.3}$$

where x_i and y_i are the individual calibration standards and and their individual detector responses and $\bar{x}$ and $\bar{y}$ are the mean standard concentration and the mean detector response respectively. Accordingly the intercept a is:

$$a = \bar{y} - b\bar{x} \tag{2.2.4}$$

The two values can then be used to give the expression for a straight line gradient:

$$y = a + bx$$

where y is the detector response to an sample of unknown concentration x. This can then be rearranged to give:

$$x = \frac{y - a}{b} \tag{2.2.5}$$

i.e. the formula for interpolation of the calibration curve to give an unknown concentration value from a measured detector response.

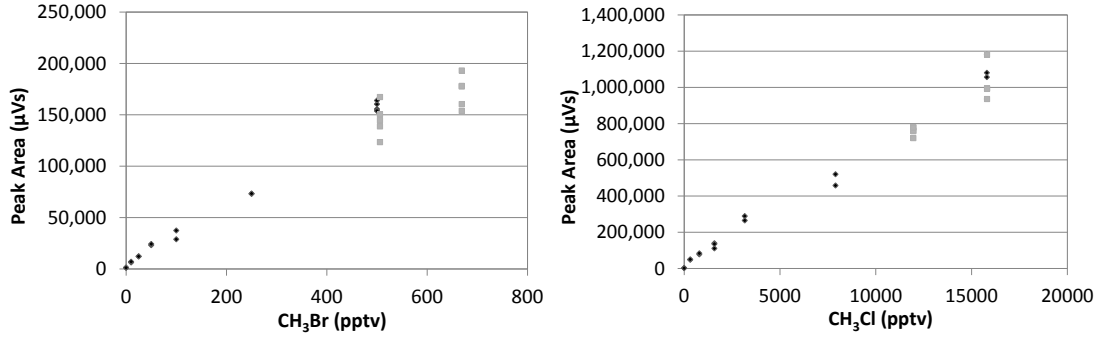
2.2.7 Intercalibration

Using standards kindly provided by Dr Kelly Redeker at the University of York, an intercalibration was carried out on the GC-ECD system used to analyse samples for CH_3X. Intercalibration methods compare one set of reference compounds, with well-known calibration characteristics, with another set of reference compounds, in order to derive accurate calibrations. This provides confidence in the calibrations and ensures consistency between the measurements of different instruments.

The certified standards used for weekly calibrations were 500$\pm$10 ppbv CH_3Br in nitrogen (Air Products Inc.) and 15.8$\pm$0.5 ppmv CH_3Cl in nitrogen (Air Liquide). The standards provided for intercalibration were 22 ppbv CH_3Br and 520 ppbv CH_3Cl. These standards were diluted in research grade nitrogen to provide a close approximation to the highest standard used in the usual full calibration (500 ppt CH_3Br/15 800 ppt CH_3Cl). Dilutions of 669 pptv CH_3Br/15 800 pptv CH_3Cl and 506 pptv CH_3Br and 11960 pptv CH_3Cl were made up and run six times each and the highest standard was run six times along with a full calibration using the other regular standards.

There was a good agreement between both sets of standards (Figure 2.6). The gradients of the linear fit to the scatter plots of each set of standard concentrations were not statistically different. The difference between the average peak area of 6 analyses of the 500 ppt and 6 analyses of the 506 ppt CH_3Br standards was 8.9% and between the two 15 800 ppt CH_3Cl standards was 3.8%. Taking into account that the variability in peak area between analyses of the same standard can

be up to 30% and that the dilution of the standards will add a degree of uncertainty, the results indicate consistency between standards.



(a) Calibration curve for CH_3Br **(b)** Calibration curve for CH_3Cl

Figure 2.6: Calibration curves for CH_3X analysis by GC-ECD using standards from Edinburgh (◆) and from York (■).

2.2.8 Stability of CH_3Br and CH_3Cl in Tedlar and Flex Foil Bags

The stability of CH_3Br and CH_3Cl gas standards in Tedlar bags and Flex Foil bags was tested in order to determine maximum storage times and to ensure that samples did not deteriorate rapidly during storage. This was relevant for field campaigns where the samples were stored for several days before analysis. The reactivity of the methyl halide molecules was not thought to be an issue, but there was the possibility that the bags might leak over longer storage periods or that methyl halides could adsorb or dissolve into the walls of the bags over time.

The concentration of methyl halides in the two bag types was monitored over time. The longest study was carried out in April and March 2010 on 5 L Tedlar and Flex Foil bags which were stored in the dark at room temperature. Concentration measurements were run together with weekly calibrations.

Dual CH_3Br/CH_3Cl standards of concentrations 25 ppt CH_3Br/790 ppt CH_3Cl (low standard) and 250 ppt CH_3Br/7900 ppt CH_3Cl (high standard) were prepared and analysed on day 1 of the study. Three 5 L Tedlar bags and three 5 L Flex Foil bags were filled with the low standard and three 5 L Tedlar bags and three 5 L Flex Foil bags were filled with the high standard. Samples were stored in the dark and kept at room temperature throughout this study. Aliquots were withdrawn for analysis on day 3, day 6, day 9, day 14, day 23 and day 36. The peak areas were normalised to the peak area of the relevant standard that was made up and analysed in the same week.

Both bag types filled with the high CH_3Br and CH_3Cl standard stayed fairly stable for over a week (see Figure 2.7). The low CH_3Br and CH_3Cl samples remained stable for 6 days

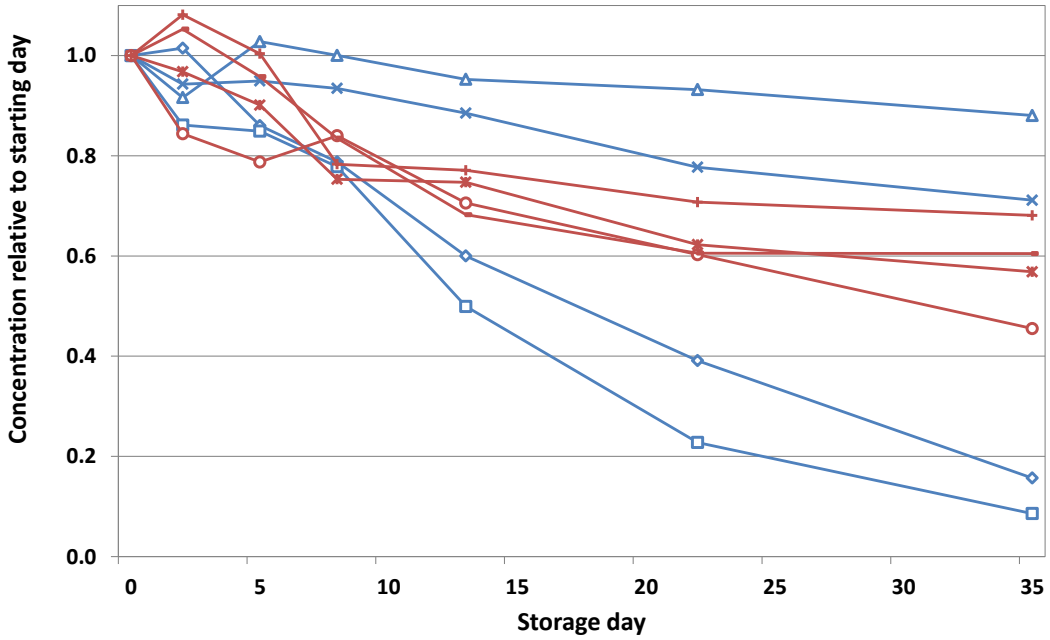


Figure 2.7: Stability study of dual CH_3Br/CH_3Cl standards at low (25 ppt CH_3Br/790 ppt CH_3Cl) and high (250 ppt CH_3Br/7900 ppt CH_3Cl) concentrations in Tedlar and Flex foil bags: 25 ppt CH_3Br in Tedlar bag ( ) and Flex foil bag ( ), 250 ppt CH_3Br in Tedlar bag ( ) and Flex foil bag ( ), 790 ppt CH_3Cl in Tedlar bag ( ) and Flex foil bag ( ) and 7900 ppt CH_3Cl in Tedlar bag ( ) and Flex foil bag ( ).

before deteriorating. All of the samples deteriorated steadily between 2 and 5 weeks, with the concentration of the low CH_3X standards decreasing more rapidly than the higher standards.

It was determined that samples should be analysed as soon as possible in order to avoid deterioration of concentrations, although concentrations remained fairly stable for the first week and higher concentrations may stay stable for up to 9 days in any type of bag. Samples were stored at room temperature and in the dark in order to mitigate deterioration. As samples were usually analysed within 2 to 3 days, a maximum concentration loss of no more than 15% is likely to have occurred for the analyses made in this work.

2.3 Biogenic Volatile Organic Compounds (BVOCs)

2.3.1 Flux measurements

Vegetation was enclosed in the same manner as for CH_3X measurements, with considerable care taken to keep plant disturbance to a minimum. After mounting the chamber on a tripod, the vegetation was carefully placed inside the chamber and enclosed. To create a dynamic enclosure

system, Teflon tubing was attached to a pump and ambient air was passed through the chamber at a rate of 12 L min^{-1} (Charles Austen Capex V2 oil-free double-ended diaphragm pump).

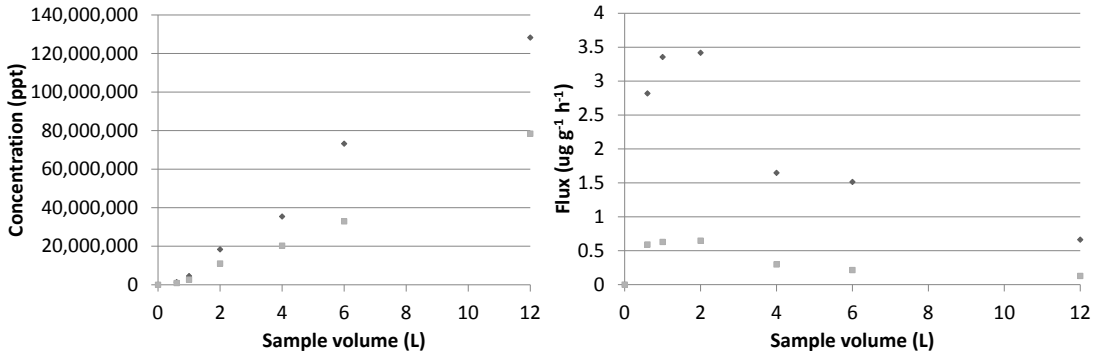
Samples were taken by pumping air from the enclosure through Teflon tubing onto adsorbent-packed tubes at a rate of 200 mL min^{-1} for a defined period of time. Three mass-flow control Pocket Pumps (210-1000 Series, SKC Inc., Eighty Four, PA, USA) were used to take the two enclosure samples (outlet) and background sample (inlet) almost concurrently. The pumps passed air through 6 mm OD stainless steel ATD tubes (L4270123, PerkinElmer, Waltham, MA, USA) packed with 200 mg poly(2,6-diphenylphenylene oxide) (Tenax® TA) (11982 SUPELCO, Sigma Aldrich, St Louis, MO, USA) and 100 mg Carbotrap® (20273 SUPELCO, Sigma Aldrich, St Louis, MO, USA). Prior to sampling, the packed tubes were conditioned at 300 °C for 15 minutes with a flow of helium.

2.3.2 Enclosure time

The linearity of the BVOC sampling process was tested by sampling increasing volumes from 0.6 L to 12 L. Measurements were taken at the fieldsite in Brattleby (described previously) using sampling points 1 and 2 in the SRC willow. The vegetation was enclosed using the small chamber (26 L) and the large chamber (66 L) and air samples were drawn at a rate of 200 mL min^{-1} for 3, 5, 10, 20, 30 and 60 minutes leading to sample volumes of 0.6 L, 1 L, 2 L, 4 L, 6 L and 12 L.

The results of these experiments (Figure 2.8a) show a linear dependency of BVOC concentration on the sample volume. When calculating fluxes using these concentrations, peak fluxes are calculated at around 10 minutes followed by a decrease after longer enclosure times due to the division of the concentration by the longer sampling time/larger volume (Figure 2.8b). It was not possible to regularly analyse samples at several enclosure times, therefore a 10 minute enclosure period was employed to provide as good a representation of the BVOC fluxes as possible. A ten minute enclosure with a sampling rate of 200 mL min^{-1} gives a 2 L sample volume which produces detectable concentrations but does not lead to under-estimation of fluxes.

This is similar to the sample volume used by Hakola et al. (1998) to measure BVOCs from tree species including willow, where a sampling rate of 60 mL min^{-1} was employed for 20 min to give a sample volume of 1.2 L. A 2 L sample volume is much lower than the lowest breakthrough volume (breakthrough volume is defined as the sampled volume corresponding to the end of the linear domain) observed in a study by Komenda et al. (2001). Breakthrough of monoterpenes was not observed until volumes greater than 18 L were reached and the lowest breakthrough volume was observed for hexane with a value of approximately 8 L.



(a) Isoprene concentration **(b)** Isoprene flux

Figure 2.8: Enclosure time series of isoprene concentrations and fluxes for increasing sample volume measured at the Brattleby fieldsite at SRC willow sampling points 1 and 2.

2.3.3 Gross and net BVOC fluxes

Net BVOC fluxes are derived from the difference between the concentration at the inlet and at the outlet, therefore some sources of inaccuracy uncertainty cancel out, such as in primary standard concentrations and their dilutions in an individual calibration curve. The major uncertainty in an individual concentration arises from the interpolations from a given calibration regression fit.

The emission rate, ER, (in $\mu g\, g^{-1}\, h^{-1}$) from a dynamic enclosure is calculated using Equation 2.3.1:

$$ER = \frac{[C_{out} - C_{in}] \times Q}{m_{dry}} \tag{2.3.1}$$

where C_{out} and C_{in} are the outlet (enclosure) and inlet (background) concentrations of the compound of interest ($\mu g\, L^{-1}$), Q is the flow rate of the purge air ($L\, h^{-1}$) and m_{dry} is the dried mass (g) of leaves enclosed.

2.3.4 GC-MS analysis system

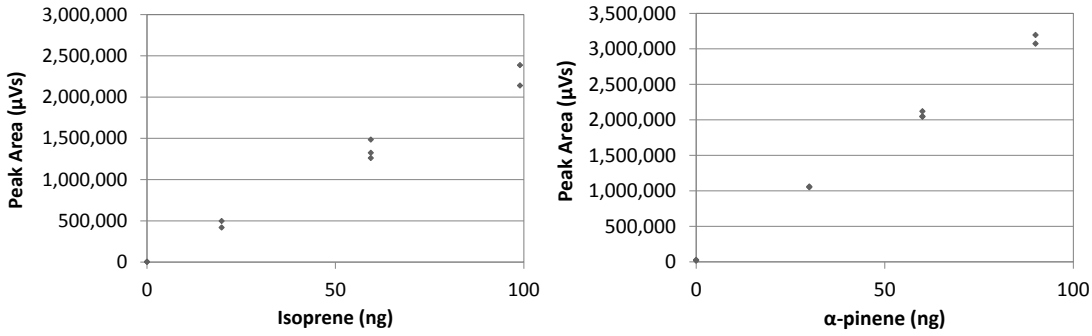
BVOC analysis in this study was carried out using gas chromatography-mass spectrometry (5890HP GC with a 5970HP mass-selective detector, Hewlett Packard, CA, USA). An Automated Thermal Desorber (ATD 400, Perkin-Elmer, MA, USA) used a flow of helium to desorb the sample from the tube (at 280 °C for 6 min) onto a Tenax TA cold trap at -30 °C. Transfer into the GC (Ultra-2 column, 100 m length, 0.2 mm I.D., 5% phenylmethyl silica, Agilent, CA, USA) was achieved by flash heating the cold trap to 300 °C for 6 min thereby

flushing the sample through a heated transfer line (200 °C). The GC was held at 35 °C for 2 minutes, ramped up to 160 °C at 3 °C min^{-1} then ramped up to 280 °C at 45 °C min^{-1} before being held at 280 °C for 10 minutes.

The mass spectrometer then allowed identification of compounds by comparison of retention times and mass spectra with literature data and quantification was achieved by comparison with a series of standards. The mass spectrometer was run in full scan mode to qualify compounds present. Fragment ions of compounds of interest were then selected for quantification. For example. quantification of α-pinene is achieved using the fragment ion at *m/z* 93. An example chromatogram is shown in Figure 2.9 (taken from Martin et al. (2003)).

2.3.5 Standard make up and calibration curves

Calibrations were carried out using dilutions of certified standards: 0.7 ppbv isoprene in nitrogen gas (BOC Gases, UK) and a 10 ng μL^{-1} mixed monoterpene (α-pinene, β-pinene, limonene, δ-3-carene, α-phellandrene and eucalyptol) in methanol standard solution (Sigma Aldrich, UK). Example calibration curves are shown in Figure 2.10.



(a) Isoprene calibration curve **(b)** α-pinene calibration curve

Figure 2.10: Calibration curves for BVOC analysis by GC-MS

Adsorbent packed tubes were loaded with small volumes of dilutions by injection whilst purging with helium to ensure effective deposition of the analyte onto the adsorbent. These dilutions made up the final calibration standards (Table 2.2). The standards were then analysed alongside each set of field samples. A set of standards was inserted between every set of around 8 field samples.

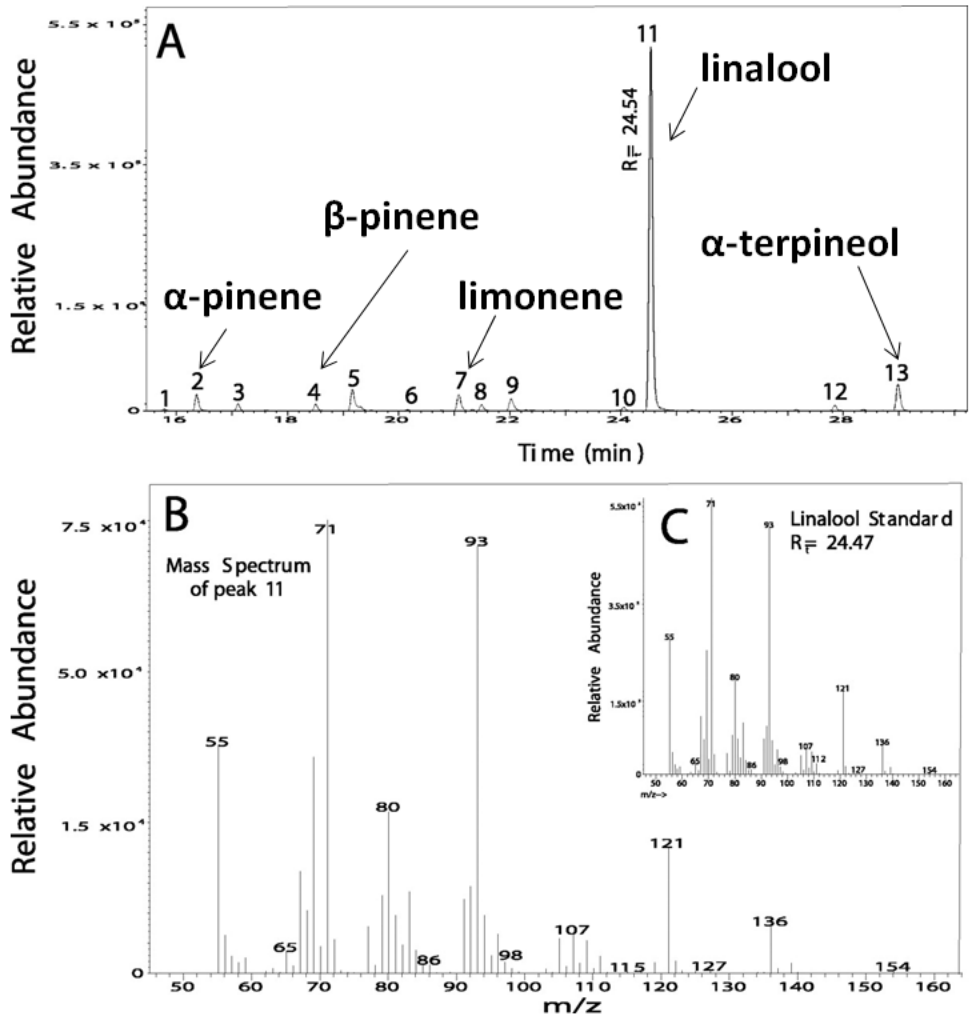


Figure 2.9: An example of the output from a GC-MS, taken from Martin et al. (2003). Chromatogram A shows the mass spectrometer output using full scan mode. The x-axis is the retention time in minutes and the y-axis is the relative abundance. A peak is selected according to retention time and the qualification of that peak can be verified by comparing chromatogram B with chromatogram C. Chromatogram B shows the mass to charge spectrum of the selected peak where the x-axis is now the mass-to-charge ratio and the y-axis is still the relative abundance. This is compared to Chromatogram C which shows the mass-to-charge ratio and relative abundance of a library reference, and from this the peak can be confirmed as being correctly identified.

Table 2.2: Calibration standards for BVOCs

Isoprene (ng)	Mixed monoterpenes (ng)
0	0
19.8	30
59.4	60
99	90

Assuming that the detector response is linear over the range of the calibration curve (which was checked visually for all calibration curves) linear regression can be used to describe the calibration curve in the same manner described for CH_3X calibrations in Section 2.2.7.

2.3.6 Quantification

Quantification of α-pinene is achieved using the fragment ion at *m/z* 93. Similarly, *m/z* 68 is used for isoprene. Monoterpenes not present in the calibration standards could be quantified using a response factor. Relative response factors were calculated by determining the relative contribution to ion *m/z* 93 of the monoterpene in relation to α-pinene as shown in Equation 2.3.2.

$$RF\ MT\ (93) = \frac{RF\ \alpha\text{-pinene}\ (93)\ \times\ Fraction\ \alpha\text{-pinene}\ (93)}{Fraction\ MT\ (93)} \tag{2.3.2}$$

where *RF* is the response factor for *m/z* 93 and *Fraction* is the contribution made by the *m/z* ion to the full mass spectrum. RF for α-pinene is known from the calibration curve. The fractional contribution of the *m/z* ion for a range of monoterpenes was calculated from relative abundances in the library mass spectra.

2.3.7 Stability of BVOCs on adsorbent packed tubes

A number of studies have shown that reasonable stability of VOCs adsorbed onto solid adsorbents can be achieved under proper storage conditions (Ciccioli et al., 1993; Janson, 1991; Lindquist, 1990; Vandendriessche, 1989). BVOC samples stored on adsorbent tubes should remain stable for months, even years, provided the tubes are capped correctly. Results of a stability study on a large number of common VOCs stored on standard $\frac{1}{4}$ inch tubes packed with 200 mg Tenax TA and loaded with approximately 10 μg of each component demonstrated negligible analyte losses after 11 months of storage (HSE, 1992).

Another study found that 1 μg each of benzene, toluene, and m-xylene on tubes packed with 200 mg Tenax TA adsorbent remained stable for up to 14 months (Vandendriessche, 1989). The effects of extended sample storage times are also reported for much lower levels of analyte. For example, data reported for tubes loaded with 4 ng monoterpenes demonstrates safe storage for at least 1 week (Janson, 1991) and data on over 100 VOCs ranging from 0.02 to 40 ng collected from rural air demonstrates safe storage for two months (Ciccioli et al., 1993).

2.4 Environmental monitoring

Previous studies have shown that CH_3X and BVOC fluxes cannot be related to the same environmental variables across all ecosystems. In salt-marsh ecosystems for example, CH_3Br fluxes have been correlated to environmental measurements such as temperature (Drewer et al., 2006) and photosynthetically active radiation (PAR) (Rhew et al., 2002). BVOC concentrations are also known to respond to environmental drivers (Schnitzler et al., 2002). In order to ascertain whether environmental factors had an influence on fluxes measured, as many drivers as possible were monitored during the enclosure period.

During each enclosure, the PAR, total solar radiation and the inner chamber temperature were electronically monitored (sampling rate between 2 s and 30 s) via a small weather-station (H21-002 Hobo Micro Station Data Logger, Onset Computer Corporation, Bourne MA, USA). An example of the output is shown in Fig. 2.11. The PAR sensor (S-LIA-M003 Photosynthetic Light Smart Sensor, Onset Computer Corporation, Bourne MA, USA) and total solar radiation sensor (S-LIB-M003 Solar Radiation Sensor, Onset Computer Corporation, Bourne MA, USA) were mounted levelly on a tripod beside the sampling point. The inner chamber temperature was recorded by a stainless steel temperature probe (S-TMB-M002 12-Bit Temp Smart Sensor, Onset Computer Corporation, Bourne MA, USA) which was inserted into the monitoring port of the chamber mentioned above. Soil temperature and moisture measurements were also made regularly. Micromet towers in the *Miscanthus* and willow field also provided continuous data on soil temperature at 5 cm depth, soil water content at 5 cm depth, rainfall and air temperature.

2.5 Other general methods

2.5.1 Soils

Soil samples collected from the field were immediately placed in air-tight zipper-bags and were kept in a fridge until analysis.

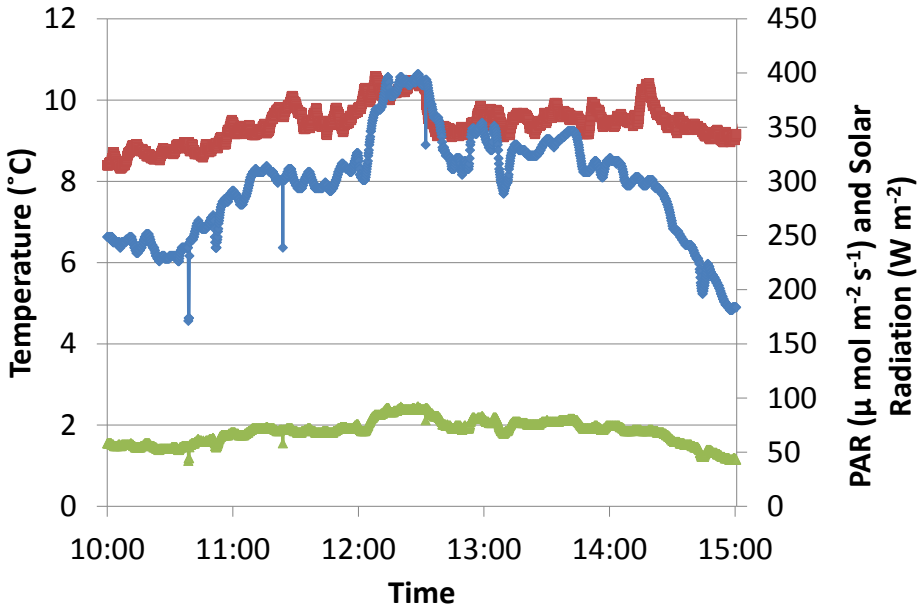


Figure 2.11: An example of the environment parameters monitored during measurements including PAR ( ), total solar radiation ( ) and the inner chamber temperature ( )

Determination of fresh weight, dry weight and water content

To measure the soil water content, 10 g of soil material was freed of any large and obvious root or plant material and placed in a pre-weighed foil tray. The masses of the tin and wet soil were recorded and the sample then dried in an oven at 105 °C to constant weight and the final weight recorded. Three replicates were measured for each sample.

pH

Measurements of soil pH were made using 10 g fresh soil mixed with 20 mL deionised water. This mixture was left for one hour before the pH was recorded with a Mp220 pH meter (Mettler Toledo, Columbus, OH, USA). Three replicates were measured for each sample.

Bulk density

Bulk density was measured by inserting a steel cutter of known volume into the soil and hammering it into the ground before removing it, scraping off soil flush with the edges and placing the soil collected into a zip-lock bag. Five replicates were taken for each bulk density measurement. The sample was dried in an oven at 105 °C to constant weight and the final weight

recorded. The bulk density was then calculated as follows:

$$\text{bulk density} = \frac{\text{(dry weight)}}{\text{(volume)}}$$

Elemental carbon and nitrogen content

For each soil sample, three replicates were analysed. Around 3 g were ground using a ball mill (Retsch, Hann, Germany). Samples were then analysed for total carbon and nitrogen on the Elementar Vario EL elemental analyser at CEH Lancaster.

2.5.2 Plant material

Determination of fresh weight and dry weight

Fresh weight of plant materials was recorded upon arrival in the laboratory. The leaves were put into paper bags and dried in an oven at 70 °Cto constant weight. The plant matter and bag were weighed immediately on a balance without prior cooling; the paper bag was emptied and also weighed.

2.6 Data analysis, statistics and quality control

2.6.1 Estimation of Errors and Uncertainties in CH_3X and BVOC Fluxes

Error sources for flux measurements

Several sources of uncertainties were encountered in the calculation of final flux values for CH_3X and BVOCs. The preparation of standards and analysis of standards and samples introduced the main sources of error, including:

- The value of the certified standards
- The dilution of the certified standards to provide a stock standard (for CH_3X calibrations)
- The dilution of a standard into a series of calibration standards
- Variability in the analytical systems such as the performance of the pre-concentration equipment, the chromatography performance and the detector
- The integration of the peaks in the chromatogram

However, as the net fluxes are derived from the difference between parallel enclosure and ambient samples, some sources of uncertainty cancel out, such as inaccuracy in primary standard concentrations and their dilutions in an individual calibration curve. The major uncertainty (s_{Δ_c}) in an individual concentration arises from the interpolations from a given calibration regression fit.

The sources of statistical uncertainty that affected the precision of the final calculated flux value were as follows:

- mixing ratio interpolated from a calibration regression fit (Δc) was often the largest single error source and is discussed in detail below
- pressure (p) was assumed to have no uncertainty associated with it
- volume (V) was given a different uncertainty value according to the measurement type conducted
  - For branch enclosures, volume uncertainty (s_V) was estimated to be 1.5×10^{-3} m^3 and 2.5×10^{-3} m^3 for small and large chambers respectively.
- temperature (T) was assumed to have an uncertainty (s_T) of 3 K
- the uncertainty of the time of enclosure (s_t) was dependent on the enclosure type and enclosure time
  - For enclosures of 3 min, s_t was assumed to be $\sim$4 seconds (0.0012 hours).
  - For enclosures of 5 min, s_t was assumed to be $\sim$8 seconds (0.0023 hours).
  - For enclosures of 10 min, s_t was assumed to be 20 seconds (0.0056 hours).
  - For enclosures of 20 min, s_t was assumed to be 30 seconds (0.0083 hours).
  - For enclosures of 30 min, s_t was assumed to be 36 seconds (0.01 hours).
- The mass of dried plant material m was another source of statistical uncertainty. Since the uncertainty s_m for branch measurements was likely to be variable, it had to be calculated separately for each enclosed branch individually.

Any other sources of error not mentioned here were dismissed as being insignificant contributors to the overall uncertainty of the calculations. The two main and also more complex sources of uncertainty, the before/after- enclosure concentration difference (Δc), and the total dry mass (m) for branch enclosures mentioned above are discussed next in more detail.

Statistical uncertainty of instrumental analysis

The preparation of standards and the analysis of standards and samples introduced several sources of uncertainty into the final flux values calculated. Identified sources of uncertainty include: the

value of the certified gas standard, the dilution of the certified standard to the working standard, the dilution of the working standard into the series of calibration standards, the performance of the analytical system and the manual integration of peaks in the chromatogram.

The uncertainty value (s_{Δ_c}) of the concentration difference between the enclosure sample and the concurrent background sample is derived from the uncertainties present in both, described above. It is assumed that any error for both values is solely due to the GC measurements and not due to variation from sample collection or storage. Apart from the uncertainty in the certified standards, the uncertainties listed are random and are accounted for when the uncertainty for an individual sample (from interpolation from the standard curve) is calculated:

$$s_{x_0} = \frac{s_{y/x}}{b}\sqrt{1+\left(\frac{1}{n}\right)+\frac{(y_0-\bar{y})^2}{b^2\sum(x_i-\bar{x})^2}} \tag{2.6.1}$$

where s_{x_0} is the standard error in the interpolated concentration, $s_{y/x}$ is the standard error in the regression line, b is the slope of the regression line and y_0 is the experimental value of y (the peak area). The values for $s_{y/x}$ and b were calculated in Microsoft Excel. Because the value of $(y_0 - \bar{y})^2$ will be larger (Equation 2.6.1) for high and low concentration samples, the range of standards was selected to ensure that most of the sample concentrations would lie in the middle of the range of standards.

The statistical uncertainty is therefore subject to any statistical error in the individual flux measurement and the standard curve used. The formula expressing this relationship is:

$$s_{x_0} = \frac{s_{y/x}}{b}\sqrt{\frac{1}{m_{\text{measurement}}}+\frac{1}{n_{\text{standards}}}+\frac{(y_0-\bar{y})^2}{b^2\sum_i(x_i-\bar{x})^2}} \tag{2.6.2}$$

where s_{x_0} is the statistical uncertainty for an individual concentration value x_0, $n_{standards}$ is the number of standards measured to construct the calibration curve used for interpolation, $m_{measurement}$ is the number of repeat measurements used to determine the sample concentration, $s_{y/x}$ is a measure of the errors in the y- direction in the calibration curve and is defined as:

$$s_{y/x} = \sqrt{\frac{\sum_i(y_i-\hat{y}_i)^2}{n_{\text{standards}}-2}} \tag{2.6.3}$$

with $\hat{y}_i$ being the y- values calculated for the individual x-values from the calibration curve with a and b from the regression line. All other symbols here were already defined in Equation (2.2.3)

The first part of Eq. (2.6.2) incorporates the size of the y-residuals between the fitted and actual detector signals from the calibration curve to measure the variability of individual measurements for known concentrations. The first and second term under the square root account for the fact that the statistical uncertainty grows smaller the larger the number of calibration and sample measurements. The last term under the square root measures how near the actual y-value of an individual sample is to the centre of the calibration curve, since the statistical error increases the further a y-value is from the centre.

Once both the statistical concentration uncertainties of a sample s_{sample} and its corresponding background/blank sample $s_{background}$ has been calculated the overall uncertainty $s_{\Delta c}$ for the concentration difference is calculated as:

$$s_{\Delta c} = \sqrt{s^2_{\text{sample}} + s^2_{\text{background}}} \tag{2.6.4}$$

Statistical uncertainty of total leaf material mass

The mass of leaves on a branch was calculated by multiplying the average mass of a number of leaves taken from a branch with the number of leaves on the branch. Assuming that the number of leaves on a branch were counted accurately then the average mass of the leaves remains as a source of uncertainty. The best statistical measure for quantification is the standard error of the mean s_{foliage} which takes account of both the variability of the average leaf mass $\bar{m}_{\text{dried leaves}}$ and of the number $n_{\text{leaves weighed}}$ of leaf samples used to derive an average value:

$$s_{\text{foliage}} = \frac{\sqrt{\sum_i (m_{i,\text{ leaf}} - \bar{m}_{\text{dried leaves}})^2 / (n_{\text{leaves weighed}} - 1)}}{\sqrt{n_{\text{leaves weighed}}}} \tag{2.6.5}$$

where $m_{i,\text{ leaf}}$ is the mass of each individual leaf that was weighed.

Final error propagation calculations

Finally, using error propagation calculations, the overall uncertainties for a flux are calculated as:

$$s_{F_{\text{branch}}} = F_{\text{branch}} \times \sqrt{(\frac{s_{\Delta c}}{\Delta c})^2 + (\frac{s_V}{V})^2 + (\frac{s_T}{T})^2 + (\frac{s_t}{t})^2 + (\frac{s_{\text{foliage}}}{m_{\text{foliage}}})^2} \tag{2.6.6}$$

where s_{Δ_c} is the uncertainty in the mixing ratio, s_V is the uncertainty in the volume, s_T is the uncertainty in the temperature, s_t is the uncertainty in the enclosure time and $s_{foliage}$ is the uncertainty in the dried leaf mass enclosed.

LOD

In this study it was important to determine the limit of detection (LOD) i.e. the lowest analyte concentration likely to be reliably distinguished by the analytical procedure. Sufficient analyte concentration must be present to produce an analytical signal that can reliably be distinguished from the signal produced in the absence of analyte. If a sample concentration was not outside of the range of the LOD it could not be stated as a significant concentration and was assumed to be zero for all further purposes. The LOD is defined here as the 95% confidence limit calculated using Equation 2.6.7:

$$\pm\left(s_{\Delta_{LOD}} \times 1.96\right) \tag{2.6.7}$$

where $s_{\Delta_{LOD}}$ can be calculated for an individual sample using:

$$s_{\Delta_{LOD}} = \sqrt{s^2_{interpolation} + s^2_{standard}} \tag{2.6.8}$$

where $s_{interpolation}$ is the value of s_{x_0} calculated using Equation 2.6.1 and $s_{standard}$ is the uncertainty in the certified standard. 1.96 is the *t* statistic for the 95% confidence limit. For methyl halides, the uncertainty in the CH_3Br standard was $\pm$2% and for the CH_3Cl standard was $\pm$3%. For BVOCs, the uncertainty in the isoprene standard was $\pm$2% and the mixed monoterpene standard was $\pm$2%.

The average LOD was 10 ppt for CH_3Br fluxes and 350 ppt CH_3Cl fluxes (Table 2.3). For example a sample mixing ratio would have to be outside of the range of 10 ppt to be considered as a net emission. If a sample mixing ratio was not outside of the range of the limit of detection it could not be stated as significantly different from the background air mixing ratio and was taken as zero. If a mixing ratio was outside the limit of detection it was a positive flux. The average LOD was between 30 and 45 ppt for BVOC fluxes (Table 2.3).

Table 2.3: Average limit of detection (LOD) for CH_3X fluxes in ppt and $ng\,g^{-1}\,h^{-1}$and BVOC fluxes in ppt and $\mu g\,g^{-1}\,h^{-1}$.

	ppt	$ng\,g^{-1}\,h^{-1}$or $\mu g\,g^{-1}\,h^{-1}$
CH_3Br	10	2.6
CH_3Cl	350	47
Isoprene	45	0.13
α-pinene	44	0.13
β-pinene	37	0.11
δ-3-carene	27	0.08
Limonene	31	0.09

2.6.2 Statistical methods

Statistical analysis of experimental results was performed using either The R Project for Statistics (a free online statistical package) or Microsoft Excel. Various functions within the R i386 2.15.1 software package were employed for most of the statistical analyses described. Linear regression fits were calculated with Microsoft Excel software. All statistical significance tests, unless stated otherwise, were performed at a significance level of $P = 0.05$.

Analysis of variation in gas fluxes in relation to sampling site and season was conducted using the Kruskal-Wallis analysis of variance. The KruskalWallis one-way analysis of variance by ranks is a non-parametric method for testing whether samples originate from the same distribution (the non-parametric version of the one-way analysis of variance ANOVA). It is useful for comparing more than two independent samples. If the Kruskal-Wallis test leads to significant results, then at least one of the samples is different from the other samples.

Correlations between different gas fluxes and correlations between gas fluxes and environmental variables were analysed using Spearman's Rank correlation. Spearman's rank correlation coefficient is a non-parametric measure of statistical dependence between two variables. It assesses how well the relationship between two variables can be described using a monotonic function. If there are no repeated data values, a perfect Spearman correlation of +1 or -1 occurs when each of the variables is a perfect monotone function of the other.

2.7 Sampling sites and characterisation

The overall aim of this study was to characterise reactive gas fluxes from perennial bioenergy crops and annual arable crops in the United Kingdom. Three different field sites were investigated, one in the East Midlands of England and two in lowland Scotland. The main fieldsite was located in Brattleby, Lincolnshire, England, and was sampled about once a month

between February 2010 and August 2012. The Arnot fieldsite in Perthshire, Scotland was sampled monthly between August 2011 and August 2012. A third site in East Grange, Fife, Scotland was also sampled monthly between March and August 2012.

2.7.1 Brattleby, Lincolnshire

Location and description

Brattleby is a small village in rural Lincolnshire, England. It is 5 miles north of Lincoln, to the west of the A15, and close to RAF Scampton (Lat: 53°18′55″N, Lon: 0°34′40″W) (Fig. 2.12a). The field site is a commercial farm located on the outskirts of the village. The site contains adjacent fields planted with the perennial bioenergy crops SRC (short rotation coppice) willow (*Salix* spp.) and *Miscanthus* (*Miscanthus x giganteus*) and the annual arable crops wheat (*Triticum aestivum*) and oilseed rape (*Brassica napus*) on rotation (Fig. 2.12b). The energy crops grown at this field site are used for co-firing at the nearby Drax power station in North Yorkshire. The fieldsite is located in a predominantly flat area and is surrounded by arable fields.



(a) Map of the United Kingdom showing the approximate location of Brattleby, Lincolnshire.



(b) Aerial picture of the Brattleby site with fields of interest distinguished.

Figure 2.12: Location of the Brattleby fieldsite and layout of the fields within the site.

Short rotation coppice willow (SRC willow) was established on around 6.5 ha in 2002 and was cut back in 2003 before it was first harvested in October 2007 and again in March 2011. The high-density plantation was established with around 15 000 stools ha^{-1} of five different varieties (Tora (30%)and Bjorn *S. viminalis x schwerinii*, Jorr, Jorunn, Orm and Ulv (*S. viminalis*)) planted at random to avoid the spread of diseases. Trees were planted in pairs of rows 1.3 m

apart, with 0.6 m spacing within each pair. Around 11 ha of *Miscanthus* was established in 2005, and is harvested annually during the spring, with the first harvest in 2007 and further harvests during the sampling period in March 2010, 2011 and 2012. *Miscanthus* rhizomes were planted at a density of 10 000 rhizomes ha^{-1}. The annual arable crop had a crop rotation of wheat to oilseed rape back to wheat during the measurement period.

Sampling sites

A total of ten sampling sites were used within each field of each crop of interest, as shown in Figure 2.13. The terrain is very similar across the fieldsite so the accessibility of the sampling site was the main consideration when choosing the sampling sites. The sites in the *Miscanthus* include plants on the edge of the plantation and within the plantation, as do those in the annual arable field. In the willow field, sites were restricted to plants on the edge of the field as it was not possible to set up the equipment within the plantation.

Edge effects on vegetation have previously been found both to be pronounced and to be insignificant and are very much site-specific (Camargo and Kapos, 1995; Young and Mitchell, 1994). A study in a Brazilian rainforest found that soil moisture was lowest at the extreme edge of the forest but was highest immediately inside the edge (Camargo and Kapos, 1995). This may be due to the influence of wind and PAR on increasing evapotranspiration at the field edge. This may consequently lead to variation in canopy height with distance from the edge. The degree of the edge effect is also dependent on the direction of the edge with wind-facing edges experiencing more severe effects (Young and Mitchell, 1994).

The influence of edge effects on trace gas emissions is not well known. Laurance et al. (1998) suggest that edge effects lead to increased emissions of some trace gases. However, their research was based on fragmentation and disturbance of large forest areas over a long time period and it is difficult to make any comparison to this work as the crops studied only grow for 1 to 3 years.

Agricultural management

Prior to conversion to bioenergy crops, the *Miscanthus* and SRC willow fields were managed identically to the annual arable crop fields. The crop rotation cycle usually employed was 3 years of wheat and 1 year of oilseed rape. Directly prior to conversion, both bioenergy crop fields had 3 years of wheat cultivation and received N-fertiliser. The bioenergy crops did not receive any N fertiliser in the duration of this research or during the establishment phase. The only disturbance was caused by the annual harvests for *Miscanthus* and three to four yearly harvest for willow. In contrast, the annual arable crops received three applications of N-fertiliser every



Figure 2.13: Location of sampling sites within fields at Brattleby. Ten sites were sampled in each field of interest.

spring (35/70/35 kg N ha^{-1} totalling 140 kg N ha^{-1} yr^{-1}). The annual crops were harvested in August, and the new crop was directly drilled into the stubble field in early September.

Soil properties

The soil association at the site is Beccles 1, fine loam over clay and the bedrock is Charnmouth mudstone formation. As the fields lie adjacent to one another, soil conditions are similar across the site. The soil pH was 7.12 ± 0.10 (standard deviation (SD) of 3 replicates) in the *Miscanthus*, 5.06 ± 0.12 in the willow and 6.32 ± 0.68 in the field with a wheat and oilseed rape rotation. Total elemental carbon content was 1.22% in *Miscanthus*, and 2.18% in willow and total elemental nitrogen content was 0.3% and 0.37% respectively. Bulk density was 1.43 ± 0.06 g cm^{-3} in *Miscanthus*, 1.35 ± 0.24 g cm^{-3} in willow and 1.22 ± 0.06 g cm^{-3} in the field with wheat and oilseed rotation.

Climate conditions

As the fields are adjacent, the climate conditions are consistent across the site. Continuous weather data is provided by both a meteorological station at Scampton, just under a mile from the site, and a meteorological tower within the site. Long-term measurements (1971 to 2000) collected at Scampton reveal a long-term mean annual minimum temperature of 5.9 °C and a long-term mean annual maximum temperature of 13.1 °C. Long-term (1963 to 2004) mean annual rainfall was 605 mm.

The meteorological tower set up in the *Miscanthus* field in 2008 provided half-hourly measurements of soil temperature and soil water content at 5 cm depth and hourly measurements of solar radiation, air temperature, pressure, wind speed, wind direction and rainfall.

December 2010 was the coldest December in 100 years, with snow falling in most areas of the UK and temperatures struggling to get above freezing during the day. These extreme end of year temperatures may have contributed to a low annual average air temperature of 8.6 °C and soil temperature of 8.7 °C. Average daily rainfall was 1.5 mm and average soil water content at 5 cm depth was 0.3 vol vol^{-1}.

Extreme weather also occurred in 2011. In June 2011 drought was declared in East Anglia with near drought conditions in the South East, South West and the Midlands. These were the driest conditions across England and Wales since 1900. A higher annual average air temperature of 10.5 °C and soil temperature of 9.8 °C were measured. Average daily rainfall was 1.2 mm, lower than 2010, and soil water content was also lower at 0.28 vol vol^{-1}.

Following drought in 2011 and early 2012, flooding occurred in many parts of the UK in spring and summer 2012, including Lincolnshire. In July, The average monthly rainfall for the Midlands (60 mm) fell in just 24 hours causing flash flooding. In the three year measurement period, the highest annual average air temperature of 12.6 °C was recorded in 2012. The soil temperature of 10.1 °C was also slightly higher than other years and despite the flooding the soil water content was 0.3 vol vol^{-1}, the same as in 2010.

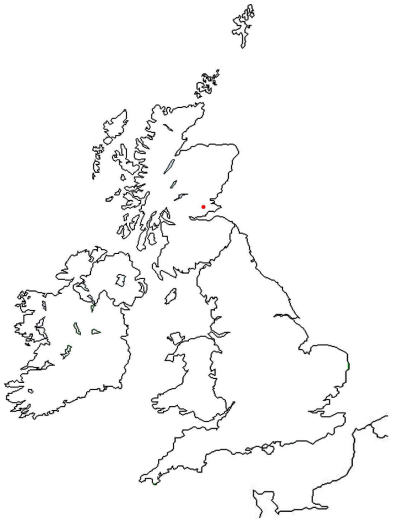
2.7.2 Greenhead of Arnot, Perthshire

Location and description

Greenhead of Arnot is a farmstead situated high on the south side of the Lomond Hills Regional Park in Perth and Kinross, Scotland (Lat: 56°20′10″N, Lon: 3°27′25″W) (Fig. 2.14a). The field itself (Little Arnot) is situated next to a burn flowing to the Arnot resevoir, previously a disused quarry. The 10 ha site contains two adjacent fields planted at random with five different varieties of willow (*Salix* spp. Tora and Sven, Olof, Torhild and Tordis (*S. schwerinii* x *S. viminalis*)) to avoid the spread of diseases.

Sampling sites

For the purposes of this research, the first field was split into two sites - field X and Y, as the terrain was markedly different within the field (see Fig. 2.14b). Field X takes in sampling points running from the top of the hill down a relatively steep slope towards the road. Field Y consists of sampling points spread along the top of the field. This is separated from the third field (field



(a) Map of the United Kingdom showing the approximate location of Arnot, Perthshire.



(b) Aerial picture of the Arnot site with fields of interest distinguished.

Figure 2.14: Location of the Arnot fieldsite and layout of the fields within the site.

Z) by a small stone dyke. A total of ten sampling sites were used within each field of interest, as shown in Figure 2.15.

Agricultural management

Prior to conversion to bioenergy crops, the fields were planted with annual crops on rotation. SRC willow was established in June 2007 and was cut back after one year but has yet to be harvested. The biomass will eventually be used for co-firing in a nearby power station. The site treated with 15 tons per hectare of lime-stabilised sewage sludge cake during the establishment phase in June 2008. This is equivalent to 548 kg N ha^{-1} if the N content is defined as 40.3 g kg^{-1} (Guo et al., 2012). No treatments were applied in the duration of this research.

Soil properties

The soil at the site is Macmerry soil of the Rowanhill soil association. The soil pH was 7.02 ± 0.20 (standard deviation (SD) of 3 replicates) in the first willow field (X), 6.82 ± 0.04 in the second (Y) and 7.29 ± 0.04 in the final field (Z). Total elemental carbon content was 3.19% in field X, 3.02% in field Y and 3.64% in field Z and total elemental nitrogen content was 0.29%, 0.28% and 0.34% respectively. Bulk density was 0.93 ± 0.09 g cm^{-3} in field X, 0.88 ± 0.09 g cm^{-3} in field Y and 0.90 ± 0.08 g cm^{-3} in field Z. The soil moisture is similar across all fields, averaging around 23%.

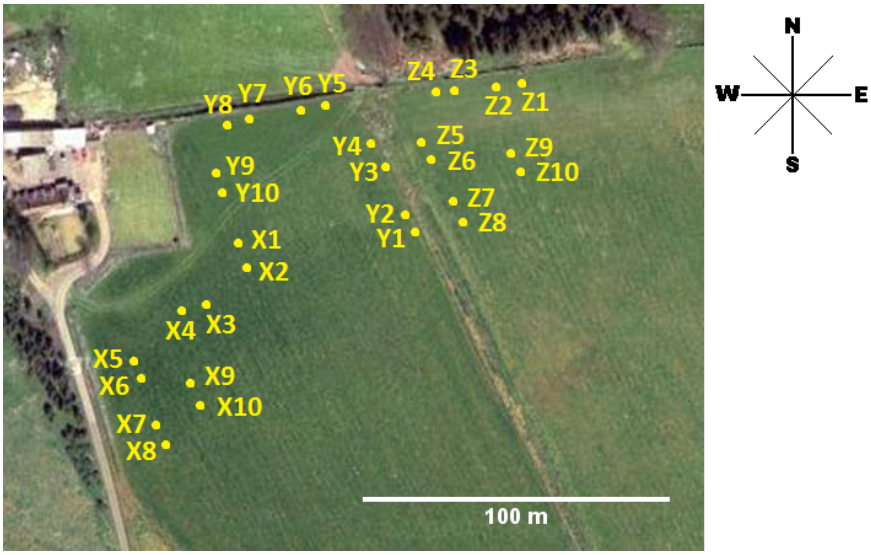


Figure 2.15: Location of sampling points within fields. There are ten sampling sites in each of the three fields X, Y and Z.

Climate conditions

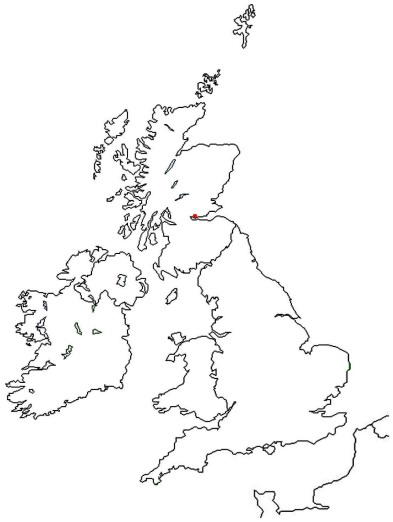
Fife is a peninsula, between the Firth of Tay to the north, Firth of Forth to the south and the North Sea to the east. Summers are relatively cool and the warming of the water over the summer results in warm winters. Continuous weather data was provided by a meteorological station at Kinross, 4 km from the site. The long-term mean annual minimum temperature (from 1981 to 2010) was 4.0 °C and the long-term mean annual maximum temperature was 12.1 °C. Mean annual rainfall across the same period was 1056 mm. The mean temperature over the 12 month period was 13.6 °C and therefore slightly higher than the previous long-term mean annual maximum temperature, and the average soil temperature was 11.7 °C.

2.7.3 East Grange, Fife

Location and description

The East Grange site is located in the south of Fife close to Blairhill and Dunfermline, a few kilometres North of the Firth of Forth (Lat: 56°05′54″N, Lon: 3°62′93″W) (see Fig. 2.16). The site has homogenous ground conditions and slope.

The SRC willow plantation was established in mid-May 2009 on around 35 ha of the site with a planting density of 15 000 stools ha^{-1}. Four varieties of willow (Tora (*S. schwerinii* x *S. viminalis*), Inger (*S. triandra* x *S. viminalis*), Tordis ((*S. schwerinii* x *S. viminalis*) x *S. viminalis*) and Sven (*S. viminalis* x (*S. schwerinii* x *S. viminalis*))) were planted in blocks. The willow was



(a) Map of the United Kingdom showing the approximate location of East Grange, Fife.



(b) Aerial picture of the East Grange site with fields of interest distinguished.

Figure 2.16: Location of the East Grange fieldsite and layout of the fields within the site.

cut back in spring 2010 but has not yet been coppiced.

Agricultural management

Prior to conversion to bioenergy crops, the land was used for agriculture with a rotation of wheat and barley. No fertiliser treatments are known to have been applied in the duration of this research but were applied to the land when it was used for annual arable crops.

Sampling sites

A total of ten sampling sites were used within the field, as shown in Figure 2.17. A range of sampling sites on the edge of the plantation and within the plantation were chosen. All of the sampling sites were located within a block planted with the Inger (*S. triandra* x *S. viminalis*) variety.

Soil properties

The soil at the site is Macmerry soil of the Rowanhill soil association. The topsoil was a mainly homogenous, well mixed, clay loam. The soil pH was 6.2 and total elemental carbon content was 3.2% and total elemental nitrogen content was 0.21%. Bulk density was $0.97 \pm 0.06\,\mathrm{g\,cm^{-3}}$ and the soil moisture was around 30%.

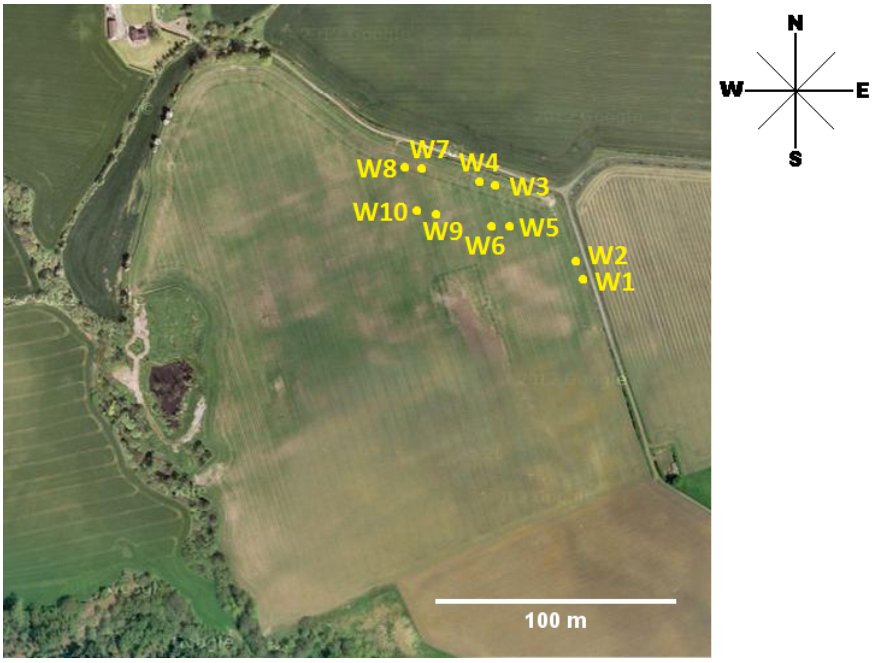


Figure 2.17: Location of sampling points within fields

Climate conditions

Continuous weather data was provided by a meteorological station at Grangemouth Refinery, about 6 km from the site. The mean daily maximum temperature over the 6 month measurement period was 14.4 °C and the mean daily minimum temperature was 7 °C. The mean monthly rainfall calculated for the same period was 90 mm. There was an average of 139 hours of sunshine a month. The mean temperature recorded at East Grange during measurements over the 6 month period was 15.1 °C and the average soil temperature was 11.9 °C. This is higher than the other fieldsites as the measurements were made during the summer months.

Chapter 3

Long term flux measurements in *Miscanthus*

3.1 Introduction

Miscanthus x giganteus is native to subtropical and tropical regions of Africa and southern Asia and is relatively new to the UK. Numerous field trials of *Miscanthus* have been carried out in northern Europe since 1983. However, the impact of growing *Miscanthus* on CH_3X and BVOC budgets has not yet been investigated. Ambitious renewable energy targets are likely to encourage the planting of large areas of arable land with *Miscanthus* so it is important to consider the impact this may have on atmospheric composition.

Much of the literature published on *Miscanthus* is based on modelling studies of potential land resources for *Miscanthus* plantations (Bauen et al., 2010; Clifton-Brown et al., 2004; Tuck et al., 2006), potential biomass yields (Price et al., 2004), potential costs (Bocquého and Jacquet, 2010), and potential CO_2 mitigation (Brandão et al., 2011; Davis et al., 2010; Hillier et al., 2009; Rowe et al., 2009). Generally, it is agreed that using *Miscanthus* plantations as a renewable energy source will have a beneficial impact on reducing GHG emissions, with one study suggesting that *Miscanthus* could provide around 10 000 kg CO_2 ha^{-1} y^{-1} of avoided CO_2 emissions (Brandão et al., 2011). However, other potent trace gases such as CH_3X and BVOCs are not considered in any of these studies.

This study is the first ever attempt to characterise CH_3X fluxes from *Miscanthus* as a bioenergy crop in the UK. Other studies have looked at comparable ecosystems such as grasslands and other C_4 plants such as switchgrass. Temperate grasslands are generally considered to be a significant sink for CH_3X although large uncertainties exist due to the lack of field measurements. A study in a temperate tallgrass prairie in Kansas, USA found that the ecosystem acted as both a source and a sink for CH_3Br and CH_3Cl (Rhew, 2011). In central North America this ecosystem type is dominated by switchgrass (*Panicum virgatum*), a C_4 plant similar to *Miscanthus* that is also used as a bioenergy crop. Studies found growing season gross uptake rates of CH_3Br and CH_3Cl in temperate tallgrass prairie to be similar to those measured in grasslands in California (Rhew and Abel, 2007) and in shortgrass steppe in Colorado (Teh et al., 2008). The average

gross uptake rates during the growing season were 504 $\pm$ 38 nmol m^{-2} day^{-1} CH_3Cl and 12 $\pm$ 3 nmol m^{-2} day^{-1} CH_3Br (Rhew and Abel, 2007). Emission rates of CH_3X were also measured with gross production ranging from 0 to 535 nmol m^{-2} day^{-1} and 1.5 to 40.7 nmol m^{-2} day^{-1} for CH_3Cl and CH_3Br, respectively. All of the above studies used static ground chambers which take into account fluxes from the soil as well as the vegetation.

At present, only one study has been published on BVOC fluxes from a *Miscanthus* plantation in the UK. Copeland et al. (2012), from this research group, found no measurable fluxes of BVOCs above the *Miscanthus* canopy using a PTR-MS and eddy correlation technique. Grasses are generally found to have lower BVOC emissions than most other plant groups (Guenther et al., 1995), although they sometimes emit oxygenated BVOCs (Davison et al., 2008; Kirstine et al., 1998; König et al., 1995). Grasslands as an ecosystem are known to emit monoterpenes such as α-pinene, β-pinene and sabinene as major species (König et al., 1995).

A study by Eller et al. (2011) found that emissions from switchgrass were dominated by oxygenated VOCs and isoprene contributed less than 8%. Isoprene and monoterpene emission rates of around 0.006 nmol m^{-2} s^{-1} from switchgrass were in the range reported for Illinois grasslands (Fukui and Doskey, 1998) but all other estimated emission rates were lower. Grasslands are typically mixtures of grasses and forbes so grassland ecosystem measurements represent a combination of the two plant groups. Measurements from grass species in southeastern Victoria, Australia, using a static chamber technique found that the emissions recorded were high in oxygenated BVOCs and extremely low in isoprene and monoterpenes (Kirstine et al., 1998). Another PTR-MS study in agricultural grassland also measured fluxes of oxygenated BVOCs which were highest immediately after harvesting (Davison et al., 2008).

A study into the influence of crop cultivation (and surface air temperature) on annual global isoprene and monoterpene emissions found that an increase in cropland led to a 7% reduction of isoprene and a 2% reduction in monoterpenes (Tanaka et al., 2012). This was mainly attributed to the reduction in broadleaf evergreen forests in Southeast Asia, which have the highest and most constant emissions of isoprene and where both temperature and radiation are high all year round. However, an increase in C_4 crop plantations in the regions of south and west Africa and South America played an important role in hindering the reduction of annual monoterpene emissions, but not isoprene emissions. This is supported by another study which also predicts that the conversion of forested areas to cropland will decrease BVOC emissions in some geographical areas (Laothawornkitkul et al., 2009).

In summary, although there are previous studies on CH_3X fluxes in comparable species and ecosystems, this is the first characterisation of CH_3X fluxes from a *Miscanthus* plantation. Studies into grasslands and grass species found both uptake and emissions of CH_3X from these ecosystems and plant types and have observed that there is a general lack of field measurements available. Previous studies into BVOC emissions from *Miscanthus* and other grass species

concluded that these plant types are generally low emitters of BVOCs but may emit small amounts of isoprene, monoterpenes and oxygenated BVOCs.

Objectives of the work described in this chapter:

- Characterisation of CH_3X and BVOC fluxes in a *Miscanthus* plantation in the East Midlands, England
- Quantification of seasonal, diurnal and temporal variations in CH_3X and BVOC fluxes within a *Miscanthus* plantation
- Identification of possible drivers of variation in CH_3X and BVOC fluxes from a *Miscanthus* plantation

3.2 Description of *Miscanthus* site and sampling points

Measurements were conducted at the Brattleby fieldsite in Lincolnshire, as described in Section 2.7.1. A total of ten sampling points were used within the *Miscanthus* field, as shown in Figure 3.1. The terrain is very similar across the site so the hydrology of the area was not considered when choosing the sampling sites, rather they were chosen at random for their accessibility. A mixture of sites on the edge of the *Miscanthus* field and within the field were chosen.

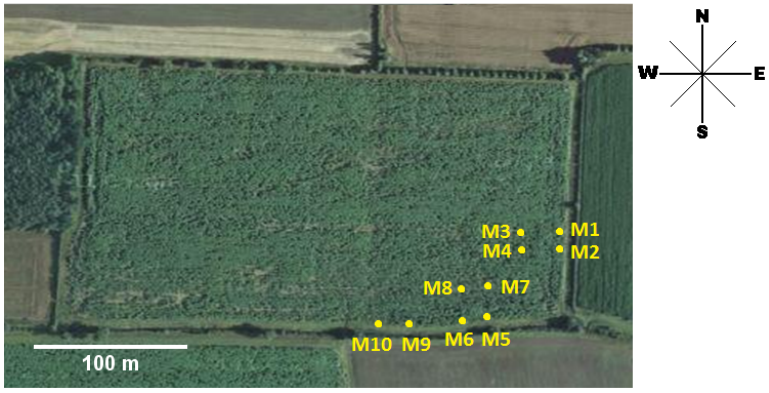


Figure 3.1: Location of sampling sites within the *Miscanthus* field at Brattleby

December 2010 saw extremely cold conditions at the fieldsite with the temperature staying below 0 °C for weeks and dropping as low as -15 °C. However, *Miscanthus* is able to survive harsh winters at temperatures as low as -33 °C and is only vulnerable to frost in the first year of establishment (Clifton-Brown and Jones, 1997; Heaton et al., 2010; Lewandowski et al., 2000). Freezing temperatures were not found to affect time of senescence or the final size of the crop (Lewandowski et al., 2000). It is therefore not very likely that the cold winter conditions affected the CH_3X and BVOC gas fluxes measured from the *Miscanthus* during 2011.

Drought was declared in the area in summer 2011 and spring 2012 followed by flooding in July 2012. *Miscanthus* has been shown to be widely tolerant to different soil moisture regimes, growing rapidly under both extremely low soil moisture conditions and in flooded conditions (**?**). However, Richter et al. (2008) concluded that sufficient water supply from the soil (soil available water capacity (AWC) ¿ 150 mm) during the main growing season was the most important factor for growth of *Miscanthus* . One study suggested that a 20% variability in biomass should be expected due to variation in weather patterns (Hastings et al., 2009). At Brattleby, there was a noticeable difference in timing of emergence and further growth stages, leaf growth and stand size of *Miscanthus* in 2010 and 2011 compared to 2012 due to drought conditions in late 2011 and early 2012. Emergence and leaf growth occurred later in 2012 compared to 2010 and 2011.

3.3 Outline of CH_3X flux measurements

Flux measurements were carried out as described in Section 2.2.1. The main body of the work carried out in the *Miscanthus* field was the characterisation of CH_3Br and CH_3Cl fluxes through regular sampling measurements. These totalled 250 measurements during 19 site visits from April 2010 to June 2012, which were made almost every month in order to capture seasonal flux variability.

Firstly, the seasonal CH_3X flux trends during each sampling year and between years are examined. Time series of seasonal net CH_3X fluxes for the years 2010, 2011 and 2012 and the respective PAR levels, ambient air temperature, soil temperature and soil water content observations at the time of measurement for each sampling site are then illustrated, incorporating seasonal, temporal and annual variation in fluxes.

Statistical analysis of the CH_3X fluxes is then presented. CH_3X fluxes are tested for significant correlations with monitored environmental parameters in order to investigate possible drivers of variation in emissions. Correlations between CH_3Br and CH_3Cl fluxes were tested for significance as was the dependence of variation in CH_3X flux on season and sampling site.

Finally, the behaviour of CH_3X fluxes throughout the day at different times of the year is examined in a separate diurnal study carried out in July 2010 and in seven sub-diurnal studies conducted in August 2010 and between June to November 2011.

3.3.1 CH_3X flux trends

CH_3Br fluxes

CH_3Br fluxes were characterised through a total of 125 measurements made during 19 site visits beginning in April 2010 and ending in June 2012. Seasonal, temporal and annual variations

in CH_3Br fluxes are investigated. Fluxes are examined by year and then collectively across all 3 calendar years. Figure 3.2 presents the CH_3Br fluxes at all ten sampling points on each sampling occasion and the mean of those values between 2010 and 2012. Figures 3.3 to 3.7 then illustrate the seasonal CH_3Br fluxes for all 10 individual sampling sites together with respective PAR levels, ambient air temperature, soil temperature and soil water content by calendar year.

In 2010, 39 measurements were made in total over the ten sampling sites (Table 3.1a). The maximum flux measured was 34 ng g^{-1} h^{-1} from site 3. Mean fluxes per site ranged from 0.4 to 8.4 ng g^{-1} h^{-1}, excluding results from sites 9 and 10 as they were only sampled once. Five of the ten highest maximum fluxes measured throughout the 3 calendar years were measured in 2010 from sites 1 - 4 and 6.

A total of 64 measurements were made in 2011 (Table 3.1b). The maximum flux measured was 15 ng g^{-1} h^{-1} from site 8. The range of mean fluxes per site was smaller than in 2010, ranging from 0.6 to 3.7 ng g^{-1} h^{-1}. Five of the ten highest maximum fluxes measured throughout the sampling period were measured in 2011 from sites 5 and 7 - 10. More measurements were also made at these sites in 2011 than in 2010, between 4 and 7 compared to between 1 and 5.

Table 3.1: Mean, median, minimum and maximum net CH_3Br fluxes during 2010 and 2011. All flux values are in $ng\,g^{-1}\,h^{-1}$. The final column gives the number of measurements made. The last row summarises all fluxes from all sites.

(a) 2010

Site	Mean	Median	Min	Max	Measurements
M1	1.99	0.00	0.00	8.21	7
M2	1.99	0.00	0.00	11.9	7
M3	8.44	0.00	0.00	33.8	4
M4	6.41	6.77	0.00	12.5	3
M5	0.41	0.00	0.00	1.24	5
M6	1.66	0.48	0.00	4.45	5
M7	1.17	0.81	0.00	2.70	3
M8	1.95	0.00	0.00	5.84	3
M9	0.62	0.62	0.62	0.62	1
M10	0.00	0.00	0.00	0.00	1
All	2.59	0.00	0.00	33.8	39

(b) 2011

Site	Mean	Median	Min	Max	Measurements
M1	1.26	0.00	0.00	5.07	7
M2	1.31	0.81	0.00	4.33	8
M3	2.03	2.12	0.00	3.86	6
M4	0.61	0.00	0.00	2.44	6
M5	2.42	0.00	0.00	8.50	6
M6	0.98	0.00	0.00	2.68	7
M7	3.70	2.71	0.00	9.39	4
M8	3.25	0.95	0.00	14.9	6
M9	1.39	0.00	0.00	4.25	7
M10	1.01	0.00	0.00	5.55	7
All	1.68	0.00	0.00	14.9	64

Out of 22 measurements made in 2012, zero fluxes were recorded at every site during every sampling occasion apart from a flux of 9.6 ng g^{-1} h^{-1} measured at site 2 in June. However, measurements finished in mid-June so it is possible that higher emission fluxes may have been detected later in the growing season, as was the case in both 2010 and 2011.

Taking into account all three calendar years during which these measurements took place, the minimum flux measured for all sampling sites was zero (Table 3.2). Maximum fluxes ranged from 4.2 to 33.8 ng g^{-1} h^{-1}. Maximum fluxes were higher in 2010 compared to 2011 and 2012 with maximum fluxes of 33.8, 14.9 and 9.6 ng g^{-1} h^{-1} recorded in 2010, 2011 and 2012, respectively. Mean fluxes varied from 0.8 to 3.2 ng g^{-1} h^{-1}. Sites with low maximum fluxes have corresponding low mean fluxes. The highest maximum emission was measured at site 3 (33.8 ng g^{-1} h^{-1} in 2010) and the lowest maximum was recorded at site 9 (4.25 ng g^{-1} h^{-1} in 2011). The mean value of all samples at all sites during the measurement period was 1.75 ng g^{-1} h^{-1}.

Table 3.2: Mean, median, minimum and maximum net CH_3Br fluxes for the entire measurement period. All flux values are given as ng g^{-1} h^{-1}. The final column gives the number of measurements made. The last row presents all fluxes from all sites.

Site	Mean	Median	Min	Max	Measurements
M1	1.26	0.00	0.00	8.21	18
M2	1.79	0.00	0.00	11.9	19
M3	3.28	0.00	0.00	33.8	14
M4	1.76	0.00	0.00	12.5	13
M5	1.38	0.00	0.00	8.50	12
M6	1.16	0.00	0.00	4.45	13
M7	2.29	1.22	0.00	9.39	8
M8	2.53	0.00	0.00	14.9	10
M9	1.15	0.00	0.00	4.25	9
M10	0.79	0.00	0.00	5.55	9
All	1.75	0.00	0.00	33.8	125

Figure 3.2 presents the CH_3Br fluxes at all ten sampling points and the mean of those values during 2010, 2011 and 2012. The minimum CH_3Br fluxes throughout the measurement period were recorded during the non-growing season between November and April. During 2010 CH_3Br emissions peaked in July and August. In 2011 peak emissions occurred later in the year, during August and September. Not enough data was available to determine when peak emissions occurred in 2012. However, fluxes in 2012 followed a similar pattern to 2011 with low fluxes during June, as compared to peak emissions for 2010 occurring in June. The earlier

peak emissions in 2010 may be due to higher air temperatures during June and July as compared to those recorded in 2011.

Figures 3.3 to 3.7 illustrate the CH_3Br fluxes for all 10 sampling sites by each individual calendar year together with the respective PAR levels, ambient air temperature, soil temperature and soil water content for the 125 measurements made between April 2010 and June 2012. The annual net CH_3Br fluxes in all ten sampling sites for each year followed a very similar pattern, rising into the summer and then falling away into the winter. However, despite following this general trend, there are distinct differences in flux patterns between years. The magnitude of peak fluxes and the timing of their occurrence varies between years and this indicates that the fluxes may be influenced by environmental parameters such as temperature and sunlight. The statistical significance of correlations between CH_3Br fluxes and environmental variables is described in Section 3.3.2.

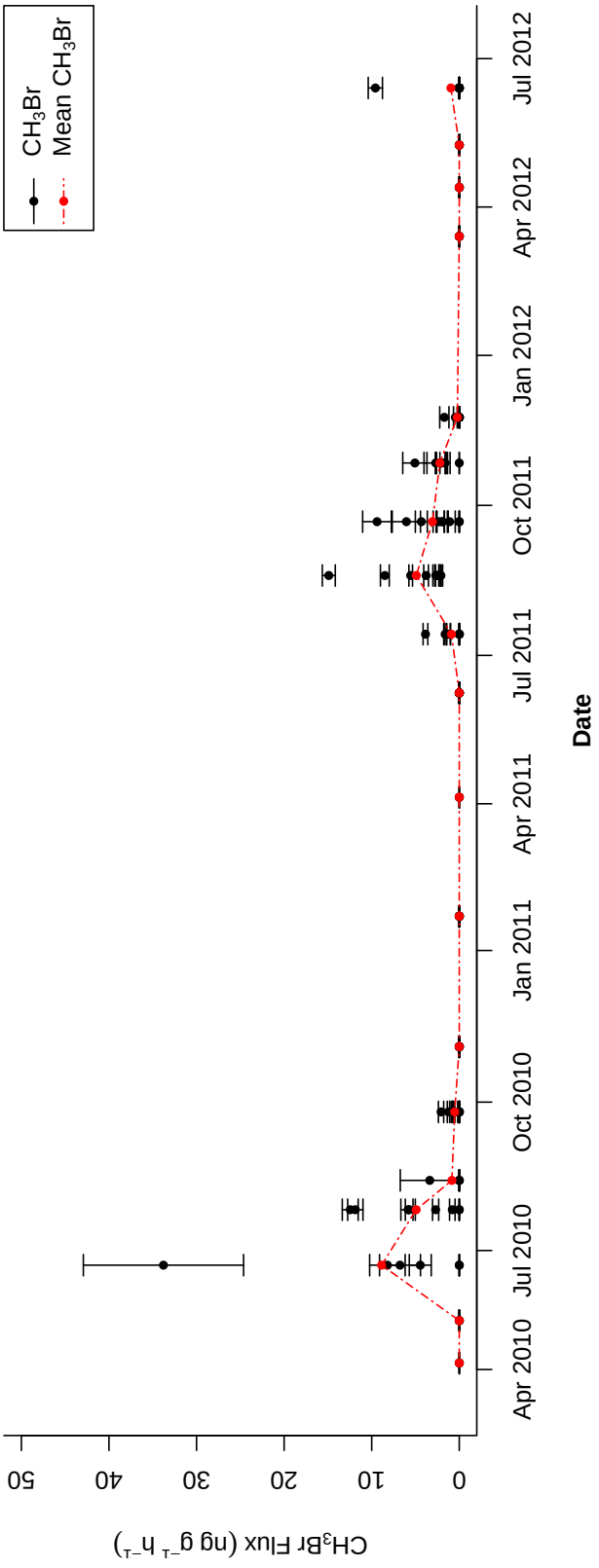


Figure 3.2: CH_3Br fluxes at all ten *Miscanthus* sampling points and the mean of those values on each sampling occasion between 2010 and 2012. Error bars incorporate analytical and sampling uncertainties (as described in Section 2.6.1).

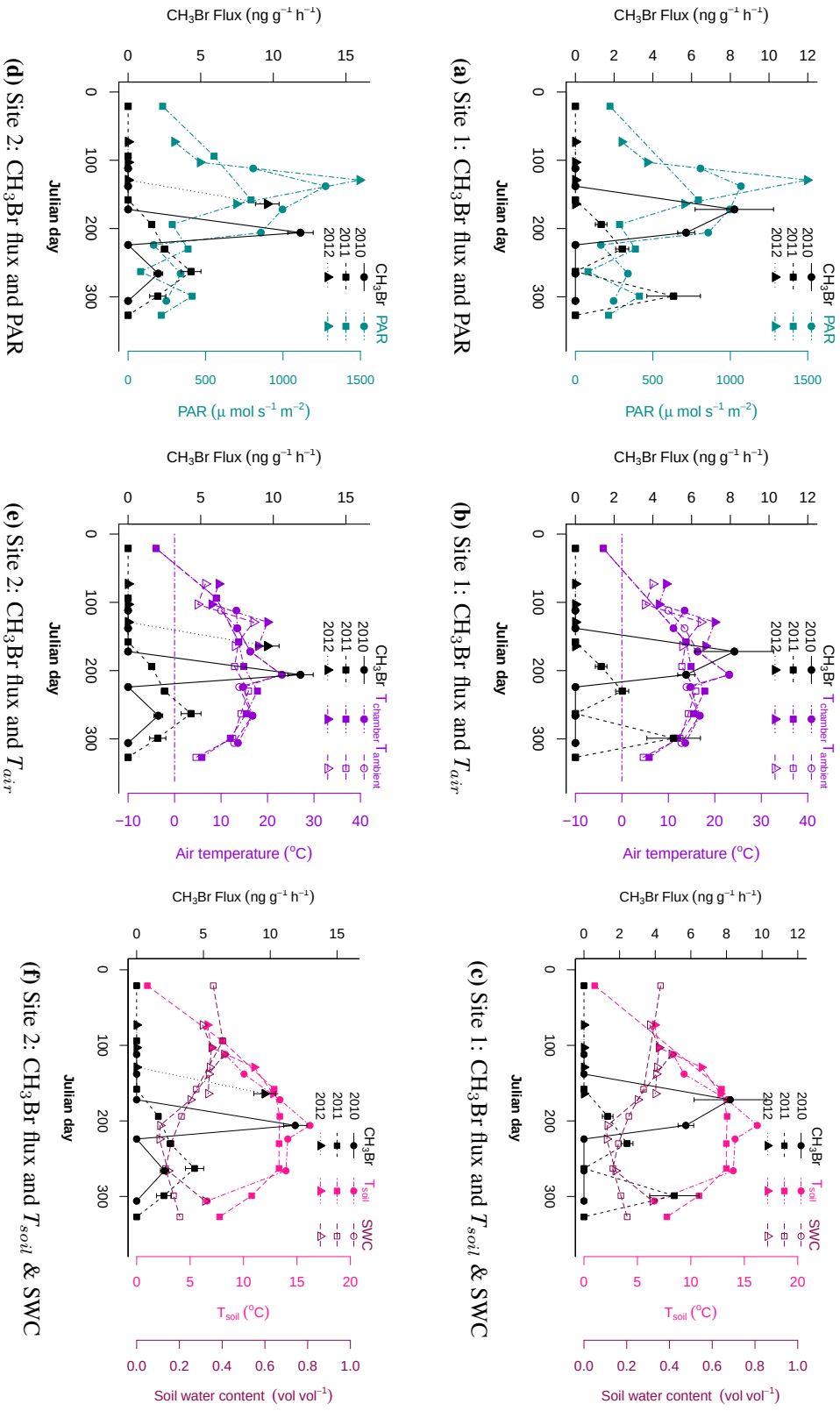
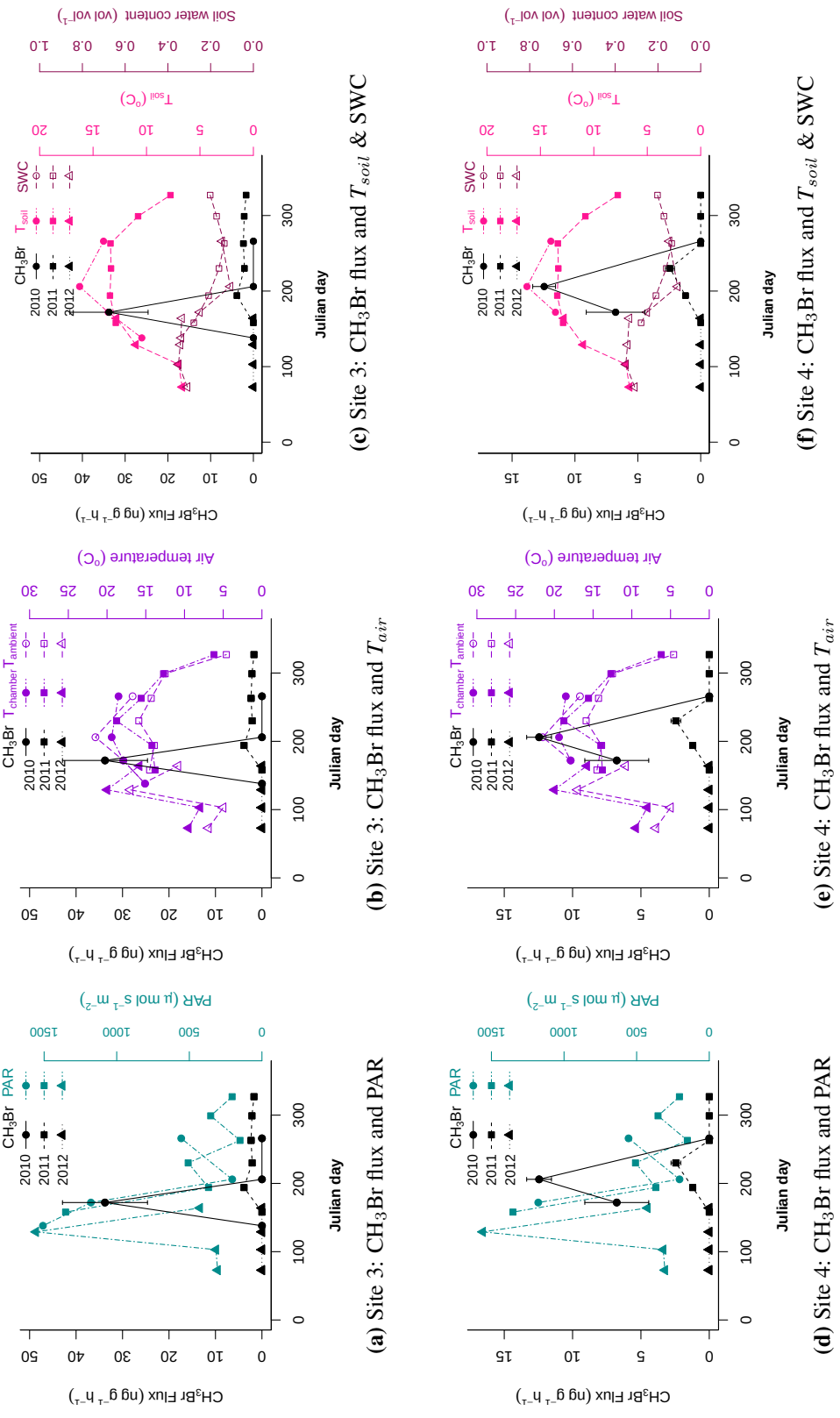


Figure 3.3: Comparison of net CH_3Br fluxes from *Miscanthus* with PAR, chamber and ambient air temperature, soil temperature and soil water content for 2010 and 2012 for sites 1 and 2. Note different y-axis scales for CH_3Br . Error bars on fluxes incorporate analytical and sampling uncertainties.



(a) Site 3: CH_3Br flux and PAR

(b) Site 3: CH_3Br flux and T_{air}

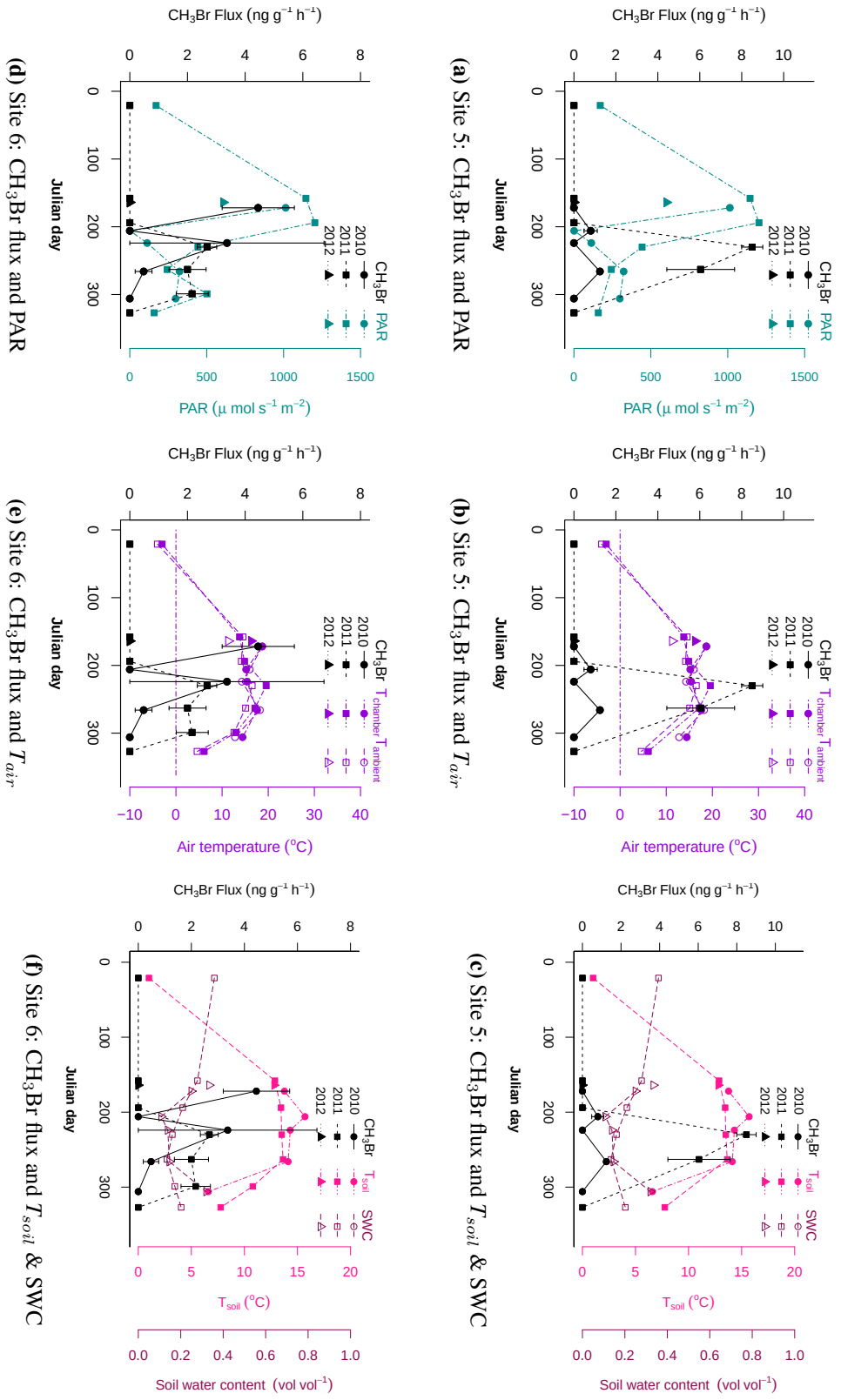
(c) Site 3: CH_3Br flux and T_{soil} & SWC

(d) Site 4: CH_3Br flux and PAR

(e) Site 4: CH_3Br flux and T_{air}

(f) Site 4: CH_3Br flux and T_{soil} & SWC

Figure 3.4: Comparison of net CH_3Br fluxes from *Miscanthus* with PAR, chamber and ambient air temperature, soil temperature and soil water content for 2010 and 2012 for sites 3 and 4. Note different y-axis scales for CH_3Br . Error bars on fluxes incorporate analytical and sampling uncertainties.



(a) Site 5: CH_3Br flux and PAR

(b) Site 5: CH_3Br flux and T_{air}

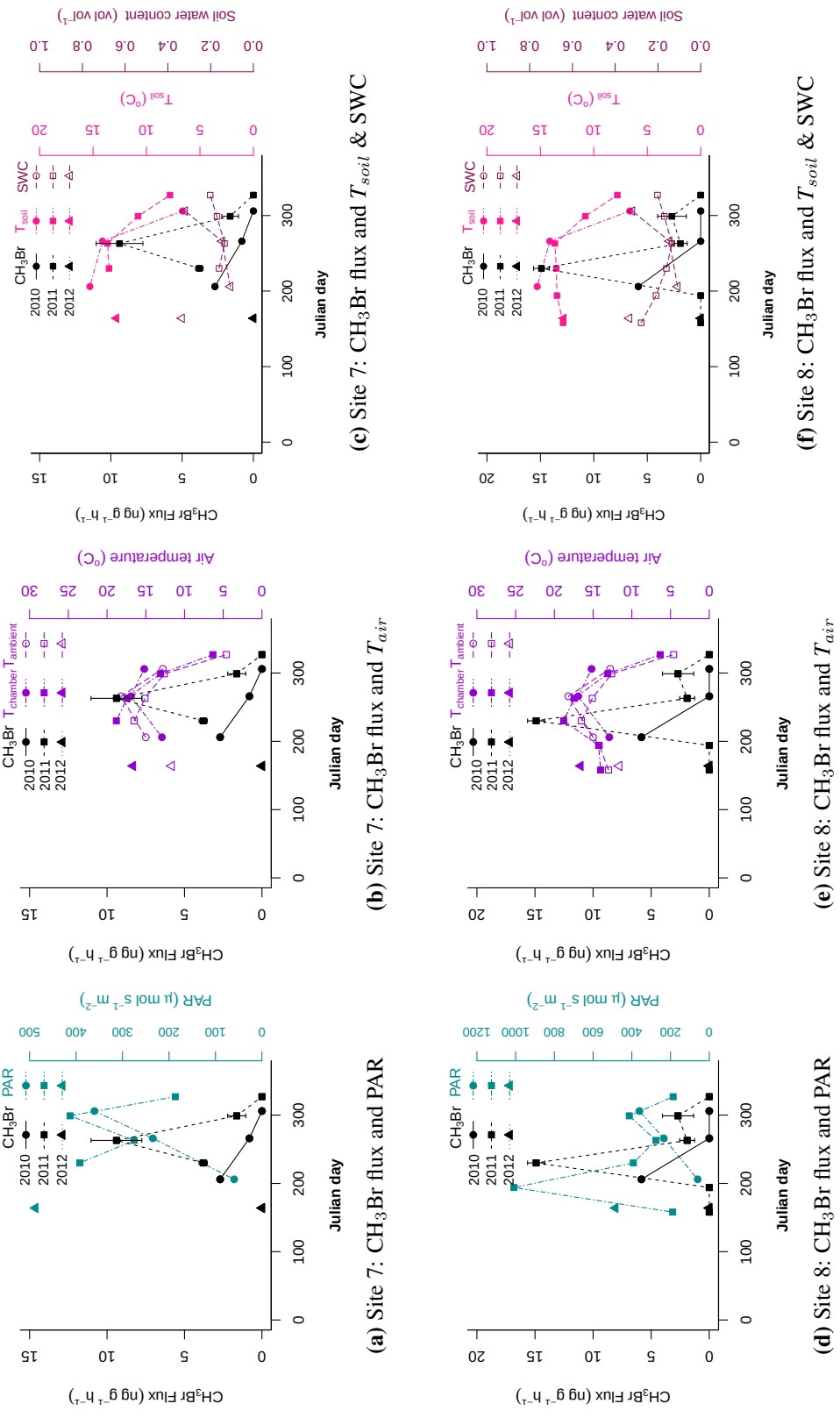
(c) Site 5: CH_3Br flux and T_{soil} & SWC

(d) Site 6: CH_3Br flux and PAR

(e) Site 6: CH_3Br flux and T_{air}

(f) Site 6: CH_3Br flux and T_{soil} & SWC

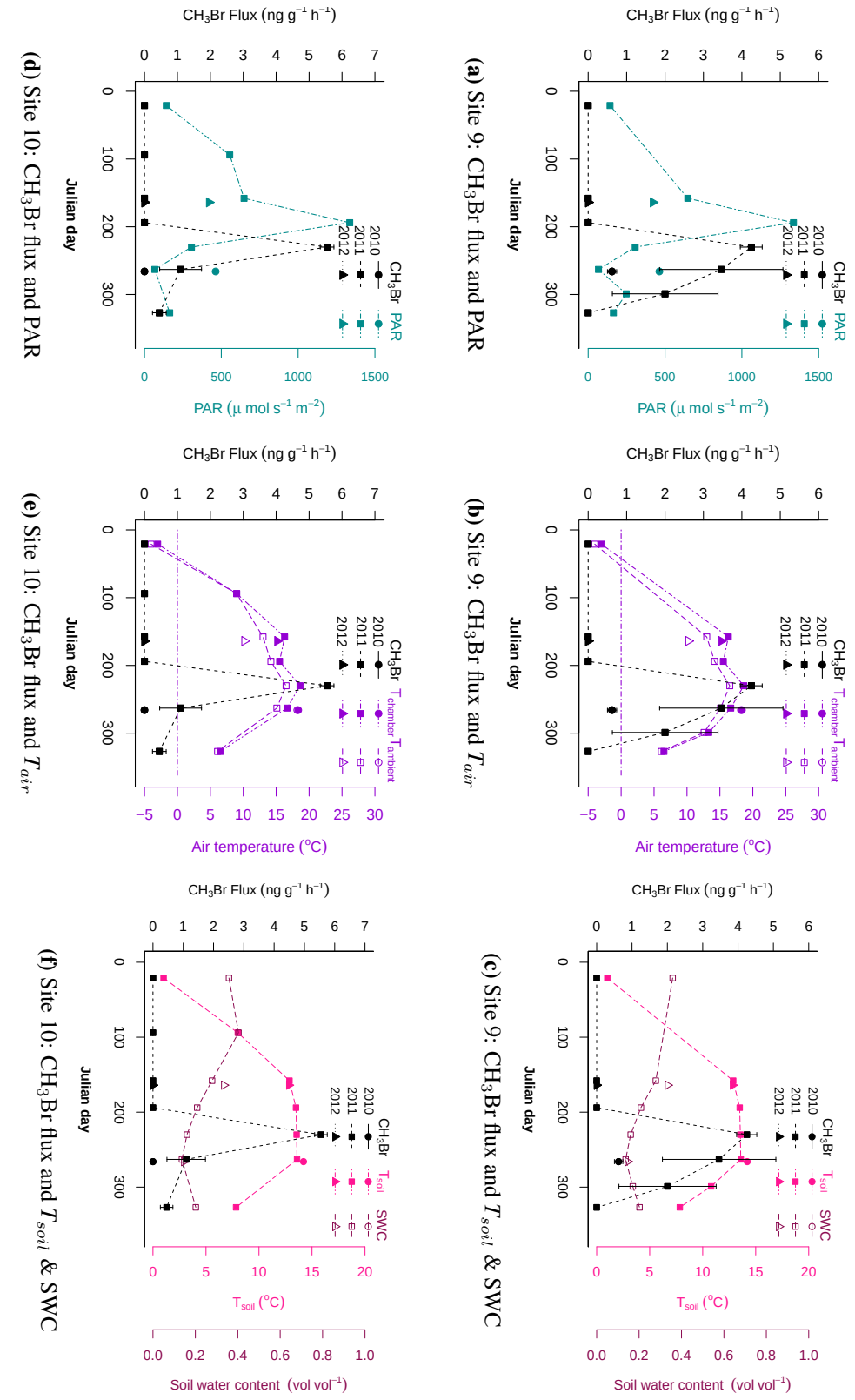
Figure 3.5: Comparison of net CH_3Br fluxes from *Miscanthus* with PAR, chamber and ambient air temperature, soil temperature and soil water content for 2010 and 2012 for sites 5 and 6. Note different y-axis scales for CH_3Br . Error bars on fluxes incorporate analytical and sampling uncertainties.



(a) Site 7: CH_3Br flux and PAR **(b)** Site 7: CH_3Br flux and T_{air} **(c)** Site 7: CH_3Br flux and T_{soil} & SWC

(d) Site 8: CH_3Br flux and PAR **(e)** Site 8: CH_3Br flux and T_{air} **(f)** Site 8: CH_3Br flux and T_{soil} & SWC

Figure 3.6: Comparison of net CH_3Br fluxes from *Miscanthus* with PAR, chamber and ambient air temperature, soil temperature and soil water content for 2010 and 2012 for sites 7 and 8. Note different y-axis scales for CH_3Br . Error bars on fluxes incorporate analytical and sampling uncertainties.



(a) Site 9: CH_3Br flux and PAR

(b) Site 9: CH_3Br flux and T_{air}

(c) Site 9: CH_3Br flux and T_{soil} & SWC

(d) Site 10: CH_3Br flux and PAR

(e) Site 10: CH_3Br flux and T_{air}

(f) Site 10: CH_3Br flux and T_{soil} & SWC

Figure 3.7: Comparison of net CH_3Br fluxes from *Miscanthus* with PAR, chamber and ambient air temperature, soil temperature and soil water content for 2010 and 2012 for sites 9 and 10. Note different y-axis scales for CH_3Br . Error bars on fluxes incorporate analytical and sampling uncertainties.

CH_3Cl fluxes

From April 2010 to June 2012, a total of 123 CH_3Cl flux measurements were made during 19 site visits. Net fluxes from each year are examined individually and then compared across the 3 year measurement period. CH_3Cl fluxes at all ten sampling points and the mean of those values on each sampling occasion between 2010 and 2012 are presented in Figure 3.8. Figures 3.9 to 3.13 illustrate the seasonal CH_3Cl fluxes for all 10 sampling sites together with respective PAR levels, ambient air temperature, soil temperature and soil water content by calendar year, capturing seasonal, temporal and annual variations.

In 2010, 39 measurements were made in total. Zero fluxes were recorded at every site except sites 6 and 9. Three non-zero fluxes were measured at site 6 and the maximum flux measured there was 45.0 ng g^{-1} h^{-1}. One non-zero flux was also recorded at site 9 (7.1 ng g^{-1} h^{-1}).

A total of 62 measurements were made in 2011 with between 4 and 7 measurements made at each site (Table 3.3a). The maximum flux measured was 118 ng g^{-1} h^{-1} from site 3. Except for site 5, all of the maximum CH_3Cl fluxes measured throughout the sampling period were measured in 2011. Mean fluxes per sampling site ranged from 2.5 to 32.1 ng g^{-1} h^{-1}.

In 2012, fluxes of 85.8, 93.7 and 42.4 ng g^{-1} h^{-1} were measured from sites 3, 5 and 6 respectively. The first was recorded in May and the following two were measured in June. The flux recorded at site 5 was the maximum recorded for that site over the sampling period. Zero fluxes were recorded at all other sites at all other times. However, measurements finished in mid-June so it is possible that high emission fluxes may have been detected later in the growing season, as was the case in both 2010 and 2011.

During the measurement period, the minimum flux measured for all sampling sites was zero. Maximum fluxes ranged from 17.4 to 118 ng g^{-1} h^{-1} (Table 3.3b). Maximum fluxes were much higher in 2011 and 2012 than in 2010. In 2010, 2011 and 2012 the maximum fluxes recorded were 45.0, 118 and 93.7 ng g^{-1} h^{-1} respectively. Mean fluxes per site varied from 1.0 to 20.9 ng g^{-1} h^{-1}. Sites with low maximum fluxes have corresponding low mean fluxes. Site 3 recorded the highest maximum CH_3Cl flux (118 ng g^{-1} h^{-1} in 2011) as well as the highest maximum CH_3Br flux. The lowest maximum flux was recorded at site 2 (17.4 ng g^{-1} h^{-1}, also in 2011) and the mean flux for all samples across all sites over the sampling period was 10.9 ng g^{-1} h^{-1}. This is over six times greater than the mean CH_3Br flux of 1.75 ng g^{-1} h^{-1}.

Table 3.3: Mean, median, minimum and maximum net CH_3Cl fluxes in 2011 and for all 3 years. All flux values are given as $ng\,g^{-1}\,h^{-1}$. The final column gives the number of measurements made. The last row summarises all fluxes from all sites.

(a) 2011

Site	Mean	Median	Min	Max	Measurements
M1	9.96	0.00	0.00	45.9	6
M2	2.49	0.00	0.00	17.4	7
M3	23.9	0.00	0.00	118	6
M4	32.1	15.80	0.00	84.0	6
M5	16.8	0.00	0.00	72.4	6
M6	12.3	0.00	0.00	67.3	7
M7	6.78	0.00	0.00	27.1	4
M8	22.6	0.00	0.00	107	6
M9	25.8	0.00	0.00	92.9	7
M10	11.3	0.00	0.00	78.8	7
All	16.5	0.00	0.00	118	62

(b) 2010, 2011 and 2012

Site	Mean	Median	Min	Max	Measurements
M1	3.52	0.00	0.00	45.9	17
M2	0.97	0.00	0.00	17.4	18
M3	16.4	0.00	0.00	118	14
M4	14.8	0.00	0.00	84.0	13
M5	16.2	0.00	0.00	93.7	12
M6	16.9	0.00	0.00	67.3	13
M7	3.39	0.00	0.00	27.1	8
M8	13.5	0.00	0.00	107	10
M9	20.9	0.00	0.00	92.9	9
M10	8.75	0.00	0.00	78.8	9
All	10.9	0.00	0.00	118	123

The minimum fluxes recorded were measured in the non-growing season between November and April (Figure 3.8). The annual net CH_3Cl fluxes at all ten sampling sites for each year followed a very similar pattern with the highest emissions occurring during the summer months and low to zero emissions occurring during the winter. During both 2010 and 2011 CH_3Cl emissions peaked in June and August. Not enough data was available to determine when peak emissions occurred in 2012. However the last measurements taken in 2012 were recorded in June and show the highest fluxes measured up to that point. This is similar to the two previous years, although relatively high fluxes were also measured in May 2012, in contrast to 2010 and 2011. Emissions in July 2011 were lower than would be expected, possibly due in part to the overcast conditions on the day the measurements were made.

Figures 3.9 to 3.13 show seasonal CH_3Cl fluxes for all 10 sites (together with respective PAR levels, ambient air temperature, chamber temperature, soil temperature and soil moisture water content for the years 2010, 2011 and 2012. Figure 3.8 presents the CH_3Cl fluxes at all ten sampling points and the mean of those values on each sampling occasion across 2010 to 2012. Overall, the CH_3Cl fluxes for all sites followed a similar pattern for each year throughout the measurement period. However, the strength of peak emissions differed for each year with much higher maximum fluxes in 2011 and 2012 compared with 2010.

In summary, the highest maximum fluxes for both CH_3Br and CH_3Cl were recorded at site 3 during different sampling years (2010 and 2011 respectively). This site is located inside the *Miscanthus* field and has similar soil and climate conditions to all other sites so there is no clear reason why it was the highest emitter. The CH_3Br and CH_3Cl fluxes from all sites followed a seasonal trend with higher emissions of 4.5 - 33.8 and 17.4 - 118 ng g^{-1} h^{-1}, respectively, during the growing season and low to zero fluxes during the non-growing season. Peak emissions differed in magnitude from year to year and the timing of their occurrence during the year also varied, suggesting that environmental parameters may be influencing variation in fluxes.

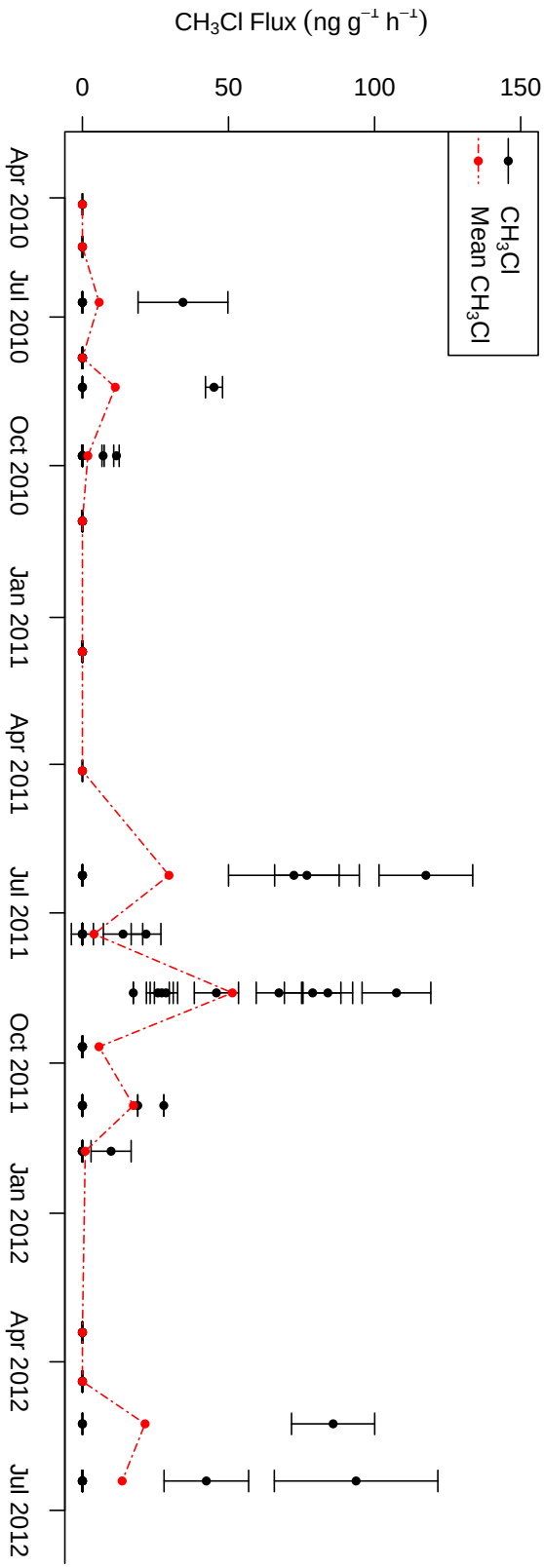


Figure 3.8: CH_3Cl fluxes at all ten *Miscanthus* sampling points and the mean of those values between 2010 and 2012. Error bars incorporate analytical and sampling uncertainties (as described in Section 2.6.1).

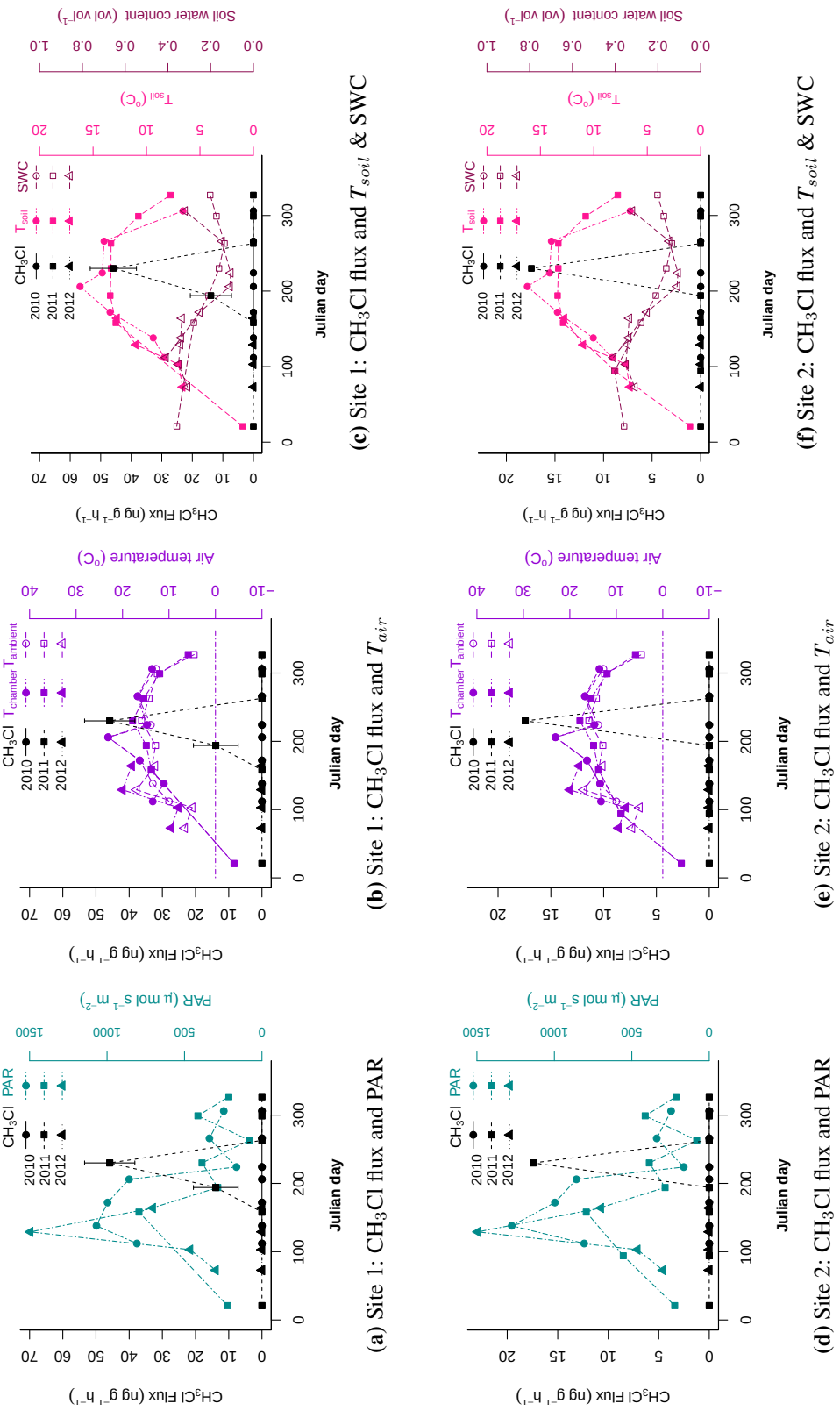
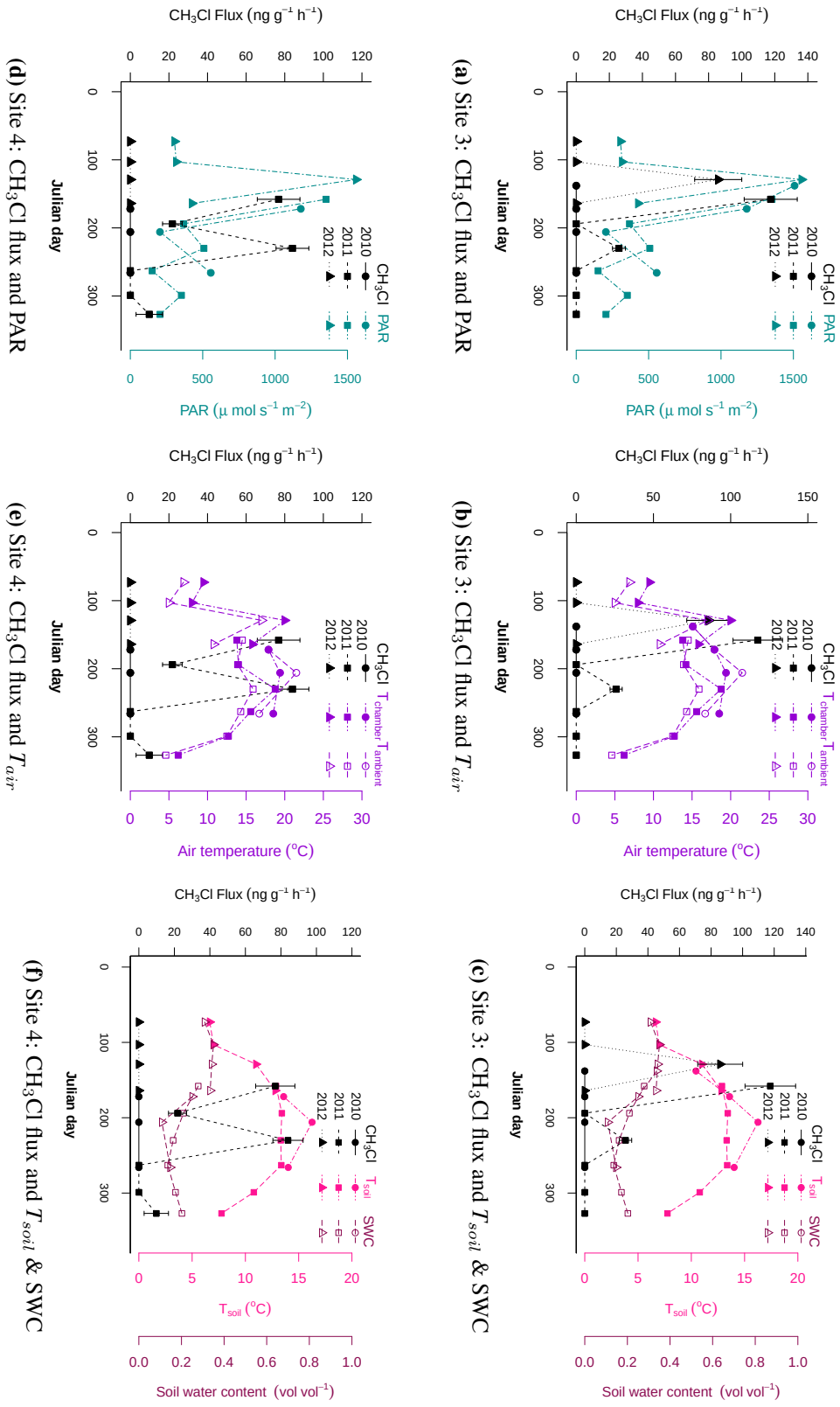


Figure 3.9: Comparison of net CH_3Cl fluxes from *Miscanthus* with PAR, chamber and ambient air temperature, soil temperature and soil water content for 2010 and 2012 for sites 1 and 2. Note different y-axis scales for CH_3Cl . Error bars on fluxes incorporate analytical and sampling uncertainties.



(a) Site 3: CH_3Cl flux and PAR

(b) Site 3: CH_3Cl flux and T_{air}

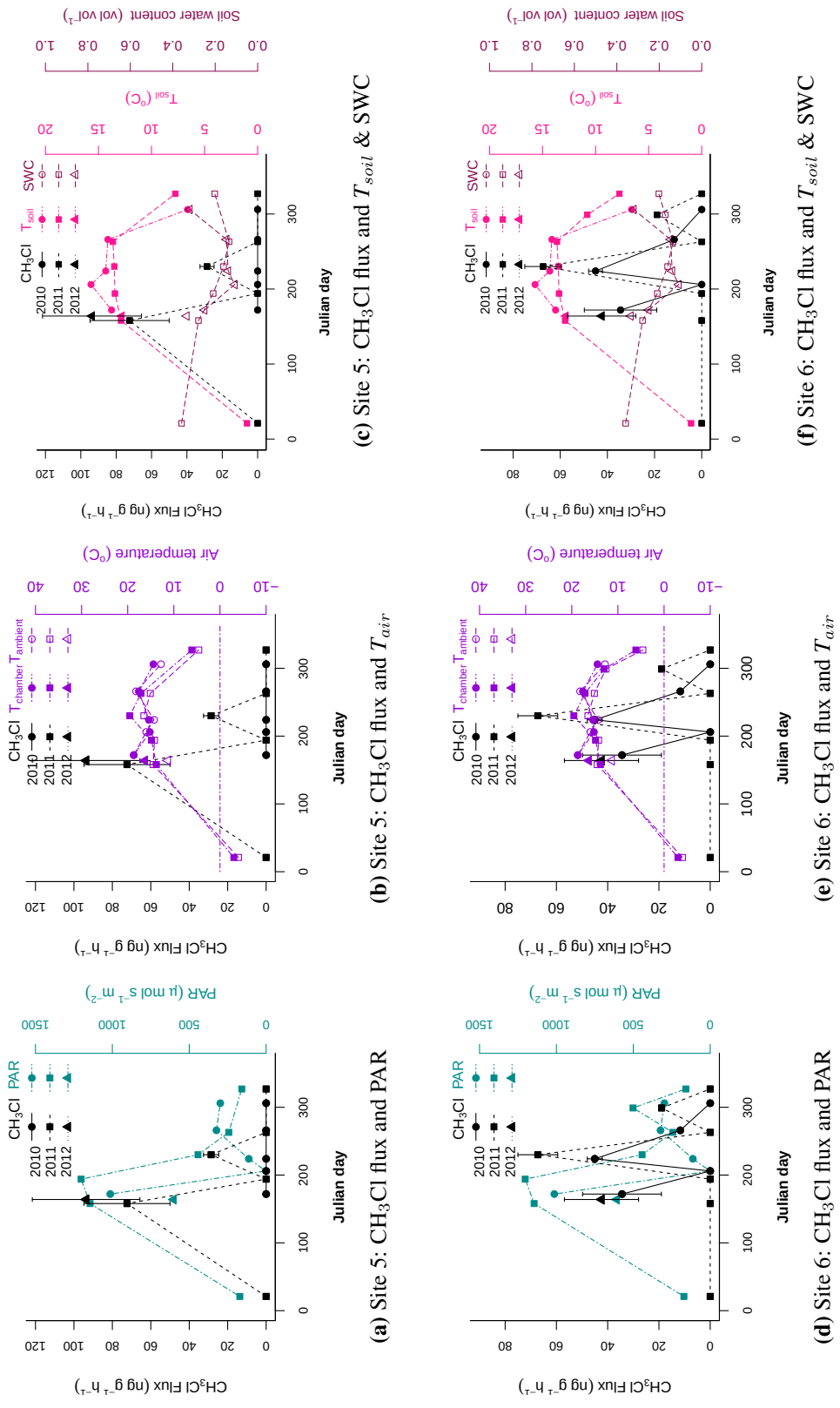
(c) Site 3: CH_3Cl flux and T_{soil} & SWC

(d) Site 4: CH_3Cl flux and PAR

(e) Site 4: CH_3Cl flux and T_{air}

(f) Site 4: CH_3Cl flux and T_{soil} & SWC

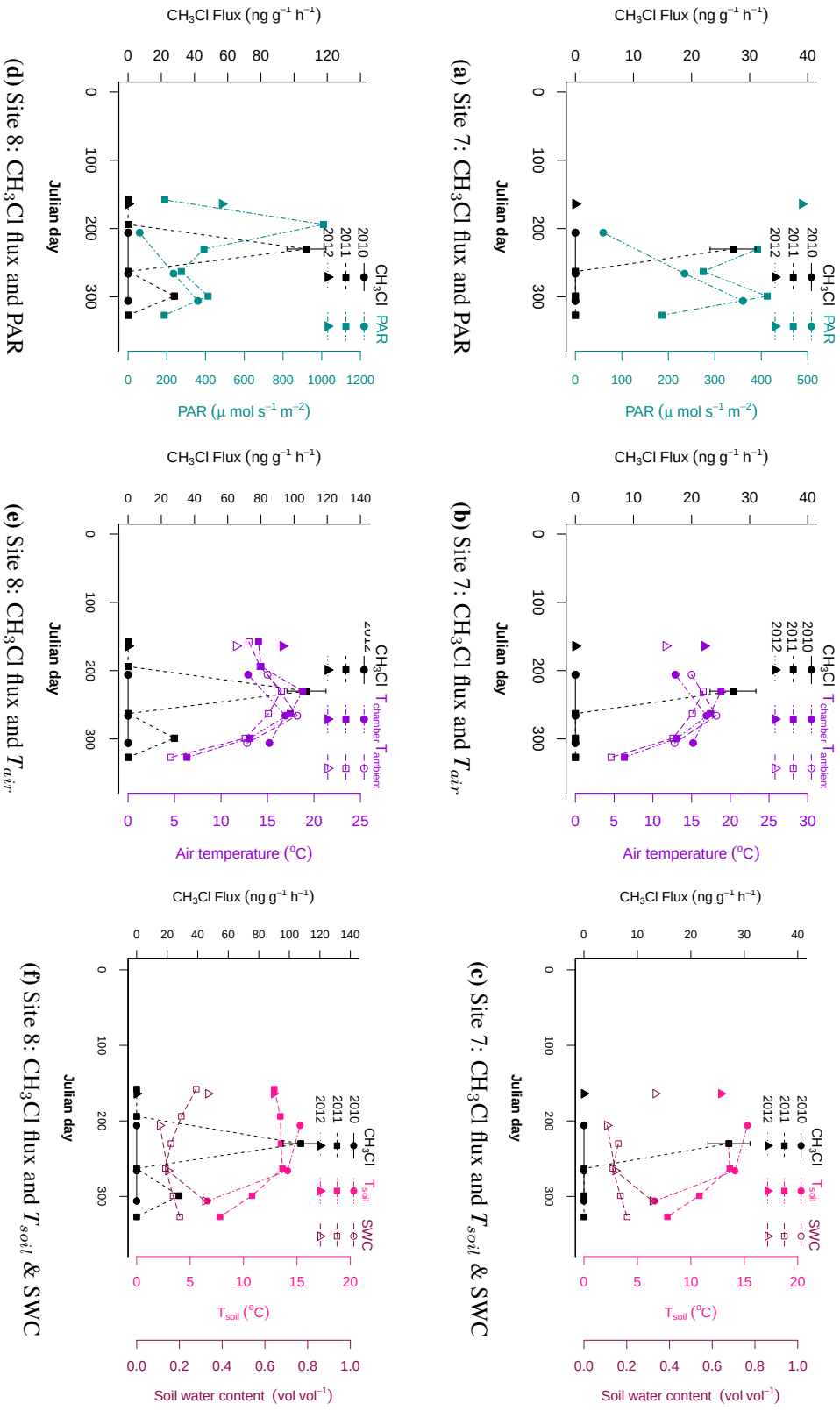
Figure 3.10: Comparison of net CH_3Cl fluxes from *Miscanthus* with PAR, chamber and ambient air temperature, soil temperature and soil water content for 2010 and 2012 for sites 3 and 4. Note different y-axis scales for CH_3Cl . Error bars on fluxes incorporate analytical and sampling uncertainties.



(a) Site 5: CH_3Cl flux and PAR **(b)** Site 5: CH_3Cl flux and T_{air} **(c)** Site 5: CH_3Cl flux and T_{soil} & SWC

(d) Site 6: CH_3Cl flux and PAR **(e)** Site 6: CH_3Cl flux and T_{air} **(f)** Site 6: CH_3Cl flux and T_{soil} & SWC

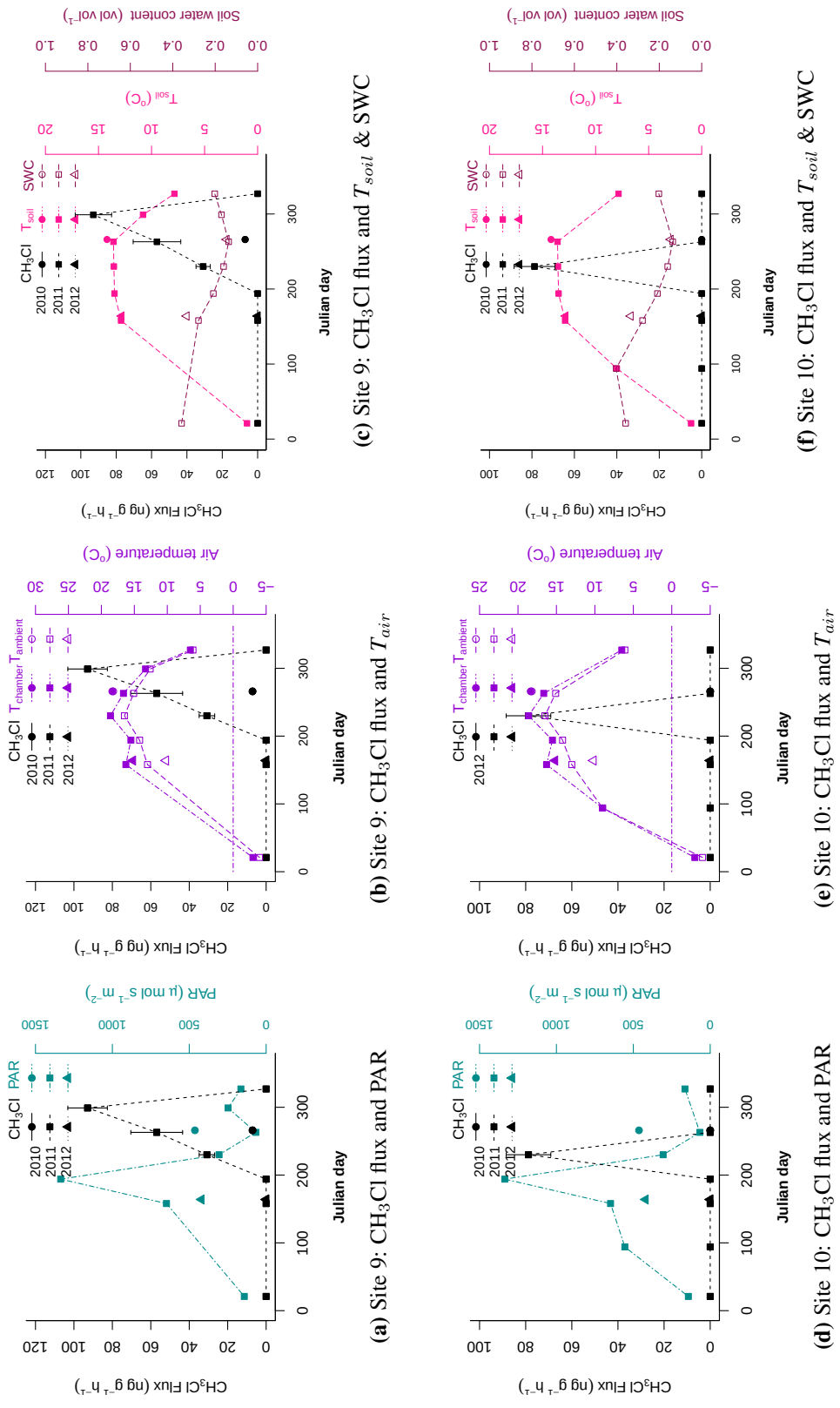
Figure 3.11: Comparison of net CH_3Cl fluxes from *Miscanthus* with PAR, chamber and ambient air temperature, soil temperature and soil water content for 2010 and 2012 for sites 5 and 6. Note different y-axis scales for CH_3Cl . Error bars on fluxes incorporate analytical and sampling uncertainties.



(a) Site 7: CH_3Cl flux and PAR **(b)** Site 7: CH_3Cl flux and T_{air} **(c)** Site 7: CH_3Cl flux and T_{soil} & SWC

(d) Site 8: CH_3Cl flux and PAR **(e)** Site 8: CH_3Cl flux and T_{air} **(f)** Site 8: CH_3Cl flux and T_{soil} & SWC

Figure 3.12: Comparison of net CH_3Cl fluxes from *Miscanthus* with PAR, chamber and ambient air temperature, soil temperature and soil water content for 2010 and 2012 for sites 7 and 8. Note different y-axis scales for CH_3Cl . Error bars on fluxes incorporate analytical and sampling uncertainties.



(a) Site 9: CH_3Cl flux and PAR

(b) Site 9: CH_3Cl flux and T_{air}

(c) Site 9: CH_3Cl flux and T_{soil} & SWC

(d) Site 10: CH_3Cl flux and PAR

(e) Site 10: CH_3Cl flux and T_{air}

(f) Site 10: CH_3Cl flux and T_{soil} & SWC

Figure 3.13: Comparison of net CH_3Cl fluxes from *Miscanthus* with PAR, chamber and ambient air temperature, soil temperature and soil water content for 2010 and 2012 for sites 9 and 10. Note different y-axis scales for CH_3Cl . Error bars on fluxes incorporate analytical and sampling uncertainties.

3.3.2 Statistical analysis of seasonal fluxes and potential drivers

Three types of analyses were carried out on the long term CH_3X time series:

- Variation in CH_3X fluxes between sites and between growing and non-growing season were analysed for significance using the Kruskal-Wallis function within the R i386 2.15.1 software package
- Correlations between CH_3Br and CH_3Cl fluxes were investigated using regression analysis
- CH_3X fluxes were also analysed for their association with measured environmental parameters

Analysis of variation according to site and season

Using multivariate ANOVA, the amount of variation in fluxes caused by different factors was investigated. The differences in CH_3X fluxes due to location (different sites in the field), season (growing and non-growing), and from the interaction between these two factors were analysed. Each year was divided into a growing season (beginning of April to end of October) and a non-growing season (the rest of the year) based on observational evidence of plant growth.

It was found that a significant amount of the variation in both CH_3Br and CH_3Cl fluxes was caused by the season that they were measured in ($p < 0.005$ for CH_3Br and CH_3Cl (Table 3.4)). Although some sites were known to be high emitters of CH_3X and other sites to be low emitters, no statistically significant difference between sites was found in the CH_3X fluxes ($p > 0.05$). There was no significant interaction between season and site.

Table 3.4: Analysis of CH_3X flux variation according to site and season derived using the Kruskal-Wallis test. Degrees of freedom (d.f), χ^2 value and p value for the effect of site, season and season-site interaction terms on CH_3Br and CH_3Cl fluxes are presented. At a significance level of 95% the null hypothesis is rejected if $p \leq 0.05$.

	CH_3Br			CH_3Cl		
	d.f	χ^2	p	d.f	χ^2	p
Season	1	21.3	<0.001	1	9.91	0.002
Site	9	3.22	0.95	9	12.6	0.181
Season*Site	9	26.7	0.112	9	24.7	0.171

Correlations between CH_3Br and CH_3Cl

Significant positive Spearman-Rank correlations between CH_3Br and CH_3Cl fluxes were found at sites 6, 8, 9 and between all sites combined (correlation coefficients (ρ) between 0.35 - 0.92

(Table 3.5)). Site 6 was generally low emitters of CH_3Br and CH_3Cl whereas site 8 was a fairly high emitter of both CH_3Br and CH_3Cl . Site 9 emitted CH_3Cl at the high end of the emissions range but emitted CH_3Br in low quantities. No trends could be distinguished between high or low emitting sites and significant correlations between CH_3Br and CH_3Cl fluxes. Overall, there was a significant correlation between the methyl halides despite individual fluxes being significantly correlated at only 3 sites.

Table 3.5: Spearman-Rank correlation coefficients (ρ) between CH_3Br and CH_3Cl fluxes at each site and the associated p value (at a significance level of 95% the null hypothesis is rejected if $p \leq 0.05$). The last row shows the ρ correlation and p value for fluxes over all sites.

Site	ρ	p
M1	0.432	0.070
M2	0.298	0.215
M3	-0.203	0.486
M4	0.213	0.485
M5	0.016	0.960
M6	0.714	0.006
M7	0.423	0.297
M8	0.702	0.024
M9	0.920	< 0.001
M10	0.651	0.058
All	0.346	< 0.001

CH_3X flux dependency on measured environmental factors

Correlations of CH_3Br and CH_3Cl fluxes with PAR and air temperature were investigated. CH_3Br and CH_3Cl fluxes were first normalised to the highest flux recorded over the measurement period before being tested for correlations with PAR, chamber air temperature, ambient air temperature, soil temperature and soil moisture.

Significant positive Spearman-Rank correlation coefficients were identified between CH_3Br fluxes and ambient air temperature, chamber air temperature and soil temperature and a significant negative correlation with soil moisture (Table 3.6). CH_3Cl fluxes were also found to be significantly correlated with ambient and chamber air temperature and with soil temperature. Correlations with PAR were not found to be significant.

This suggests that CH_3X production may be controlled via an enzymatic reaction which is not directly linked to primary metabolism. Variation in temperature produces variation in the production rate of CH_3Br via enzymatic methylation of Br^- by S-adenosyl-L-methionine

(SAM) (Manley, 2002; Ni and Hager, 1999; Saini et al., 1995; Wuosmaa and Hager, 1990). This reaction is not directly coupled to primary metabolism so no correlation to PAR would be expected.

Table 3.6: Spearman-Rank correlation coefficients between potential drivers and CH_3X fluxes during growing and non-growing season. Significant correlations ($p \leq 0.05$) are highlighted in bold.

	CH_3Br	CH_3Cl
PAR	-0.109	0.138
$\boldsymbol{T_{chamber}}$	**0.416**	**0.291**
$\boldsymbol{T_{ambient\ air}}$	**0.461**	**0.245**
$\boldsymbol{T_{soil}}$	**0.485**	**0.171**
Soil moisture	**-0.545**	-0.150

3.3.3 Diurnal and sub-diurnal trends

To investigate the behaviour of CH_3X fluxes throughout the day during different times of the year, one full diurnal and seven sub-diurnal measurement campaigns were conducted. During the full diurnal campaign measurements were taken every 6 hours over a 24 hour period. During the sub-diurnal campaigns, three measurements were taken between 9 am and 9 pm. Air temperature and PAR were recorded at 5 second intervals throughout each 12 or 24 hour sampling period. Fluxes were measured for either 2 or 4 sites during these campaigns. As well as changes to the weather in different measurement months, there were also changes to the physiology of the *Miscanthus* plants. When diurnal and sub-diurnal measurements were made in 2010 and 2011, the *Miscanthus* grew between June and September, senesced in October and became dormant in November.

CH_3Br fluxes

The CH_3Br fluxes measured during the diurnal and sub-diurnal campaigns and the respective PAR and air temperature observations are presented. These diurnal measurements allow investigation of the CH_3Br flux trends within a 12 hour or 24 hour period.

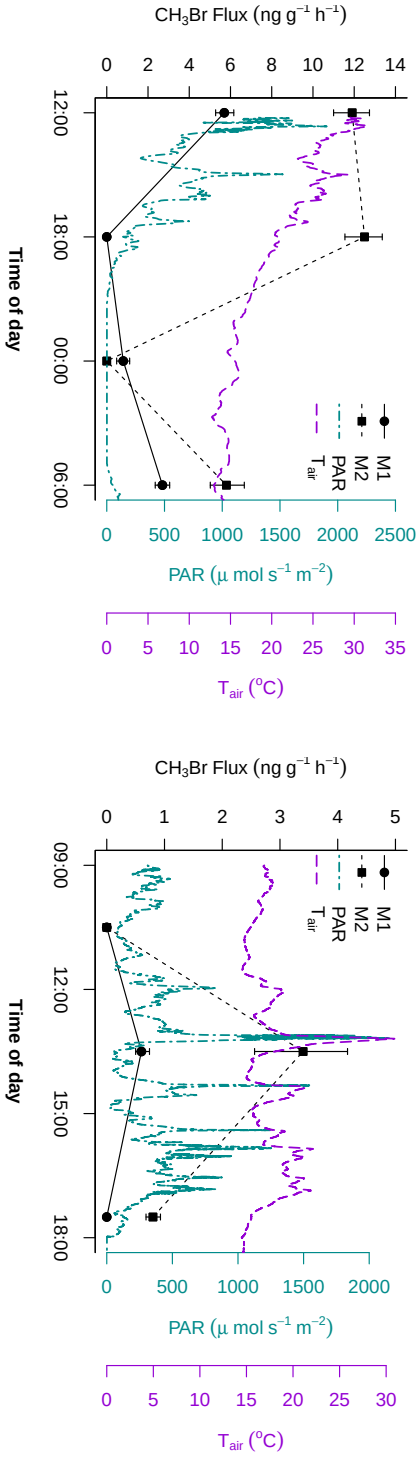
Figure 3.14a shows results from the full diurnal measurements carried out in July 2010. Sites 1 and 2 in the *Miscanthus* field were sampled every 6 hours over 24 hours on 25-26th July 2010. It was cloudy but dry during the day with PAR and air temperature at a maximum at midday on the 25th and at a minimum between 7 pm and 6 am the next day.

The trend in fluxes measured at site 1 closely follows the trend in observed PAR and air temperature. Emissions peaked at 6 ng g^{-1} h^{-1} at midday before dropping to zero at 6 pm and

increasing to 3 ng g^{-1} h^{-1} at 6 am the next day. Emissions measured at site 2 peak at 12 to 12.5 ng g^{-1} h^{-1} at midday and 6 pm respectively. No flux was measured at midnight and an emission rate of half the maximum rate was measured at 6 am.

A sub-diurnal campaign was carried out at site 1 and 2 on the 12th August 2010 (Figure 3.14b). The sky was overcast and there were frequent showers throughout the day. Observed PAR and air temperature were lowest between 9 and 11 am and from 5 pm onwards although values fluctuated a lot during the course of the day.

The measured fluxes from site 1 and 2 were very low but emissions seemed to follow the general trends in the corresponding air temperature and PAR measurements. No flux was measured from either site in the morning. Emissions peaked at around 1 pm (0.5 and 3.5 ng g^{-1} h^{-1} for site 1 and 2 respectively), corresponding to the highest PAR and air temperature observations. Emissions dropped to zero at site 1 and to a minimum at site 2 in the evening.



(a) 25-26th July 2010

(b) 12th August 2010

Figure 3.14: Diurnal and sub-diurnal CH_3Br fluxes at *Miscanthus* sites 1 and 2 together with ambient air temperature and PAR. Error bars incorporate analytical and sampling uncertainties.

The results of the six sub-diurnal campaigns carried out from June to November 2011 are illustrated in Figures 3.15 and 3.16. Variations in net CH_3Br fluxes were often small and tended not to show a clear diurnal pattern but closely followed the trends in the corresponding air temperature and PAR measurements which sometimes peaked in the morning or afternoon rather than at midday.

During the measurements on the 7th June, the weather was sunny with cloudy intervals. Fluxes from both site 1 and 2 were highest at the start of the day (8 and 24 $\mathrm{ng\,g^{-1}\,h^{-1}}$ for site 1 and 2 respectively) and low to zero at midday and at 6 pm. PAR and air temperature were also lower during the second part of the day.

The weather in July, August and September was similar with fairly sunny mornings and cloudy intervals followed by showers in the afternoon, usually around 4 pm. Fluxes measured from site 1 and 2 during the 13th July peaked at midday (just under 4 $\mathrm{ng\,g^{-1}\,h^{-1}}$) and were at a minimum at the start and end of the day. The fluxes from sites 3 and 4 didn't follow the same trends as any measured environmental parameters and were at a minimum at midday. Emissions from site 3 reached the level of the peak emissions from site 1 and 2 at 9 am (4 $\mathrm{ng\,g^{-1}\,h^{-1}}$), dipped to a minimum at midday and then peaked at 11 $\mathrm{ng\,g^{-1}\,h^{-1}}$ at 6 pm. Emissions greater than 1.5 $\mathrm{ng\,g^{-1}\,h^{-1}}$ were not measured from site 4 at any point.

During the August measurements, as in July, the sunniest portion of the day was between 9 am and 4 pm, after which rain clouds appeared. Fluxes measured from sites 1 to 4 on the 18th August all started at around 2.5 $\mathrm{ng\,g^{-1}\,h^{-1}}$ at 9 am. However, a variety of trends in fluxes from different sites occurred as the day went on. At site 1, emissions increased to 5 $\mathrm{ng\,g^{-1}\,h^{-1}}$ at midday and increased again to a maximum of 20 $\mathrm{ng\,g^{-1}\,h^{-1}}$ just before 6 pm. Emissions from site 2 and 4 were generally low and reached a minimum at midday before rising back up at 6 pm to a flux rate similar to that measured at 9 am. The opposite occurred at site 3 where a maximum of 18 $\mathrm{ng\,g^{-1}\,h^{-1}}$ was measured at midday and no emission was measured at 6 pm.

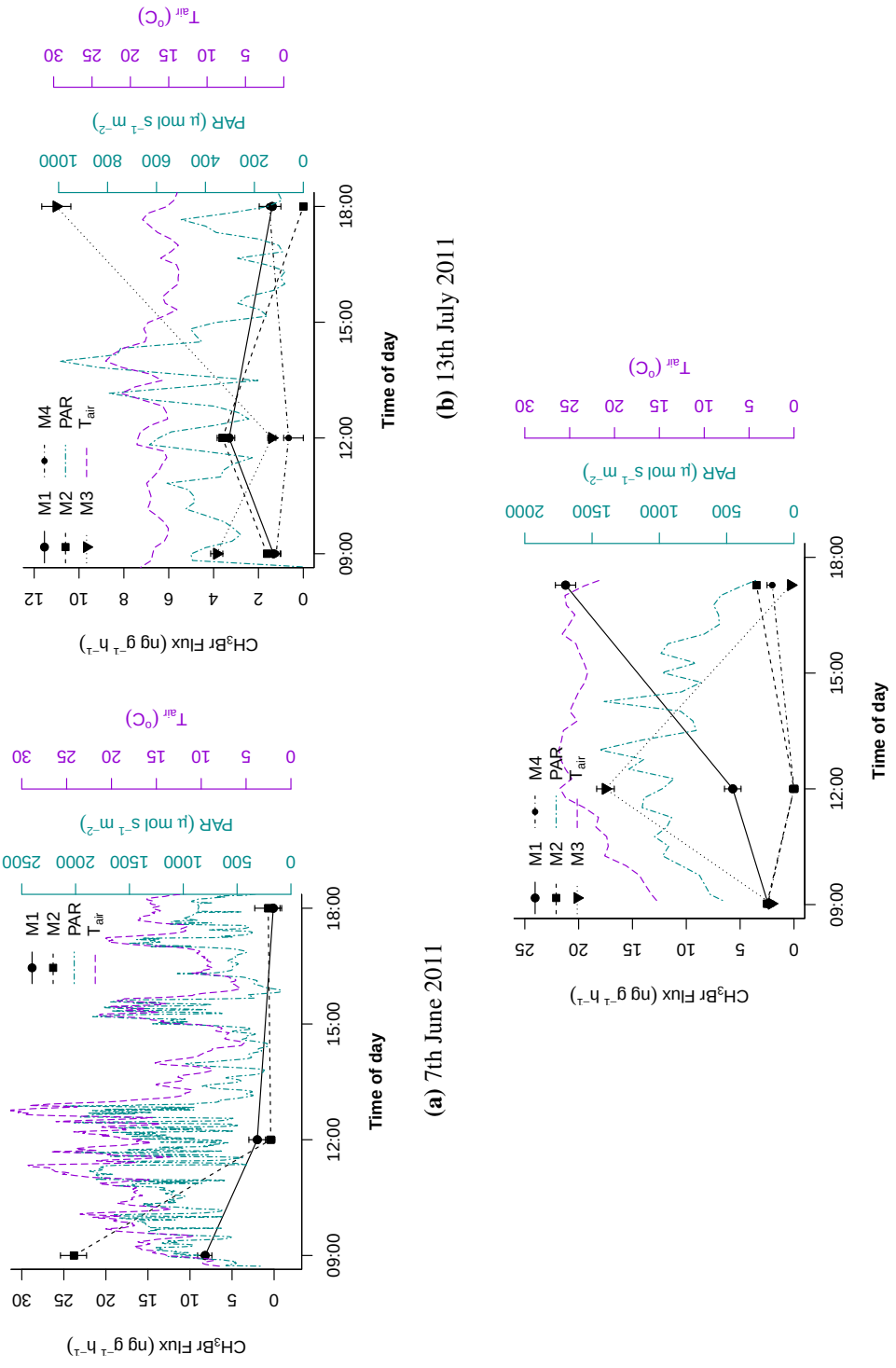
The widths of the diurnal cycles in September, October and November are narrower, corresponding to less daylight hours. On the 20th September, PAR was at a minimum between 9 and 11 am and again during a thunderstorm between 2 and 3 pm. Air temperature remained fairly steady throughout the day at around 15 °C. Emissions from sites 1 and 2 were generally low and peaked at 2.5 to 3 $\mathrm{ng\,g^{-1}\,h^{-1}}$ at 10 am and remained steady or decreased slightly at 1 pm before dropping to zero at 4 pm.

It was a sunny and fairly warm day for the time of year when measurements were made on the 26th October. PAR and air temperature were low at the start of the day but increased substantially before peaking at around 1.30 pm (800 μ mol $\mathrm{m^{-2}\,s^{-1}}$ and 20 °C respectively). The majority of the leaves on the *Miscanthus* were senescing by this time and fairly low fluxes were measured. Emissions from sites 1, 2 and 3 followed a similar pattern with minimum emissions of 0 to

2 ng g^{-1} h^{-1} in the morning and peak emissions of 2 to 5 ng g^{-1} h^{-1} around 2 pm. However at site 4 a maximum emission of 9 ng g^{-1} h^{-1} was measured at 10 am and emissions dropped to 2 ng g^{-1} h^{-1} at 2 pm and to zero at 4 pm.

The 23rd November was a cloudy and wet day. The *Miscanthus* leaves had all turned brown by this stage and very low or zero fluxes were measured, making it difficult to pick out any diurnal trend. No environmental observations were recorded from 3 pm onwards.

In summary, a clear diurnal trend was measured in July 2010 with CH_3Br emissions dropping to very low or zero during the night and peaking during the day when sunlight and air temperature are highest. Changeable weather meant that it was sometimes difficult to distinguish trends during the sub-diurnal measurement campaigns in August 2010 and June to November 2011. However, trends in CH_3Br fluxes were often found to follow trends in observed PAR and air temperature. Low fluxes were measured throughout these campaigns, similarly to those measured during the long-term time series. The lowest fluxes were recorded in November when the *Miscanthus* plants were dormant.



(a) 7th June 2011 **(b)** 13th July 2011 **(c)** 18th August 2011

Figure 3.15: Sub-diurnal CH_3Br fluxes in *Miscanthus* in June to August 2011 plotted together with ambient air temperature and PAR. Error bars incorporate analytical and sampling uncertainties. Note the different vertical scales in each figure.

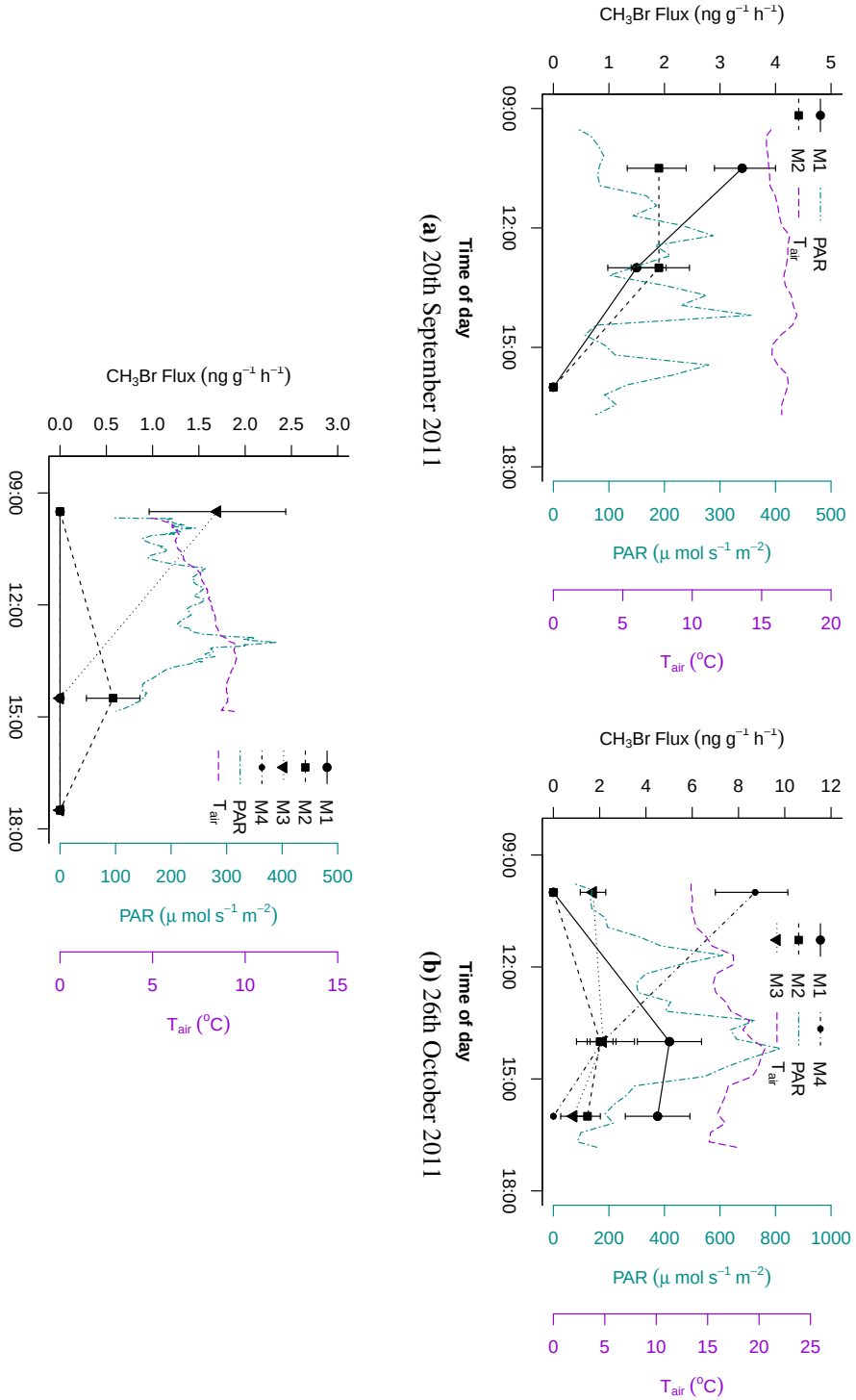


Figure 3.16: Sub-diurnal CH_3Br fluxes in *Miscanthus* in September to November 2011 plotted against ambient air temperature and PAR. Error bars incorporate analytical and sampling uncertainties. Note the different vertical scales in each figure.

CH_3Cl fluxes

CH_3Cl fluxes measured during three sub-diurnal campaigns in June, July and August 2011 are illustrated in Figure 3.17. CH_3Cl measurements from the diurnal campaign in July 2010 and the sub-diurnal campaigns in September, October and November are omitted as very little flux was detected.

On the 7th June the air temperature and PAR were highest at midday and fluctuated during the afternoon. The trend in emissions from site 1 followed the trends in air temperature and PAR. Emissions of around 15 ng g^{-1} h^{-1} were recorded at 9 am, a peak emission of 30 ng g^{-1} h^{-1} was recorded at midday and no flux was recorded at 6 pm. The trend in emissions from site 2 was slightly different with a peak emission of just under 30 ng g^{-1} h^{-1} occurring at 9 am, which had halved at midday before dropping to zero at 6 pm.

The weather in July and August was similar with fairly sunny mornings and cloudy intervals followed by showers in the afternoon, usually around 4 pm. PAR and air temperature fluctuated throughout the day on 13th July. Fluxes measured from site 1 and 2 followed a similar pattern with peak emissions at midday (20 and just under 30 ng g^{-1} h^{-1} respectively) and lower emissions at 9 am and 6 pm (around 14 ng g^{-1} h^{-1} for site 1 and zero for site 2). A peak emission of around 20 ng g^{-1} h^{-1} was measured at site 3 at 9 am and no fluxes were measured during the rest of the day.

As in July, PAR and air temperature on the 18th August were highest between 10 am and 4 pm, although they did fluctuate a great deal throughout the day. Emissions from sites 1, 2 and 3 all followed the general trends in air temperature and PAR. Emissions were highest at midday and lowest at 6 pm (between 30-90 and 0-10 ng g^{-1} h^{-1} respectively) with emissions around half the peak emissions measured at 9 am (19 to 45 ng g^{-1} h^{-1}).

Overall, the CH_3Cl fluxes measured during three sub-diurnal campaigns in June, July and August 2011 indicate a clear diurnal trend in emissions. The CH_3Cl fluxes measured during the diurnal campaign in July 2010 and the sub-diurnal campaigns in September, October and November are omitted as very little flux was detected. Fluctuations in the weather may have contributed to differences in flux trends so that peak emissions do not always occur in the middle of the day. However, trends in CH_3Cl fluxes usually closely followed trends in observed PAR and air temperature.

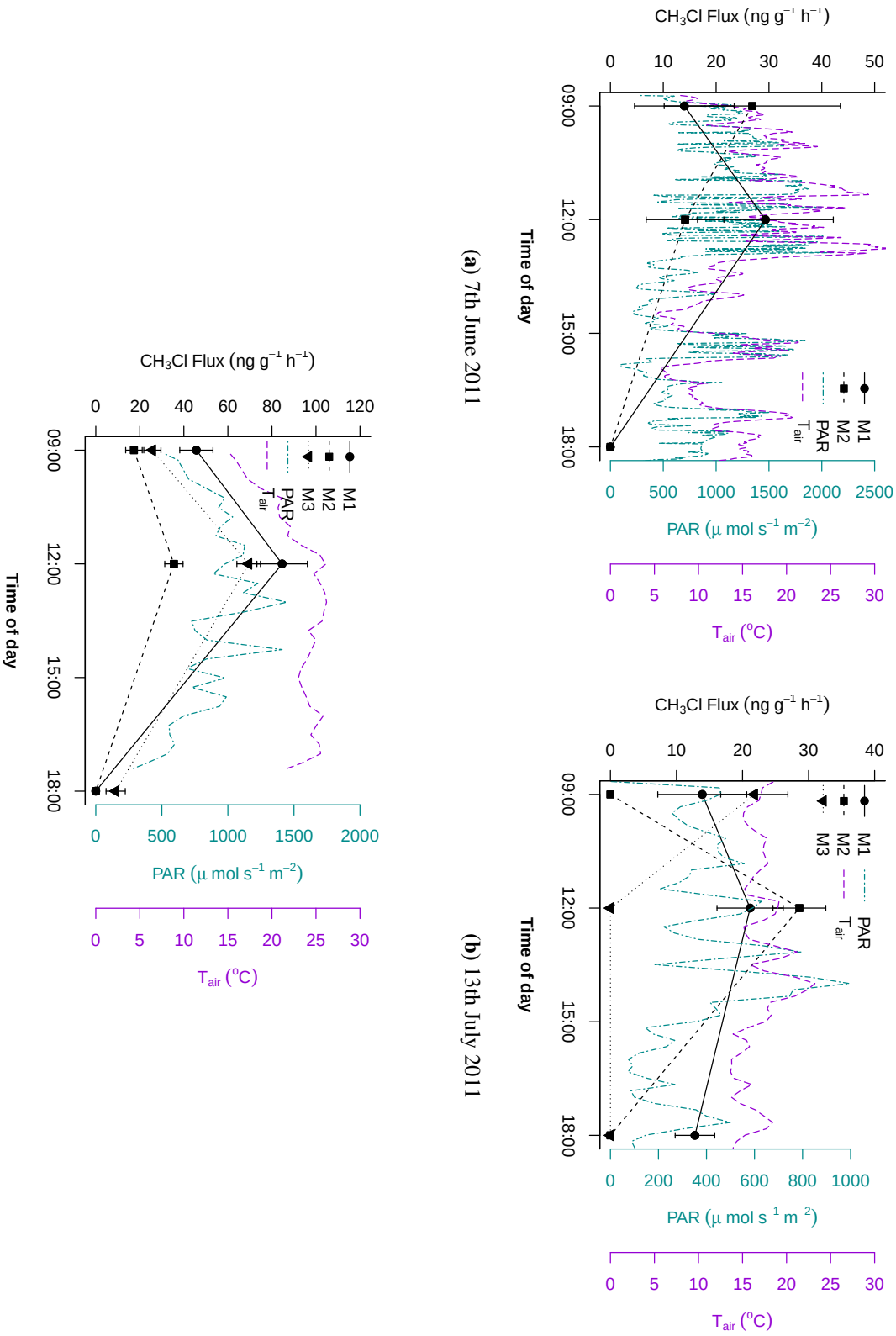


Figure 3.17: Sub-diurnal CH_3Cl fluxes in *Miscanthus* in June to August 2011 plotted against ambient air temperature and PAR. Error bars incorporate analytical and sampling uncertainties. Note the different scales used in each figure.

3.4 Outline of BVOC flux measurements in *Miscanthus*

Flux measurements were carried out as described in Section 2.3.1. Regular BVOC flux measurements were made alongside CH_3X measurements throughout 2010, 2011 and 2012. In order to capture seasonal flux variability 244 measurements were made in total over 18 site visits almost every month. The seasonal net fluxes measured during 2010 to 2012 are illustrated in time series Figures 3.19 to 3.23. In order to investigate the behaviour of BVOC fluxes throughout the day, separate sub-diurnal studies were also carried out between June and November 2011. These are presented in Figure 3.28.

3.4.1 BVOC flux trends

Isoprene

131 isoprene flux measurements were made during 18 site visits beginning in April 2010 and ending in August 2012. Fluxes are considered first by calendar year and then collectively across all 3 calendar years. Figure 3.18 presents the isoprene fluxes at all ten individual sampling points and the mean of those values on each sampling occasion between 2010 and 2012. Figures 3.19 to 3.23 illustrate the seasonal isoprene fluxes for all 10 sampling sites, together with respective PAR levels, ambient air temperature, soil temperature and soil water content by calendar year. These measurements capture the seasonal, temporal and annual variations in isoprene fluxes.

In 2010, 26 measurements were made and the maximum flux measured was 42.5 $\mu g\, g^{-1}\, h^{-1}$ from site 3 (Table 3.7a). Mean fluxes ranged from 0 to 14.7 $\mu g\, g^{-1}\, h^{-1}$. Three of the ten maximum fluxes measured throughout the campaign were measured in 2010 from sites 1, 3 and 6.

Almost three times as many measurements were made in 2011 compared to 2010 (Table 3.7b). Measured isoprene fluxes were much lower in 2011. The maximum flux measured was 6.4 $\mu g\, g^{-1}\, h^{-1}$ from site 2. Mean fluxes ranged from 0 to 0.8 $\mu g\, g^{-1}\, h^{-1}$. Seven of the ten highest maximum fluxes measured throughout the campaign were measured in 2011 from sites 2, 4, 5, and 7-10, probably due in part to a lack of summer measurements at sites 4-10 in 2010.

In 2012 there were only two non-zero fluxes recorded, 2.0 and 0.7 $\mu g\, g^{-1}\, h^{-1}$ from sites 1 and 2 respectively in August 2012. Unfortunately some measurement data from the other sites was lost due to instrument problems.

During the sampling period, annual net isoprene fluxes were very small or zero (Table 3.8). A range of fluxes from 5 to 43 $\mu g\, g^{-1}\, h^{-1}$ were measured during 2010 but have large associated uncertainties. During August in 2011 and 2012 there were maximum emissions of 6 and 2 $\mu g\, g^{-1}\, h^{-1}$ respectively with smaller associated uncertainties. Over the three calendar years

during which sampling took place, maximum emissions of under 1.5 $\mu g\, g^{-1}\, h^{-1}$ were measured in 6 out of the 10 sites.

Table 3.7: Mean, median, minimum and maximum net isoprene fluxes during 2010 and 2011. All flux values are given in $\mu g\, g^{-1}\, h^{-1}$. The final column gives the number of measurements made. The last row summarises all fluxes from all sites.

(a) 2010

Site	Mean	Median	Min	Max	Measurements
M1	5.33	0.00	0.00	28.8	6
M2	0.93	0.00	0.00	4.64	5
M3	14.7	8.08	0.00	42.5	4
M4	0.00	0.00	0.00	0.00	3
M5	0.00	0.00	0.00	0.00	2
M6	8.93	8.93	0.00	17.9	2
M7	0.00	0.00	0.00	0.00	1
M8	0.00	0.00	0.00	0.00	1
M9	0.00	0.00	0.00	0.00	1
M10	0.00	0.00	0.00	0.00	1
All	4.35	0.00	0.00	42.5	26

(b) 2011

Site	Mean	Median	Min	Max	Measurements
M1	0.14	0.00	0.00	0.83	8
M2	0.84	0.00	0.00	6.42	8
M3	0.03	0.00	0.00	0.12	8
M4	0.07	0.00	0.00	0.40	7
M5	0.05	0.00	0.00	0.35	7
M6	0.46	0.00	0.00	3.10	7
M7	0.22	0.00	0.00	1.33	7
M8	0.07	0.00	0.00	0.29	7
M9	0.12	0.00	0.00	0.62	7
M10	0.19	0.00	0.00	1.21	7
All	0.22	0.00	0.00	6.42	73

Table 3.8: Mean, median, minimum and maximum net isoprene fluxes for the entire measurement period. All flux values are given as $\mu g\, g^{-1}\, h^{-1}$. The final column gives the number of measurements made. The last row summarises all fluxes from all sites.

Site	Mean	Median	Min	Max	Measurements
M1	1.95	0.00	0.00	28.8	18
M2	0.71	0.00	0.00	6.42	17
M3	3.92	0.00	0.00	42.5	15
M4	0.04	0.00	0.00	0.40	13
M5	0.03	0.00	0.00	0.35	12
M6	1.75	0.00	0.00	17.9	12
M7	0.14	0.00	0.00	1.33	11
M8	0.05	0.00	0.00	0.29	11
M9	0.08	0.00	0.00	0.62	11
M10	0.12	0.00	0.00	1.21	11
All	1.01	0.00	0.00	42.5	131

Figure 3.18 illustrates the high fluxes measured in 2010 compared with 2011 and 2012. The emissions measured in 2011 and 2012 are dwarfed by the fluxes measured in 2010 and their large associated uncertainties which were caused in part by problems with the analytical instrumentation during summer 2010.

Measured fluxes of isoprene from each individual site across three calendar years from April 2010 to August 2012 together with PAR, air temperature, soil temperature and soil water content observations are illustrated in Figures 3.19 to 3.23. Maximum emissions of less than 1.5 $\mu g\, g^{-1}\, h^{-1}$ were recorded at sites 4, 5 and 7-10. The highest isoprene flux was measured at site 3 in 2010 (42.5 $\mu g\, g^{-1}\, h^{-1}$), which also recorded the highest CH_3Br and CH_3Cl fluxes during 2010 and 2011 respectively.

In summary, very low fluxes of isoprene were measured across the campaign and higher fluxes had large uncertainties. The low fluxes measured here are in line with the measurements of the previous EC PTR-MS study of BVOCs from above the *Miscanthus* canopy (generally undetectable fluxes with maximum isoprene emissions of 0.25 mg $m^{-2}\, h^{-1}$ (Copeland et al., 2012)). However, even from these low fluxes it is possible to distinguish a seasonal trend with highest emissions occurring during the growing season and zero fluxes during the winter.

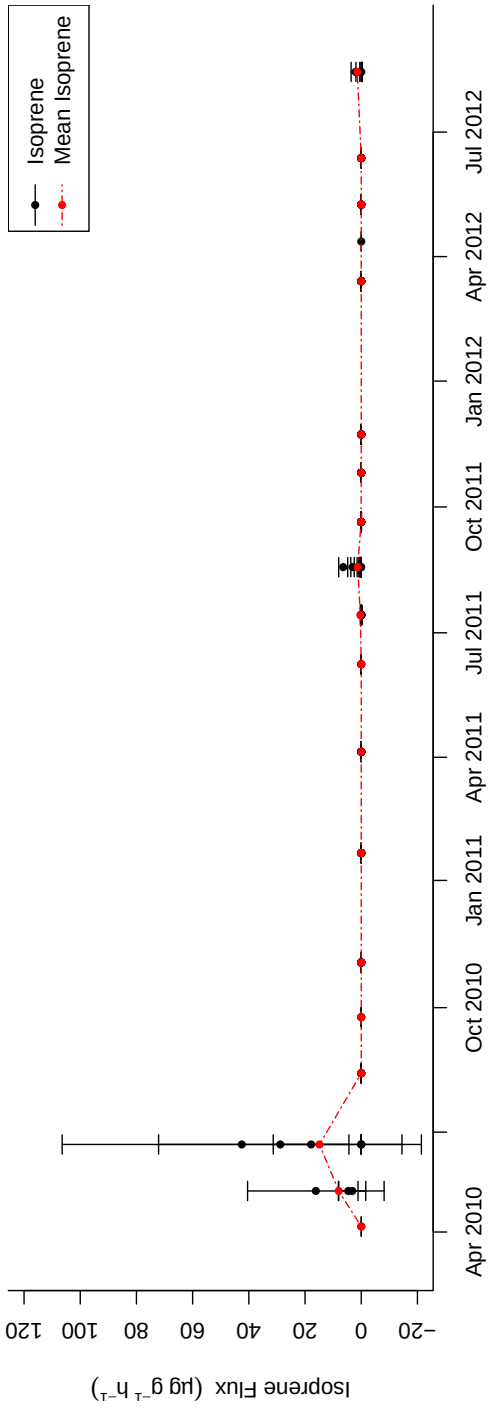
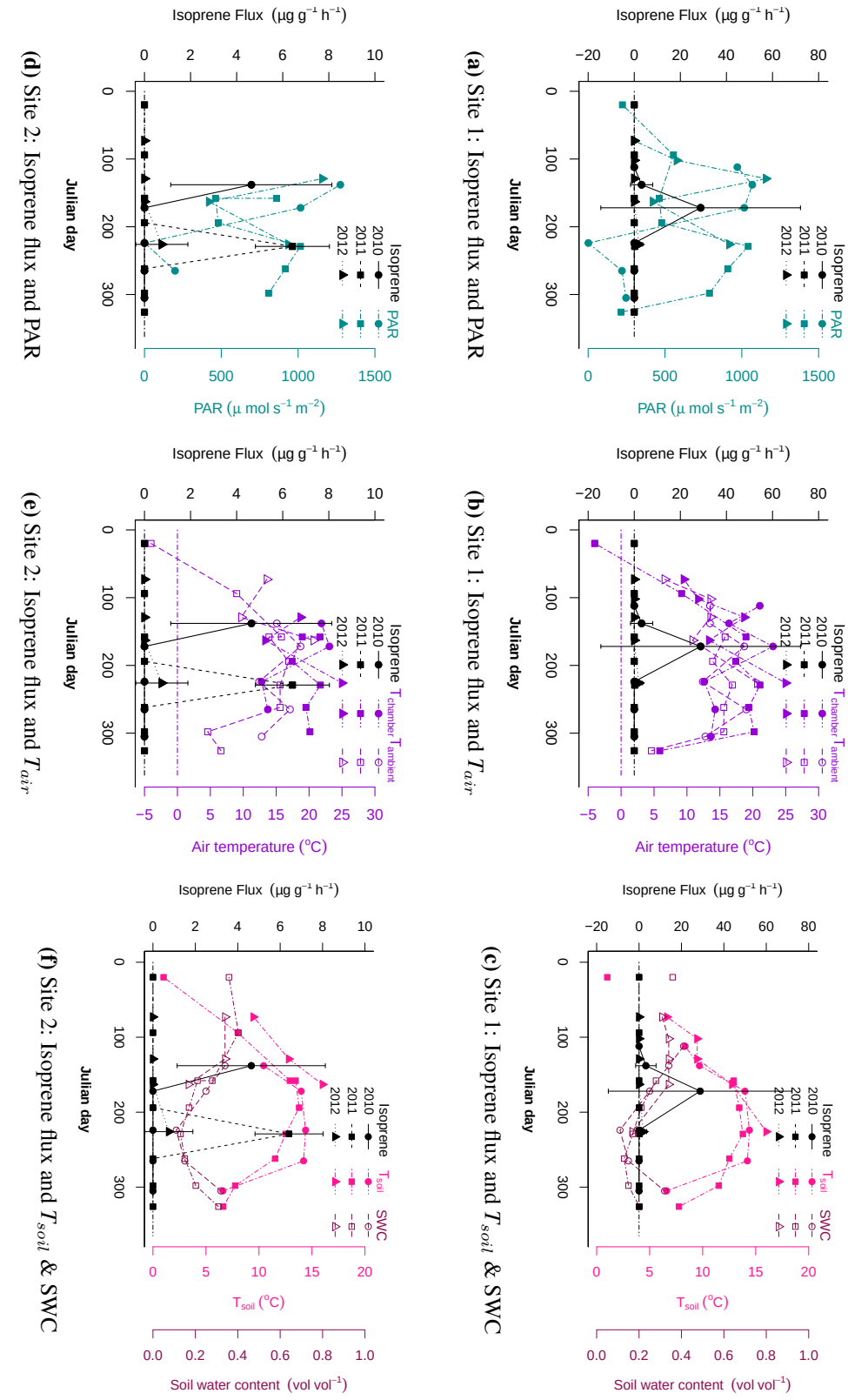


Figure 3.18: Isoprene fluxes at all ten *Miscanthus* sampling points and the mean of those values on each sampling occasion between 2010 and 2012. Error bars incorporate analytical and sampling uncertainties (as described in Section 2.6.1).



(a) Site 1: Isoprene flux and PAR

(b) Site 1: Isoprene flux and T_{air}

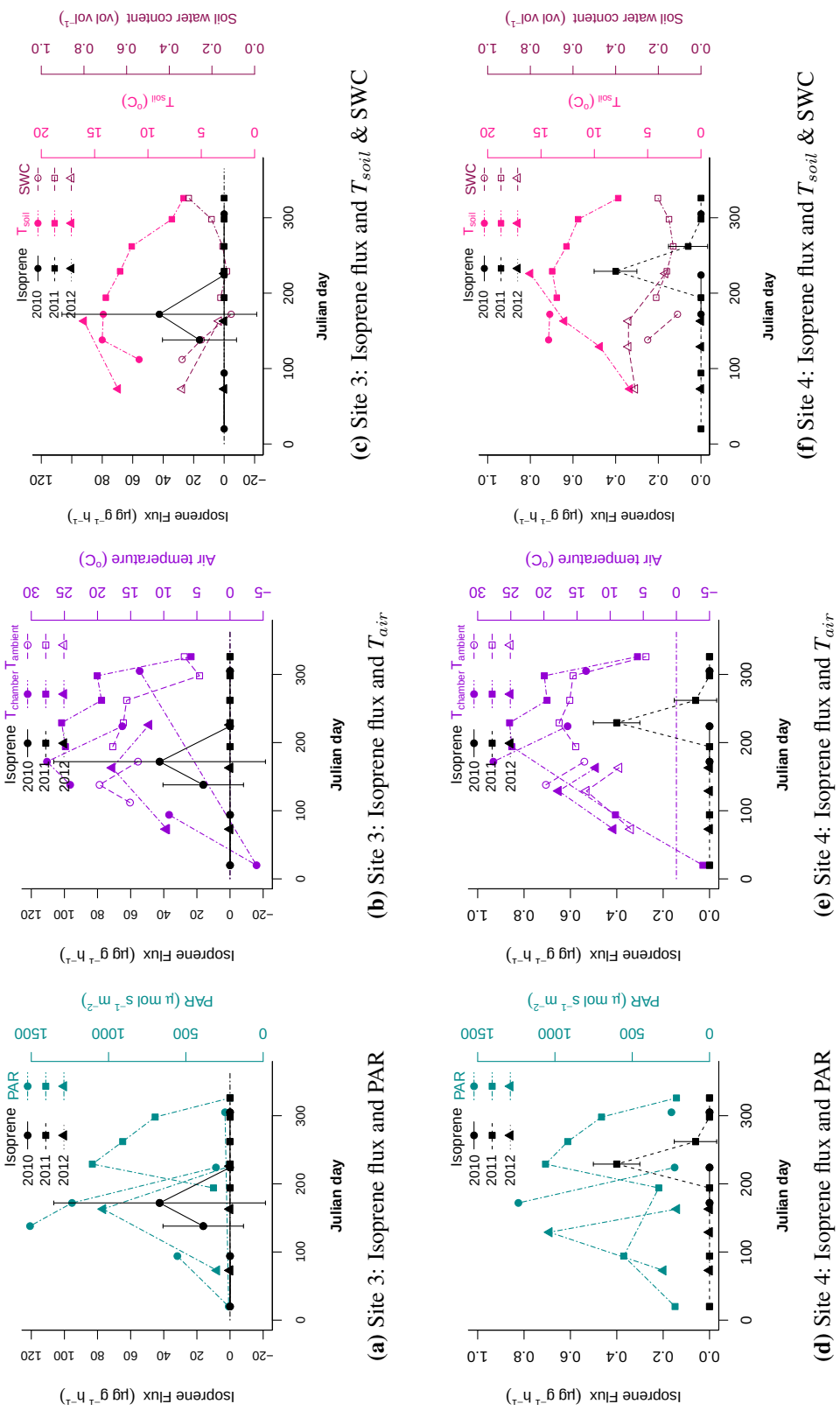
(c) Site 1: Isoprene flux and T_{soil} & SWC

(d) Site 2: Isoprene flux and PAR

(e) Site 2: Isoprene flux and T_{air}

(f) Site 2: Isoprene flux and T_{soil} & SWC

Figure 3.19: Comparison of net isoprene fluxes from *Miscanthus* with PAR, chamber and ambient air temperature, soil temperature and soil water content for 2010 and 2012 for sites 1 and 2. Note different y-axis scales for isoprene. Error bars on fluxes incorporate analytical and sampling uncertainties.



(a) Site 3: Isoprene flux and PAR

(b) Site 3: Isoprene flux and T_{air}

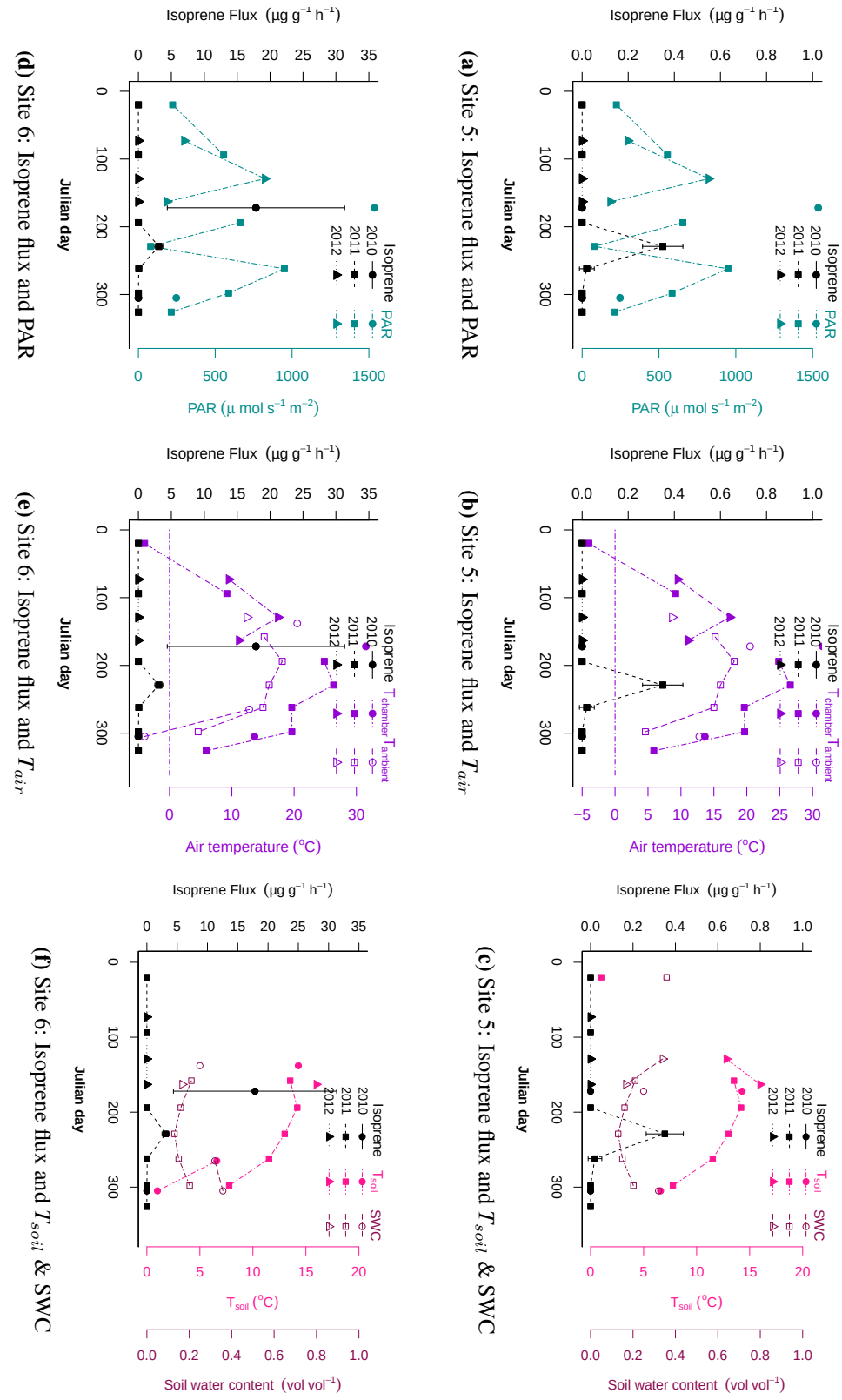
(c) Site 3: Isoprene flux and T_{soil} & SWC

(d) Site 4: Isoprene flux and PAR

(e) Site 4: Isoprene flux and T_{air}

(f) Site 4: Isoprene flux and T_{soil} & SWC

Figure 3.20: Comparison of net isoprene fluxes from *Miscanthus* with PAR, chamber and ambient air temperature, soil temperature and soil water content for 2010 and 2012 for sites 3 and 4. Note different y-axis scales for isoprene. Error bars on fluxes incorporate analytical and sampling uncertainties.



(a) Site 5: Isoprene flux and PAR

(b) Site 5: Isoprene flux and T_{air}

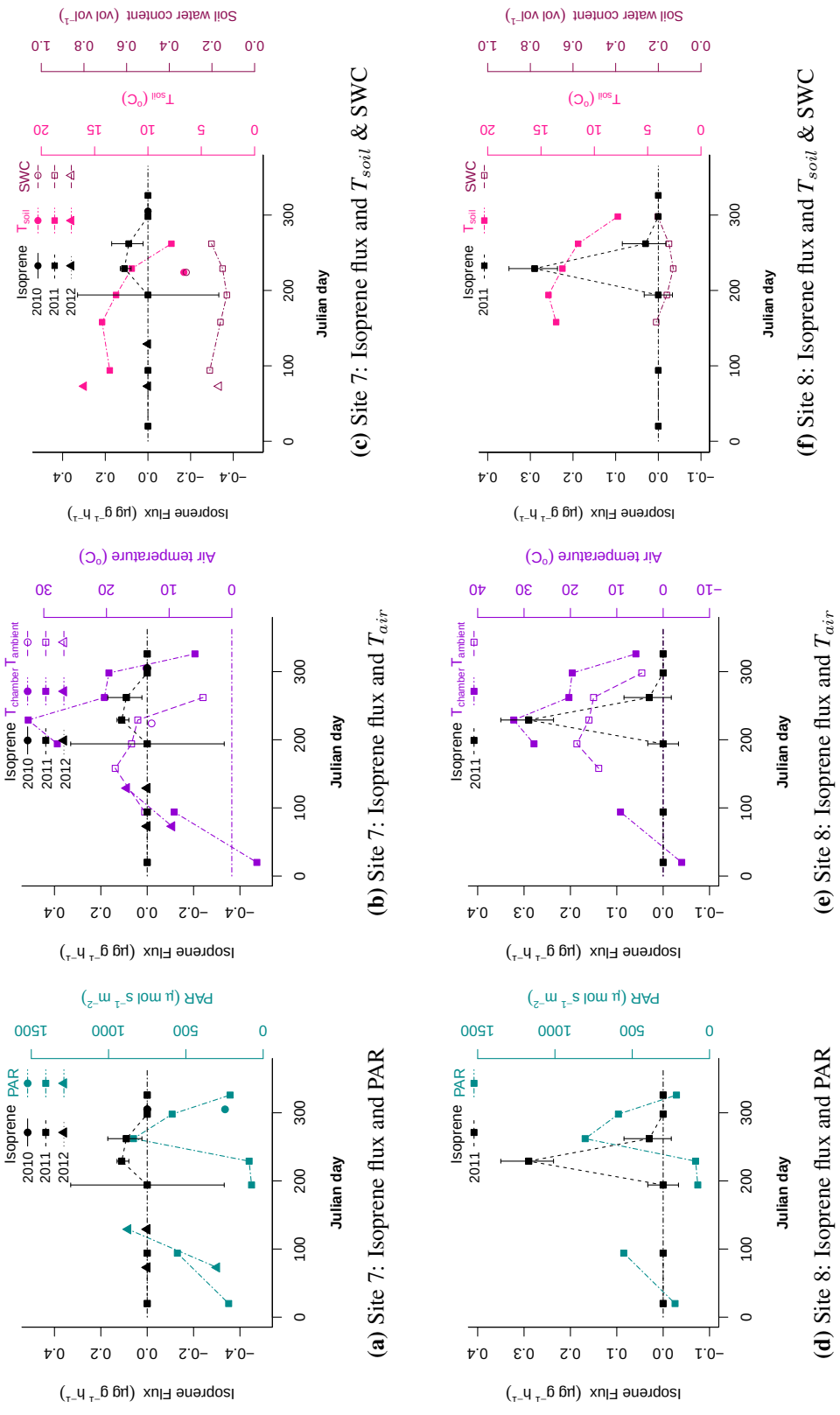
(c) Site 5: Isoprene flux and T_{soil} & SWC

(d) Site 6: Isoprene flux and PAR

(e) Site 6: Isoprene flux and T_{air}

(f) Site 6: Isoprene flux and T_{soil} & SWC

Figure 3.21: Comparison of net isoprene fluxes from *Miscanthus* with PAR, chamber and ambient air temperature, soil temperature and soil water content for 2010 and 2012 for sites 5 and 6. Note different y-axis scales for isoprene. Error bars on fluxes incorporate analytical and sampling uncertainties.



(a) Site 7: Isoprene flux and PAR

(b) Site 7: Isoprene flux and T_{air}

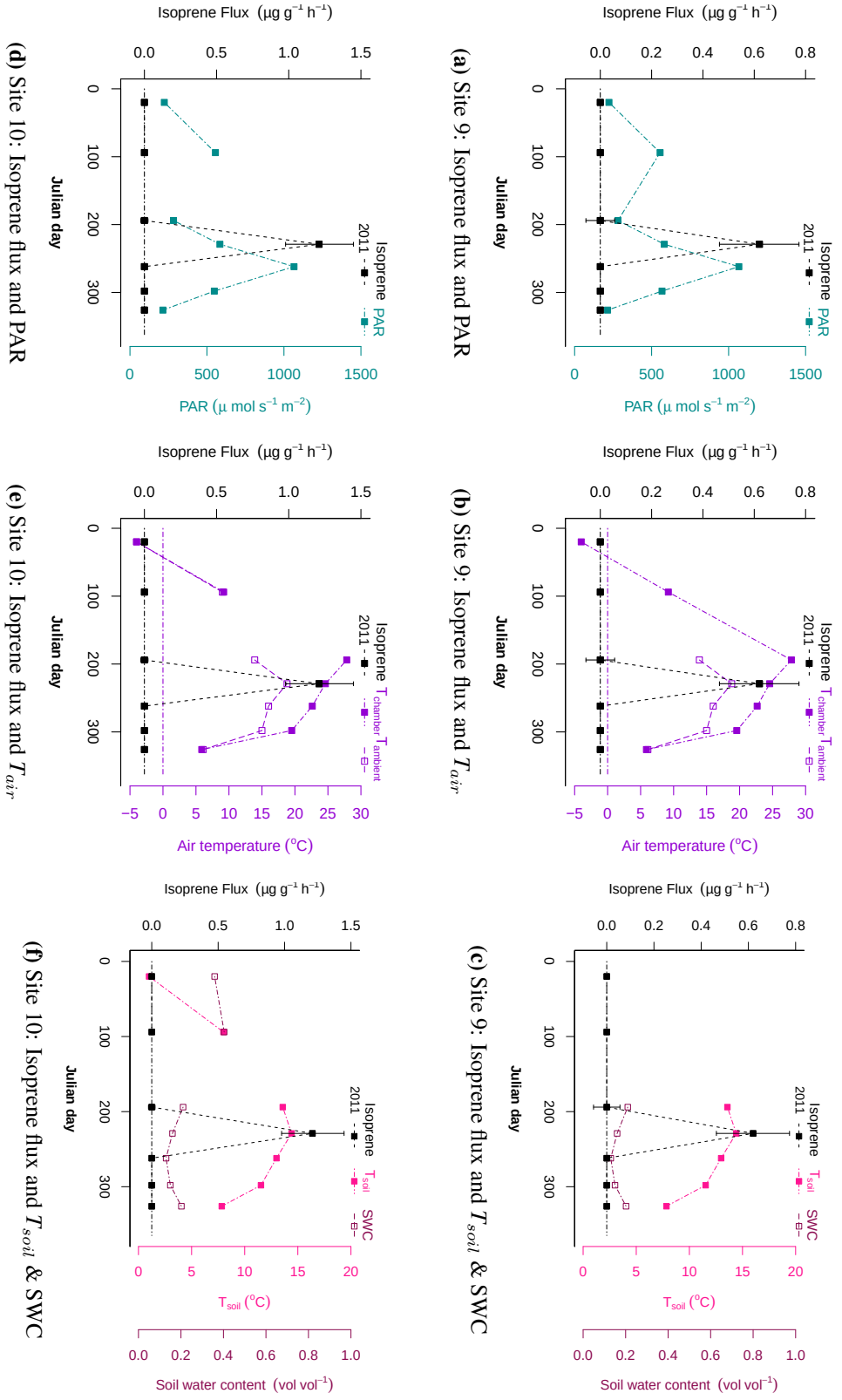
(c) Site 7: Isoprene flux and T_{soil} & SWC

(d) Site 8: Isoprene flux and PAR

(e) Site 8: Isoprene flux and T_{air}

(f) Site 8: Isoprene flux and T_{soil} & SWC

Figure 3.22: Comparison of net isoprene fluxes from *Miscanthus* with PAR, chamber and ambient air temperature, soil temperature and soil water content for 2010 and 2012 for sites 7 and 8. Note different y-axis scales for isoprene. Error bars on fluxes incorporate analytical and sampling uncertainties.



(a) Site 9: Isoprene flux and PAR

(b) Site 9: Isoprene flux and T_{air}

(c) Site 9: Isoprene flux and T_{soil} & SWC

(d) Site 10: Isoprene flux and PAR

(e) Site 10: Isoprene flux and T_{air}

(f) Site 10: Isoprene flux and T_{soil} & SWC

Figure 3.23: Comparison of net isoprene fluxes from *Miscanthus* with PAR, chamber and ambient air temperature, soil temperature and soil water content for 2010 and 2012 for sites 9 and 10. Note different y-axis scales for isoprene. Error bars on fluxes incorporate analytical and sampling uncertainties.

α-pinene

Small or zero α-pinene fluxes were measured across the three calendar years with the exception of summer 2010 (Table 3.9). Large fluxes of between 640 and 1910 $\mu g\, g^{-1}\, h^{-1}$ were measured in 2010 but have large associated uncertainties due to problems with the analytical equipment. At sites 1, 3 and 5 the uncertainties associated with these large fluxes make it unlikely that real emissions are being measured. Despite large uncertainties associated with fluxes at sites 2, 4 and 6 these are believed to be detectable emissions.

In June 2011, an emission of 2.4 $\mu g\, g^{-1}\, h^{-1}$ was measured from site 2 but no other fluxes were recorded at any other time during 2011 from any other site. Maximum emissions of between 3 and 11 $\mu g\, g^{-1}\, h^{-1}$ were measured in May, June and August of 2012. No fluxes were recorded at any time at sites 7, 8, 9 and 10.

Table 3.9: Mean, median, minimum and maximum net α-pinene fluxes for the entire measurement period. All flux values are given as $\mu g\, g^{-1}\, h^{-1}$. The final column gives the number of measurements made. The last row summarises all fluxes from all sites.

Site	Mean	Median	Min	Max	Measurements
M1	39.7	0.00	0.00	641	18
M2	97.3	0.00	0.00	1360	16
M3	104	0.00	0.00	911	14
M4	147	0.00	0.00	1910	13
M5	82.3	0.00	0.00	823	10
M6	85.2	0.00	0.00	849	10
All	64.7	0.00	0.00	1910	113

Figure 3.24 presents the α-pinene fluxes at all ten sampling points and the mean of those values on each sampling occasion across 2010 to 2012. It illustrates the high fluxes and large uncertainties measured in 2010 and the low to zero fluxes in the following two years. The times series of α-pinene fluxes against PAR and air temperature are shown in Figures 3.25 to 3.27. Correlations to environmental parameters were not investigated due to the low fluxes measured.

In summary, no significant α-pinene fluxes were measured during the sampling period apart from those recorded in summer 2010. However, these measurements have sufficiently large uncertainties that their significance is ambiguous. Overall, these measurements are consistent with a previous PTR-MS study in *Miscanthus* which did not detect any monoterpene flux from the *Miscanthus* canopy (Copeland et al., 2012).

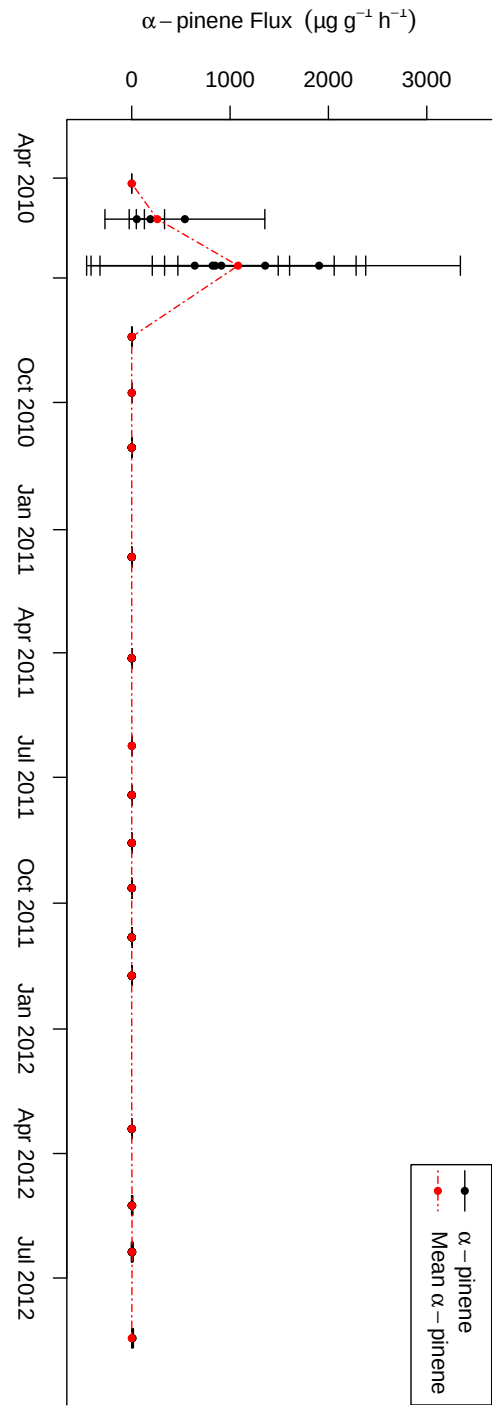
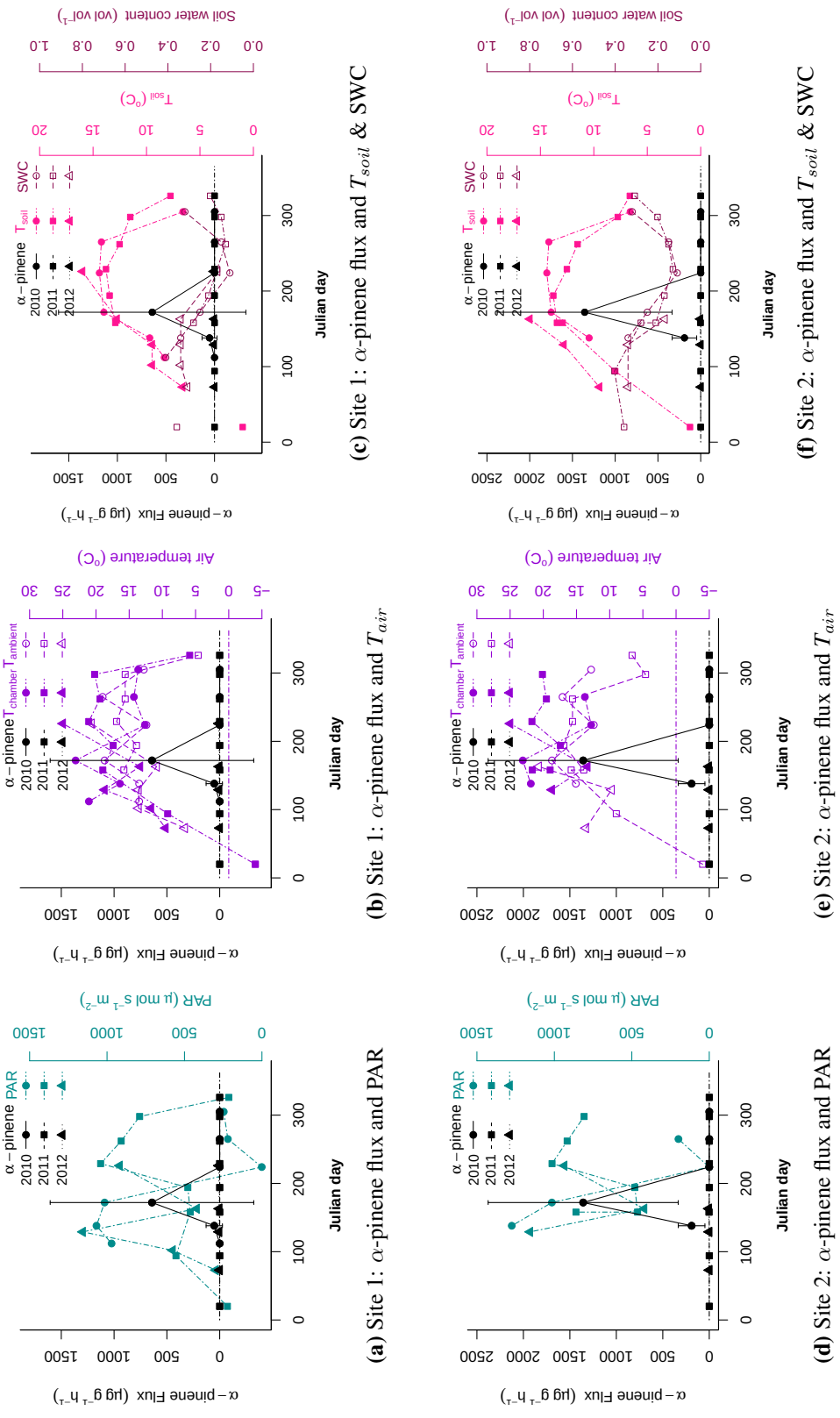


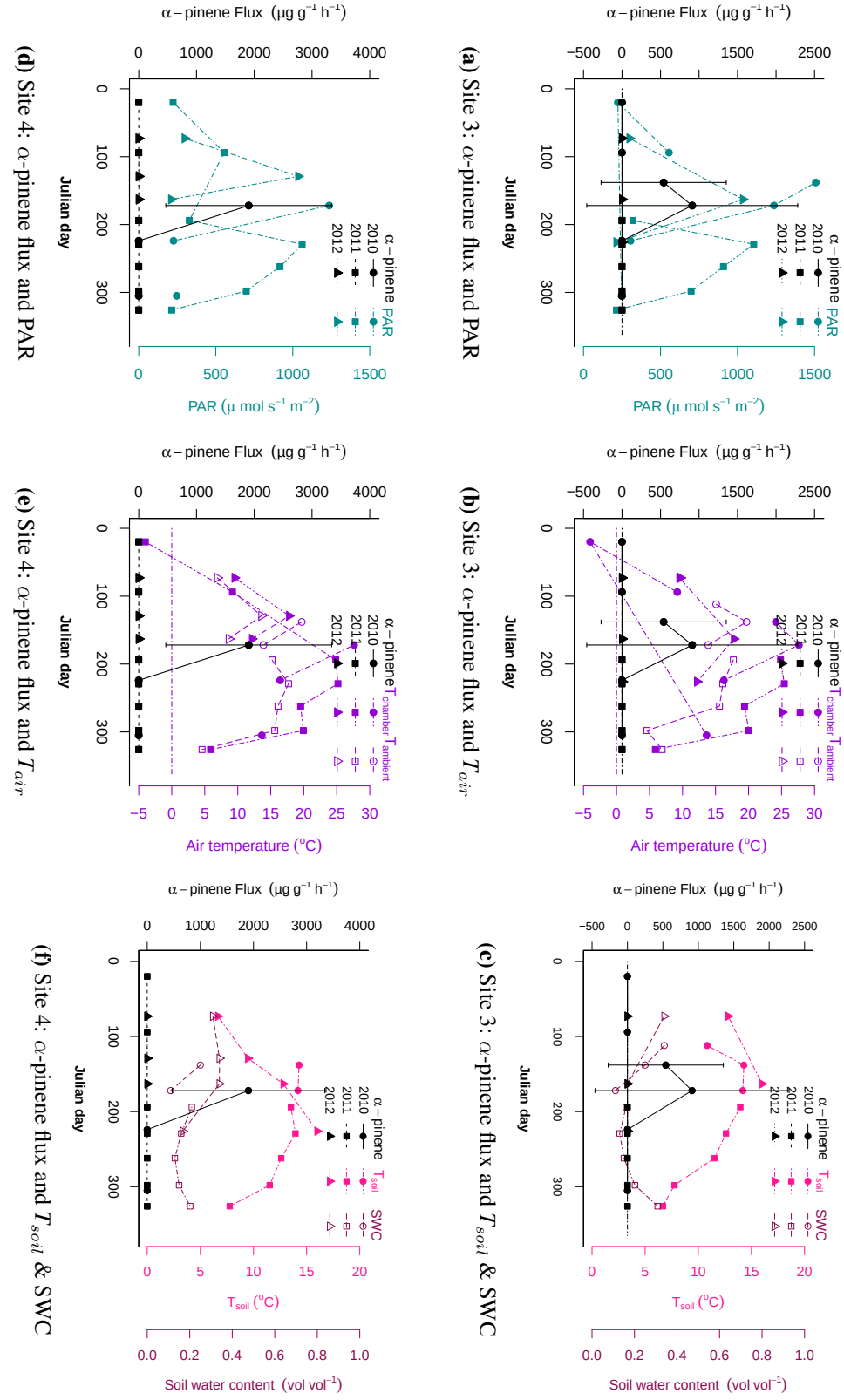
Figure 3.24: α-pinene fluxes at all ten *Miscanthus* sampling points and the mean of those values on each sampling occasion between 2010 and 2012. Error bars incorporate analytical and sampling uncertainties (as described in Section 2.6.1).



(a) Site 1: α-pinene flux and PAR **(b)** Site 1: α-pinene flux and T_{air} **(c)** Site 1: α-pinene flux and T_{soil} & SWC

(d) Site 2: α-pinene flux and PAR **(e)** Site 2: α-pinene flux and T_{air} **(f)** Site 2: α-pinene flux and T_{soil} & SWC

Figure 3.25: Comparison of net α-pinene fluxes from *Miscanthus* with PAR, chamber and ambient air temperature, soil temperature and soil water content for 2010 and 2012 for sites 1 and 2. Note different y-axis scales for α-pinene. Error bars on fluxes incorporate analytical and sampling uncertainties.



(a) Site 3: α-pinene flux and PAR

(b) Site 3: α-pinene flux and T_{air}

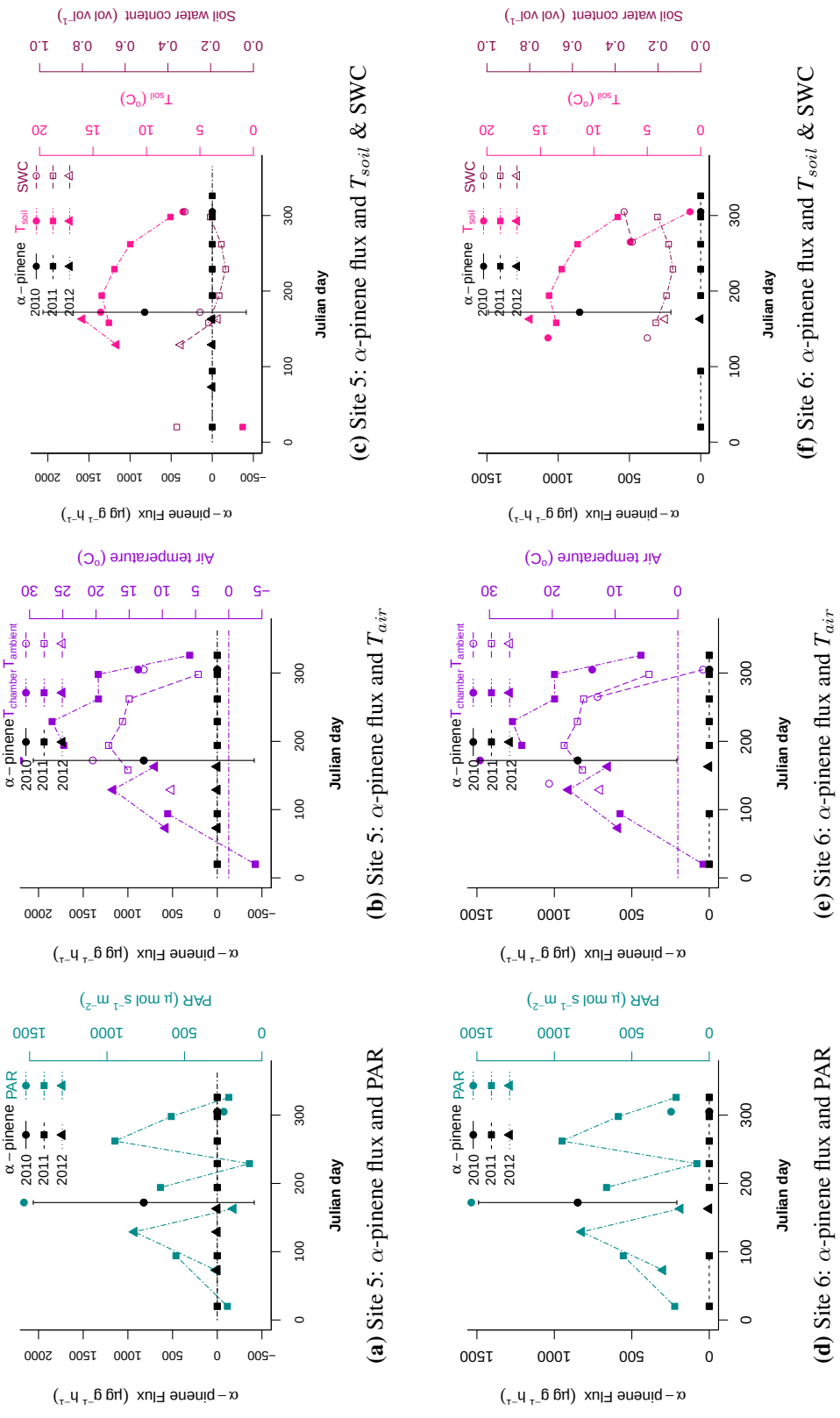
(c) Site 3: α-pinene flux and T_{soil} & SWC

(d) Site 4: α-pinene flux and PAR

(e) Site 4: α-pinene flux and T_{air}

(f) Site 4: α-pinene flux and T_{soil} & SWC

Figure 3.26: Comparison of net α-pinene fluxes from *Miscanthus* with PAR, chamber and ambient air temperature, soil temperature and soil water content for 2010 and 2012 for sites 3 and 4. Note different y-axis scales for α-pinene. Error bars on fluxes incorporate analytical and sampling uncertainties.



(a) Site 5: α-pinene flux and PAR

(b) Site 5: α-pinene flux and T_{air}

(c) Site 5: α-pinene flux and T_{soil} & SWC

(d) Site 6: α-pinene flux and PAR

(e) Site 6: α-pinene flux and T_{air}

(f) Site 6: α-pinene flux and T_{soil} & SWC

Figure 3.27: Comparison of net α-pinene fluxes from *Miscanthus* with PAR, chamber and ambient air temperature, soil temperature and soil water content for 2010 and 2012 for sites 5 and 6. Note different y-axis scales for α-pinene. Error bars on fluxes incorporate analytical and sampling uncertainties.

3.4.2 Sub-diurnal trends

To investigate the behaviour of BVOC fluxes throughout the day at different times of the year, six sub-diurnal measurement campaigns were conducted between June and November 2011. Sampling frequency varied from either three or four measurements taken between 9 am and 9 pm. Air temperature and PAR were recorded at 5 second intervals throughout each sampling period. Fluxes were measured from four sites during these campaigns. Results for isoprene fluxes are illustrated in Figure 3.28. No flux results are presented for other BVOCs such as α-pinene as there were no detectable fluxes during any of the sub-diurnal campaigns.

Small or zero isoprene fluxes were measured during six sub-diurnal campaigns from June to November 2011. No emissions were measured on the 7th June 2011, even though emissions were detected during June the previous year. On the 13th July, emissions of up to 1.5 $\mu g\, g^{-1}\, h^{-1}$ were measured from site 1 but fluxes of less than 0.3 $\mu g\, g^{-1}\, h^{-1}$ were recorded at sites 2 and 3. No diurnal trends could be distinguished.

A peak emission of just over 6 $\mu g\, g^{-1}\, h^{-1}$ was measured from site 2 on the 19th August. This emission rate was half at midday and was half again at 4 pm. Emissions from the three other sites were all lower than 1 $\mu g\, g^{-1}\, h^{-1}$ and there were no discernible trends. Zero fluxes were recorded during sub-diurnal campaigns in September, October or November 2011.

In summary, very low to zero fluxes of isoprene were recorded during the sub-diurnal measurement campaigns. No significant diurnal trends were detected in these low fluxes.

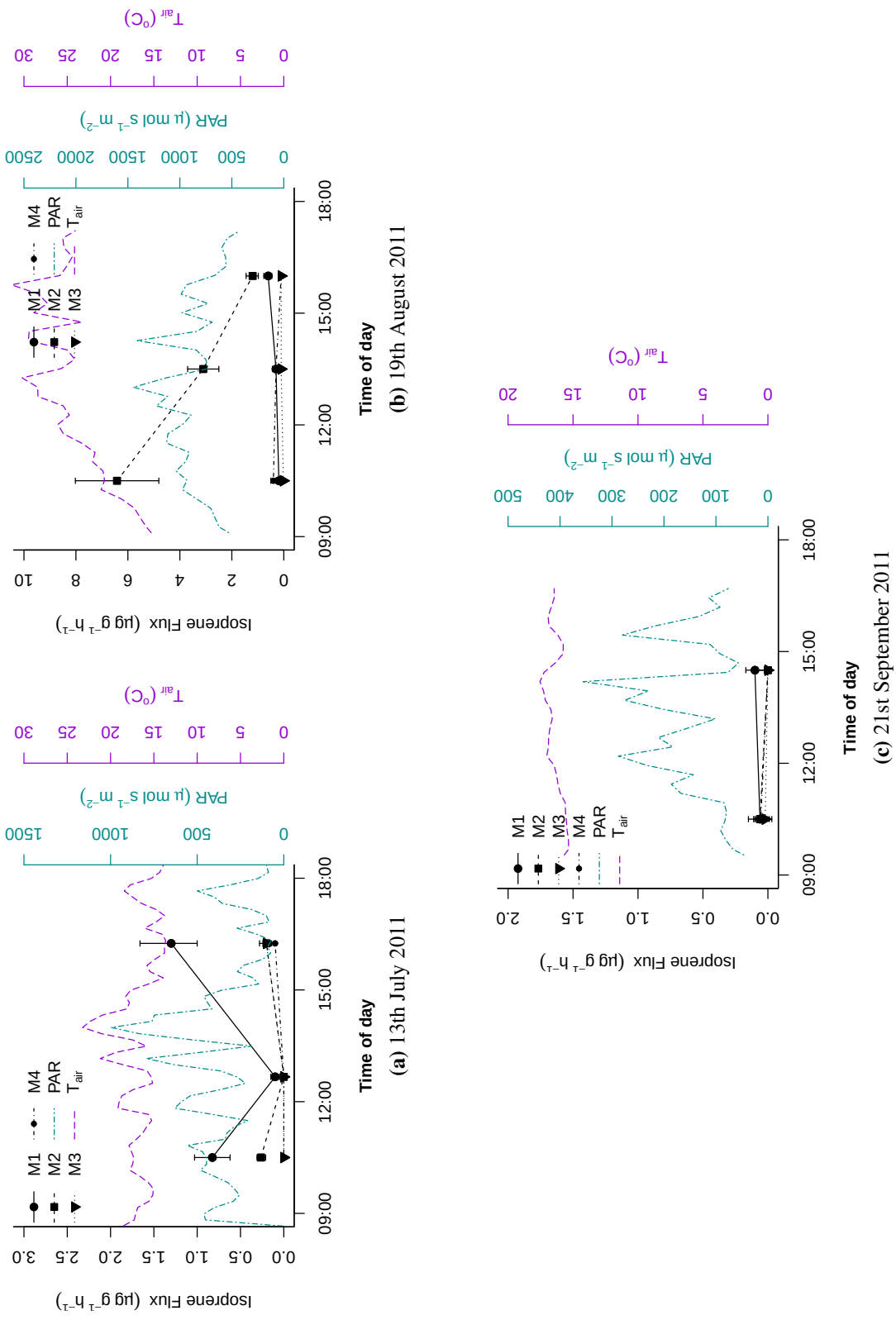


Figure 3.28: Sub-diurnal isoprene fluxes in *Miscanthus* in July to September 2011 plotted together with ambient air temperature and PAR. Error bars on fluxes incorporate analytical and sampling uncertainties. Note the different scales used in each figure.

3.5 Summary

Low annual net fluxes of CH_3Br, CH_3Cl and isoprene from *Miscanthus* were measured during the sampling period. High fluxes of α-pinene but no other monoterpenes were measured in 2010 with large associated uncertainties. However fluxes of α-pinene were not detected the following two years. The mean CH_3Br and CH_3Cl fluxes from all sites combined over measurement period were 1.75 and 10.9 ng g^{-1} h^{-1}, respectively. This is equivalent to 14 and 87 ng m^{-2} h^{-1} if it is assumed that half the plant biomass is enclosed and that there are 4 *Miscanthus* plants per square meter (Price et al., 2004). Significant positive correlations between CH_3Br and CH_3Cl fluxes were found at three individual sites and for all sites combined. However no trends could be distinguished between high or low emitting sites and significant correlations between CH_3Br and CH_3Cl fluxes.

Very low fluxes of isoprene were measured across the campaign and higher fluxes measured in 2010 had large associated uncertainties so a mean value is not presented. Fluxes of α-pinene were only measured in 2010 giving a mean flux of 65 µg g^{-1} h^{-1} or 500 ng m^{-2} h^{-1}.

As expected in accordance with the literature, significant correlations were derived between season and CH_3X and isoprene fluxes. CH_3Br, CH_3Cl and isoprene fluxes from each *Miscanthus* sampling site followed a similar pattern each year with the highest fluxes occurring during the summer and the lowest in the winter. This trend is related to the stages of plant growth during the different seasons. *Miscanthus* enters dormancy around November, is harvested during the winter and begins growing again in May/June. Maximum fluxes of CH_3Br, CH_3Cl and isoprene were measured during the growing season (May/June to September/October), between June and August, and were 33.8 and 118 ng g^{-1} h^{-1} and 42.5 µg g^{-1} h^{-1} respectively. The highest maximum fluxes for all three compounds were measured at site 3. There was high spatial variability. However there were no significant correlations between fluxes and sampling site despite some sites being high emitters and others low emitters. Significant correlations were found between CH_3X fluxes and air and soil temperatures. This indicates a general relationship between fluxes and season and with the plant growth cycle.

The magnitude of maximum emissions measured varied from year to year as did the timing of their occurrence during the growing season. This is likely due to changes in weather patterns between years including events such as frost and drought. Low to zero fluxes were recorded at all sites during the non-growing season. Minimum fluxes of zero were measured at all sites.

Diurnal CH_3X measurements indicated a likely relationship between temperature, light levels and CH_3X fluxes which decreased , although not always to zero, during the night and peaked during the day when sunlight and air temperature are highest. Changeable weather meant that it was sometimes difficult to distinguish trends during the sub-diurnal measurement campaigns in August 2010 and June to November 2011. However, trends in CH_3X fluxes were generally

found to follow trends in observed PAR and air temperature. Low CH_3X fluxes were measured throughout these campaigns, similarly to those measured during the long term time series. The lowest fluxes were recorded in November when the *Miscanthus* plants were dormant. No significant diurnal trends were detected in the low isoprene and α-pinene fluxes measured during the sub-diurnal campaigns.

3.6 Discussion

This study presents the first measurements of CH_3X and BVOCs fluxes from *Miscanthus* plants using enclosure methods. *Miscanthus* plants at this site should not be considered as an important source of these compounds. Assuming that *Miscanthus* is planted under the same soil and climate conditions present at this site, an increase in planting of *Miscanthus* for bioenergy would not impact on regional atmospheric composition for these trace gases.

Chapter 4

Long term measurements in willow

4.1 Introduction

Willow trees (*Salix spp.*) have many historic uses, including the use of willow branches in basket weaving and the use of bark as a precursor to aspirin. Now, the use of short rotation coppice (SRC) willow biomass for bioenergy production can be added to the list.

There have been a wide range of studies into SRC willow bioenergy, including the potential land resources available for planting in the UK (Bauen et al., 2010) and the potential contribution of SRC willow to both Scotland's renewable energy needs (Andersen et al., 2005) and those of the UK as a whole (Aylott et al., 2008). The potential CO_2 mitigation afforded by replacing fossil fuels with SRC willow has been the focus of many studies as this is the main driver for the uptake of bioenergy (Heller et al., 2003; Hillier et al., 2009; Rowe et al., 2009). Other environmental benefits such as the protection of ground water quality in intensively farmed areas have also been considered (Jørgensen et al., 2005).

CH_3X fluxes from willow trees have not been investigated before but a number of previous studies have examined CH_3X fluxes in woodland ecosystems containing deciduous and coniferous tree species. Most of these studies focused on fluxes from soils. Both net uptake and net emission of CH_3Br and CH_3Cl from these ecosystems have been discovered, depending on the study location and the composition of the woodland system. In a temperate woodland ecosystem in Scotland, composed of ash, beech and sycamore trees, Drewer et al. (2008) described net uptake and net emissions between -73 to +279 $\mathrm{ng\,m^{-2}\,h^{-1}}$ from static soil flux chambers, with an overall net CH_3Br emission flux of +27 $\pm$ 57 $\mathrm{ng\,m^{-2}\,h^{-1}}$.

Ambient CH_3X fluxes were investigated at conifer plantations on a temperate peatbog in Ireland by Dimmer et al. (2001), where a median daytime annual CH_3Br emission flux of +190 $\mathrm{ng\,m^{-2}\,h^{-1}}$ (with a range of average daytime annual fluxes between +30 and +740 $\mathrm{ng\,m^{-2}\,h^{-1}}$) and a median daytime annual CH_3Cl emission flux of +3900 $\mathrm{ng\,m^{-2}\,h^{-1}}$ (with a range of average daytime annual fluxes between 0 and +17000 $\mathrm{ng\,m^{-2}\,h^{-1}}$) were measured. However, at a mixed deciduous and conifer forest in New Hampshire, USA, a net

uptake of CH_3Br of -30 ng m^{-2} h^{-1} (-170 to +140 ng m^{-2} h^{-1}) was measured using a similar ambient enclosure technique (Varner et al., 2003). A global annual soil sink for CH_3Br of -22 Gg y^{-1} was estimated for deciduous and coniferous forests (Shorter et al., 1995). A similar global annual sink for CH_3Br of -38 ($\pm$ 30) Gg y^{-1} was estimated for cottonwood and deciduous shrub ecosystems (Serça et al., 1998).

A stable isotope incubation technique was employed by Rhew et al. (2003a) in order to simultaneously determine production and consumption fluxes of CH_3X in boreal forest soils from Alaska, USA. Net CH_3Br fluxes of between -39 ($\pm$ 11) ng m^{-2} h^{-1} and +9.9 ($\pm$ 5.5) ng m^{-2} h^{-1} were measured, and net CH_3Cl fluxes of between -840 ($\pm$ 310) ng m^{-2} h^{-1} and +50 ($\pm$ 30) ng m^{-2} h^{-1}. In a later study by Rhew et al. (2010), a seasonality in uptake rates was shown, with much larger uptake occurring during wet winter months (-40 $\pm$ 4.2 ng m^{-2} h^{-1} for CH_3Br and -2700 $\pm$ 360 ng m^{-2} h^{-1} for CH_3Cl) than in summer (5 to 7% of winter uptake values).

There are very few studies of CH_3X fluxes from trees. Measurements of CH_3Cl fluxes from leaves and above canopy measurements in tropical forests in Malaysia were used to estimate a canopy scale CH_3Cl flux of about 0.0014 ng m^{-2} h^{-1} (Saito et al., 2008). Using the canopy-scale flux, global CH_3Cl emission by tropical forests was estimated to be 1.3 Tg y^{-1}, representing approximately 30% of the global emissions. The study also found that 21% of the 117 tree species investigated were CH_3Cl emitters.

Another study by Blei et al. (2010a) measured fluxes of CH_3X from tropical plant branches and leaf litter during summer in Malaysian Borneo. The tree species measured determined the magnitude of CH_3X fluxes, with the highest emitting species *Shorea pilosa* emitting CH_3Br and CH_3Cl fluxes of 2.7 $\pm$ 0.6 and 65 $\pm$ 17 ng g^{-1} h^{-1}, respectively. Mean CH_3Br and CH_3Cl emissions for 18 plant species were 0.4 and 19 ng g^{-1} h^{-1}, respectively.

Fluxes of BVOCs from various willow species are well documented, although these studies focus on natural and decorative varieties rather than the commercial varieties used for bioenergy plantations and are commonly based on short-term measurements. Willow is known to be a high isoprene emitter with estimated standard emission rates (see following equation 4.1.1 for calculation) of between 12 and 115 µg $g^{-1}_{dryweight}$ h^{-1} measured using different techniques for common varieties including tea-leaf willow (*Salix phylicifolia*) (see Table 4.1).

Table 4.1: Comparison of literature values for standardised isoprene emission rates from different willow species using different methods of measurement. REA corresponds to Relaxed Eddy Accumulation.

Species	Standard emission rate ($\mu g\ g^{-1}_{dry\ weight}\ h^{-1}$)	Location	Measurement type	Reference
Salix spp.	20	East Midlands, UK	Canopy-scale, PTR-MS	Copeland et al. (2012)
Salix spp.	28	NW Mediterranean	Branch enclosure	Owen and Hewitt (2000)
Salix spp.	54.7	Wisconsin, USA	Leaf, branch, canopy & landscape	Isebrands et al. (1999)
Salix spp.	22.7	West Midlands, UK	Leaf, branch, canopy & landscape	Owen et al. (2003)
Salix alba	41	Tartu, Estonia	Branch enclosure	Niinemets et al. (2010)
Salix alba	37.2	-	-	Karl et al. (2009)
Salix alba	18	Portugal	Branch enclosure, lab conditions	Pio et al. (1993)
Salix babylonica	115	California, USA	-	Miller et al. (1983)
Salix caprea	36	Tartu, Estonia	Leaf cuvette, canopy-scale	Niinemets et al. (2010)
Salix caprea	18.9	-	Branch enclosure	Karl et al. (2009)
Salix caroliniana	12.5	Florida, USA	Air-exchange branch enclosure	Zimmerman (1979)
Salix discolor	90.7	Wisconsin, USA	Leaf, branch, canopy & landscape	Isebrands et al. (1999)
Salix humulis	40.5	Wisconsin, USA	Leaf, branch, canopy & landscape	Isebrands et al. (1999)
Salix nigra	25.2	Greenhouse	Whole plant, air-exchange chamber	Evans et al. (1982)
Salix petiolaris	101.5	Wisconsin, USA	Leaf, branch, canopy & landscape	Isebrands et al. (1999)
Salix phylicifolia	32	Vantaa, Finland	Branch enclosure	Hakola et al. (1998)
Salix subsericea	56.8	Wisconsin, USA	Leaf, branch, canopy & landscape	Isebrands et al. (1999)
Salix viminalis	12	Västergötland, Sweden	Canopy-scale, REA	Olofsson et al. (2005)

As isoprene emission from plants is strongly influenced by light and leaf temperature, an emission is often expressed as a standard emission factor (ϵ) normalised to a standard leaf temperature of 303 K and PAR flux of 1000 μmol m^{-2} s^{-1}, as described by the G95 algorithm (Guenther et al., 1995):

$$\epsilon = \frac{F}{D\,\gamma} \tag{4.1.1}$$

where *D* is foliar density (g$_{dryweight}$ m^{-2}) and γ is a non-dimensional activity adjustment factor to account for the effect of light and temperature:

$$\gamma = C_L\,C_T \tag{4.1.2}$$

The light dependence, C_L, is defined by:

$$C_L = \frac{\alpha\,C_{L1}\,Q}{\sqrt{1\,+\,\alpha^2\,Q^2}} \tag{4.1.3}$$

where α (0.0027) and C_{L1} (1.066) are empirical coefficients and *Q* is PAR flux (μmol m^{-2} s^{-1}). The temperature dependence C_T, is defined by:

$$C_T = exp\,\frac{C_{T1}\,(T - T_s)}{\frac{exp\,(C_{T2}\,(T - T_M)}{R\,T_s\,T}} \tag{4.1.4}$$

where *T* is leaf temperature (K), T_s is leaf temperature at standard conditions (303 K), *R* is the universal gas constant (8.314 J K^{-1} mol^{-1}), and C_{T1} (95000 J mol^{-1}), C_{T2} (230000 J mol^{-1}) and T_M (314 K) are empirical coefficients.

Leaf, branch, canopy and landscape-scale studies involving willow species have also been carried out, with one study in Wisconsin, USA, concluding that willow species were among the highest isoprene emitters out of the 30 different species that were studied (average standard isoprene emission rate of 54 µg g_{dw}^{-1} h^{-1} for four willow species) (Isebrands et al., 1999). In a similar manner, an isoprene emission rate of 22.7 µg g_{dw}^{-1} h^{-1} was calculated for willow species in the West Midlands, UK (Owen et al., 2003).

Using a PTR-MS and eddy correlation technique, Copeland et al. (2012) measured a peak midday isoprene emission rate equivalent to 20 µg g_{dw}^{-1} h^{-1} at the Brattleby fieldsite discussed in this thesis, whilst Olofsson et al. (2005) measured a similar rate of 12 µg g_{dw}^{-1} h^{-1} in Västergötland, Sweden. As these were canopy-averaged emissions factors which included leaves in the shade as well as those in direct sunlight, the standard emission factors calculated were lower than those calculated in individual branch or leaf-level experiments.

A whole host of leaf cuvette measurements made at different canopy locations in Tartu, Estonia,

were collated in a model in order to obtain whole canopy isoprene emission rates (Niinemets et al., 2010). This study found an isoprene emission rate of 36 μg g_{dw}^{-1} h^{-1} for *Salix caprea* and of 41 μg g_{dw}^{-1} h^{-1} for *Salix alba*.

A small emission potential for monoterpenes from willow of 0.33 μg g_{dw}^{-1} h^{-1} was calculated from measurements made in Vantaa, Finland (Hakola et al., 1998, 1999). These emissions occur in spring during the early stages of leaf development and bud break before summer begins and the mature leaves start to intensively produce isoprene (Kesselmeier and Staudt, 1999). A monoterpene emission rate of 1.00 μg g_{dw}^{-1} h^{-1} was measured for willow species in the West Midlands, UK (Guenther et al., 2000; Owen et al., 2003). In the East Midlands, Copeland et al. (2012) measured small quantities of the monoterpenes α-pinene and limonene using a GC-MS technique. An emission potential of 1.5 μg g_{dw}^{-1} h^{-1} for oxygenated VOCs has been assigned to all boreal vegetation including willow species (Guenther et al., 1995; Simpson et al., 1999).

Biotrophic fungal infection in willow leaves is known to affect VOC emissions, reducing isoprene emissions to a third of emissions from uninfected leaves (Toome et al., 2010). Total monoterpene emissions did not change in infected plants, although infection increased the amount of the stress-signalling compound (Z)-β-ocimene. This compound was also identified during branch enclosures of willow species in the Mediterranean, although no connection was made with fungal infection (Owen et al., 2001).

Investigations into CH_3X fluxes from woodland soils have been carried out previously, but no data is known to exist on CH_3X fluxes from the vegetation, i.e. the willow trees themselves. The literature on BVOC fluxes from willow species is fairly extensive, although previous studies have focussed on natural species rather than commercially grown varieties. Willow is a known emitter of high quantities of isoprene as well as small amounts of monoterpenes and oygenated VOCs.

Objectives of the work described in this chapter:

- Characterisation of CH_3X and BVOC fluxes in SRC willow in the East Midlands, England and in Perthshire and Fife, Scotland
- Quantification of seasonal, diurnal and temporal variations in CH_3X and BVOC fluxes within SRC willow plantations
- Identification of possible drivers of variation in CH_3X and BVOC fluxes from SRC willow
- Comparison of CH_3X and BVOC fluxes between different SRC willow in Scotland and England

4.2 Brattleby

4.2.1 Site description

Measurements were conducted at the Brattleby fieldsite in Lincolnshire, as described in Section 2.7.1. A total of ten sampling points were used within the SRC willow field, as shown in Figure 4.1. Sampling sites were chosen across one side of the field at the edge of the field for ease of access.



Figure 4.1: Location of the sampling points within the SRC willow field at Brattleby.

December 2010 saw extremely cold conditions at the fieldsite with the temperature staying below 0 °Cfor weeks and dropping as low as -15 °C. However, as a result of hardening, dormant shoots of willow can tolerate winter temperatures as low as -85 °C(Von Fircks, 1994). Fertilisation studies have shown that nitrogen supply could delay cold acclimation and make the trees more sensitive to frost (Von Fircks, 1994). A study in an Estonian bioenergy willow plantation found dieback to be related to a synergistic effect of frost and bacterial infection, possibly aggravated by fertilisation (**?**). However no fertiliser was applied to the SRC willow at the Brattleby fieldsite and there was no noticeable effect of frost on the timing of growth stages the following year and the development of buds, branches and leaves.

Drought was declared in the area in summer 2011 and spring 2012 followed by flooding in July 2012. One study found that drought resistance of willow was negatively related to maximum growth yields, most likely due to resources being diverted away from leaf production to the production of denser wood (Wikberg and Ögren, 2004). However, the level of drought stress

that willow plants could tolerate varied considerably between different clones. The drought resistance of different clones was shown to affect their growth, even under favourable conditions, suggesting a resource trade-off of investment in wood density and root growth against growth and water use.

Drought occurred during first year of growth of the coppiced SRC willow. This may have affected the growth rate and total biomass reached. However there is not enough data to confirm whether this occurred at this site as measurements were taken at different stages of the coppicing cycle.

4.2.2 Outline of CH_3X flux measurements

A total of 155 measurements were made during 19 site visits between April 2010 and June 2012. These measurements were made almost every month in order to capture seasonal flux variability. Flux measurements were carried out as described in Section 2.2.1.

Firstly, the seasonal CH_3X flux trends during each sampling year are examined. Variation between years during the sampling period is discussed. Time series of seasonal net CH_3X fluxes for the years 2010, 2011 and 2012 and the respective PAR, ambient and chamber air temperature, soil temperature and soil water content observations at the time of measurement for each sampling site are then illustrated, incorporating seasonal, temporal and annual variation in fluxes.

Statistical analysis of the CH_3X fluxes is then presented. CH_3X fluxes are tested for significant correlations with monitored environmental parameters in order to investigate possible drivers of emissions. Correlations between CH_3Br and CH_3Cl fluxes were tested for significance as was the dependence of variation in CH_3X flux on season and sampling site.

Finally, the behaviour of CH_3X fluxes throughout the day at different times of the year is examined in separate sub-diurnal studies conducted between June and November 2011 (Figures 4.14 and 4.15).

4.2.3 CH_3X flux trends

CH_3Br

CH_3Br fluxes were characterised through a total of 155 measurements made during 19 site visits beginning in April 2010 and ending in June 2012. Seasonal, temporal and annual variations in CH_3Br fluxes are investigated. Fluxes are examined by year and then collectively across all 3 calendar years. Figure 4.2 presents the CH_3Br fluxes at all ten sampling points on each sampling occasion and the mean of those values across 2010 to 2012. Figures 4.3 to 4.7 then

illustrate the seasonal CH_3Br fluxes for all 10 sampling sites with respective PAR, ambient and chamber air temperature, soil temperature and soil water content observations.

In Figure 4.2, a seasonal trend is evident, with higher fluxes during the summer months and low to zero fluxes during the winter. Generally, CH_3Br fluxes were low (< 3.9 ng g^{-1} h^{-1}) with outlying fluxes of 7.9, 8.9 and 34 ng g^{-1} h^{-1}. Fluxes measured in 2011 were generally higher than those measured in 2010 and 2012. This may be due to the growth stage of the willow trees. The willow trees were coppiced in winter 2010 so measurements taken in 2011 were from younger trees compared to measurements taken from trees with three year's growth in 2010 and at least a year's growth 2012.

Zero fluxes were measured in April 2010. During summer 2010 (May to September), fluxes of between 0 and 2.1 ng g^{-1} h^{-1} were measured. Zero fluxes were measured during winter 2010/2011 (November 2010, January and April 2011). Fluxes of between zero and 7.9ng g^{-1} h^{-1} were measured during June to August 2011. Fluxes of between zero and 3.9 ng g^{-1} h^{-1} were measured in October 2011, with one very high flux of 34 ng g^{-1} h^{-1}. Zero fluxes were measured in November 2011 and March 2012. Zero fluxes were measured during April 2012 with the exception of one high flux of 8.9 ng g^{-1} h^{-1}. Fluxes of between zero and 1.1 ng g^{-1} h^{-1} were measured in May and June 2012. Mean summer fluxes varied between zero and 4.3 ng g^{-1} h^{-1} during 2010, 2011 and 2012.

Time series of CH_3Br fluxes from each individual site between April 2010 and June 2012 together with the concurrent PAR, ambient and chamber air temperature, soil temperature and soil water content observations are illustrated in Figures 4.3 to 4.7. These figures show both the seasonal trend in fluxes from individual sampling sites and the variation in fluxes between calendar years. The statistical significance of correlations between CH_3Br fluxes and environmental variables is described in Section 4.2.4.

In 2010, 43 measurements were made in total over the ten sampling sites (Table 4.2a). The maximum flux measured was 2.1 ng g^{-1} h^{-1} from site 2. Mean fluxes per site ranged from 0 to 0.4 ng g^{-1} h^{-1}, excluding results from sites 9 and 10 as they were only sampled once. A mean flux of 0.2 ng g^{-1} h^{-1} was calculated from fluxes measured at all sites during 2010.

72 measurements were made in total in 2011 (Table 4.2b). Fluxes were slightly higher than those measured in 2010. The maximum flux recorded was 34 ng g^{-1} h^{-1} which was again measured site 2. The range of mean fluxes per site ranged from 0 to 4.7 ng g^{-1} h^{-1}. A mean flux of 0.9 ng g^{-1} h^{-1} was calculated from fluxes measured at all sites during 2011. Seven of the ten highest maximum fluxes measured throughout the sampling period were measured in 2011 from sites 1 - 3, 5 and 8 - 10.

Another 40 measurements were made in 2012, with fluxes similar to those measured in 2010 and 2011 (Table 4.2c). The maximum flux measured was 8.9 ng g^{-1} h^{-1} from site 7. Mean

fluxes per site ranged from 0 to 2.2 ng g^{-1} h^{-1}. A mean flux of 0.3 ng g^{-1} h^{-1} was calculated from fluxes measured at all sites during 2012.

Mean CH_3Br fluxes between 0.1 and 2.3 ng g^{-1} h^{-1} were measured from sites 1 to 10 (Table 4.2d). Higher maximum CH_3Br fluxes were measured at sites 2, 7 and 10 (7.9 to 34 ng g^{-1} h^{-1}) and lower maximum fluxes at other sites (between 0.9 and 3.9 ng g^{-1} h^{-1}).

The highest maximum flux of 34 ng g^{-1} h^{-1} was measured at site 2 in 2011. The minimum flux recorded at all sites was zero. A mean emission of 0.6 ng g^{-1} h^{-1} was calculated from fluxes measured at all sites during the measurement period. A median value of zero was calculated for almost every site and for measurements at all sites combined.

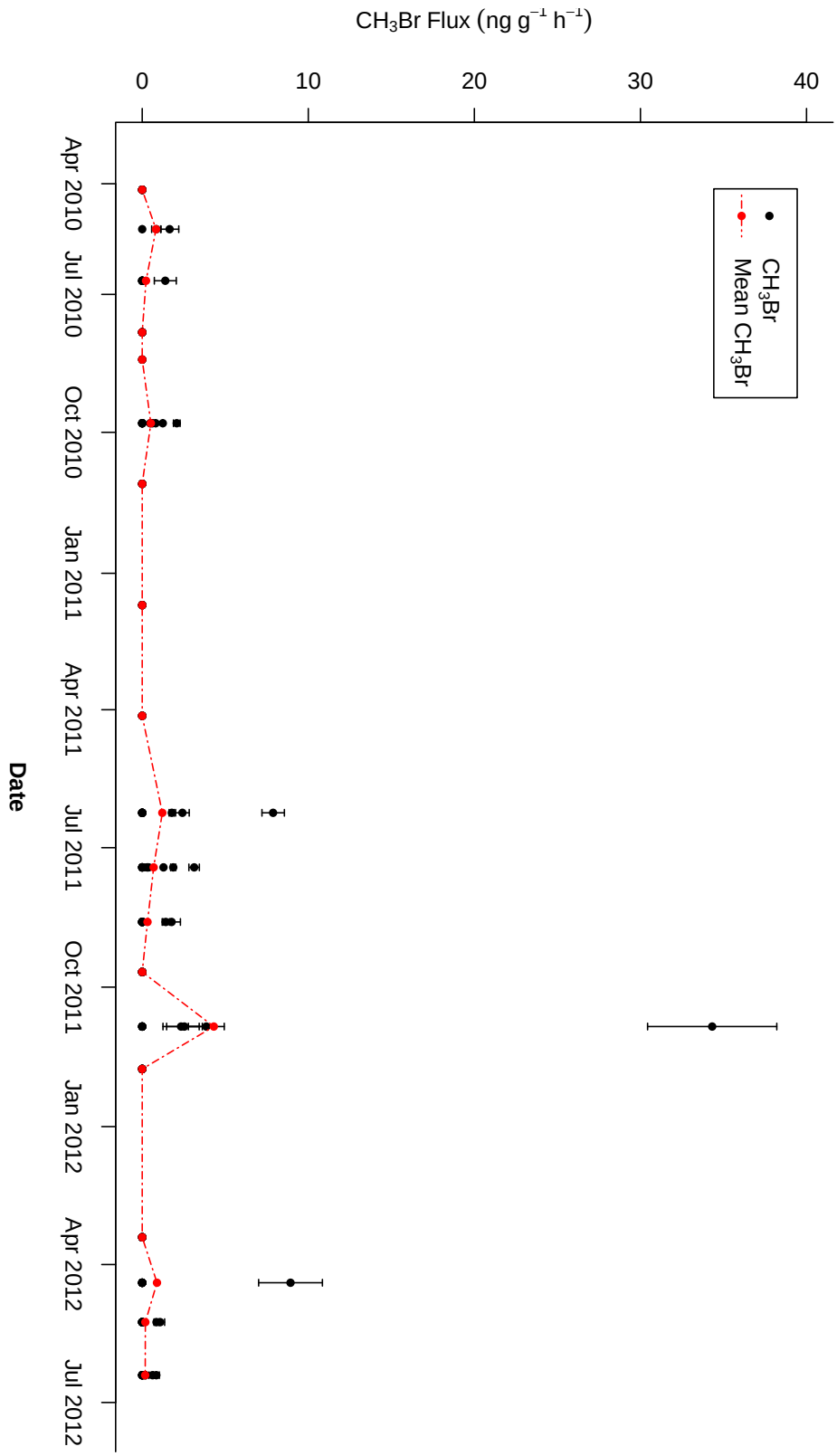


Figure 4.2: CH_3Br fluxes from willow at the Brattleby fieldsite at all ten sampling points and the mean of those values on each sampling occasion between 2010 and 2012. Error bars on fluxes incorporate analytical and sampling uncertainties (as described in Section 2.6.1).

Table 4.2: Mean, median, minimum and maximum net CH_3Br fluxes from SRC willow at Brattleby during (a) 2010, (b) 2011, (c) 2012 and (d) 2010 - 2012. All flux values are in $ng\,g^{-1}\,h^{-1}$. The final column in each table gives the number of measurements made. The last row summarises all fluxes from all sites.

(a) CH_3Br flux ($ng\,g^{-1}\,h^{-1}$) - 2010

Site	Mean	Median	Min	Max	Number
W1	0.20	0.00	0.00	1.39	7
W2	0.42	0.00	0.00	2.08	5
W3	0.00	0.00	0.00	0.00	6
W4	0.24	0.00	0.00	1.65	7
W5	0.25	0.00	0.00	1.24	5
W6	0.22	0.00	0.00	0.85	6
W7	0.27	0.00	0.00	0.81	3
W8	0.00	0.00	0.00	0.00	2
W9	0.62	0.62	0.62	0.62	1
W10	0.00	0.00	0.00	0.00	1
All	0.21	0.00	0.00	2.08	43

(b) CH_3Br flux ($ng\,g^{-1}\,h^{-1}$) - 2011

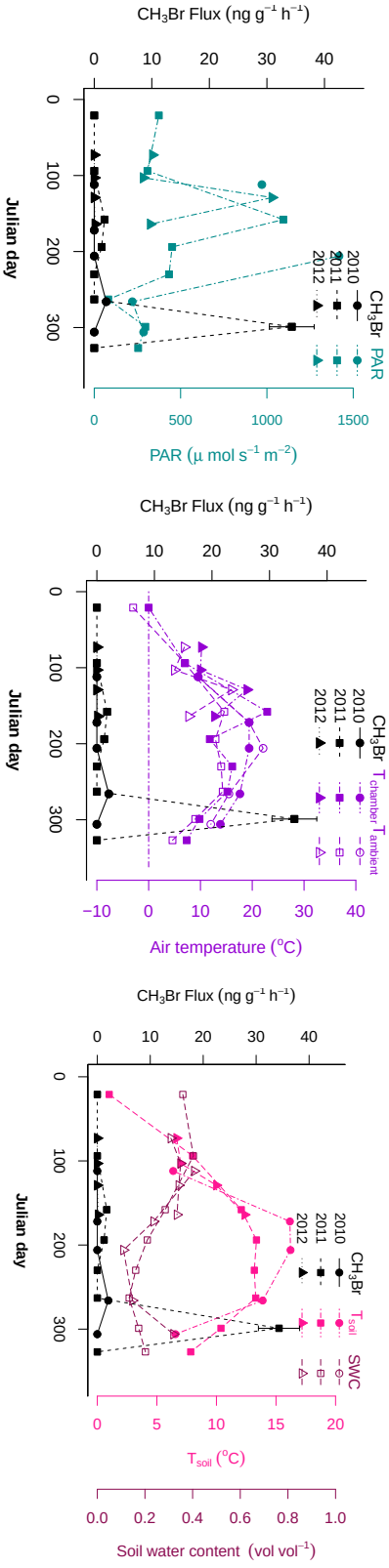
Site	Mean	Median	Min	Max	Number
W1	0.83	0.00	0.00	2.42	8
W2	4.67	0.00	0.00	34.3	8
W3	0.39	0.00	0.00	3.13	8
W4	0.00	0.00	0.00	0.00	7
W5	0.48	0.00	0.00	3.86	8
W6	0.00	0.00	0.00	0.00	8
W7	0.05	0.00	0.00	0.30	6
W8	0.20	0.00	0.00	1.42	7
W9	0.30	0.00	0.00	1.77	6
W10	1.80	0.18	0.00	7.88	6
All	0.91	0.00	0.00	34.3	72

(c) CH_3Br flux ($ng\,g^{-1}\,h^{-1}$) - 2012

Site	Mean	Median	Min	Max	Number
W1	0.21	0.00	0.00	0.85	4
W2	0.04	0.00	0.00	0.16	4
W3	0.00	0.00	0.00	0.00	4
W4	0.32	0.10	0.00	1.08	4
W5	0.00	0.00	0.00	0.00	4
W6	0.37	0.31	0.00	0.86	4
W7	2.23	0.00	0.00	8.93	4
W8	0.00	0.00	0.00	0.00	4
W9	0.00	0.00	0.00	0.00	4
W10	0.00	0.00	0.00	0.00	4
All	0.32	0.00	0.00	8.93	40

(d) CH_3Br flux ($ng\,g^{-1}\,h^{-1}$) - 2010 to 2012

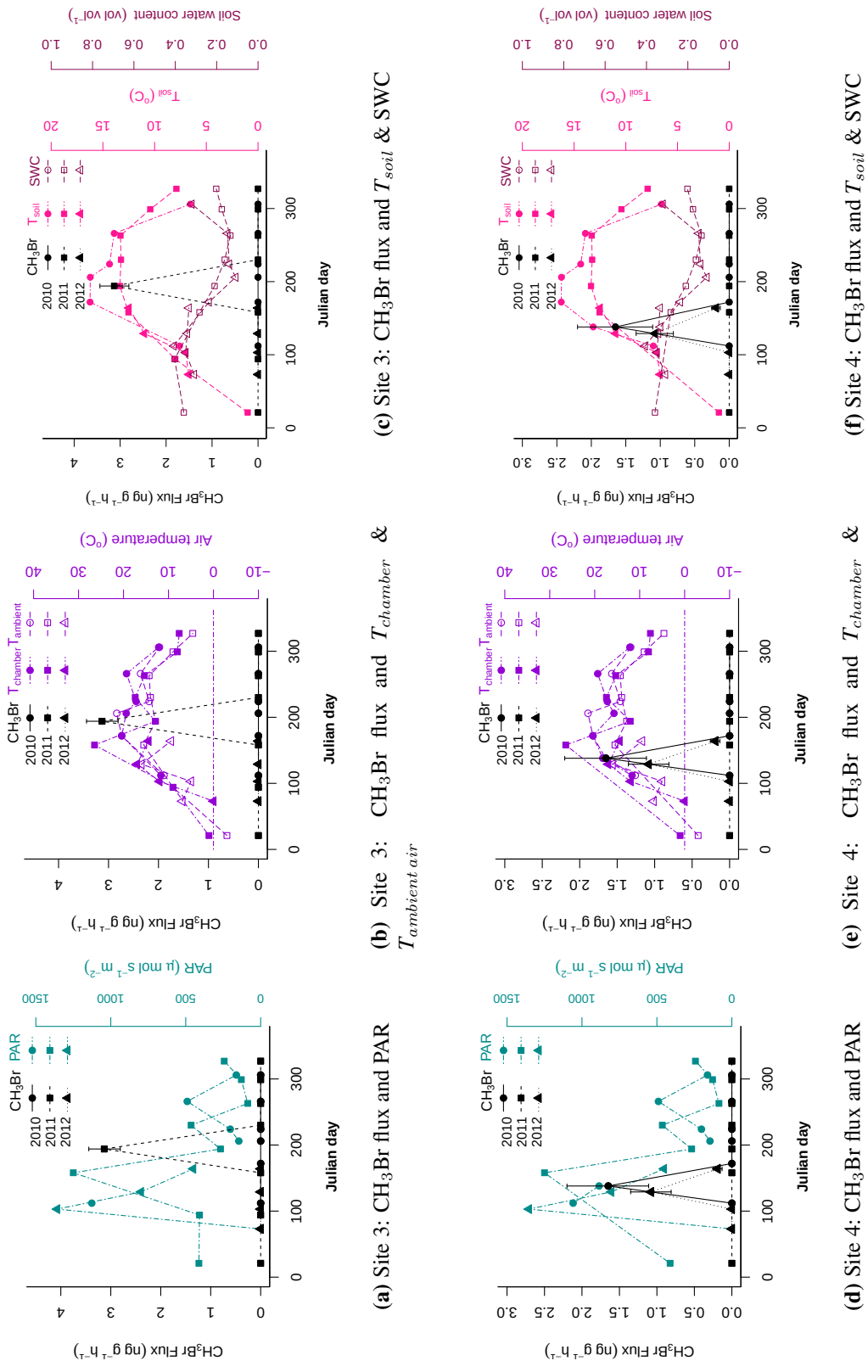
Site	Mean	Median	Min	Max	Number
W1	0.47	0.00	0.00	2.42	19
W2	2.33	0.00	0.00	34.3	17
W3	0.17	0.00	0.00	3.13	18
W4	0.16	0.00	0.00	1.65	18
W5	0.30	0.00	0.00	3.86	17
W6	0.16	0.00	0.00	0.86	18
W7	0.77	0.00	0.00	8.93	13
W8	0.11	0.00	0.00	1.42	13
W9	0.22	0.00	0.00	1.77	11
W10	0.98	0.00	0.00	7.88	11
All	0.56	0.00	0.00	34.3	155



(a) Site 1: CH_3Br flux and PAR **(b)** Site 1: CH_3Br flux and $T_{chamber}$ & $T_{ambient\,air}$ **(c)** Site 1: CH_3Br flux and T_{soil} & SWC

(d) Site 2: CH_3Br flux and PAR **(e)** Site 2: CH_3Br flux and $T_{chamber}$ & $T_{ambient\,air}$ **(f)** Site 2: CH_3Br flux and T_{soil} & SWC

Figure 4.3: Comparison of net CH_3Br fluxes from willow with PAR, chamber and ambient air temperature, soil temperature and soil water content (SWC) for 2010, 2011 and 2012 for sites 1 and 2. Note different y-axis scales for CH_3Br. Error bars on fluxes incorporate analytical and sampling uncertainties.



(a) Site 3: CH_3Br flux and PAR

(b) Site 3: CH_3Br flux and $T_{chamber}$ & $T_{ambient\ air}$

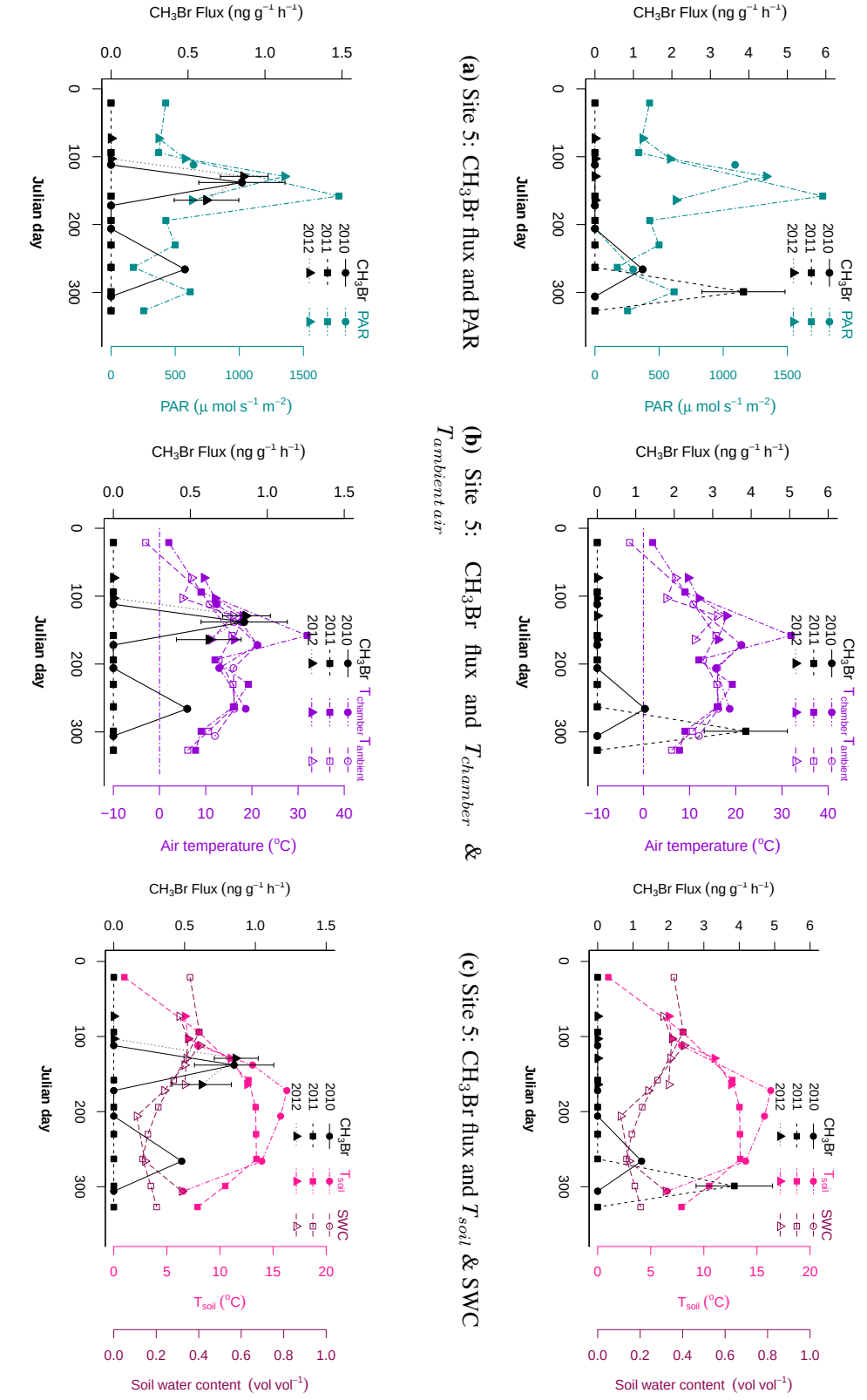
(c) Site 3: CH_3Br flux and T_{soil} & SWC

(d) Site 4: CH_3Br flux and PAR

(e) Site 4: CH_3Br flux and $T_{chamber}$ & $T_{ambient\ air}$

(f) Site 4: CH_3Br flux and T_{soil} & SWC

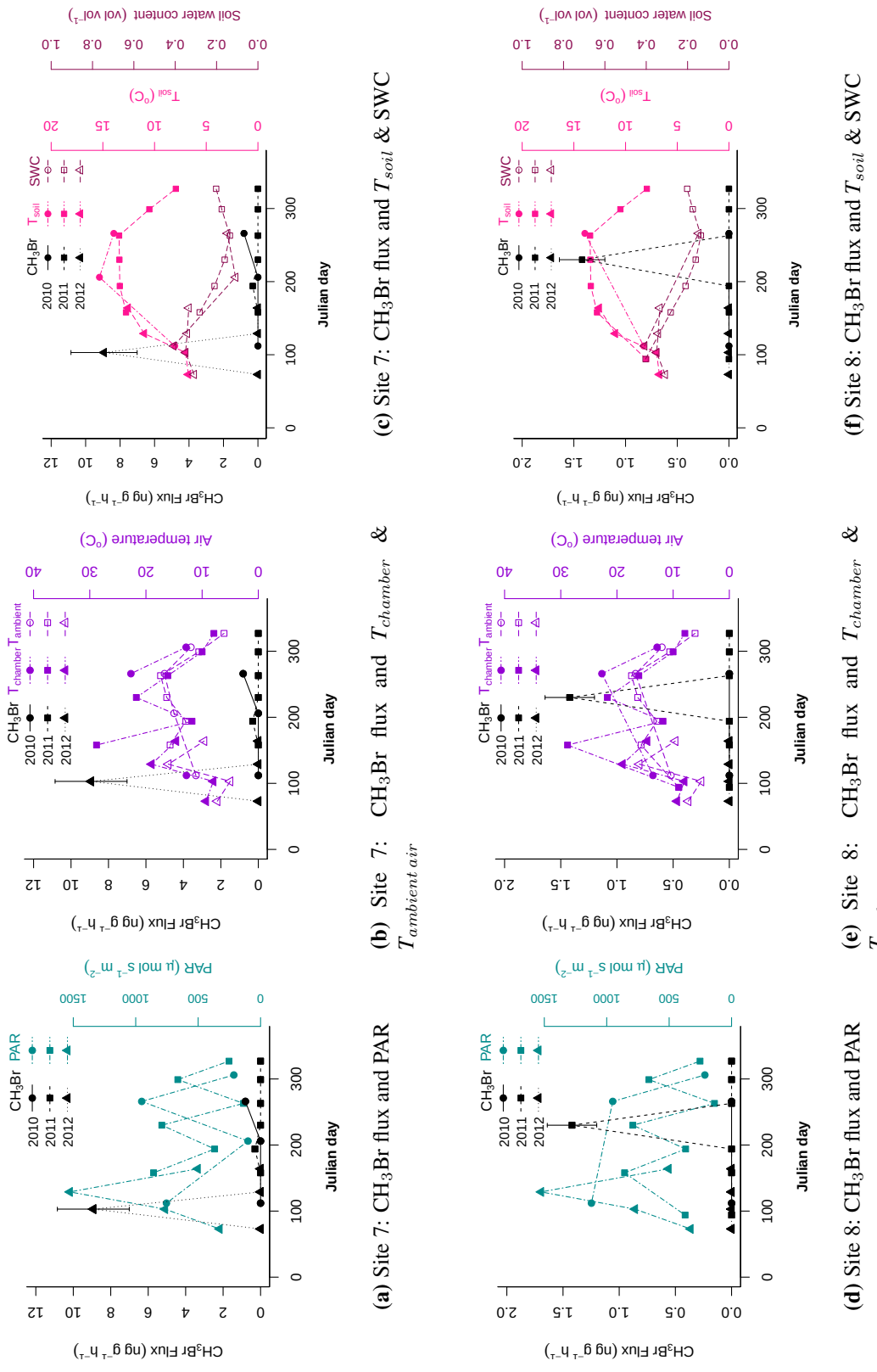
Figure 4.4: Comparison of net CH_3Br fluxes from willow with PAR, chamber and ambient air temperature, soil temperature and soil water content (SWC) for 2010, 2011 and 2012 for sites 3 and 4. Note different y-axis scales for CH_3Br. Error bars on fluxes incorporate analytical and sampling uncertainties.



(a) Site 5: CH_3Br flux and PAR **(b)** Site 5: CH_3Br flux and $T_{chamber}$ & $T_{ambient\,air}$ **(c)** Site 5: CH_3Br flux and T_{soil} & SWC

(d) Site 6: CH_3Br flux and PAR **(e)** Site 6: CH_3Br flux and $T_{chamber}$ & $T_{ambient\,air}$ **(f)** Site 6: CH_3Br flux and T_{soil} & SWC

Figure 4.5: Comparison of net CH_3Br fluxes from willow with PAR, chamber and ambient air temperature, soil temperature and soil water content (SWC) for 2010, 2011 and 2012 for sites 5 and 6. Note different y-axis scales for CH_3Br. Error bars on fluxes incorporate analytical and sampling uncertainties.



(a) Site 7: CH_3Br flux and PAR

(b) Site 7: CH_3Br flux and $T_{chamber}$ & $T_{ambient\ air}$

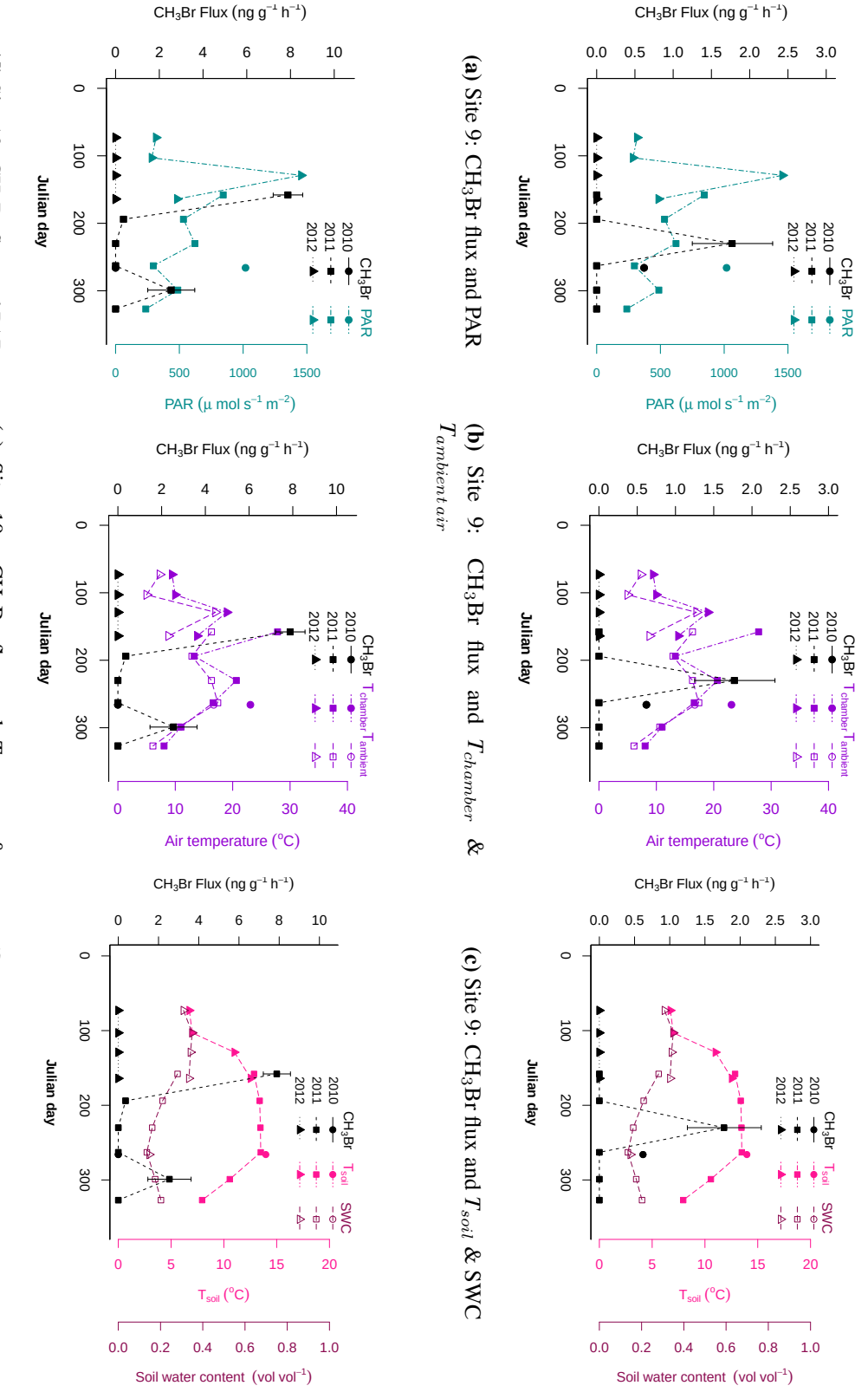
(c) Site 7: CH_3Br flux and T_{soil} & SWC

(d) Site 8: CH_3Br flux and PAR

(e) Site 8: CH_3Br flux and $T_{chamber}$ & $T_{ambient\ air}$

(f) Site 8: CH_3Br flux and T_{soil} & SWC

Figure 4.6: Comparison of net CH_3Br fluxes from willow with PAR, chamber and ambient air temperature, soil temperature and soil water content (SWC) for 2010, 2011 and 2012 for sites 7 and 8. Note different y-axis scales for CH_3Br. Error bars on fluxes incorporate analytical and sampling uncertainties.



(a) Site 9: CH_3Br flux and PAR

(b) Site 9: CH_3Br flux and $T_{chamber}$ & $T_{ambient\,air}$

(c) Site 9: CH_3Br flux and T_{soil} & SWC

(d) Site 10: CH_3Br flux and PAR

(e) Site 10: CH_3Br flux and $T_{chamber}$ & $T_{ambient\,air}$

(f) Site 10: CH_3Br flux and T_{soil} & SWC

Figure 4.7: Comparison of net CH_3Br fluxes from willow with PAR, chamber and ambient air temperature, soil temperature and soil water content (SWC) for 2010, 2011 and 2012 for sites 9 and 10. Note different y-axis scales for CH_3Br. Error bars on fluxes incorporate analytical and sampling uncertainties.

CH_3Cl

CH_3Cl fluxes were characterised through a total of 154 measurements made during 19 site visits beginning in April 2010 and ending in June 2012. Seasonal, temporal and annual variations in CH_3Cl fluxes are investigated. Fluxes are examined by year and then collectively across all 3 calendar years. Figure 4.8 presents the CH_3Cl fluxes at all ten sampling points on each sampling occasion and the mean of those values across 2010 to 2012. Figures 4.9 to 4.13 then illustrate the seasonal CH_3Cl fluxes for all 10 sampling sites with respective PAR, ambient and chamber air temperature, soil temperature and soil water content observations.

A seasonal trend is evident in Figure 4.8, with higher fluxes during the summer months and zero fluxes during the winter. Generally, CH_3Cl fluxes were low (< 50 ng g^{-1} h^{-1}) with two outlying peak fluxes of 100 and 190 ng g^{-1} h^{-1}. Fluxes measured in 2011 were much higher than those measured in 2010 and 2012. This is the same pattern as for the CH_3Br fluxes and is again likely to be associated with the growth stage of the willow trees. The willow trees were coppiced in winter 2010 so measurements taken in 2011 were from younger trees compared to measurements taken from trees with three year's growth in 2010 and at least a year's growth 2012.

Zero fluxes were measured between April and July 2010. One non-zero flux of 14 ng g^{-1} h^{-1} was measured in August 2010 and fluxes of 2.7 and 7.0 ng g^{-1} h^{-1} were measured in September. Zero fluxes were measured during winter 2010/2011 (November 2010 and April 2011).

High fluxes were measured during the summer of 2011. In June, fluxes of between zero and 46 ng g^{-1} h^{-1} were measured. Lower fluxes of between zero and 6.8 ng g^{-1} h^{-1} were measured in July. Fluxes then increased to between zero and 190 ng g^{-1} h^{-1} in August. Zero fluxes were measured in September, with the exception of one site where a flux of 35 ng g^{-1} h^{-1} was measured.

Zero fluxes were measured during winter 2011/2012 (October 2011 to April 2012). Only one non-zero flux of 20 ng g^{-1} h^{-1} was measured in May 2012 and two non-zero fluxes of 13 and 15 ng g^{-1} h^{-1} were measured in June 2012. During 2010, 2011 and 2012, mean summer fluxes varied between zero and 48 ng g^{-1} h^{-1}, which is over ten times the highest mean CH_3Br flux measured.

Time series of CH_3Cl fluxes from each individual site between April 2010 and June 2012 together with the concurrent PAR, ambient and chamber air temperature, soil temperature and soil water content observations are illustrated in Figures 4.9 to 4.13 . These figures show both the seasonal trend in fluxes from individual sampling sites and the variation in fluxes between calendar years. The statistical significance of correlations between CH_3Cl fluxes and environmental variables is described in Section 4.2.4.

In 2010, 43 measurements were made in total over the ten sampling sites (Table 4.3a). The maximum flux measured was 14 ng g^{-1} h^{-1} from site 3. Mean fluxes per site ranged from 0 to 2.3 ng g^{-1} h^{-1}, excluding results from sites 9 and 10 as they were only sampled once. A mean flux of 0.6 ng g^{-1} h^{-1} was calculated from fluxes measured at all sites during 2010.

A total of 71 measurements were made in 2011 (Table 4.3b). Fluxes were generally much higher than in 2010. The maximum flux measured was 100 ng g^{-1} h^{-1} from site 9. The range of mean fluxes per site ranged from 0.6 to 36 ng g^{-1} h^{-1}. A mean flux of 9.6 ng g^{-1} h^{-1} was calculated from fluxes measured at all sites during 2011, over 15 times higher than in 2010. Nine out of the ten highest maximum fluxes measured throughout the sampling period were measured in 2011 from sites 2 - 10.

Another 40 measurements were made in 2012, with only 4 non-zero fluxes which were measured at sites 1 and 9 (Table 4.3c). The maximum flux measured was 20 ng g^{-1} h^{-1} from site 9 in May, with the next highest flux of 15 ng g^{-1} h^{-1} measured from the same site in June. A CH_3Cl flux of 13 ng g^{-1} h^{-1} was measured at site 1 in June, the highest flux measured at site 1.

Mean CH_3Cl fluxes between 0.9 and 17 ng g^{-1} h^{-1} were measured from sites 1 to 10 during 2010 to 2012 (Table 4.3d). Higher maximum CH_3Cl fluxes were measured at sites 3, 6, 7 and 9 (41 to 190 ng g^{-1} h^{-1}) and lower maximum fluxes at other sites (between 13 and 34 ng g^{-1} h^{-1}).

The highest maximum flux of 190 ng g^{-1} h^{-1} was measured at site 7 in 2011. The minimum flux recorded at all sites was zero. A mean emission of 4.9 ng g^{-1} h^{-1} was calculated from fluxes measured at all sites during the measurement period. A median value of zero was calculated for almost every site and for measurements at all sites combined.

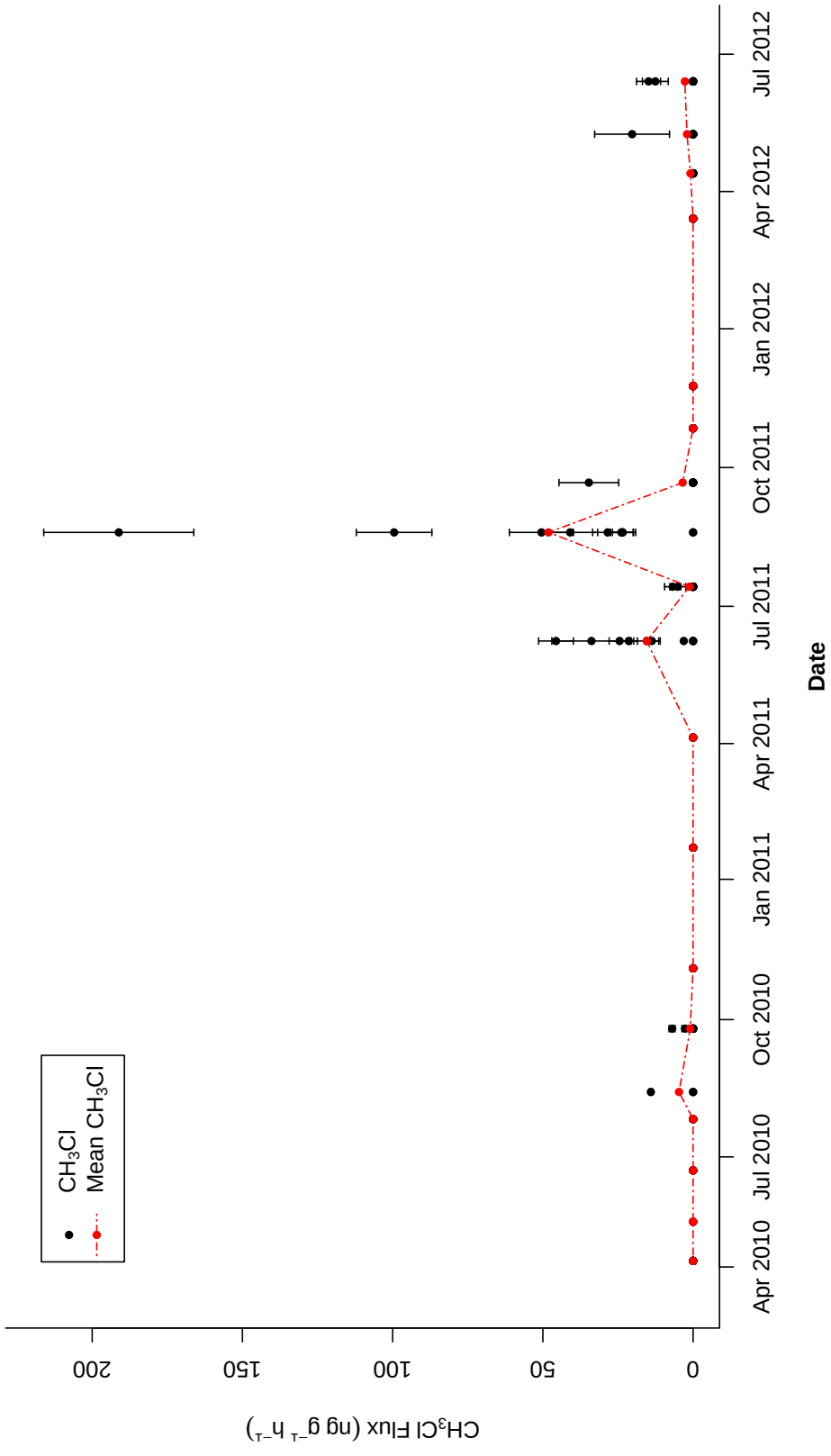


Figure 4.8: CH_3Cl fluxes from willow at the Brattleby fieldsite at all ten sampling points and the mean of those values on each sampling occasion between 2010 and 2012. Error bars on fluxes incorporate analytical and sampling uncertainties (as described in Section 2.6.1).

Table 4.3: Mean, median, minimum and maximum net CH_3Cl fluxes from SRC willow at Brattleby during (a) 2010, (b) 2011, (c) 2012 and (d) 2010 - 2012. All flux values are in $ng\,g^{-1}\,h^{-1}$. The final column in each table gives the number of measurements made. The last row summarises all fluxes from all sites.

(a) CH_3Cl flux ($ng\,g^{-1}\,h^{-1}$) - 2010

Site	Mean	Median	Min	Max	Number
W1	0.00	0.00	0.00	0.00	7
W2	0.00	0.00	0.00	0.00	5
W3	2.34	0.00	0.00	14.1	6
W4	0.00	0.00	0.00	0.00	7
W5	0.00	0.00	0.00	0.00	4
W6	1.40	0.00	0.00	6.98	5
W7	0.00	0.00	0.00	0.00	4
W8	0.00	0.00	0.00	0.00	3
W9	2.66	2.66	2.66	2.66	1
W10	0.00	0.00	0.00	0.00	1
All	0.55	0.00	0.00	14.1	43

(b) CH_3Cl flux ($ng\,g^{-1}\,h^{-1}$) - 2011

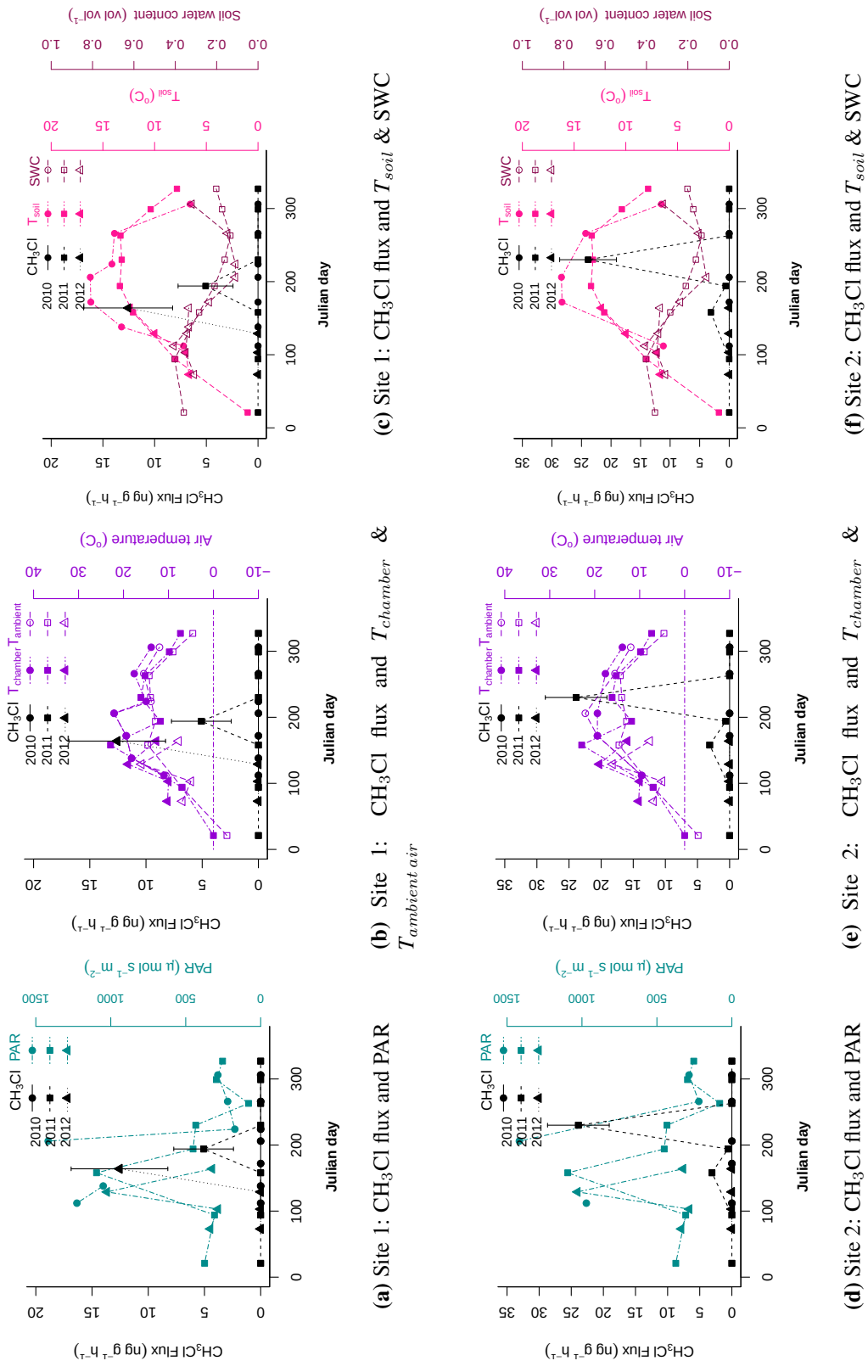
Site	Mean	Median	Min	Max	Number
W1	0.63	0.00	0.00	5.07	8
W2	2.99	0.00	0.00	23.9	8
W3	10.6	0.00	0.00	50.5	8
W4	7.37	3.40	0.00	23.6	6
W5	2.68	0.00	0.00	21.4	8
W6	7.03	0.00	0.00	40.9	8
W7	35.9	0.00	0.00	191	6
W8	8.90	0.00	0.00	33.8	7
W9	24.2	0.00	0.00	99.5	6
W10	3.90	0.00	0.00	23.4	6
All	9.61	0.00	0.00	191	71

(c) CH_3Cl flux ($ng\,g^{-1}\,h^{-1}$) - 2012

Site	Mean	Median	Min	Max	Number
W1	3.14	0.00	0.00	12.6	4
W2	0.00	0.00	0.00	0.00	4
W3	0.00	0.00	0.00	0.00	4
W4	0.00	0.00	0.00	0.00	4
W5	0.00	0.00	0.00	0.00	4
W6	0.00	0.00	0.00	0.00	4
W7	0.00	0.00	0.00	0.00	4
W8	0.00	0.00	0.00	0.00	4
W9	8.78	7.41	0.00	20.3	4
W10	0.00	0.00	0.00	0.00	4
All	1.19	0.00	0.00	20.3	40

(d) CH_3Cl flux ($ng\,g^{-1}\,h^{-1}$) - 2010 to 2012

Site	Mean	Median	Min	Max	Number
W1	0.93	0.00	0.00	12.6	19
W2	1.41	0.00	0.00	23.9	17
W3	5.51	0.00	0.00	50.5	18
W4	2.60	0.00	0.00	23.6	17
W5	1.34	0.00	0.00	21.4	16
W6	3.72	0.00	0.00	40.9	17
W7	15.4	0.00	0.00	191	14
W8	4.45	0.00	0.00	33.8	14
W9	16.6	0.00	0.00	99.5	11
W10	2.13	0.00	0.00	23.4	11
All	4.90	0.00	0.00	191	154



(a) Site 1: CH_3Cl flux and PAR

(b) Site 1: CH_3Cl flux and $T_{chamber}$ & $T_{ambient\ air}$

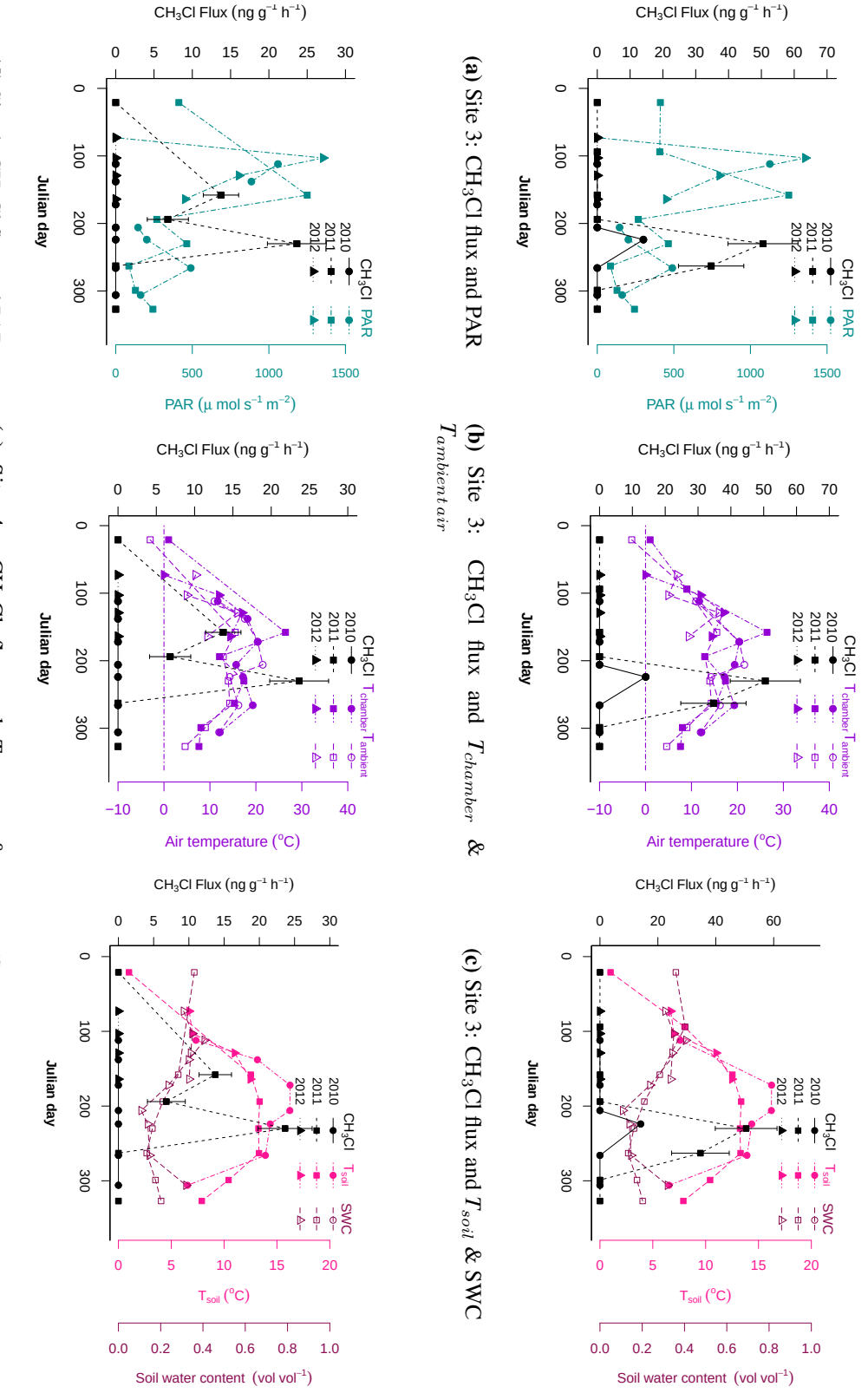
(c) Site 1: CH_3Cl flux and T_{soil} & SWC

(d) Site 2: CH_3Cl flux and PAR

(e) Site 2: CH_3Cl flux and $T_{chamber}$ & $T_{ambient\ air}$

(f) Site 2: CH_3Cl flux and T_{soil} & SWC

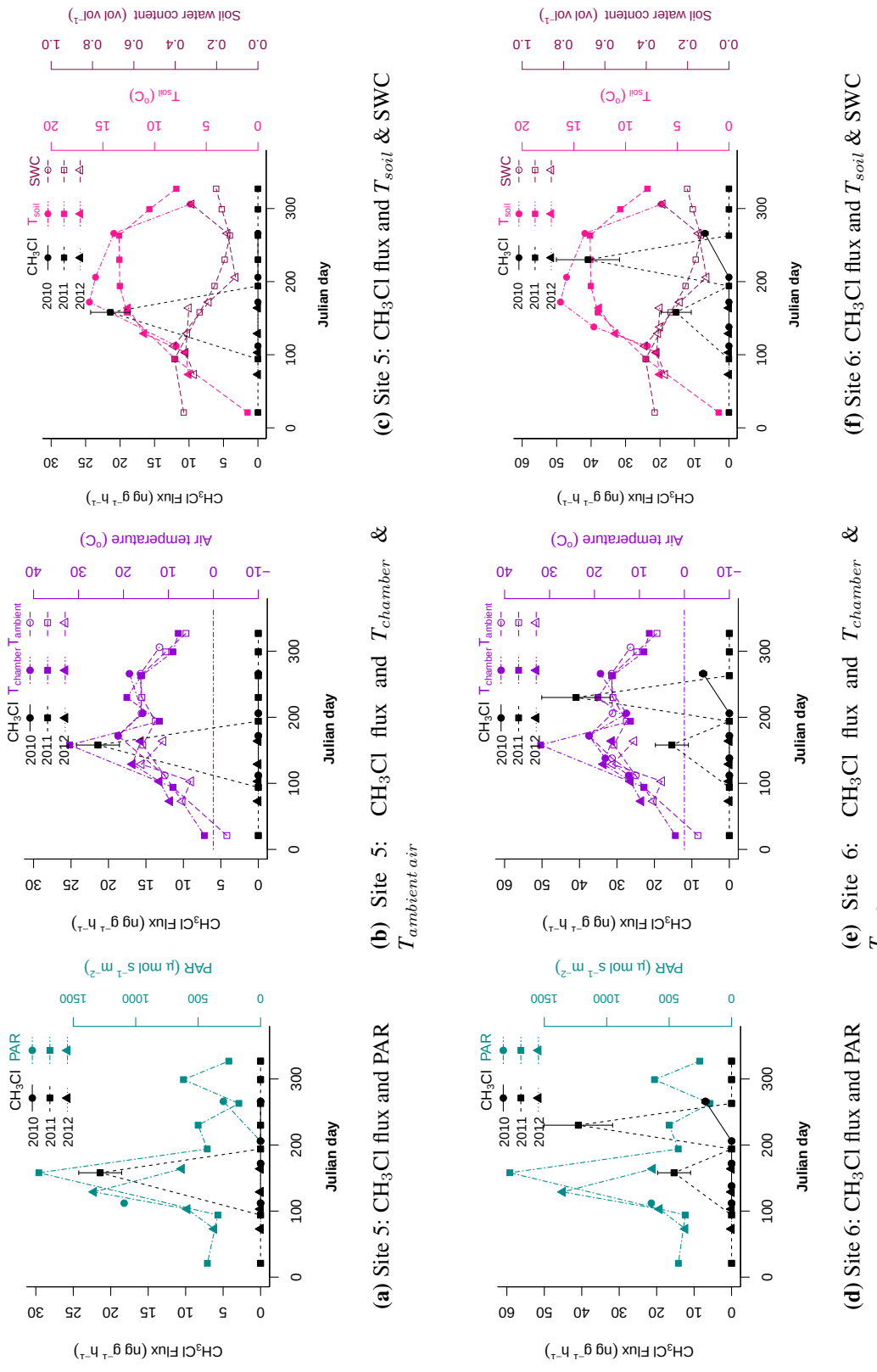
Figure 4.9: Comparison of net CH_3Cl fluxes from willow with PAR, chamber and ambient air temperature, soil temperature and soil water content (SWC) for 2010, 2011 and 2012 for sites 1 and 2. Note different y-axis scales for CH_3Cl. Error bars on fluxes incorporate analytical and sampling uncertainties.



(a) Site 3: CH_3Cl flux and PAR **(b)** Site 3: CH_3Cl flux and $T_{chamber}$ & $T_{ambient\,air}$ **(c)** Site 3: CH_3Cl flux and T_{soil} & SWC

(d) Site 4: CH_3Cl flux and PAR **(e)** Site 4: CH_3Cl flux and $T_{chamber}$ & $T_{ambient\,air}$ **(f)** Site 4: CH_3Cl flux and T_{soil} & SWC

Figure 4.10: Comparison of net CH_3Cl fluxes from willow with PAR, chamber and ambient air temperature, soil temperature and soil water content (SWC) for 2010, 2011 and 2012 for sites 3 and 4. Note different y-axis scales for CH_3Cl. Error bars on fluxes incorporate analytical and sampling uncertainties.



(a) Site 5: CH_3Cl flux and PAR

(b) Site 5: CH_3Cl flux and $T_{chamber}$ & $T_{ambient\ air}$

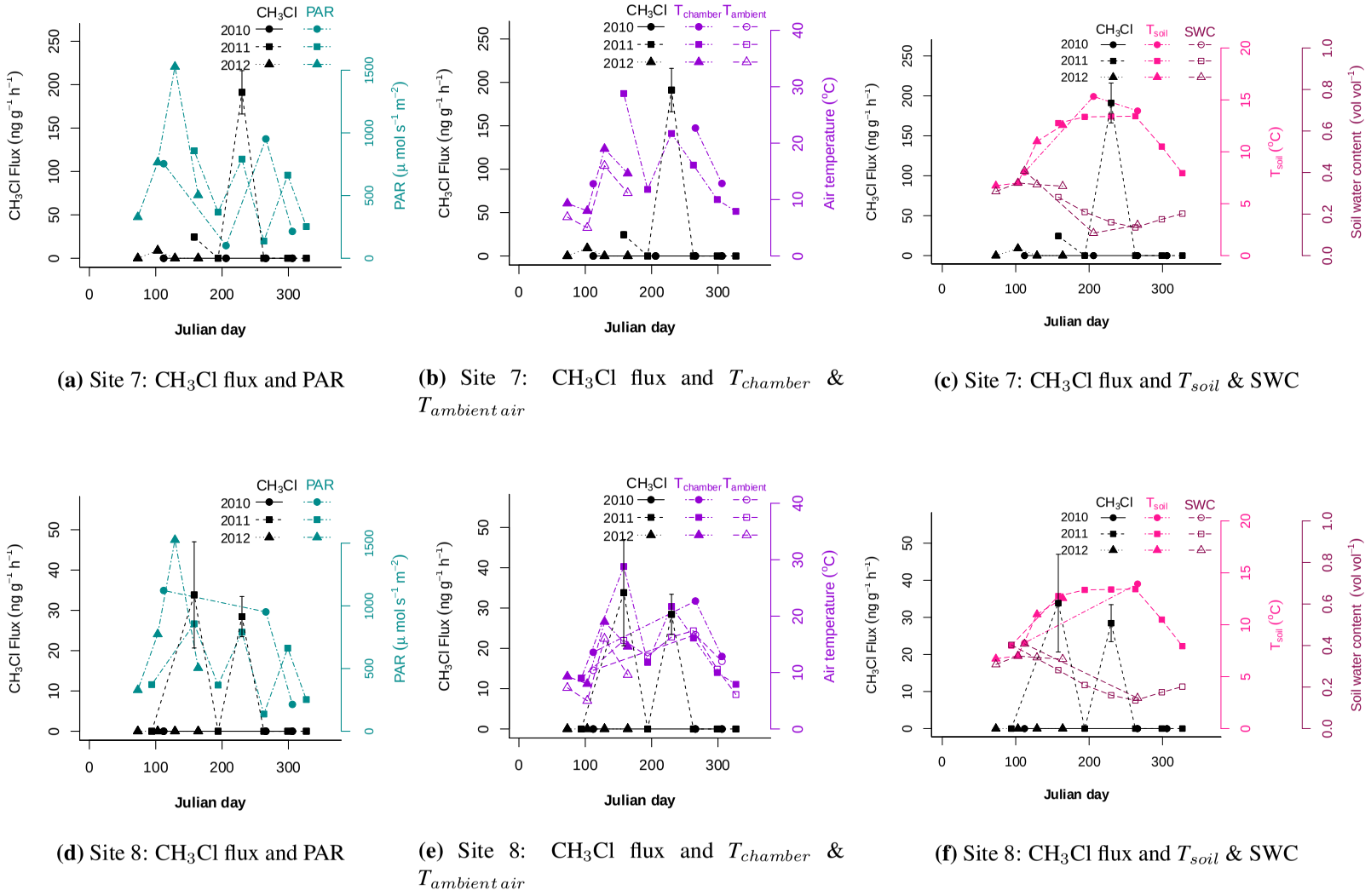
(c) Site 5: CH_3Cl flux and T_{soil} & SWC

(d) Site 6: CH_3Cl flux and PAR

(e) Site 6: CH_3Cl flux and $T_{chamber}$ & $T_{ambient\ air}$

(f) Site 6: CH_3Cl flux and T_{soil} & SWC

Figure 4.11: Comparison of net CH_3Cl fluxes from willow with PAR, chamber and ambient air temperature, soil temperature and soil water content (SWC) for 2010, 2011 and 2012 for sites 5 and 6. Note different y-axis scales for CH_3Cl. Error bars on fluxes incorporate analytical and sampling uncertainties.



(a) Site 7: CH_3Cl flux and PAR

(b) Site 7: CH_3Cl flux and $T_{chamber}$ & $T_{ambient\,air}$

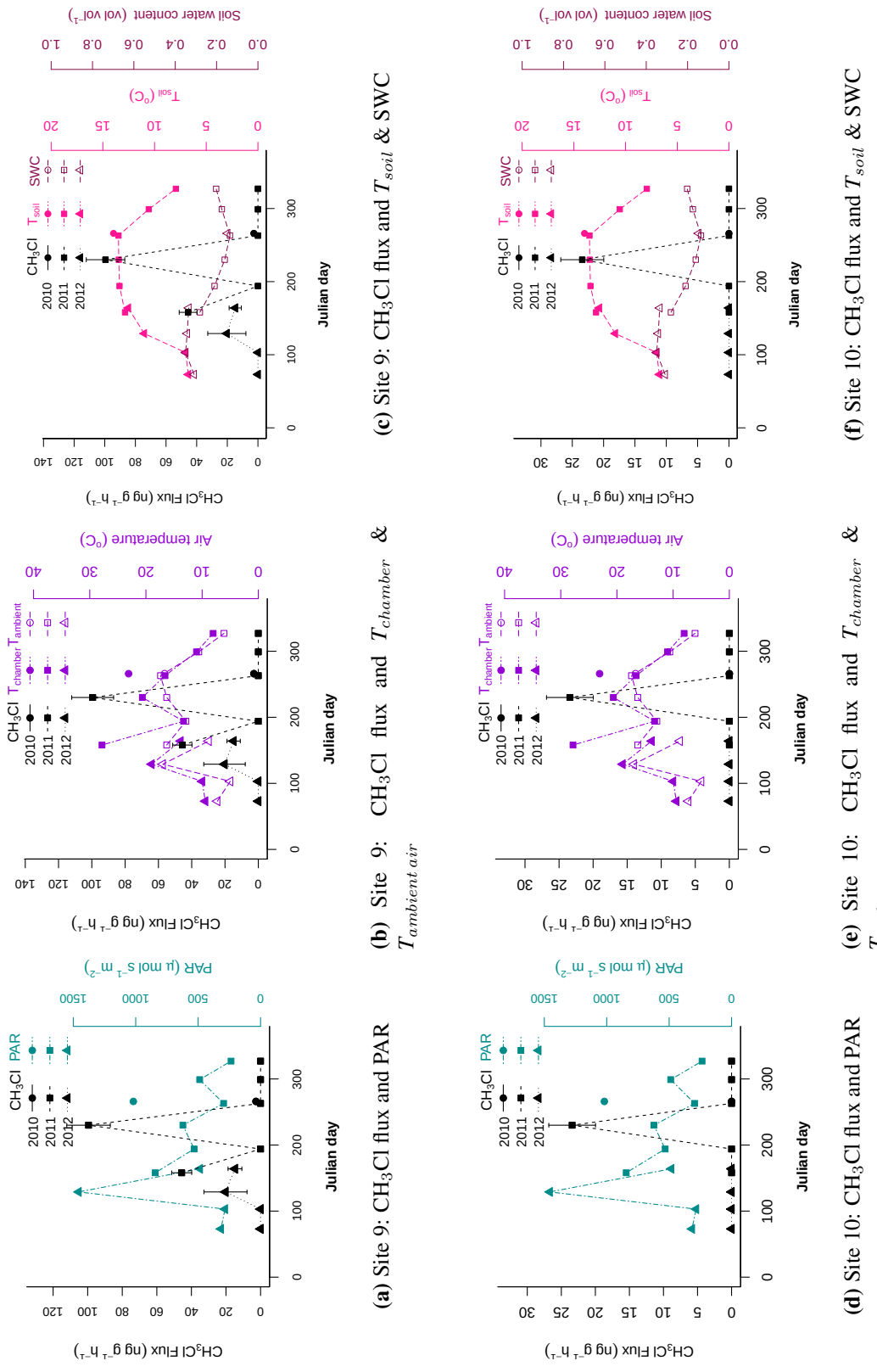
(c) Site 7: CH_3Cl flux and T_{soil} & SWC

(d) Site 8: CH_3Cl flux and PAR

(e) Site 8: CH_3Cl flux and $T_{chamber}$ & $T_{ambient\,air}$

(f) Site 8: CH_3Cl flux and T_{soil} & SWC

Figure 4.12: Comparison of net CH_3Cl fluxes from willow with PAR, chamber and ambient air temperature, soil temperature and soil water content (SWC) for 2010, 2011 and 2012 for sites 7 and 8. Note different y-axis scales for CH_3Cl. Error bars on fluxes incorporate analytical and sampling uncertainties.



(a) Site 9: CH_3Cl flux and PAR

(b) Site 9: CH_3Cl flux and $T_{chamber}$ & $T_{ambient\ air}$

(c) Site 9: CH_3Cl flux and T_{soil} & SWC

(d) Site 10: CH_3Cl flux and PAR

(e) Site 10: CH_3Cl flux and $T_{chamber}$ & $T_{ambient\ air}$

(f) Site 10: CH_3Cl flux and T_{soil} & SWC

Figure 4.13: Comparison of net CH_3Cl fluxes from willow with PAR, chamber and ambient air temperature, soil temperature and soil water content (SWC) for 2010, 2011 and 2012 for sites 9 and 10. Note different y-axis scales for CH_3Cl. Error bars on fluxes incorporate analytical and sampling uncertainties.

4.2.4 Statistical analysis of seasonal fluxes and potential drivers

Three types of analyses were carried out on the long-term CH_3X time series:

- Variation in CH_3X fluxes between sites and between growing and non-growing season were analysed for significance using the Kruskal-Wallis function within the R i386 2.15.1 software package
- Correlations between CH_3Br and CH_3Cl fluxes were investigated using regression analysis
- CH_3X fluxes were also analysed for their association with measured environmental parameters

Analysis of variation according to site and season

The significance of the variation in CH_3X fluxes due to location (different sites in the field), season (growing and non-growing), and from the interaction between these two factors was analysed using the Kruskal-Wallis test. Each year was divided into a growing season (beginning of April to end of October) and a non-growing season (the rest of the year) based on observational evidence of plant growth.

Variation in both CH_3Br and CH_3Cl fluxes with season were found to be significant (Table 4.4). Variation in CH_3X fluxes between sites was not found to be significant, as indicated by observation of the data. There was no significant interaction between season and site.

Table 4.4: Analysis of CH_3X flux variation according to site and season derived using Kruskal-Wallis. The degrees of freedom (d.f), χ^2 value and p value for the effect of site, season and season-site interaction terms on CH_3Br and CH_3Cl fluxes are presented. At a significance level of 95% the null hypothesis is rejected if $p \leq 0.05$.

	CH_3Br			CH_3Cl		
	d.f	χ^2	p	d.f	χ^2	p
Season	1	10.2	0.001	1	8.63	0.003
Site	9	6.48	0.691	9	9.30	0.410
Season*Site	9	20.0	0.392	9	20.1	0.387

Correlations between CH_3Br and CH_3Cl

Only two significant correlations were found between CH_3Br and CH_3Cl fluxes with Spearman's rank correlation coefficients (ρ) of 0.48 and 0.61 with corresponding p values of 0.04 and 0.03 at sites 1 and 8 respectively (Table 4.5). During the three years of measurements, site 1 emitted

average fluxes of both CH_3Br and CH_3Cl whereas site 8 emitted fairly high fluxes of CH_3Cl but low CH_3Br fluxes. No general relationship between magnitude of CH_3Br and CH_3Cl fluxes and correlation of CH_3X could therefore be determined.

Table 4.5: Spearman's rank correlation coefficients (ρ) between CH_3Br and CH_3Cl fluxes at each site and the associated p value (at a significance level of 95% the null hypothesis is rejected if $p \leq 0.05$). The last row shows the ρ correlation and p value for fluxes over all sites.

Site	ρ	p
W1	0.480	0.038
W2	0.296	0.249
W3	-0.108	0.670
W4	-0.212	0.414
W5	-0.097	0.720
W6	0.007	0.977
W7	-0.230	0.449
W8	0.613	0.026
W9	0.515	0.105
W10	-0.191	0.574
All	0.115	0.157

CH_3X flux association with measured environmental factors

Correlations of CH_3Br and CH_3Cl fluxes and observed environmental variables were investigated. CH_3Br and CH_3Cl fluxes were first normalised to the highest flux recorded over the three year measurement period before being tested for correlations with PAR, chamber and ambient air temperature, soil temperature and soil moisture.

Significant positive correlation between CH_3X fluxes and PAR, chamber temperature, ambient air temperature and soil temperature were derived, with Spearman's rank correlation coefficients of between 0.167 and 0.395 and corresponding p values of < 0.05 (Table 4.6). No significant correlations were derived between CH_3X fluxes and soil moisture.

Table 4.6: Spearman's rank correlation coefficients between potential drivers and CH_3X fluxes. Significant correlations ($p \leq 0.05$) are highlighted in bold.

Factor	CH_3Br	CH_3Cl
PAR	**0.167**	**0.213**
$\boldsymbol{T_{chamber}}$	**0.179**	**0.395**
$\boldsymbol{T_{ambient\ air}}$	**0.175**	**0.237**
$\boldsymbol{T_{soil}}$	**0.199**	**0.260**
Soil moisture	-0.090	**-0.193**

4.2.5 Sub-diurnal trends

To investigate the behaviour of CH_3X fluxes throughout the day during different times of the year, one full diurnal and seven sub-diurnal measurement campaigns were conducted. During the full diurnal campaign measurements were taken every 6 hours over a 24 hour period. During the sub-diurnal campaigns, three measurements were taken between 9 am and 9 pm. Air temperature and PAR were recorded throughout each 12 or 24 hour sampling period. Fluxes were measured for either 2 or 4 sites during these campaigns. As well as changes to the weather in different measurement months, there were also changes to the physiology of the willow plants. When diurnal and sub-diurnal measurements were made in 2010 and 2011, buds break occurred in March, branches and leaves grew between April and September, leaves senesced in October and fell off in November.

CH_3Br

Of the diurnal and sub-diurnal measurements conducted, only a few produced interesting results. Results from four sub-diurnal studies conducted between June and October 2011 are presented in Figure 4.14. The first of these was carried out at sites 1 and 2 on the 7th June 2011 (Figure 4.14a). CH_3Br fluxes from both site 1 and 2 were highest at the start of the day (just over and just under 3 ng g^{-1} h^{-1} for site 1 and 2 respectively) and zero at 1 pm and 5.30 pm. PAR and air temperature were also lower during the later part of the day.

A similar trend in fluxes was evident from measurements at sites 1 and 2 on the 13th July 2011 (Figure 4.14b). Fluxes of 1.3 and 1.9 ng g^{-1} h^{-1} were measured at 9 am then dropped to zero at 1 pm and 5 pm. On this occasion there was no apparent relation between fluxes measured and the observed environmental variables.

The trend of high fluxes in the morning and zero fluxes in the afternoon was found to be reversed during measurements made at sites 1 to 4 on the 18th August 2011 (Figure 4.14c). Zero fluxes were measured at all sites at 9 am, before they rose to between zero and 2 ng g^{-1} h^{-1} at 1 pm, and increased to between 3 and 5 ng g^{-1} h^{-1} at sites 1 and 3 and a maximum of 17 ng g^{-1} h^{-1} at site 2 at 4 pm. PAR and air temperature were at a minimum at this time, suggesting no correlation between the sunlight and temperature levels and the fluxes measured.

The flux measurements made at sites 1 to 4 on the 26th October 2011 follow a similar trend to those measured in June and July with the highest fluxes in the morning and zero fluxes in the afternoon (Figure 4.14d). Fluxes of between zero and 3 ng g^{-1} h^{-1} were measured at sites 1 and 3 at 9.30 am while at site 2 a much higher flux of 35 ng g^{-1} h^{-1} was measured. Fluxes at all sites then dropped to zero at 1.30 pm and 3.30 pm.

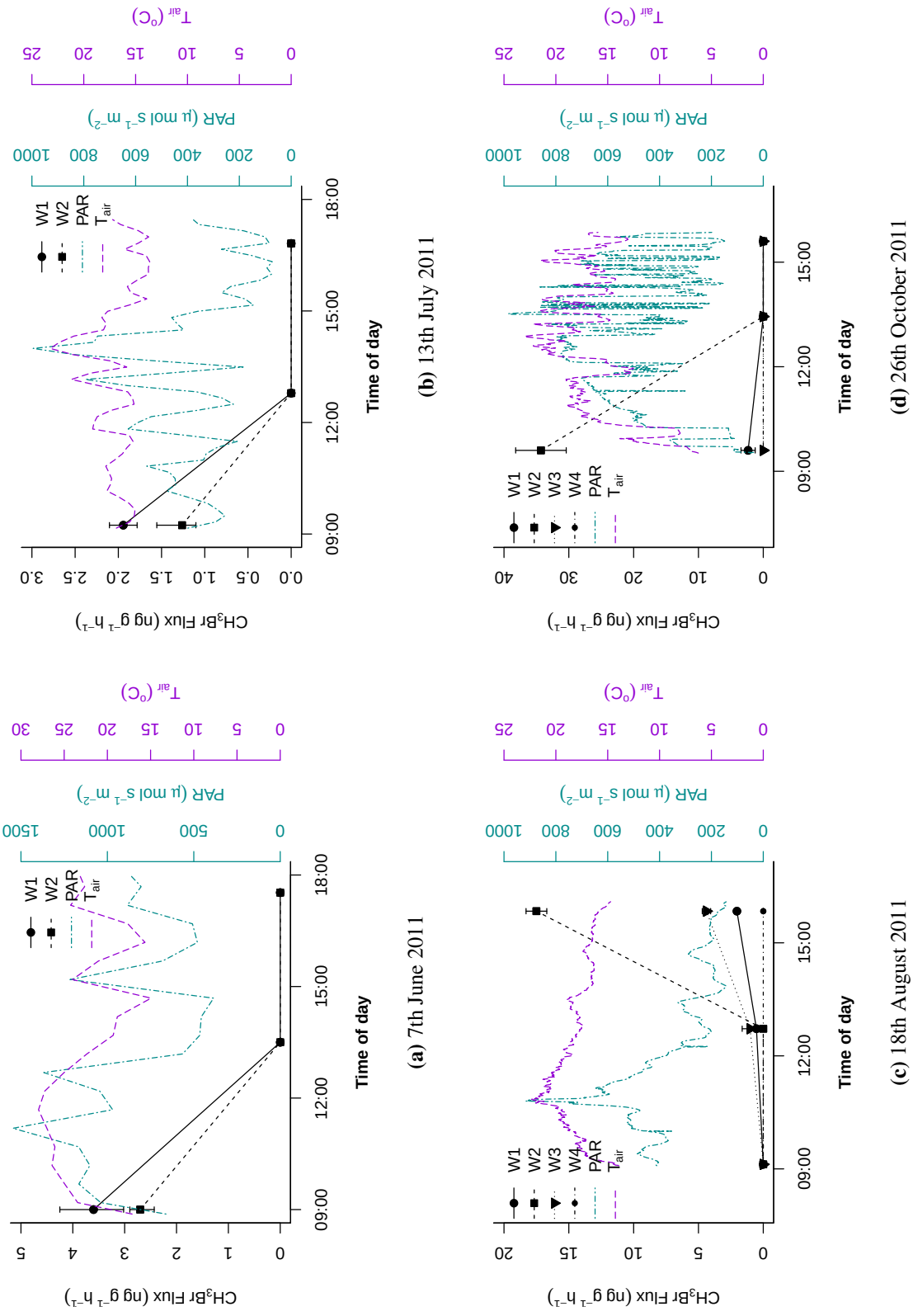


Figure 4.14: Sub-diurnal CH_3Br fluxes at Brattleby SRC willow sites 1-2 or 1-4 in June, July, August and October 2011 with ambient air temperature and PAR. Error bars incorporate analytical and sampling uncertainties. Note the different vertical scales in each figure.

CH_3Cl

Results from four sub-diurnal studies conducted in June, July, August and September 2011 are presented in Figure 4.15. The first of these was carried out at sites 1 and 2 on the 7th June 2011 (Figure 4.15a). CH_3Cl fluxes at both site 1 and 2 were highest in the middle of the day, with a flux of 60 ng g^{-1} h^{-1} measured at site 1 and a lower flux of 9 ng g^{-1} h^{-1} measured at site 2 at 1 pm. Zero fluxes were measured from both sites at 9 am and 5.30 pm. The trend in fluxes did not appear to correlate to any trends in the PAR levels and air temperature.

The reverse trend in fluxes was found at site 1 on the 13th July 2011 (Figure 4.15b). Fluxes of around 10 ng g^{-1} h^{-1} were measured at the start and end of the day and this dropped to around 5 ng g^{-1} h^{-1} in the middle of the day. Zero fluxes were measured throughout the day at site 2. Fluxes appeared to be totally independent of the observed environmental variables.

Measurements made on the 18th August 2011 at sites 1 to 4 show several different trends in fluxes (Figure 4.15c). At site 1 a zero flux was measured in the morning. This increased slightly to 22 ng g^{-1} h^{-1} at 1 pm and dropped slightly to 17 ng g^{-1} h^{-1} at 4 pm. A similar trend was found at site 3, where a flux of 40 ng g^{-1} h^{-1} was measured in the morning, this increased to 116 ng g^{-1} h^{-1} at 1 pm and then fell again to 48 ng g^{-1} h^{-1} in the afternoon. A flux of 24 ng g^{-1} h^{-1} was measured from site 2 at 9 am. This increased almost four-fold to 85 ng g^{-1} h^{-1} at 1 pm and increased again to 100 ng g^{-1} h^{-1} at 4 pm. At site 4 a flux of 19 ng g^{-1} h^{-1} was measured at 9 am, similar to that measured at site 2. This dropped to zero at midday and then increased six-fold to 119 ng g^{-1} h^{-1} in the afternoon.

On the 20th September 2011, zero fluxes were measured from site 1 and 2 throughout the day (Figure 4.15d). One non-zero flux of 32 ng g^{-1} h^{-1} was measured from site 3 at 9 am and one non-zero flux of 12 ng g^{-1} h^{-1} from site 4 at midday.

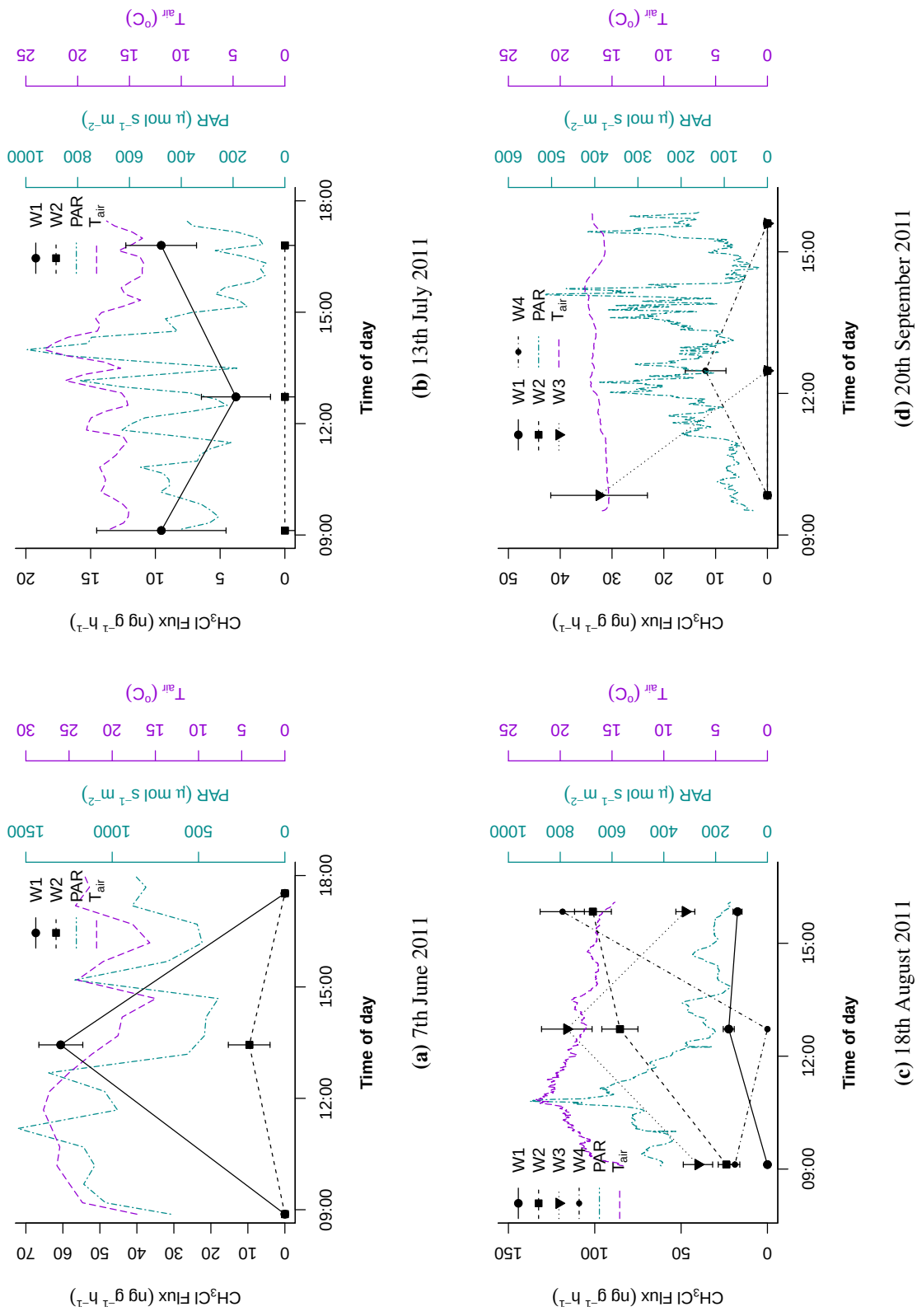


Figure 4.15: Sub-diurnal CH_3Cl fluxes at Brattleby SRC willow sites 1 - 2 or 1 - 4 in June, July, August and September 2011 with ambient air temperature and PAR. Error bars on fluxes incorporate analytical and sampling uncertainties. Note the different scales used in each figure.

4.2.6 Outline of BVOC flux measurements

A total of 132 measurements were made during 19 site visits between April 2010 and August 2012. These measurements were made almost every month in order to capture seasonal flux variability. Flux measurements were carried out as described in Section 2.3.1.

Firstly, the seasonal BVOC flux trends during each sampling year are examined for isoprene, α-pinene, β-pinene, limonene and δ-3-carene. The variation between years during the sampling period is discussed. Time series of seasonal net BVOC fluxes for the years 2010, 2011 and 2012 and the respective PAR, ambient and chamber air temperature, soil temperature and soil water content observations at the time of measurement for each sampling site are then illustrated, incorporating seasonal, temporal and annual variation in fluxes.

Statistical analysis of the BVOC fluxes is then presented. BVOC fluxes are tested for significant correlations with monitored environmental parameters in order to investigate possible drivers of emissions. Correlations between various BVOC fluxes were tested for significance as was the association of variation in BVOC flux with season and sampling site.

Thirdly, the behaviour of BVOC fluxes throughout the day at different times of the year is examined in separate sub-diurnal studies in August and September 2011 and presented in Figure 4.46.

4.2.7 BVOC flux trends

Isoprene

A total of 132 isoprene flux measurements were made during 19 site visits beginning in April 2010 and ending in August 2012. Fluxes are considered first by calendar year and then collectively across all 3 calendar years. Figure 4.16 presents the isoprene fluxes at all ten sampling points and the mean of those values on each sampling occasion across 2010 to 2012. There is a clear seasonal trend, with higher fluxes during the summer and zero fluxes over the winter. The fluxes of isoprene measured from the willow were generally high, with much higher fluxes measured in 2010 compared to 2011 and 2012, albeit with much larger associated uncertainties than in the following years. This is a different trend to the CH_3X fluxes, where fluxes were highest in 2011, and is probably related to the growth stage of the willow trees. The willow trees were coppiced in winter 2010 so measurements taken in 2011 were from younger trees compared to measurements taken from trees with three year's growth in 2010 and at least a year's growth 2012.

Fluxes reached up to 160 $\mu g\, g^{-1}\, h^{-1}$ in April 2010. The maximum flux then increased six-fold to 1100 $\mu g\, g^{-1}\, h^{-1}$ in May, with a minimum flux of 270 $\mu g\, g^{-1}\, h^{-1}$. Fluxes then almost

doubled again in June, with fluxes of between 630 and 1960 $\mu g\, g^{-1}\, h^{-1}$. Fluxes dropped dramatically to between zero and 23 $\mu g\, g^{-1}\, h^{-1}$ in August but rose again to between 270 and 360 $\mu g\, g^{-1}\, h^{-1}$ in September. Zero fluxes were measured over winter between November 2010 and April 2011.

In June 2011 fluxes of zero and 9.6$\mu g\, g^{-1}\, h^{-1}$ were measured. Fluxes increased to between zero and 41 $\mu g\, g^{-1}\, h^{-1}$ in July and remained fairly similar but slightly higher in August with a range of 4.6 to 49 $\mu g\, g^{-1}\, h^{-1}$. In September fluxes fell to between zero and 12 $\mu g\, g^{-1}\, h^{-1}$ and fell again in October to between 0.2 to 3.9 $\mu g\, g^{-1}\, h^{-1}$. Zero fluxes were measured during the winter between November 2011 and March 2012.

Fluxes increased marginally in April 2012 to between zero and 1.87 $\mu g\, g^{-1}\, h^{-1}$. The range of fluxes increased again in May to between 0.5 to 14 $\mu g\, g^{-1}\, h^{-1}$ before they decreased slightly in June to between 0.1 to 4.1 $\mu g\, g^{-1}\, h^{-1}$. There was a sharp increase in fluxes measured during August with fluxes of between 16 and 280 $\mu g\, g^{-1}\, h^{-1}$, the highest measured during 2011 and 2012. Measurements finished in August so it is possible that high emission fluxes may also have been detected later in the growing season, as was the case in 2010. Mean summer fluxes varied between 2.3 and 1100 $\mu g\, g^{-1}\, h^{-1}$ during 2010, 2011 and 2012.

Time series of isoprene fluxes from each individual site across three calendar years from April 2010 to August 2012 with concurrent PAR, ambient and chamber air temperature, soil temperature and soil water content observations are illustrated in Figures 4.17 to 4.21.

In 2010, 25 measurements were made in total and the maximum flux measured was 1960 $\mu g\, g^{-1}\, h^{-1}$ from site 3 (Table 4.7a). Mean fluxes ranged from 0 to 760 $\mu g\, g^{-1}\, h^{-1}$. All but three of the ten maximum fluxes measured throughout the campaign were measured in 2010. The three exceptions were site 5, which was measured only once in April of that year, and site 9 and 10 which were not sampled in 2010. A mean flux of 360 $\mu g\, g^{-1}\, h^{-1}$ was calculated from all fluxes recorded at all sites during 2010.

Isoprene fluxes measured were generally lower in 2011 with a mean flux of 6.5 $\mu g\, g^{-1}\, h^{-1}$ calculated for all sites on all dates, in comparison to 360 $\mu g\, g^{-1}\, h^{-1}$ for 2010, although more measurements were taken during the winter months in 2011 (Table 4.7b). A total of 58 measurements were made between January and November. The highest mean fluxes were measured at sites 1, 3, 4 and 7 - 9 (between 7.2 and 11 $\mu g\, g^{-1}\, h^{-1}$) and lower mean fluxes at the remaining sites (1.4 to 4.2 $\mu g\, g^{-1}\, h^{-1}$). The highest maximum flux was measured at site 4 (49 $\mu g\, g^{-1}\, h^{-1}$) and the lowest maximum at site 6 (5.5 $\mu g\, g^{-1}\, h^{-1}$).

49 measurements were taken between March and August 2012 (Table 4.7c). The mean flux calculated for all measurements at all sites was 17 $\mu g\, g^{-1}\, h^{-1}$ which is over double that calculated in 2011 but much lower than that calculated for 2010. Higher mean fluxes were measured at sites 4 to 9 (between 13 and 59 $\mu g\, g^{-1}\, h^{-1}$) and lower mean fluxes at the remaining

sites (4.6 to 8.9 $\mu g\, g^{-1}\, h^{-1}$). The highest maximum flux of 280 $\mu g\, g^{-1}\, h^{-1}$ was measured at site 5 and the lowest maximum flux of 16 $\mu g\, g^{-1}\, h^{-1}$ was measured at site 10.

Mean isoprene fluxes between 4.1 and 200 $\mu g\, g^{-1}\, h^{-1}$ were measured from sites 1 to 10 during 2010 to 2012 (Table 4.7d). Slightly lower fluxes were measured at sites 2, 5, 6 and 10 (mean fluxes of under 5 $\mu g\, g^{-1}\, h^{-1}$) and higher fluxes were measured at the remaining sites (mean fluxes of between 7.2 and 10 $\mu g\, g^{-1}\, h^{-1}$). Higher maximum isoprene fluxes were measured at sites 1 - 4 and 6 (630 to 1960 $\mu g\, g^{-1}\, h^{-1}$) and lower maximum fluxes at other sites (between 16 and 280 $\mu g\, g^{-1}\, h^{-1}$). The highest maximum flux of 1960 $\mu g\, g^{-1}\, h^{-1}$ was measured at site 3 in 2010. The minimum flux recorded at all sites was zero. A mean emission of 77 $\mu g\, g^{-1}\, h^{-1}$ was calculated from fluxes measured at all sites during the measurement period.

Trends in isoprene fluxes appear to follow trends in the observed environmental variables, with increased PAR levels and air and soil temperatures leading to higher fluxes. The statistical significance of correlations between isoprene fluxes and environmental variables is described in Section 4.2.8.

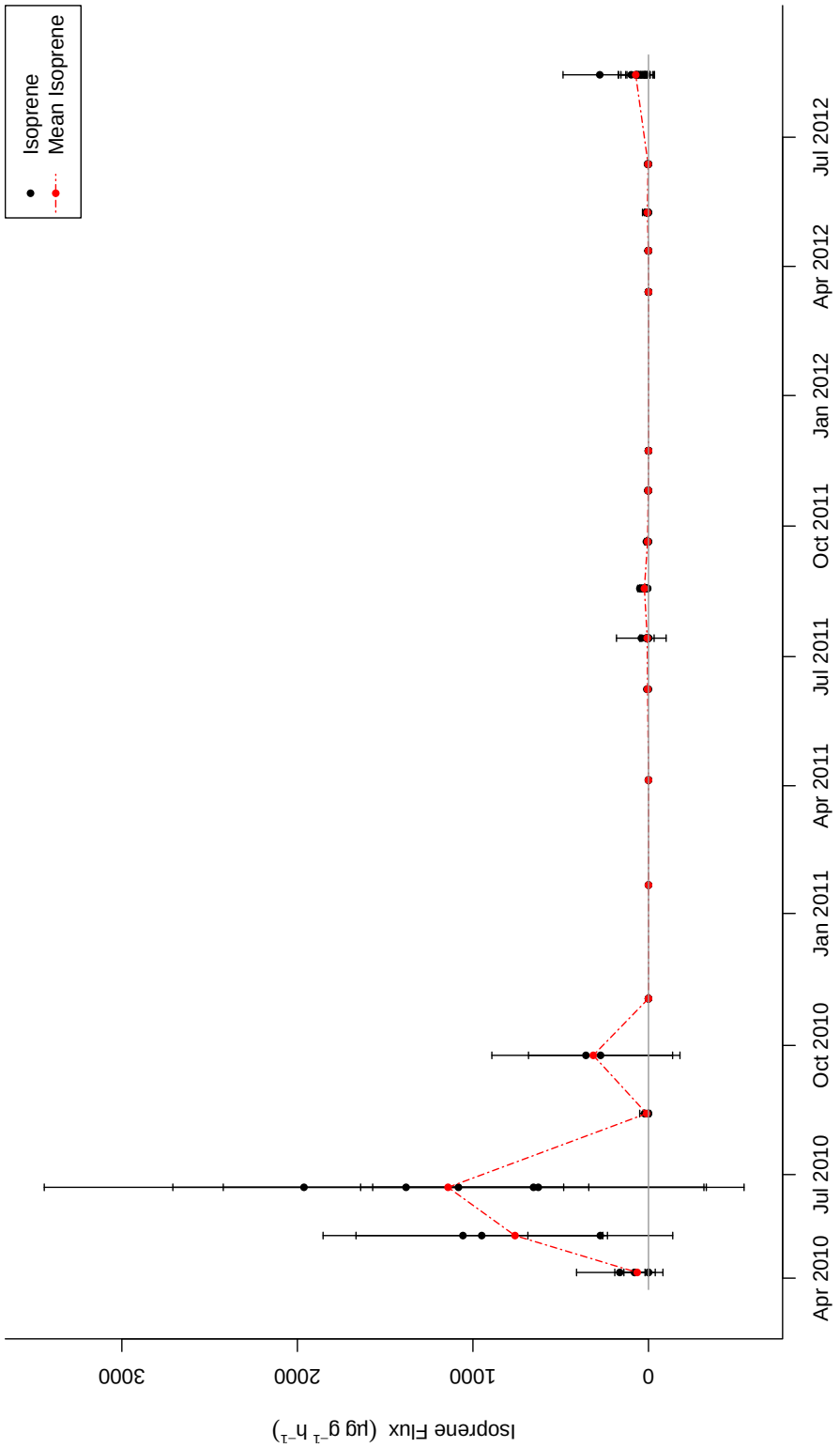


Figure 4.16: Isoprene fluxes from willow at the Brattleby fieldsite at all ten sampling points and the mean of those values on each sampling occasion from 2010 to 2012. Error bars on fluxes incorporate analytical and sampling uncertainties (as described in Section 2.6.1).

Table 4.7: Mean, median, minimum and maximum net isoprene fluxes from SRC willow at Brattleby during (a) 2010, (b) 2011, (c) 2012 and (d) 2010 - 2012. All flux values are in $\mu g\, g^{-1}\, h^{-1}$. The final column in each table gives the number of measurements made. The last row summarises all fluxes from all sites.

(a) Isoprene flux ($\mu g\, g^{-1}\, h^{-1}$) - 2010

Site	Mean	Median	Min	Max	Number
W1	447	176	0.00	1380	6
W2	298	176	0.00	1080	6
W3	760	538	0.00	1960	4
W4	226	22.9	0.00	655	3
W5	0.00	0.00	0.00	0.00	1
W6	628	628	628	628	1
W7	0.00	0.00	0.00	0.00	2
W8	81.8	81.8	0.00	164	2
All	359	76.7	0.00	1960	25

(b) Isoprene flux ($\mu g\, g^{-1}\, h^{-1}$) - 2011

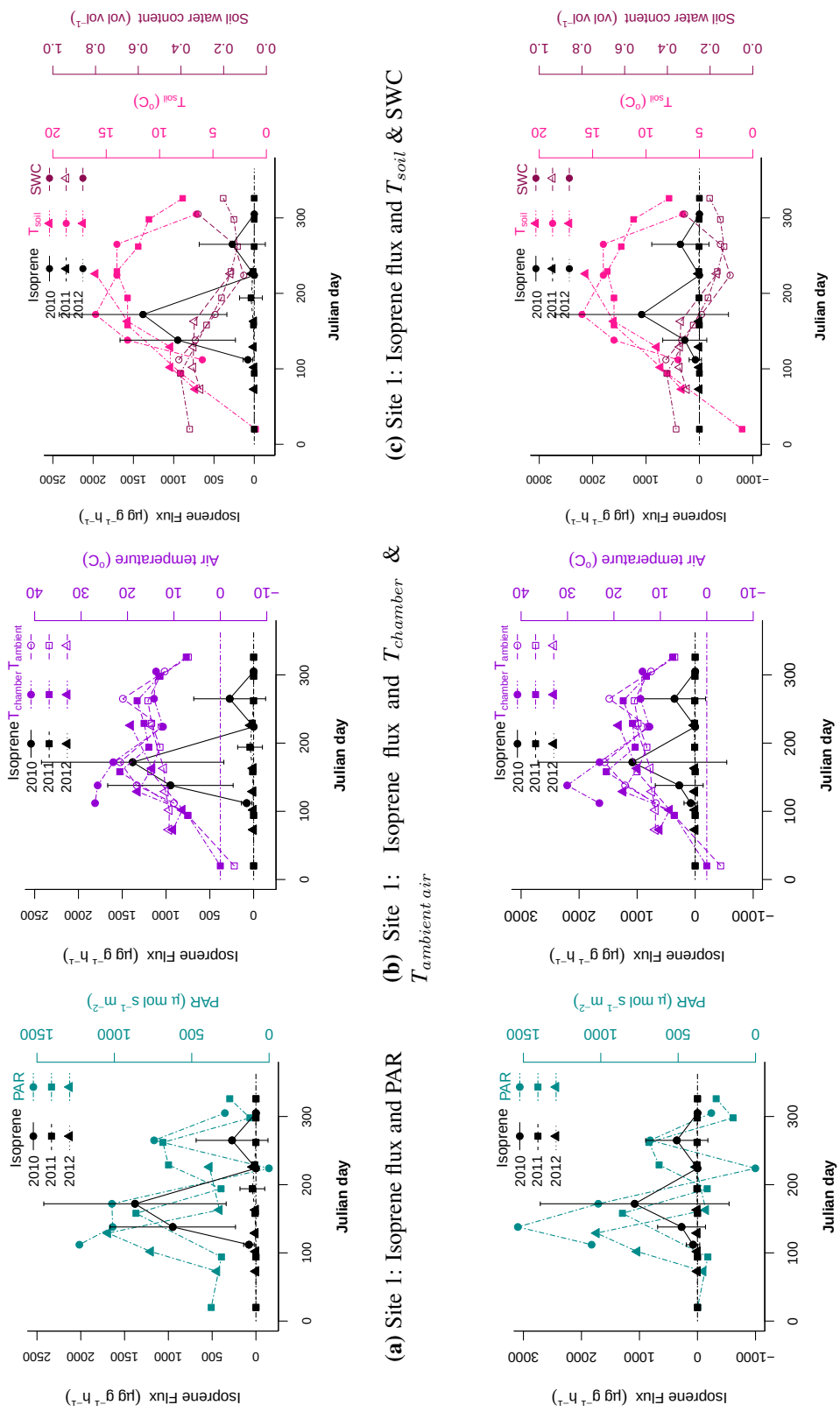
Site	Mean	Median	Min	Max	Number
W1	8.27	0.44	0.00	40.9	8
W2	3.76	1.96	0.00	11.0	8
W3	7.19	0.34	0.00	40.8	7
W4	10.9	0.84	0.00	49.2	5
W5	4.16	0.15	0.00	18.8	6
W6	1.43	0.00	0.00	5.50	6
W7	10.4	4.91	0.00	40.4	5
W8	8.86	1.41	0.00	40.3	5
W9	7.44	8.34	0.00	13.1	4
W10	3.53	3.25	0.00	7.61	4
All	6.46	0.90	0.00	49.2	58

(c) Isoprene flux ($\mu g\, g^{-1}\, h^{-1}$) - 2012

Site	Mean	Median	Min	Max	Number
W1	8.94	3.76	0.00	33.3	5
W2	5.75	4.11	0.00	17.9	5
W3	8.25	2.38	0.00	30.9	5
W4	16.6	0.66	0.00	67.9	5
W5	58.8	1.87	0.00	278	5
W6	14.6	3.26	0.00	62.7	5
W7	15.0	0.50	0.00	73.9	5
W8	12.6	0.70	0.00	49.0	4
W9	20.6	1.24	0.00	98.4	5
W10	4.55	2.78	0.00	16.3	5
All	16.7	1.84	0.00	278	49

(d) Isoprene flux ($\mu g\, g^{-1}\, h^{-1}$) - 2010 to 2012

Site	Mean	Median	Min	Max	Number
W1	147	3.76	0.00	1380	19
W2	97.3	4.11	0.00	1080	19
W3	196	1.81	0.00	1960	16
W4	62.7	0.84	0.00	655	13
W5	26.6	0.59	0.00	278	12
W6	59.1	2.37	0.00	628	12
W7	10.6	0.62	0.00	73.9	12
W8	23.5	0.79	0.00	164	11
W9	14.7	3.20	0.00	98.4	9
W10	4.09	2.78	0.00	16.3	9
All	77.1	1.62	0.00	1960	132



(a) Site 1: Isoprene flux and PAR

(b) Site 1: Isoprene flux and $T_{chamber}$ & $T_{ambient\ air}$

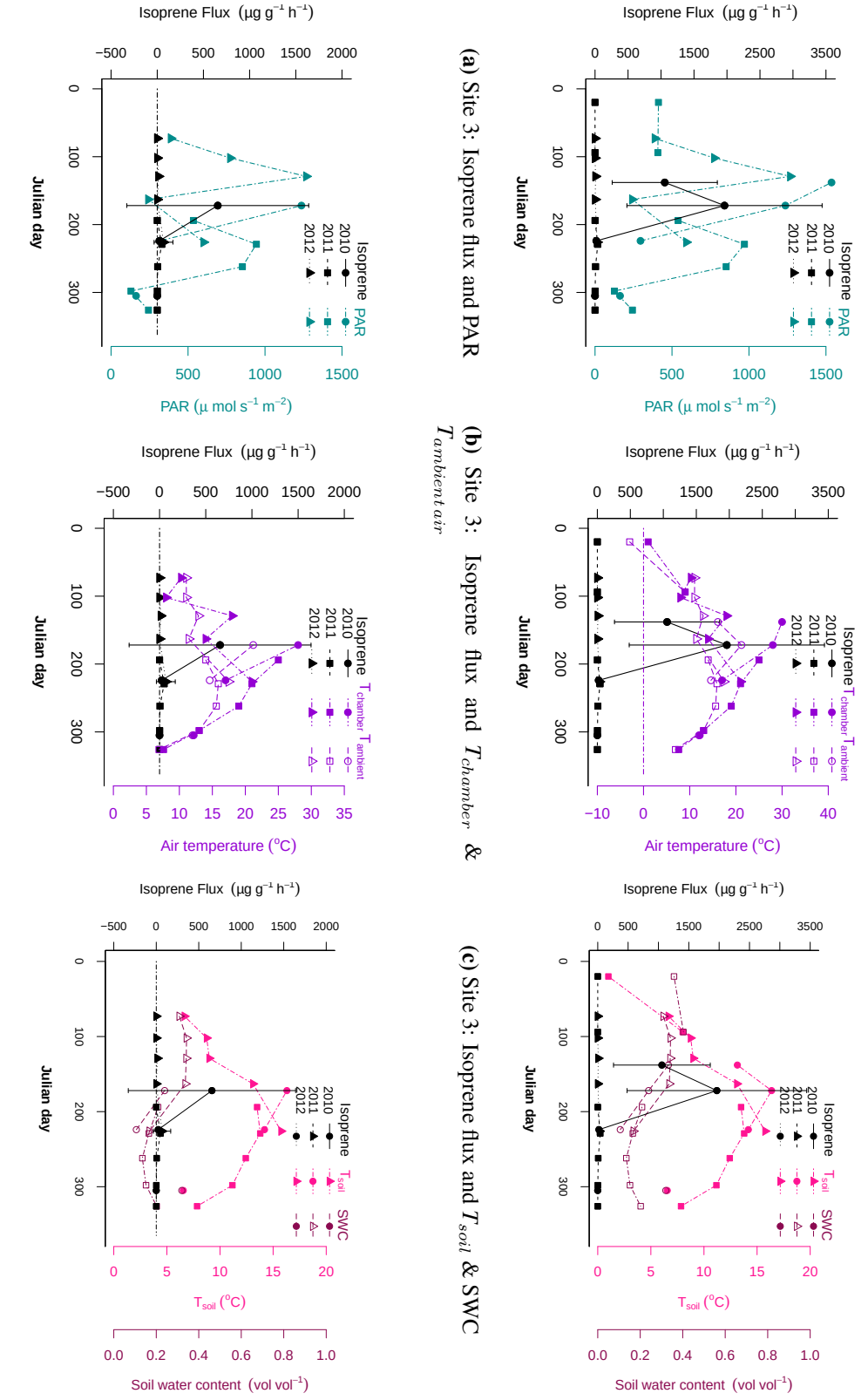
(c) Site 1: Isoprene flux and T_{soil} & SWC

(d) Site 2: Isoprene flux and PAR

(e) Site 2: Isoprene flux and $T_{chamber}$ & $T_{ambient\ air}$

(f) Site 2: Isoprene flux and T_{soil} & SWC

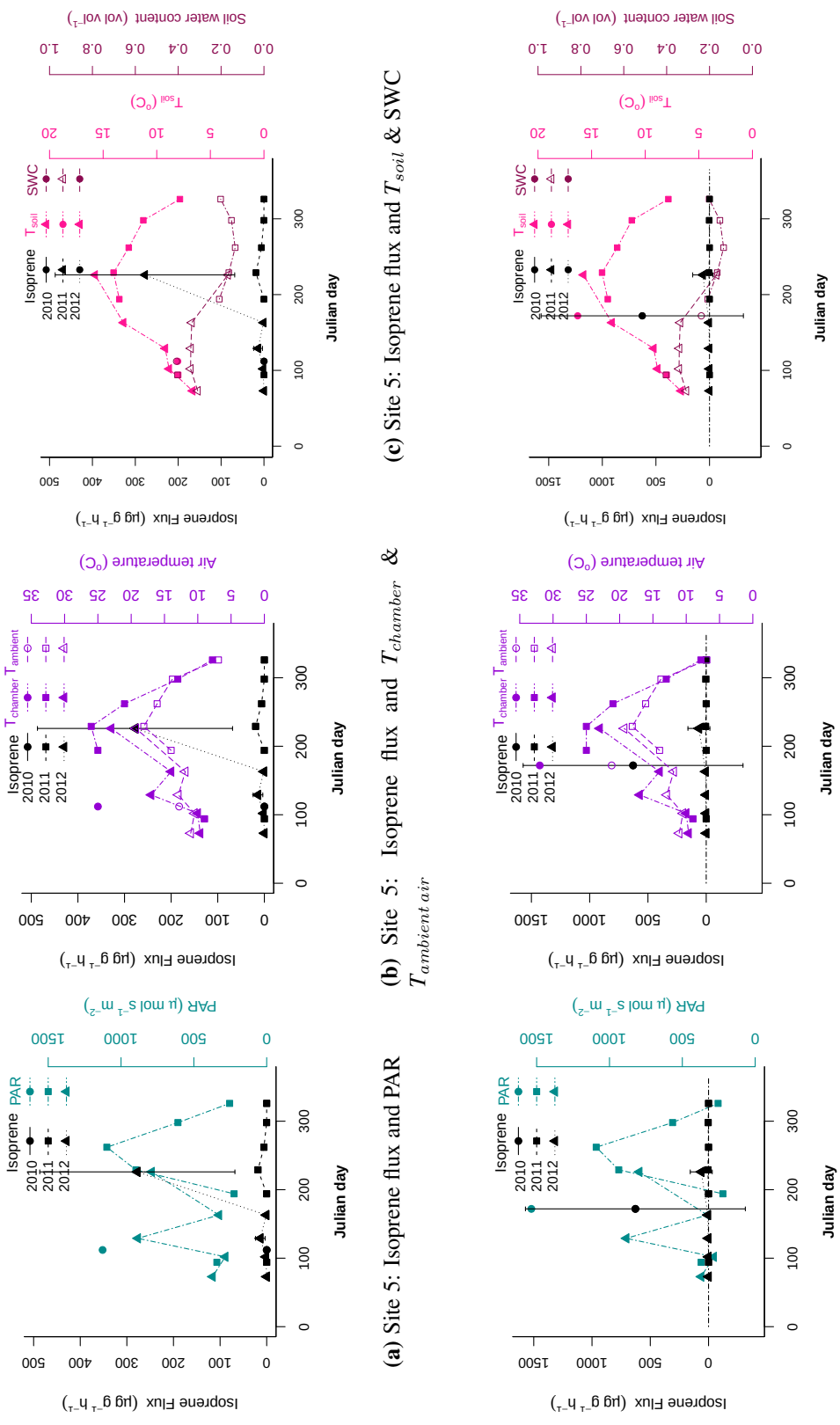
Figure 4.17: Comparison of net isoprene fluxes from willow with PAR, chamber and ambient air temperature, soil temperature and soil water content (SWC) for 2010, 2011 and 2012 for sites 1 and 2. Note different y-axis scales for isoprene. Error bars on fluxes incorporate analytical and sampling uncertainties.



(a) Site 3: Isoprene flux and PAR **(b)** Site 3: Isoprene flux and $T_{chamber}$ & $T_{ambient\,air}$ **(c)** Site 3: Isoprene flux and T_{soil} & SWC

(d) Site 4: Isoprene flux and PAR **(e)** Site 4: Isoprene flux and $T_{chamber}$ & $T_{ambient\,air}$ **(f)** Site 4: Isoprene flux and T_{soil} & SWC

Figure 4.18: Comparison of net isoprene fluxes from willow with PAR, chamber and ambient air temperature, soil temperature and soil water content (SWC) for 2010, 2011 and 2012 for sites 3 and 4. Note different y-axis scales for isoprene. Error bars on fluxes incorporate analytical and sampling uncertainties.



(a) Site 5: Isoprene flux and PAR

(b) Site 5: Isoprene flux and $T_{chamber}$ & $T_{ambient\ air}$

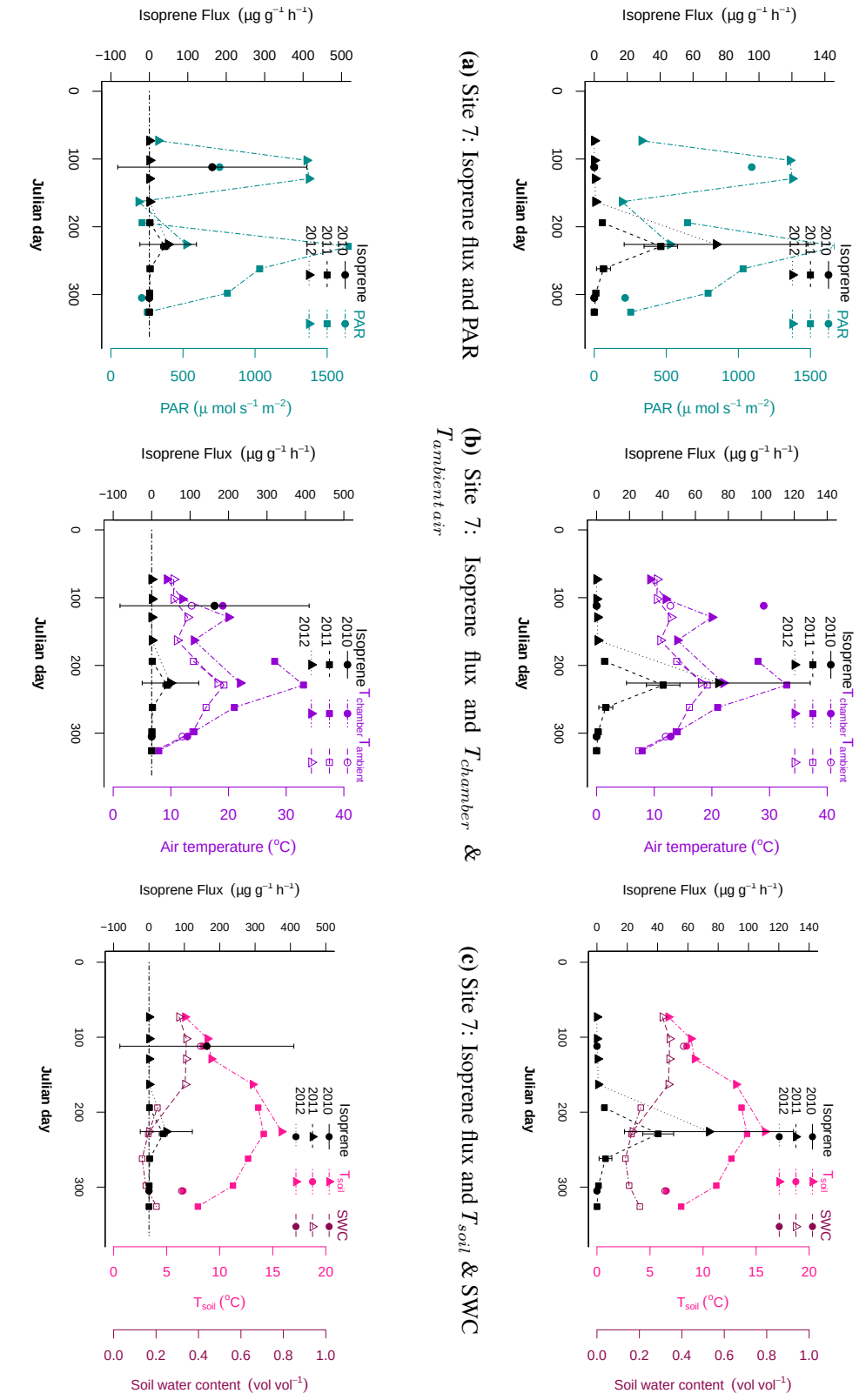
(c) Site 5: Isoprene flux and T_{soil} & SWC

(d) Site 6: Isoprene flux and PAR

(e) Site 6: Isoprene flux and $T_{chamber}$ & $T_{ambient\ air}$

(f) Site 6: Isoprene flux and T_{soil} & SWC

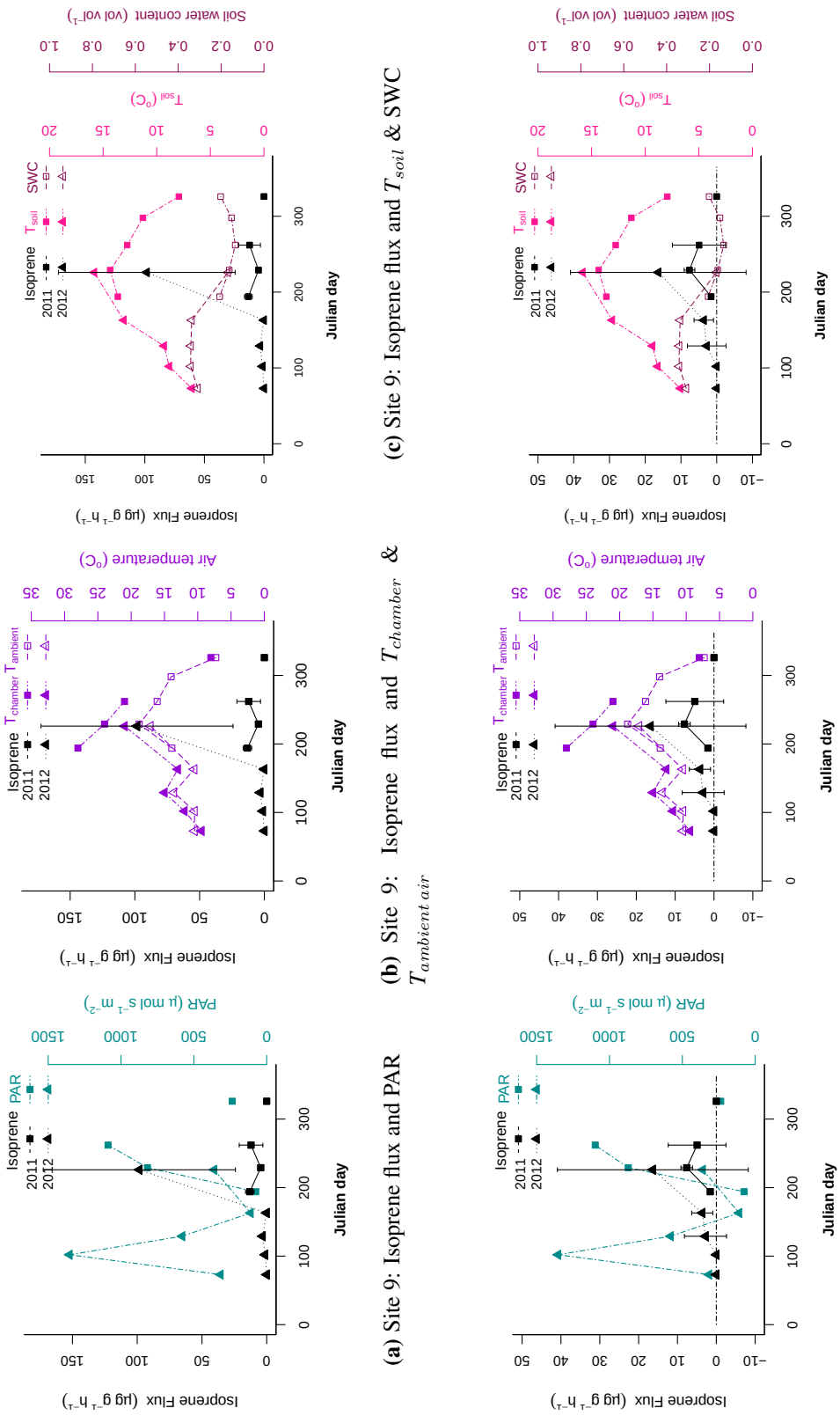
Figure 4.19: Comparison of net isoprene fluxes from willow with PAR, chamber and ambient air temperature, soil temperature and soil water content (SWC) for 2010, 2011 and 2012 for sites 5 and 6. Note different y-axis scales for isoprene. Error bars on fluxes incorporate analytical and sampling uncertainties.



(a) Site 7: Isoprene flux and PAR **(b)** Site 7: Isoprene flux and $T_{chamber}$ & $T_{ambient\,air}$ **(c)** Site 7: Isoprene flux and T_{soil} & SWC

(d) Site 8: Isoprene flux and PAR **(e)** Site 8: Isoprene flux and $T_{chamber}$ & $T_{ambient\,air}$ **(f)** Site 8: Isoprene flux and T_{soil} & SWC

Figure 4.20: Comparison of net isoprene fluxes from willow with PAR, chamber and ambient air temperature, soil temperature and soil water content (SWC) for 2010, 2011 and 2012 for sites 7 and 8. Note different y-axis scales for isoprene. Error bars on fluxes incorporate analytical and sampling uncertainties.



(a) Site 9: Isoprene flux and PAR

(b) Site 9: Isoprene flux and $T_{chamber}$ & $T_{ambient\ air}$

(c) Site 9: Isoprene flux and T_{soil} & SWC

(d) Site 10: Isoprene flux and PAR

(e) Site 10: Isoprene flux and $T_{chamber}$ & $T_{ambient\ air}$

(f) Site 10: Isoprene flux and T_{soil} & SWC

Figure 4.21: Comparison of net isoprene fluxes from willow with PAR, chamber and ambient air temperature, soil temperature and soil water content (SWC) for 2011 and 2012 for sites 9 and 10. Note different y-axis scales for isoprene. Error bars on fluxes incorporate analytical and sampling uncertainties.

α-pinene

Results are presented from 132 α-pinene flux measurements made during 19 site visits beginning in April 2010 and ending in August 2012. Fluxes are considered first by calendar year and then collectively across all 3 calendar years. Figure 4.22 presents the α-pinene fluxes at all ten sampling points and the mean of those values on each sampling occasion across 2010 to 2012. There is a seasonal trend in α-pinene fluxes with higher fluxes during summer and zero fluxes during winter, although this is somewhat obscured by the high values measured in 2010. Fluxes measured in 2010 were an order of magnitude higher than those measured in 2011 and 2012, with large associated uncertainties. This may be due to growth stage of the plants, as trees measured in 2010 had 3 to 4 years growth but the trees measured in 2011 and 2012 were younger, with a few months growth and around a year's growth, respectively, after they were coppiced in winter 2010.

Time series of α-pinene fluxes from each individual site across three calendar years from April 2010 to August 2012 with concurrent PAR, ambient and chamber air temperature, soil temperature and soil water content observations are illustrated in Figures 4.23 to 4.27.

α-pinene fluxes reached up to 591 $\mu g\, g^{-1}\, h^{-1}$ in April 2010. The maximum flux then increased to 803 $\mu g\, g^{-1}\, h^{-1}$ in May, with a minimum flux of 22 $\mu g\, g^{-1}\, h^{-1}$. Fluxes remained high in June, with a range of fluxes of between 239 and 683 $\mu g\, g^{-1}\, h^{-1}$. Fluxes dropped to zero in August and remained at zero over winter (between November 2010 and April 2011).

Eight sampling trips were made between January and November 2011, with zero fluxes measured at every site on every occasion. The SRC willow was coppiced in March 2011 and the plants grew from around 30 cm in April to around 3 m in November 2011. Non-zero fluxes were only measured again in March 2012, when a maximum α-pinene flux of 0.56 $\mu g\, g^{-1}\, h^{-1}$ was measured. Fluxes increased slightly in April to between 0.43 and 2.2 $\mu g\, g^{-1}\, h^{-1}$ and remained the same in May, with a range of fluxes between 0.34 and 2.9 $\mu g\, g^{-1}\, h^{-1}$. Fluxes increased substantially in June, with fluxes reaching a maximum of 83 $\mu g\, g^{-1}\, h^{-1}$. In August fluxes dropped again to under half of the maximum flux measured in June, with a range of fluxes between 0.1 and 37 $\mu g\, g^{-1}\, h^{-1}$ measured. Mean summer fluxes varied between zero in 2011 and 536 $\mu g\, g^{-1}\, h^{-1}$ during 2010.

In 2010, 25 measurements were made in total and the maximum flux measured was 803 $\mu g\, g^{-1}\, h^{-1}$ from site 3, where the highest isoprene flux was also measured in 2010 (Table 4.8a). Mean fluxes ranged from 130 to 296 $\mu g\, g^{-1}\, h^{-1}$. All of the maximum fluxes measured throughout the campaign were measured in 2010 with the exception of sites 9 and 10 which were not sampled in 2010. A mean flux of 228 $\mu g\, g^{-1}\, h^{-1}$ was calculated from all fluxes recorded at all sites during 2010.

49 measurements were taken between March and August 2012 (Table 4.8b). The mean flux

calculated for all measurements at all sites was 6.2 $\mu g\, g^{-1}\, h^{-1}$ which is two orders of magnitude lower than that calculated for 2010. Higher mean fluxes were measured at sites 1 - 3 and 5 - 6 (between 6.7 and 18 $\mu g\, g^{-1}\, h^{-1}$) and lower mean fluxes at the remaining sites (0.9 to 2.5 $\mu g\, g^{-1}\, h^{-1}$). The highest maximum flux of 83 $\mu g\, g^{-1}\, h^{-1}$ was measured at site 2 and the lowest maximum flux of 2.5 $\mu g\, g^{-1}\, h^{-1}$ was measured at site 8. A mean flux of 46 $\mu g\, g^{-1}\, h^{-1}$ was calculated from all results from all three years.

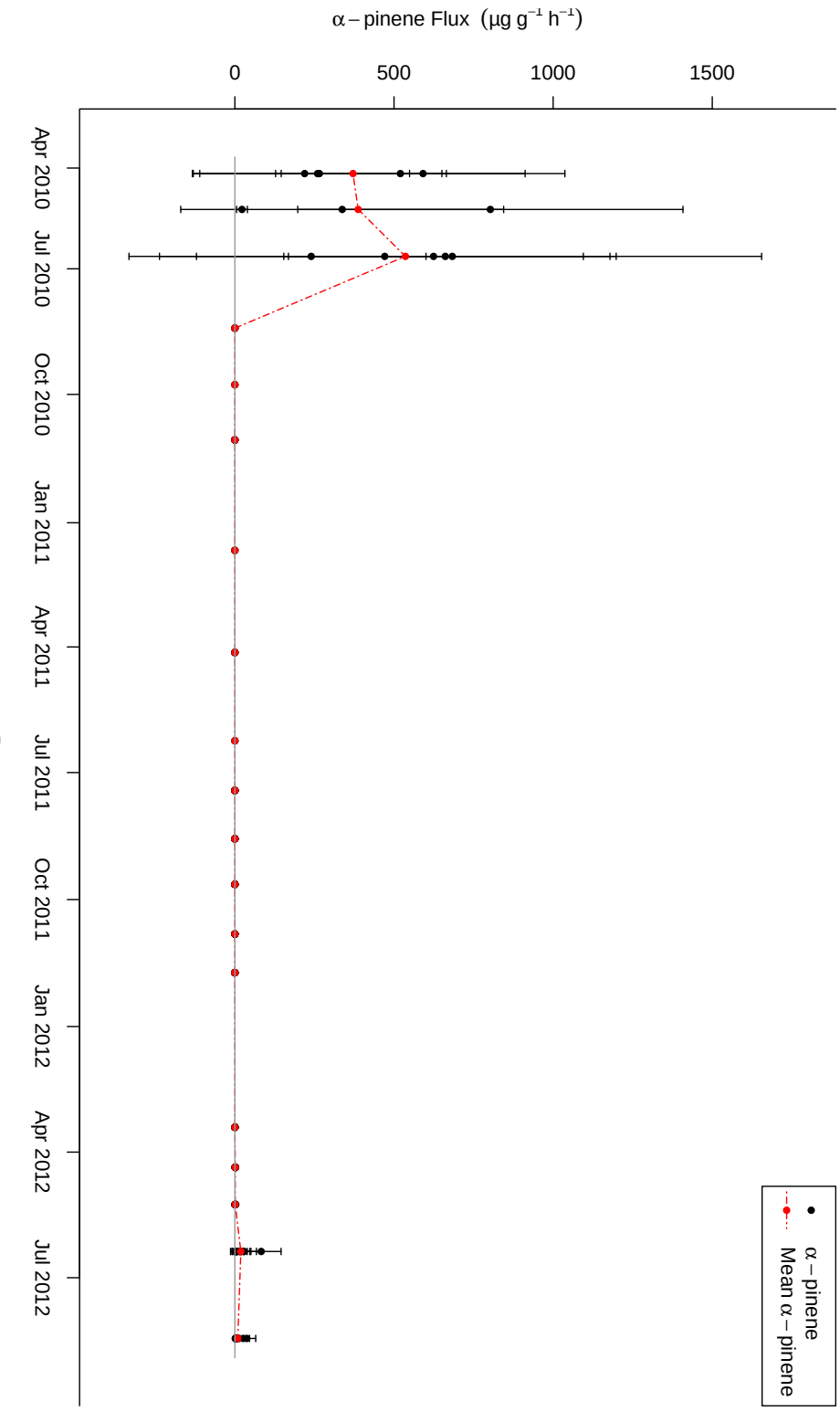


Figure 4.22: α-pinene fluxes from willow at the Brattleby fieldsite at all ten sampling points and the mean of those values on each sampling occasion from 2010 to 2012. Error bars on fluxes incorporate analytical and sampling uncertainties (as described in Section 2.6.1).

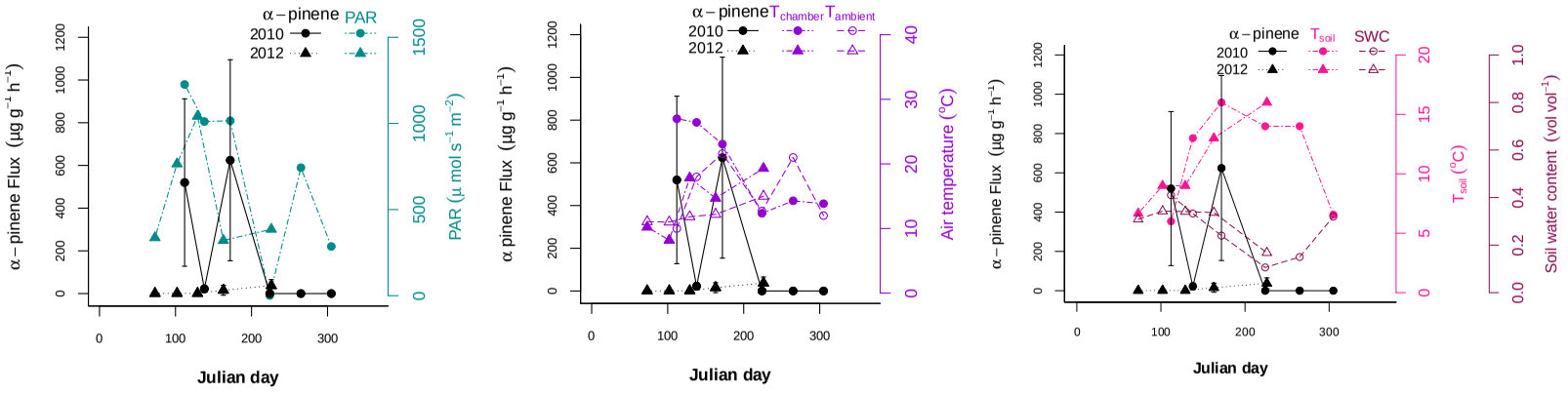
Table 4.8: Mean, median, minimum and maximum net α-pinene fluxes from SRC willow in Brattleby during 2010 (a) and 2012 (b). All flux values are in $\mu g\, g^{-1}\, h^{-1}$. The final column gives the number of measurements made. The last row summarises all fluxes from all sites.

(a) α-pinene flux ($\mu g\, g^{-1}\, h^{-1}$) - 2010

Site	Mean	Median	Min	Max	Number
W1	194	11.2	0.00	624	6
W2	203	110	0.00	661	6
W3	371	342	0.00	803	4
W4	157	0.00	0.00	471	3
W5	265	265	265	265	1
W6	240	240	240	240	1
W7	296	296	0.00	591	2
W8	130	130	0.00	260	2
All	228	22.4	0.00	803	25

(b) α-pinene flux ($\mu g\, g^{-1}\, h^{-1}$) - 2012

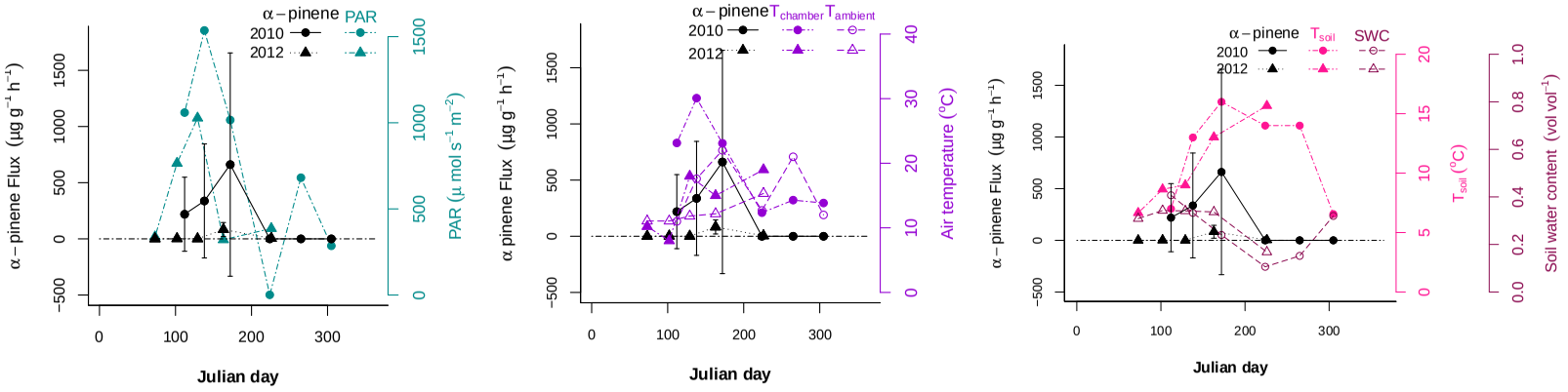
Site	Mean	Median	Min	Max	Number
W1	11.0	0.78	0.56	37.3	5
W2	17.8	1.64	0.16	82.8	5
W3	7.86	1.99	0.31	27.0	5
W4	0.94	0.34	0.06	3.43	5
W5	10.0	2.87	0.00	26.2	5
W6	6.71	1.50	0.00	28.8	5
W7	1.29	1.24	0.00	3.00	5
W8	1.37	1.48	0.00	2.53	4
W9	1.36	0.94	0.37	2.67	5
W10	2.46	1.24	0.00	8.61	5
All	6.18	1.24	0.00	82.8	49



(a) Site 1: α-pinene flux and PAR

(b) Site 1: α-pinene flux and $T_{chamber}$ & $T_{ambient\,air}$

(c) Site 1: α-pinene flux and T_{soil} & SWC

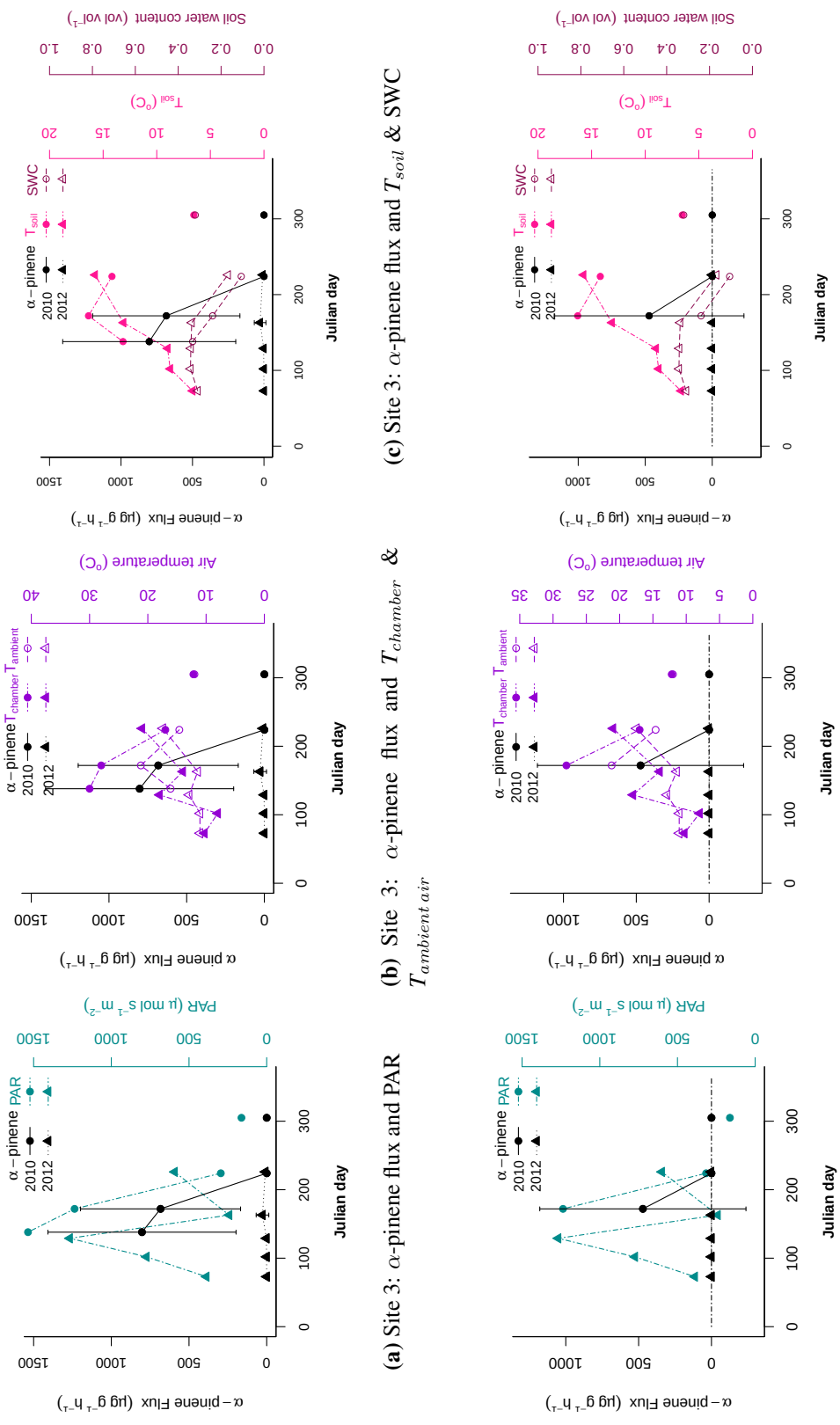


(d) Site 2: α-pinene flux and PAR

(e) Site 2: α-pinene flux and $T_{chamber}$ & $T_{ambient\,air}$

(f) Site 2: α-pinene flux and T_{soil} & SWC

Figure 4.23: Comparison of net α-pinene fluxes from willow with PAR, chamber and ambient air temperature, soil temperature and soil water content (SWC) for 2010 and 2012 for sites 1 and 2. Note different y-axis scales for α-pinene. Error bars on fluxes incorporate analytical and sampling uncertainties.



(a) Site 3: α-pinene flux and PAR

(b) Site 3: α-pinene flux and $T_{chamber}$ & $T_{ambient\ air}$

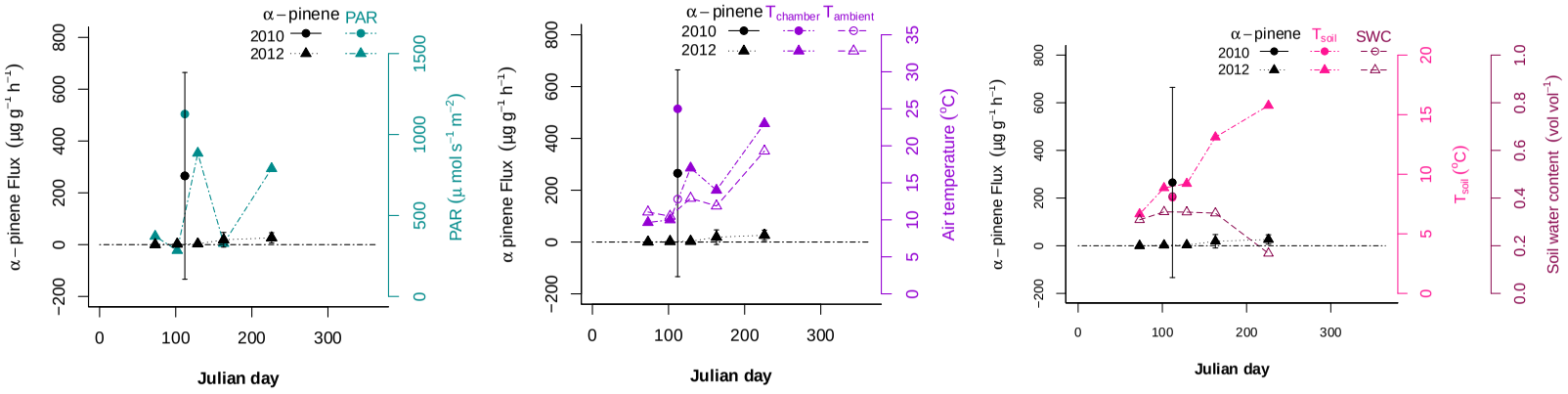
(c) Site 3: α-pinene flux and T_{soil} & SWC

(d) Site 4: α-pinene flux and PAR

(e) Site 4: α-pinene flux and $T_{chamber}$ & $T_{ambient\ air}$

(f) Site 4: α-pinene flux and T_{soil} & SWC

Figure 4.24: Comparison of net α-pinene fluxes from willow with PAR, chamber and ambient air temperature, soil temperature and soil water content (SWC) for 2010 and 2012 for sites 3 and 4. Note different y-axis scales for α-pinene. Error bars on fluxes incorporate analytical and sampling uncertainties.



(a) Site 5: α-pinene flux and PAR

(b) Site 5: α-pinene flux and $T_{chamber}$ & $T_{ambient\,air}$

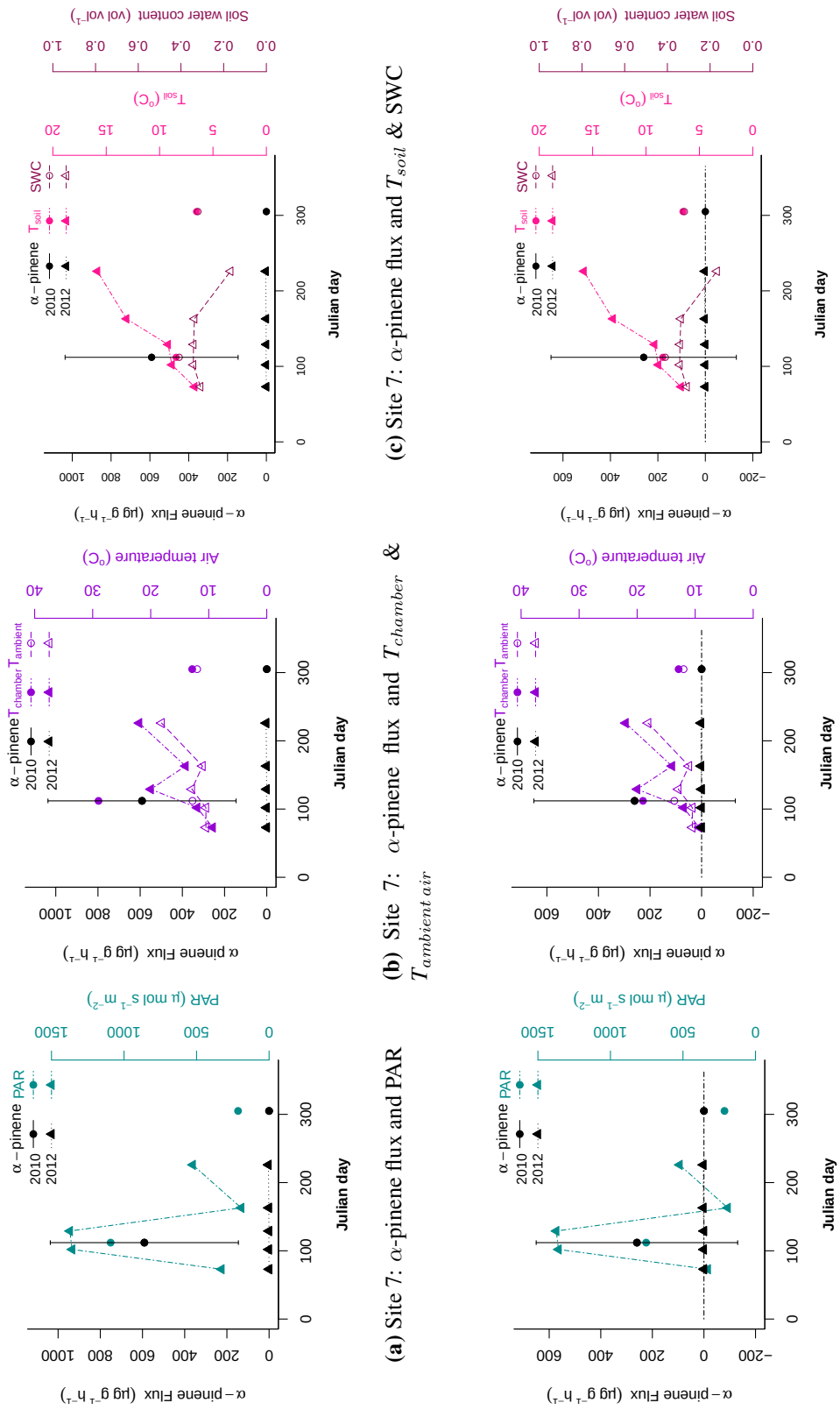
(c) Site 5: α-pinene flux and T_{soil} & SWC

(d) Site 6: α-pinene flux and PAR

(e) Site 6: α-pinene flux and $T_{chamber}$ & $T_{ambient\,air}$

(f) Site 6: α-pinene flux and T_{soil} & SWC

Figure 4.25: Comparison of net α-pinene fluxes from willow with PAR, chamber and ambient air temperature, soil temperature and soil water content (SWC) for 2010 and 2012 for sites 5 and 6. Note different y-axis scales for α-pinene. Error bars on fluxes incorporate analytical and sampling uncertainties.



(a) Site 7: α-pinene flux and PAR

(b) Site 7: α-pinene flux and $T_{chamber}$ & $T_{ambient\ air}$

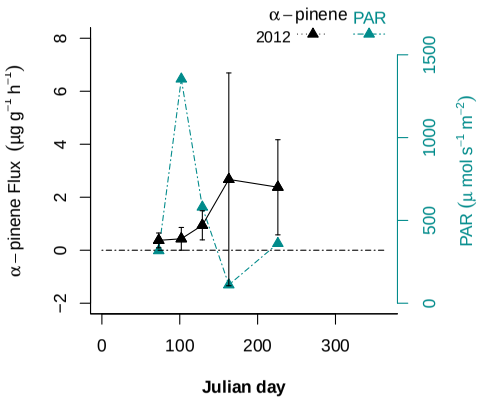
(c) Site 7: α-pinene flux and T_{soil} & SWC

(d) Site 8: α-pinene flux and PAR

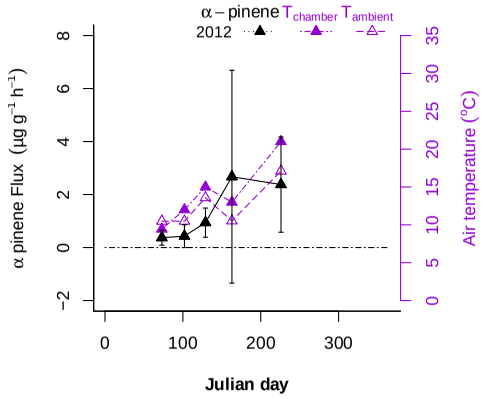
(e) Site 8: α-pinene flux and $T_{chamber}$ & $T_{ambient\ air}$

(f) Site 8: α-pinene flux and T_{soil} & SWC

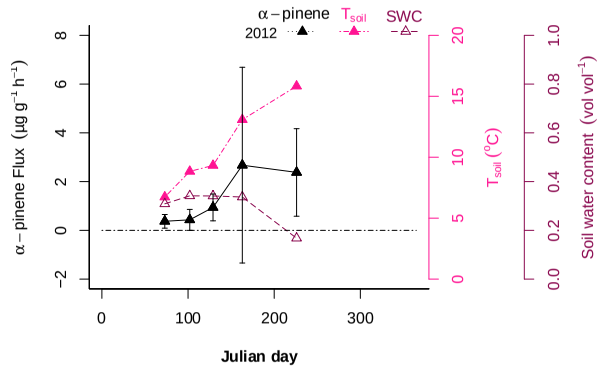
Figure 4.26: Comparison of net α-pinene fluxes from willow with PAR, chamber and ambient air temperature, soil temperature and soil water content (SWC) for 2010 and 2012 for sites 7 and 8. Note different y-axis scales for α-pinene. Error bars on fluxes incorporate analytical and sampling uncertainties.



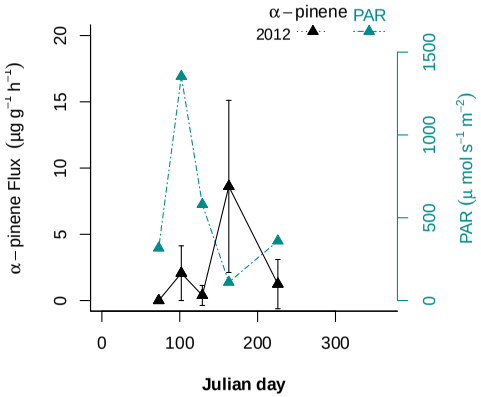
(a) Site 9: α-pinene flux and PAR



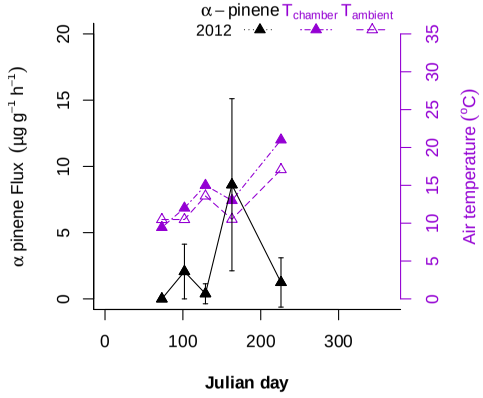
(b) Site 9: α-pinene flux and $T_{chamber}$ & $T_{ambient\,air}$



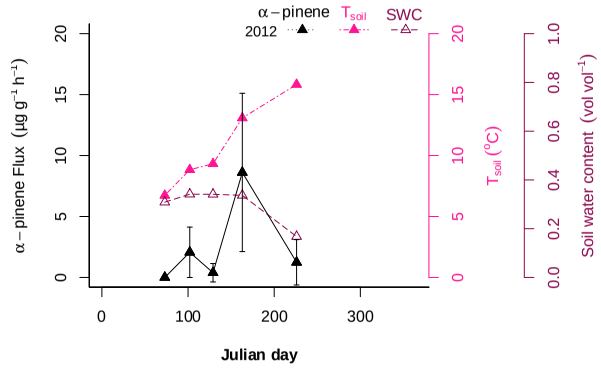
(c) Site 9: α-pinene flux and T_{soil} & SWC



(d) Site 10: α-pinene flux and PAR



(e) Site 10: α-pinene flux and $T_{chamber}$ & $T_{ambient\,air}$



(f) Site 10: α-pinene flux and T_{soil} & SWC

Figure 4.27: Comparison of net α-pinene fluxes from willow with PAR, chamber and ambient air temperature, soil temperature and soil water content (SWC) for 2012 for sites 9 and 10. Note different y-axis scales for α-pinene. Error bars on fluxes incorporate analytical and sampling uncertainties.

β-pinene

From the 132 β-pinene flux measurements made between April 2010 and ending in August 2012, a seasonal trend is somewhat apparent (Figure 4.28). Higher values were measured in summer 2010 and summer 2012, although the 2010 values are obscured by the high values measured in 2010, and zero fluxes during winter. Fluxes measured in 2010 were one or two orders of magnitude higher than those measured in 2012, with large associated uncertainties. Similarly to other BVOC fluxes, this is likely to be due to the growth stage of the willow trees.

Time series of β-pinene fluxes from each individual site across three calendar years from April 2010 to August 2012 with concurrent PAR, ambient and chamber air temperature, soil temperature and soil water content observations are illustrated in Figures 4.29 to 4.33.

β-pinene fluxes of between 28 and 53 $\mu g\, g^{-1}\, h^{-1}$ were measured in April 2010. A wider range of fluxes were measured in May, with a minimum flux of zero and a maximum of 125 $\mu g\, g^{-1}\, h^{-1}$. Fluxes remained high in June, with a range of fluxes of between 38 and 96 $\mu g\, g^{-1}\, h^{-1}$. Fluxes dropped to zero in August and remained at zero over winter (between November 2010 and April 2011) and throughout 2011.

Non-zero fluxes were only measured again in June 2012, with β-pinene fluxes of between 0.1 and 5 $\mu g\, g^{-1}\, h^{-1}$ measured. In August fluxes dropped back to zero. Mean summer fluxes varied between zero in 2011, 1.7 $\mu g\, g^{-1}\, h^{-1}$ in 2012 and 72 $\mu g\, g^{-1}\, h^{-1}$ during 2010.

The maximum β-pinene flux measured in 2010 was 125 $\mu g\, g^{-1}\, h^{-1}$ from site 3, where the highest isoprene and α-pinene fluxes were also measured (Table 4.9a). Mean fluxes ranged from 14 to 55 $\mu g\, g^{-1}\, h^{-1}$. All of the maximum fluxes measured throughout the campaign were measured in 2010 with the exception of sites 9 and 10 which were not sampled in 2010. A mean flux of 29 $\mu g\, g^{-1}\, h^{-1}$ was calculated from all fluxes recorded at all sites during 2010.

The mean β-pinene flux calculated for all measurements at all sites in 2012 was 0.35$\mu g\, g^{-1}\, h^{-1}$, which is two orders of magnitude lower than that calculated for 2010 (Table 4.9b). Fluxes were similar at all sites (mean fluxes between 0.1 and 5 $\mu g\, g^{-1}\, h^{-1}$). A mean flux of 5.5$\mu g\, g^{-1}\, h^{-1}$ was calculated from all results from all three years.

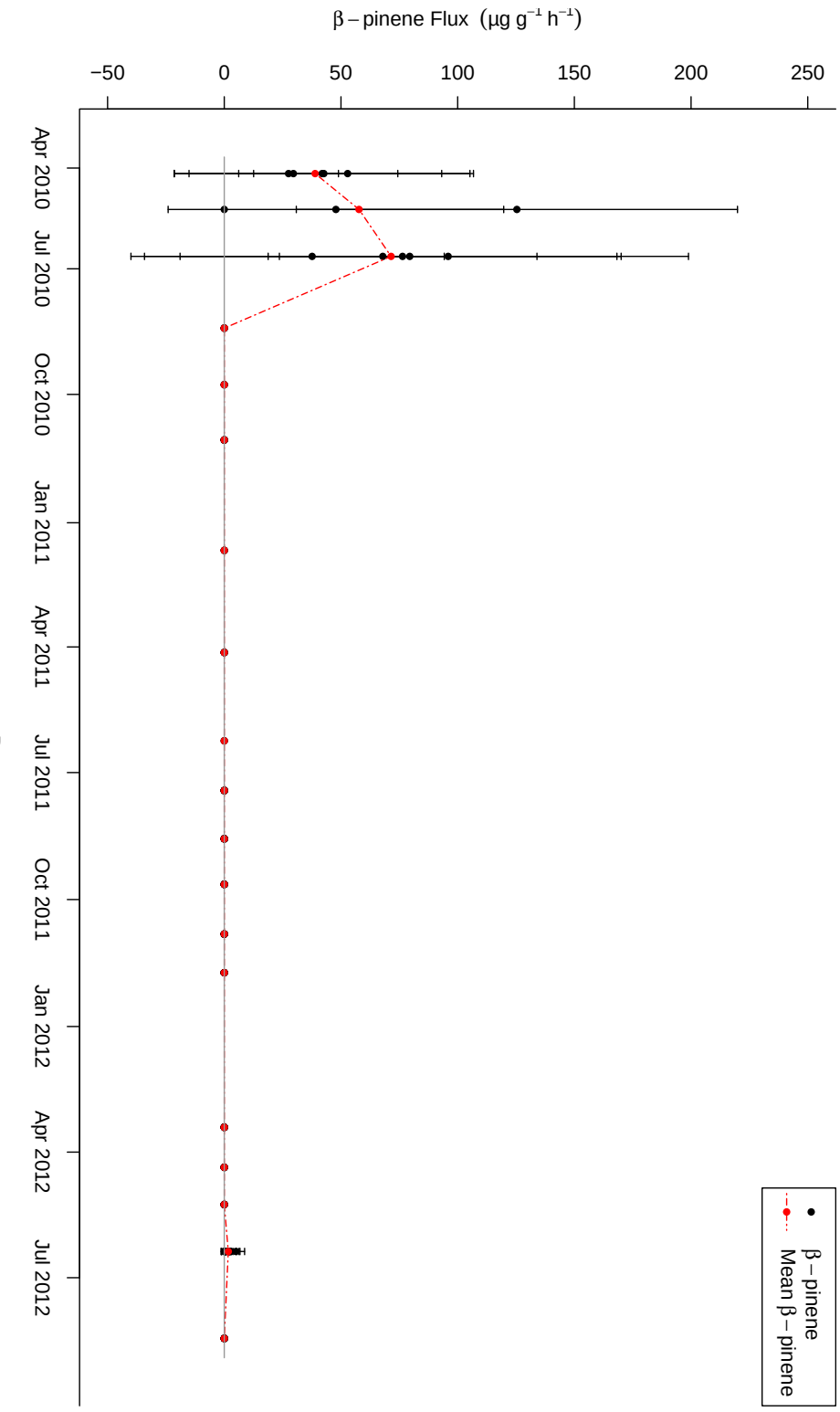


Figure 4.28: β-pinene fluxes from willow at the Brattleby fieldsite at all ten sampling points and the mean of those values on each sampling occasion from 2010 to 2012. Error bars on fluxes incorporate analytical and sampling uncertainties (as described in Section 2.6.1).

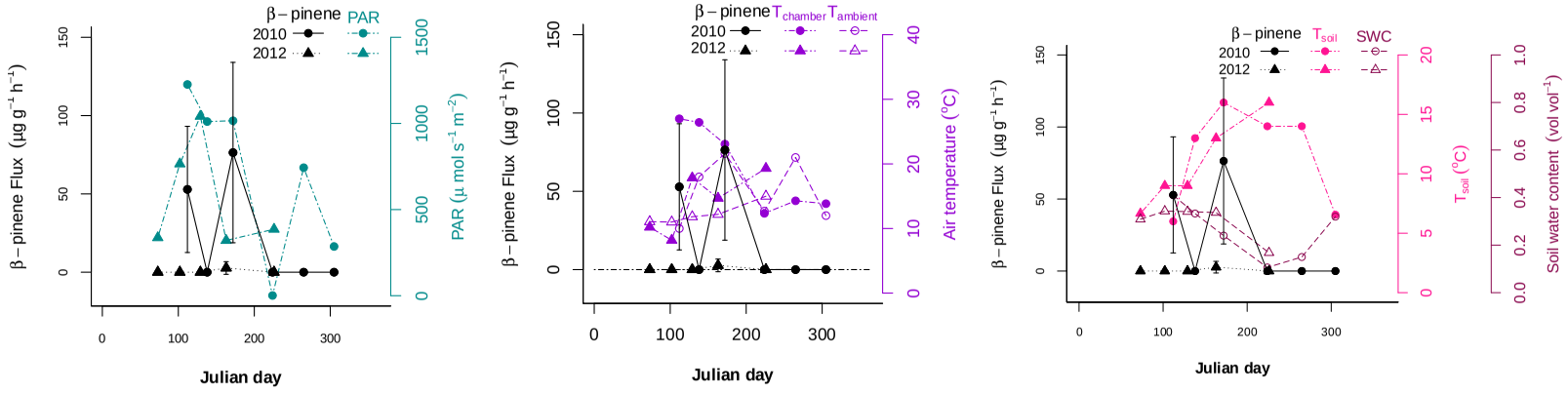
Table 4.9: Mean, median, minimum and maximum net β-pinene fluxes from SRC willow at Brattleby during 2010 (a) and 2012 (b). All flux values are in $\mu g\, g^{-1}\, h^{-1}$. The final column gives the number of measurements made. The last row summarises all fluxes from all sites.

(a) β-pinene flux ($\mu g\, g^{-1}\, h^{-1}$) - 2010

Site	Mean	Median	Min	Max	Number
W1	21.5	0.00	0.00	76.4	6
W2	26.2	14.8	0.00	79.5	6
W3	55.3	48.0	0.00	125	4
W4	22.6	0.00	0.00	67.9	3
W5	41.9	41.9	41.9	41.9	1
W6	37.7	37.7	37.7	37.7	1
W7	13.8	13.8	0.00	27.6	2
W8	21.3	21.3	0.00	42.7	2
All	29.0	0.00	0.00	125	25

(b) β-pinene flux ($\mu g\, g^{-1}\, h^{-1}$) - 2012

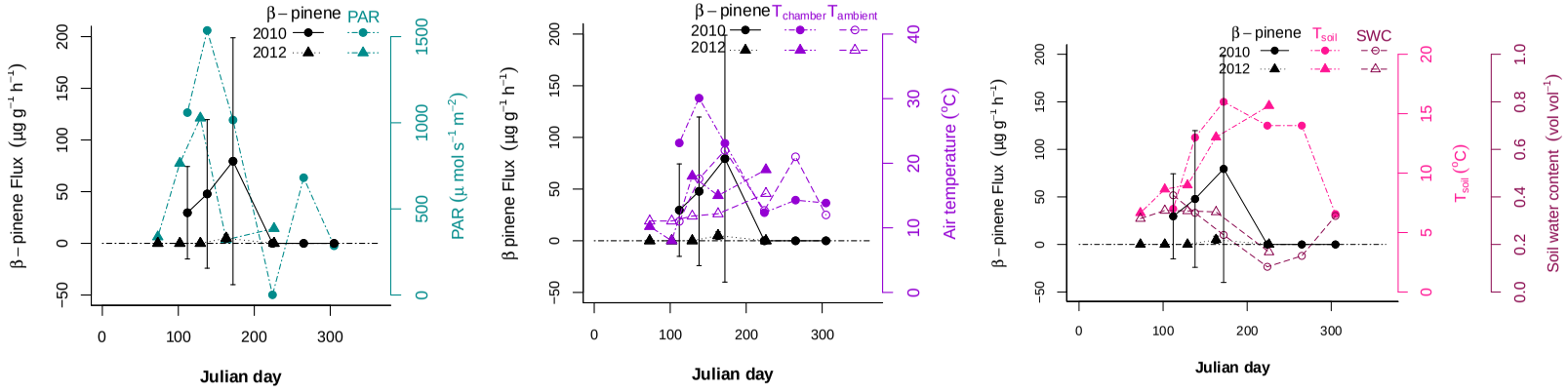
Site	Mean	Median	Min	Max	Number
W1	0.54	0.00	0.00	2.69	5
W2	0.99	0.00	0.00	4.96	5
W3	0.42	0.00	0.00	2.12	5
W4	0.02	0.00	0.00	0.08	5
W5	0.50	0.00	0.00	2.52	5
W6	0.42	0.00	0.00	2.12	5
W7	0.06	0.00	0.00	0.32	5
W8	0.10	0.00	0.00	0.40	4
W9	0.05	0.00	0.00	0.27	5
W10	0.34	0.00	0.00	1.69	5
All	0.35	0.00	0.00	4.96	49



(a) Site 1: β-pinene flux and PAR

(b) Site 1: β-pinene flux and $T_{chamber}$ & $T_{ambient\,air}$

(c) Site 1: β-pinene flux and T_{soil} & SWC

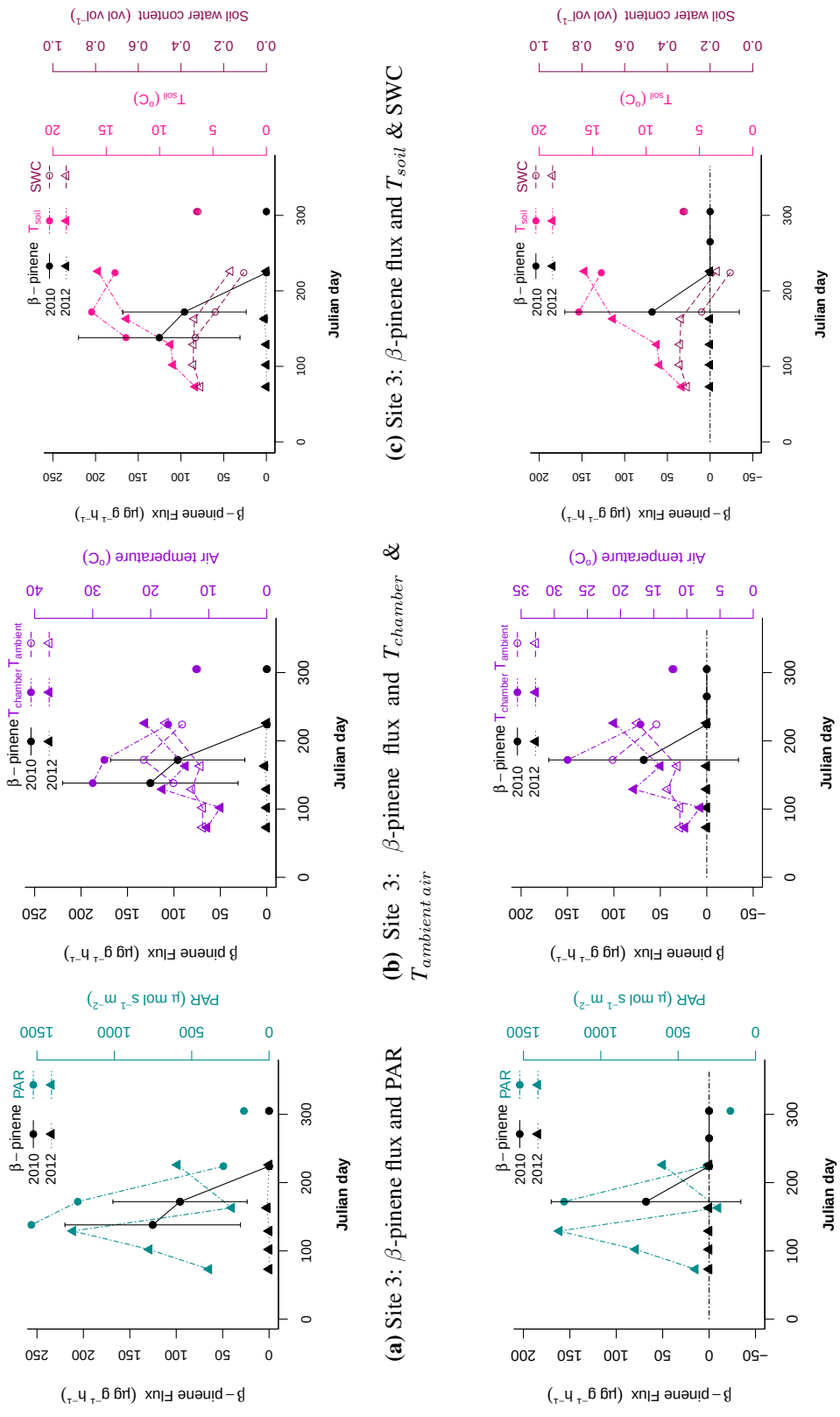


(d) Site 2: β-pinene flux and PAR

(e) Site 2: β-pinene flux and $T_{chamber}$ & $T_{ambient\,air}$

(f) Site 2: β-pinene flux and T_{soil} & SWC

Figure 4.29: Comparison of net β-pinene fluxes from willow with PAR, chamber and ambient air temperature, soil temperature and soil water content (SWC) for 2010 and 2012 for sites 1 and 2. Note different y-axis scales for β-pinene. Error bars on fluxes incorporate analytical and sampling uncertainties.



(a) Site 3: β-pinene flux and PAR

(b) Site 3: β-pinene flux and $T_{chamber}$ & $T_{ambient\ air}$

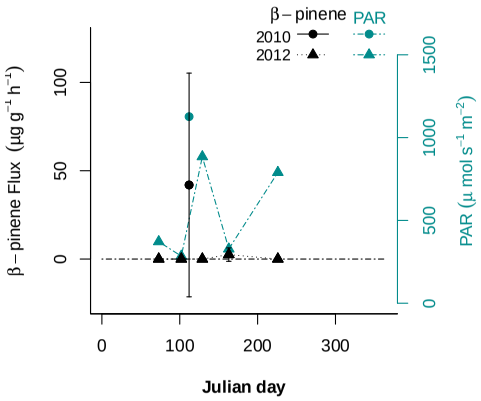
(c) Site 3: β-pinene flux and T_{soil} & SWC

(d) Site 4: β-pinene flux and PAR

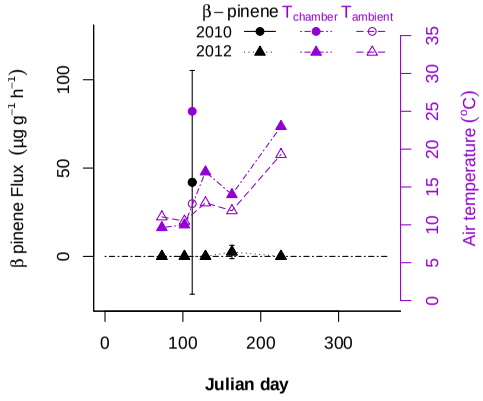
(e) Site 4: β-pinene flux and $T_{chamber}$ & $T_{ambient\ air}$

(f) Site 4: β-pinene flux and T_{soil} & SWC

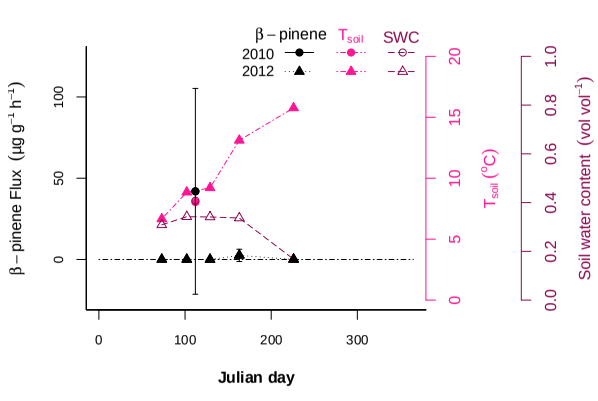
Figure 4.30: Comparison of net β-pinene fluxes from willow with PAR, chamber and ambient air temperature, soil temperature and soil water content (SWC) for 2010 and 2012 for sites 3 and 4. Note different y-axis scales for β-pinene. Error bars on fluxes incorporate analytical and sampling uncertainties.



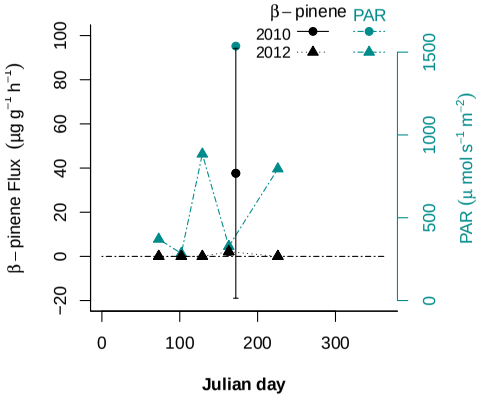
(a) Site 5: β-pinene flux and PAR



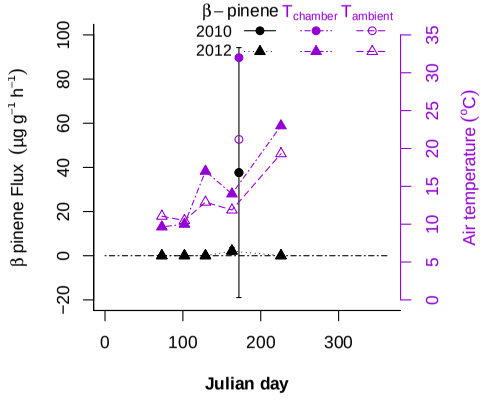
(b) Site 5: β-pinene flux and $T_{chamber}$ & $T_{ambient\,air}$



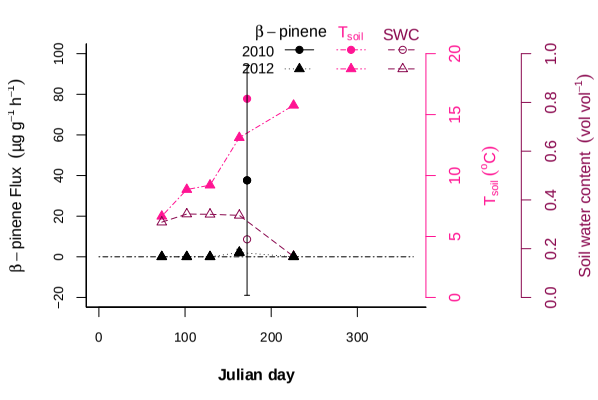
(c) Site 5: β-pinene flux and T_{soil} & SWC



(d) Site 6: β-pinene flux and PAR

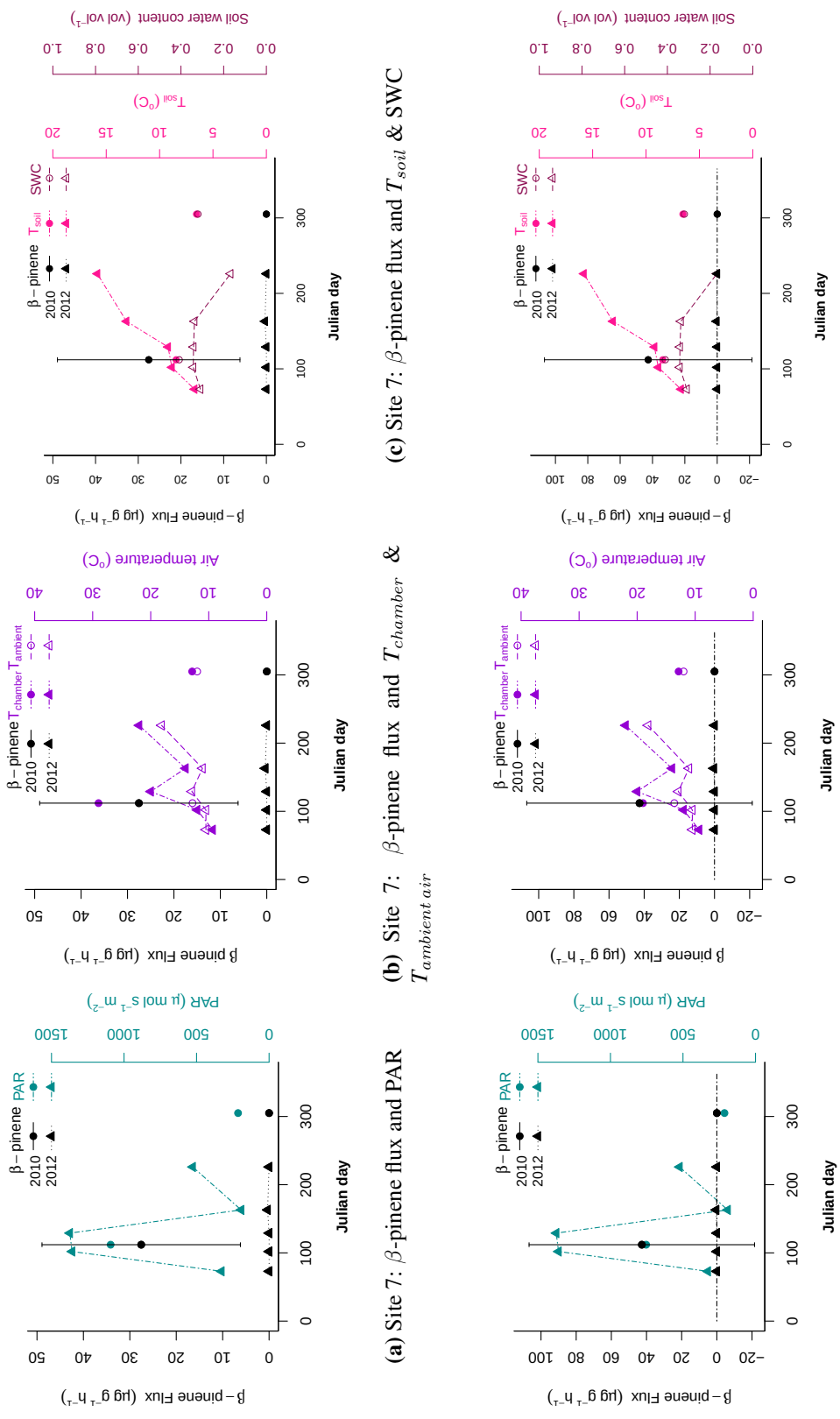


(e) Site 6: β-pinene flux and $T_{chamber}$ & $T_{ambient\,air}$



(f) Site 6: β-pinene flux and T_{soil} & SWC

Figure 4.31: Comparison of net β-pinene fluxes from willow with PAR, chamber and ambient air temperature, soil temperature and soil water content (SWC) for 2010 and 2012 for sites 5 and 6. Note different y-axis scales for β-pinene. Error bars on fluxes incorporate analytical and sampling uncertainties.



(a) Site 7: β-pinene flux and PAR

(b) Site 7: β-pinene flux and $T_{chamber}$ & $T_{ambient\ air}$

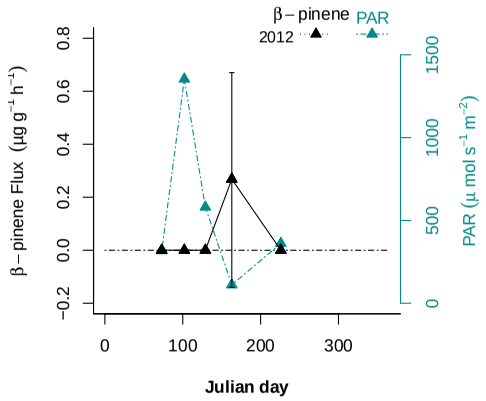
(c) Site 7: β-pinene flux and T_{soil} & SWC

(d) Site 8: β-pinene flux and PAR

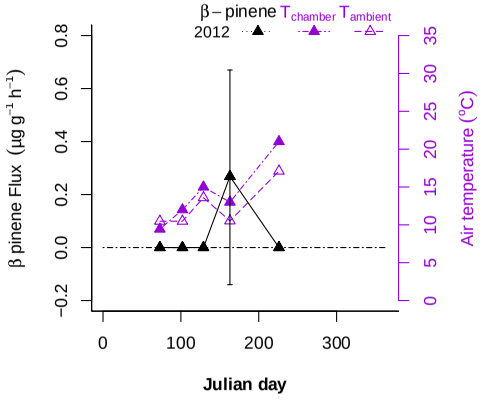
(e) Site 8: β-pinene flux and $T_{chamber}$ & $T_{ambient\ air}$

(f) Site 8: β-pinene flux and T_{soil} & SWC

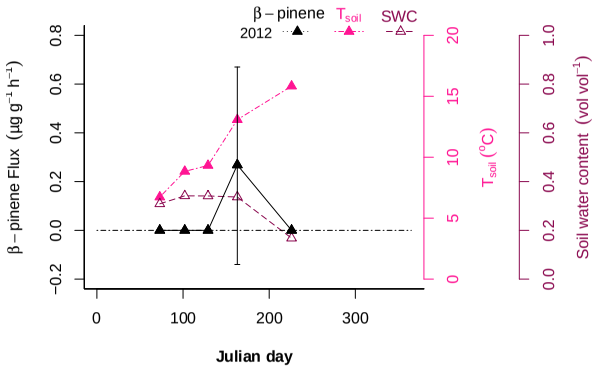
Figure 4.32: Comparison of net β-pinene fluxes from willow with PAR, chamber and ambient air temperature, soil temperature and soil water content (SWC) for 2010 and 2012 for sites 7 and 8. Note different y-axis scales for β-pinene. Error bars on fluxes incorporate analytical and sampling uncertainties.



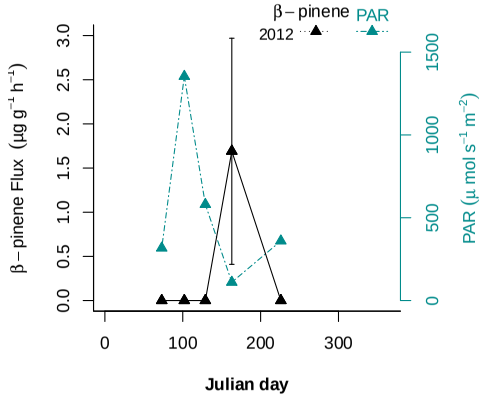
(a) Site 9: β-pinene flux and PAR



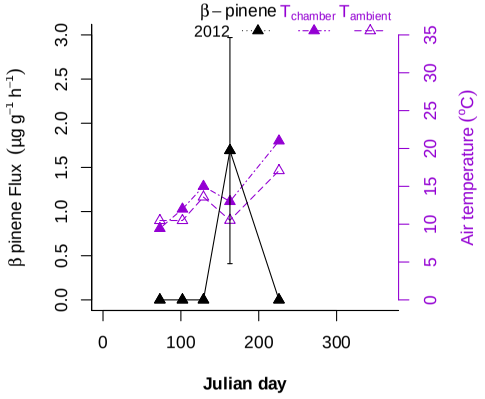
(b) Site 9: β-pinene flux and $T_{chamber}$ & $T_{ambient\,air}$



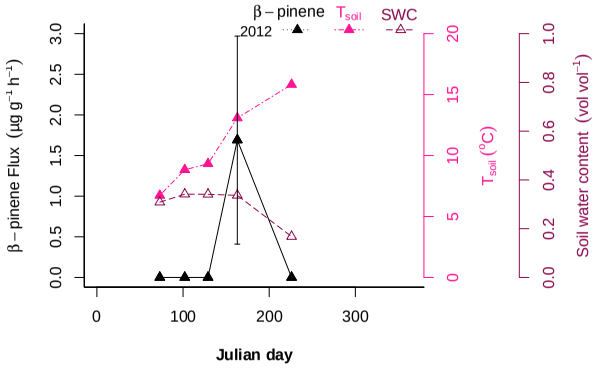
(c) Site 9: β-pinene flux and T_{soil} & SWC



(d) Site 10: β-pinene flux and PAR



(e) Site 10: β-pinene flux and $T_{chamber}$ & $T_{ambient\,air}$



(f) Site 10: β-pinene flux and T_{soil} & SWC

Figure 4.33: Comparison of net β-pinene fluxes from willow with PAR, chamber and ambient air temperature, soil temperature and soil water content (SWC) for 2012 for sites 9 and 10. Note different y-axis scales for β-pinene. Error bars on fluxes incorporate analytical and sampling uncertainties.

Limonene

Similarly to β-pinene, a seasonal trend was suggested by the limonene fluxes measured (132 flux measurements made between April 2010 and ending in August 2012). Higher fluxes were measured in summer and zero fluxes in winter (Figure 4.34). However, unlike isoprene, α-pinene and β-pinene fluxes, limonene fluxes were higher in 2012 than in 2010. As with the other BVOCs mentioned, zero fluxes were measured throughout 2011. This is most likely due to the growth stage of the plant, as the trees were coppiced in winter 2010 and the vegetation was therefore young when measurements were taken in 2011. The higher fluxes of limonene in 2012 from younger trees may also be linked to the physiology of the trees as the composition of the BVOCs emitted from vegetation has previously been shown to change with growth stage (Hakola et al., 1998; Kesselmeier and Staudt, 1999).

Time series of limonene fluxes from each individual site across three calendar years from April 2010 to August 2012 with concurrent PAR, ambient and chamber air temperature, soil temperature and soil water content observations are illustrated in Figures 4.35 to 4.39.

Limonene fluxes of between 6.4 and 31 $\mu g\, g^{-1}\, h^{-1}$ were measured in April 2010. Lower fluxes were measured in May, with a range of fluxes between zero and 17 $\mu g\, g^{-1}\, h^{-1}$. Fluxes decreased again in June, with a range of fluxes of between zero and 9 $\mu g\, g^{-1}\, h^{-1}$. Fluxes dropped to zero in August and remained at zero over winter (between November 2010 and April 2011) and throughout all measurements in 2011.

Non-zero fluxes were only measured again in April 2012, when a maximum limonene flux of 0.5 $\mu g\, g^{-1}\, h^{-1}$ was measured. Fluxes dropped to zero in May and then increased significantly in June, with a range of fluxes between 1.2 and 73 $\mu g\, g^{-1}\, h^{-1}$. Fluxes increased substantially again in August with a range of fluxes between zero and 80 $\mu g\, g^{-1}\, h^{-1}$ measured. Mean summer fluxes varied between zero in 2011, 17 $\mu g\, g^{-1}\, h^{-1}$ in 2010 and 22 $\mu g\, g^{-1}\, h^{-1}$ during 2012.

The maximum limonene flux measured in 2010 was 31 $\mu g\, g^{-1}\, h^{-1}$ from site 7 (Table 4.10a). Mean fluxes ranged from 2.1 to 15 $\mu g\, g^{-1}\, h^{-1}$. A mean flux of 4.5 $\mu g\, g^{-1}\, h^{-1}$ was calculated from all fluxes recorded at all sites during 2010.

The mean limonene flux calculated for all measurements at all sites in 2012 was 7.8 $\mu g\, g^{-1}\, h^{-1}$, which is almost twice that calculated for 2010 (Table 4.10b). Higher mean fluxes were measured at sites 1 - 3 (between 9 and 20 $\mu g\, g^{-1}\, h^{-1}$) and lower at sites 4 - 10 (between 0.3 and 7 $\mu g\, g^{-1}\, h^{-1}$). The maximum limonene flux measured in 2012 was 80 $\mu g\, g^{-1}\, h^{-1}$ which is over double that measured in 2010. All of the maximum fluxes measured throughout the campaign were measured in 2012 with the exception of sites 4 and 8. A mean flux of 3.7 $\mu g\, g^{-1}\, h^{-1}$ was calculated from all results from all three years.

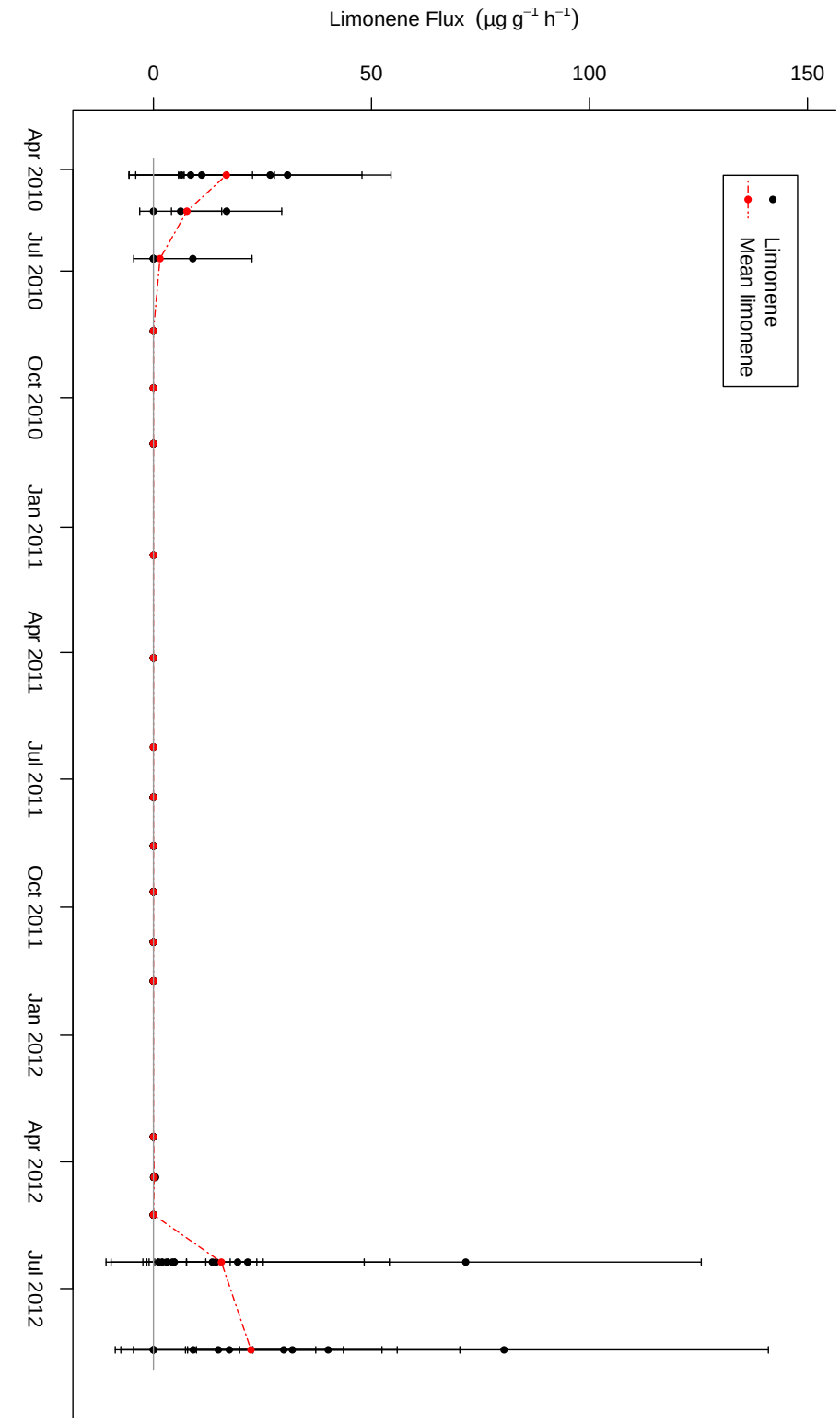


Figure 4.34: Limonene fluxes from willow at the Brattleby fieldsite at all ten sampling points and the mean of those values on each sampling occasion from 2010 to 2012. Error bars on fluxes incorporate analytical and sampling uncertainties (as described in Section 2.6.1).

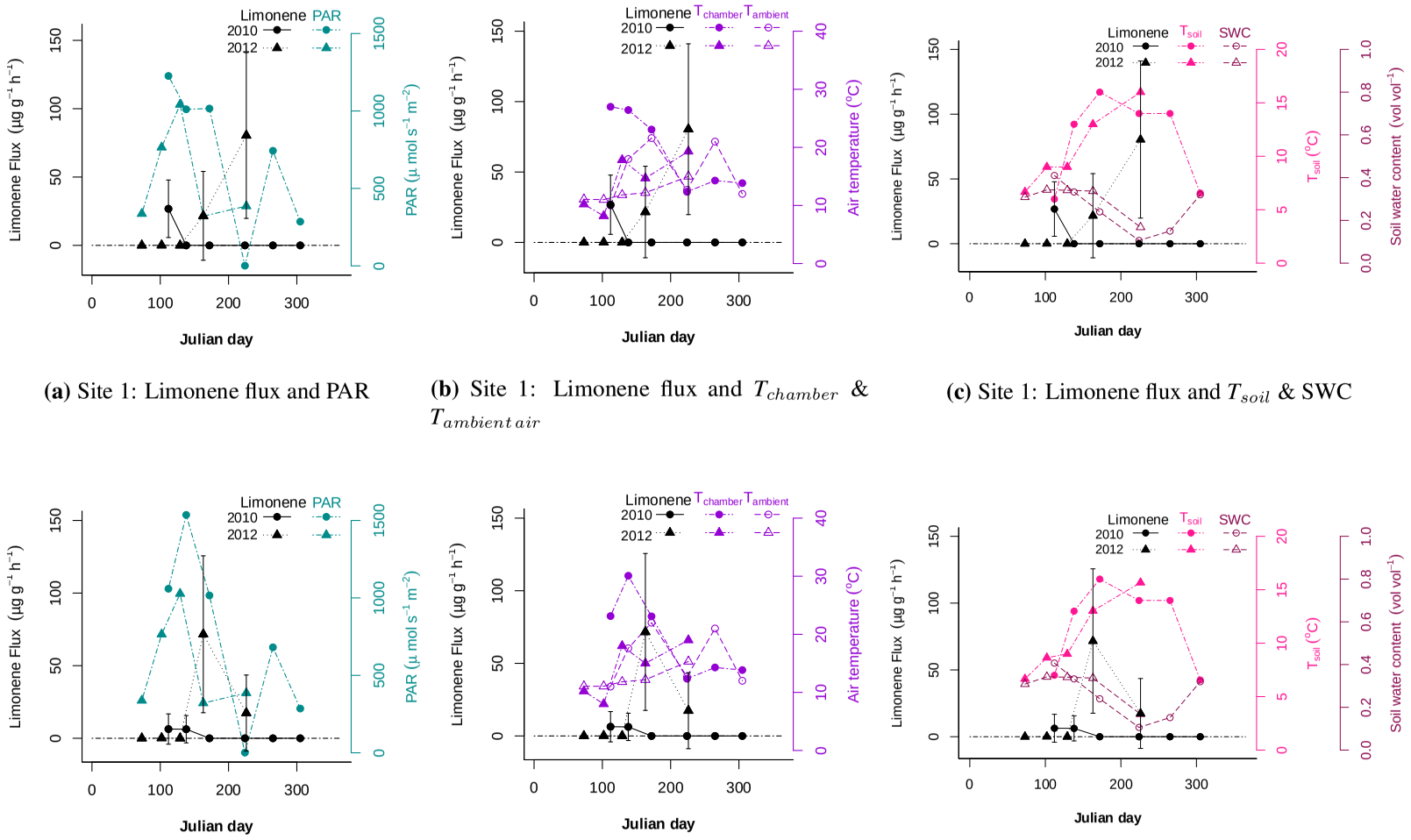
Table 4.10: Mean, median, minimum and maximum net limonene fluxes from SRC willow at Brattleby during 2010 (a) and 2012 (b). All flux values are in $\mu g\, g^{-1}\, h^{-1}$. The final column gives the number of measurements made. The last row summarises all fluxes from all sites.

(a) Limonene flux ($\mu g\, g^{-1}\, h^{-1}$) - 2010

Site	Mean	Median	Min	Max	Number
W1	4.46	0.00	0.00	26.8	6
W2	2.10	0.00	0.00	6.36	6
W3	4.19	0.00	0.00	16.8	4
W4	3.01	0.00	0.00	9.03	3
W5	4.28	4.28	0.00	8.55	1
W6	0.00	0.00	0.00	0.00	1
W7	15.4	15.4	0.00	30.8	2
W8	5.54	5.54	0.00	11.1	2
All	4.45	0.00	0.00	30.8	25

(b) Limonene flux ($\mu g\, g^{-1}\, h^{-1}$) - 2012

Site	Mean	Median	Min	Max	Number
W1	20.4	0.06	0.00	80.4	5
W2	17.8	0.14	0.00	71.6	5
W3	9.02	0.24	0.00	40.1	5
W4	0.25	0.00	0.00	1.18	5
W5	3.88	0.00	0.00	19.3	5
W6	2.90	0.00	0.00	14.4	5
W7	7.04	0.33	0.00	31.9	5
W8	3.38	2.20	0.00	9.12	4
W9	6.38	0.06	0.00	29.9	5
W10	5.77	0.47	0.00	14.9	5
All	7.77	0.06	0.00	80.4	49



(a) Site 1: Limonene flux and PAR

(b) Site 1: Limonene flux and $T_{chamber}$ & $T_{ambient\,air}$

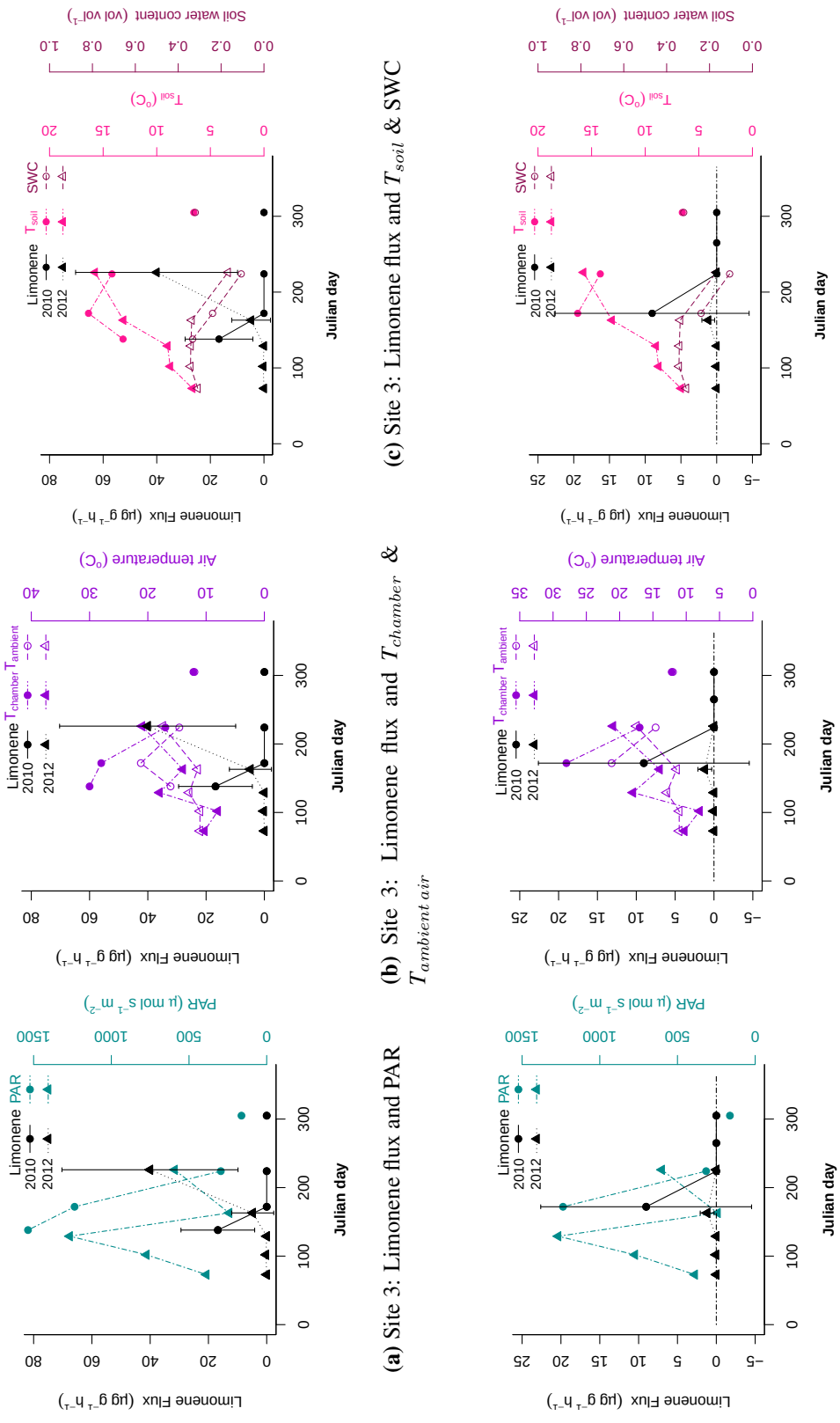
(c) Site 1: Limonene flux and T_{soil} & SWC

(d) Site 2: Limonene flux and PAR

(e) Site 2: Limonene flux and $T_{chamber}$ & $T_{ambient\,air}$

(f) Site 2: Limonene flux and T_{soil} & SWC

Figure 4.35: Comparison of net limonene fluxes from willow with PAR, chamber and ambient air temperature, soil temperature and soil water content (SWC) for 2010 and 2012 for sites 1 and 2. Note different y-axis scales for limonene. Error bars on fluxes incorporate analytical and sampling uncertainties.



(a) Site 3: Limonene flux and PAR

(b) Site 3: Limonene flux and $T_{chamber}$ & $T_{ambient\ air}$

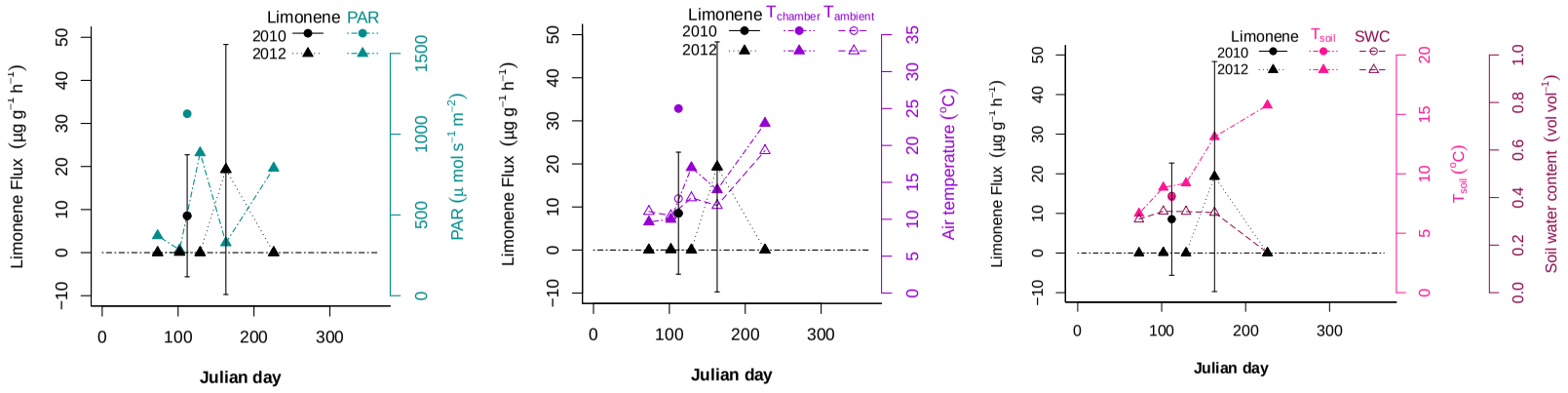
(c) Site 3: Limonene flux and T_{soil} & SWC

(d) Site 4: Limonene flux and PAR

(e) Site 4: Limonene flux and $T_{chamber}$ & $T_{ambient\ air}$

(f) Site 4: Limonene flux and T_{soil} & SWC

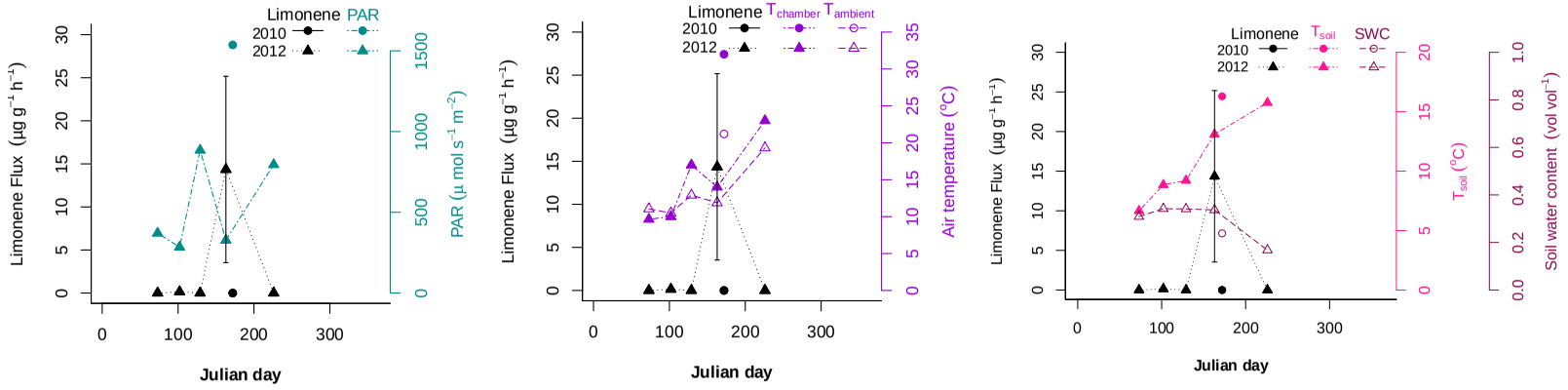
Figure 4.36: Comparison of net limonene fluxes from willow with PAR, chamber and ambient air temperature, soil temperature and soil water content (SWC) for 2010 and 2012 for sites 3 and 4. Note different y-axis scales for limonene. Error bars on fluxes incorporate analytical and sampling uncertainties.



(a) Site 5: Limonene flux and PAR

(b) Site 5: Limonene flux and $T_{chamber}$ & $T_{ambient\,air}$

(c) Site 5: Limonene flux and T_{soil} & SWC

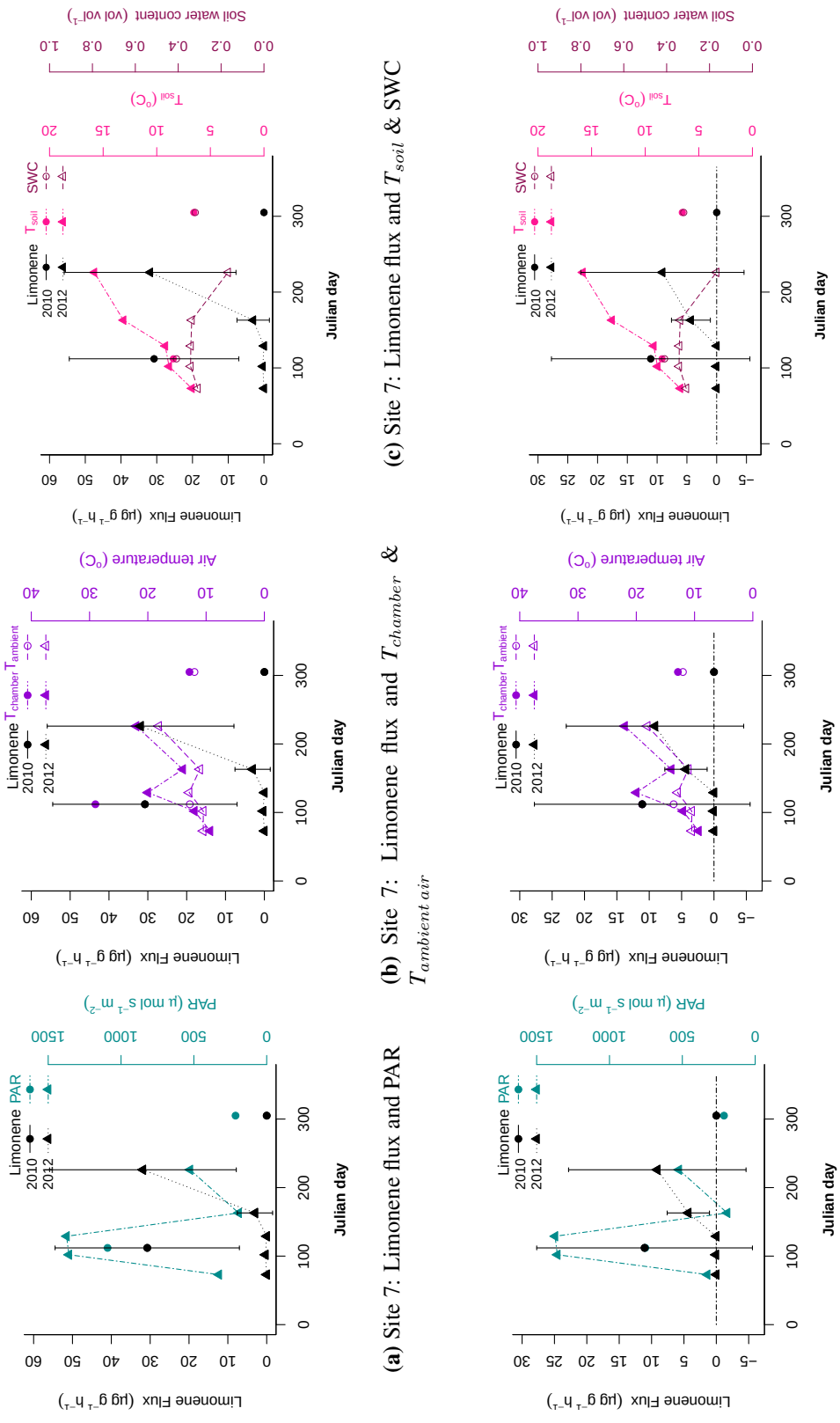


(d) Site 6: Limonene flux and PAR

(e) Site 6: Limonene flux and $T_{chamber}$ & $T_{ambient\,air}$

(f) Site 6: Limonene flux and T_{soil} & SWC

Figure 4.37: Comparison of net limonene fluxes from willow with PAR, chamber and ambient air temperature, soil temperature and soil water content (SWC) for 2010 and 2012 for sites 5 and 6. Note different y-axis scales for limonene. Error bars on fluxes incorporate analytical and sampling uncertainties.



(a) Site 7: Limonene flux and PAR

(b) Site 7: Limonene flux and $T_{chamber}$ & $T_{ambient\ air}$

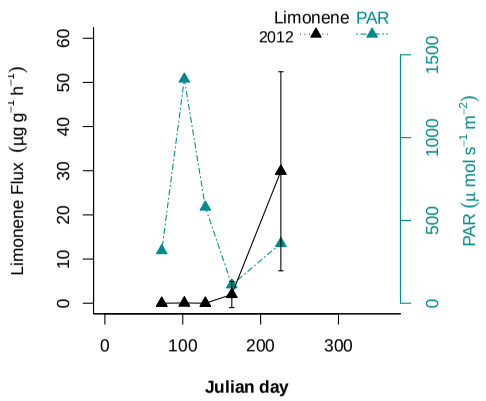
(c) Site 7: Limonene flux and T_{soil} & SWC

(d) Site 8: Limonene flux and PAR

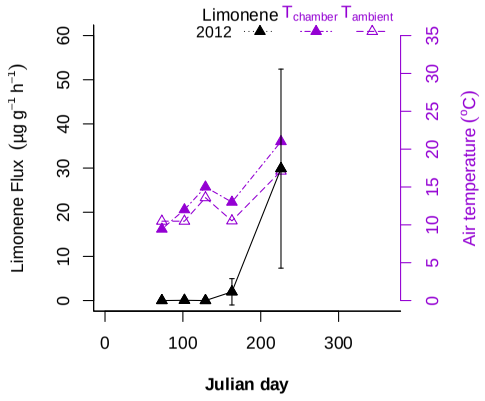
(e) Site 8: Limonene flux and $T_{chamber}$ & $T_{ambient\ air}$

(f) Site 8: Limonene flux and T_{soil} & SWC

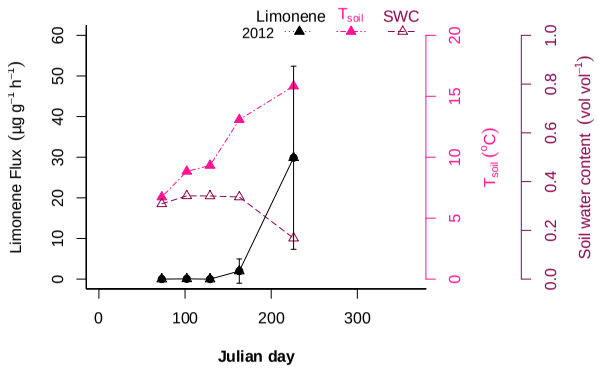
Figure 4.38: Comparison of net limonene fluxes from willow with PAR, chamber and ambient air temperature, soil temperature and soil water content (SWC) for 2010 and 2012 for sites 7 and 8. Note different y-axis scales for limonene. Error bars on fluxes incorporate analytical and sampling uncertainties.



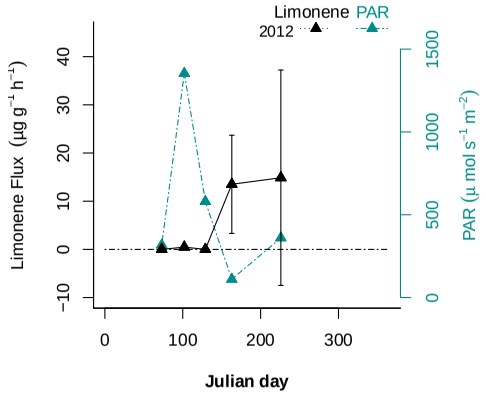
(a) Site 9: Limonene flux and PAR



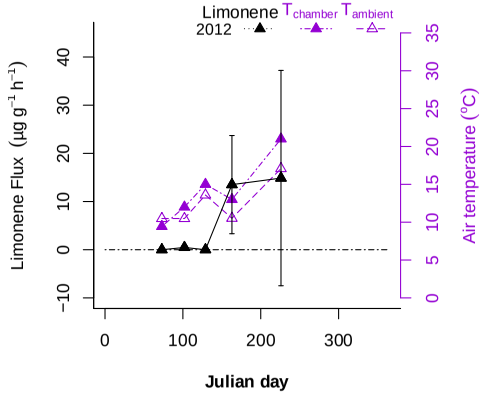
(b) Site 9: Limonene flux and $T_{chamber}$ & $T_{ambient\,air}$



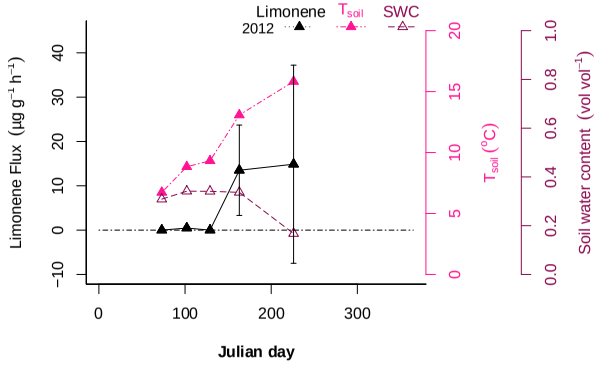
(c) Site 9: Limonene flux and T_{soil} & SWC



(d) Site 10: Limonene flux and PAR



(e) Site 10: Limonene flux and $T_{chamber}$ & $T_{ambient\,air}$



(f) Site 10: Limonene flux and T_{soil} & SWC

Figure 4.39: Comparison of net limonene fluxes from willow with PAR, chamber and ambient air temperature, soil temperature and soil water content (SWC) for 2012 for sites 9 and 10. Note different y-axis scales for limonene. Error bars on fluxes incorporate analytical and sampling uncertainties.

δ-3-carene

A seasonal trend is suggested in the δ-3-carene fluxes measured between April 2010 and ending in August 2012 (Figure 4.40). Higher fluxes were measured in summer and zero fluxes in winter. As with fluxes of isoprene, α-pinene and β-pinene δ-3-carene fluxes were higher in 2010 than in 2012 and zero fluxes were measured throughout 2011, likely due to the growth stage of the plant.

The seasonal trend in δ-3-carene fluxes is somewhat obscured by the high values measured in 2010. Fluxes measured in 2010 were an order of magnitude higher than those measured in 2012, with large associated uncertainties.

Fluxes ranged between 5.4 and 268 $\mu g\, g^{-1}\, h^{-1}$ in April 2010. A similar range of 48 to 260 $\mu g\, g^{-1}\, h^{-1}$ was measured in May. Fluxes remained high in June, with a range of fluxes of between 49 and 119 $\mu g\, g^{-1}\, h^{-1}$. Fluxes dropped to zero in August and remained at zero over winter (between November 2010 and April 2011) and throughout 2011.

Non-zero fluxes were only measured again in June 2012, when a range of fluxes between zero and 17 $\mu g\, g^{-1}\, h^{-1}$ was measured. Fluxes increased slightly in August to between 2.5 and 22 $\mu g\, g^{-1}\, h^{-1}$. Mean summer fluxes varied between zero in 2011, 7.1 $\mu g\, g^{-1}\, h^{-1}$ in 2012 and 133 $\mu g\, g^{-1}\, h^{-1}$ during 2010.

The maximum δ-3-carene flux measured in 2010 was 268 $\mu g\, g^{-1}\, h^{-1}$ from site 7, where the highest limonene flux was also measured (Table 4.11a). Mean fluxes ranged from 19 to 134 $\mu g\, g^{-1}\, h^{-1}$. A mean flux of 57 $\mu g\, g^{-1}\, h^{-1}$ was calculated from all fluxes recorded at all sites during 2010. All of the maximum fluxes measured throughout the campaign were measured in 2010 with the exception of sites 9 and 10 which were not measured in 2010.

The mean δ-3-carene flux calculated for all measurements at all sites in 2012 was 2.2 $\mu g\, g^{-1}\, h^{-1}$, which is an order of magnitude lower than that calculated for 2010 (Table 4.11b). Higher mean fluxes were measured at sites 1-3 and 5 (between 2.4 and 5.2 $\mu g\, g^{-1}\, h^{-1}$) and lower at the remaining sites (between 0.67 and 1.5 $\mu g\, g^{-1}\, h^{-1}$). A mean flux of 11 $\mu g\, g^{-1}\, h^{-1}$ was calculated from all results from all three years.

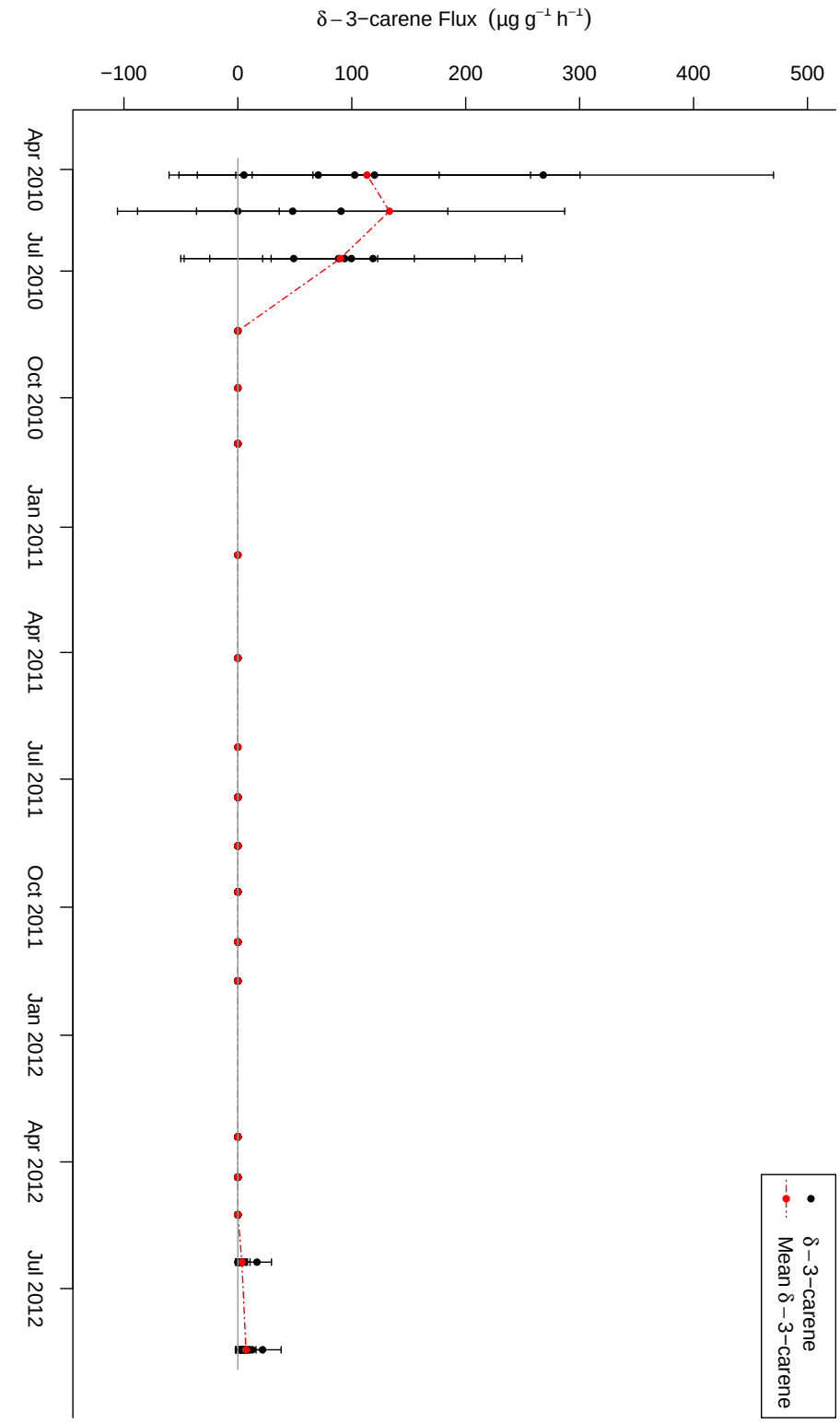


Figure 4.40: δ-3-carene fluxes from willow at the Bratleby fieldsite at all ten sampling points and the mean of those values on each sampling occasion from 2010 to 2012. Error bars on fluxes incorporate analytical and sampling uncertainties (as described in Section 2.6.1).

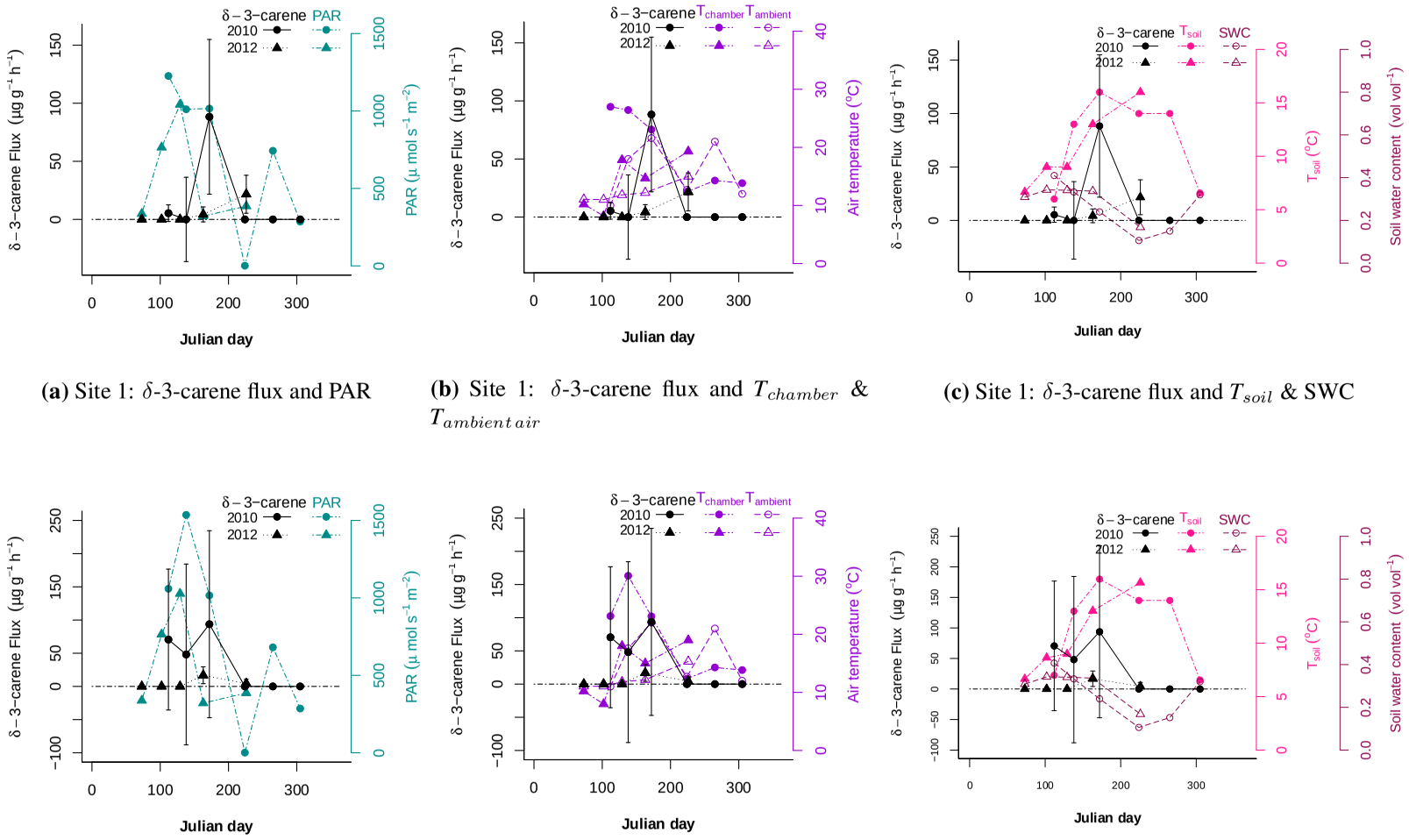
Table 4.11: Mean, median, minimum and maximum net δ-3-carene fluxes from SRC willow at Brattleby during 2010 (a) and 2012 (b). All flux values are in $\mu g\, g^{-1}\, h^{-1}$. The final column gives the number of measurements made. The last row summarises all fluxes from all sites.

(a) δ-3-carene flux ($\mu g\, g^{-1}\, h^{-1}$) - 2010

Site	Mean	Median	Min	Max	Number
W1	18.7	0.00	0.00	88.3	5
W2	35.4	24.1	0.00	93.7	6
W3	52.3	45.3	0.00	119	4
W4	90.0	49.8	0.00	260	4
W5	103	103	103	103	1
W6	49.1	49.1	49.1	49.1	1
W7	134	134	0.00	268	2
W8	60.0	60.00	0.00	120	2
All	56.6	5.35	0.00	268	25

(b) δ-3-carene flux ($\mu g\, g^{-1}\, h^{-1}$) - 2012

Site	Mean	Median	Min	Max	Number
W1	5.19	0.00	0.00	21.7	5
W2	4.23	0.00	0.00	16.8	5
W3	2.35	0.00	0.00	9.08	5
W4	0.67	0.00	0.00	3.33	5
W5	3.12	0.00	0.00	12.7	5
W6	1.54	0.00	0.00	4.82	5
W7	1.32	0.00	0.00	6.22	5
W8	1.14	0.90	0.00	2.76	4
W9	1.16	0.00	0.00	5.24	5
W10	0.67	0.00	0.00	2.46	5
All	2.16	0.00	0.00	21.7	49



(a) Site 1: δ-3-carene flux and PAR

(b) Site 1: δ-3-carene flux and $T_{chamber}$ & $T_{ambient\,air}$

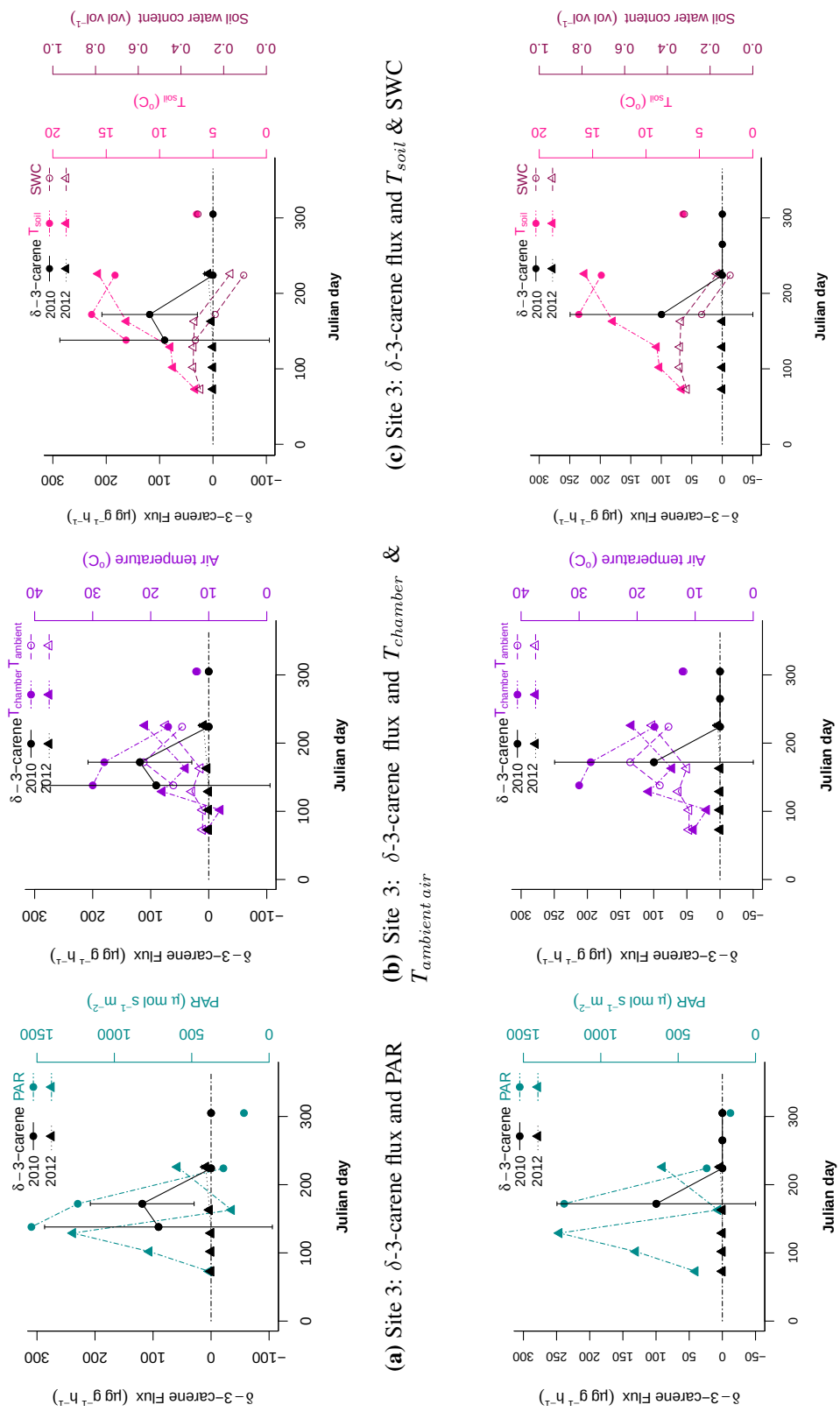
(c) Site 1: δ-3-carene flux and T_{soil} & SWC

(d) Site 2: δ-3-carene flux and PAR

(e) Site 2: δ-3-carene flux and $T_{chamber}$ & $T_{ambient\,air}$

(f) Site 2: δ-3-carene flux and T_{soil} & SWC

Figure 4.41: Comparison of net δ-3-carene fluxes from willow with PAR, chamber and ambient air temperature, soil temperature and soil water content (SWC) for 2010 and 2012 for sites 1 and 2. Note different y-axis scales for δ-3-carene. Error bars on fluxes incorporate analytical and sampling uncertainties.



(a) Site 3: δ-3-carene flux and PAR

(b) Site 3: δ-3-carene flux and $T_{chamber}$ & $T_{ambient\ air}$

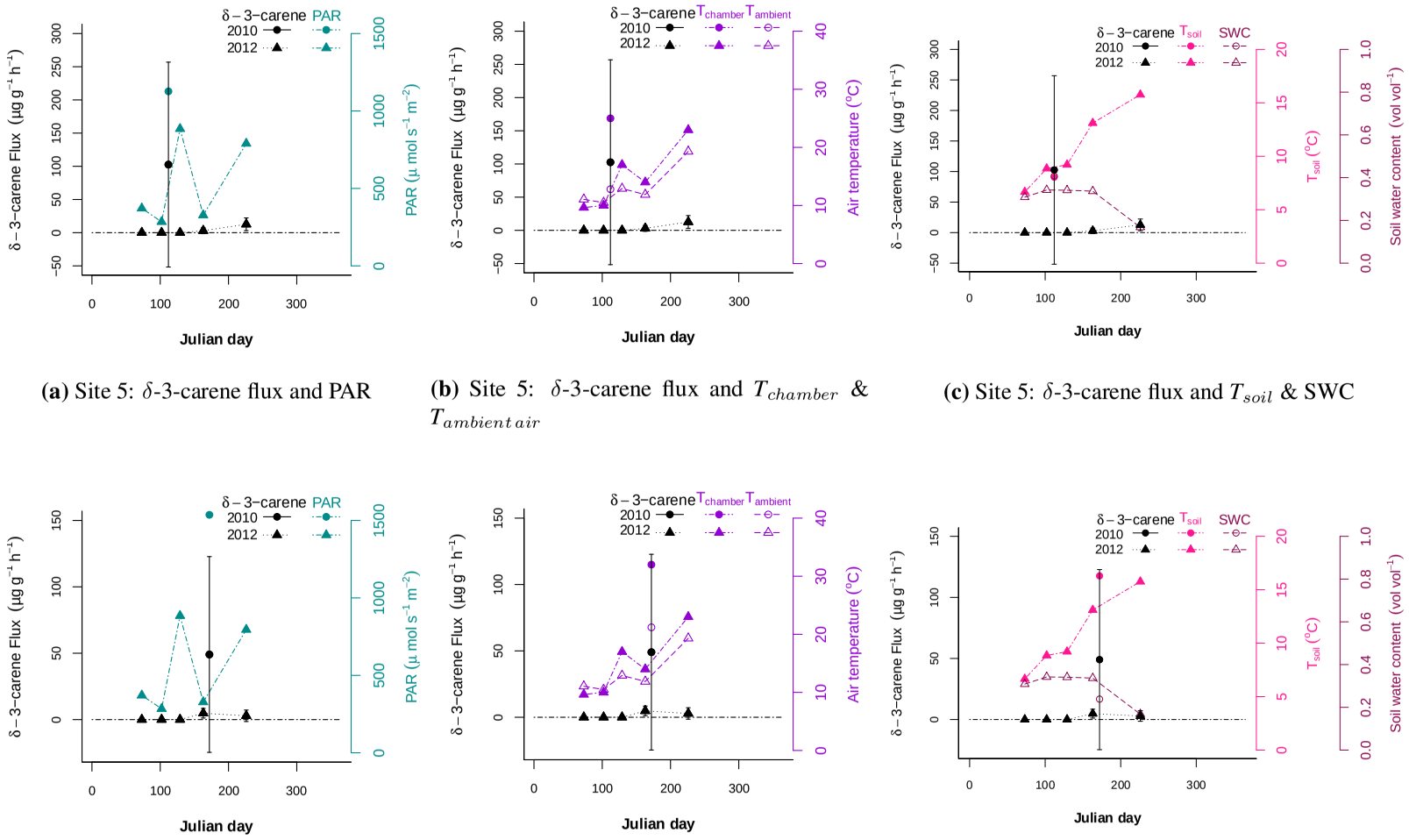
(c) Site 3: δ-3-carene flux and T_{soil} & SWC

(d) Site 4: δ-3-carene flux and PAR

(e) Site 4: δ-3-carene flux and $T_{chamber}$ & $T_{ambient\ air}$

(f) Site 4: δ-3-carene flux and T_{soil} & SWC

Figure 4.42: Comparison of net δ-3-carene fluxes from willow with PAR, chamber and ambient air temperature, soil temperature and soil water content (SWC) for 2010 and 2012 for sites 3 and 4. Note different y-axis scales for δ-3-carene. Error bars on fluxes incorporate analytical and sampling uncertainties.



(a) Site 5: δ-3-carene flux and PAR

(b) Site 5: δ-3-carene flux and $T_{chamber}$ & $T_{ambient\,air}$

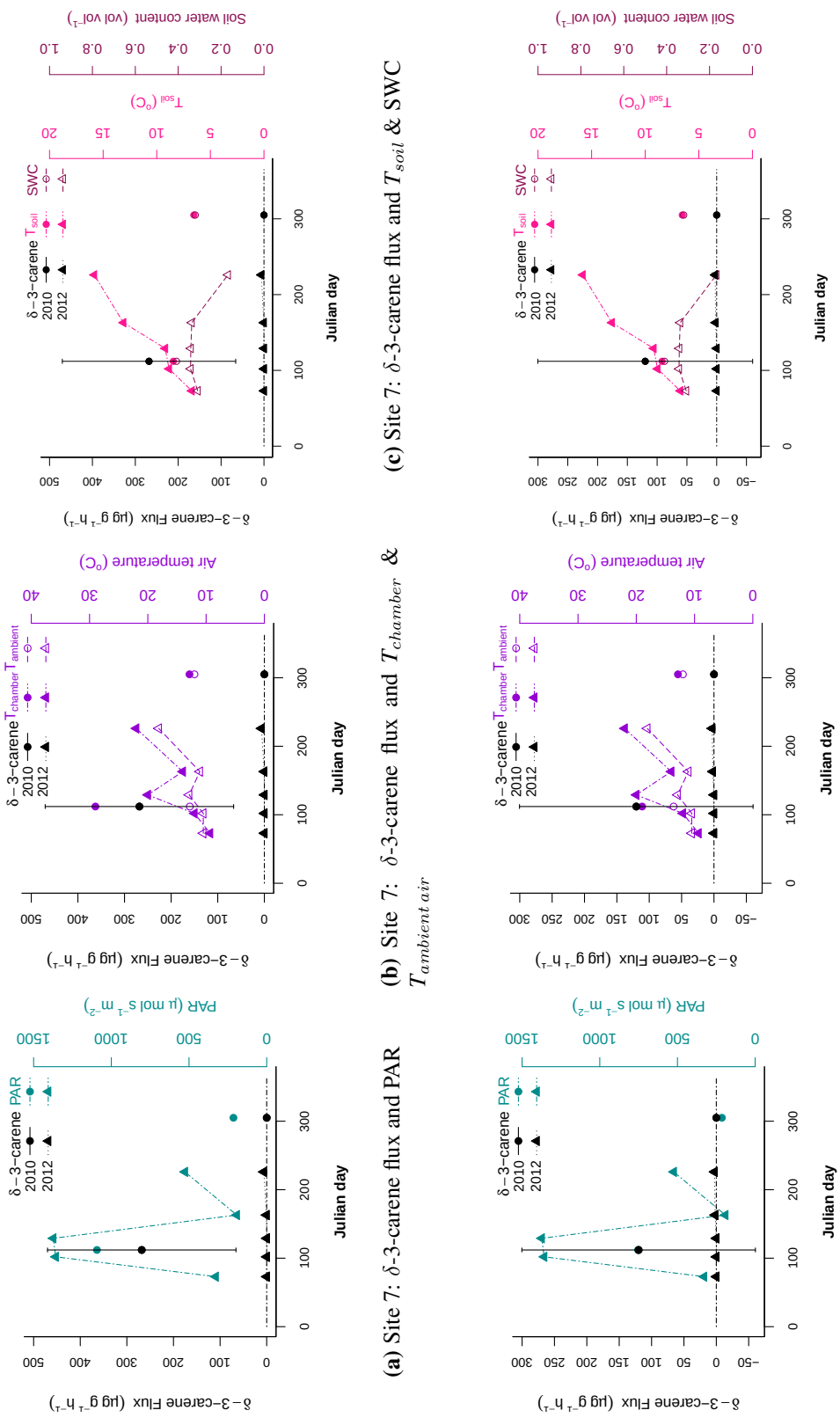
(c) Site 5: δ-3-carene flux and T_{soil} & SWC

(d) Site 6: δ-3-carene flux and PAR

(e) Site 6: δ-3-carene flux and $T_{chamber}$ & $T_{ambient\,air}$

(f) Site 6: δ-3-carene flux and T_{soil} & SWC

Figure 4.43: Comparison of net δ-3-carene fluxes from willow with PAR, chamber and ambient air temperature, soil temperature and soil water content (SWC) for 2010 and 2012 for sites 5 and 6. Note different y-axis scales for δ-3-carene. Error bars on fluxes incorporate analytical and sampling uncertainties.



(a) Site 7: δ-3-carene flux and PAR

(b) Site 7: δ-3-carene flux and $T_{chamber}$ & $T_{ambient\ air}$

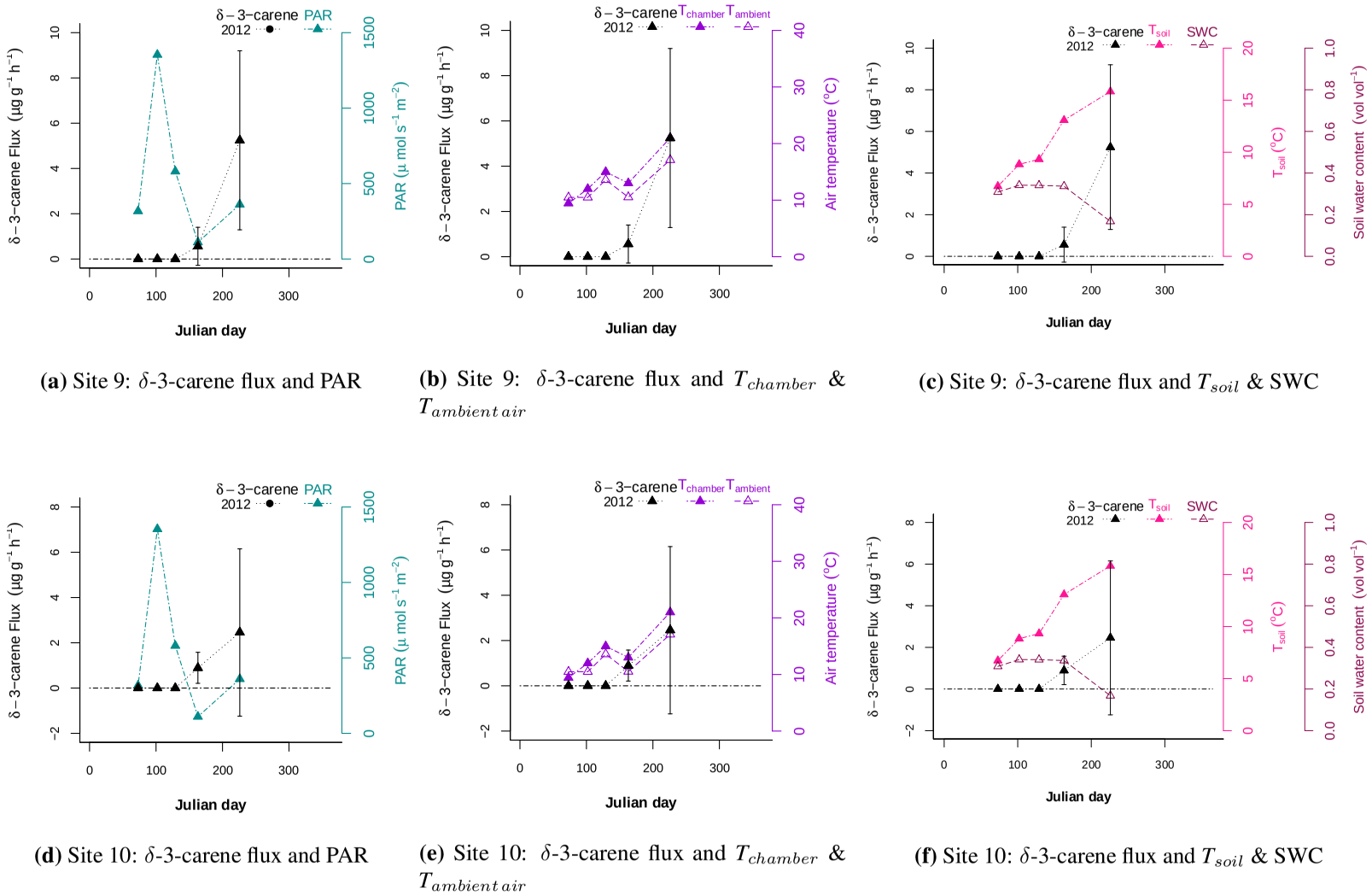
(c) Site 7: δ-3-carene flux and T_{soil} & SWC

(d) Site 8: δ-3-carene flux and PAR

(e) Site 8: δ-3-carene flux and $T_{chamber}$ & $T_{ambient\ air}$

(f) Site 8: δ-3-carene flux and T_{soil} & SWC

Figure 4.44: Comparison of net δ-3-carene fluxes from willow with PAR, chamber and ambient air temperature, soil temperature and soil water content (SWC) for 2010 and 2012 for sites 7 and 8. Note different y-axis scales for δ-3-carene. Error bars on fluxes incorporate analytical and sampling uncertainties.



(a) Site 9: δ-3-carene flux and PAR

(b) Site 9: δ-3-carene flux and $T_{chamber}$ & $T_{ambient\,air}$

(c) Site 9: δ-3-carene flux and T_{soil} & SWC

(d) Site 10: δ-3-carene flux and PAR

(e) Site 10: δ-3-carene flux and $T_{chamber}$ & $T_{ambient\,air}$

(f) Site 10: δ-3-carene flux and T_{soil} & SWC

Figure 4.45: Comparison of net δ-3-carene fluxes from willow with PAR, chamber and ambient air temperature, soil temperature and soil water content (SWC) for 2012 for sites 9 and 10. Note different y-axis scales for δ-3-carene. Error bars on fluxes incorporate analytical and sampling uncertainties.

4.2.8 Statistical analysis of seasonal fluxes and potential drivers

Three types of analyses were carried out on the long term BVOC time series:

- Variation in BVOC fluxes between sites and between growing and non-growing season were analysed for significance using the Kruskal-Wallis function within the R i386 2.15.1 software package
- BVOC fluxes were also analysed for their association with measured environmental parameters
- Correlations between various BVOC fluxes were investigated using regression analysis

Analysis of variation according to site and season

The significance of the variation in isoprene, α-pinene, β-pinene, limonene and δ-3-carene fluxes due to location (different sites in the field), season (growing and non-growing), and from the interaction between these two factors was analysed using Kruskal-Wallis. Each year was divided into a growing season (beginning of April to end of October) and a non-growing season (the rest of the year) based on observational evidence of plant growth.

Fluxes of isoprene, α-pinene, β-pinene, limonene and δ-3-carene were found to vary significantly with season with χ^2 values of between 7 and 51 and corresponding $p < 0.05$ (Table 4.12). BVOC fluxes were not found to vary significantly with site. There was a significant interaction between season and site with isoprene fluxes but not other BVOC fluxes.

Table 4.12: Analysis of isoprene, α-pinene, β-pinene, limonene and δ-3-carene flux variation according to site and season derived using Kruskal-Wallis. Degrees of freedom (D.f) and χ^2 value for the effect of site, season and season-site interaction terms on BVOC fluxes in 2010 and 2012. Significant variation in BVOC flux ($p \leq 0.05$) is highlighted in bold.

	Season	Site	Season*Site
D.f	1	9	9
Isoprene	**51.3**	2.82	**55.3**
α-pinene	**13.8**	0.786	15.5
β-pinene	**7.14**	1.22	8.76
Limonene	**12.6**	2.17	16.0
δ-3-carene	**10.8**	1.15	12.3

BVOC flux association with measured environmental factors

Significant correlations between fluxes of all BVOCs (isoprene, α-pinene, β-pinene, limonene and δ-3-carene) and PAR and soil temperature were identified, with ρ values of between 0.2

and 0.7 and corresponding p values < 0.05 (Table 4.13). All BVOC fluxes except limonene were significantly correlated with chamber temperature, and all BVOC fluxes except limonene and β-pinene with ambient air temperature. Fluxes of all BVOCs were also correlated with soil moisture with the exception of δ-3-carene.

Table 4.13: Spearman's rank correlation coefficients between potential drivers and isoprene, α-pinene, β-pinene, limonene and δ-3-carene fluxes. Significant correlations ($p \leq 0.05$) are highlighted in bold.

Factor	Isoprene	α-pinene	β-pinene	limonene	δ-3-carene
PAR	**0.421**	**0.203**	0.140	0.032	**0.170**
$\boldsymbol{T}_{chamber}$	**0.680**	**0.335**	**0.299**	0.149	**0.414**
$\boldsymbol{T}_{ambient\ air}$	**0.713**	**0.212**	0.101	0.008	**0.310**
$\boldsymbol{T}_{soil}$	**0.643**	**0.292**	**0.183**	**0.200**	**0.397**
Soil moisture	**-0.288**	**0.245**	**0.257**	**0.262**	0.105

Correlations between different BVOCs

Significant positive Spearman's Rank correlation coefficients were identified between all BVOC compounds at all sites combined. Isoprene and α-pinene/β-pinene/δ-3-carene fluxes were significantly correlated at 4 out of 10 sites (Table 4.14). Isoprene fluxes were not significantly correlated with limonene at any individual sites but were significantly correlated for all sites combined.

α-pinene and β-pinene fluxes were significantly correlated at 7 out of 10 sites and overall. The correlations which were not significant were at the two sites with the fewest measurements (9 and 10) and site 4, where the correlation is close to significant. α-pinene fluxes were also significantly correlated with limonene/δ-3-carene fluxes at 9 sites and at all sites combined.

β-pinene fluxes were significantly correlated with limonene at 5 sites and overall and with δ-3-carene fluxes at 6 sites and at all sites combined. Limonene and δ-3-carene fluxes were significantly correlated at 8 sites and at all sites combined.

Table 4.14: Spearman's Rank correlation coefficients (ρ) between isoprene, α-pinene, β-pinene, limonene and δ-3-carene fluxes and for fluxes over all sites. Significant correlation coefficients ($p \leq 0.05$) are highlighted in bold.

bVOC compound	W1	W2	W3	W4	W5	W6	W7	W8	W9	W10	All
Isoprene & α-pinene	**0.591**	**0.468**	**0.51**	0.388	0.262	**0.8**	-0.081	0.546	-0.057	0.13	**0.431**
Isoprene & β-pinene	**0.492**	**0.483**	**0.534**	0.29	-0.254	**0.613**	-0.223	0.301	-0.275	0.139	**0.3**
Isoprene & Limonene	0.292	0.296	0.225	0.202	-0.121	0.223	0.047	0.546	0.189	0.322	**0.231**
Isoprene & δ-3-carene	**0.529**	**0.574**	**0.641**	**0.633**	0.07	**0.78**	0.105	0.542	0.275	0.557	**0.477**
α-pinene & β-pinene	**0.725**	**0.739**	**0.751**	0.456	**0.659**	**0.725**	**0.593**	**0.704**	0.572	0.6	**0.676**
α-pinene & Limonene	**0.658**	**0.703**	**0.698**	**0.594**	**0.665**	0.516	**0.919**	**1**	**0.786**	**0.857**	**0.729**
α-pinene & δ-3-carene	**0.809**	**0.828**	**0.83**	**0.684**	**0.85**	**0.85**	**0.798**	**0.907**	**0.739**	0.65	**0.804**
β-pinene & Limonene	**0.526**	0.465	0.459	**0.848**	**0.84**	0.393	**0.62**	**0.704**	0.488	0.488	**0.569**
β-pinene & δ-3-carene	**0.862**	**0.892**	**0.85**	0.5	**0.776**	**0.854**	**0.776**	**0.776**	0.562	0.562	**0.789**
Limonene & δ-3-carene	**0.709**	**0.659**	**0.651**	0.391	**0.602**	0.296	**0.895**	**0.907**	**0.868**	**0.868**	**0.689**

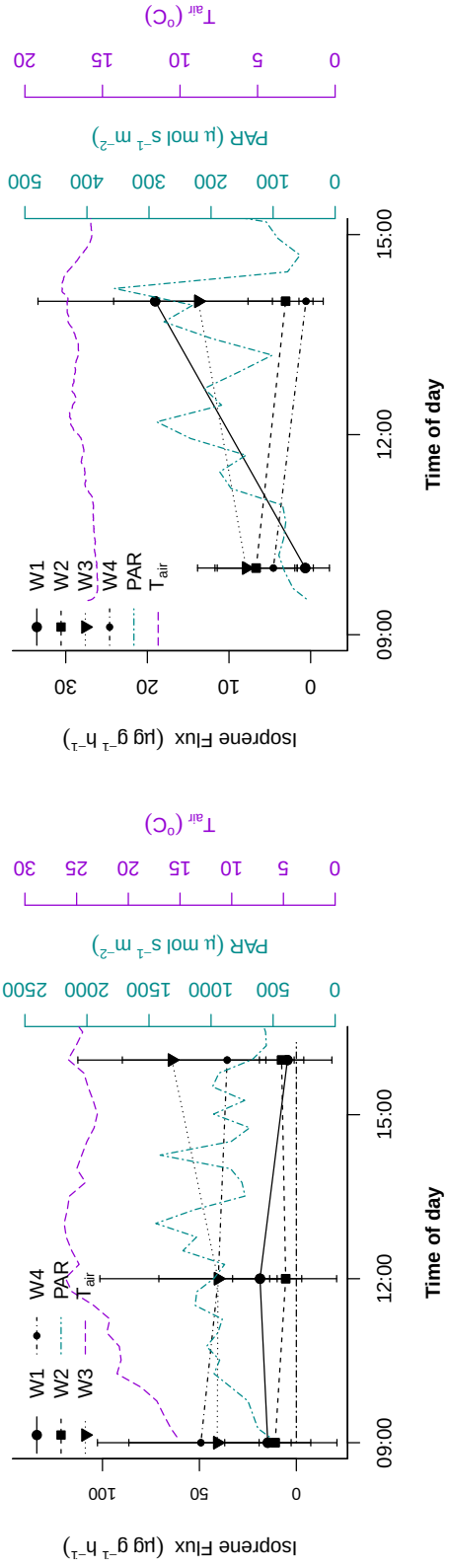
4.2.9 Sub-diurnal trends in isoprene

To investigate the behaviour of BVOC fluxes throughout the day during different times of the year, one full diurnal and seven sub-diurnal measurement campaigns were conducted. During the full diurnal campaign measurements were taken every 6 hours over a 24 hour period. During the sub-diurnal campaigns, three measurements were taken between 9 am and 9 pm. Air temperature and PAR were recorded throughout each 12 or 24 hour sampling period. Fluxes were measured for either 2 or 4 sites during these campaigns. Results from two sub-diurnal studies conducted in August and September 2011 are presented in Figure 4.46.

As well as changes to the weather in different measurement months, there were also changes to the physiology of the willow plants. When diurnal and sub-diurnal measurements were made in 2010 and 2011, catkins grew on the willow in February and March, trees and leaves grew between April and September, leaves senesced in October and fell off in November.

Isoprene fluxes were measured at sites 1 to 4 on the 18th August 2011 (Figure 4.46a). Fluxes at site 1 were fairly steady at around 20 $\mu g\, g^{-1}\, h^{-1}$ in the early part of the day between 9 am and noon before they dropped to 5 $\mu g\, g^{-1}\, h^{-1}$ at 3 pm. Site 2 started off at a similar magnitude of flux in the morning, dropped to around 8 $\mu g\, g^{-1}\, h^{-1}$ at midday and rose slightly to 12 $\mu g\, g^{-1}\, h^{-1}$ in the afternoon. At 9 am, a flux of 40 $\mu g\, g^{-1}\, h^{-1}$ was measured at site 3. This remained steady at midday before the flux increased to 65 $\mu g\, g^{-1}\, h^{-1}$ in the afternoon. A flux of 50 $\mu g\, g^{-1}\, h^{-1}$ was measured at site 4, this dropped to 40 $\mu g\, g^{-1}\, h^{-1}$ at midday and dropped again to 38 $\mu g\, g^{-1}\, h^{-1}$ in the afternoon. PAR and air temperature were low at the start of the day and remained generally high during the measurements at midday and in the afternoon. The isoprene fluxes measured appeared to vary independently of observed sunlight and temperature levels.

The flux measurements made at sites 1 to 4 on the 19th September 2011 started between 1 and 8 $\mu g\, g^{-1}\, h^{-1}$ at 10 am (Figure 4.46b). At sites 1 and 3 fluxes then increased to 19 and 14 $\mu g\, g^{-1}\, h^{-1}$, respectively. Fluxes at sites 2 and 4 decreased to 3 and 1 $\mu g\, g^{-1}\, h^{-1}$, respectively. Very low PAR and low air temperatures were observed at around 10 am and gradually increased during the day, with a maximum PAR of 380 μmol $m^{-2}\, s^{-1}$ and maximum air temperature of 17°C.



(a) 18th August 2011

(b) 19th September 2011

Figure 4.46: Sub-diurnal isoprene fluxes from Brattleby willow sites 1-4 in August and September 2011 with ambient air temperature and PAR. Error bars incorporate analytical and sampling uncertainties. Note the different vertical scales in each figure.

4.3 Arnot

4.3.1 Site description

Measurements were conducted at the Arnot fieldsite in Fife, as described in Section 2.7.2. Although the site has only two separate fields, for the purposes of this research the first field was split into two sites as the terrain was markedly different within the field. These were labelled fields "X", "Y" and the second field labelled "Z". Field "X" takes in sampling points running from the top of the hill down a relatively steep slope towards the road. Field "Y" consists of sampling points spread along the top of the field and down the eastern edge. This is separated from the third field "Z" by a small stone dyke. There are ten sampling points along the western edge of field, along the top and within the field. A total of ten sampling points are used within each field of interest, with a maximum of 30 sampling points used as shown in Figure 4.47.

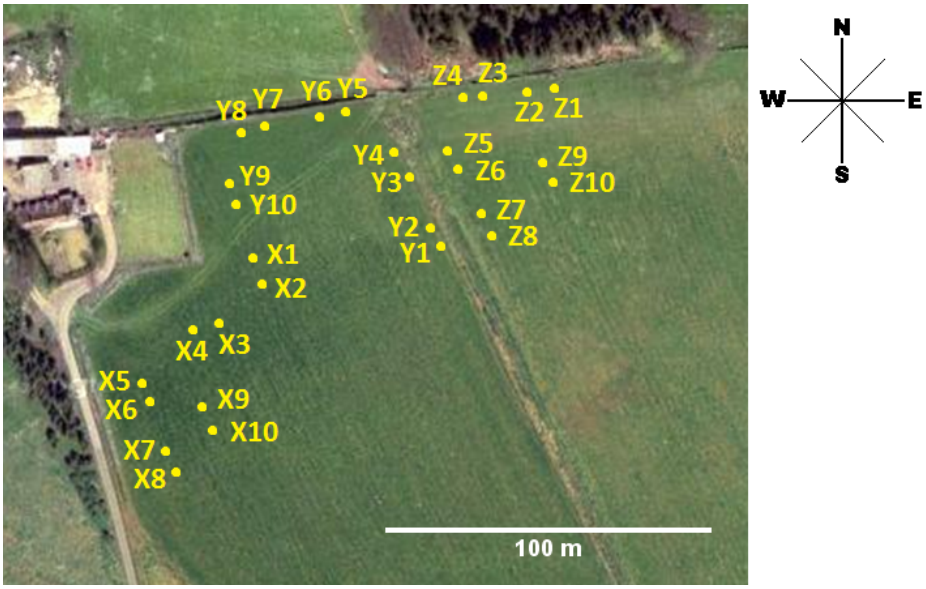


Figure 4.47: Location of sampling points within the SRC willow fields at Arnot.

4.3.2 Outline of CH_3X flux measurements

A total of 132 measurements were made during 8 site visits between August 2011 and June 2012. Firstly, the CH_3X flux trends over the measurement period are examined. Time series of seasonal net CH_3X fluxes and the respective PAR, ambient and chamber air temperature, soil temperature and soil water content observations at the time of measurement for each sampling site are then illustrated, incorporating seasonal and temporal variation in fluxes.

Statistical analysis of the CH_3X fluxes is then presented. CH_3X fluxes are tested for significant

correlations with monitored environmental parameters in order to investigate possible drivers of emissions. Correlations between CH_3Br and CH_3Cl fluxes were tested for significance as was the association of variation in CH_3X flux with season and sampling site.

CH_3Br

The CH_3Br fluxes measured between August 2011 and June 2012 at all thirty willow sampling points and the mean of those values on each sampling occasion are illustrated in Figure 4.48. Fluxes were highest later in the year in 2011, peaking in October, and earlier in the year in 2012, peaking in March. Generally, CH_3Br fluxes were low (less than 10 ng g^{-1} h^{-1}) with peak fluxes of 23 to 32 ng g^{-1} h^{-1}.

Zero fluxes were measured at all sites in August 2011, with the exception of a flux of 1ng g^{-1} h^{-1} measured at site X1. Fluxes of between zero and 2 ng g^{-1} h^{-1} were measured in September. The range increased to between zero and 23 ng g^{-1} h^{-1} in October before falling again to zero to 17 ng g^{-1} h^{-1} in November. In March 2012, fluxes of between zero and 32 ng g^{-1} h^{-1} were measured. Only zero fluxes were measured in April. Fluxes of between zero and 5 ng g^{-1} h^{-1} were measured in May, and in June 2012. Mean fluxes varied between zero and 4.5 ng g^{-1} h^{-1}.

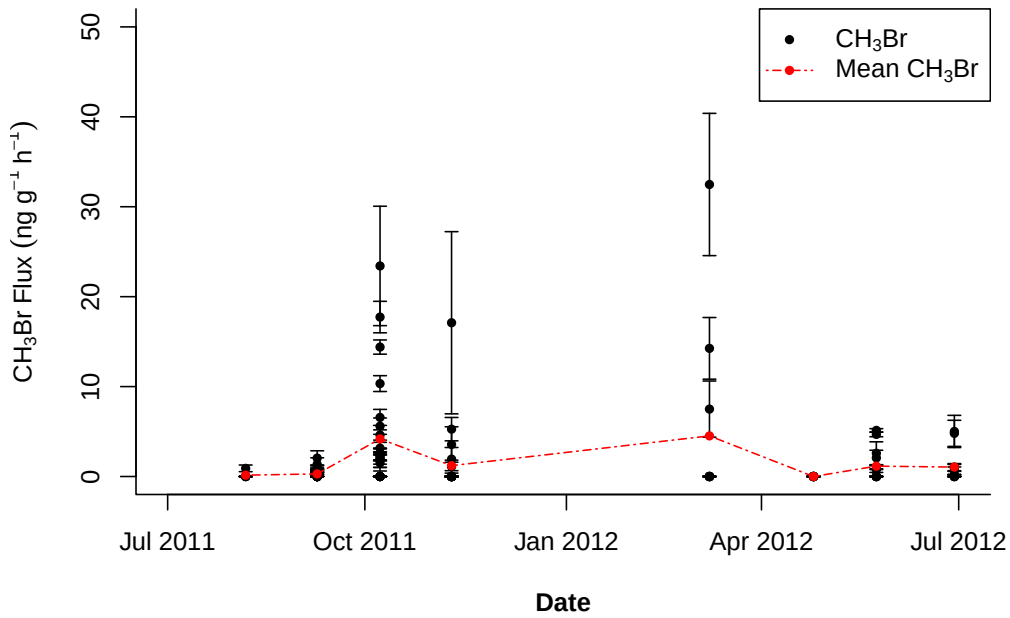


Figure 4.48: CH_3Br fluxes from willow at the Arnot fieldsite at all thirty sampling points and the mean of those values on each sampling occasion from 2011 to 2012. Error bars on fluxes incorporate analytical and sampling uncertainties (as described in Section 2.6.1).

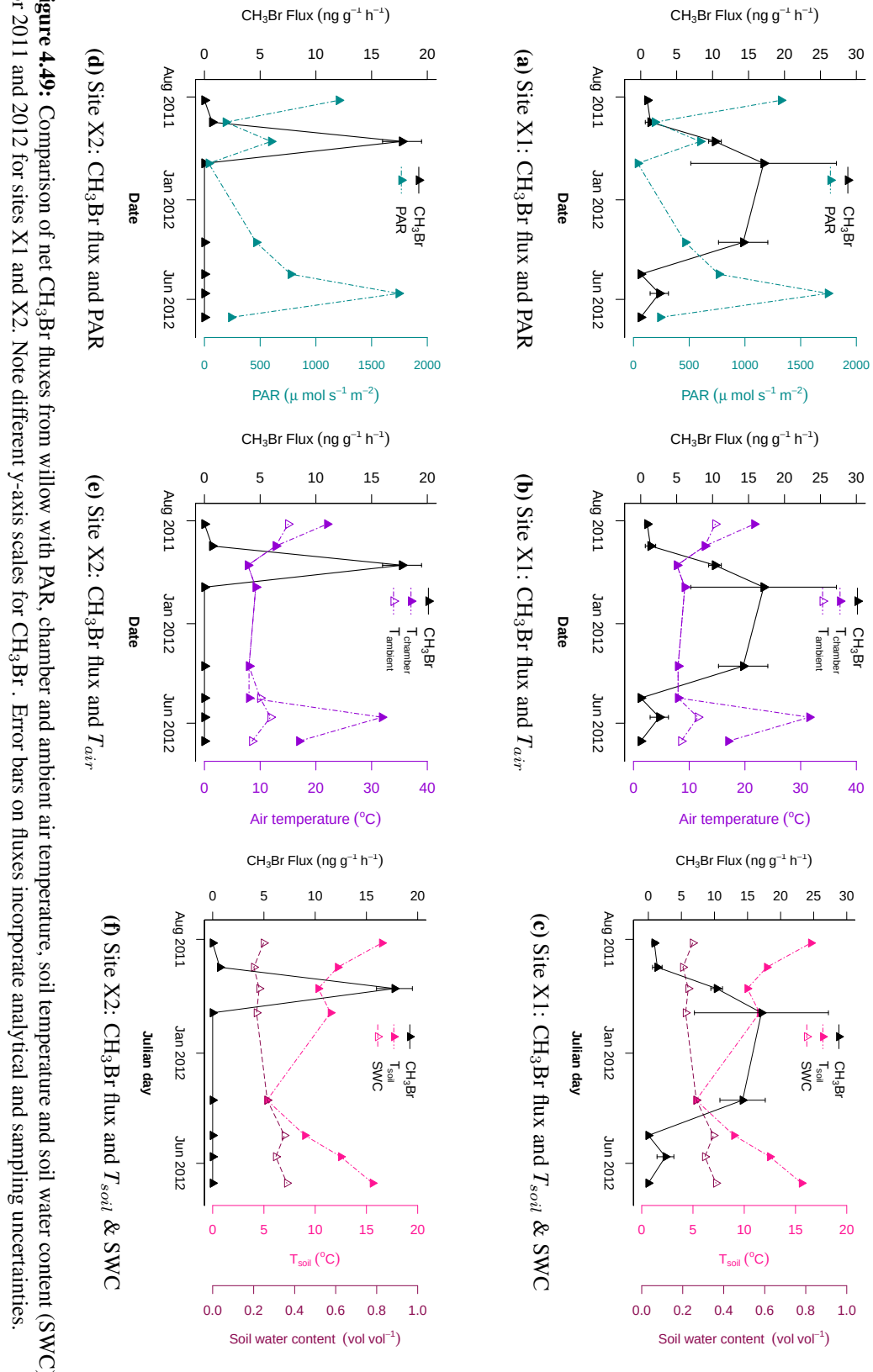
Time series of CH_3Br fluxes from each individual site between August 2011 and June 2012 together with the concurrent PAR, ambient and chamber air temperature, soil temperature and soil water content observations are illustrated in Figures 4.49 to 4.63. The statistical significance of correlations between CH_3Br fluxes and environmental variables is described in Section 4.3.3.

Similar mean CH_3Br fluxes were calculated for all fields, varying between zero and 9.6 ng g^{-1} h^{-1} (Table 4.15). Sites X9 and X10, Y9 and Y10 and Z9 and Z10 were excluded as they were measured only once. Higher mean CH_3Br fluxes (between 1 and 9.6 ng g^{-1} h^{-1}) were measured at sites X1 - 3, X5 and X8, Y1 - 2, Y4, and Y7 and Z1 - 2 and Z5. Lower mean fluxes (< 1 ng g^{-1} h^{-1}) were measured at the remaining sites. Median fluxes of between zero and 5.3 ng g^{-1} h^{-1} were calculated. The highest maximum flux of 33 ng g^{-1} h^{-1} was measured at site Z1 in March 2012. The minimum flux recorded at all sites was zero.

Mean fluxes of 2.6, 0.9 and 1.5 ng g^{-1} h^{-1} were calculated from all fluxes measured during the measurement period combined for Fields X, Y and X, respectively. A median of zero was calculated for all fields. An overall mean CH_3Br flux of 1.7 ng g^{-1} h^{-1} was calculated from fluxes measured at all sites during the measurement period.

Table 4.15: Mean, median, minimum and maximum net CH_3Br fluxes from SRC willow at Arnot during 2011 to 2012. All flux values are in $ng\,g^{-1}\,h^{-1}$. The final column gives the number of measurements made. The last row summarises all fluxes from all sites.

Site	Mean	Median	Min	Max	Number
Willow X1	5.82	1.97	0.00	17.1	8
Willow X2	2.30	0.00	0.00	17.7	8
Willow X3	1.08	0.00	0.00	6.57	7
Willow X4	0.84	0.00	0.00	5.01	7
Willow X5	1.14	0.25	0.00	3.16	3
Willow X6	0.81	0.00	0.00	2.42	3
Willow X7	0.62	0.00	0.00	1.85	3
Willow X8	9.56	5.27	0.00	23.4	3
Willow X9	0.00	0.00	0.00	0.00	1
Willow X10	0.00	0.00	0.00	0.00	1
All X	2.61	0.00	0.00	23.4	44
Willow Y1	1.88	0.00	0.00	14.4	8
Willow Y2	1.28	0.00	0.00	5.60	8
Willow Y3	0.02	0.00	0.00	0.14	7
Willow Y4	1.26	0.00	0.00	4.80	7
Willow Y5	0.00	0.00	0.00	0.00	4
Willow Y6	0.56	0.00	0.00	2.24	4
Willow Y7	1.73	0.58	0.00	4.62	3
Willow Y8	0.00	0.00	0.00	0.00	3
Willow Y9	1.00	1.00	1.00	1.00	1
Willow Y10	0.00	0.00	0.00	0.00	1
All Y	0.93	0.00	0.00	14.4	46
Willow Z1	4.94	0.00	0.00	32.5	8
Willow Z2	1.95	0.94	0.00	7.50	8
Willow Z3	0.29	0.00	0.00	2.05	7
Willow Z4	0.12	0.00	0.00	0.82	7
Willow Z5	1.02	0.55	0.00	2.51	3
Willow Z6	0.00	0.00	0.00	0.00	3
Willow Z7	0.00	0.00	0.00	0.00	3
Willow Z8	0.69	0.00	0.00	2.08	3
Willow Z9	0.61	0.61	0.61	0.61	1
Willow Z10	0.75	0.75	0.75	0.75	1
All Z	1.46	0.00	0.00	32.5	44
Overall	1.65	0.00	0.00	32.5	132



(a) Site X1: CH_3Br flux and PAR

(b) Site X1: CH_3Br flux and T_{air}

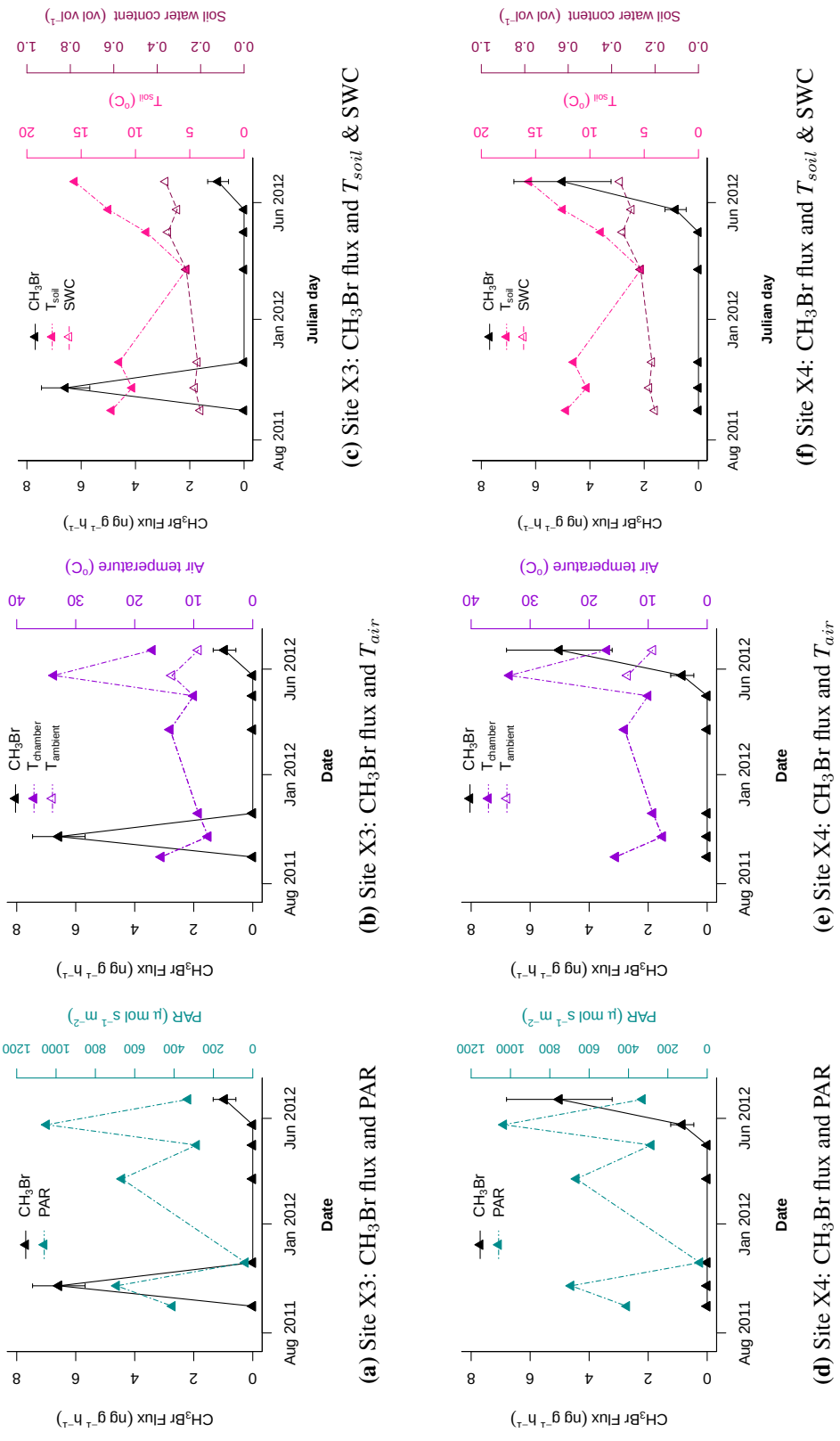
(c) Site X1: CH_3Br flux and T_{soil} & SWC

(d) Site X2: CH_3Br flux and PAR

(e) Site X2: CH_3Br flux and T_{air}

(f) Site X2: CH_3Br flux and T_{soil} & SWC

Figure 4.49: Comparison of net CH_3Br fluxes from willow with PAR, chamber and ambient air temperature, soil temperature and soil water content (SWC) for 2011 and 2012 for sites X1 and X2. Note different y-axis scales for CH_3Br . Error bars on fluxes incorporate analytical and sampling uncertainties.



(a) Site X3: CH_3Br flux and PAR

(b) Site X3: CH_3Br flux and T_{air}

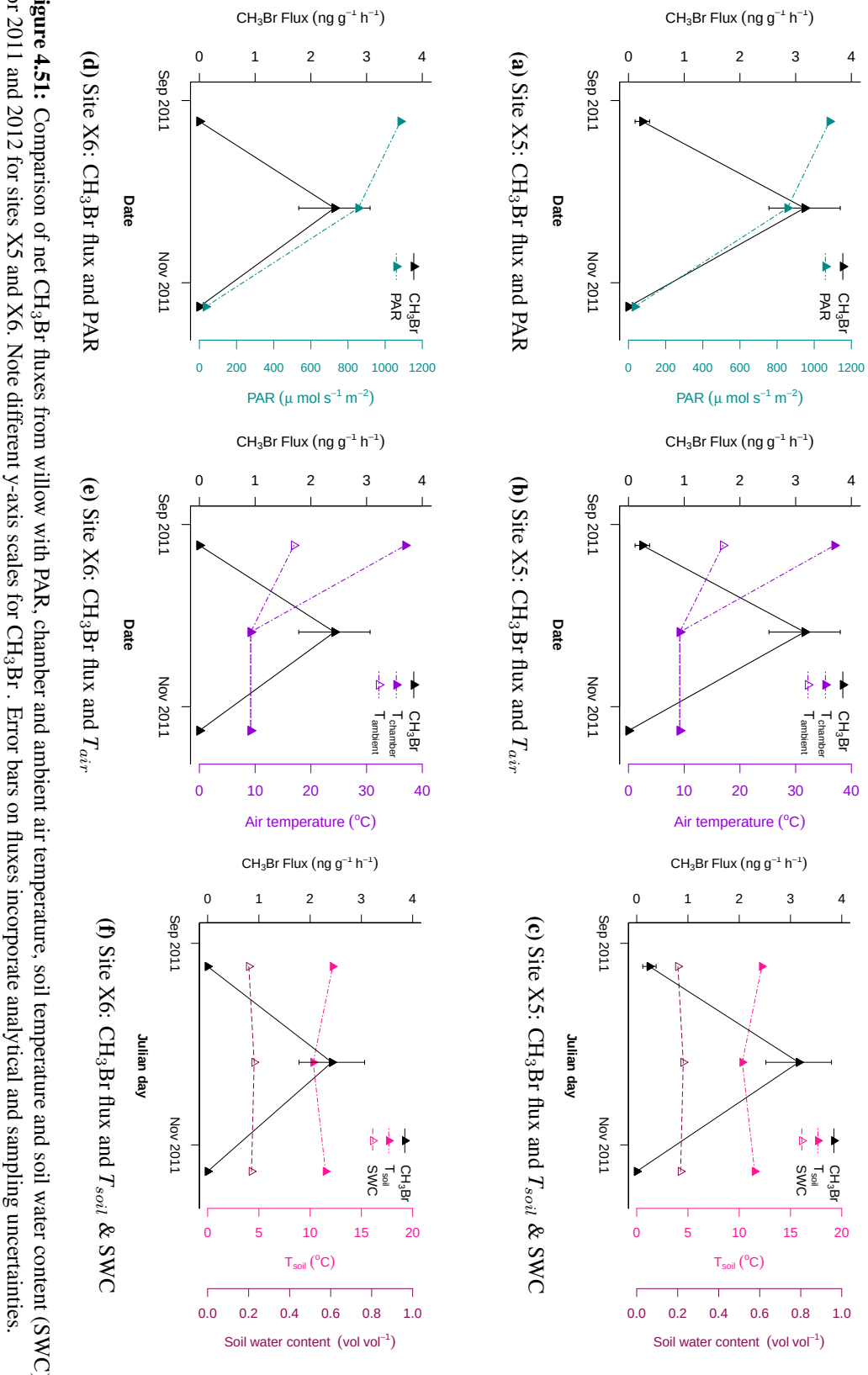
(c) Site X3: CH_3Br flux and T_{soil} & SWC

(d) Site X4: CH_3Br flux and PAR

(e) Site X4: CH_3Br flux and T_{air}

(f) Site X4: CH_3Br flux and T_{soil} & SWC

Figure 4.50: Comparison of net CH_3Br fluxes from willow with PAR, chamber and ambient air temperature, soil temperature and soil water content (SWC) for 2011 and 2012 for sites X3 and X4. Note different y-axis scales for CH_3Br . Error bars on fluxes incorporate analytical and sampling uncertainties.



(a) Site X5: CH_3Br flux and PAR

(b) Site X5: CH_3Br flux and T_{air}

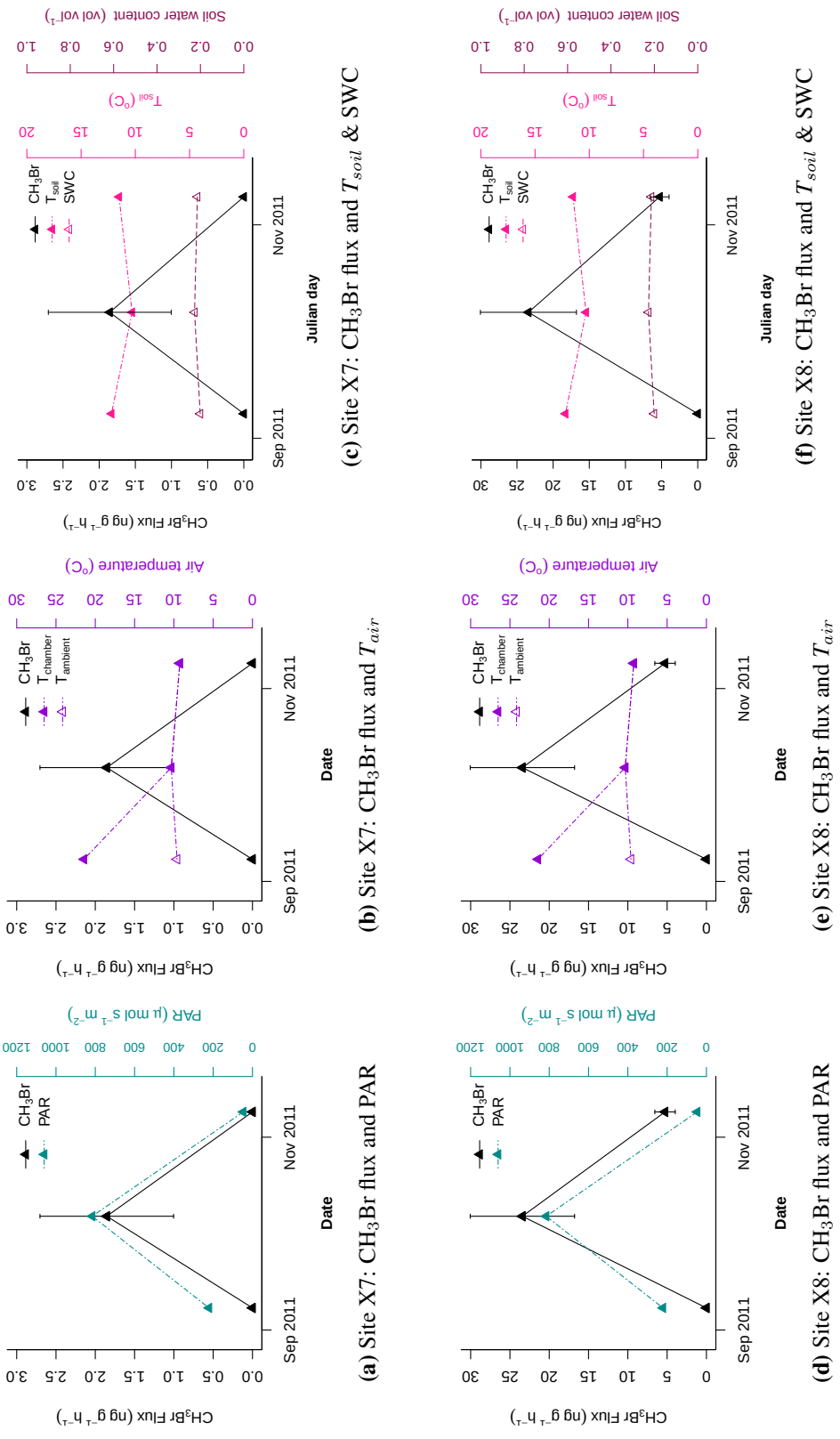
(c) Site X5: CH_3Br flux and T_{soil} & SWC

(d) Site X6: CH_3Br flux and PAR

(e) Site X6: CH_3Br flux and T_{air}

(f) Site X6: CH_3Br flux and T_{soil} & SWC

Figure 4.51: Comparison of net CH_3Br fluxes from willow with PAR, chamber and ambient air temperature, soil temperature and soil water content (SWC) for 2011 and 2012 for sites X5 and X6. Note different y-axis scales for CH_3Br . Error bars on fluxes incorporate analytical and sampling uncertainties.



(a) Site X7: CH_3Br flux and PAR

(b) Site X7: CH_3Br flux and T_{air}

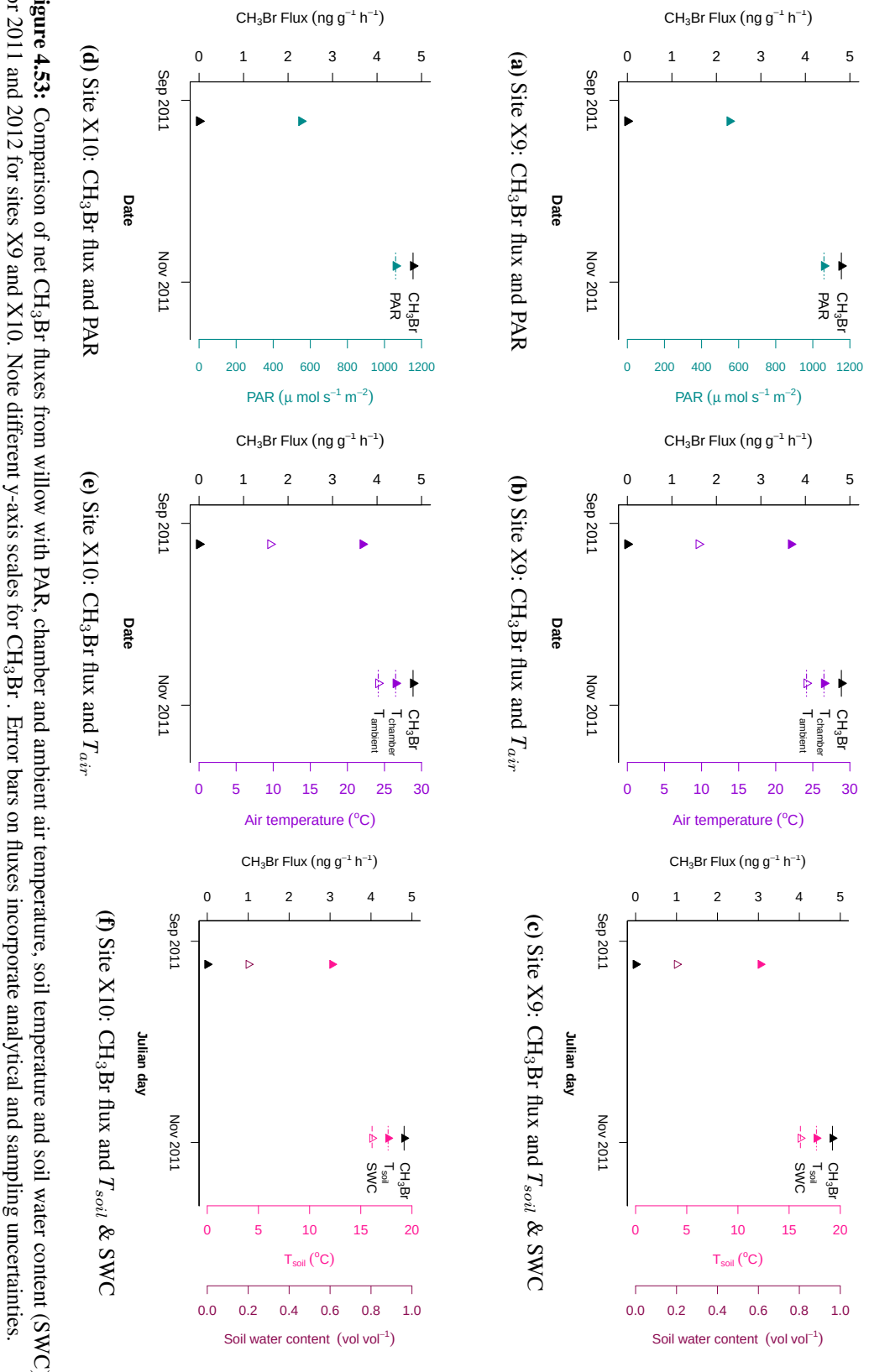
(c) Site X7: CH_3Br flux and T_{soil} & SWC

(d) Site X8: CH_3Br flux and PAR

(e) Site X8: CH_3Br flux and T_{air}

(f) Site X8: CH_3Br flux and T_{soil} & SWC

Figure 4.52: Comparison of net CH_3Br fluxes from willow with PAR, chamber and ambient air temperature, soil temperature and soil water content (SWC) for 2011 and 2012 for sites X7 and X8. Note different y-axis scales for CH_3Br . Error bars on fluxes incorporate analytical and sampling uncertainties.



(a) Site X9: CH_3Br flux and PAR

(b) Site X9: CH_3Br flux and T_{air}

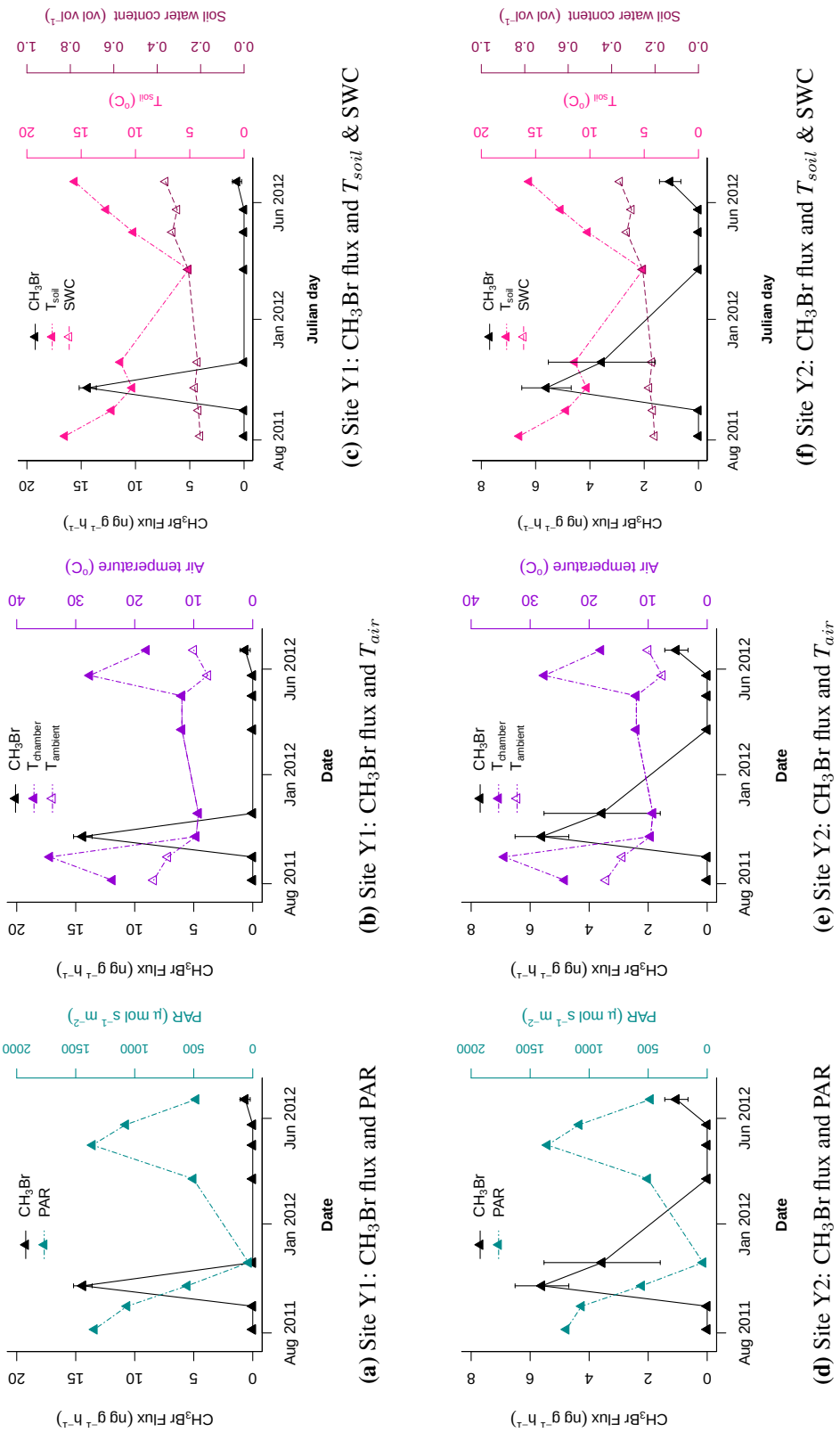
(c) Site X9: CH_3Br flux and T_{soil} & SWC

(d) Site X10: CH_3Br flux and PAR

(e) Site X10: CH_3Br flux and T_{air}

(f) Site X10: CH_3Br flux and T_{soil} & SWC

Figure 4.53: Comparison of net CH_3Br fluxes from willow with PAR, chamber and ambient air temperature, soil temperature and soil water content (SWC) for 2011 and 2012 for sites X9 and X10. Note different y-axis scales for CH_3Br . Error bars on fluxes incorporate analytical and sampling uncertainties.



(a) Site Y1: CH_3Br flux and PAR

(b) Site Y1: CH_3Br flux and T_{air}

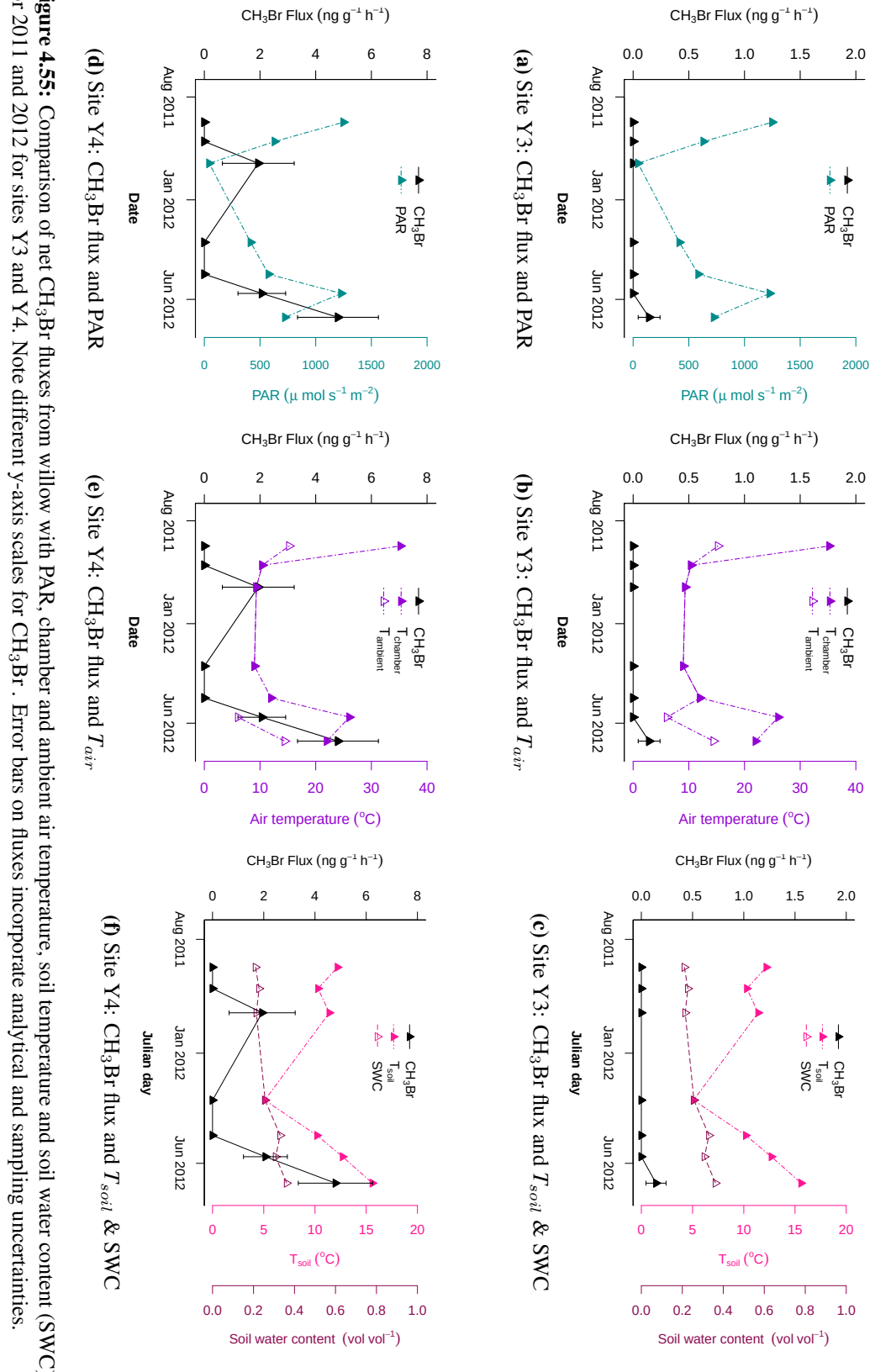
(c) Site Y1: CH_3Br flux and T_{soil} & SWC

(d) Site Y2: CH_3Br flux and PAR

(e) Site Y2: CH_3Br flux and T_{air}

(f) Site Y2: CH_3Br flux and T_{soil} & SWC

Figure 4.54: Comparison of net CH_3Br fluxes from willow with PAR, chamber and ambient air temperature, soil temperature and soil water content (SWC) for 2011 and 2012 for sites Y1 and Y2. Note different y-axis scales for CH_3Br . Error bars on fluxes incorporate analytical and sampling uncertainties.



(a) Site Y3: CH_3Br flux and PAR

(b) Site Y3: CH_3Br flux and T_{air}

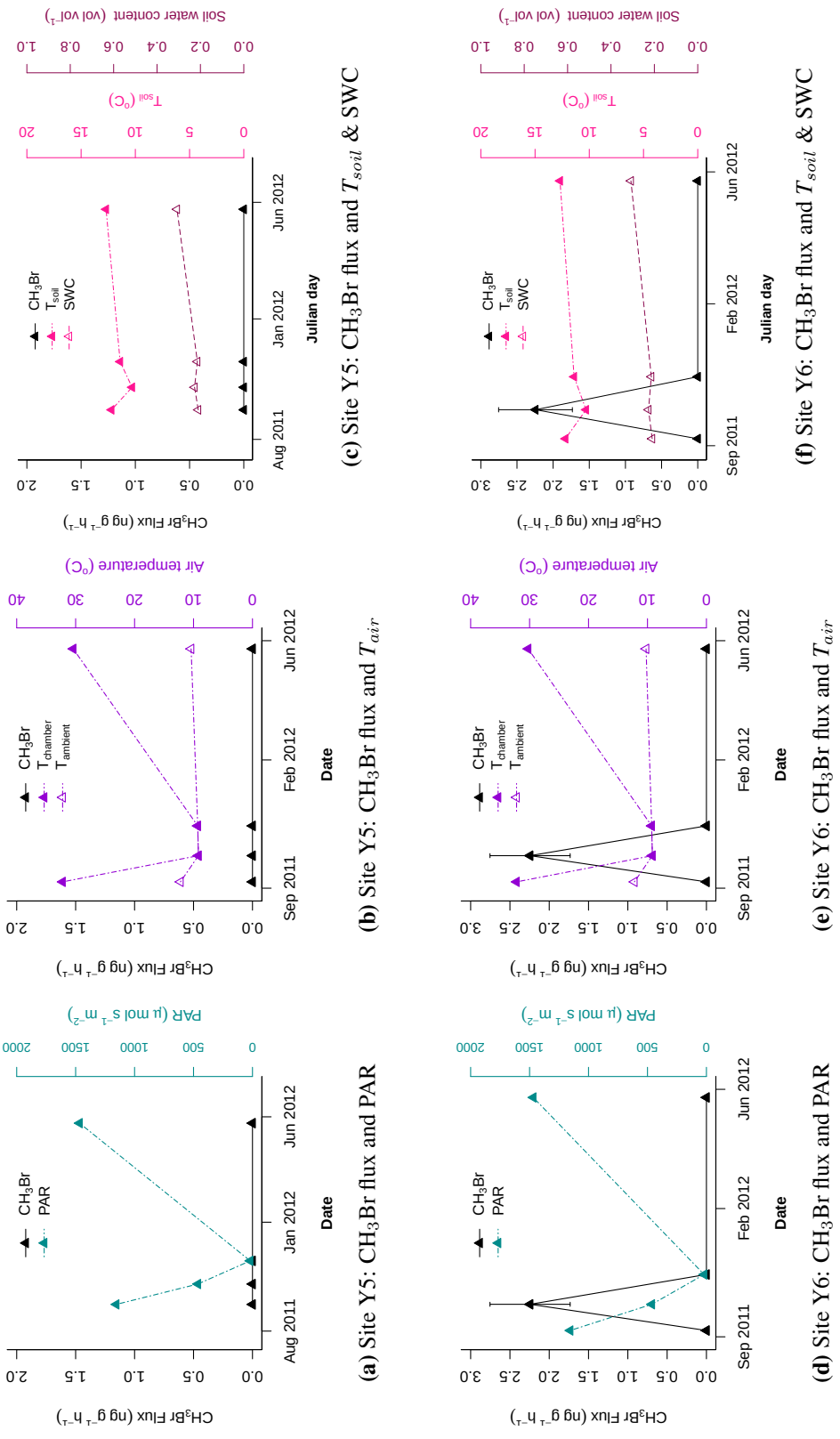
(c) Site Y3: CH_3Br flux and T_{soil} & SWC

(d) Site Y4: CH_3Br flux and PAR

(e) Site Y4: CH_3Br flux and T_{air}

(f) Site Y4: CH_3Br flux and T_{soil} & SWC

Figure 4.55: Comparison of net CH_3Br fluxes from willow with PAR, chamber and ambient air temperature, soil temperature and soil water content (SWC) for 2011 and 2012 for sites Y3 and Y4. Note different y-axis scales for CH_3Br . Error bars on fluxes incorporate analytical and sampling uncertainties.



(a) Site Y5: CH_3Br flux and PAR

(b) Site Y5: CH_3Br flux and T_{air}

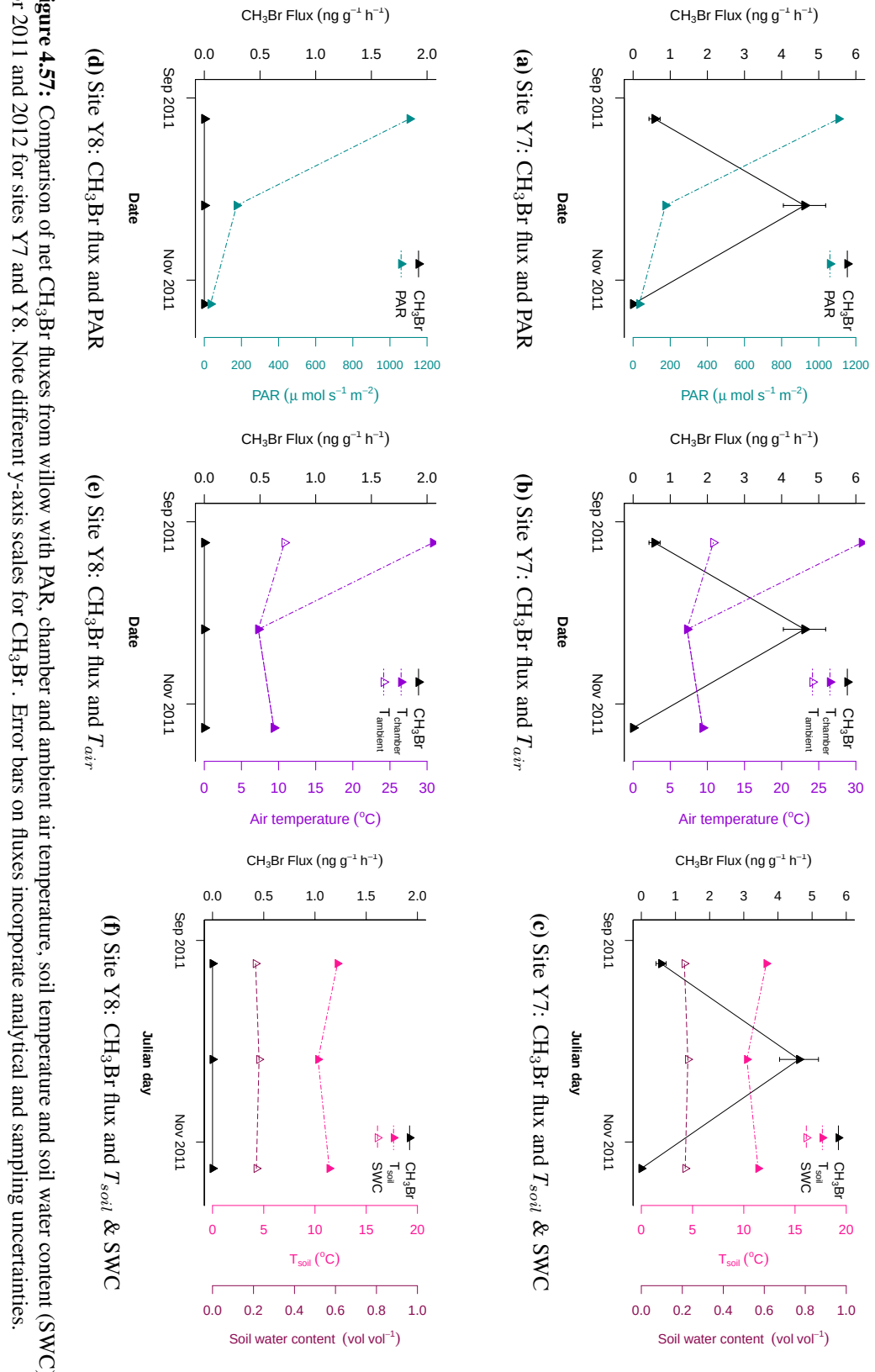
(c) Site Y5: CH_3Br flux and T_{soil} & SWC

(d) Site Y6: CH_3Br flux and PAR

(e) Site Y6: CH_3Br flux and T_{air}

(f) Site Y6: CH_3Br flux and T_{soil} & SWC

Figure 4.56: Comparison of net CH_3Br fluxes from willow with PAR, chamber and ambient air temperature, soil temperature and soil water content (SWC) for 2011 and 2012 for sites Y5 and Y6. Note different y-axis scales for CH_3Br . Error bars on fluxes incorporate analytical and sampling uncertainties.



(a) Site Y7: CH_3Br flux and PAR

(b) Site Y7: CH_3Br flux and T_{air}

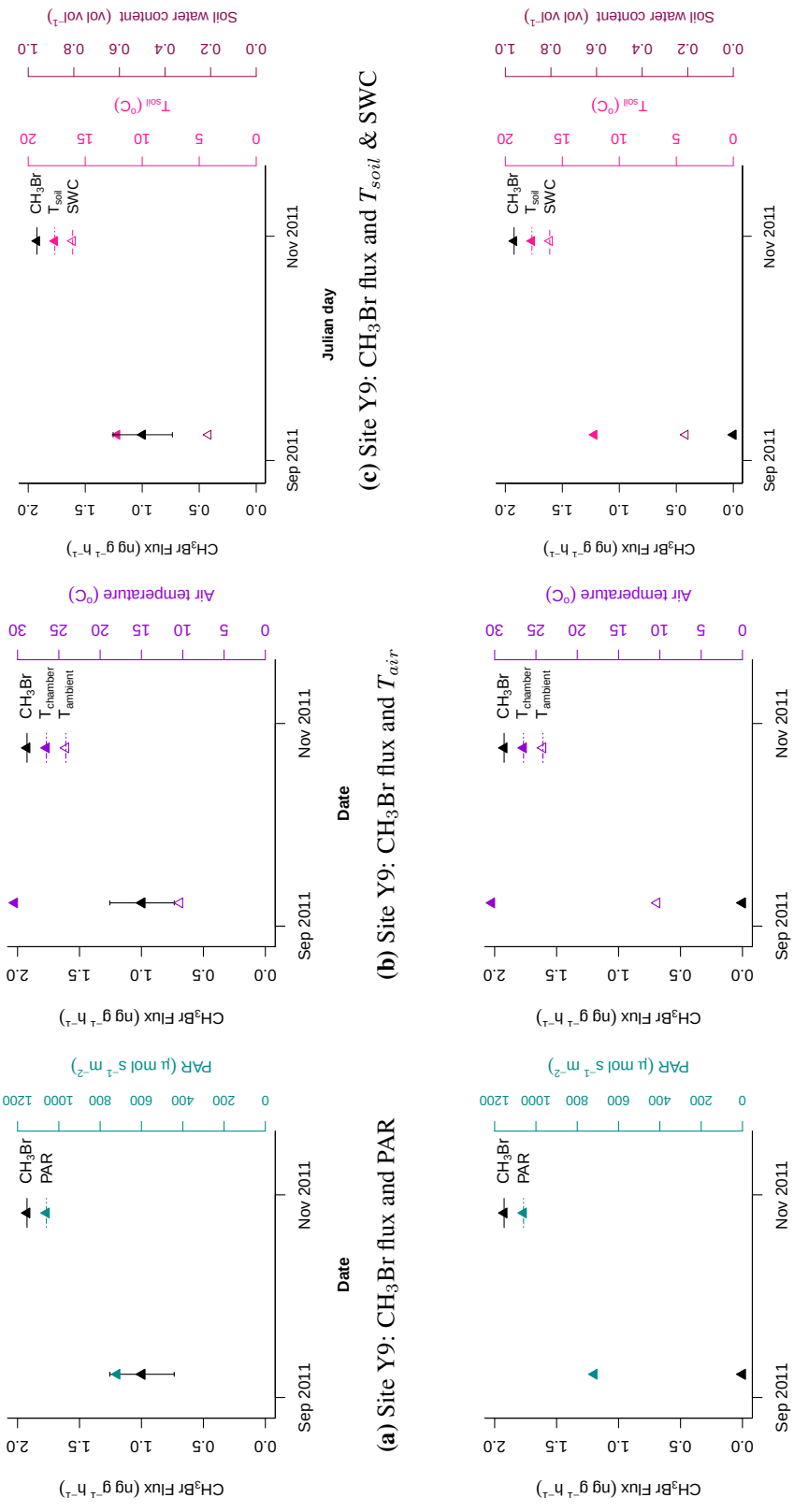
(c) Site Y7: CH_3Br flux and T_{soil} & SWC

(d) Site Y8: CH_3Br flux and PAR

(e) Site Y8: CH_3Br flux and T_{air}

(f) Site Y8: CH_3Br flux and T_{soil} & SWC

Figure 4.57: Comparison of net CH_3Br fluxes from willow with PAR, chamber and ambient air temperature, soil temperature and soil water content (SWC) for 2011 and 2012 for sites Y7 and Y8. Note different y-axis scales for CH_3Br . Error bars on fluxes incorporate analytical and sampling uncertainties.



(a) Site Y9: CH_3Br flux and PAR

(b) Site Y9: CH_3Br flux and T_{air}

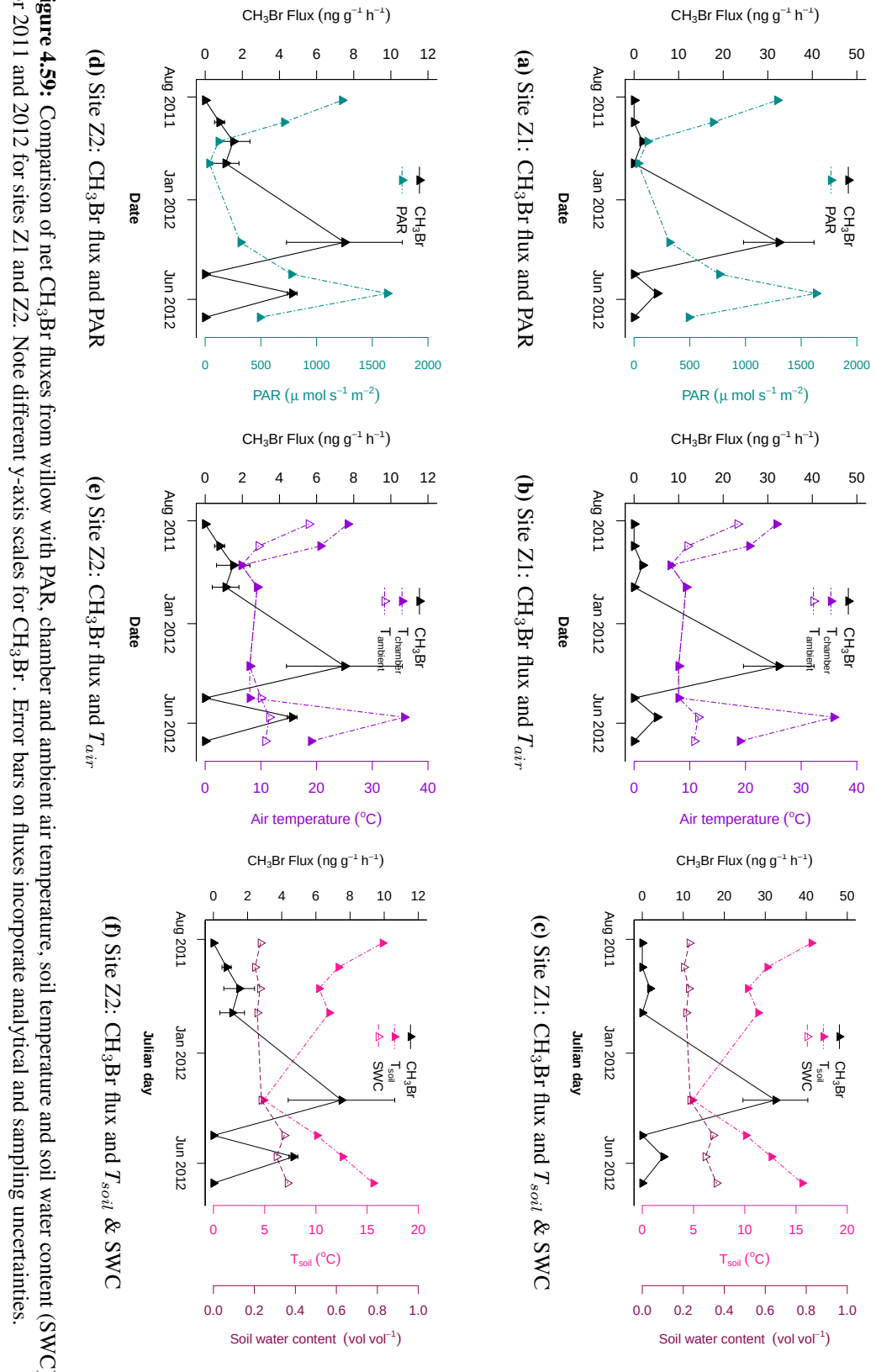
(c) Site Y9: CH_3Br flux and T_{soil} & SWC

(d) Site Y10: CH_3Br flux and PAR

(e) Site Y10: CH_3Br flux and T_{air}

(f) Site Y10: CH_3Br flux and T_{soil} & SWC

Figure 4.58: Comparison of net CH_3Br fluxes from willow with PAR, chamber and ambient air temperature, soil temperature and soil water content (SWC) for 2011 and 2012 for sites Y9 and Y10. Note different y-axis scales for CH_3Br . Error bars on fluxes incorporate analytical and sampling uncertainties.



(a) Site Z1: CH_3Br flux and PAR

(b) Site Z1: CH_3Br flux and T_{air}

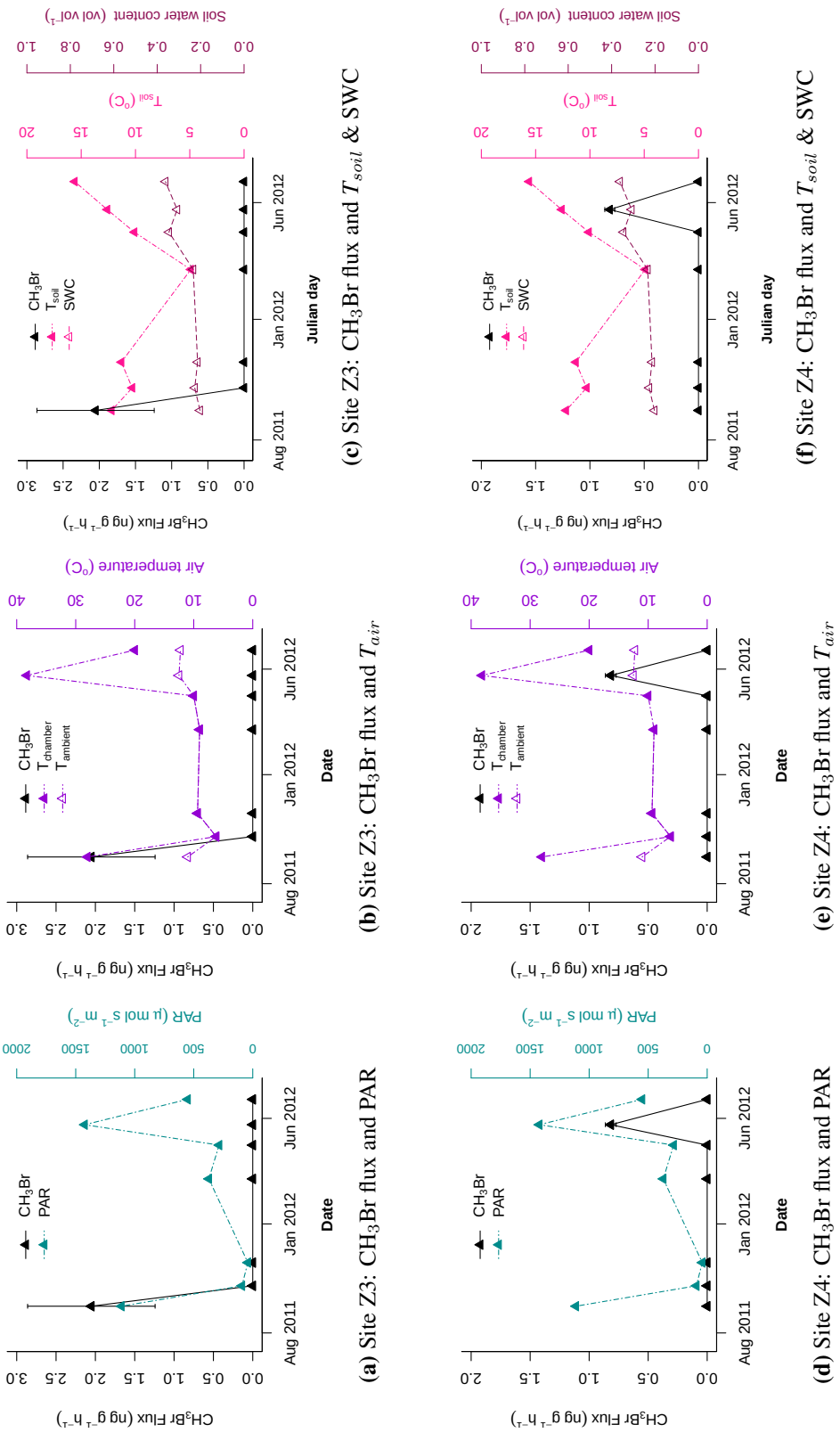
(c) Site Z1: CH_3Br flux and T_{soil} & SWC

(d) Site Z2: CH_3Br flux and PAR

(e) Site Z2: CH_3Br flux and T_{air}

(f) Site Z2: CH_3Br flux and T_{soil} & SWC

Figure 4.59: Comparison of net CH_3Br fluxes from willow with PAR, chamber and ambient air temperature, soil temperature and soil water content (SWC) for 2011 and 2012 for sites Z1 and Z2. Note different y-axis scales for CH_3Br . Error bars on fluxes incorporate analytical and sampling uncertainties.



(a) Site Z3: CH_3Br flux and PAR

(b) Site Z3: CH_3Br flux and T_{air}

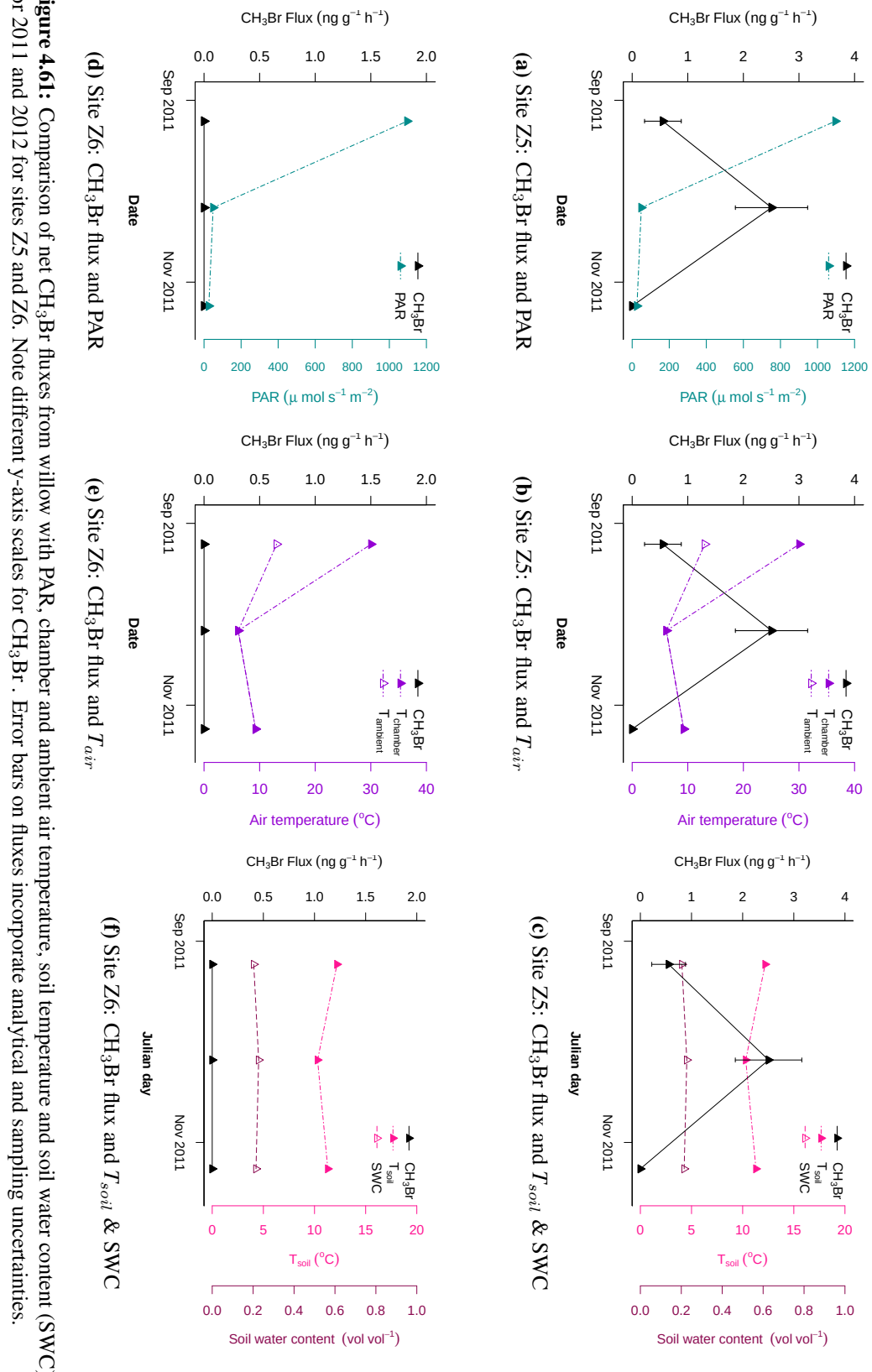
(c) Site Z3: CH_3Br flux and T_{soil} & SWC

(d) Site Z4: CH_3Br flux and PAR

(e) Site Z4: CH_3Br flux and T_{air}

(f) Site Z4: CH_3Br flux and T_{soil} & SWC

Figure 4.60: Comparison of net CH_3Br fluxes from willow with PAR, chamber and ambient air temperature, soil temperature and soil water content (SWC) for 2011 and 2012 for sites Z3 and Z4. Note different y-axis scales for CH_3Br . Error bars on fluxes incorporate analytical and sampling uncertainties.



(a) Site Z5: CH_3Br flux and PAR

(b) Site Z5: CH_3Br flux and T_{air}

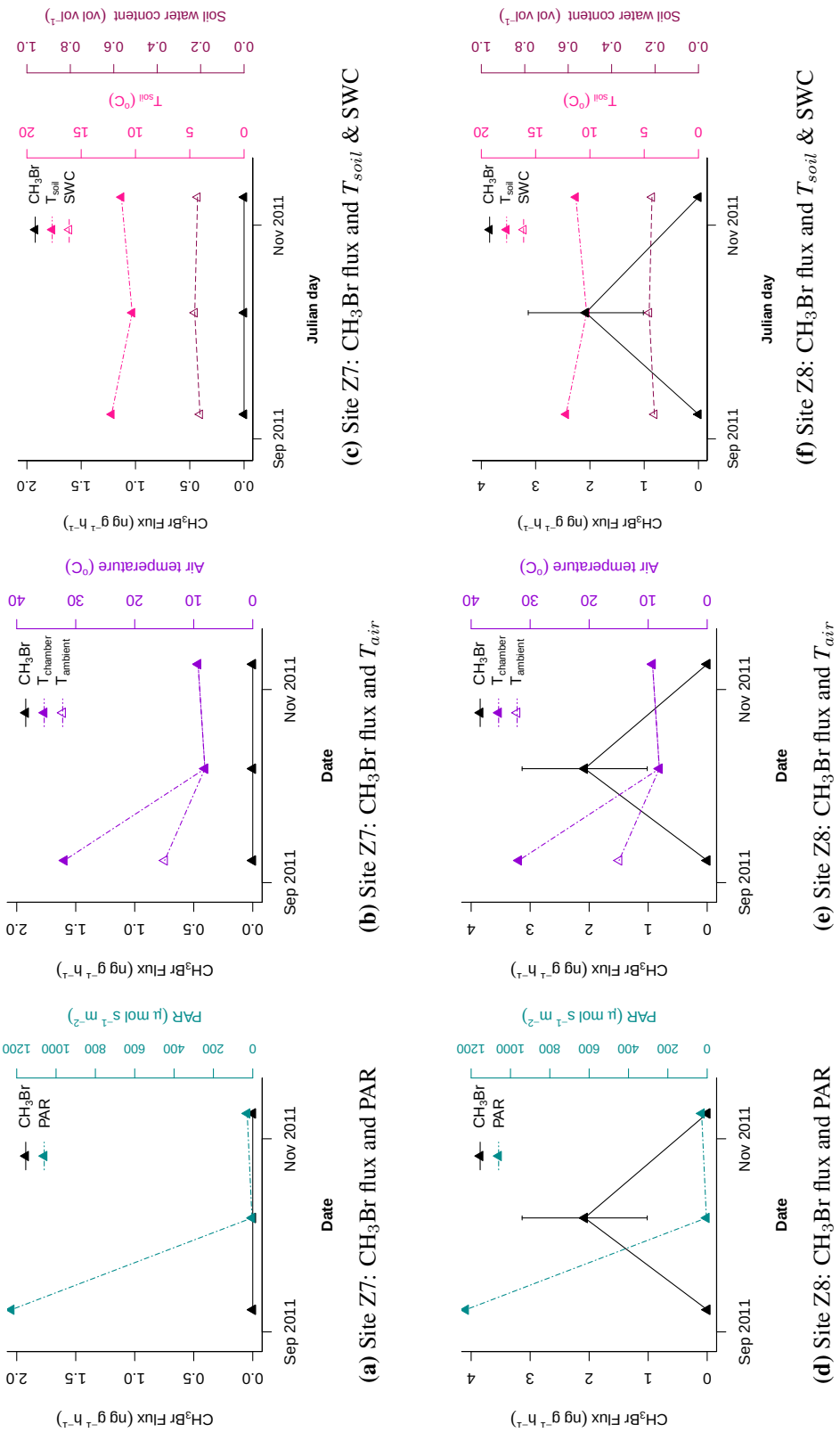
(c) Site Z5: CH_3Br flux and T_{soil} & SWC

(d) Site Z6: CH_3Br flux and PAR

(e) Site Z6: CH_3Br flux and T_{air}

(f) Site Z6: CH_3Br flux and T_{soil} & SWC

Figure 4.61: Comparison of net CH_3Br fluxes from willow with PAR, chamber and ambient air temperature, soil temperature and soil water content (SWC) for 2011 and 2012 for sites Z5 and Z6. Note different y-axis scales for CH_3Br . Error bars on fluxes incorporate analytical and sampling uncertainties.



(a) Site Z7: CH_3Br flux and PAR

(b) Site Z7: CH_3Br flux and T_{air}

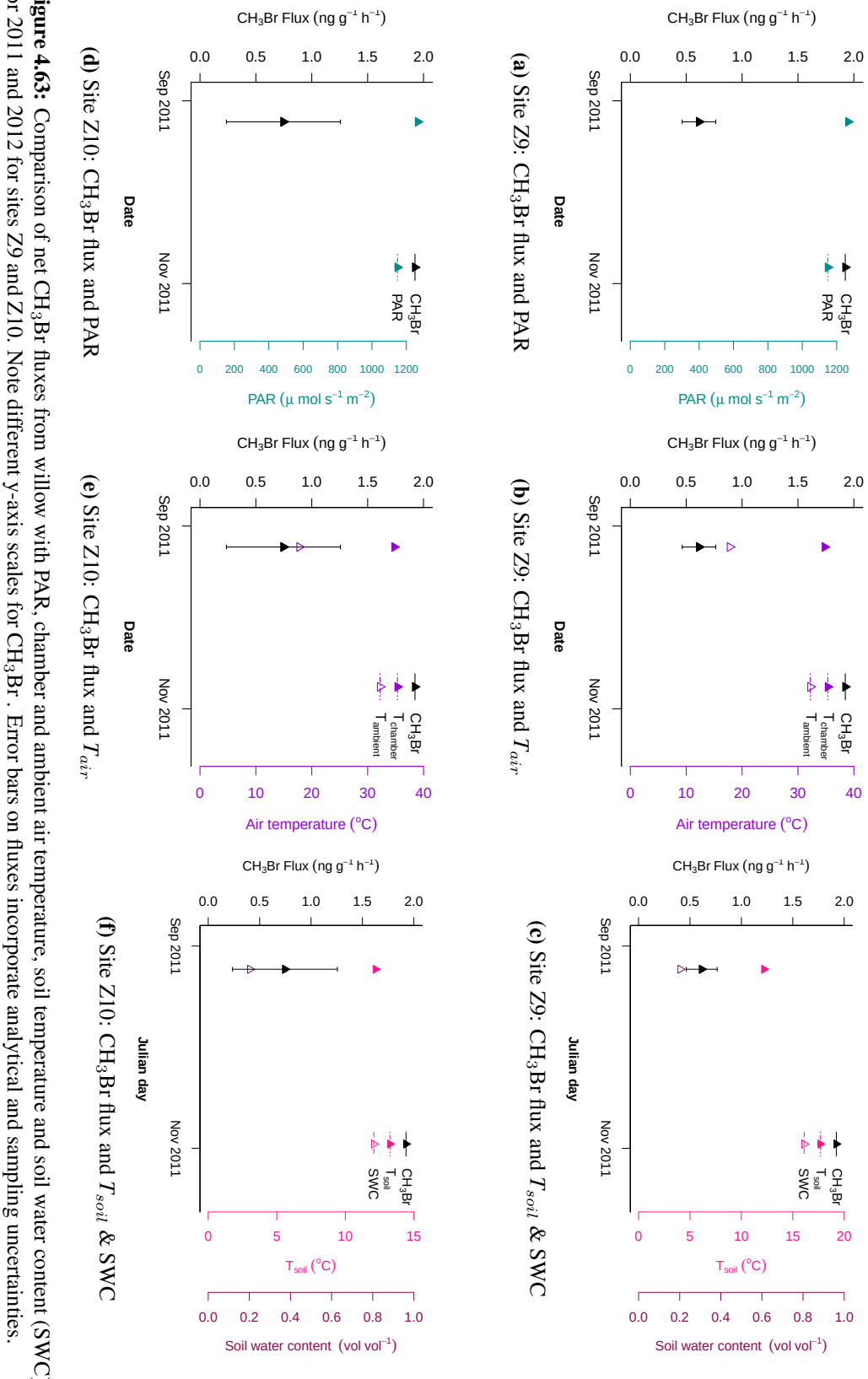
(c) Site Z7: CH_3Br flux and T_{soil} & SWC

(d) Site Z8: CH_3Br flux and PAR

(e) Site Z8: CH_3Br flux and T_{air}

(f) Site Z8: CH_3Br flux and T_{soil} & SWC

Figure 4.62: Comparison of net CH_3Br fluxes from willow with PAR, chamber and ambient air temperature, soil temperature and soil water content (SWC) for 2011 and 2012 for sites Z7 and Z8. Note different y-axis scales for CH_3Br . Error bars on fluxes incorporate analytical and sampling uncertainties.



(a) Site Z9: CH_3Br flux and PAR

(b) Site Z9: CH_3Br flux and T_{air}

(c) Site Z9: CH_3Br flux and T_{soil} & SWC

(d) Site Z10: CH_3Br flux and PAR

(e) Site Z10: CH_3Br flux and T_{air}

(f) Site Z10: CH_3Br flux and T_{soil} & SWC

Figure 4.63: Comparison of net CH_3Br fluxes from willow with PAR, chamber and ambient air temperature, soil temperature and soil water content (SWC) for 2011 and 2012 for sites Z9 and Z10. Note different y-axis scales for CH_3Br . Error bars on fluxes incorporate analytical and sampling uncertainties.

CH_3Cl

CH_3Cl fluxes measured between August 2011 and June 2012 at all sampling points and the mean of those values on each sampling occasion during 2011 and 2012 are illustrated in Figure 4.64. CH_3Cl fluxes were highest in November 2011 and May 2012. Fluxes generally ranged between zero and 70 ng g^{-1} h^{-1}, with the exception of two high fluxes of 120 and 158 ng g^{-1} h^{-1} measured in November 2011.

In August 2011, fluxes of between zero and 15 ng g^{-1} h^{-1} were measured. Fluxes of between zero and 56 ng g^{-1} h^{-1} were measured in September. In October, fluxes of 23 ng g^{-1} h^{-1} were measured at two sites and zero fluxes at all other sites. Fluxes of between zero and 158 ng g^{-1} h^{-1} were measured in November. Zero fluxes were measured in March and April 2012. Fluxes of between zero and 58 ng g^{-1} h^{-1} were measured in May, and between zero and 71 ng g^{-1} h^{-1} in June 2012. Mean fluxes varied between zero and 19 ng g^{-1} h^{-1}.

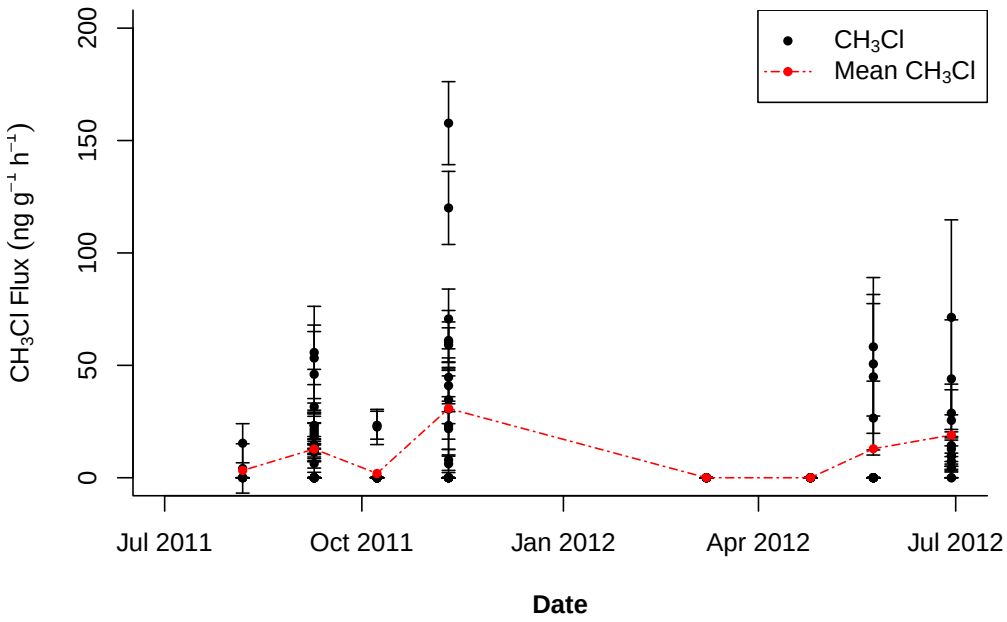


Figure 4.64: CH_3Cl fluxes from willow at the Arnot fieldsite at all thirty sampling points and the mean of those values on each sampling occasion from 2011 to 2012. Error bars on fluxes incorporate analytical and sampling uncertainties (as described in Section 2.6.1).

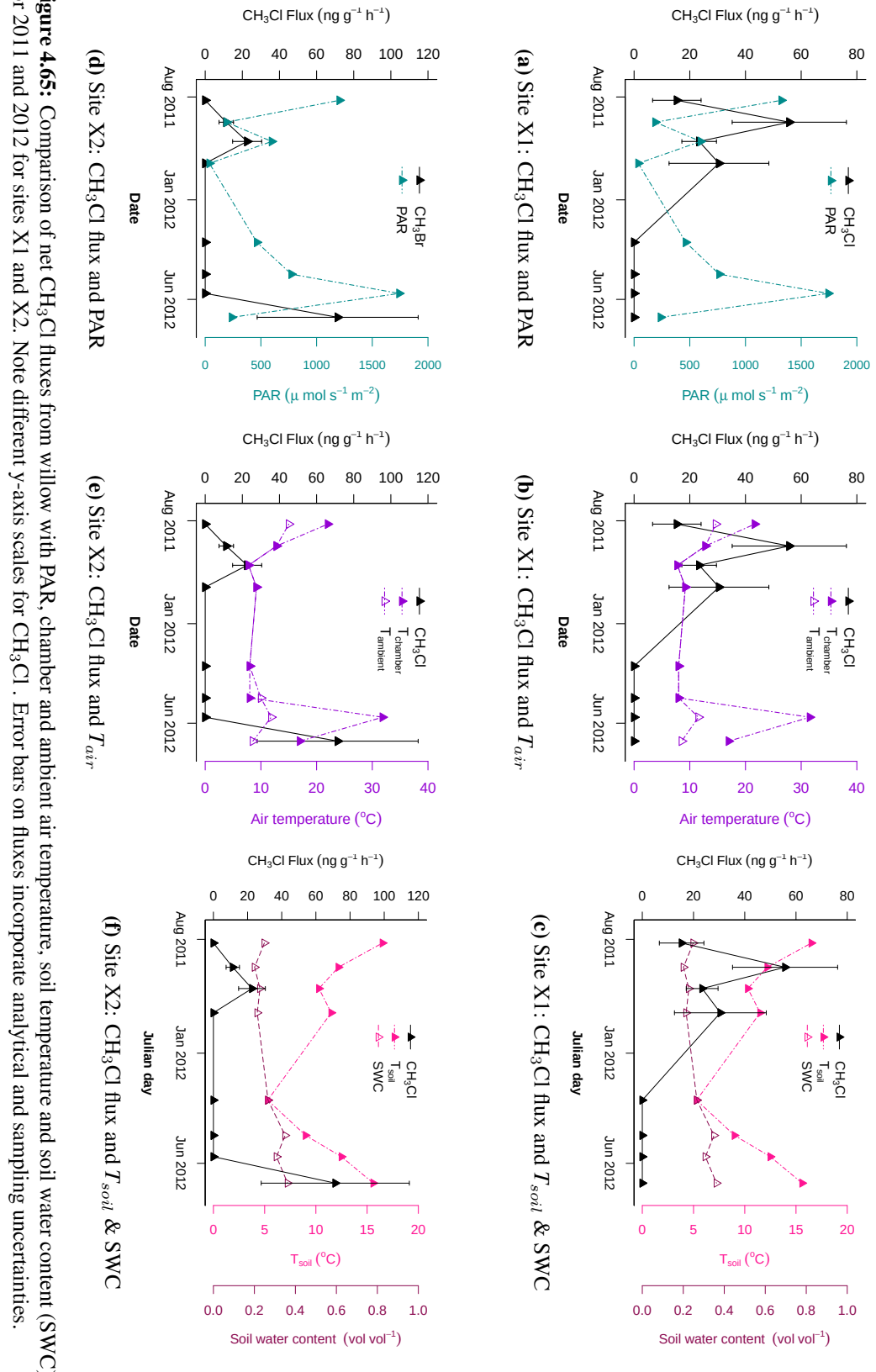
Time series of CH_3Cl fluxes from each individual site between August 2011 and June 2012 together with the concurrent PAR, ambient and chamber air temperature, soil temperature and soil water content observations are illustrated in Figures 4.65 to 4.79. The statistical significance of correlations between CH_3Cl fluxes and environmental variables is described in Section 4.3.3.

Mean CH_3Cl fluxes were very similar in all three fields, with a range of fluxes between zero and 31 ng g^{-1} h^{-1} (Table 4.16), excluding sites X9 and X10, Y9 and Y10 and Z9 and Z10 as they were measured only once. Higher mean CH_3Cl fluxes (between 4.7 and 43 ng g^{-1} h^{-1}) were measured at sites X1 - 5, Y1 - 6 and Z1 - 5 and Z8. Mean fluxes of zero were measured at the remaining 9 sites. Median fluxes of between zero and 25 ng g^{-1} h^{-1} were calculated. The highest maximum flux of 158 ng g^{-1} h^{-1} was measured at site Y3 in August 2011. The minimum flux recorded at all sites was zero.

Mean fluxes of 11, 13 and 11 ng g^{-1} h^{-1} were calculated from all fluxes measured during the measurement period combined for fields X, Y and X, respectively. An overall mean CH_3Cl flux of 12 ng g^{-1} h^{-1} was calculated from fluxes measured at all sites during the measurement period, about 7 times the overall mean calculated for CH_3Br.

Table 4.16: Mean, median, minimum and maximum net CH_3Cl fluxes from SRC willow at Arnot during 2011 to 2012. All flux values are in $ng\,g^{-1}\,h^{-1}$. The final column gives the number of measurements made. The last row summarises all fluxes from all sites.

Site	Mean	Median	Min	Max	Number
Willow X1	15.6	7.68	0.00	55.7	8
Willow X2	13.2	0.00	0.00	71.4	8
Willow X3	12.1	0.00	0.00	60.3	7
Willow X4	6.38	0.00	0.00	44.7	7
Willow X5	31.3	23.3	0.00	70.6	3
Willow X6	0.00	0.00	0.00	0.00	3
Willow X7	0.00	0.00	0.00	0.00	3
Willow X8	0.00	0.00	0.00	0.00	3
Willow X9	0.00	0.00	0.00	0.00	1
Willow X10	46.0	46.0	46.0	46.0	1
All X	11.4	0.00	0.00	71.4	44
Willow Y1	4.68	0.00	0.00	20.5	8
Willow Y2	6.92	0.00	0.00	41.0	8
Willow Y3	26.3	0.00	0.00	158	7
Willow Y4	19.2	0.00	0.00	59.1	7
Willow Y5	42.7	25.3	0.00	120	4
Willow Y6	5.82	0.00	0.00	23.3	4
Willow Y7	0.00	0.00	0.00	0.00	3
Willow Y8	0.00	0.00	0.00	0.00	3
Willow Y9	0.00	0.00	0.00	0.00	1
Willow Y10	0.00	0.00	0.00	0.00	1
All Y	13.2	0.00	0.00	158	46
Willow Z1	18.1	0.00	0.00	61.1	8
Willow Z2	9.06	3.70	0.00	44.9	8
Willow Z3	12.1	0.00	0.00	53.2	7
Willow Z4	9.57	0.00	0.00	28.7	7
Willow Z5	6.42	0.00	0.00	19.3	3
Willow Z6	0.00	0.00	0.00	0.00	3
Willow Z7	13.7	6.36	0.00	34.7	3
Willow Z8	9.80	6.23	0.00	23.2	3
Willow Z9	14.6	14.6	14.6	14.6	1
Willow Z10	18.3	18.3	18.3	18.3	1
All Z	11.2	0.00	0.00	61.1	44
Overall	11.9	0.00	0.00	158	132



(a) Site X1: CH_3Cl flux and PAR

(b) Site X1: CH_3Cl flux and T_{air}

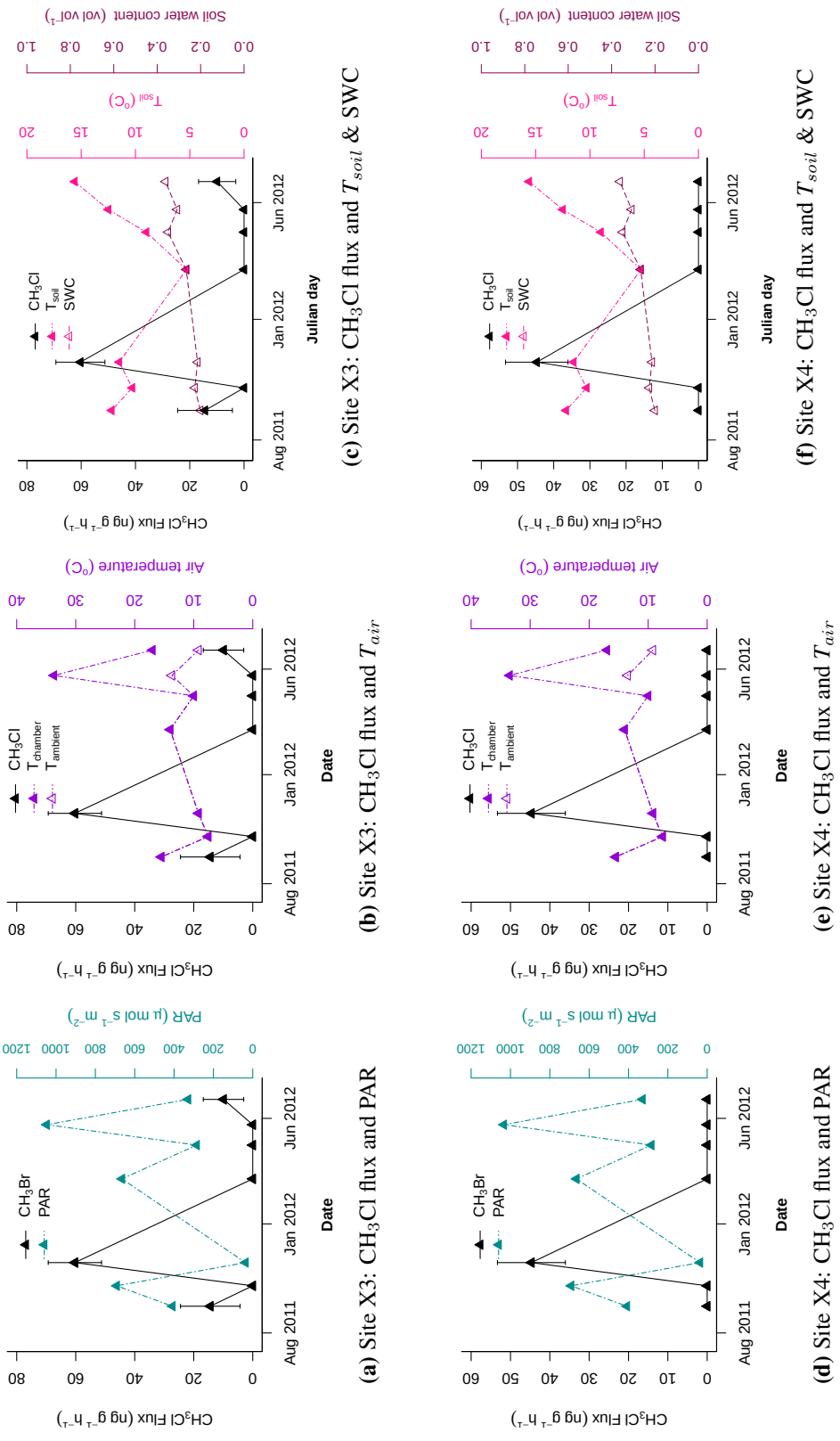
(c) Site X1: CH_3Cl flux and T_{soil} & SWC

(d) Site X2: CH_3Cl flux and PAR

(e) Site X2: CH_3Cl flux and T_{air}

(f) Site X2: CH_3Cl flux and T_{soil} & SWC

Figure 4.65: Comparison of net CH_3Cl fluxes from willow with PAR, chamber and ambient air temperature, soil temperature and soil water content (SWC) for 2011 and 2012 for sites X1 and X2. Note different y-axis scales for CH_3Cl . Error bars on fluxes incorporate analytical and sampling uncertainties.



(a) Site X3: CH_3Cl flux and PAR

(b) Site X3: CH_3Cl flux and T_{air}

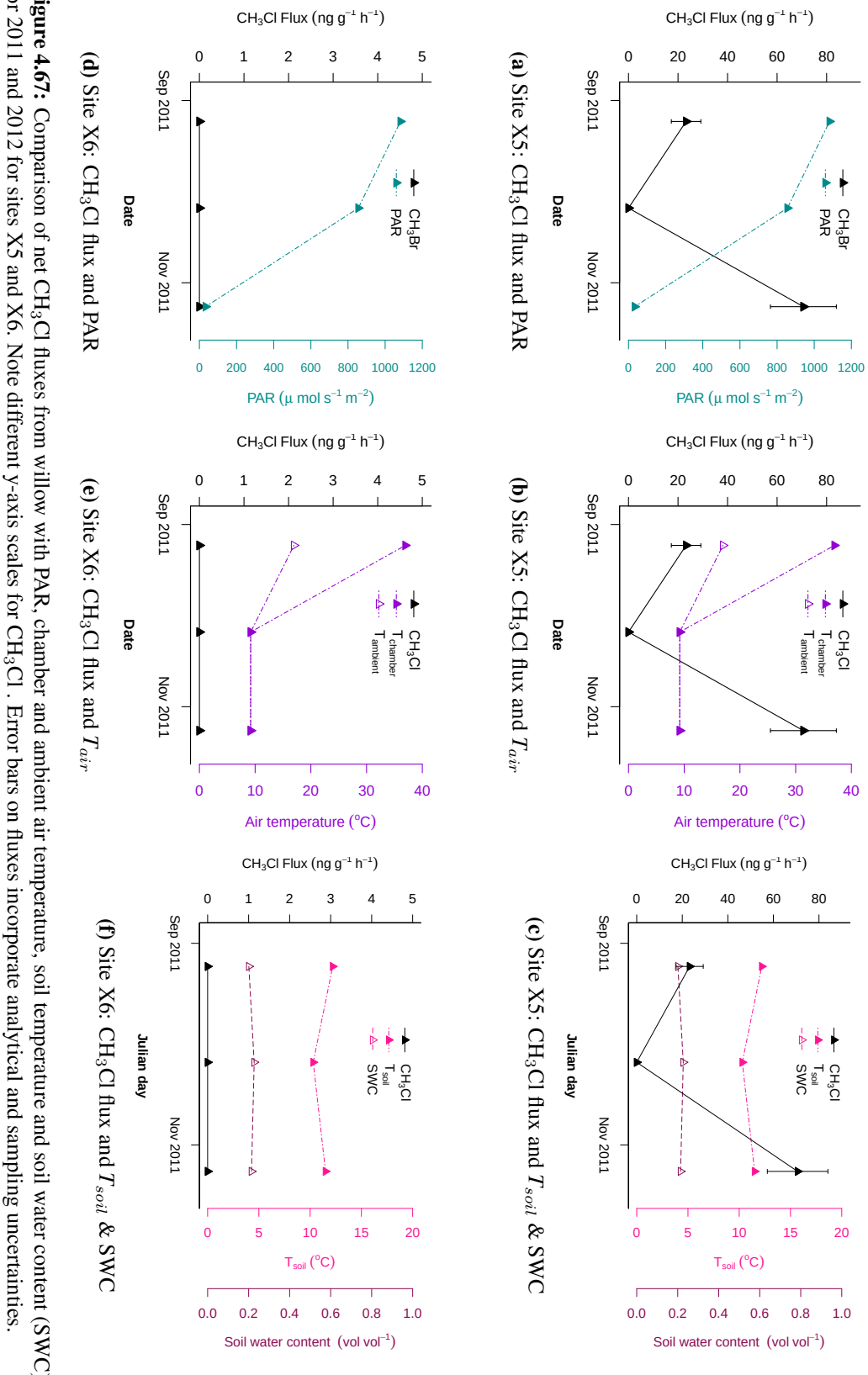
(c) Site X3: CH_3Cl flux and T_{soil} & SWC

(d) Site X4: CH_3Cl flux and PAR

(e) Site X4: CH_3Cl flux and T_{air}

(f) Site X4: CH_3Cl flux and T_{soil} & SWC

Figure 4.66: Comparison of net CH_3Cl fluxes from willow with PAR, chamber and ambient air temperature, soil temperature and soil water content (SWC) for 2011 and 2012 for sites X3 and X4. Note different y-axis scales for CH_3Cl . Error bars on fluxes incorporate analytical and sampling uncertainties.



(a) Site X5: CH_3Cl flux and PAR

(b) Site X5: CH_3Cl flux and T_{air}

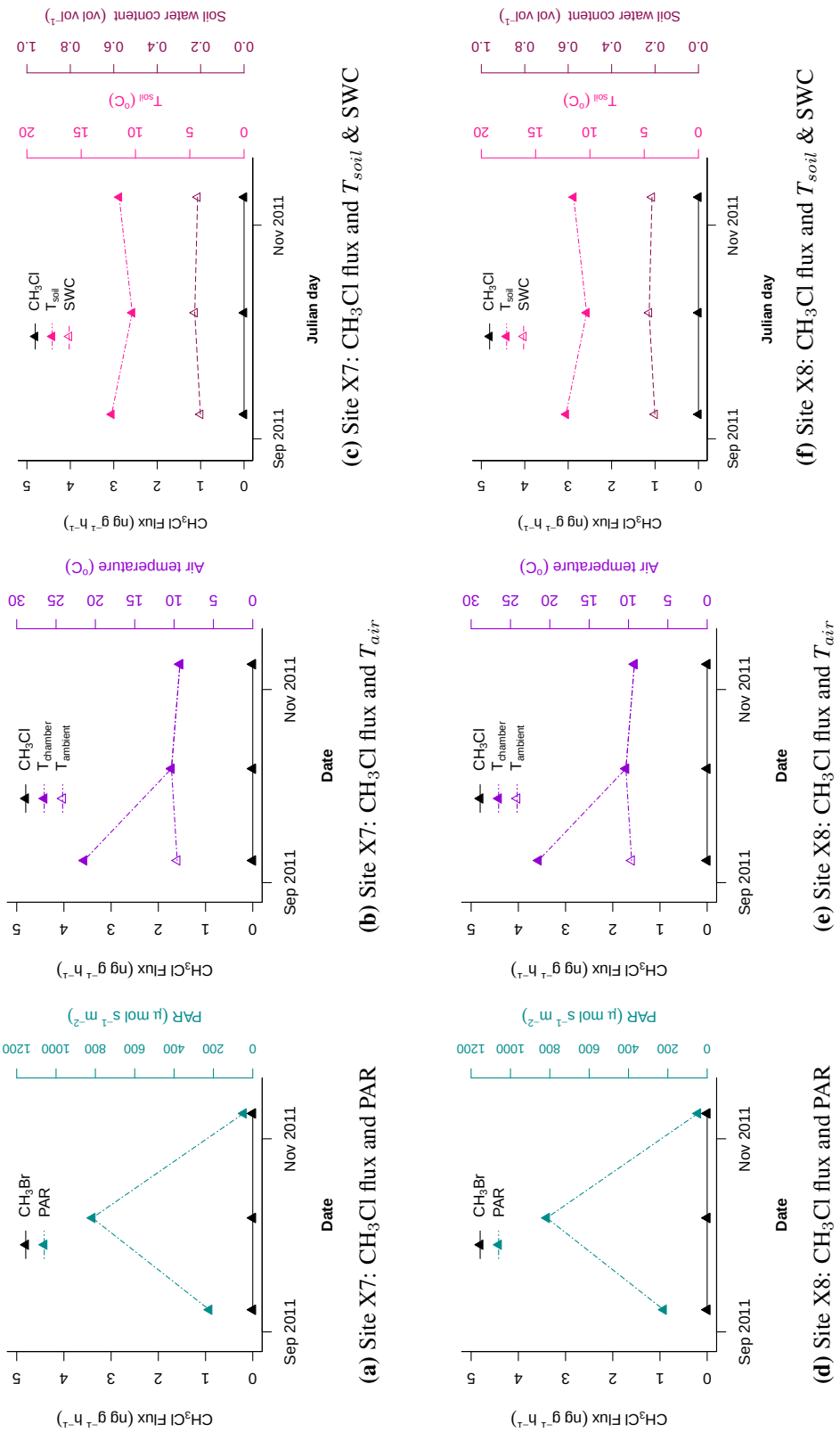
(c) Site X5: CH_3Cl flux and T_{soil} & SWC

(d) Site X6: CH_3Cl flux and PAR

(e) Site X6: CH_3Cl flux and T_{air}

(f) Site X6: CH_3Cl flux and T_{soil} & SWC

Figure 4.67: Comparison of net CH_3Cl fluxes from willow with PAR, chamber and ambient air temperature, soil temperature and soil water content (SWC) for 2011 and 2012 for sites X5 and X6. Note different y-axis scales for CH_3Cl . Error bars on fluxes incorporate analytical and sampling uncertainties.



(a) Site X7: CH_3Cl flux and PAR

(b) Site X7: CH_3Cl flux and T_{air}

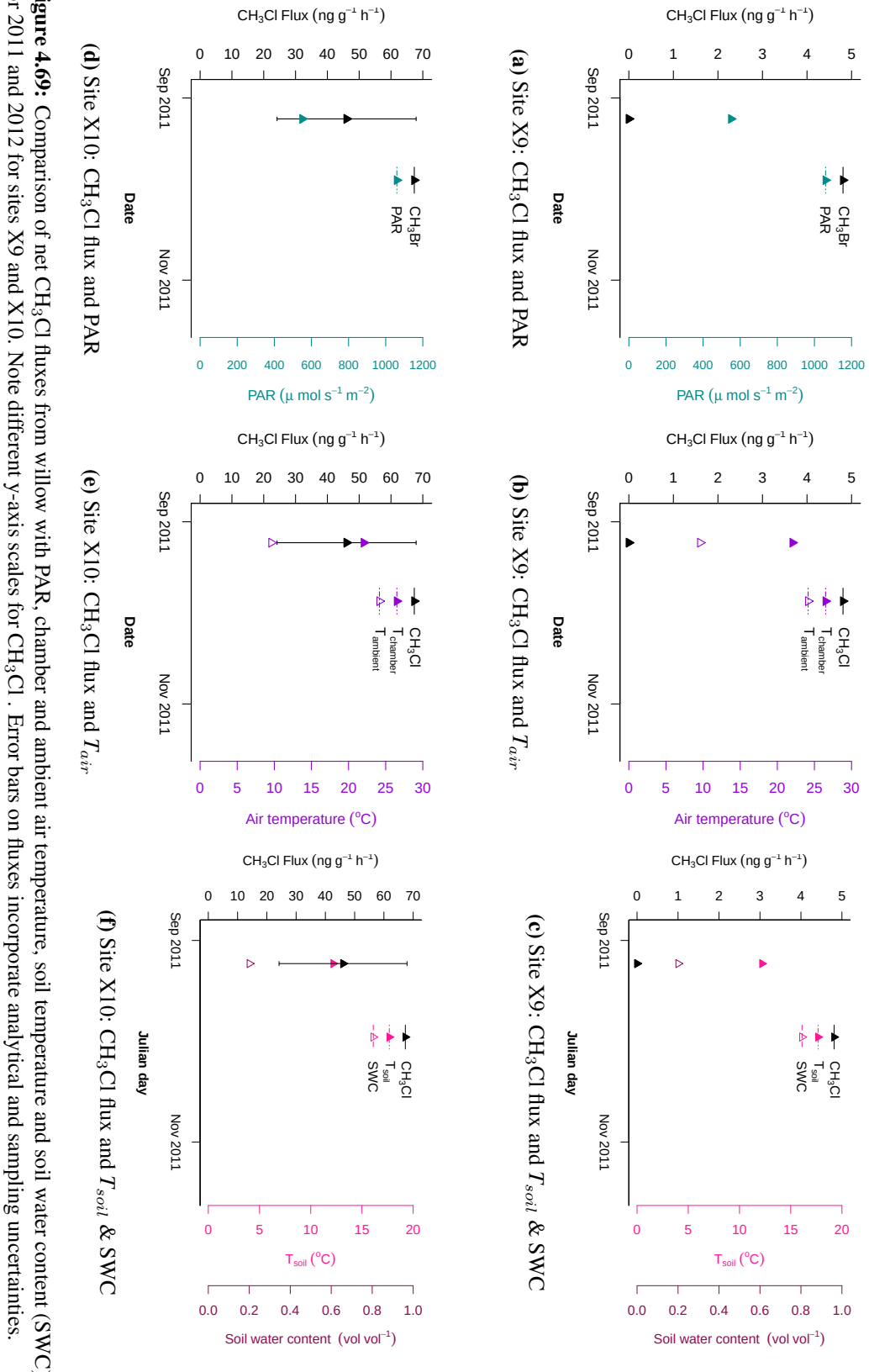
(c) Site X7: CH_3Cl flux and T_{soil} & SWC

(d) Site X8: CH_3Cl flux and PAR

(e) Site X8: CH_3Cl flux and T_{air}

(f) Site X8: CH_3Cl flux and T_{soil} & SWC

Figure 4.68: Comparison of net CH_3Cl fluxes from willow with PAR, chamber and ambient air temperature, soil temperature and soil water content (SWC) for 2011 and 2012 for sites X7 and X8. Note different y-axis scales for CH_3Cl . Error bars on fluxes incorporate analytical and sampling uncertainties.



(a) Site X9: CH_3Cl flux and PAR

(b) Site X9: CH_3Cl flux and T_{air}

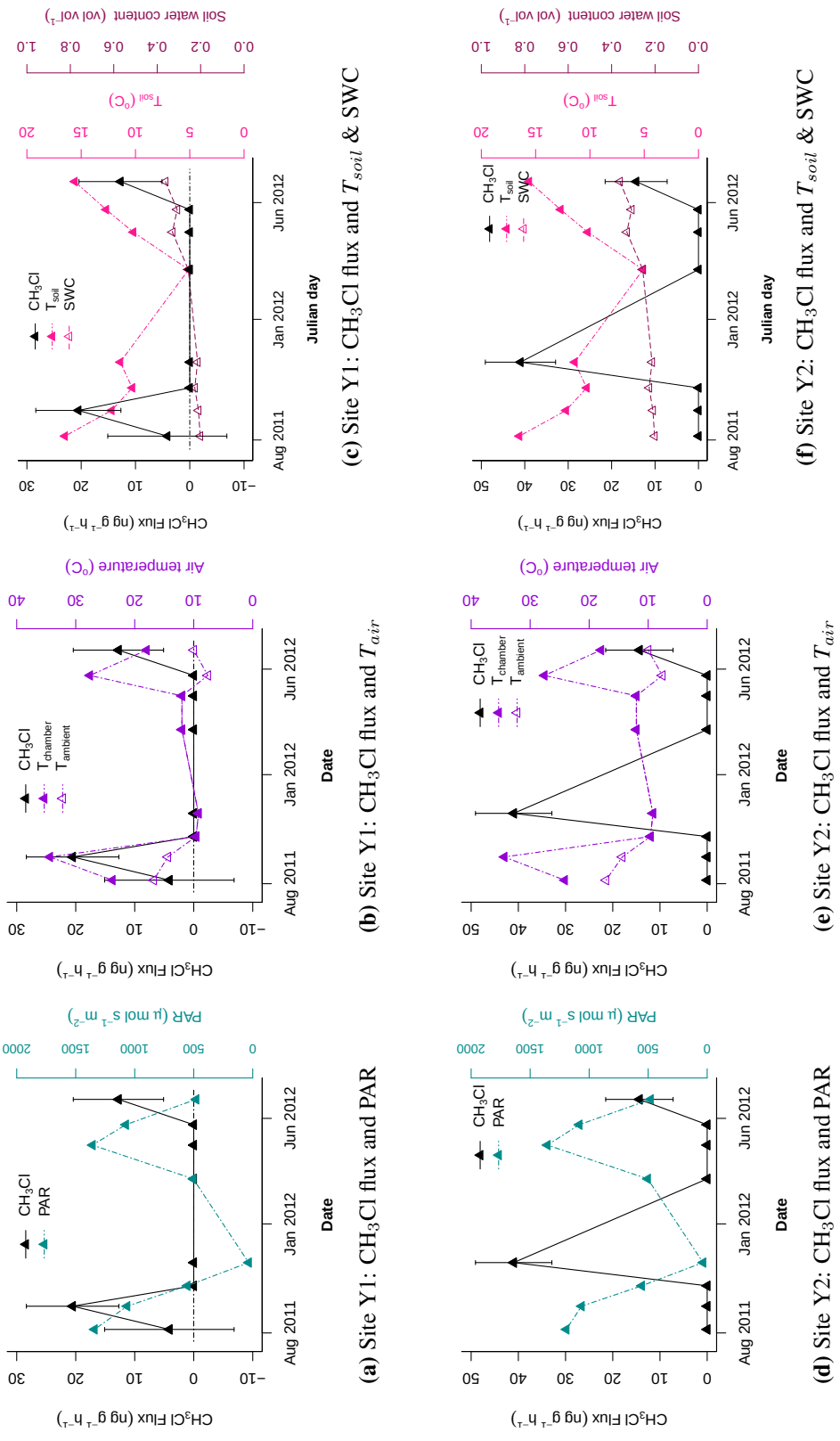
(c) Site X9: CH_3Cl flux and T_{soil} & SWC

(d) Site X10: CH_3Cl flux and PAR

(e) Site X10: CH_3Cl flux and T_{air}

(f) Site X10: CH_3Cl flux and T_{soil} & SWC

Figure 4.69: Comparison of net CH_3Cl fluxes from willow with PAR, chamber and ambient air temperature, soil temperature and soil water content (SWC) for 2011 and 2012 for sites X9 and X10. Note different y-axis scales for CH_3Cl . Error bars on fluxes incorporate analytical and sampling uncertainties.



(a) Site Y1: CH_3Cl flux and PAR

(b) Site Y1: CH_3Cl flux and T_{air}

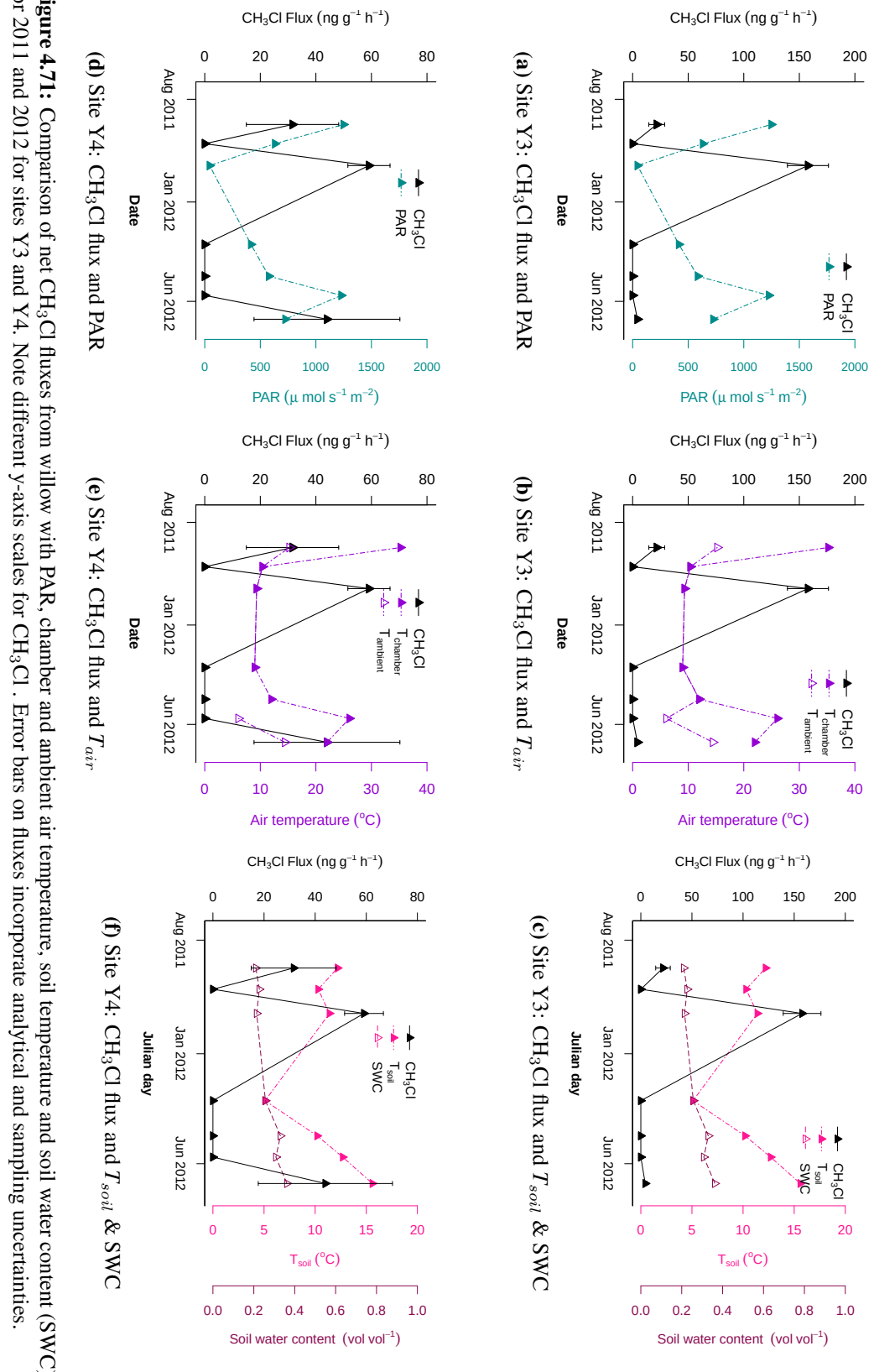
(c) Site Y1: CH_3Cl flux and T_{soil} & SWC

(d) Site Y2: CH_3Cl flux and PAR

(e) Site Y2: CH_3Cl flux and T_{air}

(f) Site Y2: CH_3Cl flux and T_{soil} & SWC

Figure 4.70: Comparison of net CH_3Cl fluxes from willow with PAR, chamber and ambient air temperature, soil temperature and soil water content (SWC) for 2011 and 2012 for sites Y1 and Y2. Note different y-axis scales for CH_3Cl . Error bars on fluxes incorporate analytical and sampling uncertainties.



(a) Site Y3: CH_3Cl flux and PAR

(b) Site Y3: CH_3Cl flux and T_{air}

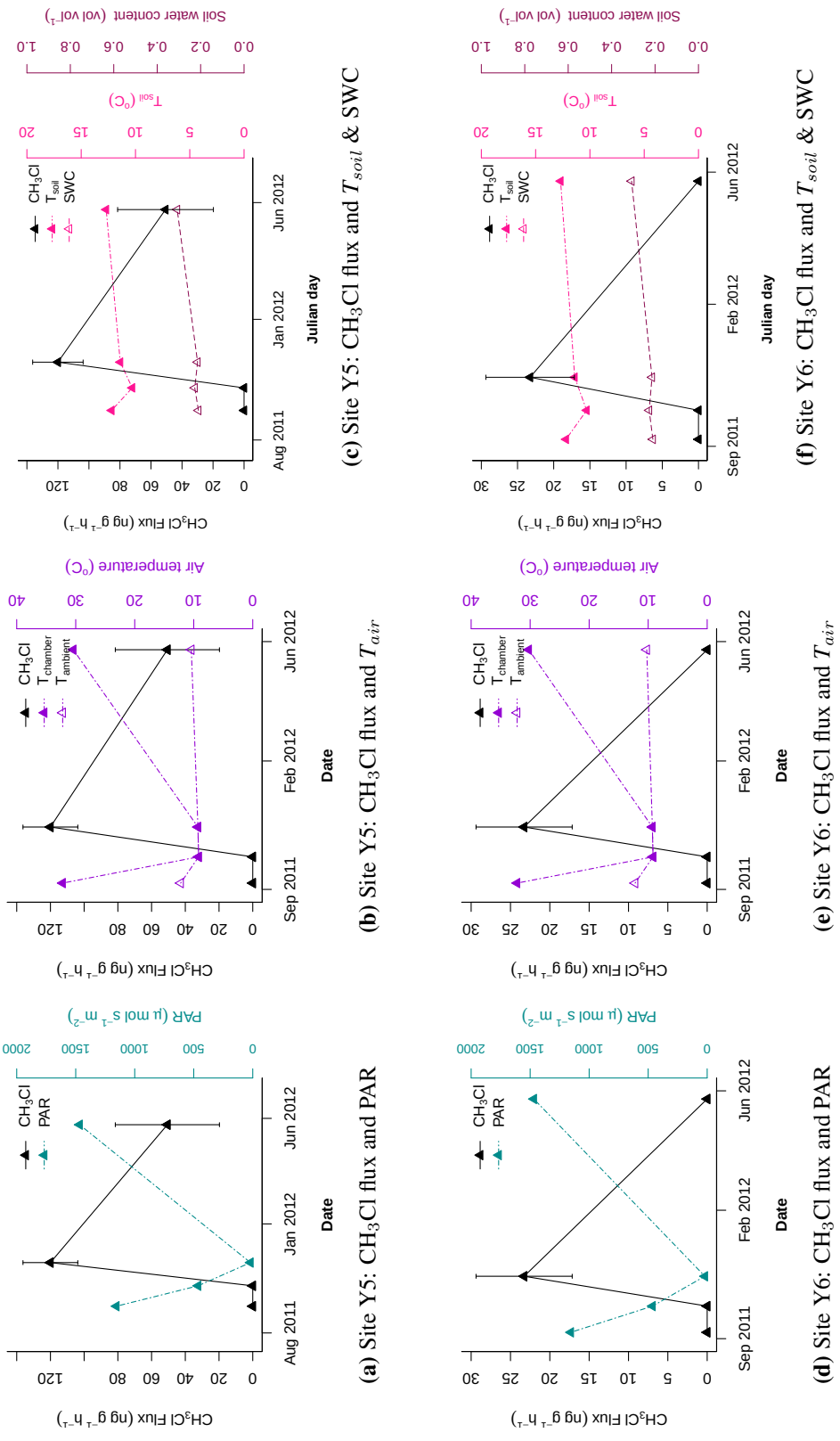
(c) Site Y3: CH_3Cl flux and T_{soil} & SWC

(d) Site Y4: CH_3Cl flux and PAR

(e) Site Y4: CH_3Cl flux and T_{air}

(f) Site Y4: CH_3Cl flux and T_{soil} & SWC

Figure 4.71: Comparison of net CH_3Cl fluxes from willow with PAR, chamber and ambient air temperature, soil temperature and soil water content (SWC) for 2011 and 2012 for sites Y3 and Y4. Note different y-axis scales for CH_3Cl . Error bars on fluxes incorporate analytical and sampling uncertainties.



(a) Site Y5: CH_3Cl flux and PAR

(b) Site Y5: CH_3Cl flux and T_{air}

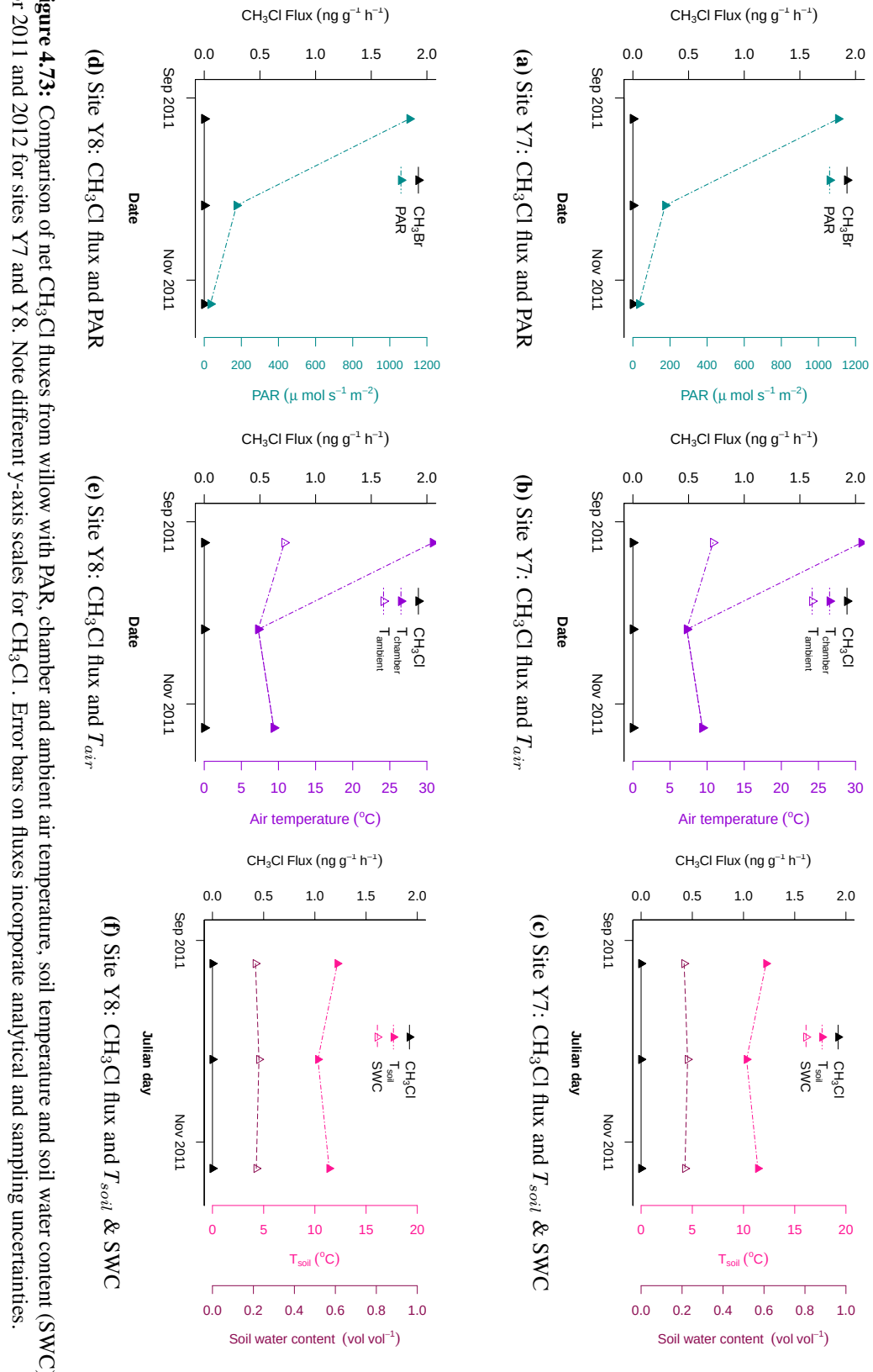
(c) Site Y5: CH_3Cl flux and T_{soil} & SWC

(d) Site Y6: CH_3Cl flux and PAR

(e) Site Y6: CH_3Cl flux and T_{air}

(f) Site Y6: CH_3Cl flux and T_{soil} & SWC

Figure 4.72: Comparison of net CH_3Cl fluxes from willow with PAR, chamber and ambient air temperature, soil temperature and soil water content (SWC) for 2011 and 2012 for sites Y5 and Y6. Note different y-axis scales for CH_3Cl . Error bars on fluxes incorporate analytical and sampling uncertainties.



(a) Site Y7: CH_3Cl flux and PAR

(b) Site Y7: CH_3Cl flux and T_{air}

(c) Site Y7: CH_3Cl flux and T_{soil} & SWC

(d) Site Y8: CH_3Cl flux and PAR

(e) Site Y8: CH_3Cl flux and T_{air}

(f) Site Y8: CH_3Cl flux and T_{soil} & SWC

Figure 4.73: Comparison of net CH_3Cl fluxes from willow with PAR, chamber and ambient air temperature, soil temperature and soil water content (SWC) for 2011 and 2012 for sites Y7 and Y8. Note different y-axis scales for CH_3Cl . Error bars on fluxes incorporate analytical and sampling uncertainties.

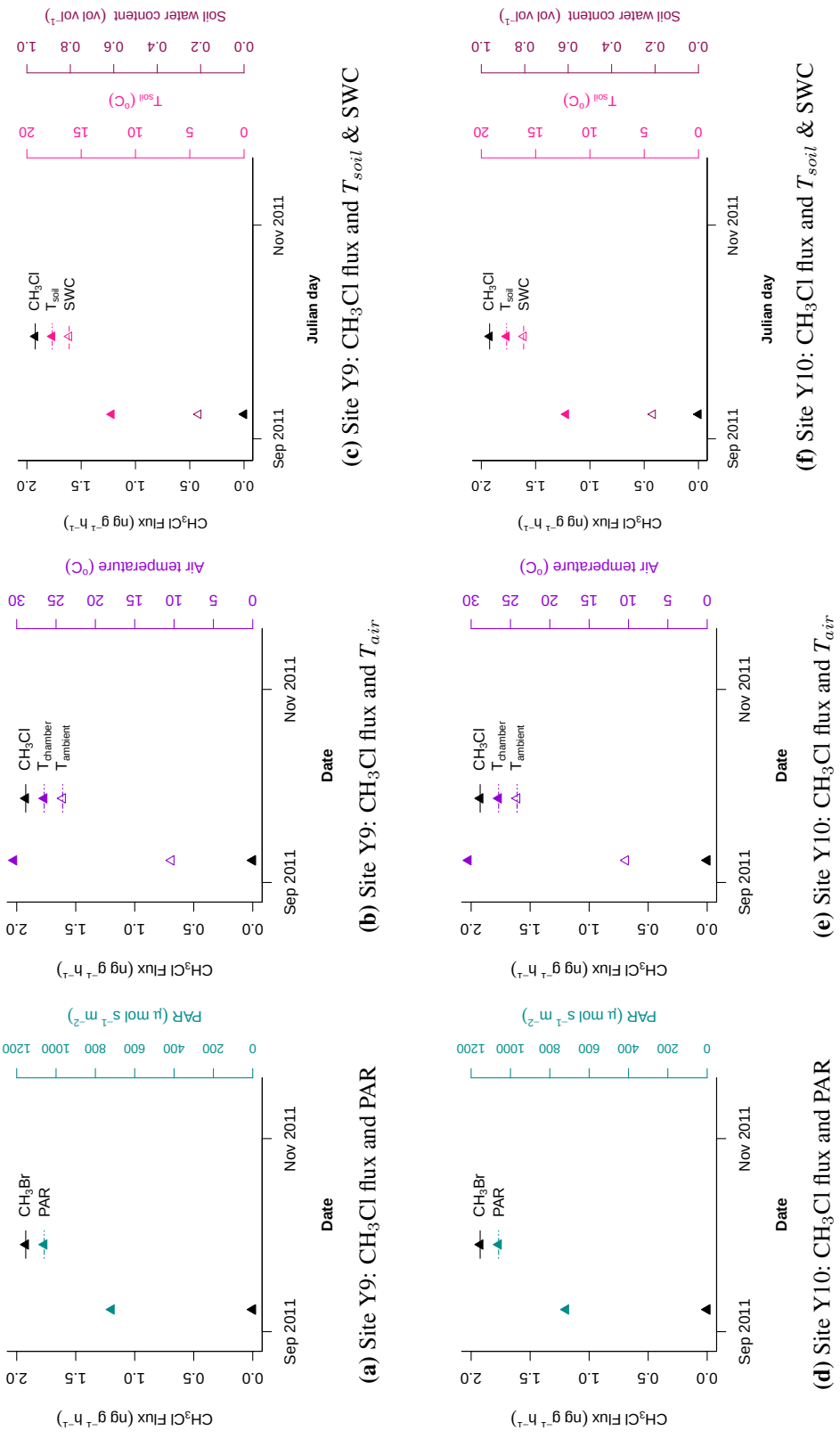
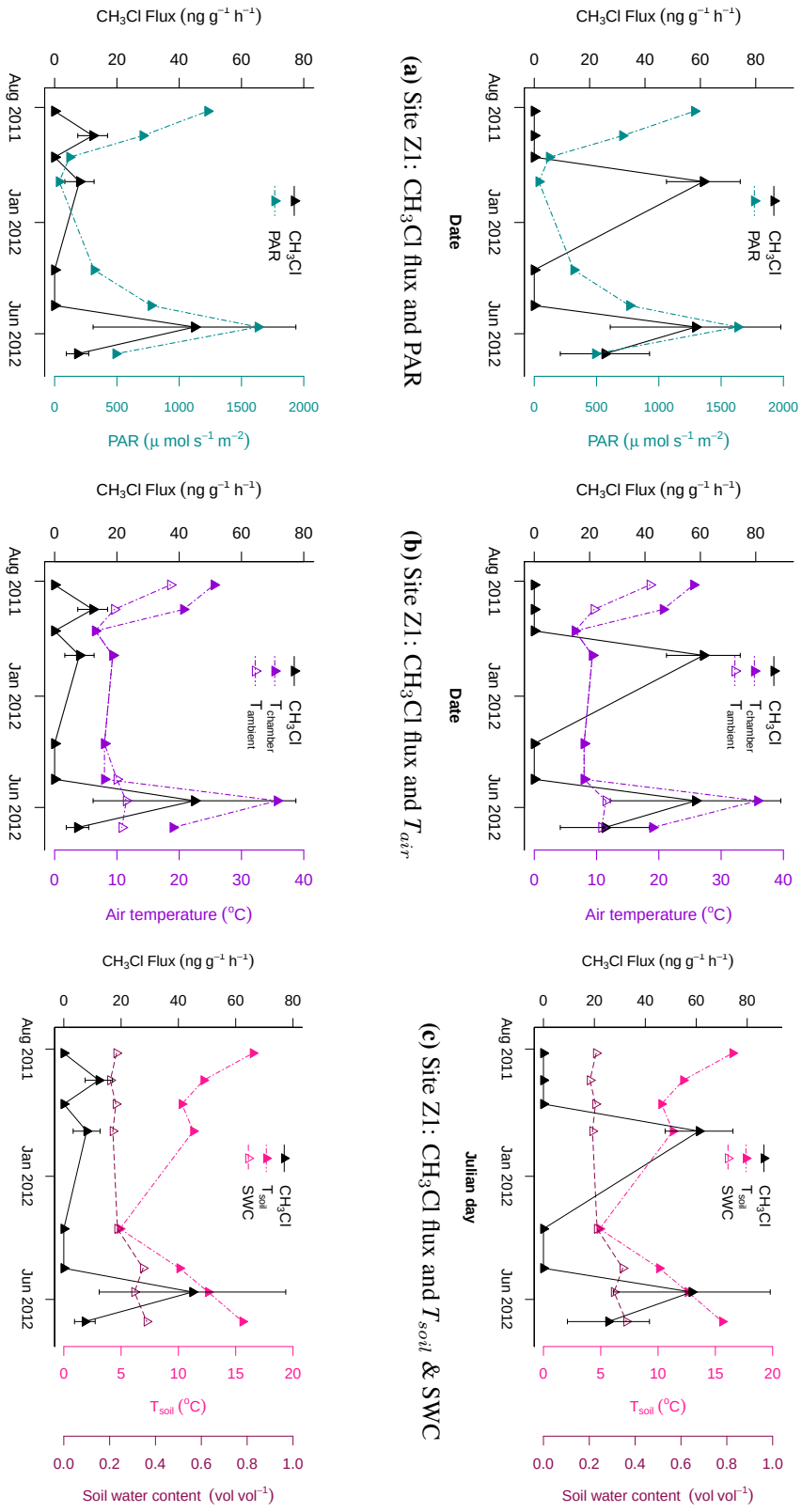


Figure 4.74: Comparison of net CH_3Cl fluxes from willow with PAR, chamber and ambient air temperature, soil temperature and soil water content (SWC) for 2011 and 2012 for sites Y9 and Y10. Note different y-axis scales for CH_3Cl . Error bars on fluxes incorporate analytical and sampling uncertainties.



(a) Site Z1: CH_3Cl flux and PAR

(b) Site Z1: CH_3Cl flux and T_{air}

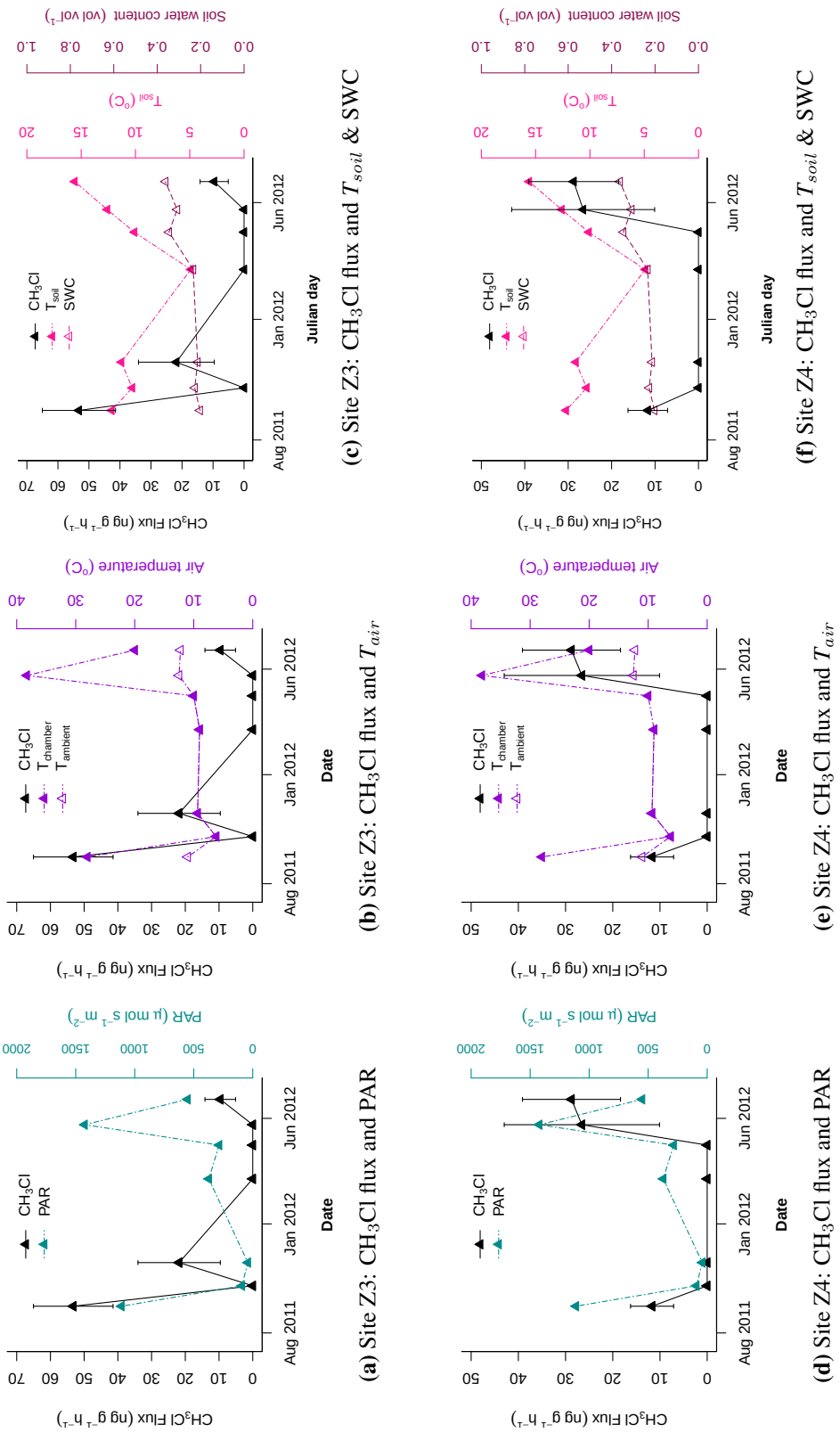
(c) Site Z1: CH_3Cl flux and T_{soil} & SWC

(d) Site Z2: CH_3Cl flux and PAR

(e) Site Z2: CH_3Cl flux and T_{air}

(f) Site Z2: CH_3Cl flux and T_{soil} & SWC

Figure 4.75: Comparison of net CH_3Cl fluxes from willow with PAR, chamber and ambient air temperature, soil temperature and soil water content (SWC) for 2011 and 2012 for sites Z1 and Z2. Note different y-axis scales for CH_3Cl . Error bars on fluxes incorporate analytical and sampling uncertainties.



(a) Site Z3: CH_3Cl flux and PAR

(b) Site Z3: CH_3Cl flux and T_{air}

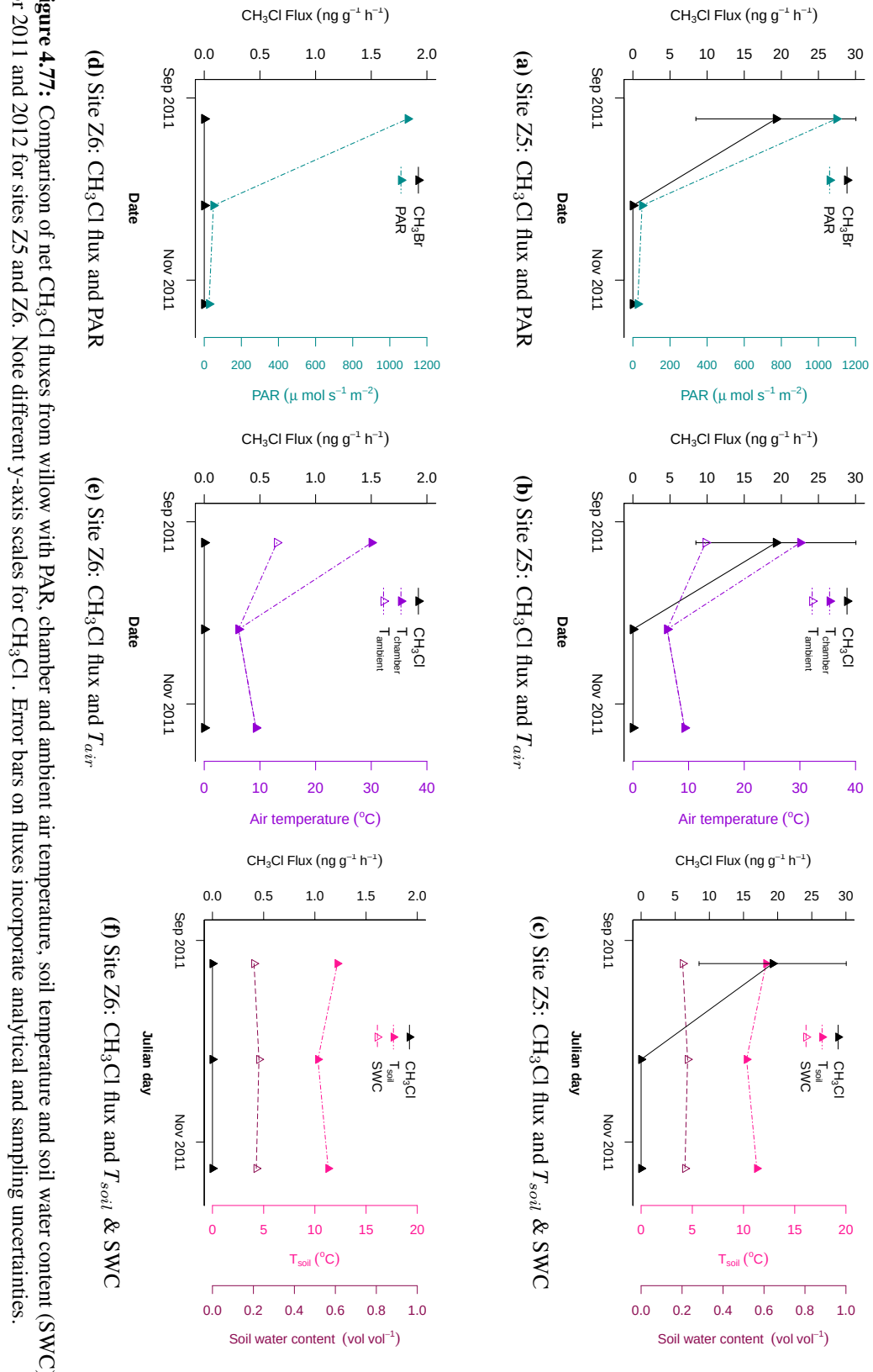
(c) Site Z3: CH_3Cl flux and T_{soil} & SWC

(d) Site Z4: CH_3Cl flux and PAR

(e) Site Z4: CH_3Cl flux and T_{air}

(f) Site Z4: CH_3Cl flux and T_{soil} & SWC

Figure 4.76: Comparison of net CH_3Cl fluxes from willow with PAR, chamber and ambient air temperature, soil temperature and soil water content (SWC) for 2011 and 2012 for sites Z3 and Z4. Note different y-axis scales for CH_3Cl . Error bars on fluxes incorporate analytical and sampling uncertainties.



(a) Site Z5: CH_3Cl flux and PAR

(b) Site Z5: CH_3Cl flux and T_{air}

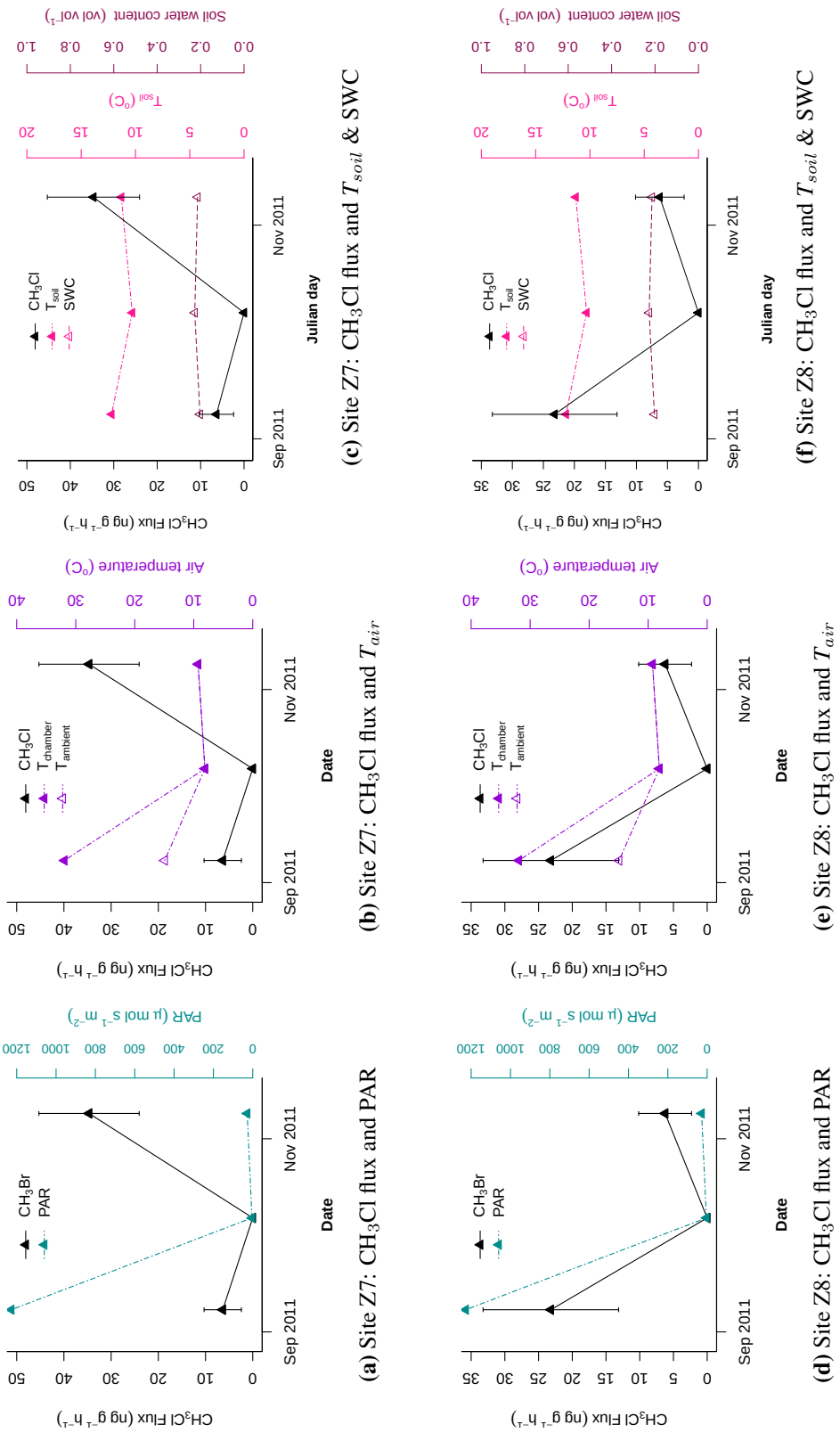
(c) Site Z5: CH_3Cl flux and T_{soil} & SWC

(d) Site Z6: CH_3Cl flux and PAR

(e) Site Z6: CH_3Cl flux and T_{air}

(f) Site Z6: CH_3Cl flux and T_{soil} & SWC

Figure 4.77: Comparison of net CH_3Cl fluxes from willow with PAR, chamber and ambient air temperature, soil temperature and soil water content (SWC) for 2011 and 2012 for sites Z5 and Z6. Note different y-axis scales for CH_3Cl . Error bars on fluxes incorporate analytical and sampling uncertainties.



(a) Site Z7: CH_3Cl flux and PAR

(b) Site Z7: CH_3Cl flux and T_{air}

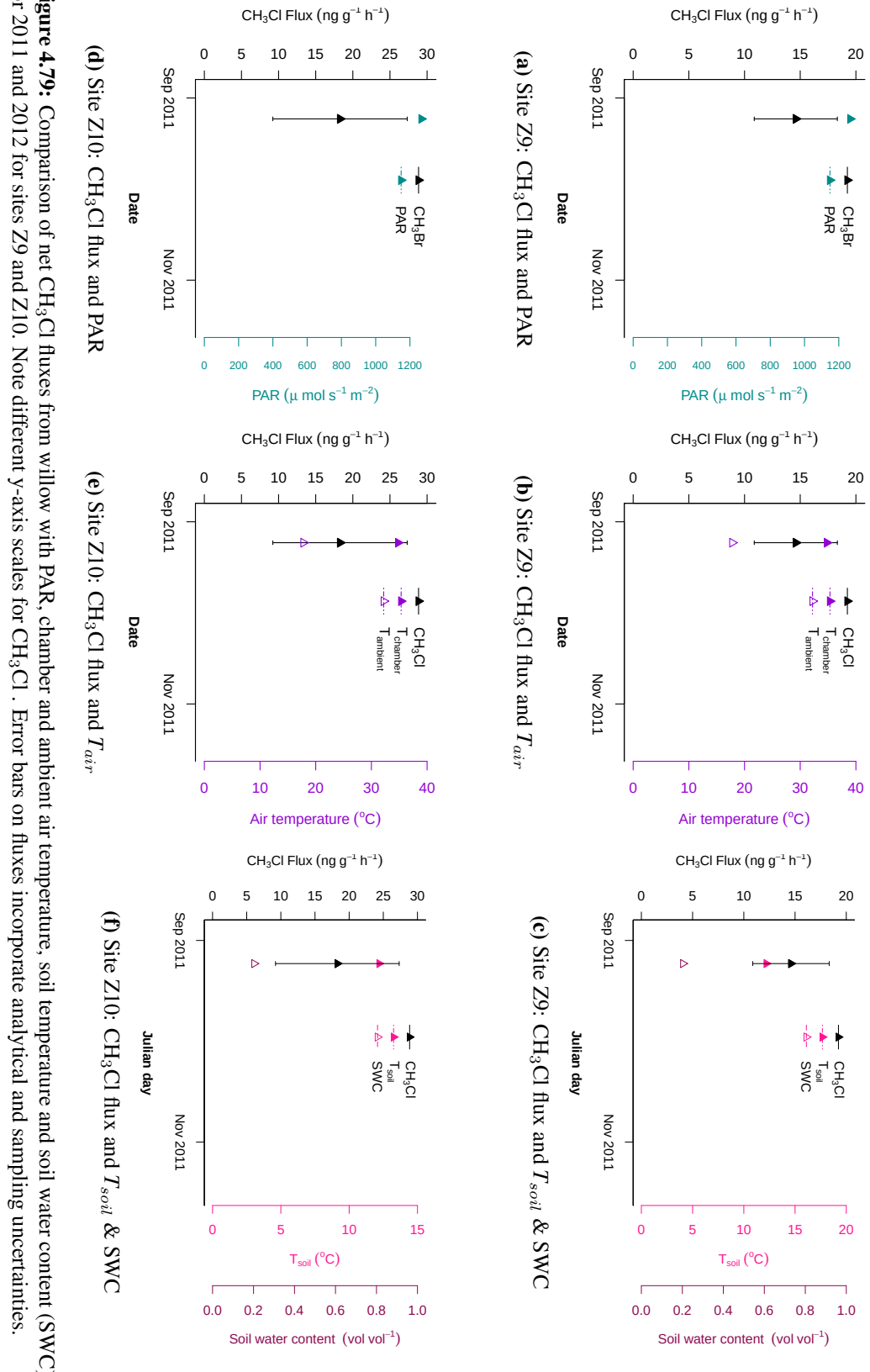
(c) Site Z7: CH_3Cl flux and T_{soil} & SWC

(d) Site Z8: CH_3Cl flux and PAR

(e) Site Z8: CH_3Cl flux and T_{air}

(f) Site Z8: CH_3Cl flux and T_{soil} & SWC

Figure 4.78: Comparison of net CH_3Cl fluxes from willow with PAR, chamber and ambient air temperature, soil temperature and soil water content (SWC) for 2011 and 2012 for sites Z7 and Z8. Note different y-axis scales for CH_3Cl . Error bars on fluxes incorporate analytical and sampling uncertainties.



(a) Site Z9: CH_3Cl flux and PAR

(b) Site Z9: CH_3Cl flux and T_{air}

(c) Site Z9: CH_3Cl flux and T_{soil} & SWC

(d) Site Z10: CH_3Cl flux and PAR

(e) Site Z10: CH_3Cl flux and T_{air}

(f) Site Z10: CH_3Cl flux and T_{soil} & SWC

Figure 4.79: Comparison of net CH_3Cl fluxes from willow with PAR, chamber and ambient air temperature, soil temperature and soil water content (SWC) for 2011 and 2012 for sites Z9 and Z10. Note different y-axis scales for CH_3Cl . Error bars on fluxes incorporate analytical and sampling uncertainties.

4.3.3 Statistical analysis of seasonal fluxes and potential drivers

Three types of analyses were carried out on the long term CH_3X time series:

- Variation in CH_3X fluxes between sites and between growing and non-growing season were analysed for significance using the Kruskal-Wallis function within the R i386 2.15.1 software package
- Correlations between CH_3Br and CH_3Cl fluxes were investigated using regression analysis
- CH_3X fluxes were also analysed for their association with measured environmental parameters

Analysis of variation according to site and season

The significance of the variation in CH_3X fluxes due to location (different sites in the field), season (growing and non-growing), and from the interaction between these two factors was analysed using the Kruskal-Wallis test. Each year was divided into a growing season (beginning of April to end of October) and a non-growing season (November to March) based on observational evidence of plant growth.

Variation in CH_3Br fluxes was found to be significantly associated with season with $\chi^2 = 7.04$ and corresponding p value = 0.008 (Table 4.17). This was not true for CH_3Cl fluxes, and no other significant correlations between site or season-site interaction terms were identified.

Table 4.17: Analysis of CH_3X flux variation according to site and season derived using the Kruskal-Wallis test. Degrees of freedom (d.f), χ^2 value and p value for the effect of site, season and season-site interaction terms on CH_3Br and CH_3Cl fluxes are presented. At a significance level of 95% the null hypothesis is rejected if $p \leq 0.05$.

	CH_3Br			CH_3Cl		
	d.f	χ^2	p	d.f	χ^2	p
Season	1	7.04	0.008	1	0.311	0.577
Site	29	31.9	0.323	29	24.4	0.711
Season*Site	29	49.2	0.622	29	45.2	0.768

Correlations between CH_3Br and CH_3Cl

Correlations of CH_3Br fluxes with CH_3Cl fluxes at individual sites and over all sites were tested for significance. Two significant positive correlations between CH_3Br and CH_3Cl fluxes were found at sites X2 and Y4 with a Spearman's rank correlation coefficient (ρ) of 1 and 0.875 respectively (Table 4.18). The CH_3Br and CH_3Cl fluxes measured at these sites between

August 2011 and June 2012 were similar to those measured at other sites. No other significant correlations were derived.

Table 4.18: Spearman's rank correlation coefficients (ρ) between CH_3Br and CH_3Cl fluxes at each site and the associated p value (at a significance level of 95% the null hypothesis is rejected if $p \leq 0.05$). The number of pairs of measurements (n) contributing to the correlation and derived p value is stated in the last column. The last row shows the ρ correlation and p value for fluxes over all sites.

	ρ	r	n
X1	0.370	0.370	8
X2	**1.000**	**0.000**	**8**
X3	-0.396	0.510	7
X4	-0.250	0.685	7
X5	-1.000	0.333	3
Y1	-0.310	0.550	8
Y2	-0.287	0.581	8
Y4	**0.875**	**0.050**	**7**
Y6	-0.775	0.225	4
Z1	-0.310	0.550	8
Z2	0.133	0.802	8
Z3	-0.250	0.685	7
Z8	-0.866	0.333	3
All	0.001	0.989	132

CH_3X flux association with measured environmental factors

Correlations of measured CH_3Br and CH_3Cl fluxes with concurrent observations of PAR, internal chamber and external ambient air temperature, soil temperature and soil water content (SWC) at 5 cm were investigated. CH_3X fluxes were first normalised to the highest flux recorded over the measurement period.

CH_3Cl fluxes were significantly correlated with ambient air temperature, internal chamber temperature, soil temperature and soil moisture, with Spearman's rank correlation coefficients (ρ) between -0.2 and 0.4 (Table 4.19). No significant correlations were found for CH_3Br fluxes.

Table 4.19: Spearman's rank correlation coefficients between potential drivers and CH_3X fluxes from willow. Significant correlations ($p \leq 0.05$) are highlighted in bold.

Factor	CH_3Br	CH_3Cl
PAR	0.080	-0.028
$\boldsymbol{T}_{chamber}$	-0.064	**0.231**
$\boldsymbol{T}_{ambient\,air}$	-0.111	**0.238**
$\boldsymbol{T}_{soil}$	0.012	**0.366**
Soil moisture	0.030	**-0.200**

4.3.4 Outline of BVOC flux measurements

A total of 94 measurements were made during 7 site visits between September 2011 and August 2012. Firstly, the BVOC flux trends during each sampling year are examined for isoprene, α-pinene, limonene and δ-3-carene (β-pinene was not detected). Time series of seasonal net BVOC fluxes for 2011 and 2012 and the respective PAR, ambient and chamber air temperature, soil temperature and soil water content observations at the time of measurement for each sampling site are then illustrated, incorporating seasonal and temporal variation in fluxes.

Statistical analysis of the BVOC fluxes is then presented. BVOC fluxes are tested for significant correlations with monitored environmental parameters in order to investigate possible drivers of emissions. Correlations between the various BVOC fluxes measured were tested for significance as was the association of variation in BVOC flux with season and sampling site.

Isoprene

The isoprene fluxes measured between September 2011 and August 2012 at 24 of 30 willow sampling points and the mean of those values on each sampling occasion are illustrated in Figure 4.80.

Fluxes of between zero and 12 $\mu g\,g^{-1}\,h^{-1}$ were measured at the start of September 2011. Zero fluxes were measured in November 2011 and March 2012. In late April 2012, fluxes of between zero and 41 $\mu g\,g^{-1}\,h^{-1}$ were measured. Fluxes increased dramatically in May, rising to between zero and 269 $\mu g\,g^{-1}\,h^{-1}$. Fluxes dropped to between zero and 10 $\mu g\,g^{-1}\,h^{-1}$ at the end of June, and increased again to between zero and 105 $\mu g\,g^{-1}\,h^{-1}$ at the end of August 2012. Mean fluxes varied between zero and 95 $\mu g\,g^{-1}\,h^{-1}$.

Time series of isoprene fluxes from each individual site between August 2011 and June 2012 together with the concurrent PAR, ambient and chamber air temperature, soil temperature and soil water content (SWC) observations are illustrated in Figures 4.81 to 4.88. The statistical

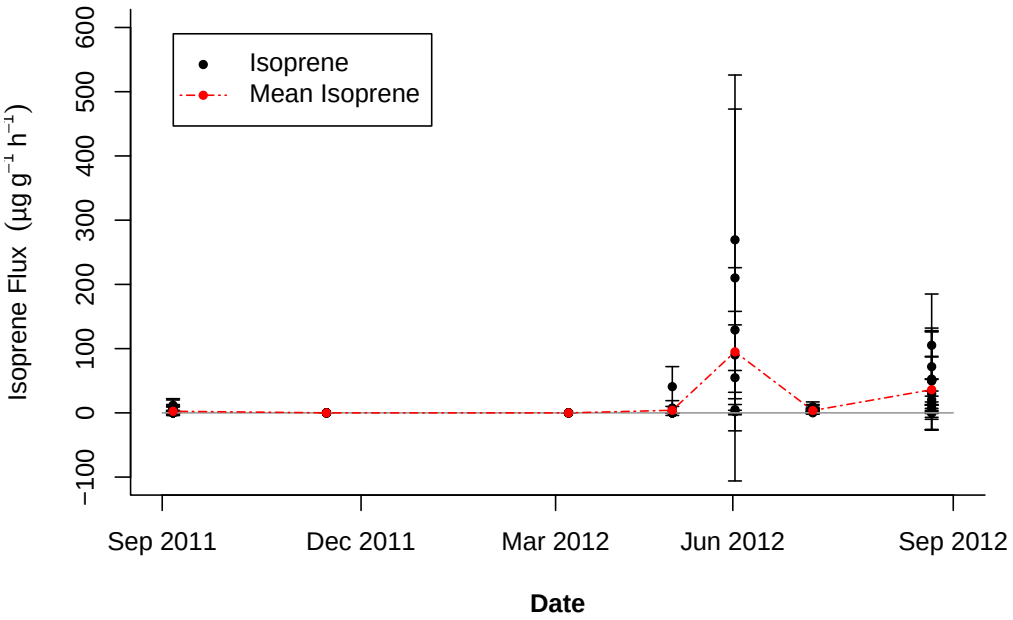


Figure 4.80: Isoprene fluxes from willow at the Arnot fieldsite at 24 sampling points and the mean of those values on each sampling occasion from 2011 to 2012. Error bars on fluxes incorporate analytical and sampling uncertainties (as described in Section 2.6.1).

significance of correlations between isoprene fluxes and environmental variables is described in Section 4.3.5.

Mean isoprene fluxes of between 0.5 and 30 $\mu g\, g^{-1}\, h^{-1}$ were measured in field X, excluding sites which were measured only once (Table 4.20). A total of 30 measurements were made in field X with higher mean fluxes of between 8.4 and 30 $\mu g\, g^{-1}\, h^{-1}$ measured at sites X2 and X3 and lower fluxes of between 0.5 and 1.7 $\mu g\, g^{-1}\, h^{-1}$ at sites X1 and X4. The highest maximum of 129 $\mu g\, g^{-1}\, h^{-1}$ was measured at site X3 and the lowest of 0.35 at site X6. At sites with more than one measurement, the minimum flux was zero or very close to zero. A mean flux of 9.1 $\mu g\, g^{-1}\, h^{-1}$ was calculated from all fluxes measured in field X during the measurement period combined. A median of 0.78 $\mu g\, g^{-1}\, h^{-1}$ was also calculated.

In field Y, mean isoprene fluxes of between 0.51 and 47 $\mu g\, g^{-1}\, h^{-1}$ were measured (Table 4.20), slightly higher than those measured in field X. A total of 36 measurements were made with higher mean fluxes of between 17 and 47 $\mu g\, g^{-1}\, h^{-1}$ measured at sites Y3-6 and mean fluxes of 0.51 to 8.4 $\mu g\, g^{-1}\, h^{-1}$ measured at the remaining sites. The highest maximum of 269 $\mu g\, g^{-1}\, h^{-1}$ was measured at site Y3 and the lowest of 1 $\mu g\, g^{-1}\, h^{-1}$ at site Y7. The minimum flux measured at all sites was zero or very close to zero. A mean flux of 23 $\mu g\, g^{-1}\, h^{-1}$ was calculated from all fluxes measured in field Y during the measurement period combined,

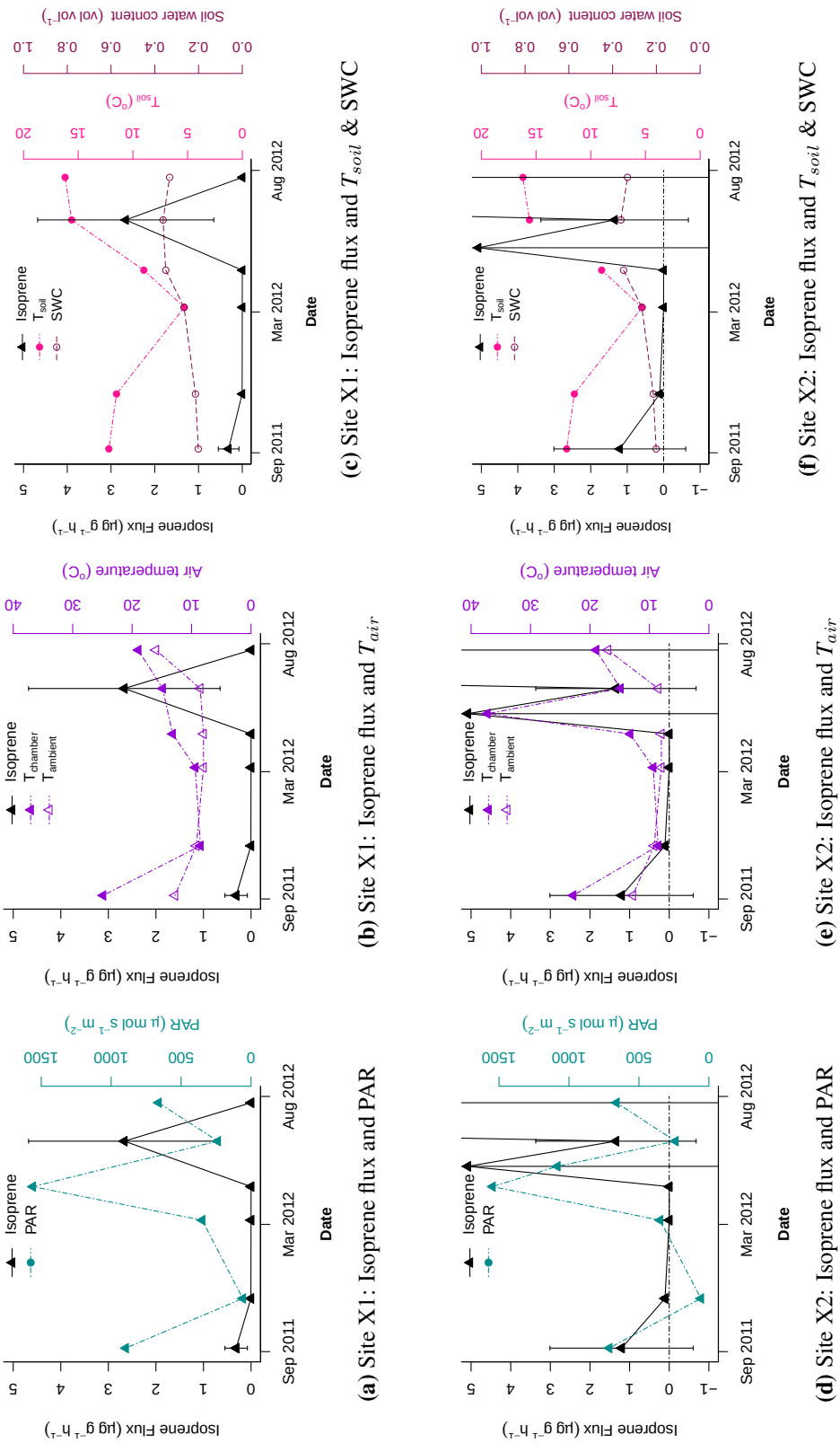
over twice that calculated for field X. The calculated median of 0.07 $\mu g\, g^{-1}\, h^{-1}$ was and order of magnitude lower than for field X.

Excluding sites which were measured only once, mean isoprene fluxes of between 1.7 and 18 $\mu g\, g^{-1}\, h^{-1}$ were measured in field Z (Table 4.20), slightly lower than those measured in fields X and Y. A total of 28 measurements were made with higher mean fluxes of between 10 and 18 $\mu g\, g^{-1}\, h^{-1}$ measured at sites Z1-3 and a lower mean fluxes of 1.7 $\mu g\, g^{-1}\, h^{-1}$ measured at site Z4. The highest maximum of 90 $\mu g\, g^{-1}\, h^{-1}$ was measured at site Z1 and the lowest of 0.04 $\mu g\, g^{-1}\, h^{-1}$ at site Z6. At sites with more than one measurement, the minimum flux was zero. A mean flux of 11 $\mu g\, g^{-1}\, h^{-1}$ was calculated from all fluxes measured in field Y during the measurement period combined, closest in value to that calculated for field X than to field Y. A median value of 1.4 $\mu g\, g^{-1}\, h^{-1}$ was also calculated, almost double that for field X and twenty times that calculated for field Y.

The overall mean calculated from the combination of all measurements made in all three fields was 15 $\mu g\, g^{-1}\, h^{-1}$. A median value of 0.28 $\mu g\, g^{-1}\, h^{-1}$ was calculated and the maximum flux measured was 269 $\mu g\, g^{-1}\, h^{-1}$.

Table 4.20: Mean, median, minimum and maximum net isoprene fluxes from SRC willow at Arnot during 2011 to 2012. All flux values are in $\mu g\, g^{-1}\, h^{-1}$. The final column gives the number of measurements made. The last row summarises all fluxes from all sites.

Site	Mean	Median	Min	Max	Number
Willow X1	0.50	0.00	0.00	2.66	6
Willow X2	8.38	1.20	0.00	50.9	7
Willow X3	30.1	5.24	0.01	129	6
Willow X4	1.74	0.17	0.00	7.50	7
Willow X5	5.60	5.60	5.60	5.60	1
Willow X6	0.35	0.35	0.35	0.35	1
Willow X7	6.46	6.46	6.46	6.46	1
Willow X8	5.13	5.13	5.13	5.13	1
All X	9.06	0.78	0.00	129	30
Willow Y1	8.42	0.03	0.00	50.4	6
Willow Y2	3.95	0.04	0.00	20.6	6
Willow Y3	46.6	0.06	0.00	269	7
Willow Y4	37.8	0.25	0.00	210	7
Willow Y5	35.4	0.83	0.00	105	3
Willow Y6	17.2	0.52	0.01	51.1	3
Willow Y7	0.51	0.51	0.00	1.02	2
Willow Y8	4.45	4.45	0.00	8.90	2
All Y	23.1	0.07	0.00	269	36
Willow Z1	18.3	0.11	0.00	90.1	7
Willow Z2	10.2	1.37	0.00	54.8	7
Willow Z3	16.8	2.48	0.00	71.9	5
Willow Z4	1.73	1.50	0.00	3.58	5
Willow Z5	0.21	0.21	0.21	0.21	1
Willow Z6	0.04	0.04	0.04	0.04	1
Willow Z7	12.5	12.5	12.5	12.5	1
Willow Z8	8.10	8.10	8.10	8.10	1
All Z	11.2	1.44	0.00	90.1	28
Overall	15.1	0.28	0.00	269	94



(a) Site X1: Isoprene flux and PAR

(b) Site X1: Isoprene flux and T_{air}

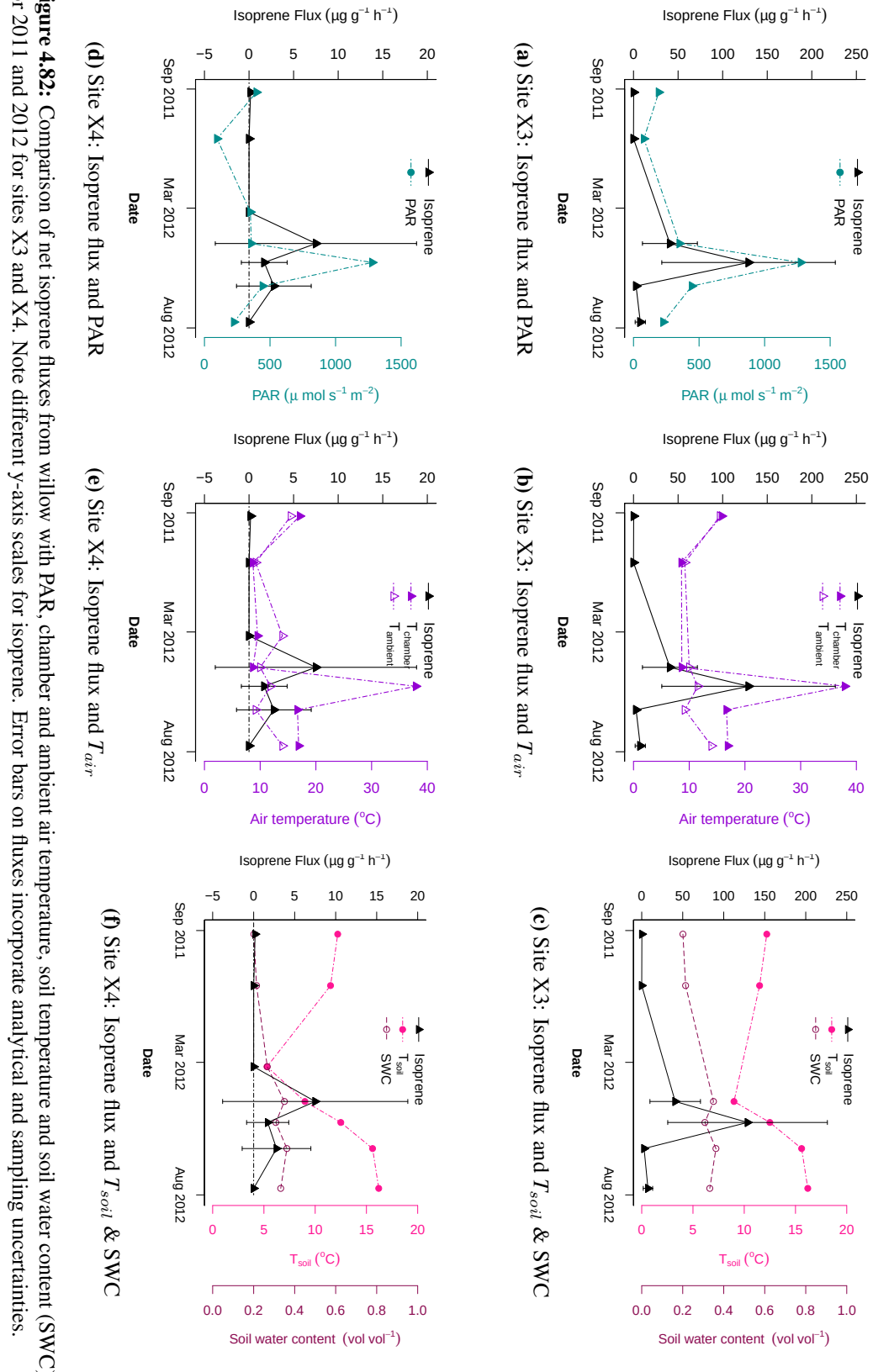
(c) Site X1: Isoprene flux and T_{soil} & SWC

(d) Site X2: Isoprene flux and PAR

(e) Site X2: Isoprene flux and T_{air}

(f) Site X2: Isoprene flux and T_{soil} & SWC

Figure 4.81: Comparison of net isoprene fluxes from willow with PAR, chamber and ambient air temperature, soil temperature and soil water content (SWC) for 2011 and 2012 for sites X1 and X2. Note different y-axis scales for isoprene. Error bars on fluxes incorporate analytical and sampling uncertainties.



(a) Site X3: Isoprene flux and PAR

(b) Site X3: Isoprene flux and T_{air}

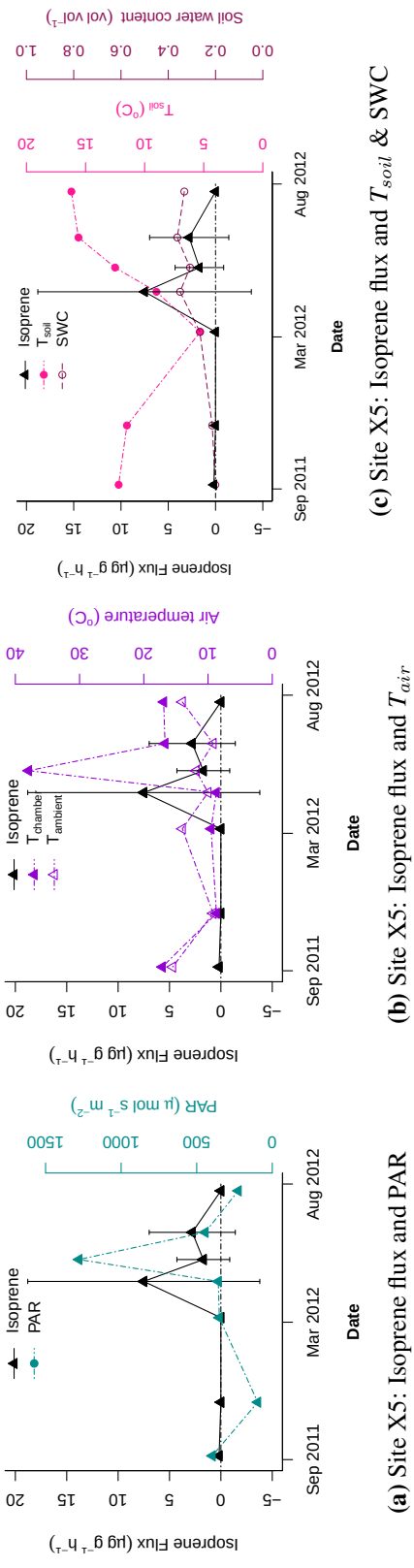
(c) Site X3: Isoprene flux and T_{soil} & SWC

(d) Site X4: Isoprene flux and PAR

(e) Site X4: Isoprene flux and T_{air}

(f) Site X4: Isoprene flux and T_{soil} & SWC

Figure 4.82: Comparison of net isoprene fluxes from willow with PAR, chamber and ambient air temperature, soil temperature and soil water content (SWC) for 2011 and 2012 for sites X3 and X4. Note different y-axis scales for isoprene. Error bars on fluxes incorporate analytical and sampling uncertainties.

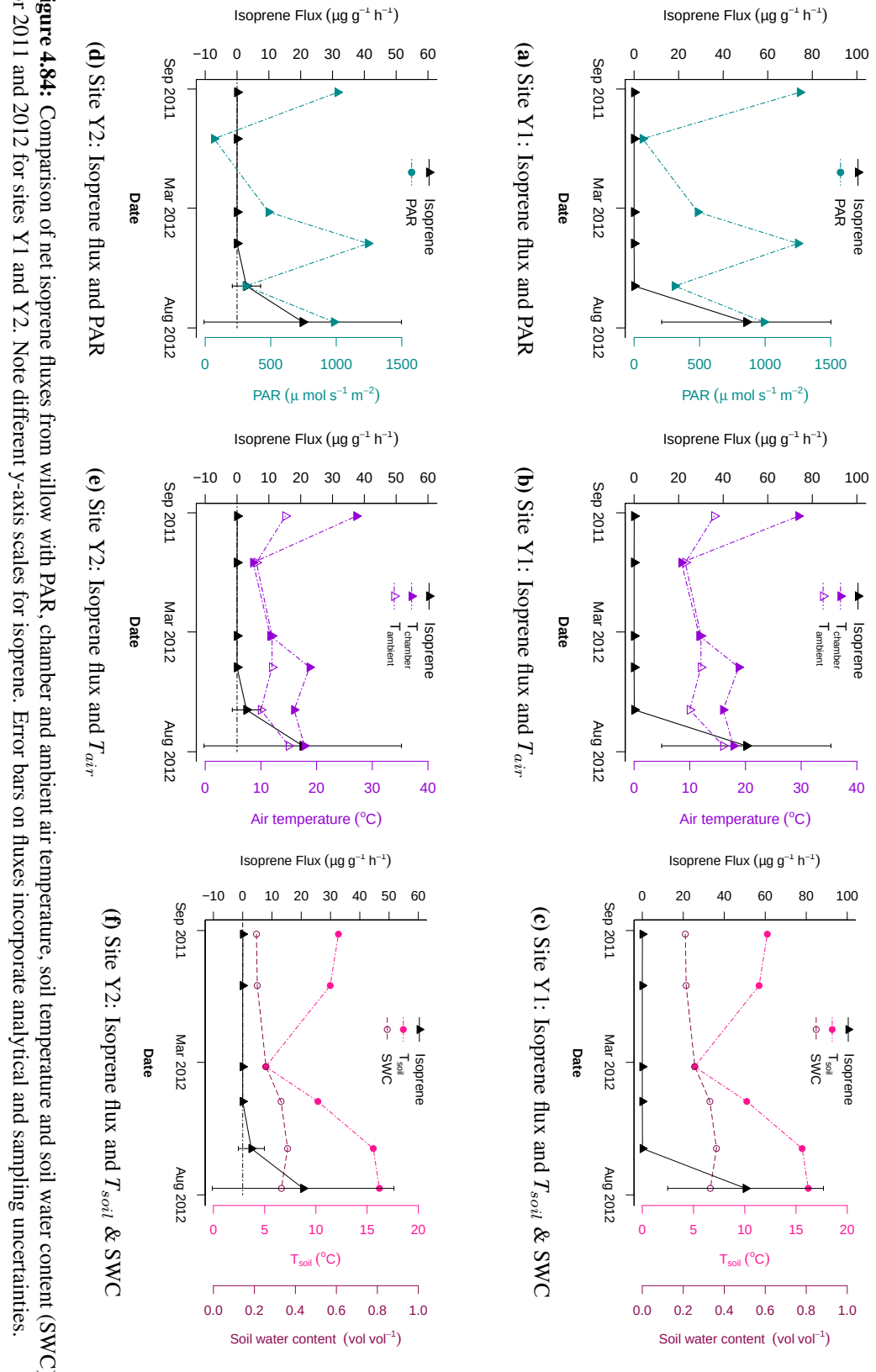


(a) Site X5: Isoprene flux and PAR

(b) Site X5: Isoprene flux and T_{air}

(c) Site X5: Isoprene flux and T_{soil} & SWC

Figure 4.83: Comparison of net isoprene fluxes from willow with PAR, chamber and ambient air temperature, soil temperature and soil water content (SWC) for 2011 and 2012 for site X5. Error bars on fluxes incorporate analytical and sampling uncertainties.



(a) Site Y1: Isoprene flux and PAR

(b) Site Y1: Isoprene flux and T_{air}

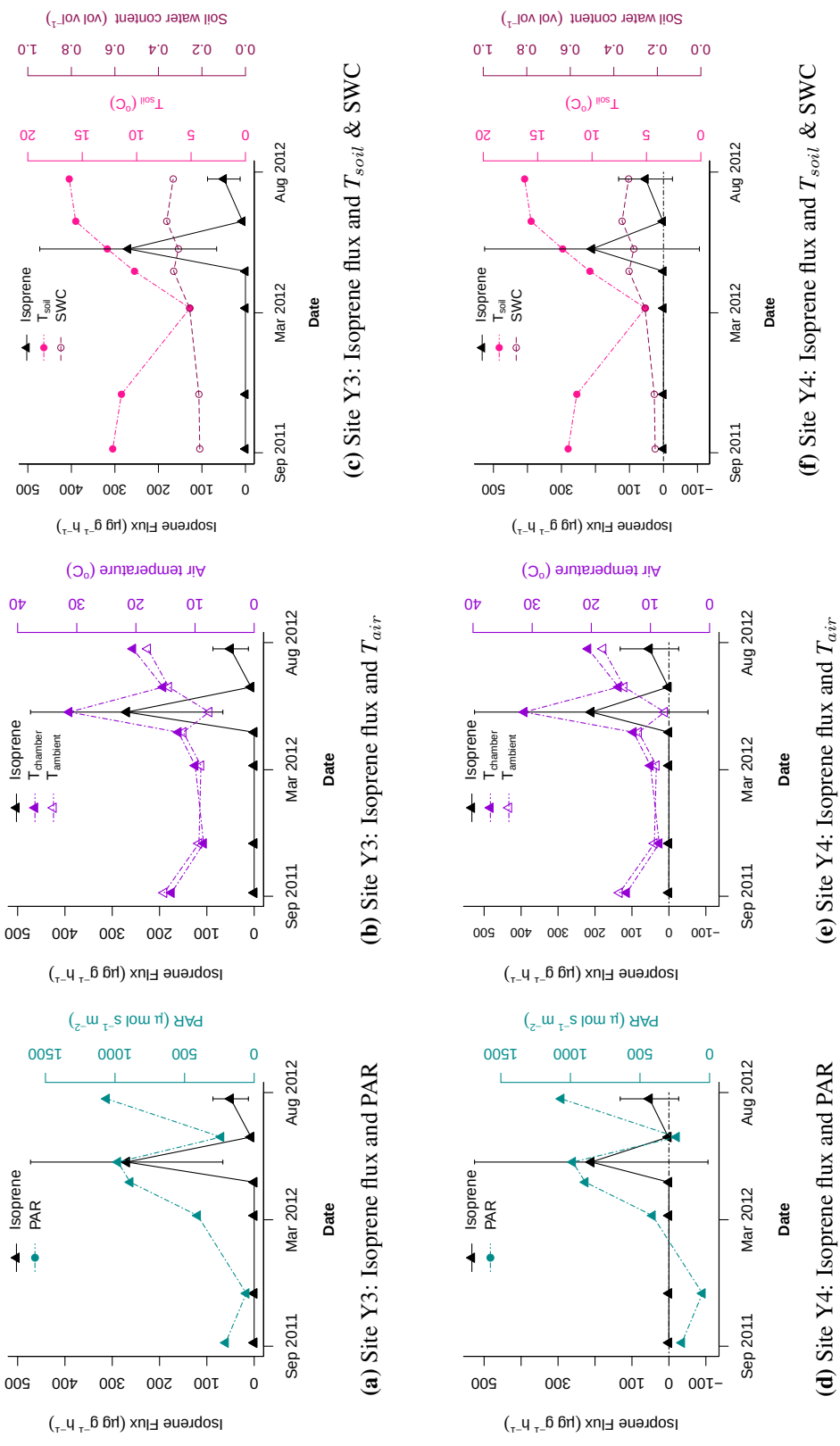
(c) Site Y1: Isoprene flux and T_{soil} & SWC

(d) Site Y2: Isoprene flux and PAR

(e) Site Y2: Isoprene flux and T_{air}

(f) Site Y2: Isoprene flux and T_{soil} & SWC

Figure 4.84: Comparison of net isoprene fluxes from willow with PAR, chamber and ambient air temperature, soil temperature and soil water content (SWC) for 2011 and 2012 for sites Y1 and Y2. Note different y-axis scales for isoprene. Error bars on fluxes incorporate analytical and sampling uncertainties.



(a) Site Y3: Isoprene flux and PAR

(b) Site Y3: Isoprene flux and T_{air}

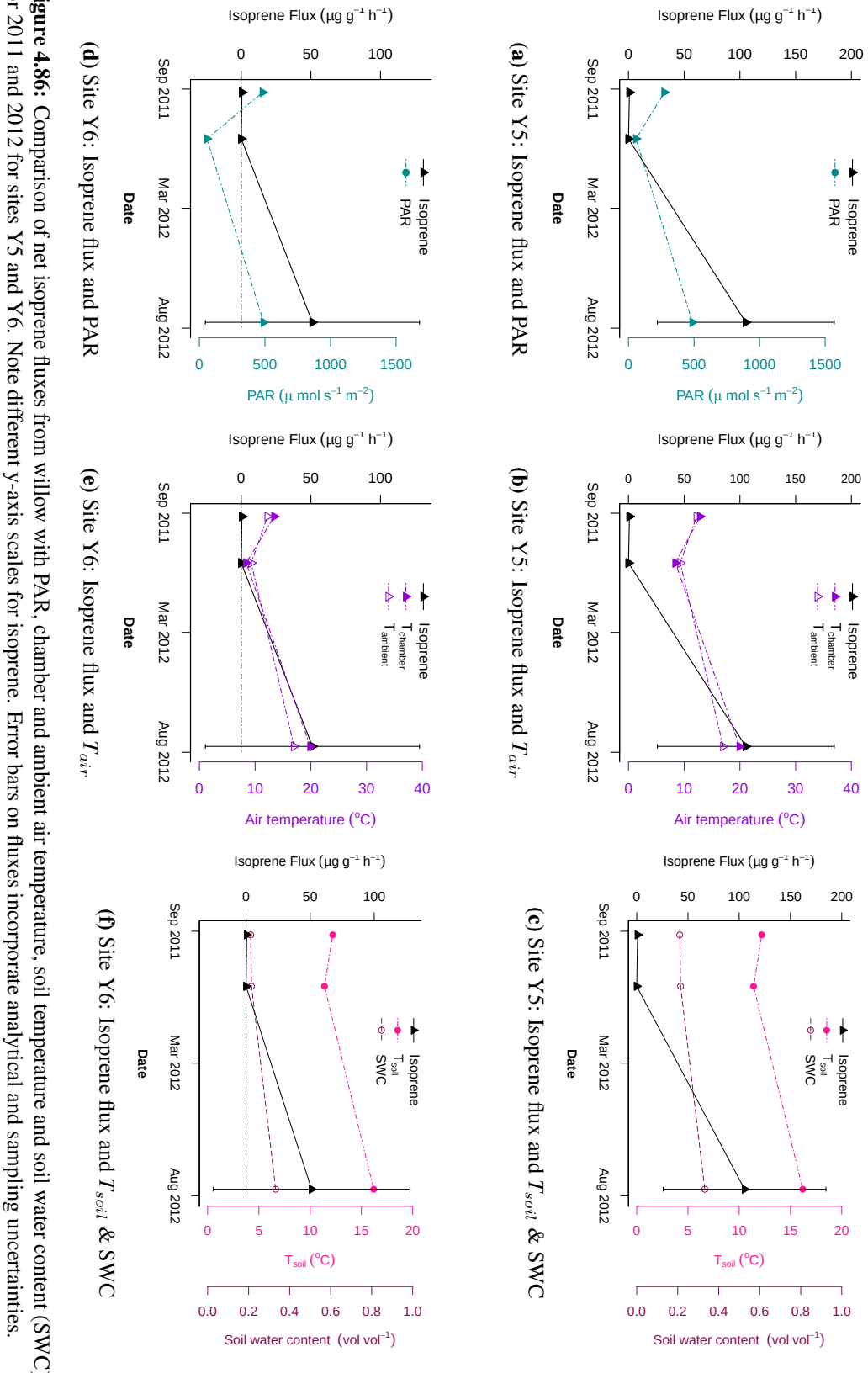
(c) Site Y3: Isoprene flux and T_{soil} & SWC

(d) Site Y4: Isoprene flux and PAR

(e) Site Y4: Isoprene flux and T_{air}

(f) Site Y4: Isoprene flux and T_{soil} & SWC

Figure 4.85: Comparison of net isoprene fluxes from willow with PAR, chamber and ambient air temperature, soil temperature and soil water content (SWC) for 2011 and 2012 for sites Y3 and Y4. Note different y-axis scales for isoprene. Error bars on fluxes incorporate analytical and sampling uncertainties.



(a) Site Y5: Isoprene flux and PAR

(b) Site Y5: Isoprene flux and T_{air}

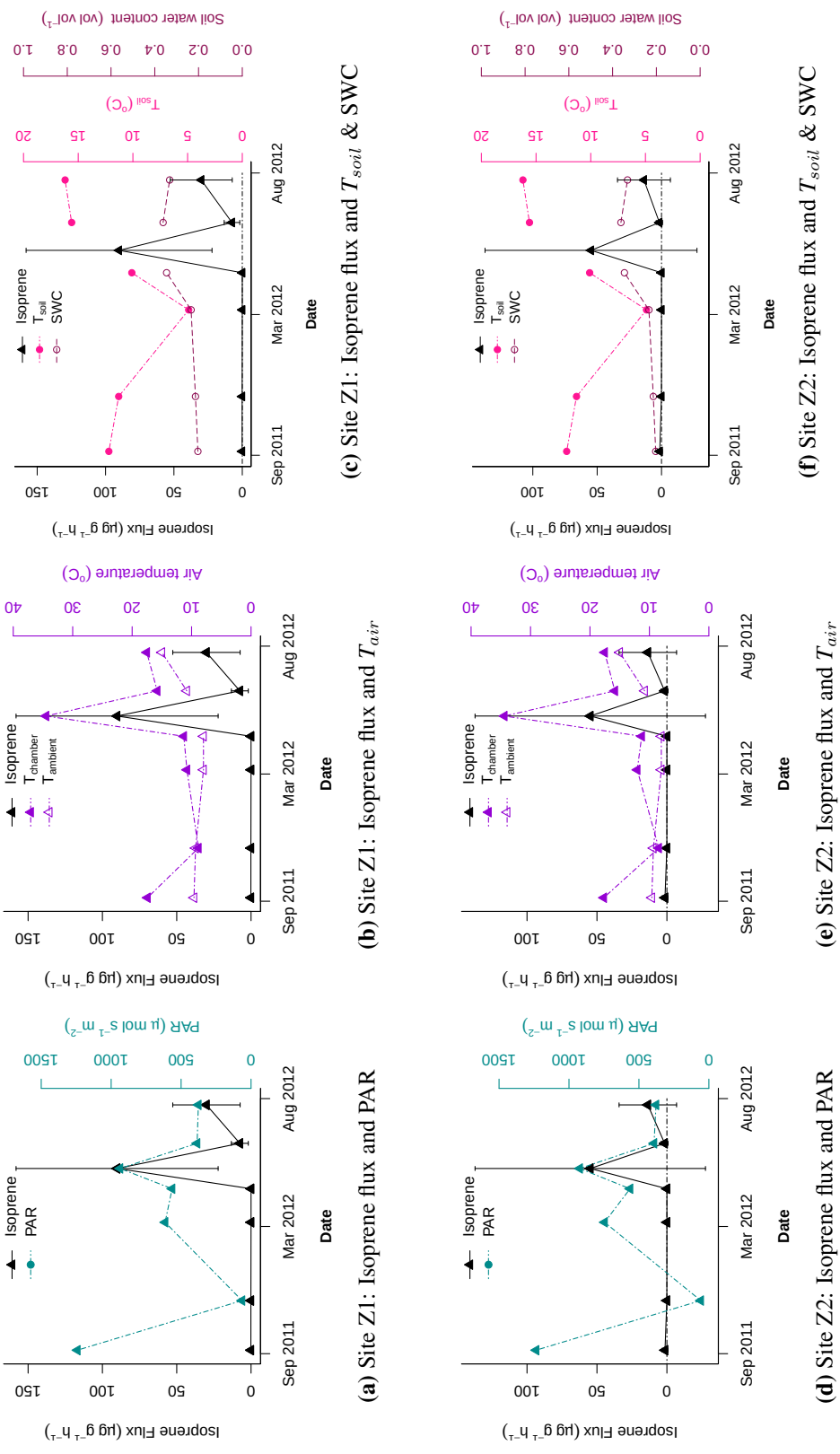
(c) Site Y5: Isoprene flux and T_{soil} & SWC

(d) Site Y6: Isoprene flux and PAR

(e) Site Y6: Isoprene flux and T_{air}

(f) Site Y6: Isoprene flux and T_{soil} & SWC

Figure 4.86: Comparison of net isoprene fluxes from willow with PAR, chamber and ambient air temperature, soil temperature and soil water content (SWC) for 2011 and 2012 for sites Y5 and Y6. Note different y-axis scales for isoprene. Error bars on fluxes incorporate analytical and sampling uncertainties.



(a) Site Z1: Isoprene flux and PAR

(b) Site Z1: Isoprene flux and T_{air}

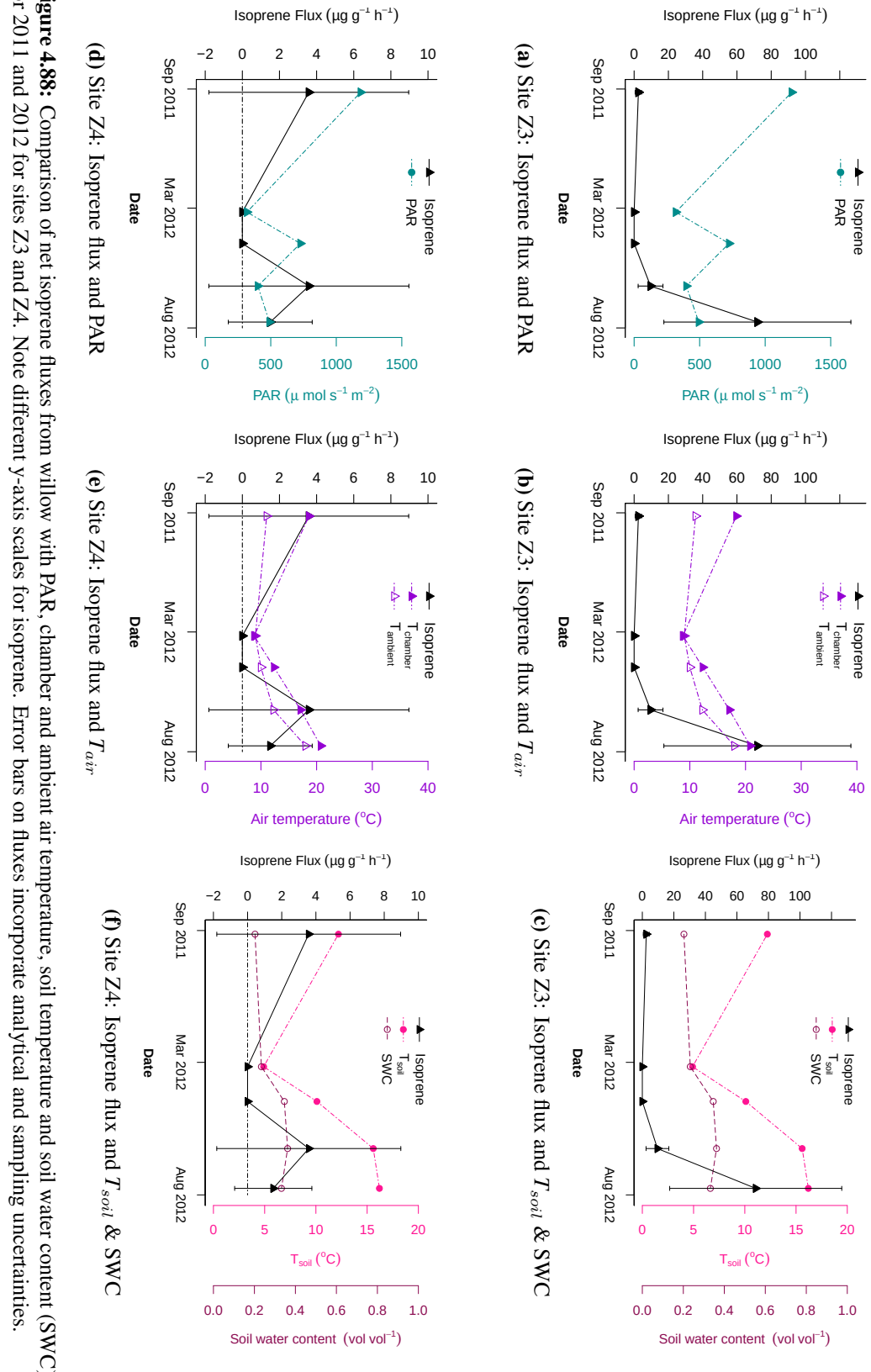
(c) Site Z1: Isoprene flux and T_{soil} & SWC

(d) Site Z2: Isoprene flux and PAR

(e) Site Z2: Isoprene flux and T_{air}

(f) Site Z2: Isoprene flux and T_{soil} & SWC

Figure 4.87: Comparison of net isoprene fluxes from willow with PAR, chamber and ambient air temperature, soil temperature and soil water content (SWC) for 2011 and 2012 for sites Z1 and Z2. Note different y-axis scales for isoprene. Error bars on fluxes incorporate analytical and sampling uncertainties.



(a) Site Z3: Isoprene flux and PAR

(b) Site Z3: Isoprene flux and T_{air}

(c) Site Z3: Isoprene flux and T_{soil} & SWC

(d) Site Z4: Isoprene flux and PAR

(e) Site Z4: Isoprene flux and T_{air}

(f) Site Z4: Isoprene flux and T_{soil} & SWC

Figure 4.88: Comparison of net isoprene fluxes from willow with PAR, chamber and ambient air temperature, soil temperature and soil water content (SWC) for 2011 and 2012 for sites Z3 and Z4. Note different y-axis scales for isoprene. Error bars on fluxes incorporate analytical and sampling uncertainties.

α-pinene

The α-pinene fluxes measured between September 2011 and August 2012 at 24 of 30 willow sampling points and the mean of those values on each sampling occasion are illustrated in Figure 4.89.

Zero fluxes were measured between September 2011 and March 2012, similarly to isoprene fluxes except for the small isoprene fluxes measured in September. In late April 2012, fluxes of between 19 and 100 $\mu g\, g^{-1}\, h^{-1}$ were measured. Fluxes dropped in May, decreasing to between 0.18 and 2.9 $\mu g\, g^{-1}\, h^{-1}$. Fluxes dropped again at the end of June, to between zero and 1 $\mu g\, g^{-1}\, h^{-1}$ then increased at the end of August 2012 to between 0.69 and 11 $\mu g\, g^{-1}\, h^{-1}$. Mean fluxes varied between zero and 50 $\mu g\, g^{-1}\, h^{-1}$.

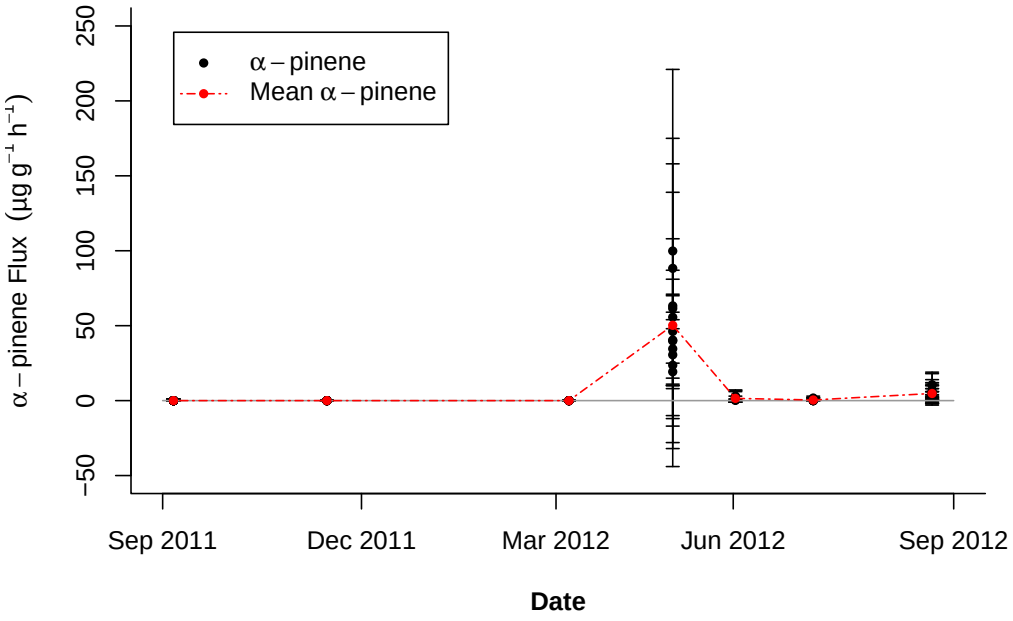


Figure 4.89: α-pinene fluxes from willow at the Arnot fieldsite at 24 sampling points and the mean of those values on each sampling occasion from 2011 to 2012. Error bars on fluxes incorporate analytical and sampling uncertainties (as described in Section 2.6.1).

Time series of α-pinene fluxes from each individual site between August 2011 and June 2012 together with the concurrent PAR, ambient and chamber air temperature, soil temperature and soil water content (SWC) observations are illustrated in Figures 4.90 to 4.97. The statistical significance of correlations between α-pinene fluxes and environmental variables is described in Section 4.3.5.

Mean α-pinene fluxes of between 9 and 18 $\mu g\, g^{-1}\, h^{-1}$ were measured in field X at sites X1-4

(Table 4.21). Sites X5-8, Y7-8 and Z5-8 were excluded as they were measured only once and produced zero fluxes. Median fluxes of between zero and 0.87 $\mu g\, g^{-1}\, h^{-1}$ were calculated. The highest maximum flux of 100 $\mu g\, g^{-1}\, h^{-1}$ was measured at site X3, where the highest isoprene flux was also measured, and the lowest of 56 $\mu g\, g^{-1}\, h^{-1}$ at site X4. The minimum flux measured at every site was zero. A mean flux of 10 $\mu g\, g^{-1}\, h^{-1}$ was calculated from all fluxes measured in field X during the measurement period combined. A median of zero was also calculated.

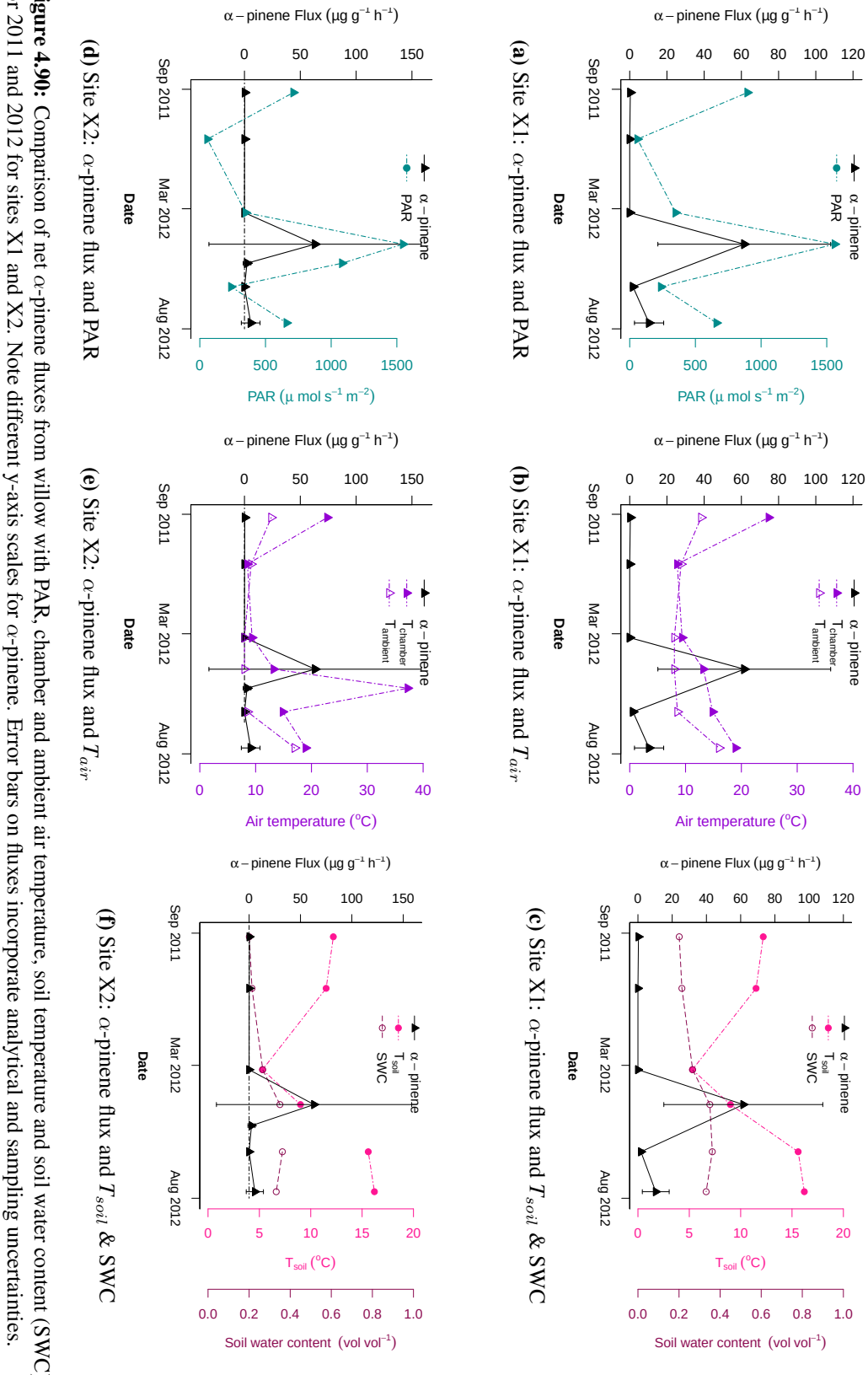
In field Y, mean α-pinene fluxes varied between 0.23 and 16 $\mu g\, g^{-1}\, h^{-1}$ at sites Y1-6 (Table 4.21). Median fluxes of between zero and 0.61 $\mu g\, g^{-1}\, h^{-1}$ were calculated. The highest maximum flux of 88 $\mu g\, g^{-1}\, h^{-1}$ was measured at site Y2 and the lowest of 0.69 $\mu g\, g^{-1}\, h^{-1}$ at site Y6, where no measurements were taken during the peak emission period at the end of April 2012. The minimum flux measured at every site was zero. A mean flux of 6.2 $\mu g\, g^{-1}\, h^{-1}$ was calculated from all fluxes measured in field Y during the measurement period combined, slightly lower than that calculated for field X. A median of zero was also calculated.

A small range of mean fluxes were measured in field Z, between 5.3 and 9.4 $\mu g\, g^{-1}\, h^{-1}$ (Table 4.21). Median fluxes of between zero and 0.53 $\mu g\, g^{-1}\, h^{-1}$ were calculated. The highest maximum flux of 40 $\mu g\, g^{-1}\, h^{-1}$ was measured at site Z3 and the lowest of 24 $\mu g\, g^{-1}\, h^{-1}$ at site Z4. The minimum flux measured at every site was zero. A mean flux of 5.4 $\mu g\, g^{-1}\, h^{-1}$ was calculated from all fluxes measured in field Y during the measurement period combined, similar to that calculated for field X. A median of zero was also calculated.

The overall mean α-pinene flux calculated from the combination of all measurements made in all three fields was 7.3 $\mu g\, g^{-1}\, h^{-1}$, around half of that calculated for isoprene. A median value of zero was calculated and the maximum flux measured was 100 $\mu g\, g^{-1}\, h^{-1}$.

Table 4.21: Mean, median, minimum and maximum net α-pinene fluxes from SRC willow at Arnot during 2011 to 2012. All flux values are in $\mu g\, g^{-1}\ h^{-1}$. The final column gives the number of measurements made. The last row summarises all fluxes from all sites.

Site	Mean	Median	Min	Max	Number
Willow X1	12.3	0.87	0.00	61.6	6
Willow X2	10.2	0.00	0.00	63.2	7
Willow X3	17.6	0.52	0.00	99.9	6
Willow X4	9.02	0.33	0.00	55.7	7
All X	10.4	0.00	0.00	99.9	30
Willow Y1	7.26	0.00	0.00	39.9	6
Willow Y2	15.6	0.21	0.00	88.3	6
Willow Y3	7.18	0.00	0.00	46.2	7
Willow Y4	3.43	0.61	0.00	19.2	7
Willow Y5	3.52	0.00	0.00	10.6	3
Willow Y6	0.23	0.00	0.00	0.69	3
All Y	6.18	0.00	0.00	88.3	36
Willow Z1	5.25	0.53	0.00	30.6	7
Willow Z2	5.53	0.18	0.00	34.6	7
Willow Z3	9.40	0.00	0.00	40.4	5
Willow Z4	5.52	0.00	0.00	23.6	5
All Z	5.35	0.00	0.00	40.4	28
Overall	7.29	0.00	0.00	99.9	94



(a) Site X1: α-pinene flux and PAR

(b) Site X1: α-pinene flux and T_{air}

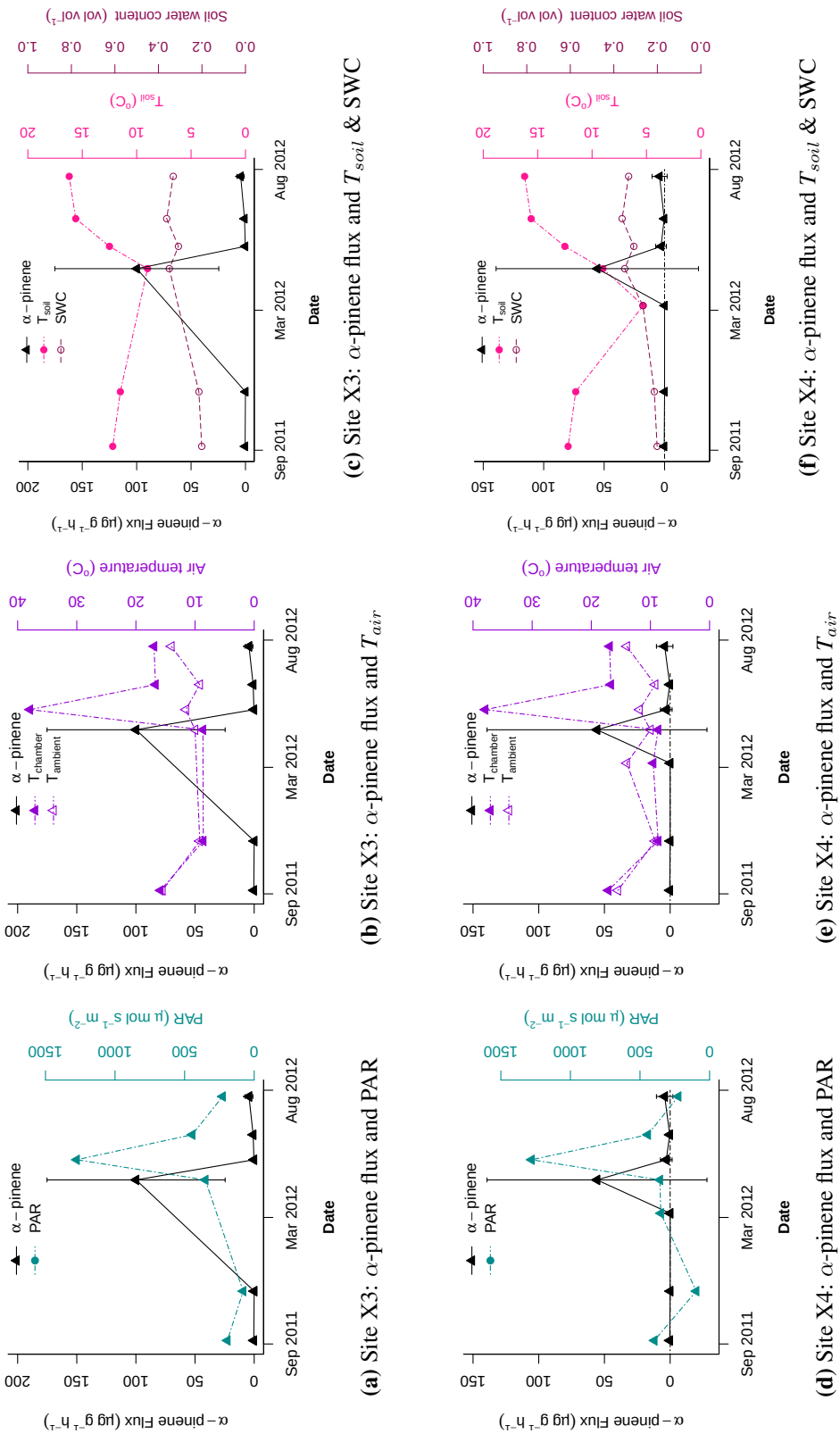
(c) Site X1: α-pinene flux and T_{soil} & SWC

(d) Site X2: α-pinene flux and PAR

(e) Site X2: α-pinene flux and T_{air}

(f) Site X2: α-pinene flux and T_{soil} & SWC

Figure 4.90: Comparison of net α-pinene fluxes from willow with PAR, chamber and ambient air temperature, soil temperature and soil water content (SWC) for 2011 and 2012 for sites X1 and X2. Note different y-axis scales for α-pinene. Error bars on fluxes incorporate analytical and sampling uncertainties.



(a) Site X3: α-pinene flux and PAR

(b) Site X3: α-pinene flux and T_{air}

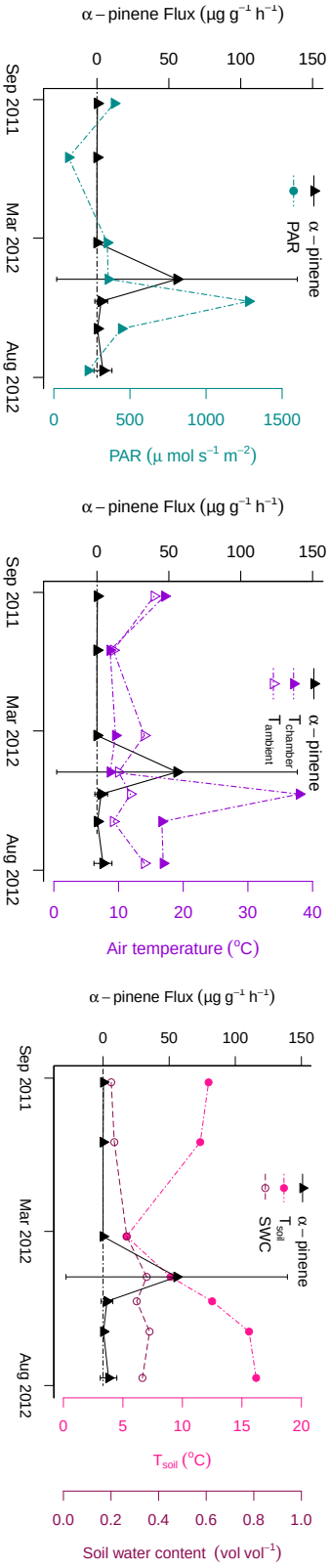
(c) Site X3: α-pinene flux and T_{soil} & SWC

(d) Site X4: α-pinene flux and PAR

(e) Site X4: α-pinene flux and T_{air}

(f) Site X4: α-pinene flux and T_{soil} & SWC

Figure 4.91: Comparison of net α-pinene fluxes from willow with PAR, chamber and ambient air temperature, soil temperature and soil water content (SWC) for 2011 and 2012 for sites X3 and X4. Note different y-axis scales for α-pinene. Error bars on fluxes incorporate analytical and sampling uncertainties.

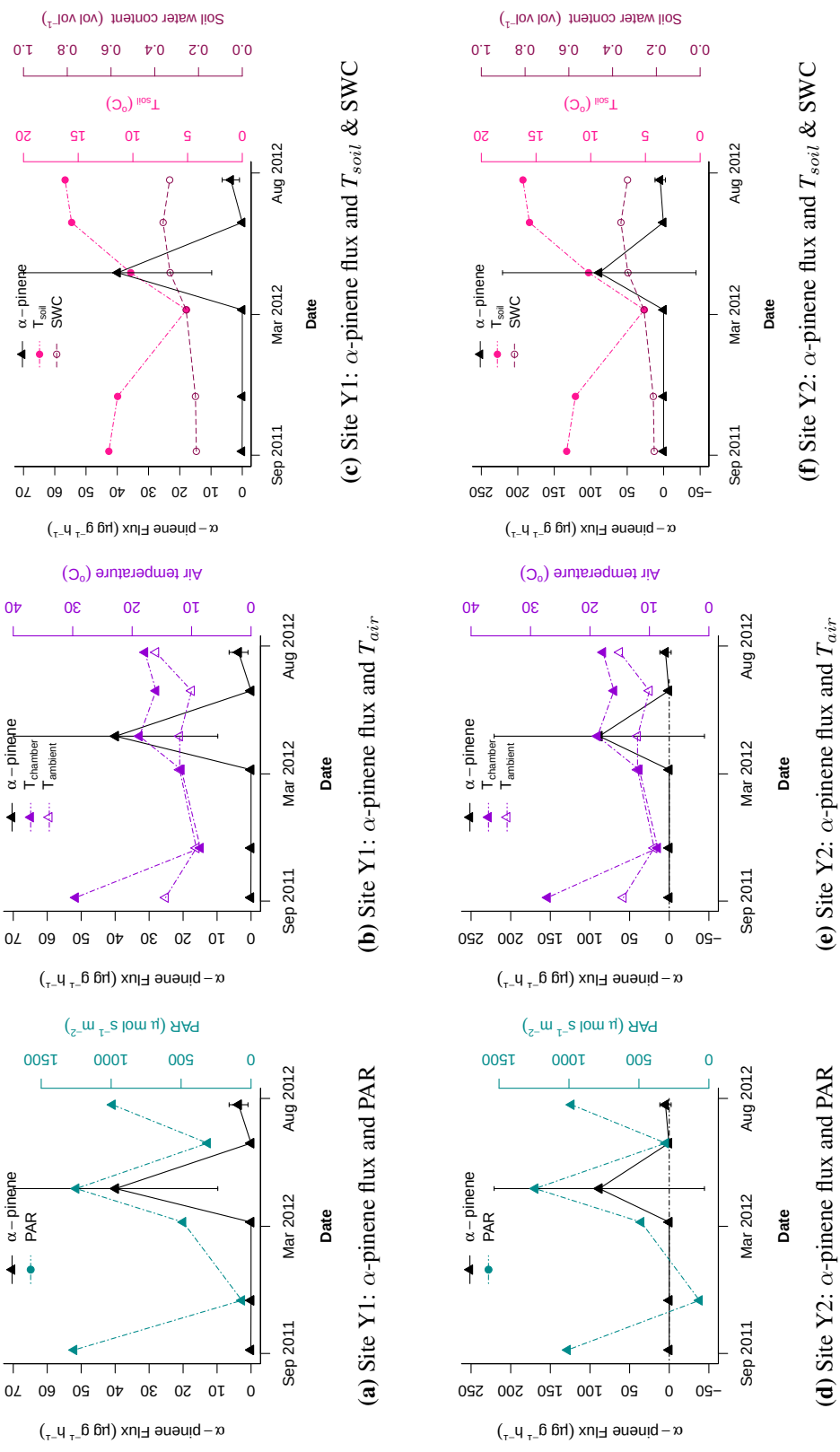


(a) Site X5: α-pinene flux and PAR

(b) Site X5: α-pinene flux and T_{air}

(c) Site X5: α-pinene flux and T_{soil} & SWC

Figure 4.92: Comparison of net α-pinene fluxes from willow with PAR, chamber and ambient air temperature, soil temperature and soil water content (SWC) for 2011 and 2012 for site X5. Error bars on fluxes incorporate analytical and sampling uncertainties.



(a) Site Y1: α-pinene flux and PAR

(b) Site Y1: α-pinene flux and T_{air}

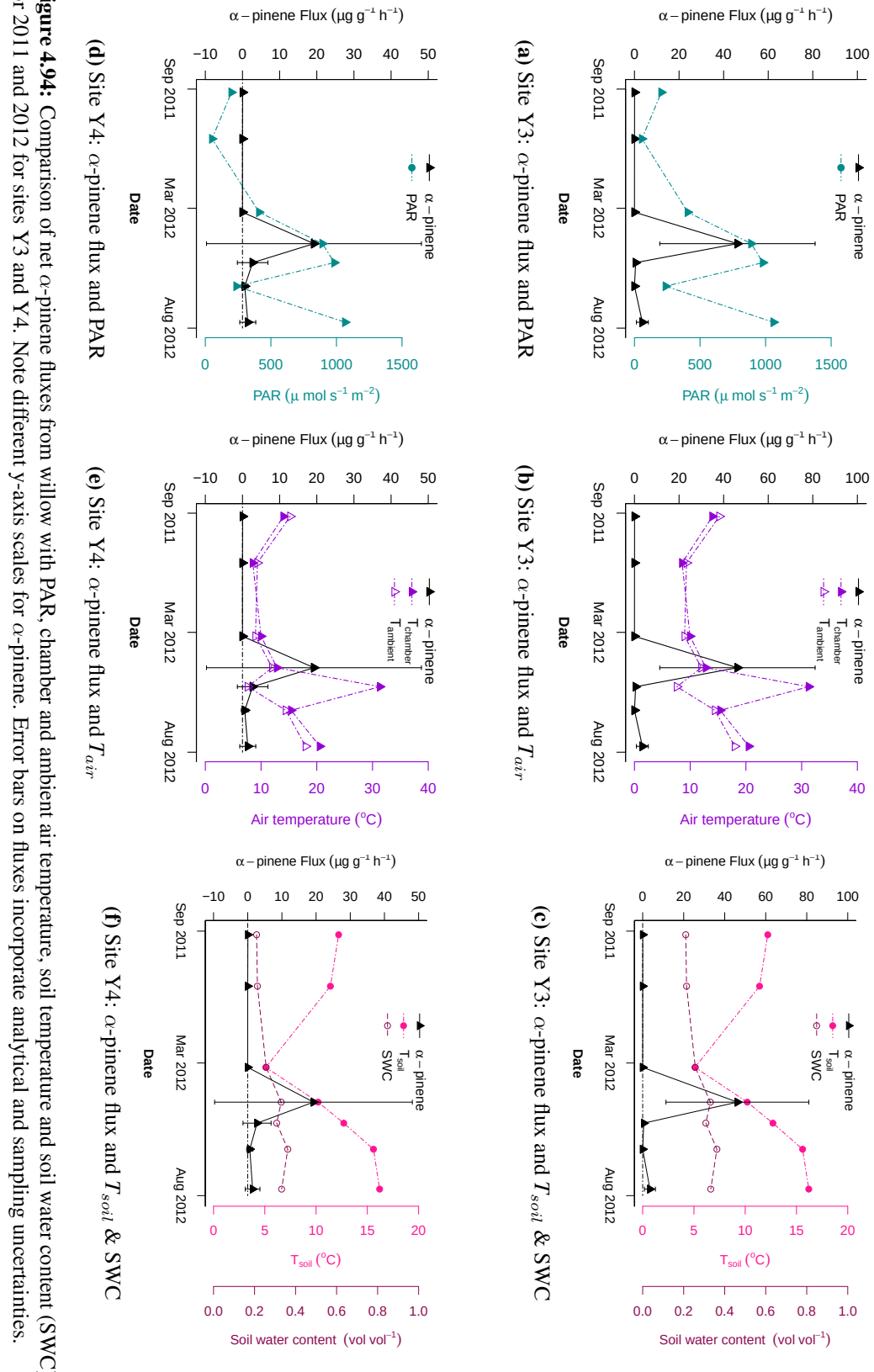
(c) Site Y1: α-pinene flux and T_{soil} & SWC

(d) Site Y2: α-pinene flux and PAR

(e) Site Y2: α-pinene flux and T_{air}

(f) Site Y2: α-pinene flux and T_{soil} & SWC

Figure 4.93: Comparison of net α-pinene fluxes from willow with PAR, chamber and ambient air temperature, soil temperature and soil water content (SWC) for 2011 and 2012 for sites Y1 and Y2. Note different y-axis scales for α-pinene. Error bars on fluxes incorporate analytical and sampling uncertainties.



(a) Site Y3: α-pinene flux and PAR

(b) Site Y3: α-pinene flux and T_{air}

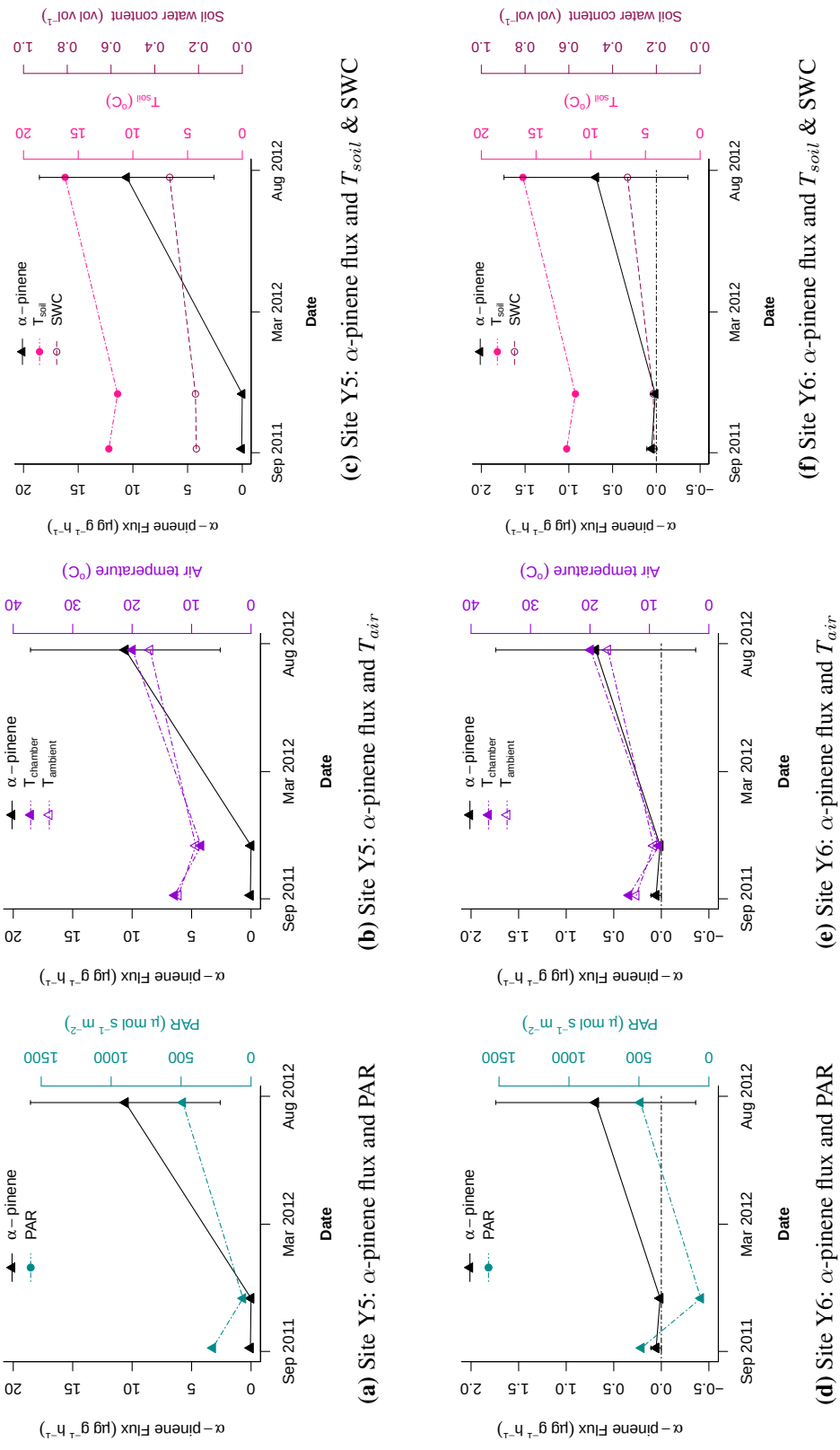
(c) Site Y3: α-pinene flux and T_{soil} & SWC

(d) Site Y4: α-pinene flux and PAR

(e) Site Y4: α-pinene flux and T_{air}

(f) Site Y4: α-pinene flux and T_{soil} & SWC

Figure 4.94: Comparison of net α-pinene fluxes from willow with PAR, chamber and ambient air temperature, soil temperature and soil water content (SWC) for 2011 and 2012 for sites Y3 and Y4. Note different y-axis scales for α-pinene. Error bars on fluxes incorporate analytical and sampling uncertainties.



(a) Site Y5: α-pinene flux and PAR

(b) Site Y5: α-pinene flux and T_{air}

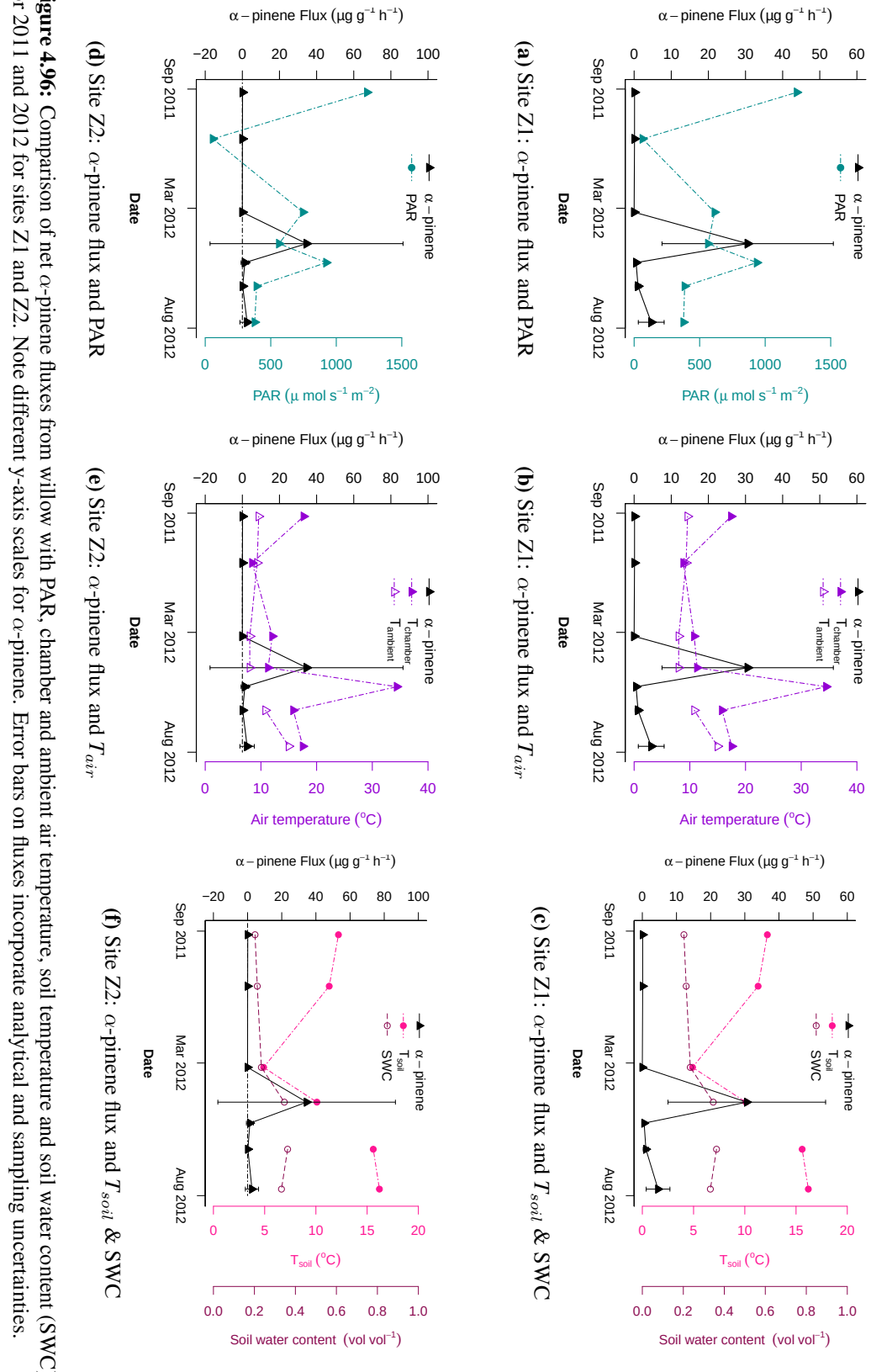
(c) Site Y5: α-pinene flux and T_{soil} & SWC

(d) Site Y6: α-pinene flux and PAR

(e) Site Y6: α-pinene flux and T_{air}

(f) Site Y6: α-pinene flux and T_{soil} & SWC

Figure 4.95: Comparison of net α-pinene fluxes from willow with PAR, chamber and ambient air temperature, soil temperature and soil water content (SWC) for 2011 and 2012 for sites Y5 and Y6. Note different y-axis scales for α-pinene. Error bars on fluxes incorporate analytical and sampling uncertainties.



(a) Site Z1: α-pinene flux and PAR

(b) Site Z1: α-pinene flux and T_{air}

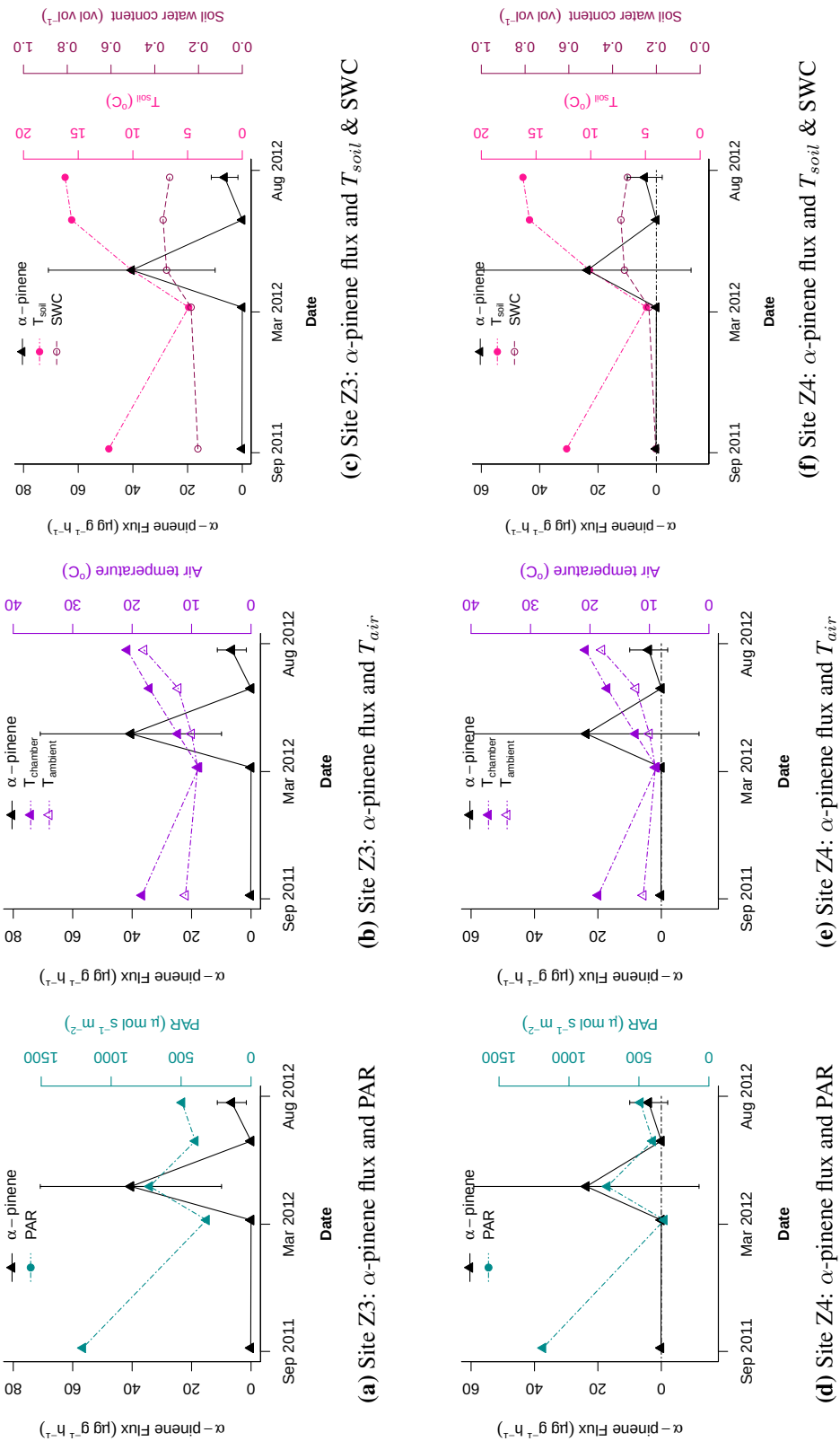
(c) Site Z1: α-pinene flux and T_{soil} & SWC

(d) Site Z2: α-pinene flux and PAR

(e) Site Z2: α-pinene flux and T_{air}

(f) Site Z2: α-pinene flux and T_{soil} & SWC

Figure 4.96: Comparison of net α-pinene fluxes from willow with PAR, chamber and ambient air temperature, soil temperature and soil water content (SWC) for 2011 and 2012 for sites Z1 and Z2. Note different y-axis scales for α-pinene. Error bars on fluxes incorporate analytical and sampling uncertainties.



(a) Site Z3: α-pinene flux and PAR

(b) Site Z3: α-pinene flux and T_{air}

(c) Site Z3: α-pinene flux and T_{soil} & SWC

(d) Site Z4: α-pinene flux and PAR

(e) Site Z4: α-pinene flux and T_{air}

(f) Site Z4: α-pinene flux and T_{soil} & SWC

Figure 4.97: Comparison of net α-pinene fluxes from willow with PAR, chamber and ambient air temperature, soil temperature and soil water content (SWC) for 2011 and 2012 for sites Z3 and Z4. Note different y-axis scales for α-pinene. Error bars on fluxes incorporate analytical and sampling uncertainties.

Limonene

The limonene fluxes measured between September 2011 and August 2012 at 24 of 30 willow sampling points and the mean of those values on each sampling occasion are illustrated in Figure 4.98.

Zero fluxes were measured between September 2011 and March 2012, similarly to α-pinene. In late April 2012, fluxes of between zero and 7 $\mu g\, g^{-1}\, h^{-1}$ were measured. Fluxes dropped slightly in May, decreasing to between 1.1 and 4.8 $\mu g\, g^{-1}\, h^{-1}$. Fluxes remained the same in June, varying between 0.77 and 4.5 $\mu g\, g^{-1}\, h^{-1}$ then increased greatly at the end of August 2012 to between 3.8 and 33 $\mu g\, g^{-1}\, h^{-1}$. Mean fluxes varied between zero and 12 $\mu g\, g^{-1}\, h^{-1}$.

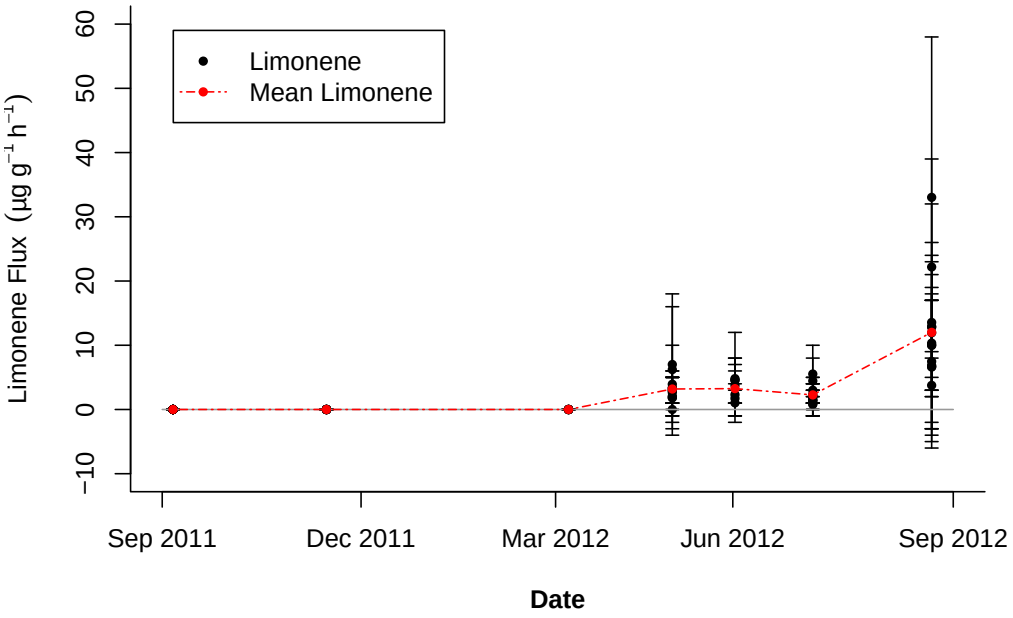


Figure 4.98: Limonene fluxes from willow at the Arnot fieldsite at 24 sampling points and the mean of those values on each sampling occasion from 2011 to 2012. Error bars on fluxes incorporate analytical and sampling uncertainties (as described in Section 2.6.1).

Time series of limonene fluxes from each individual site between August 2011 and June 2012 together with the concurrent PAR, ambient and chamber air temperature, soil temperature and soil water content (SWC) observations are illustrated in Figures 4.99 to 4.106. The statistical significance of correlations between limonene fluxes and environmental variables is described in Section 4.3.5.

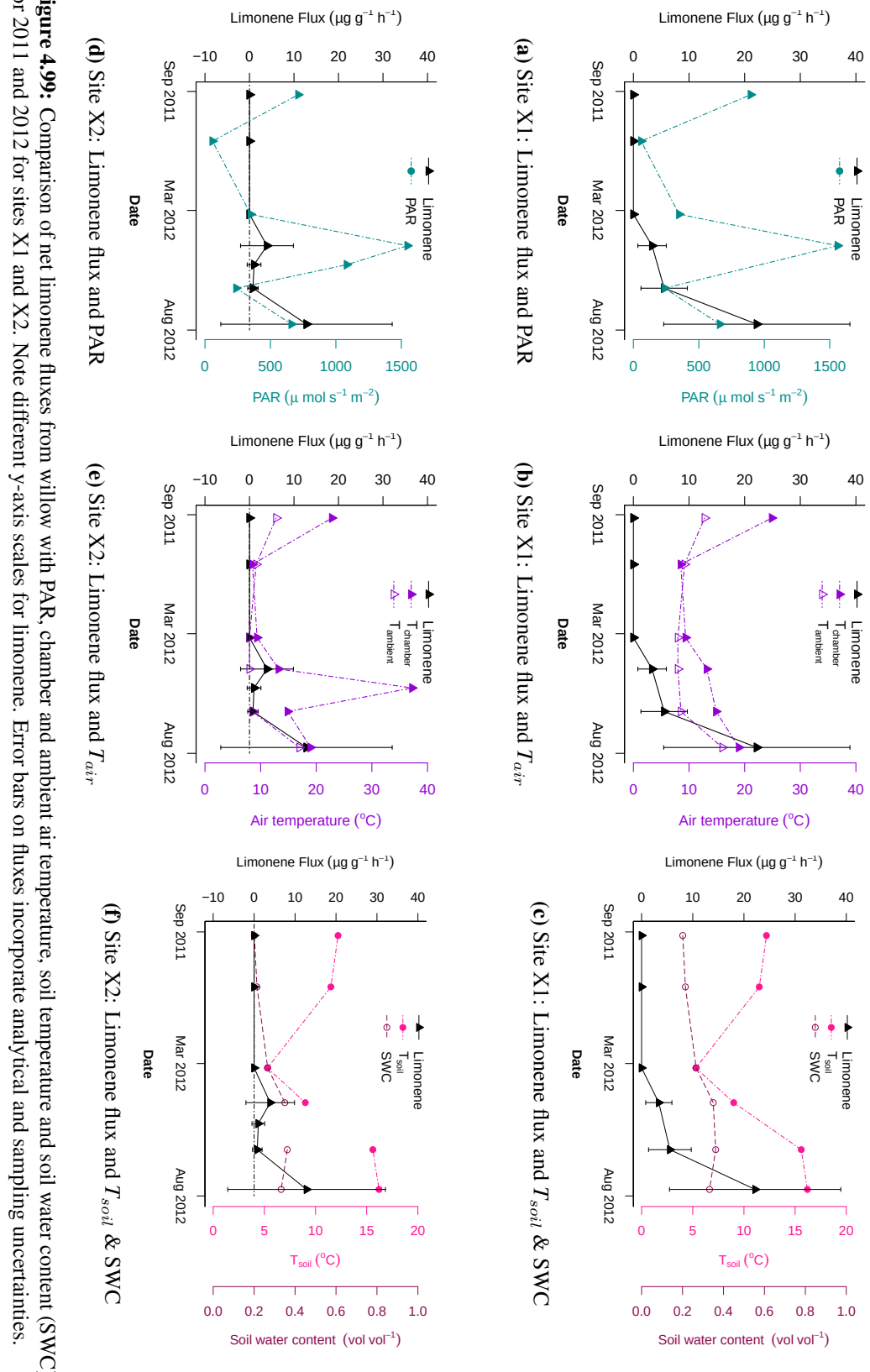
Mean limonene fluxes were similar in all fields, varying between 1.2 and 11 $\mu g\, g^{-1}\, h^{-1}$ (Table 4.22). Sites X5-8, Y7-8 and Z5-8 were excluded as they were measured only once and produced

zero fluxes. Median fluxes of between zero and 3 $\mu g\, g^{-1}\, h^{-1}$ were calculated. The highest maximum flux of 33 $\mu g\, g^{-1}\, h^{-1}$ was measured at site Y5 and the lowest maximum flux of 3.8 $\mu g\, g^{-1}\, h^{-1}$ was measured at site Z2. The minimum flux measured at every site was zero. Mean fluxes of 3, 2.99 and 2.1 $\mu g\, g^{-1}\, h^{-1}$ were calculated from all fluxes measured during the measurement period combined for fields X, Y and X, respectively. A median of zero was calculated for fields X and Y and a median flux of 0.45 $\mu g\, g^{-1}\, h^{-1}$ was calculated for field Z.

The overall mean limonene flux calculated from the combination of all measurements made in all three fields was 2.7 $\mu g\, g^{-1}\, h^{-1}$ around half of that calculated for α-pinene. A median value of zero was calculated and the maximum flux was 33 $\mu g\, g^{-1}\, h^{-1}$.

Table 4.22: Mean, median, minimum and maximum net limonene fluxes from SRC willow at Arnot during 2011 to 2012. All flux values are in $\mu g\, g^{-1}\, h^{-1}$. The final column gives the number of measurements made. The last row summarises all fluxes from all sites.

Site	Mean	Median	Min	Max	Number
Willow X1	5.18	1.68	0.00	22.2	6
Willow X2	2.65	0.77	0.00	12.8	7
Willow X3	3.36	1.05	0.00	13.6	6
Willow X4	2.89	1.37	0.00	10.3	7
All X	3.00	0.00	0.00	22.2	30
Willow Y1	2.79	0.94	0.00	11.9	6
Willow Y2	2.62	1.01	0.00	7.01	6
Willow Y3	2.83	2.37	0.00	9.96	7
Willow Y4	2.22	1.37	0.00	7.48	7
Willow Y5	11.0	0.00	0.00	33.0	3
Willow Y6	2.28	0.00	0.00	6.85	3
All Y	2.99	0.00	0.00	33.0	36
Willow Z1	2.88	3.00	0.00	10.0	7
Willow Z2	1.18	0.90	0.00	3.76	7
Willow Z3	4.08	3.03	0.00	12.9	5
Willow Z4	1.99	1.51	0.00	6.60	5
All Z	2.10	0.45	0.00	12.9	28
Overall	2.73	0.00	0.00	33.0	94



(a) Site X1: Limonene flux and PAR

(b) Site X1: Limonene flux and T_{air}

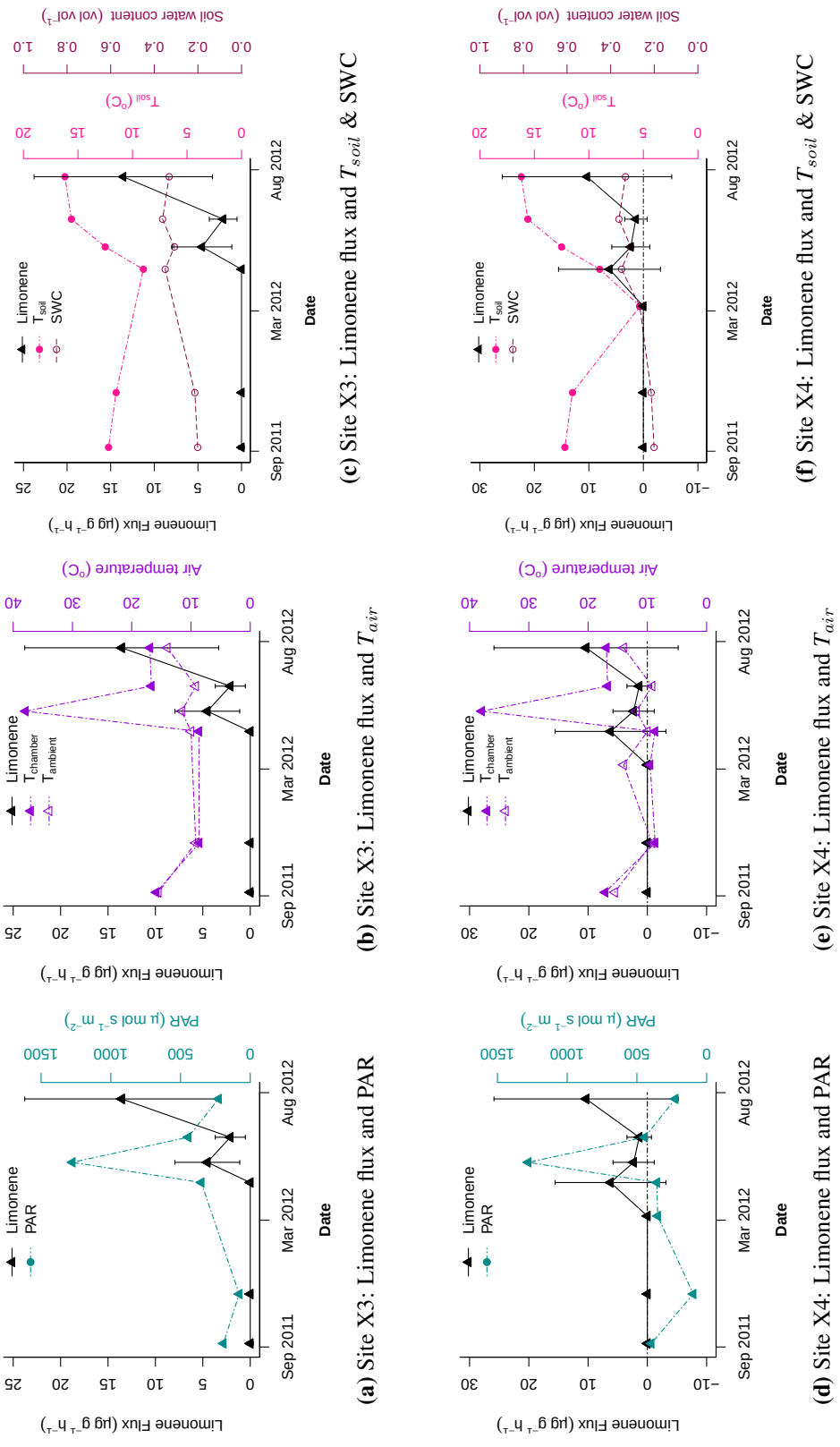
(c) Site X1: Limonene flux and T_{soil} & SWC

(d) Site X2: Limonene flux and PAR

(e) Site X2: Limonene flux and T_{air}

(f) Site X2: Limonene flux and T_{soil} & SWC

Figure 4.99: Comparison of net limonene fluxes from willow with PAR, chamber and ambient air temperature, soil temperature and soil water content (SWC) for 2011 and 2012 for sites X1 and X2. Note different y-axis scales for limonene. Error bars on fluxes incorporate analytical and sampling uncertainties.



(a) Site X3: Limonene flux and PAR

(b) Site X3: Limonene flux and T_{air}

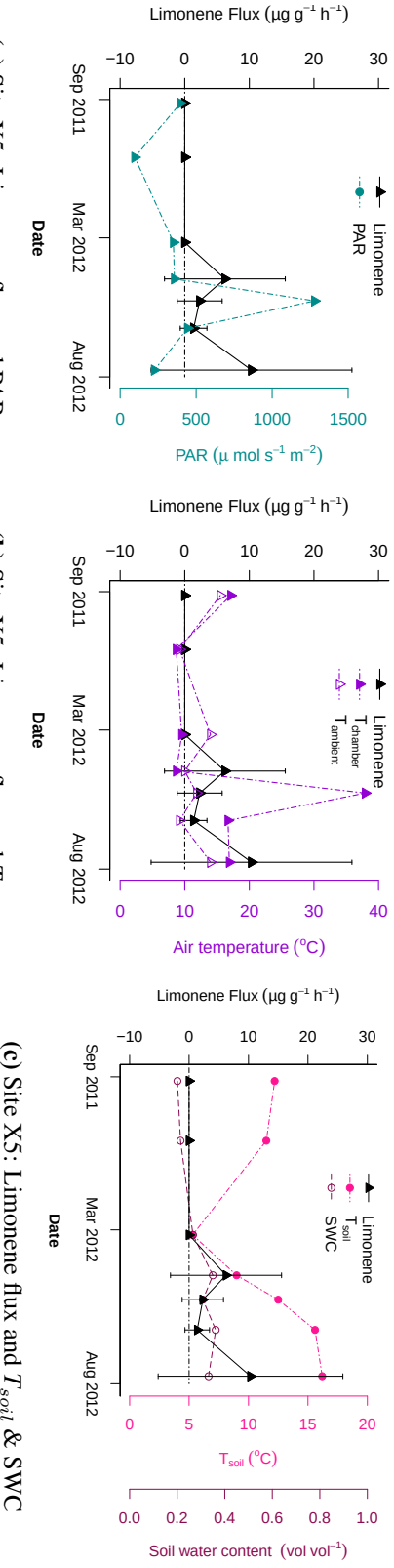
(c) Site X3: Limonene flux and T_{soil} & SWC

(d) Site X4: Limonene flux and PAR

(e) Site X4: Limonene flux and T_{air}

(f) Site X4: Limonene flux and T_{soil} & SWC

Figure 4.100: Comparison of net limonene fluxes from willow with PAR, chamber and ambient air temperature, soil temperature and soil water content (SWC) for 2011 and 2012 for sites X3 and X4. Note different y-axis scales for limonene. Error bars on fluxes incorporate analytical and sampling uncertainties.

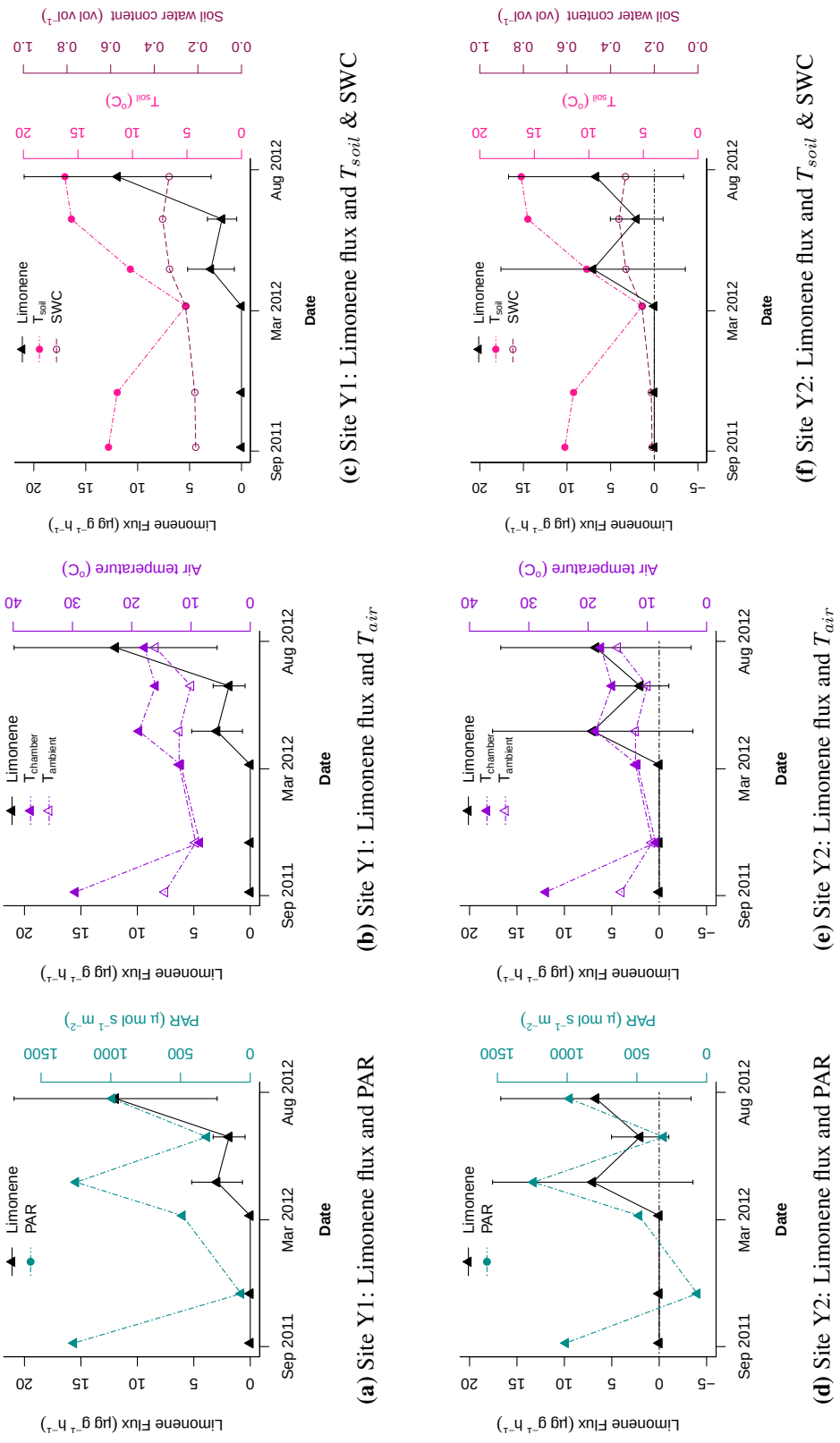


(a) Site X5: Limonene flux and PAR

(b) Site X5: Limonene flux and T_{air}

(c) Site X5: Limonene flux and T_{soil} & SWC

Figure 4.101: Comparison of net limonene fluxes from willow with PAR, chamber and ambient air temperature, soil temperature and soil water content (SWC) for 2011 and 2012 for site X5. Error bars on fluxes incorporate analytical and sampling uncertainties.



(a) Site Y1: Limonene flux and PAR

(b) Site Y1: Limonene flux and T_{air}

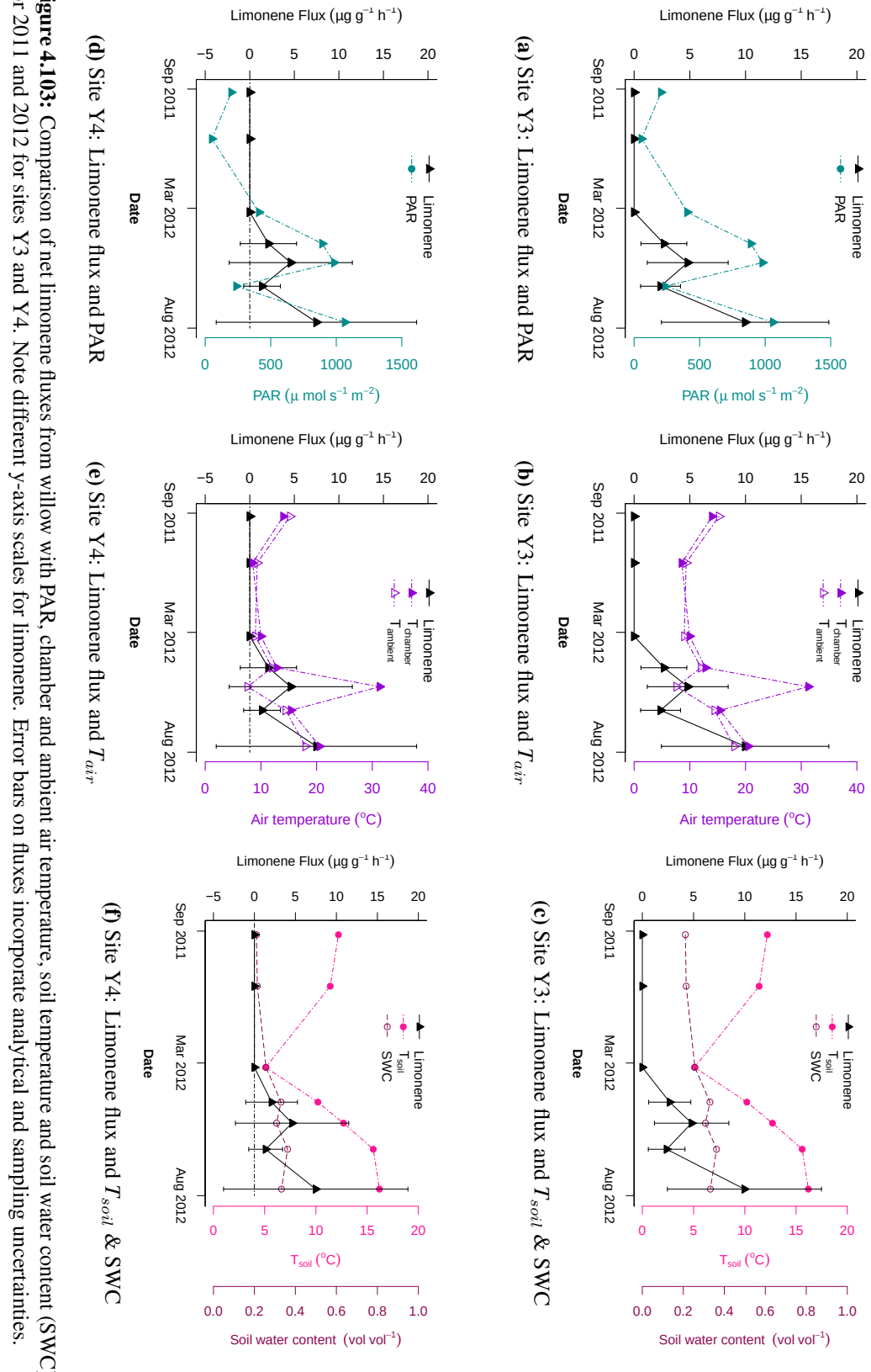
(c) Site Y1: Limonene flux and T_{soil} & SWC

(d) Site Y2: Limonene flux and PAR

(e) Site Y2: Limonene flux and T_{air}

(f) Site Y2: Limonene flux and T_{soil} & SWC

Figure 4.102: Comparison of net limonene fluxes from willow with PAR, chamber and ambient air temperature, soil temperature and soil water content (SWC) for 2011 and 2012 for sites Y1 and Y2. Note different y-axis scales for limonene. Error bars on fluxes incorporate analytical and sampling uncertainties.



(a) Site Y3: Limonene flux and PAR

(b) Site Y3: Limonene flux and T_{air}

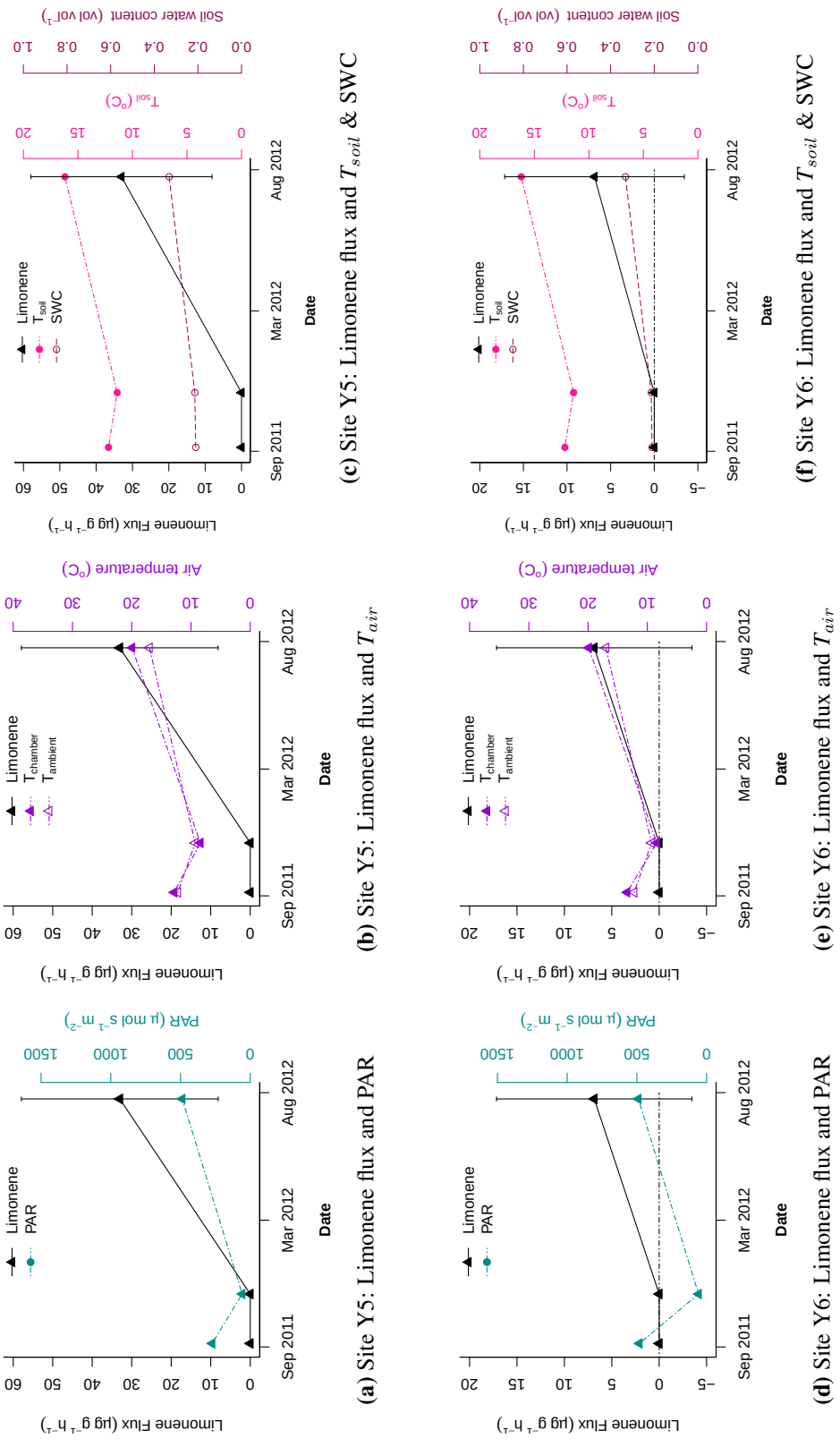
(c) Site Y3: Limonene flux and T_{soil} & SWC

(d) Site Y4: Limonene flux and PAR

(e) Site Y4: Limonene flux and T_{air}

(f) Site Y4: Limonene flux and T_{soil} & SWC

Figure 4.103: Comparison of net limonene fluxes from willow with PAR, chamber and ambient air temperature, soil temperature and soil water content (SWC) for 2011 and 2012 for sites Y3 and Y4. Note different y-axis scales for limonene. Error bars on fluxes incorporate analytical and sampling uncertainties.



(a) Site Y5: Limonene flux and PAR

(b) Site Y5: Limonene flux and T_{air}

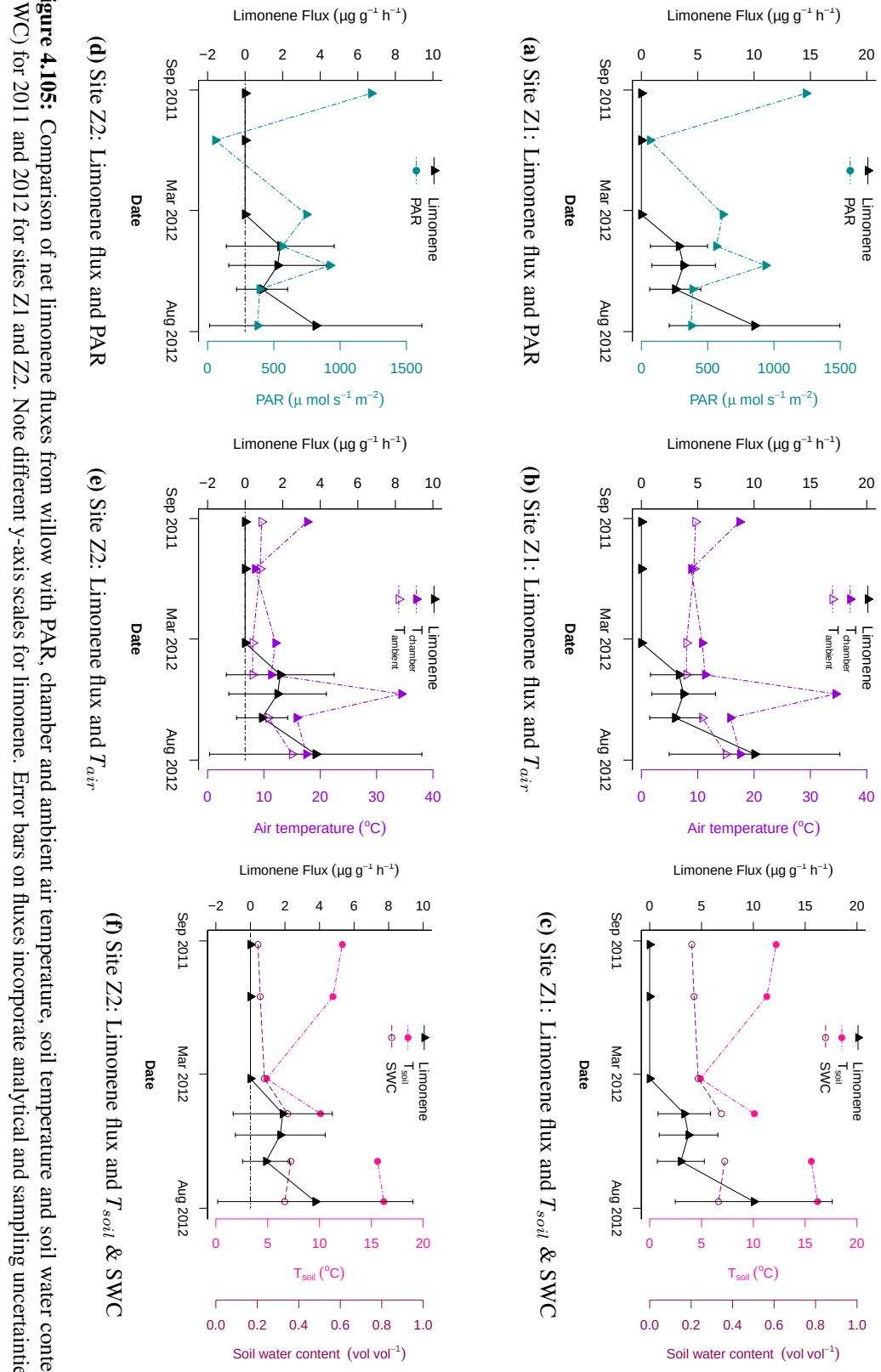
(c) Site Y5: Limonene flux and T_{soil} & SWC

(d) Site Y6: Limonene flux and PAR

(e) Site Y6: Limonene flux and T_{air}

(f) Site Y6: Limonene flux and T_{soil} & SWC

Figure 4.104: Comparison of net limonene fluxes from willow with PAR, chamber and ambient air temperature, soil temperature and soil water content (SWC) for 2011 and 2012 for sites Y5 and Y6. Note different y-axis scales for limonene. Error bars on fluxes incorporate analytical and sampling uncertainties.



(a) Site Z1: Limonene flux and PAR

(b) Site Z1: Limonene flux and T_{air}

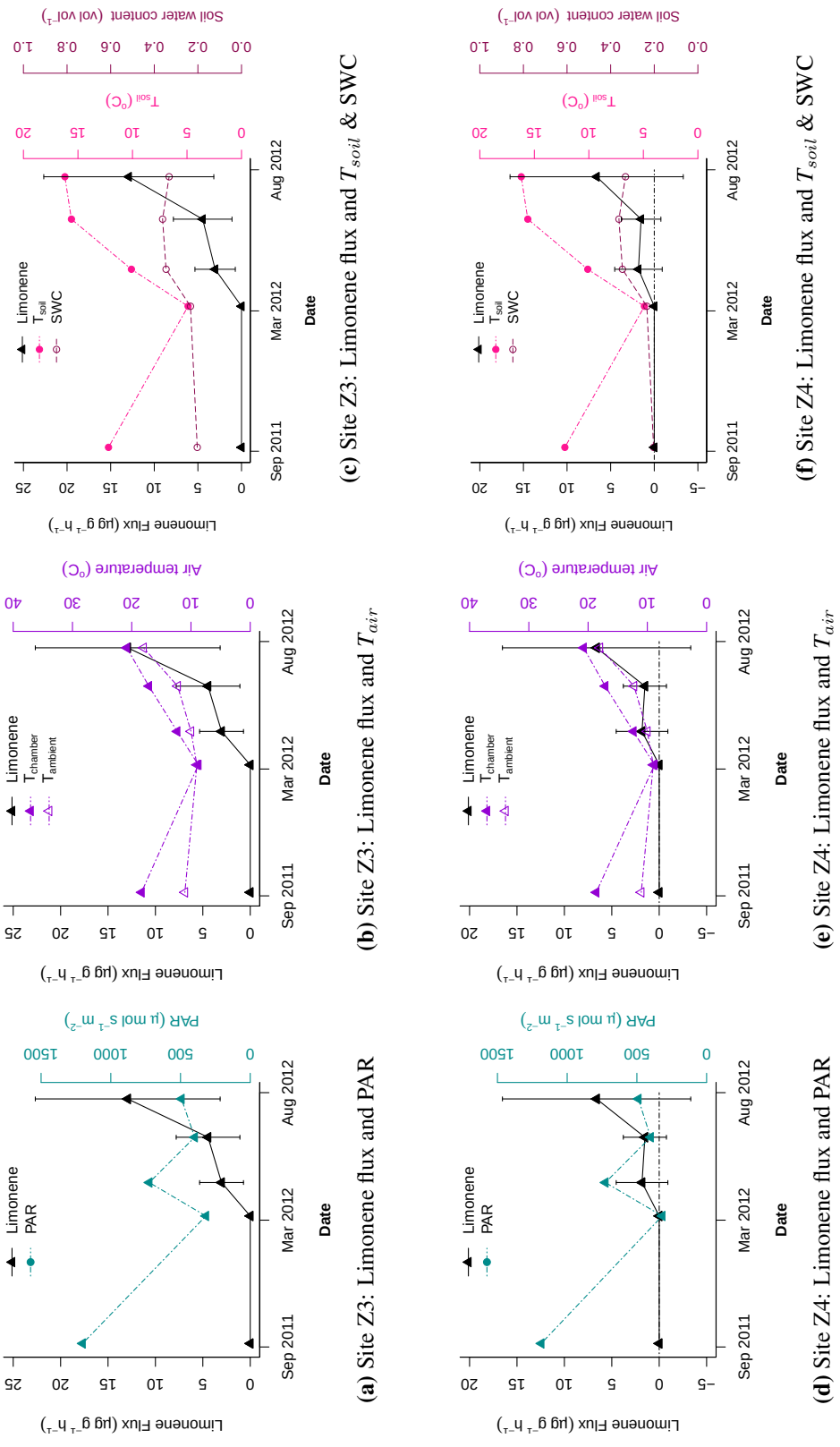
(c) Site Z1: Limonene flux and T_{soil} & SWC

(d) Site Z2: Limonene flux and PAR

(e) Site Z2: Limonene flux and T_{air}

(f) Site Z2: Limonene flux and T_{soil} & SWC

Figure 4.105: Comparison of net limonene fluxes from willow with PAR, chamber and ambient air temperature, soil temperature and soil water content (SWC) for 2011 and 2012 for sites Z1 and Z2. Note different y-axis scales for limonene. Error bars on fluxes incorporate analytical and sampling uncertainties.



(a) Site Z3: Limonene flux and PAR

(b) Site Z3: Limonene flux and T_{air}

(c) Site Z3: Limonene flux and T_{soil} & SWC

(d) Site Z4: Limonene flux and PAR

(e) Site Z4: Limonene flux and T_{air}

(f) Site Z4: Limonene flux and T_{soil} & SWC

Figure 4.106: Comparison of net limonene fluxes from willow with PAR, chamber and ambient air temperature, soil temperature and soil water content (SWC) for 2011 and 2012 for sites Z3 and Z4. Note different y-axis scales for limonene. Error bars on fluxes incorporate analytical and sampling uncertainties.

δ-3-carene

The δ-3-carene fluxes measured between September 2011 and August 2012 at 24 of 30 willow sampling points and the mean of those values on each sampling occasion are illustrated in Figure 4.107.

Zero fluxes were measured between September 2011 and April 2012, similarly to isoprene, α-pinene and limonene, except that non-zero fluxes of these compounds were measured in April 2012. Fluxes varied between zero and 1.4 $\mu g\, g^{-1}\, h^{-1}$ in May 2012. Fluxes dropped slightly at the end of June, to between zero and 0.47 $\mu g\, g^{-1}\, h^{-1}$ then increased significantly at the end of August 2012 to between zero and 13 $\mu g\, g^{-1}\, h^{-1}$. Mean fluxes varied between zero and 3.1 $\mu g\, g^{-1}\, h^{-1}$.

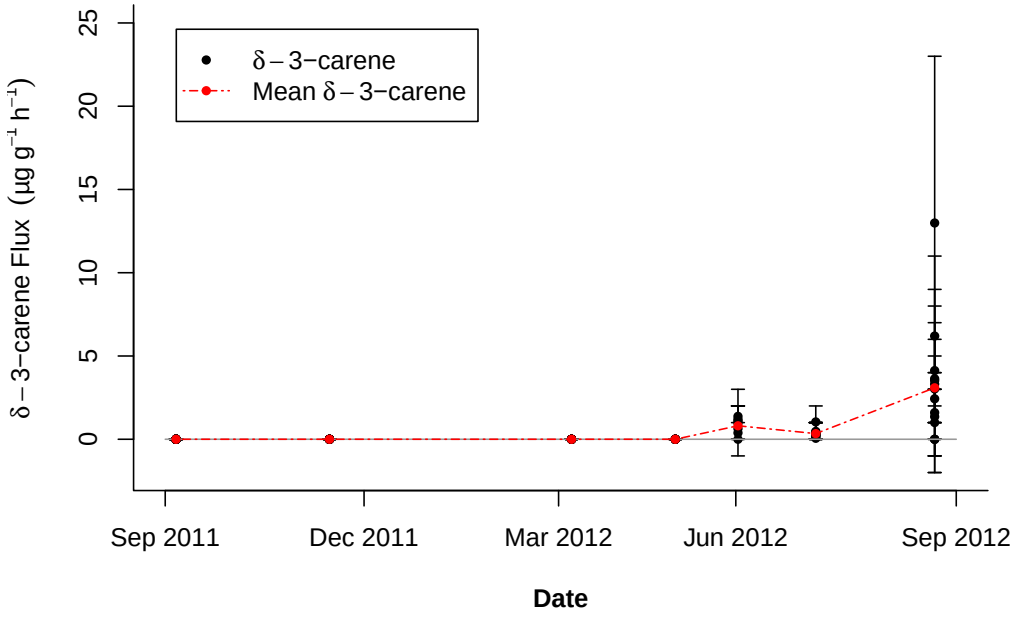


Figure 4.107: δ-3-carene fluxes from willow at the Arnot fieldsite at 24 sampling points and the mean of those values on each sampling occasion from 2011 to 2012. Error bars on fluxes incorporate analytical and sampling uncertainties (as described in Section 2.6.1).

Time series of δ-3-carene fluxes from each individual site between August 2011 and June 2012 together with the concurrent PAR, ambient and chamber air temperature, soil temperature and soil water content (SWC) observations are illustrated in Figures 4.108 to 4.115. The statistical significance of correlations between δ-3-carene fluxes and environmental variables is described in Section 4.3.5.

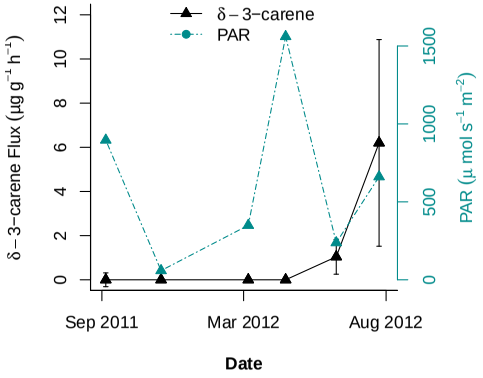
Similar mean δ-3-carene fluxes were measured in all fields, varying between zero and

1.2 $\mu g\, g^{-1}\, h^{-1}$ (Table 4.23). Sites X5-8, Y7-8 and Z5-8 were excluded as they were measured only once and produced zero fluxes. Median fluxes of between zero and 0.19 $\mu g\, g^{-1}\, h^{-1}$ were calculated. The highest maximum flux of 13 $\mu g\, g^{-1}\, h^{-1}$ was measured at site Y5 and the lowest maximum flux of zero was measured at site Y6. The minimum flux measured at every site was zero. Mean fluxes of 0.56, 0.71 and 0.38 $\mu g\, g^{-1}\, h^{-1}$ were calculated from all fluxes measured during the measurement period combined for fields X, Y and X, respectively. A median of zero was calculated for all fields.

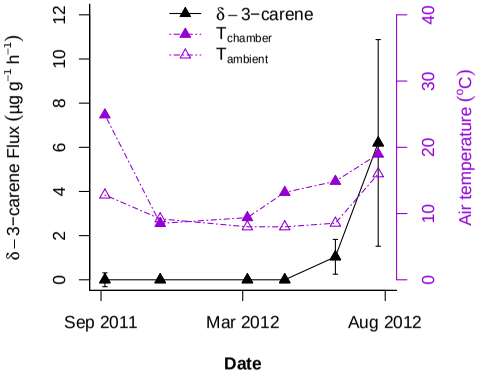
The overall mean δ-3-carene flux calculated from the combination of all measurements made in all three fields was 0.56 $\mu g\, g^{-1}\, h^{-1}$ less than a tenth of that calculated for α-pinene and almost a fifth of the value for limonene. A median value of zero was calculated and the maximum flux was 13 $\mu g\, g^{-1}\, h^{-1}$.

Table 4.23: Mean, median, minimum and maximum net δ-3-carene fluxes from SRC willow at Arnot during 2011 to 2012. All flux values are in $\mu g\, g^{-1}\, h^{-1}$. The final column gives the number of measurements made. The last row summarises all fluxes from all sites.

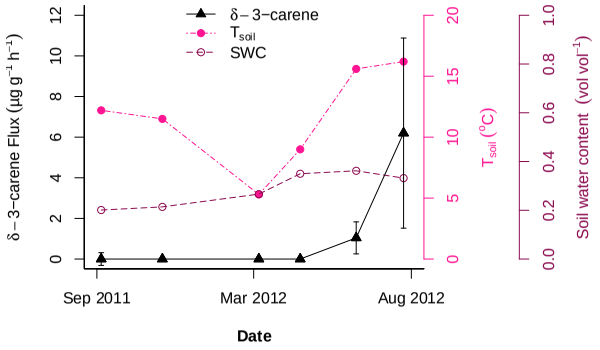
Site	Mean	Median	Min	Max	Number
Willow X1	1.21	0.00	0.00	6.20	6
Willow X2	0.49	0.00	0.00	3.31	7
Willow X3	0.85	0.19	0.00	3.53	6
Willow X4	0.14	0.00	0.00	0.64	7
All X	0.56	0.00	0.00	6.20	30
Willow Y1	0.04	0.00	0.00	0.22	6
Willow Y2	0.68	0.00	0.00	3.64	6
Willow Y3	0.75	0.00	0.00	4.13	7
Willow Y4	0.43	0.00	0.00	1.38	7
Willow Y5	4.33	0.00	0.00	13.0	3
Willow Y6	0.00	0.00	0.00	0.00	3
All Y	0.71	0.00	0.00	13.0	36
Willow Z1	0.55	0.00	0.00	2.43	7
Willow Z2	0.23	0.00	0.00	1.00	7
Willow Z3	0.67	0.00	0.00	3.02	5
Willow Z4	0.37	0.00	0.00	1.60	5
All Z	0.38	0.00	0.00	3.02	28
Overall	0.56	0.00	0.00	13.0	94



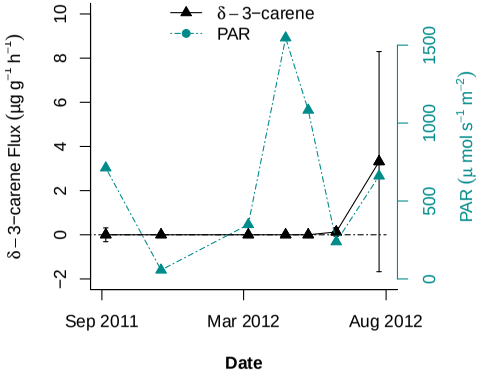
(a) Site X1: δ-3-carene flux and PAR



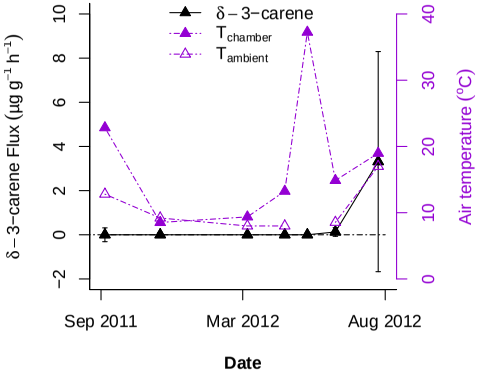
(b) Site X1: δ-3-carene flux and T_{air}



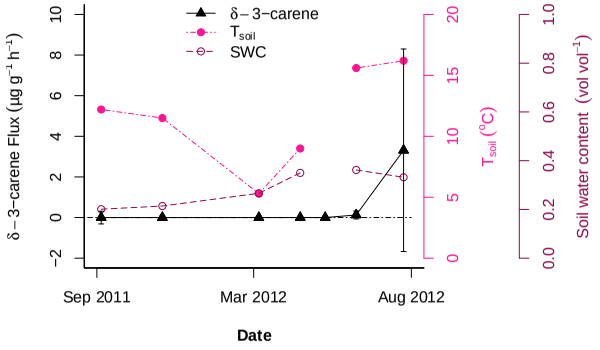
(c) Site X1: δ-3-carene flux and T_{soil} & SWC



(d) Site X2: δ-3-carene flux and PAR

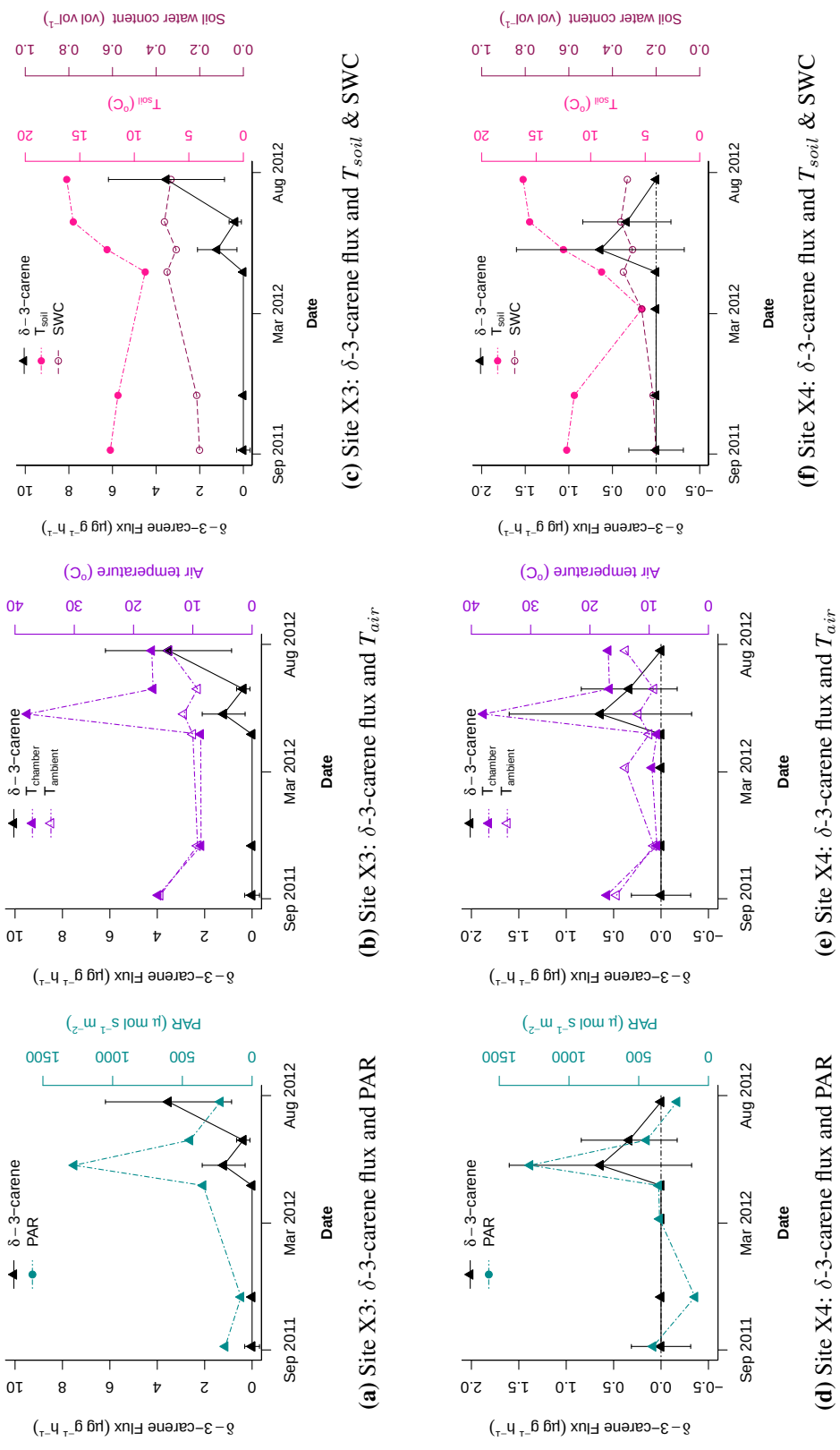


(e) Site X2: δ-3-carene flux and T_{air}



(f) Site X2: δ-3-carene flux and T_{soil} & SWC

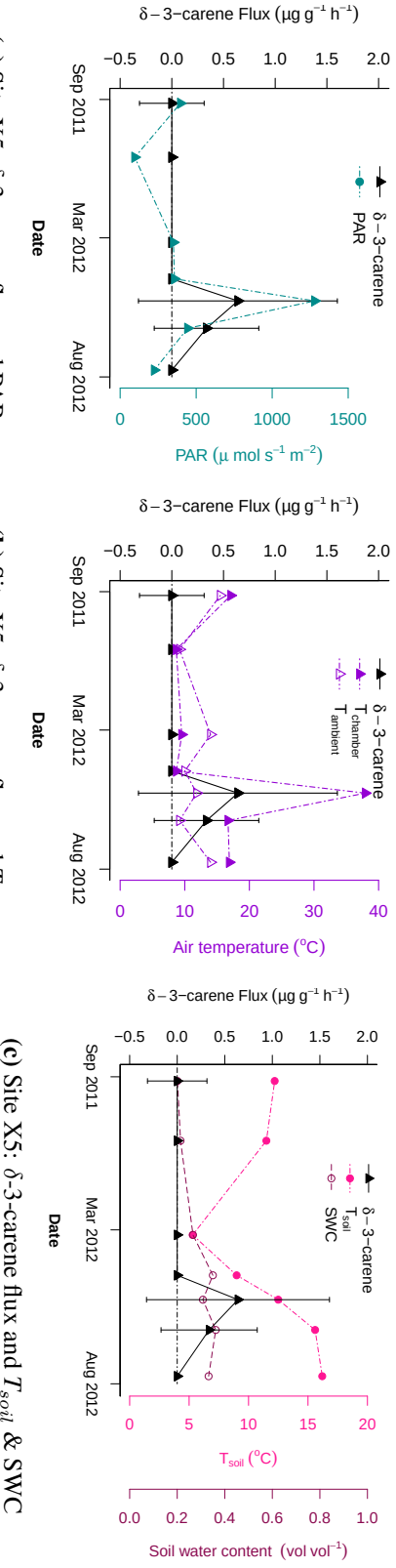
Figure 4.108: Comparison of net δ-3-carene fluxes from willow with PAR, chamber and ambient air temperature, soil temperature and soil water content (SWC) for 2011 and 2012 for sites X1 and X2. Note different y-axis scales for δ-3-carene. Error bars on fluxes incorporate analytical and sampling uncertainties.



(a) Site X3: δ-3-carene flux and PAR **(b)** Site X3: δ-3-carene flux and T_{air} **(c)** Site X3: δ-3-carene flux and T_{soil} & SWC

(d) Site X4: δ-3-carene flux and PAR **(e)** Site X4: δ-3-carene flux and T_{air} **(f)** Site X4: δ-3-carene flux and T_{soil} & SWC

Figure 4.109: Comparison of net δ-3-carene fluxes from willow with PAR, chamber and ambient air temperature, soil temperature and soil water content (SWC) for 2011 and 2012 for sites X3 and X4. Note different y-axis scales for δ-3-carene. Error bars on fluxes incorporate analytical and sampling uncertainties.

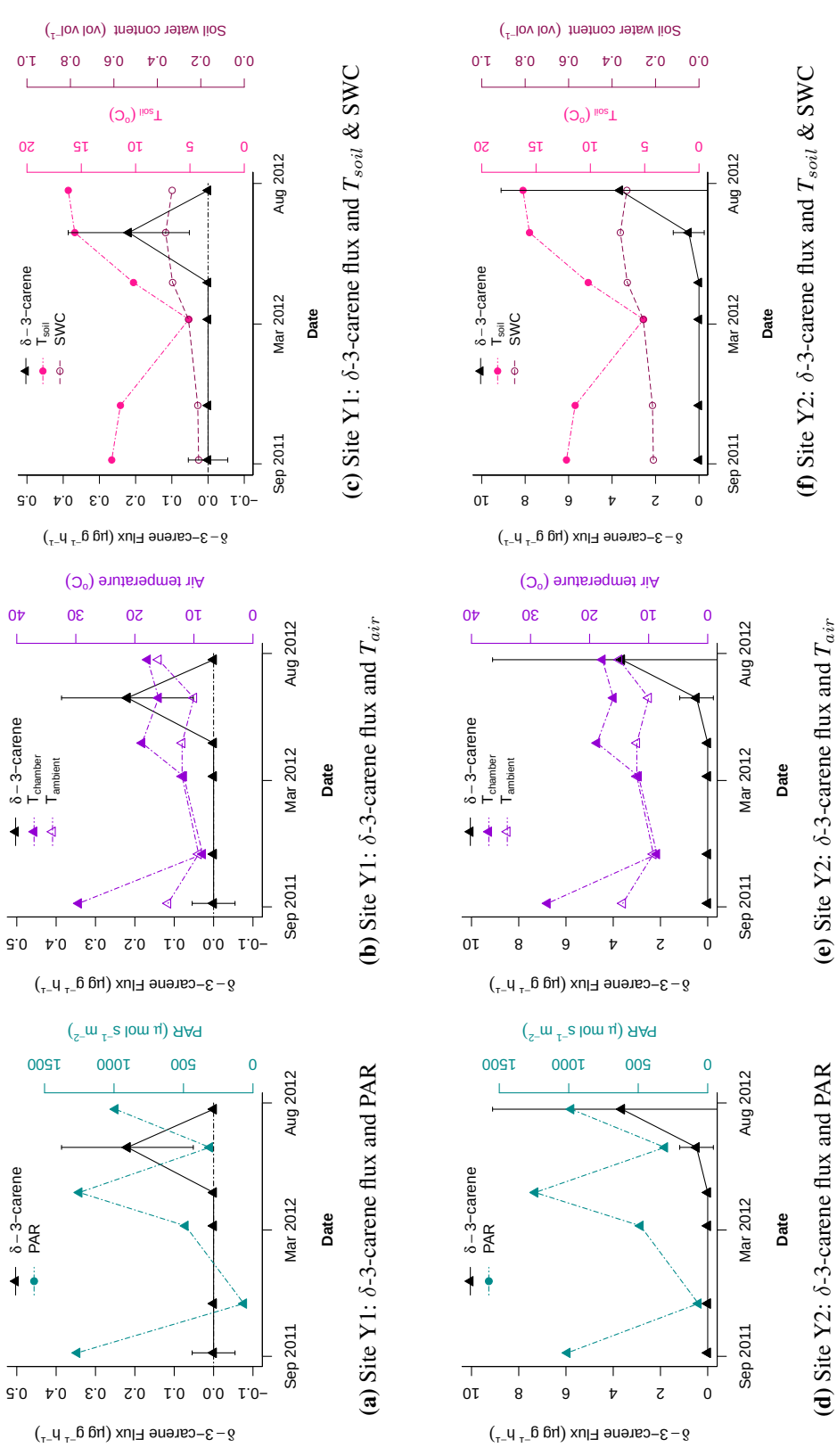


(a) Site X5: δ-3-carene flux and PAR

(b) Site X5: δ-3-carene flux and T_{air}

(c) Site X5: δ-3-carene flux and T_{soil} & SWC

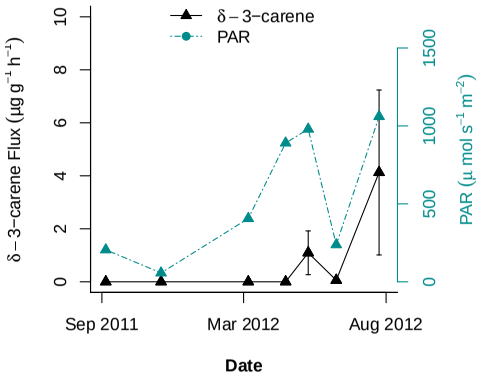
Figure 4.110: Comparison of net δ-3-carene fluxes from willow with PAR, chamber and ambient air temperature, soil temperature and soil water content (SWC) for 2011 and 2012 for site X5. Error bars on fluxes incorporate analytical and sampling uncertainties.



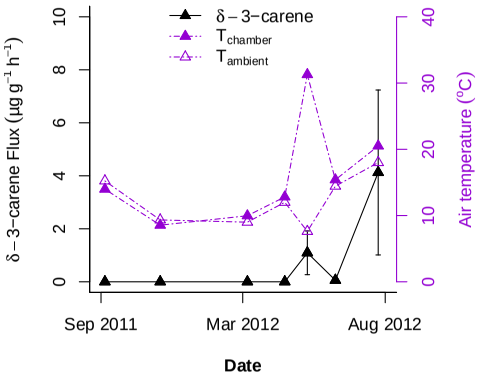
(a) Site Y1: δ-3-carene flux and PAR **(b)** Site Y1: δ-3-carene flux and T_{air} **(c)** Site Y1: δ-3-carene flux and T_{soil} & SWC

(d) Site Y2: δ-3-carene flux and PAR **(e)** Site Y2: δ-3-carene flux and T_{air} **(f)** Site Y2: δ-3-carene flux and T_{soil} & SWC

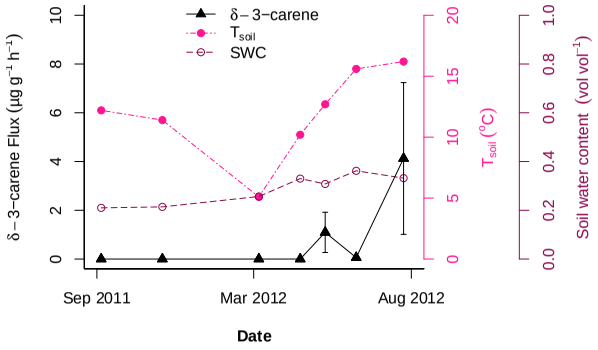
Figure 4.111: Comparison of net δ-3-carene fluxes from willow with PAR, chamber and ambient air temperature, soil temperature and soil water content (SWC) for 2011 and 2012 for sites Y1 and Y2. Note different y-axis scales for δ-3-carene. Error bars on fluxes incorporate analytical and sampling uncertainties.



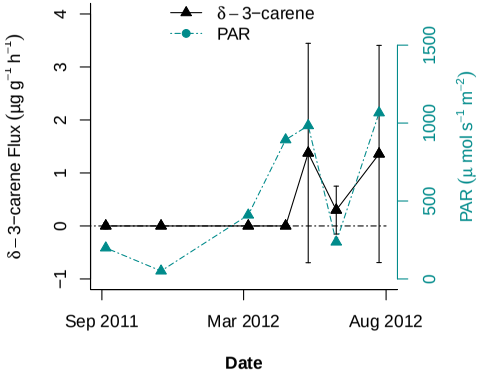
(a) Site Y3: δ-3-carene flux and PAR



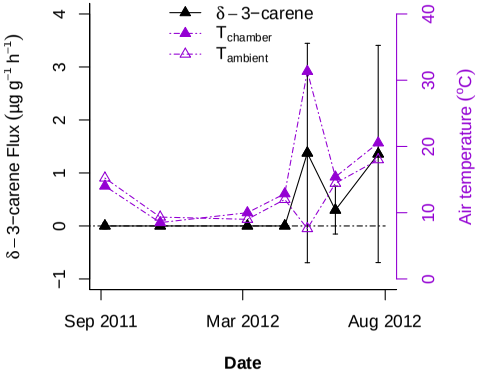
(b) Site Y3: δ-3-carene flux and T_{air}



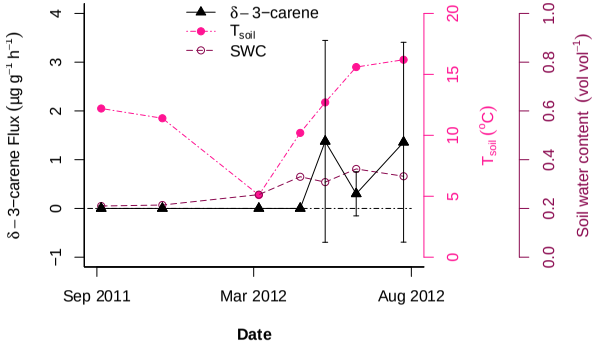
(c) Site Y3: δ-3-carene flux and T_{soil} & SWC



(d) Site Y4: δ-3-carene flux and PAR

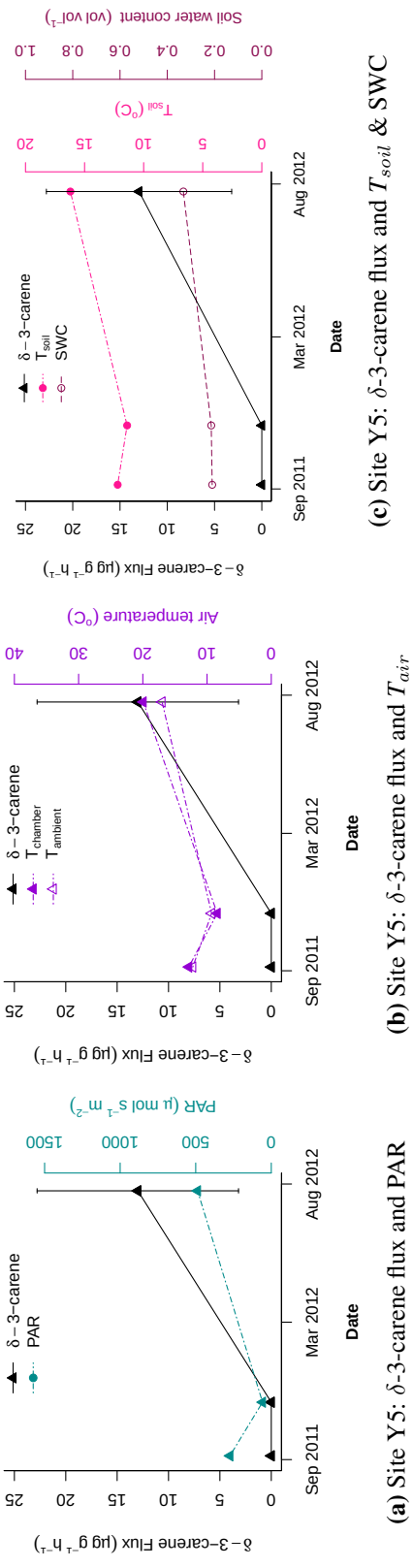


(e) Site Y4: δ-3-carene flux and T_{air}



(f) Site Y4: δ-3-carene flux and T_{soil} & SWC

Figure 4.112: Comparison of net δ-3-carene fluxes from willow with PAR, chamber and ambient air temperature, soil temperature and soil water content (SWC) for 2011 and 2012 for sites Y3 and Y4. Note different y-axis scales for δ-3-carene. Error bars on fluxes incorporate analytical and sampling uncertainties.

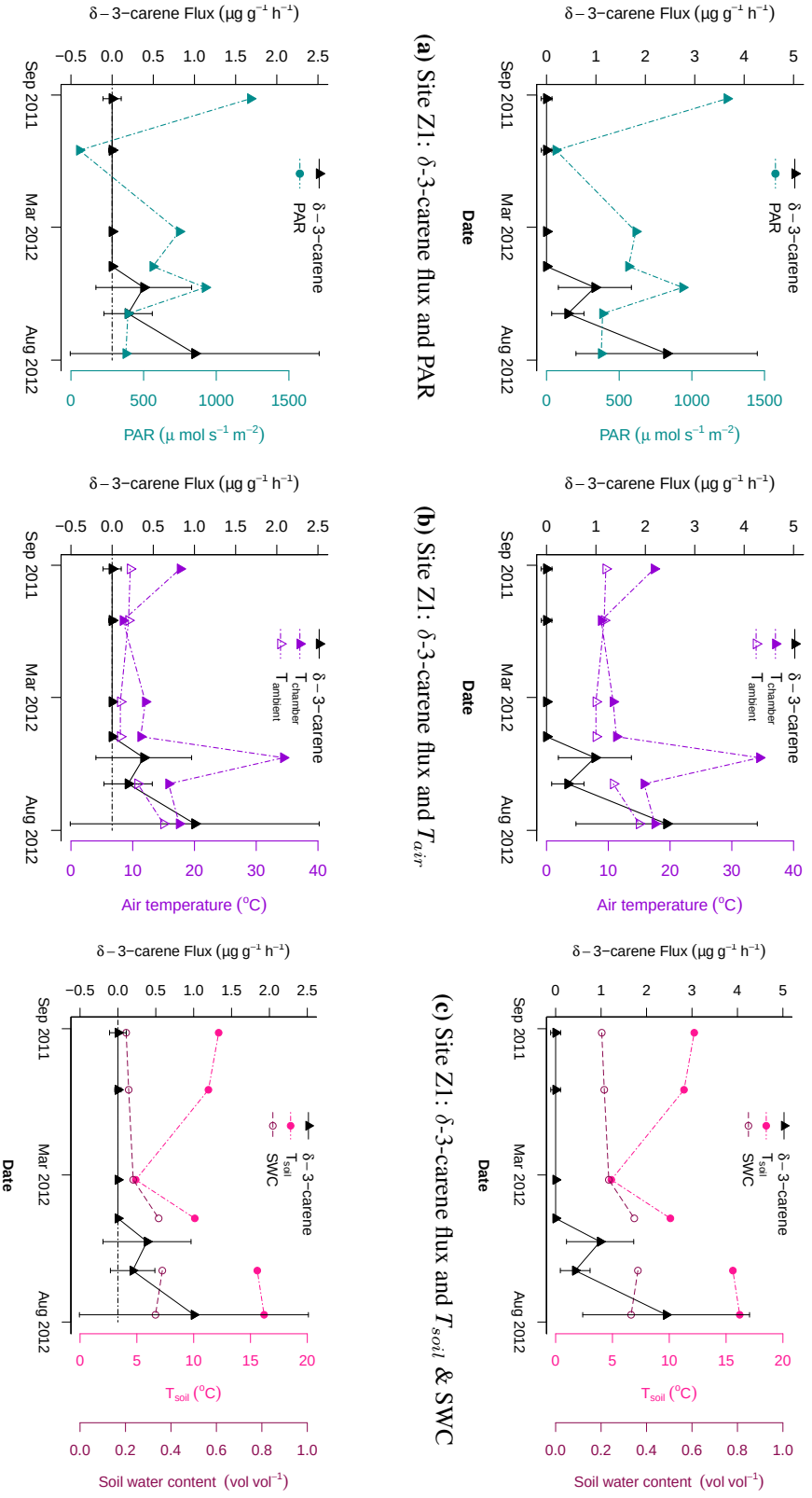


(a) Site Y5: δ-3-carene flux and PAR

(b) Site Y5: δ-3-carene flux and T_{air}

(c) Site Y5: δ-3-carene flux and T_{soil} & SWC

Figure 4.113: Comparison of net δ-3-carene fluxes from willow with PAR, chamber and ambient air temperature, soil temperature and soil water content (SWC) for 2011 and 2012 for sites 5. Note different y-axis scales for δ-3-carene. Error bars on fluxes incorporate analytical and sampling uncertainties.



(a) Site Z1: δ-3-carene flux and PAR

(b) Site Z1: δ-3-carene flux and T_{air}

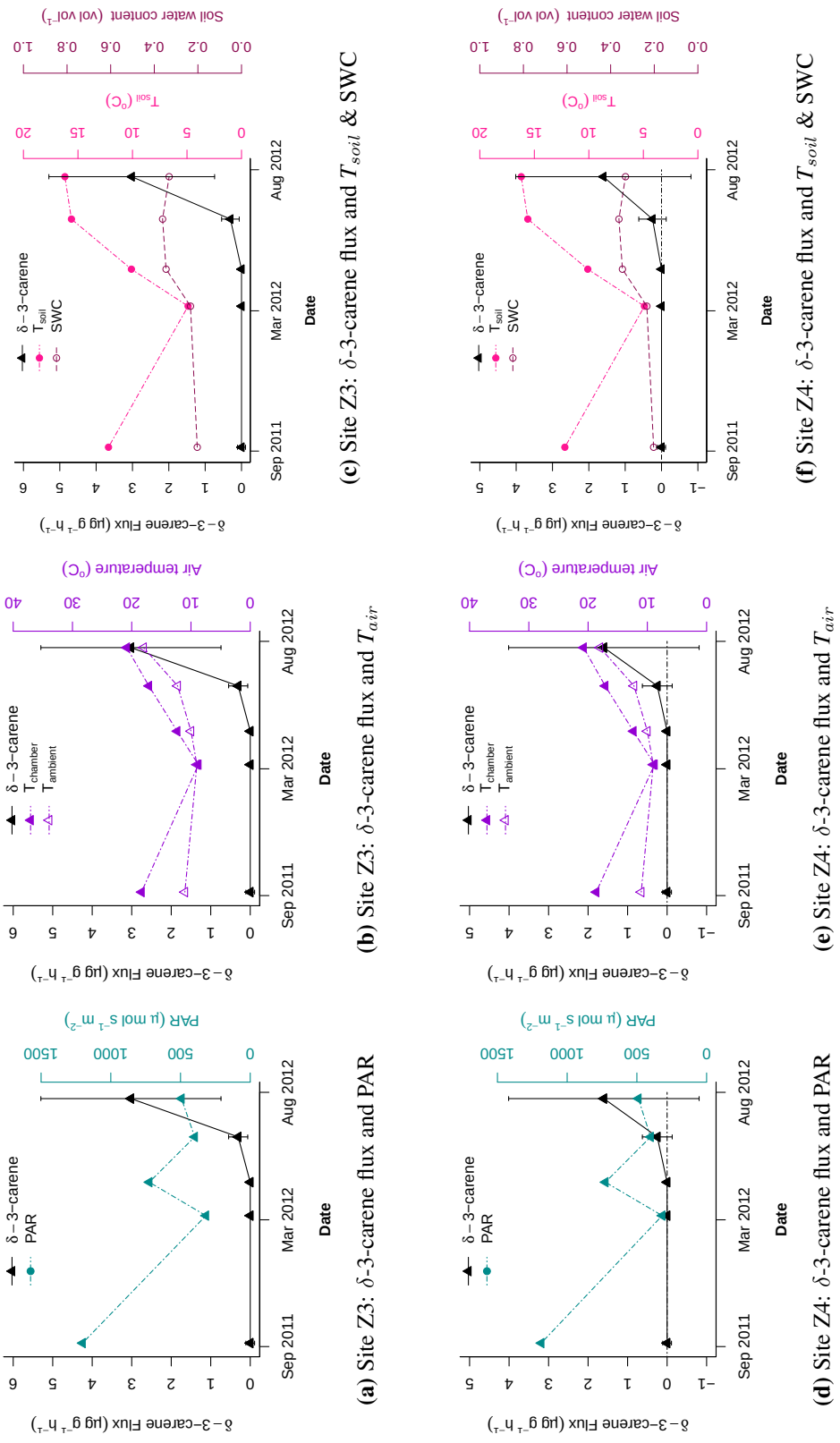
(c) Site Z1: δ-3-carene flux and T_{soil} & SWC

(d) Site Z2: δ-3-carene flux and PAR

(e) Site Z2: δ-3-carene flux and T_{air}

(f) Site Z2: δ-3-carene flux and T_{soil} & SWC

Figure 4.114: Comparison of net δ-3-carene fluxes from willow with PAR, chamber and ambient air temperature, soil temperature and soil water content (SWC) for 2011 and 2012 for sites Z1 and Z2. Note different y-axis scales for δ-3-carene. Error bars on fluxes incorporate analytical and sampling uncertainties.



(a) Site Z3: δ-3-carene flux and PAR

(b) Site Z3: δ-3-carene flux and T_{air}

(c) Site Z3: δ-3-carene flux and T_{soil} & SWC

(d) Site Z4: δ-3-carene flux and PAR

(e) Site Z4: δ-3-carene flux and T_{air}

(f) Site Z4: δ-3-carene flux and T_{soil} & SWC

Figure 4.115: Comparison of net δ-3-carene fluxes from willow with PAR, chamber and ambient air temperature, soil temperature and soil water content (SWC) for 2011 and 2012 for sites Z3 and Z4. Note different y-axis scales for δ-3-carene. Error bars on fluxes incorporate analytical and sampling uncertainties.

4.3.5 Statistical analysis of seasonal fluxes and potential drivers

Three types of analyses were carried out on the long term BVOC time series:

- Variation in BVOC fluxes between sites and between growing and non-growing season were analysed for significance using the Kruskal-Wallis function within the R i386 2.15.1 software package
- Correlations between various BVOC fluxes were investigated using regression analysis
- BVOC fluxes were also analysed for their association with measured environmental parameters

Analysis of variation according to site and season

The significance of the variation in isoprene, α-pinene, limonene and δ-3-carene fluxes due to location (different sites in the field), season (growing and non-growing), and from the interaction between these two factors was analysed using multivariate ANOVA. Each year was divided into a growing season (beginning of April to end of September) and a non-growing season (November to March) based on observational evidence of plant growth.

Fluxes of all BVOCs (isoprene, α-pinene, limonene and δ-3-carene) were found to vary significantly with season with χ^2 values beween 14 and 28 and corresponding $p < 0.05$ (Table 4.24). No significant variation in fluxes was associated with site or season-site interaction terms.

Table 4.24: Analysis of isoprene, α-pinene, limonene and δ-3-carene flux variation according to site and season derived using Kruskal-Wallis. Degrees of freedom (D.f) and χ^2 values for the effect of site, season and season-site interaction terms on BVOC fluxes in 2011 and 2012 are presented. Significant variation in BVOC flux ($p \leq 0.05$) is highlighted in bold.

	Season	Site	Season*Site
D.f	1	23	23
Isoprene	**27.9**	14.3	30.2
α-pinene	**22.6**	11.1	29.8
Limonene	**26.1**	11.7	35.1
δ-3-carene	**14.4**	10.8	24.7

Correlations between different BVOCs

Fluxes of the four BVOC compounds identified (isoprene, α-pinene, limonene and δ-3-carene) were tested for correlations with each other. Significant positive correlation coefficients were identified between all BVOC fluxes with ρ values between 0.3 and 0.8 with corresponding p values of < 0.005 (Table 4.25).

Table 4.25: Spearman's rank correlation coefficients (ρ) and their corresponding *p* values for correlations between isoprene, α-pinene, limonene and δ-3-carene fluxes for fluxes at all sites combined.

BVOC compound	ρ	p
Isoprene & α-pinene	0.326	0.001
Isoprene & limonene	0.534	< 0.001
Isoprene & δ-3-carene	0.668	< 0.001
α-pinene & limonene	0.833	< 0.001
α-pinene & δ-3-carene	0.437	< 0.001
Limonene & δ-3-carene	0.723	< 0.001

BVOC flux association with measured environmental factors

Fluxes of isoprene, α-pinene, limonene and δ-3-carene were tested for correlations with PAR, chamber and ambient temperature, soil temperature and soil moisture.

α-pinene, limonene and δ-3-carene but not isoprene were found to be significantly correlated with chamber temperature (Table 4.26). A significant correlation between α-pinene flux and PAR was identified, and between limonene and soil moisture.

Table 4.26: Spearman's rank correlation coefficients (ρ) between potential drivers and isoprene, α-pinene, limonene and δ-3-carene fluxes during the growing season. Significant correlations ($p \leq 0.05$) are highlighted in bold.

Factor	Isoprene	α-pinene	Limonene	δ-3-carene
PAR	-0.013	**0.208**	0.190	0.155
$\boldsymbol{T}_{chamber}$	0.144	**0.266**	**0.232**	**0.314**
$\boldsymbol{T}_{ambient\ air}$	0.07	0.100	-0.091	-0.148
$\boldsymbol{T}_{soil}$	0.204	0.079	0.152	**0.219**
Soil moisture	0.061	-0.060	**0.316**	0.138

4.4 East Grange

4.4.1 Site description

Measurements were conducted at the East Grange fieldsite, as described in Section 2.7.3. A total of ten sampling points on the edge of the field and within the field were used, as shown in Figure 4.116.

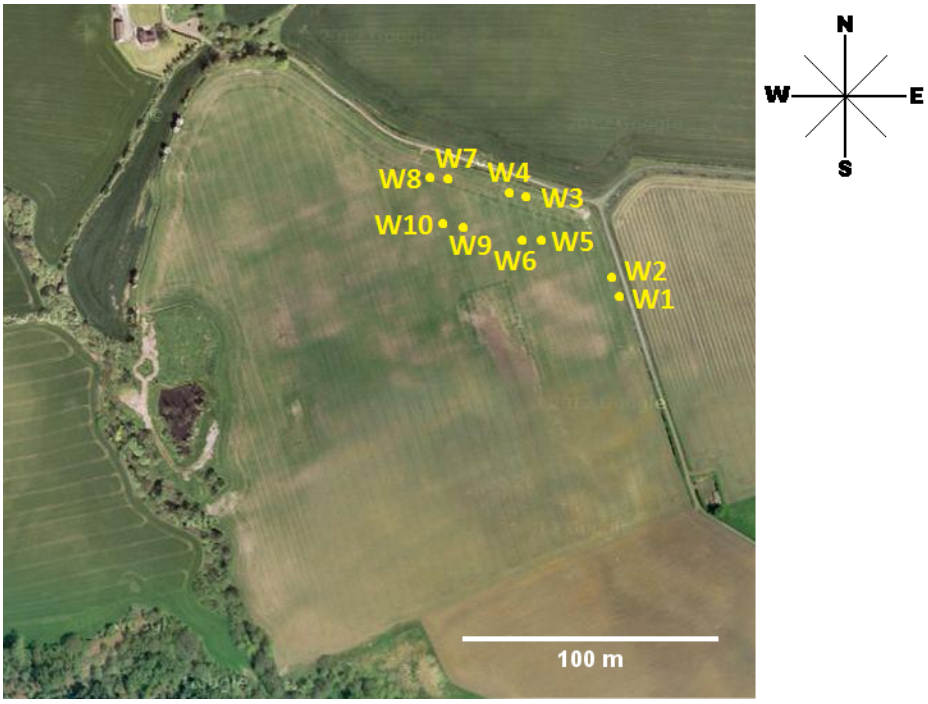


Figure 4.116: Location of sampling points within the SRC willow field in East Grange.

4.4.2 Outline of CH_3X flux measurements

A total of 40 measurements were made during 4 site visits between March and June 2012. Firstly, the CH_3X flux trends over the measurement period are examined. Time series of mean CH_3X fluxes together with the respective PAR, ambient air temperature, soil temperature and soil water content observations at the time of measurement for each sampling site are then illustrated.

CH_3Br

Measurements began at the end of March 2012, when zero fluxes were measured at all sites, as shown in Fig. 4.118. CH_3Br fluxes were present at the end of April, with a range between zero

and 5.5 ng g^{-1} h^{-1}. Fluxes decreased slightly in May to between zero and 1.8 ng g^{-1} h^{-1} but increased again at the end of June to between zero and 4.9 ng g^{-1} h^{-1}.

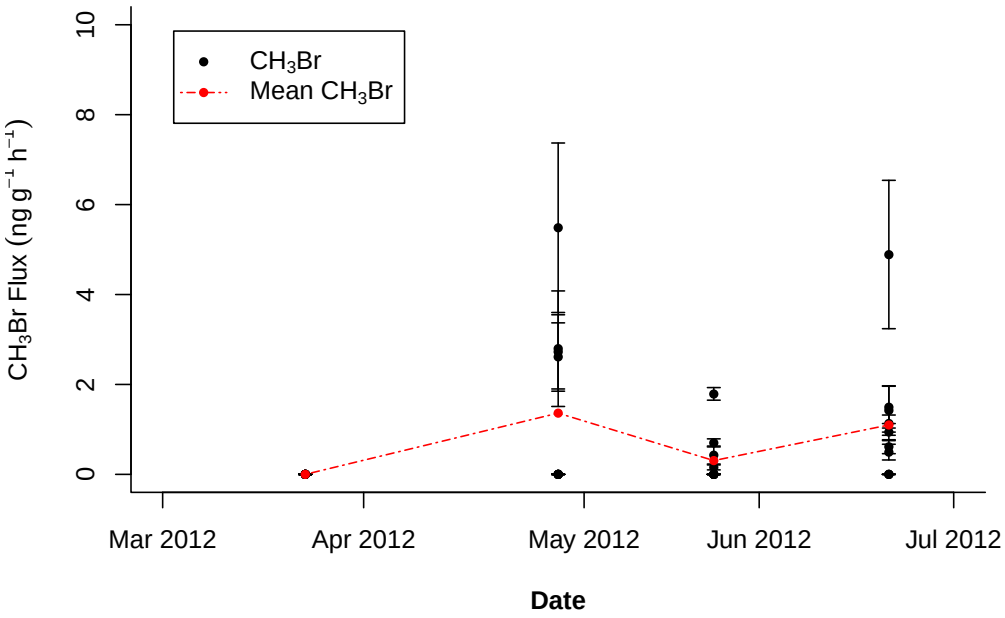


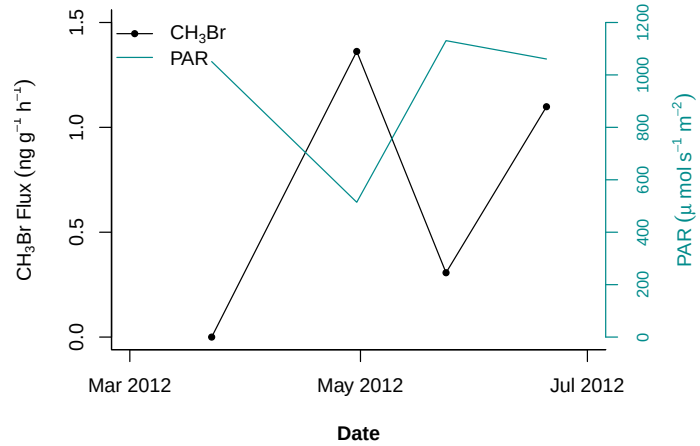
Figure 4.117: CH_3Br fluxes from willow at the East Grange fieldsite at all ten sampling points and the mean of those values on each sampling occasion in 2012. Error bars on fluxes incorporate analytical and sampling uncertainties (as described in Section 2.6.1).

The mean CH_3Br flux calculated for individual sites ranged between zero and 1.5 ng g^{-1} h^{-1} (Table 4.27). The maximum flux of 5.5 ng g^{-1} h^{-1} was measured at site 3. The minimum flux measured at all sites was zero. A mean of 0.69 ng g^{-1} h^{-1} was calculated for all measurements made combined.

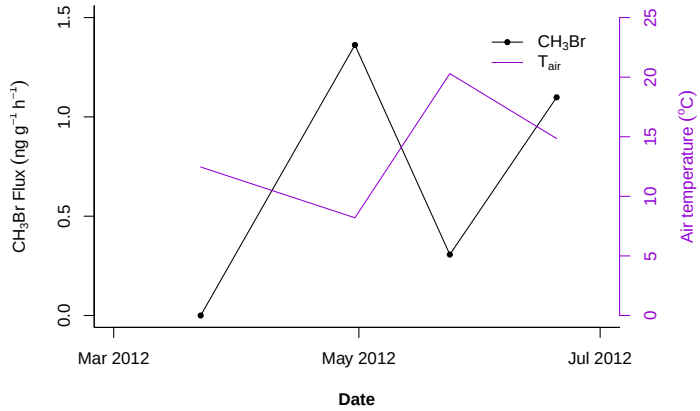
Time series of mean CH_3Br fluxes together with the respective mean PAR, ambient air temperature, soil temperature and soil water content observations are illustrated in Figure 4.118. The mean CH_3Br fluxes do not appear to follow any trends in the measured environmental variables.

Table 4.27: Mean, median, minimum and maximum net CH_3Br fluxes from SRC willow at East Grange during 2012. All flux values are in $ng\,g^{-1}\,h^{-1}$. The final column gives the number of measurements made. The last row summarises all fluxes from all sites.

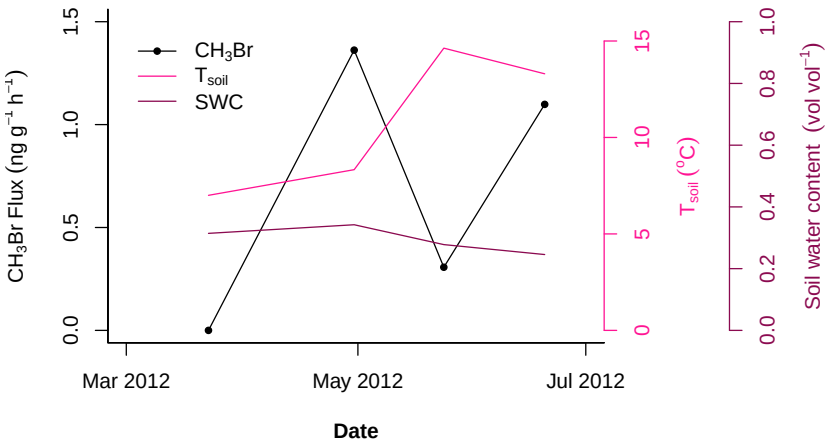
Site	Mean	Median	Min	Max	Number
W1	0.12	0.00	0.00	0.49	4
W2	0.92	0.47	0.00	2.73	4
W3	1.48	0.21	0.00	5.49	4
W4	0.81	0.31	0.00	2.61	4
W5	0.00	0.00	0.00	0.00	4
W6	0.32	0.08	0.00	1.13	4
W7	1.52	1.64	0.00	2.80	4
W8	0.18	0.00	0.00	0.70	4
W9	1.22	0.00	0.00	4.89	4
W10	0.36	0.00	0.00	1.42	4
All	0.69	0.00	0.00	5.49	40



(a) CH_3Br flux and PAR



(b) CH_3Br flux and $T_{ambient\ air}$



(c) CH_3Br flux and T_{soil} & SWC

Figure 4.118: Comparison of mean CH_3Br fluxes from willow at East Grange with mean PAR, ambient air temperature, soil temperature and soil water content (SWC). Error bars on fluxes incorporate analytical and sampling uncertainties.

CH_3Cl

Few non-zero CH_3Cl fluxes measured during the sampling period, as illustrated in Figure 4.119. Zero fluxes were measured throughout sampling in March, April and May. Two non-zero fluxes 15 and 53 ng g^{-1} h^{-1} were measured in June at sites 6 and 10 respectively.

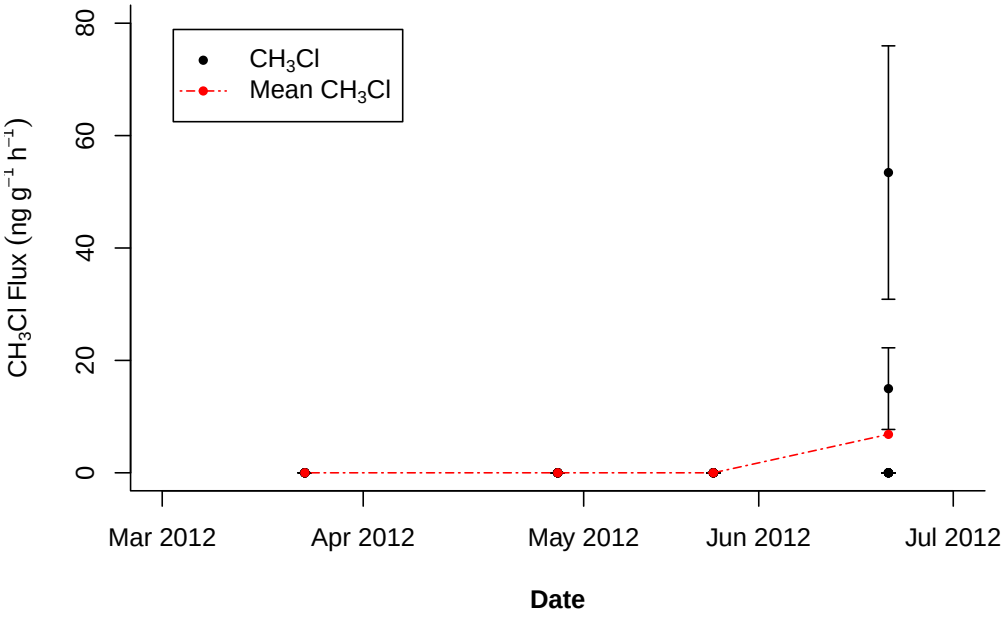


Figure 4.119: CH_3Cl fluxes from willow at the East Grange fieldsite at all ten sampling points and the mean of those values on each sampling occasion in 2012. Error bars on fluxes incorporate analytical and sampling uncertainties (as described in Section 2.6.1).

4.4.3 Outline of BVOC flux measurements

A total of 50 measurements were made during 5 site visits between March and August 2012. Fluxes were generally low, with some small fluxes of isoprene, α-pinene and limonene measured but no β-pinene or δ-3-carene. No isoprene fluxes were measured in March and only one non-zero flux of 0.5 $\mu g\, g^{-1}\, h^{-1}$ was measured at the end of April (Figure 4.120). Fluxes increased to between zero and 1 $\mu g\, g^{-1}\, h^{-1}$ in May and then again to between 0.6 and 3.8 $\mu g\, g^{-1}\, h^{-1}$ in June. The highest fluxes were measured in August, between zero and 4.6 $\mu g\, g^{-1}\, h^{-1}$. Large associated uncertainties for these fluxes suggest that these are not important fluxes of isoprene.

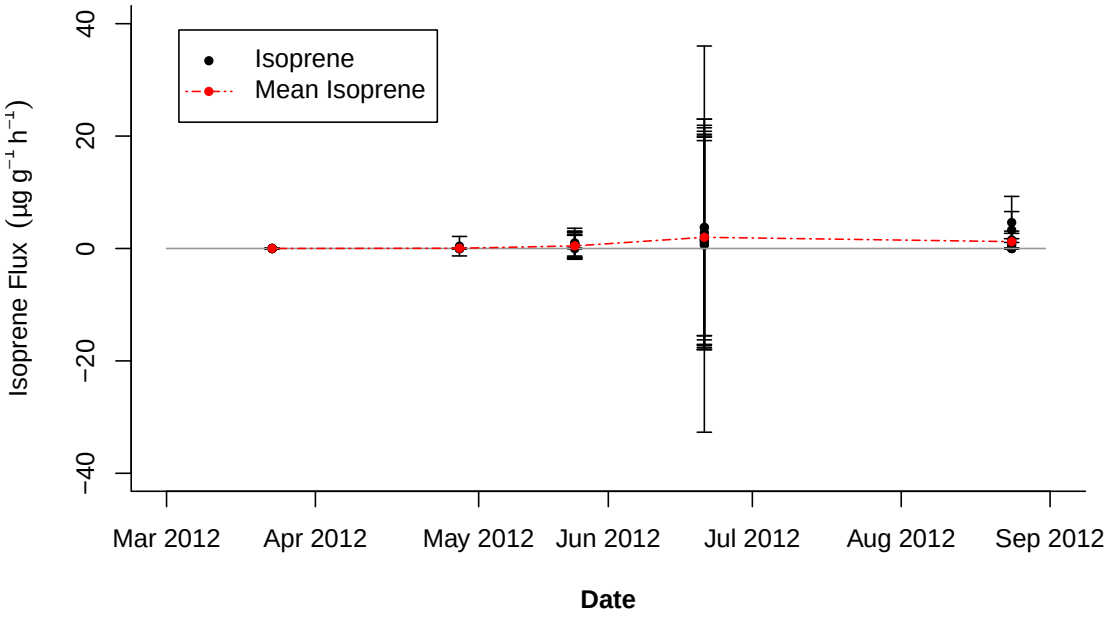


Figure 4.120: Isoprene fluxes from willow at the East Grange fieldsite at all ten sampling points and the mean of those values on each sampling occasion in 2012. Error bars on fluxes incorporate analytical and sampling uncertainties (as described in Section 2.6.1).

No α-pinene fluxes were measured in March (Figure 4.121). Fluxes varied between 2 and 20 $\mu g\, g^{-1}\, h^{-1}$ at the end of April then decreased to between zero and 0.7 $\mu g\, g^{-1}\, h^{-1}$ in May. Fluxes fell again in June to between zero and 0.4 $\mu g\, g^{-1}\, h^{-1}$ and again in August to between zero and 0.1 $\mu g\, g^{-1}\, h^{-1}$. Large associated uncertainties for these fluxes suggest that these are not important fluxes of α-pinene.

Time series of mean isoprene and α-pinene fluxes together with the respective mean PAR, ambient air temperature, soil temperature and soil water content observations are illustrated

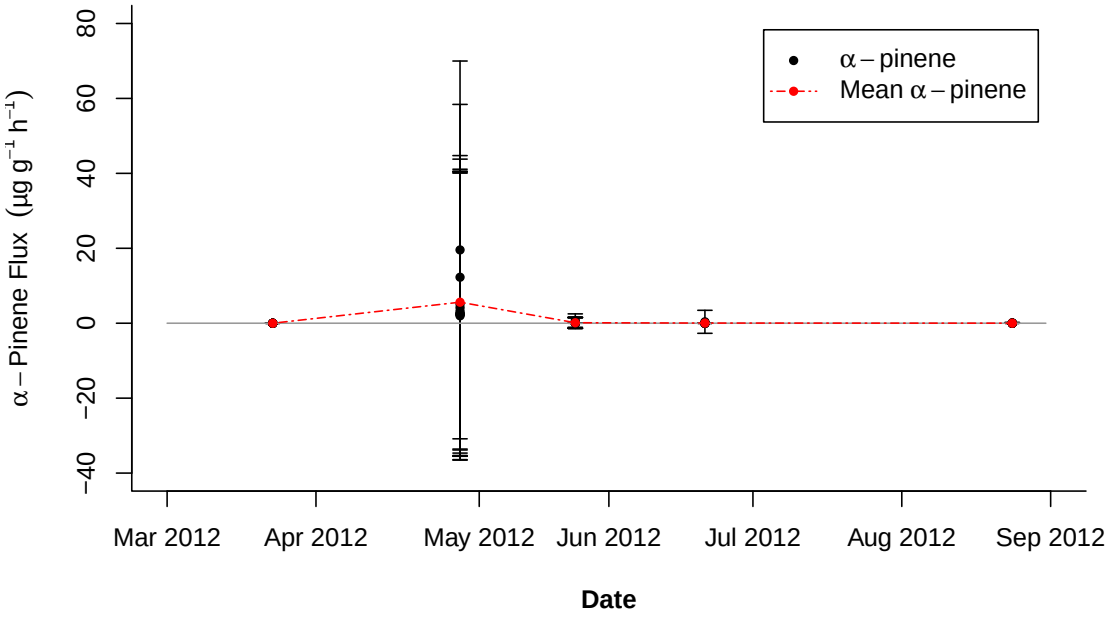
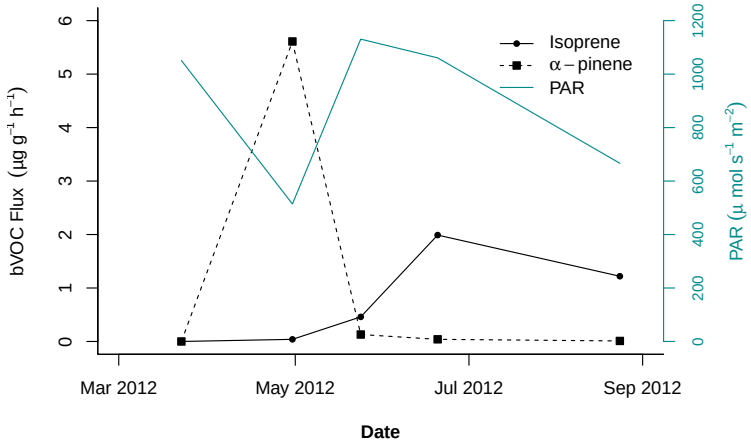


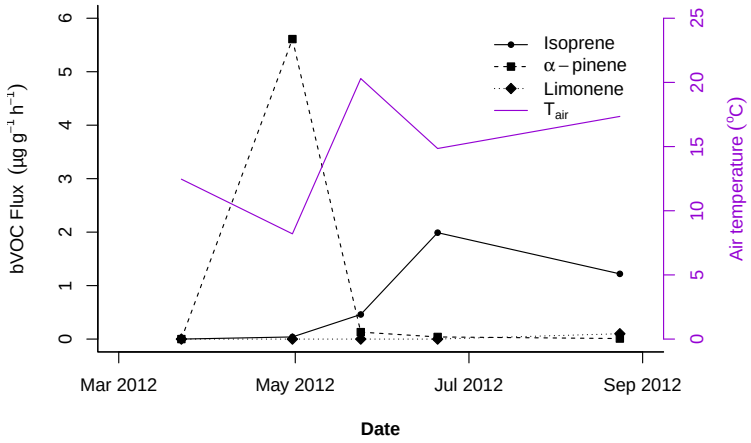
Figure 4.121: α-pinene fluxes from willow at the East Grange fieldsite at all ten sampling points and the mean of those values on each sampling occasion in 2012. Error bars on fluxes incorporate analytical and sampling uncertainties (as described in Chapter 2).

in Figure 4.122. The mean BVOC fluxes do not appear to follow any trends in the measured environmental variables.

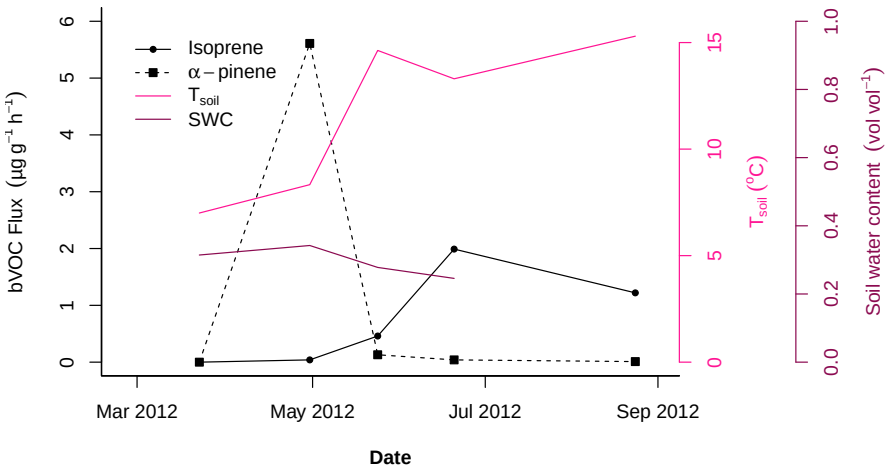
Fluxes of limonene were only detected in August 2012. Fluxes of between 0.11 and 0.39 $\mu g\, g^{-1}\, h^{-1}$ were measured at 4 sites with zero fluxes at all other sites.



(a) BVOC flux and PAR



(b) BVOC flux and $T_{ambient\,air}$



(c) BVOC flux and T_{soil} & SWC

Figure 4.122: Comparison of mean isoprene and α-pinene fluxes from willow at East Grange with mean PAR, ambient air temperature, soil temperature and soil water content (SWC). Error bars on fluxes incorporate analytical and sampling uncertainties.

4.5 Summary

Out of the three fieldsites used in this study, annual mean net CH_3X fluxes were highest at the Arnot fieldsite (Table 4.28). Annual mean fluxes of all BVOCs were highest at the Brattleby fieldsite. Fluxes measured at the East Grange site were generally low, although the annual mean net CH_3Br flux was slightly higher than that calculated for the Brattleby measurements.

Table 4.28: Annual mean net fluxes of CH_3Br and CH_3Cl in $ng\,g^{-1}\,h^{-1}$ and annual mean net fluxes of isoprene, α-pinene, β-pinene, limonene and δ-3-carene in $\mu g\,g^{-1}\,h^{-1}$ from willow measurements made in Brattleby, Arnot and East Grange. ND = Not detected.

	Site		
Flux	Brattleby	Arnot	East Grange
CH_3Br	0.56	1.65	0.69
CH_3Cl	4.90	11.9	1.71
Isoprene	77.1	15.1	0.74
α-pinene	45.5	7.29	1.16
β-pinene	5.50	ND	ND
Limonene	3.68	2.73	0.02
δ-3-carene	11.3	0.56	ND

A seasonal trend was evident in the fluxes of all compounds measured at all fieldsites, with higher fluxes during the summer months and low to zero fluxes during the winter. At the Brattleby fieldsite, there were some interesting variations in the magnitude of fluxes between the years of measurement, 2010 to 2012. This is likely to be due to the growth stage of the willow trees. The willow trees were coppiced in winter 2010 so measurements taken in 2011 were from younger trees compared to measurements taken from trees with three year's growth in 2010 and at least a year's growth in 2012.

The CH_3Br fluxes at Brattleby followed a clear seasonal trend, with higher fluxes during the summer months and low to zero fluxes during the winter. Generally, CH_3Br fluxes were low with the highest fluxes occurring in 2011. At Arnot, fluxes were highest later in the year in 2011, peaking in October, and earlier in the year in 2012, peaking in March. CH_3Br fluxes measured at East Grange were very low, with zero fluxes at the start of the year and slightly higher fluxes in April to June 2012.

Fluxes of CH_3Cl from all sites followed a similar pattern to the corresponding CH_3Br fluxes. Generally, CH_3Cl fluxes were low and again fluxes measured in 2011 were much higher than those measured in 2010 and 2012. The highest mean summer flux of CH_3Cl was over ten times the highest CH_3Br flux. CH_3Cl fluxes from Arnot were again highest later in 2011, peaking in November 2011 and again in May 2012. The vegetation at the East Grange fieldsite was not

found to be an important source of CH_3Cl as few non-zero CH_3Cl fluxes were measured during the sampling period.

Only a handful of significant correlations were found between fluxes of CH_3Br and CH_3Cl at the various fieldsites. There was no general trend for CH_3X fluxes to be correlated at low, high or average CH_3X emitting sites. Generally, significant correlations were identified between CH_3X fluxes and season but not site. Significant positive correlation between CH_3X fluxes and PAR, chamber temperature, ambient air temperature and soil temperature were derived.

The isoprene fluxes from Brattleby followed the same seasonal trend as the CH_3X fluxes, with higher fluxes during the summer and zero fluxes over the winter. The fluxes of isoprene measured from the willow were generally high, with much higher fluxes measured in 2010 compared to 2011 and 2012. This is a different trend to the CH_3X fluxes, where fluxes were highest in 2011, and is probably related to the age of the willow trees as described above.

The isoprene measurements from the Arnot fieldsite also followed a seasonal trend, with fluxes highest in summer 2012 and low between September 2011 and March 2012. Mean fluxes were lower than those measured in Brattleby (a maximum of 95 $\mu g\, g^{-1}\, h^{-1}$ at Arnot compared to a maximum of 1140 $\mu g\, g^{-1}\, h^{-1}$ at Brattleby). Low fluxes of isoprene and other BVOCs were measured at the East Grange fieldsite. These fluxes also appeared to follow a seasonal trend with low to zero fluxes in March and April and higher fluxes in May to August.

Generally, fluxes of α-pinene of under 100 $\mu g\, g^{-1}\, h^{-1}$ were measured at all fieldsites with the exception of measurements made in Brattleby in 2010 which revealed fluxes of an order of magnitude higher than those measured in 2011 and 2012. A range fluxes of α-pinene following the seasonal trend were measured in Arnot. Fluxes of α-pinene were measured in East Grange but were much lower than those measured at the other two fieldsites.

Fluxes of β-pinene were measured in Brattleby but were not detected in either Arnot nor East Grange. Similarly to α-pinene, fluxes of β-pinene measured in Brattleby in 2010 were one or two orders of magnitude higher than those measured in 2012, with large associated uncertainties.

Limonene fluxes were measured in Brattleby and Arnot but not in East Grange. Limonene fluxes in Brattleby followed a different trend to the other BVOCs measured with higher fluxes measured in 2012 than in 2010. As with the other BVOCs mentioned, zero fluxes were measured throughout 2011. Limonene fluxes measured in Arnot were of a similar magnitude to those measured in Brattleby.

Similarly to isoprene, α-pinene and β-pinene fluxes, δ-3-carene fluxes measured in Brattleby were higher in 2010 than in 2012 and zero fluxes were measured throughout 2011. The seasonal trend in δ-3-carene fluxes is somewhat obscured by the high values measured in 2010. Fluxes measured in 2010 were an order of magnitude higher than those measured in 2012, with large

associated uncertainties. Smaller fluxes of δ-3-carene were measured at Arnot but none were detected in East Grange.

Fluxes of all BVOCs (isoprene, α-pinene, β-pinene, limonene and δ-3-carene) were found to vary significantly with season but not site. The majority of BVOCs were positively significantly correlated with air temperature, inside the chamber or outside ambient air temperature. Some significant correlations were also found between BVOC fluxes and PAR and with soil temperature and soil moisture.

4.6 Discussion

This study presents the first measurements of CH_3X fluxes from willow trees using branch enclosure methods. Net emission fluxes measured from vegetation were found to be similar to those measured from soils. Converting fluxes in $\mathrm{ng\,g^{-1}\,h^{-1}}$ to $\mathrm{ng\,m^{-2}\,h^{-1}}$ using a foliar density of 150 g $\mathrm{m^{-2}}$ (Karl et al., 2009), net CH_3Br ranged from 84 $\mathrm{ng\,m^{-2}\,h^{-1}}$ at Brattleby to 248 $\mathrm{ng\,m^{-2}\,h^{-1}}$ at the Arnot fieldsite. These results are comparable to the values of between 57 and 140 $\mathrm{ng\,m^{-2}\,h^{-1}}$ measured from conifer plantation forest floor sites (Dimmer et al., 2001), temperate woodland soils (Drewer et al., 2008) and temperate forest soils (Varner et al., 2003).

Net CH_3Cl fluxes varied between 735 $\mathrm{ng\,m^{-2}\,h^{-1}}$ at Brattleby to 1790 $\mathrm{ng\,m^{-2}\,h^{-1}}$ at the Arnot fieldsite. Again these measurements are in agreement with previous net CH_3Cl fluxes of between 50 and 3900 $\mathrm{ng\,m^{-2}\,h^{-1}}$ measured from conifer plantation forest floor sites (Dimmer et al., 2001) and boreal forest soils (Rhew et al., 2003b).

This work also confirms the field measurements which indicate that willow trees are an important source of isoprene. Net fluxes of isoprene of between 1 and 77$\mathrm{\mu g\,g^{-1}\,h^{-1}}$ were measured, which are similar to previously measured net fluxes of between 12 and 115$\mathrm{\mu g\,g^{-1}\,h^{-1}}$(Copeland et al., 2012; Evans et al., 1982; Hakola et al., 1998; Isebrands et al., 1999; Karl et al., 2009; Niinemets et al., 2010; Olofsson et al., 2005; Owen and Hewitt, 2000; Owen et al., 2003; Pio et al., 1993; Miller et al., 1983; Zimmerman, 1979). Expressing the isoprene flux on a per area basis, a range between 111 to 11600 $\mathrm{ng\,m^{-2}\,h^{-1}}$ was measured.

Unlike CH_3X fluxes, fluxes of isoprene, α-pinene, β-pinene and δ-3-carene from Brattleby willow were highest from the older plants. Limonene fluxes were the exception, with higher fluxes measured from younger plants. This inter-annual variation in fluxes may be due to changes in climate between years, as limonene fluxes were found to be correlated to different environmental variables than the other BVOC fluxes, as discussed in Section 4.2.8. The differences in fluxes between years might also be due to the age of the SRC willow plants. The rate of BVOC emissions has previously been shown to vary with plant age (Street et al., 1997). Studies on *Pinus* and *Camellia* species have also observed variation in the composition of BVOC

emissions with plant age with younger plants emitting a wider range of monoterpenes (Kim et al., 2005; Nunes and Pio, 2001). However, another study of coniferous plants of different ages found no variation in BVOC composition with age (Lim et al., 2008).

Fluxes of α-pinene measured fit with the range of monoterpene fluxes described by previous measurements. Net α-pinene fluxes of between 1.2 and 7.3 $\mu g\, g^{-1}\, h^{-1}$ were measured at Arnot and East Grange, respectively, in agreement with the range of monoterpene fluxes of between 2.8 and 10 $\mu g\, g^{-1}\, h^{-1}$ measured by Hakola et al. (1998, 1999). The 46 $\mu g\, g^{-1}\, h^{-1}$ net α-pinene flux measured at the Brattleby fieldsite was slightly higher than previous measurements, possibly due to differences in the age of vegetation during measurements. The trees measured in the study by Hakola et al. (1998) were young and around 1 to 1.5 m in height. The largest fluxes of α-pinene measured in Brattleby were measured in 2010 when the trees were older and reached up to at least 3 m in height. Fluxes of β-pinene, limonene and δ-3-carene all fell within the 2.8 to 10 $\mu g\, g^{-1}\, h^{-1}$ monoterpene fluxes previously described (Hakola et al., 1998, 1999)) although some net fluxes were below this range. Expressing the BVOC fluxes on a per area basis, the range of fluxes measured were: α-pinene 170 to 6800 $ng\, m^{-2}\, h^{-1}$, β-pinene to 825 $ng\, m^{-2}\, h^{-1}$, limonene 400 $ng\, m^{-2}\, h^{-1}$ and δ-3-carene to 80 to 1700 $ng\, m^{-2}\, h^{-1}$.

Measurements made at three fieldsites across the UK allow comparison of fluxes under different soil and climate conditions. CH_3X fluxes were highest at the Arnot fieldsite and BVOC fluxes highest at the Brattleby fieldsite. Higher fluxes of CH_3X at Arnot may be due to the greater amount of rainfall that the soil receives, an average of 73 mm day^{-1} over the measurement period compared to an average of 50 mm day^{-1} at the Brattleby site.

Higher BVOC fluxes at Brattleby are likely to be due to differences in climate, namely higher temperatures and more hours of sunshine than at the two sites in Scotland. An average of 128 hours of sunshine per month were recorded at Brattleby compared to 114 at Arnot. The maximum air temperature in Brattleby was over 1 °C higher than in Arnot, 14.6 °C compared to 13.2 °C. Statistical analyses show that there are strong correlations between the environmental variables measured and the BVOC fluxes.

Chapter 5

Annual arable crops

5.1 Introduction

Fields of wheat (*Triticum aestivum*) and yellow flowering oilseed rape (*Brassica napus*) are a common sight across the UK. A record area of 0.7 Mha of oilseed rape was planted in the UK in 2011 due to increased demand for use in biofuel, with the overall annual average price around 50% higher than in 2010 (DEFRA, 2012). Better cereal prices also led to an increase in the total area of wheat crops planted in the UK from 1.94 Mha in 2010 to 1.97 Mha in 2011. The contribution of these crops to the CH_3X and BVOC budgets is therefore important to consider.

A study by Itoh et al. (2009) found that halide ion methyltransferase (HMT) activity, involved in the formation of methyl halides, is present in several families of higher plants including Poaceae, which includes wheat, and Brassicaceae, which includes oilseed rape. However, no emissions of CH_3Br or CH_3Cl from wheat were observed in vivo or in vitro due to the low levels of HMT activity in wheat (210 U $g^{-1}_{fresh\,tissue}$, where one unit (U) of enzyme activity was defined as the amount of the enzyme that catalyzed the formation of 1 pmol of CH_3X in one minute at 30 °C). The high activity of HMT activity in oilseed rape (2600 U $g^{-1}_{fresh\,tissue}$) suggested that this species may emit CH_3X in significant quantities.

The formation of methyl halides from higher plants was studied in a survey of 118 different species, with the highest activities found in the Brassicaceae family (Saini et al., 1995). Production rates of 33 nmol day^{-1} g^{-1} fresh weight and 0.51 nmol day^{-1} g^{-1} fresh weight for CH_3Br and CH_3Cl respectively were measured from leaf disks of wild cabbage (*Brassica oleracea*, a member of the Brassicaceae family). In anther study on *B.oleracea*, an indication of the rate of production of CH_3Br and CH_3Cl was given by the activity of HMT with Br^- (7 x 10^{-2} nanokatals mg^{-1} mM^{-1}) and Cl^- (4.6 x 10^{-2} nanokatals mg^{-1} mM^{-1}) (1 katal = amount of enzyme which catalyzes the conversion of one mole of substrate(s) under assay conditions) (Attieh et al., 1995).

A later study by Gan et al. (1998) investigated CH_3Br fluxes from oilseed rape and estimated an annual CH_3Br flux of 6.6 $\pm$ 1.8 Gg y^{-1}. Although CH_3Cl fluxes were not measured in the

study, it was suggested that due to the same reaction pathway being utilised for both CH_3Br and CH_3Cl production and the presence of Cl^- in the soil, oilseed rape could also prove to be a significant source of CH_3Cl.

Formation of BVOCs by these annual arable crops has also been studied previously. Dynamic plant enclosures were used by König et al. (1995) to investigate fluxes of BVOCs from agricultural plant species during and after blossoming. Total plant emission fluxes of 201.5, 320.5 and 10.9 ng g^{-1} h^{-1} were assigned for non-blossoming oilseed rape, blossoming oilseed rape and wheat, respectively, using GC-MS-FID analysis. From these measurements, an emission rate of 0.01 μg g^{-1} h^{-1} was calculated for wheat, similar to the rate of 0.041 μg g^{-1} h^{-1} calculated by Lamb et al. (1993) but lower than the rate of 0.1 μg g^{-1} h^{-1} calculated by Winer et al. (1992). Differences in these calculated emission rate may be due to differences in growth stage and weather events such as rainfall occurring during the measurements.

In agreement with a previous study by Winer et al. (1992), König et al. (1995) did not detect any fluxes of isoprene or sesquiterpenes from either oilseed rape or wheat. Monoterpenes were emitted at a rate of 37 and 34 ng g^{-1} h^{-1} from non-blossoming and blossoming oilseed rape respectively but no emissions were detected from wheat. Oxygenated BVOCs accounted for around 65% of total emissions from oilseed rape and 100% for wheat.

The major components of the oxygenated BVOC emissions from wheat were identified as cis-3-hexenylacetate and 3-hexen-l-ol (Buttery et al., 1985). Cis-3-hexenylacetate was also the main oxygenated BVOC emitted by oilseed rape. König et al. (1995) also looked at the effects of blossoming on emission rates of BVOCs from oilseed rape. It was found that emissions of individual compounds such as β-pinene and cis-3-hexenylacetate were 4 to 5 times higher in the blossoming oilseed rape than in the sample after blossoming. During blossoming, esters were the most abundant compounds emitted whereas after blossoming emissions of alcohols were more dominant.

There have been several studies into CH_3X and BVOC fluxes from annual arable crops such as wheat and oilseed rape in the USA (Buttery et al., 1985; Gan et al., 1998; Winer et al., 1992), Canada (Attieh et al., 1995; Saini et al., 1995) and a study conducted in Austria (König et al., 1995). This is the first study to measure emissions of these species from plantations in the UK. Wheat is not considered to be a significant emitter of CH_3X but oilseed rape is known to emit high amounts of CH_3Br and is also believed to emit CH_3Cl in significant quantities. No significant emissions of isoprene, monoterpenes or sesquiterpenes have previously been measured from wheat, although they are known to be emitters of oxygenated BVOCs. Oxygenated BVOCs are also the major emission species from oilseed rape, with different compounds found to dominate during and after blossoming.

Objectives of the work described in this chapter:

- Characterisation of CH_3X and BVOC fluxes from the annual arable crops wheat and oilseed rape in the East Midlands, England
- Quantification of seasonal, diurnal and temporal variations in CH_3X and BVOC fluxes within both annual arable crops
- Identification of possible drivers of CH_3X and BVOC fluxes from both annual arable crops

5.2 Description of annual arable crop site and sampling points

Measurements were conducted at the Brattleby fieldsite in Lincolnshire, as described in Section 2.7.1. A total of ten sampling sites were used within the annual arable crop field, as shown in Figure 5.1. The annual arable field was planted with wheat between May and August 2010 and April to June 2012 and with oilseed rape from November 2010 to July 2011. Sampling sites were chosen across one side of the field and incorporated plants within and at the edge of the field. The sites were chosen in order to limit damage to crops caused by walking over the field as it is a commercially farmed field as well as for ease of access with bulky equipment.

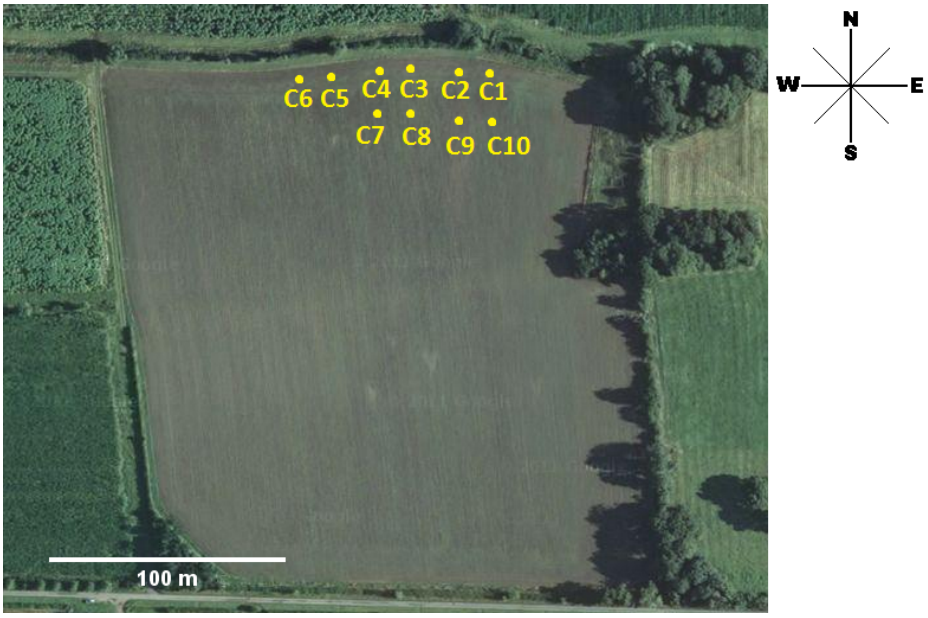


Figure 5.1: Location of the sampling points within the annual arable crop field at Brattleby.

5.3 Outline of CH_3X and BVOC flux measurements in wheat

CH_3X and BVOC flux measurements were carried out as described in Sections 2.2.1 and 2.3.1. These totalled 35 measurements of CH_3X fluxes from the wheat crop between May and August 2010 and between April and June 2012. 29 measurements of BVOC fluxes were made in total encompassing measurements made in May 2010 and between May and August 2012. The results of the CH_3X flux measurements are presented first followed by the results of the BVOC measurements.

Seasonal and temporal trends in BVOC fluxes from wheat are examined using time series of α-pinene and limonene fluxes plotted together with the concurrent PAR, ambient and chamber air temperature, soil temperature and soil water content observations for each individual sampling site.

Statistical analysis was carried out to determine whether BVOC fluxes had significant spatial and temporal variation. Correlations between BVOC fluxes and monitored environmental parameters were tested for significance in order to determine possible drivers of emissions.

5.3.1 CH_3X flux trends in wheat

Of the 35 CH_3Br measurements made in the wheat crop in May, July and August 2010 and April, May and June 2012, only two non-zero fluxes were recorded. In July 2010 an emission of 1.13 ng g^{-1} h^{-1} was measured in site 2 and an emission of 2.79 ng g^{-1} h^{-1} was measured in site 10 in July 2012. No CH_3Cl fluxes were detected. No seasonal, temporal or diurnal trends could be distinguished from these low emissions.

5.3.2 BVOC flux trends in wheat

Of the 29 measurements made in wheat in May 2010 and in May, June and August 2012, only two non-zero isoprene fluxes of 5.83 and 5.99 µg g^{-1} h^{-1} were measured in 2010 from sites 1 and 3 respectively. No other significant fluxes were detected. These results are in agreement with previous measurements of BVOC fluxes from wheat which did not find any significant isoprene fluxes (König et al., 1995; Winer et al., 1992).

Despite previous studies suggesting that wheat does not emit monoterpenes (König et al., 1995), small fluxes of various monoterpenes were measured during this study. These included α-pinene, limonene, β-pinene and δ-3-carene.

α-pinene

The α-pinene fluxes from all sites combined in 2010 in 2012 and the mean of those values on each sampling occasion are illustrated in Figure 5.2. In May 2010, fluxes of between 164 and 422 $\mu g\, g^{-1}\, h^{-1}$ were recorded with large associated uncertainties. Fluxes measured in 2012 were generally lower with the highest emissions occurring in May (peak emission flux of 157 $\mu g\, g^{-1}\, h^{-1}$), low to zero emission fluxes in June, and emission fluxes of between 10 and 27 $\mu g\, g^{-1}\, h^{-1}$ in August.

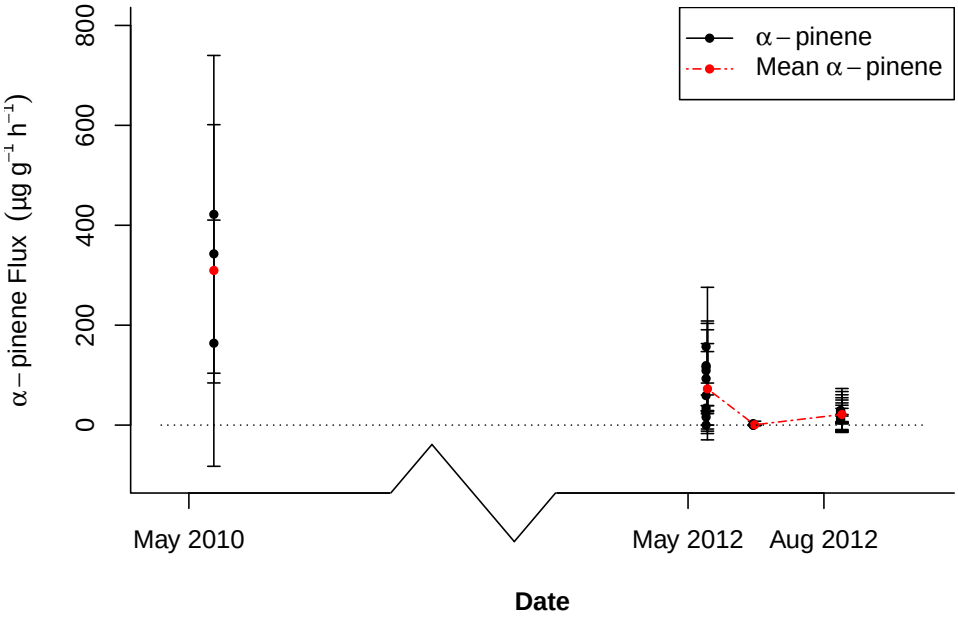


Figure 5.2: α-pinene fluxes from wheat at all ten sampling points and the mean of those values on each sampling occasion between 2010 and 2012. Error bars on fluxes incorporate analytical and sampling uncertainties (as described in Section 2.6.1).

Time series of α-pinene fluxes from each individual site in May 2010 and between May and August 2012 together with the concurrent PAR, ambient and chamber air temperature, soil temperature and soil water content observations are illustrated in Figures 5.3 to 5.7. These figures show both the seasonal trend in fluxes from individual sampling sites and the variation in fluxes between calendar years.

Lower α-pinene fluxes were measured at sites 4, 6, 8 and 10 (mean fluxes between and 16.7 and 31.4 $\mu g\, g^{-1}\, h^{-1}$) and higher fluxes were recorded at sites 1-3, 5, 7 and 9 (mean fluxes between 43.0 and 115 $\mu g\, g^{-1}\, h^{-1}$) (Table 5.1). Maximum emission fluxes varied between 17.7

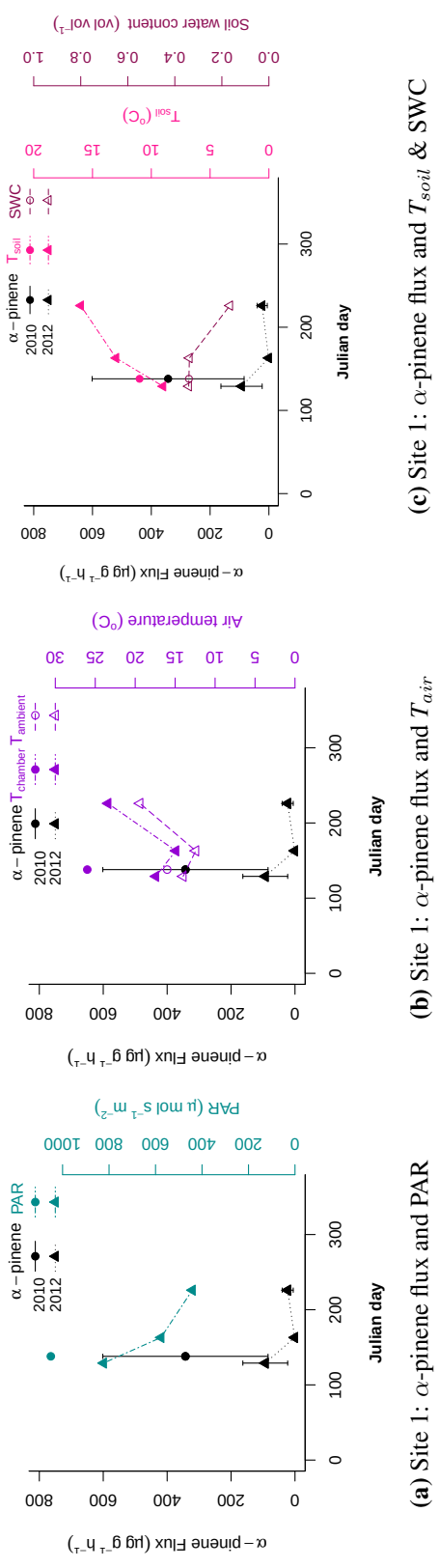
and 58.8 $\mu g\, g^{-1}\, h^{-1}$ for lower emitting sites and 109 to 422 $\mu g\, g^{-1}\, h^{-1}$ for higher emitting sites.

There is no discernible reason for differences in mean fluxes from different sites as plant growth stage and soil and climate conditions were almost identical at all sites. However, sites 1 to 3 are likely to have a bias towards higher values as high fluxes were measured from these sites in 2010 but no measurements were taken at other sites during 2010 due to instrument problems. The highest maximum emission of 422 $\mu g\, g^{-1}\, h^{-1}$ was measured at site 2 in 2010. Minimum emissions recorded were between zero and 29.3 $\mu g\, g^{-1}\, h^{-1}$. A mean emission of 64.5 $\mu g\, g^{-1}\, h^{-1}$ was calculated from fluxes measured at all sites during the measurement period.

Table 5.1: Mean, median, minimum and maximum net α-pinene fluxes from wheat for 2010 and 2012 combined. All flux values are in $\mu g\, g^{-1}\, h^{-1}$. The final column gives the number of measurements made. The last row summarises all fluxes from all sites.

Site	Mean	Median	Min	Max	Number
WHE1	115	57.8	0.67	343	4
WHE2	112	13.4	0.00	422	4
WHE3	77.1	72.3	0.00	164	4
WHE4	26.9	21.9	0.00	58.8	3
WHE5	43.0	10.3	0.00	119	3
WHE6	17.2	24.1	3.12	24.2	3
WHE7	84.7	84.7	12.1	157	2
WHE8	31.4	31.4	29.3	33.6	2
WHE9	63.9	63.9	19.1	109	2
WHE10	16.7	16.7	15.6	17.7	2
All	64.5	24.1	0.00	422	29

The low α-pinene fluxes in June 2012 coincided with lower air temperature observations (15 °C) at the field site during measurements. During the high emissions in August, the air temperature was around 10 °C higher than in June at just under 25 °C. It was difficult to distinguish any relationships between α-pinene fluxes and the observed PAR levels and soil parameters. The statistical significance of correlations between α-pinene fluxes and environmental variables is described in Section 5.3.3.



(a) Site 1: α-pinene flux and PAR

(b) Site 1: α-pinene flux and T_{air}

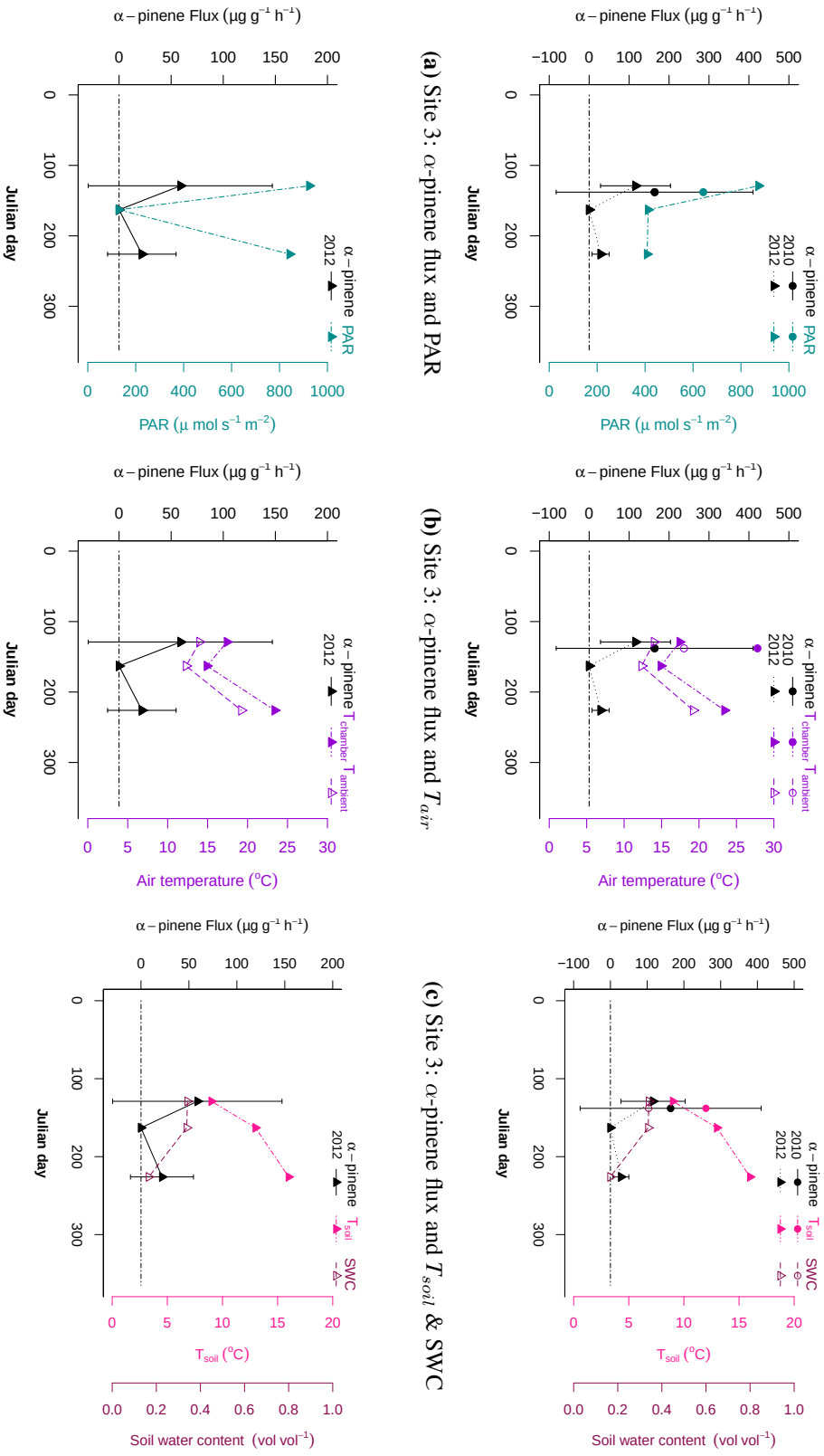
(c) Site 1: α-pinene flux and T_{soil} & SWC

(d) Site 2: α-pinene flux and PAR

(e) Site 2: α-pinene flux and T_{air}

(f) Site 2: α-pinene flux and T_{soil} & SWC

Figure 5.3: Comparison of net α-pinene fluxes from wheat with PAR, chamber and ambient air temperature, soil temperature and soil water content for 2010 and 2012 for sites 1 and 2. Note different y-axis scales for α-pinene. Error bars on fluxes incorporate analytical and sampling uncertainties.



(a) Site 3: α-pinene flux and PAR

(b) Site 3: α-pinene flux and T_{air}

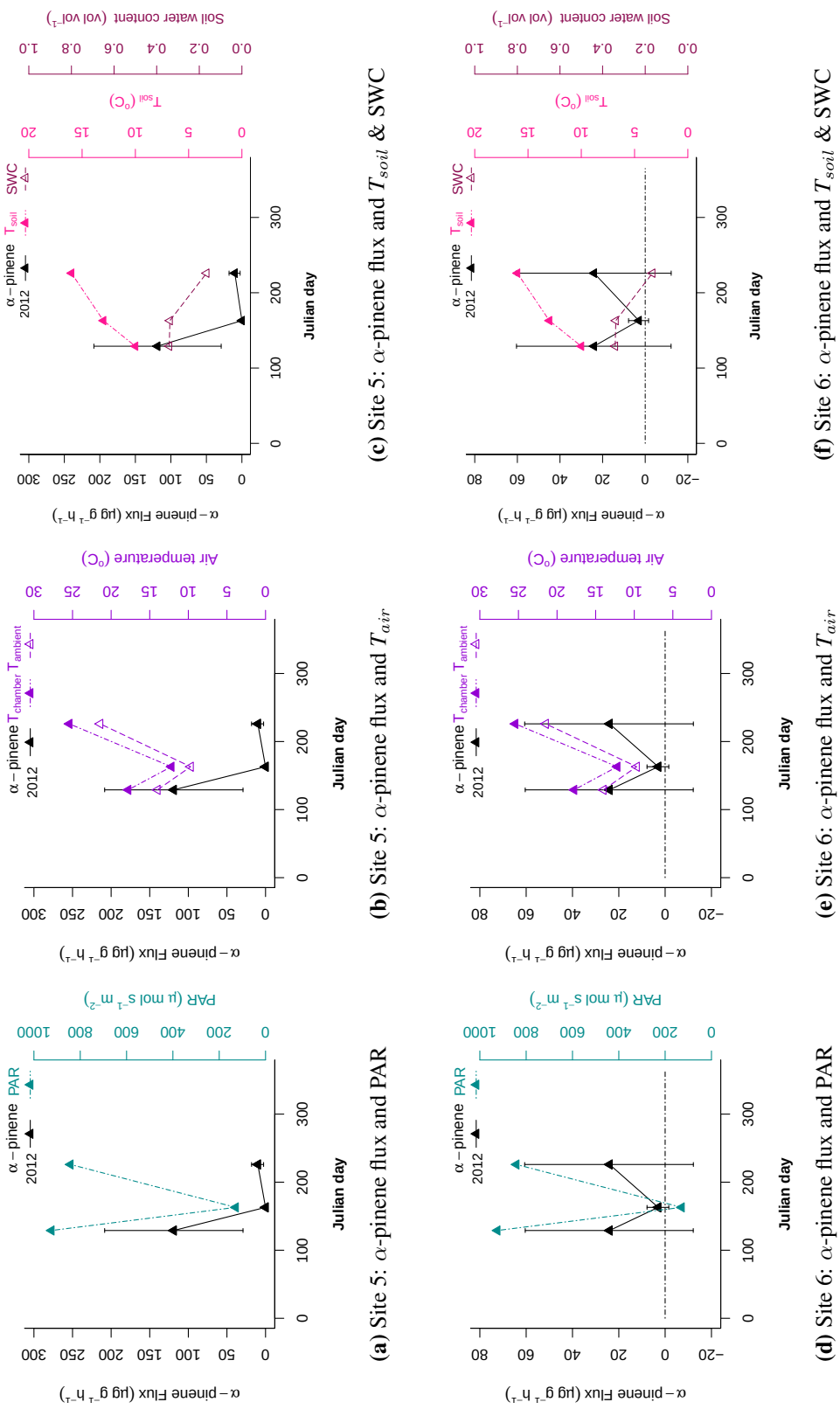
(c) Site 3: α-pinene flux and T_{soil} & SWC

(d) Site 4: α-pinene flux and PAR

(e) Site 4: α-pinene flux and T_{air}

(f) Site 4: α-pinene flux and T_{soil} & SWC

Figure 5.4: Comparison of net α-pinene fluxes from wheat with PAR, chamber and ambient air temperature, soil temperature and soil water content for 2010 and 2012 for sites 3 and 4. Note different y-axis scales for α-pinene. Error bars on fluxes incorporate analytical and sampling uncertainties. Colour-coded dashed lines denote zero on appropriate y-axis.



(a) Site 5: α-pinene flux and PAR

(b) Site 5: α-pinene flux and T_{air}

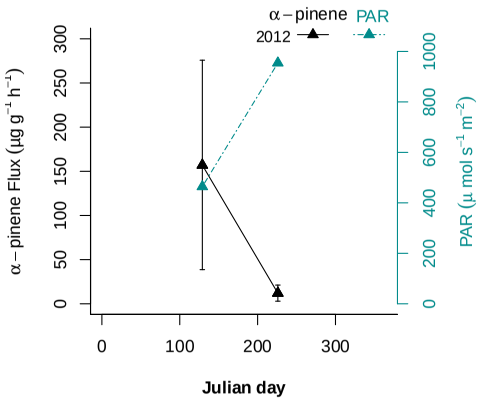
(c) Site 5: α-pinene flux and T_{soil} & SWC

(d) Site 6: α-pinene flux and PAR

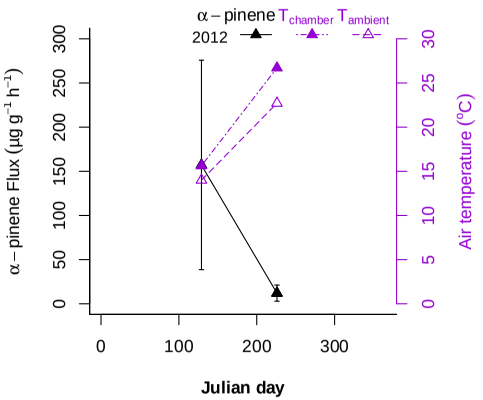
(e) Site 6: α-pinene flux and T_{air}

(f) Site 6: α-pinene flux and T_{soil} & SWC

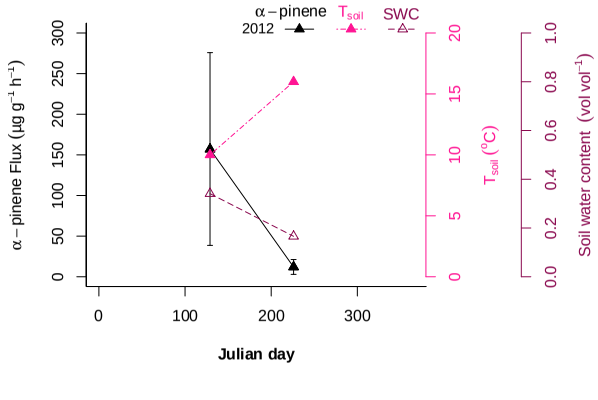
Figure 5.5: Comparison of net α-pinene fluxes from wheat with PAR, chamber and ambient air temperature, soil temperature and soil water content for 2010 and 2012 for sites 5 and 6. Note different y-axis scales for α-pinene. Error bars on fluxes incorporate analytical and sampling uncertainties. Colour-coded dashed lines denote zero on appropriate y-axis.



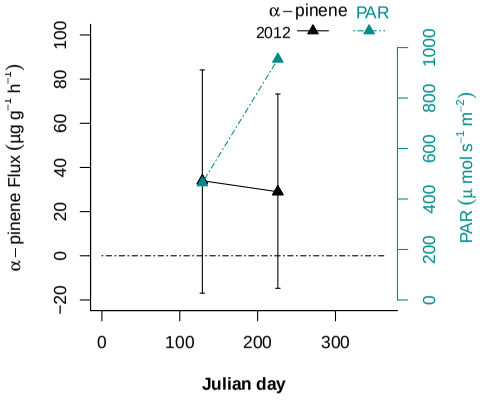
(a) Site 7: α-pinene flux and PAR



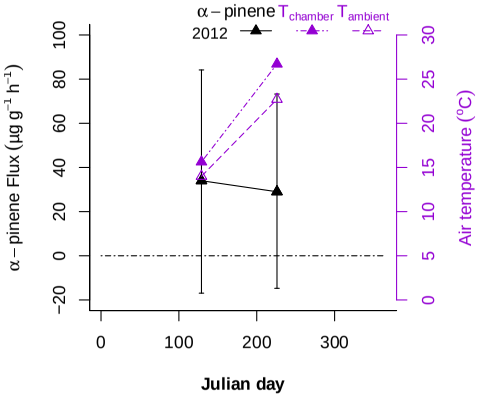
(b) Site 7: α-pinene flux and T_{air}



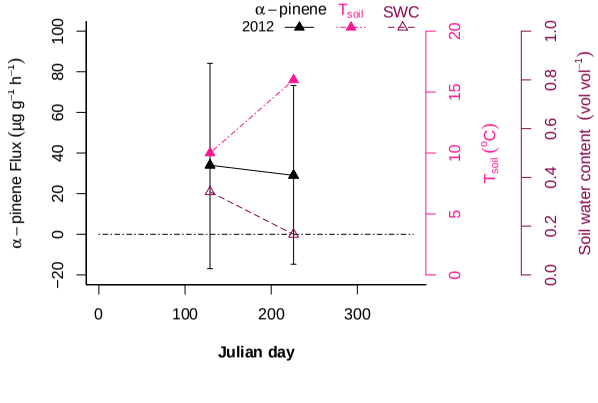
(c) Site 7: α-pinene flux and T_{soil} & SWC



(d) Site 8: α-pinene flux and PAR

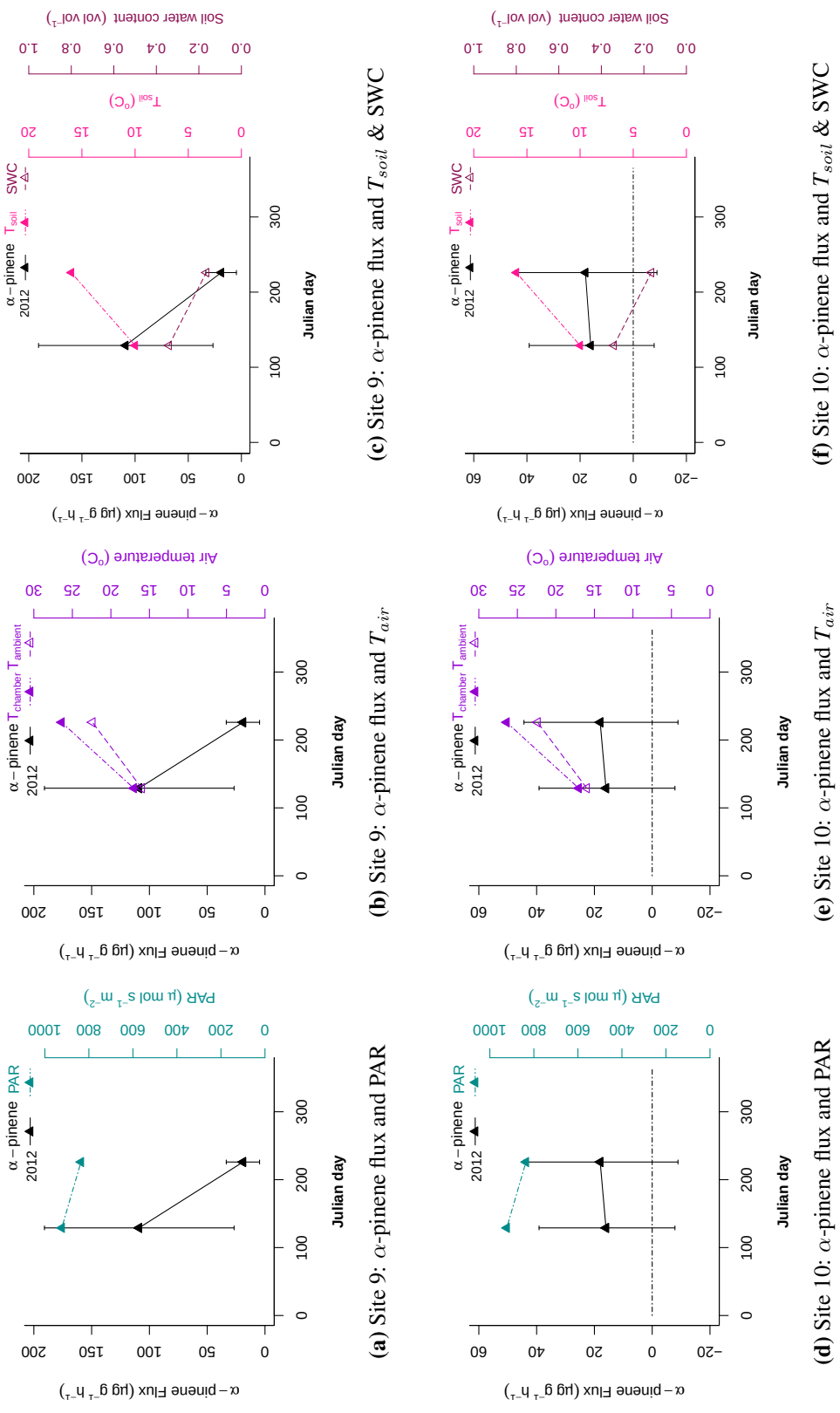


(e) Site 8: α-pinene flux and T_{air}



(f) Site 8: α-pinene flux and T_{soil} & SWC

Figure 5.6: Comparison of net α-pinene fluxes from wheat with PAR, chamber and ambient air temperature, soil temperature and soil water content for 2010 and 2012 for sites 7 and 8. Note different y-axis scales for α-pinene. Error bars on fluxes incorporate analytical and sampling uncertainties. Colour-coded dashed lines denote zero on appropriate y-axis.



(a) Site 9: α-pinene flux and PAR

(b) Site 9: α-pinene flux and T_{air}

(c) Site 9: α-pinene flux and T_{soil} & SWC

(d) Site 10: α-pinene flux and PAR

(e) Site 10: α-pinene flux and T_{air}

(f) Site 10: α-pinene flux and T_{soil} & SWC

Figure 5.7: Comparison of net α-pinene fluxes from wheat with PAR, chamber and ambient air temperature, soil temperature and soil water content for 2010 and 2012 for sites 9 and 10. Note different y-axis scales for α-pinene. Error bars on fluxes incorporate analytical and sampling uncertainties. Colour-coded dashed lines denote zero on appropriate y-axis.

Limonene

The limonene fluxes from all sites combined in 2010 and 2012 and the mean of the fluxes on each sampling occasion are illustrated in Figure 5.8. In May 2010, limonene fluxes of between 6.2 and 16.8 $\mu g\, g^{-1}\, h^{-1}$ were measured. Fluxes measured in May 2012 were all zero with the exception of site 9 where a flux of 10.8 $\mu g\, g^{-1}\, h^{-1}$ was measured. Fluxes of between 0 and 4.29 $\mu g\, g^{-1}\, h^{-1}$ were measured in June. Much higher fluxes were measured in August however, with emissions of between 47.6 and 104 $\mu g\, g^{-1}\, h^{-1}$ measured.

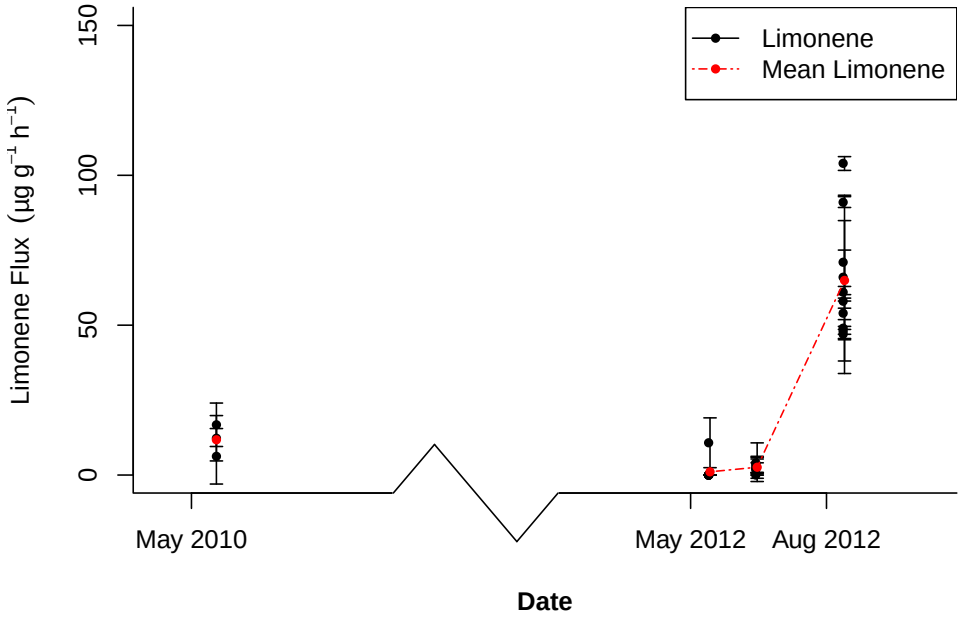


Figure 5.8: Limonene fluxes in wheat at all ten sampling points and the mean of those values on each sampling occasion between 2010 and 2012. Error bars on fluxes incorporate analytical and sampling uncertainties (as described in Section 2.6.1).

Time series of limonene fluxes from each individual site in May 2010 and between May and August 2012 together with the concurrent PAR, ambient and chamber air temperature, soil temperature and soil water content observations are illustrated in Figures 5.9 to 5.13. These figures show both the seasonal trend in fluxes and the variation in fluxes between calendar years.

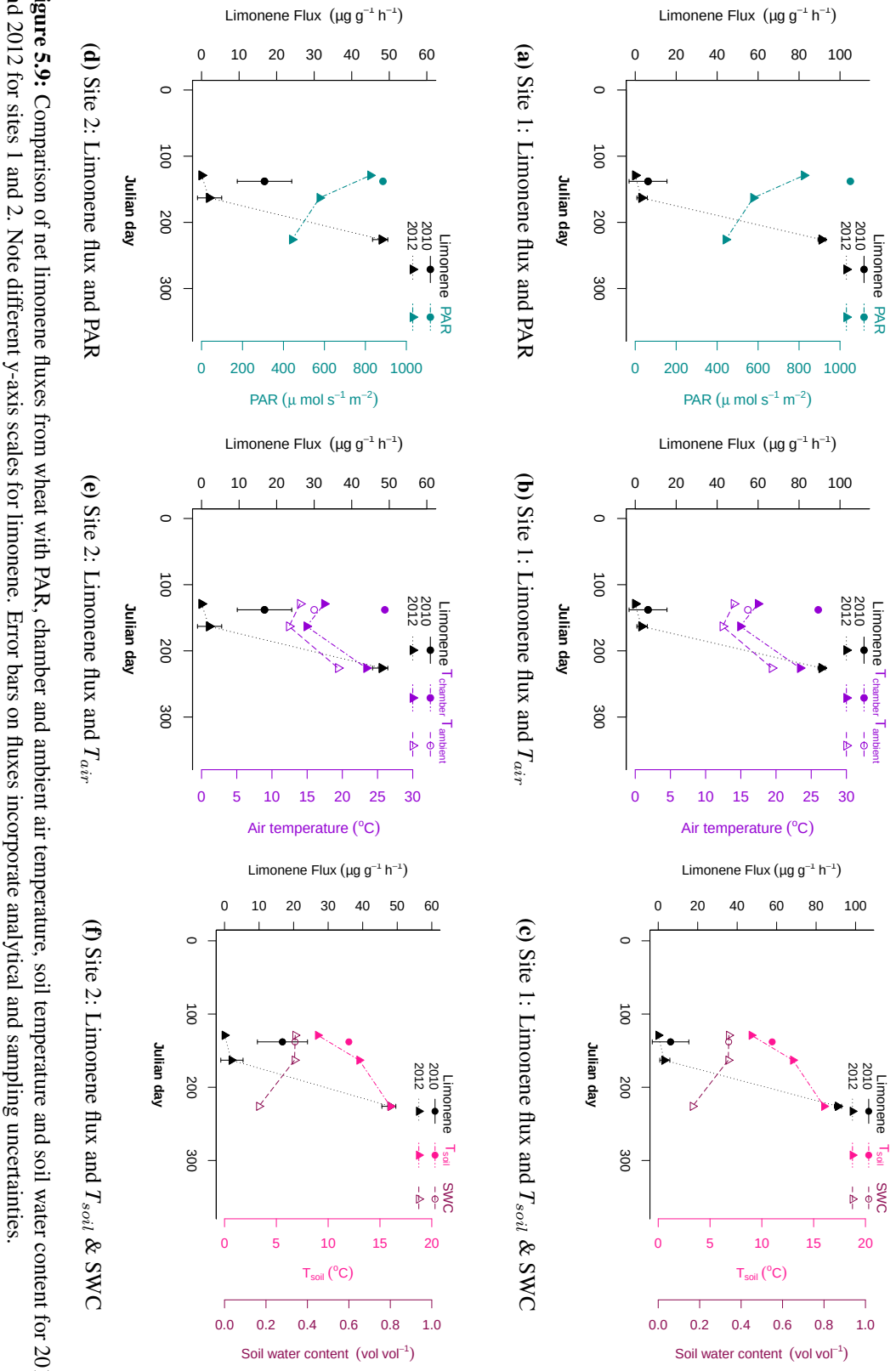
Slightly lower limonene fluxes were measured at sites 2 and 4-7 (mean fluxes between 16.5 and 23.4 $\mu g\, g^{-1}\, h^{-1}$) and higher fluxes were recorded at sites 1, 3 and 8-10 (mean fluxes between 25.2 and 41.1 $\mu g\, g^{-1}\, h^{-1}$) (Table 5.2). Maximum fluxes varied between 47.6 and 57.9 $\mu g\, g^{-1}\, h^{-1}$at lower emitting sites and between 54.5 and 104 $\mu g\, g^{-1}\, h^{-1}$at higher emitting

sites. The highest maximum emission flux of 104 $\mu g\, g^{-1}\, h^{-1}$ was measured at site 3 in 2012. Minimum emission fluxes recorded were between zero and 10.8 $\mu g\, g^{-1}\, h^{-1}$. A mean emission flux of 24.5 $\mu g\, g^{-1}\, h^{-1}$ was calculated from fluxes measured at all sites during the measurement period.

Table 5.2: Mean, median, minimum and maximum net limonene fluxes from wheat for 2010 and 2012 combined. All flux values are in $\mu g\, g^{-1}\, h^{-1}$. The final column gives the number of measurements made. The last row summarises all fluxes from all sites.

Site	Mean	Median	Min	Max	Number
WHE1	25.2	4.80	0.00	91.1	4
WHE2	16.6	9.46	0.00	47.6	4
WHE3	29.9	7.92	0.00	104	4
WHE4	16.5	0.00	0.00	49.4	3
WHE5	21.1	2.32	0.00	61.0	3
WHE6	20.7	4.29	0.00	57.9	3
WHE7	23.4	23.4	0.00	46.9	2
WHE8	32.9	32.9	0.00	65.7	2
WHE9	41.1	41.1	10.8	71.5	2
WHE10	27.2	27.2	0.00	54.5	2
All	24.5	4.29	0.00	104	29

Similarly to the lower α-pinene fluxes, the lower limonene fluxes measured in June 2012 coincided with lower air temperature observations of around 15 °C in comparison to air temperatures of just under 25 °C observed during measurements of high emission fluxes in August. There were no obvious relationships between measured PAR levels and limonene fluxes. However, higher soil temperatures and lower soil water contents appeared to be linked with higher limonene fluxes. The statistical significance of correlations between limonene fluxes and environmental variables is described in Section 5.3.3.



(a) Site 1: Limonene flux and PAR

(b) Site 1: Limonene flux and T_{air}

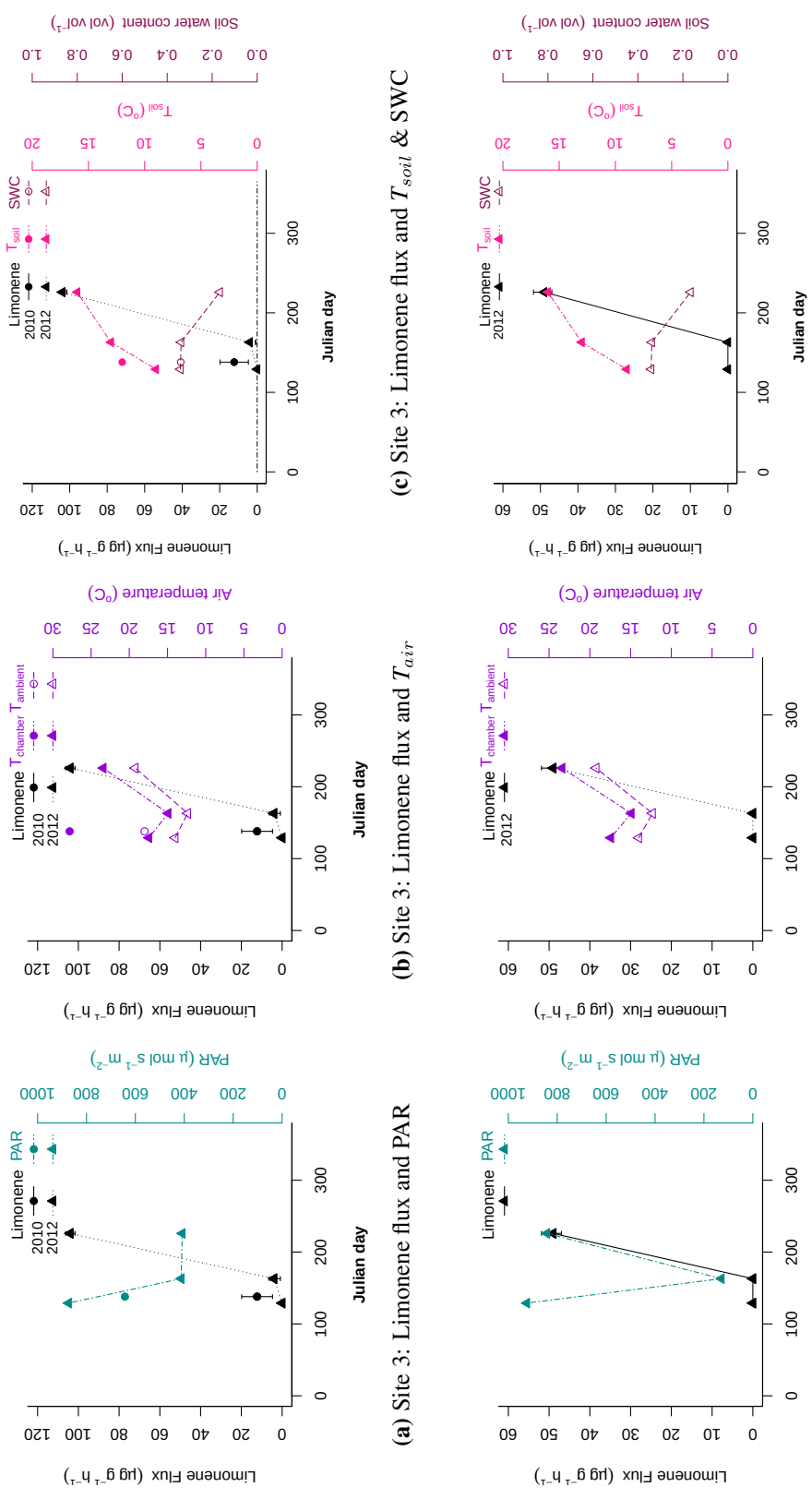
(c) Site 1: Limonene flux and T_{soil} & SWC

(d) Site 2: Limonene flux and PAR

(e) Site 2: Limonene flux and T_{air}

(f) Site 2: Limonene flux and T_{soil} & SWC

Figure 5.9: Comparison of net limonene fluxes from wheat with PAR, chamber and ambient air temperature, soil temperature and soil water content for 2010 and 2012 for sites 1 and 2. Note different y-axis scales for limonene. Error bars on fluxes incorporate analytical and sampling uncertainties.



(a) Site 3: Limonene flux and PAR

(b) Site 3: Limonene flux and T_{air}

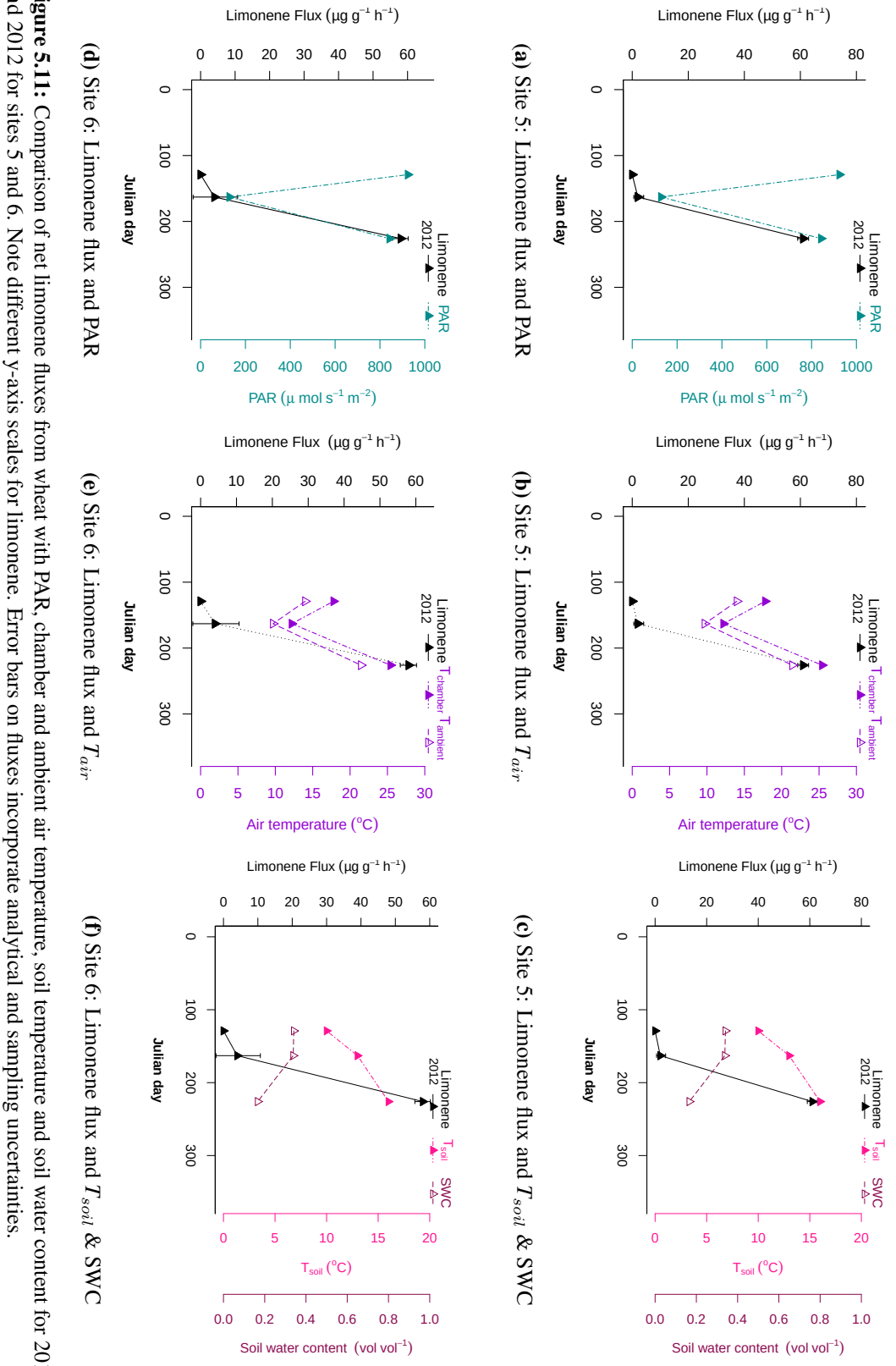
(c) Site 3: Limonene flux and T_{soil} & SWC

(d) Site 4: Limonene flux and PAR

(e) Site 4: Limonene flux and T_{air}

(f) Site 4: Limonene flux and T_{soil} & SWC

Figure 5.10: Comparison of net limonene fluxes from wheat with PAR, chamber and ambient air temperature, soil temperature and soil water content for 2010 and 2012 for sites 3 and 4. Note different y-axis scales for limonene. Error bars on fluxes incorporate analytical and sampling uncertainties.



(a) Site 5: Limonene flux and PAR

(b) Site 5: Limonene flux and T_{air}

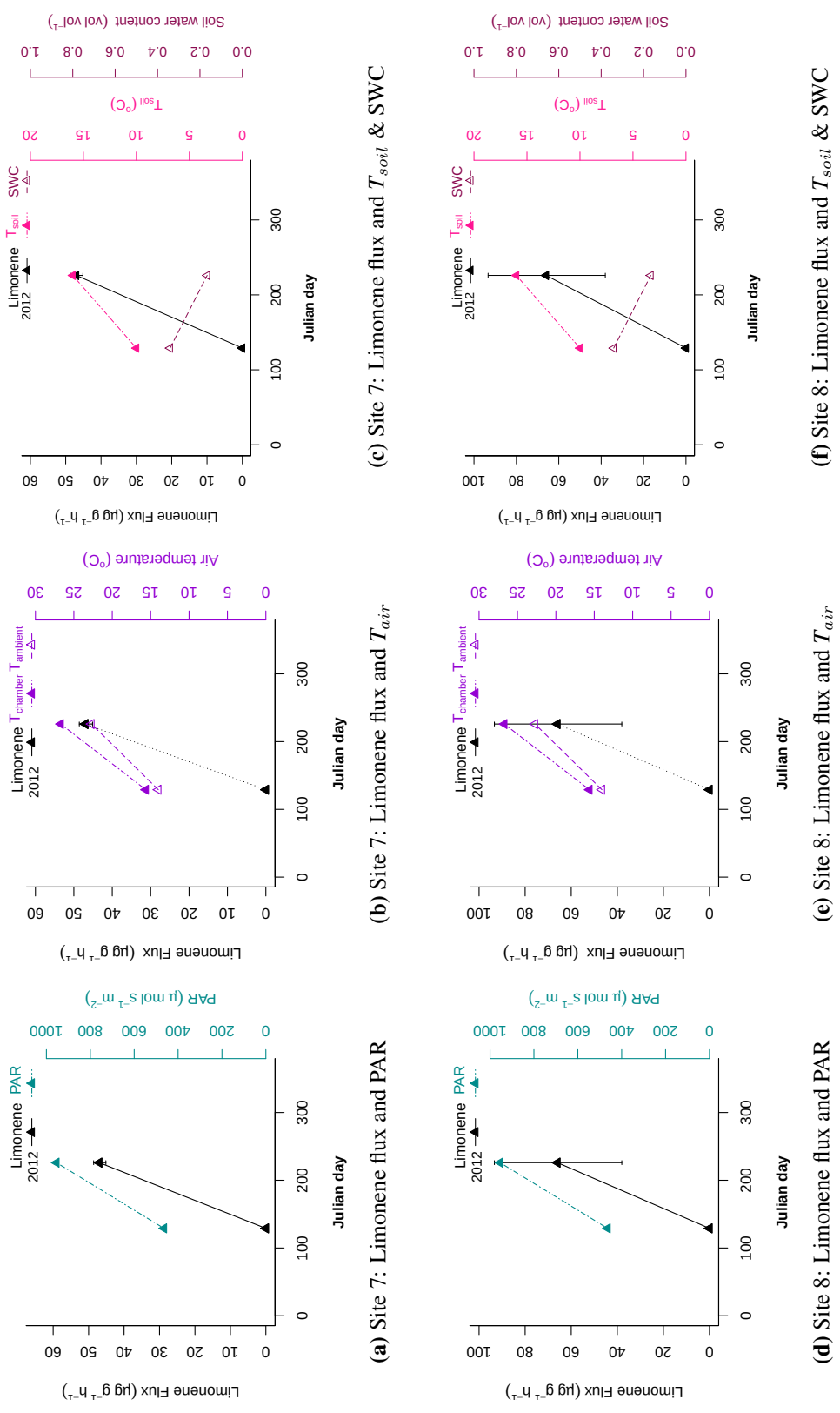
(c) Site 5: Limonene flux and T_{soil} & SWC

(d) Site 6: Limonene flux and PAR

(e) Site 6: Limonene flux and T_{air}

(f) Site 6: Limonene flux and T_{soil} & SWC

Figure 5.11: Comparison of net limonene fluxes from wheat with PAR, chamber and ambient air temperature, soil temperature and soil water content for 2010 and 2012 for sites 5 and 6. Note different y-axis scales for limonene. Error bars on fluxes incorporate analytical and sampling uncertainties.



(a) Site 7: Limonene flux and PAR

(b) Site 7: Limonene flux and T_{air}

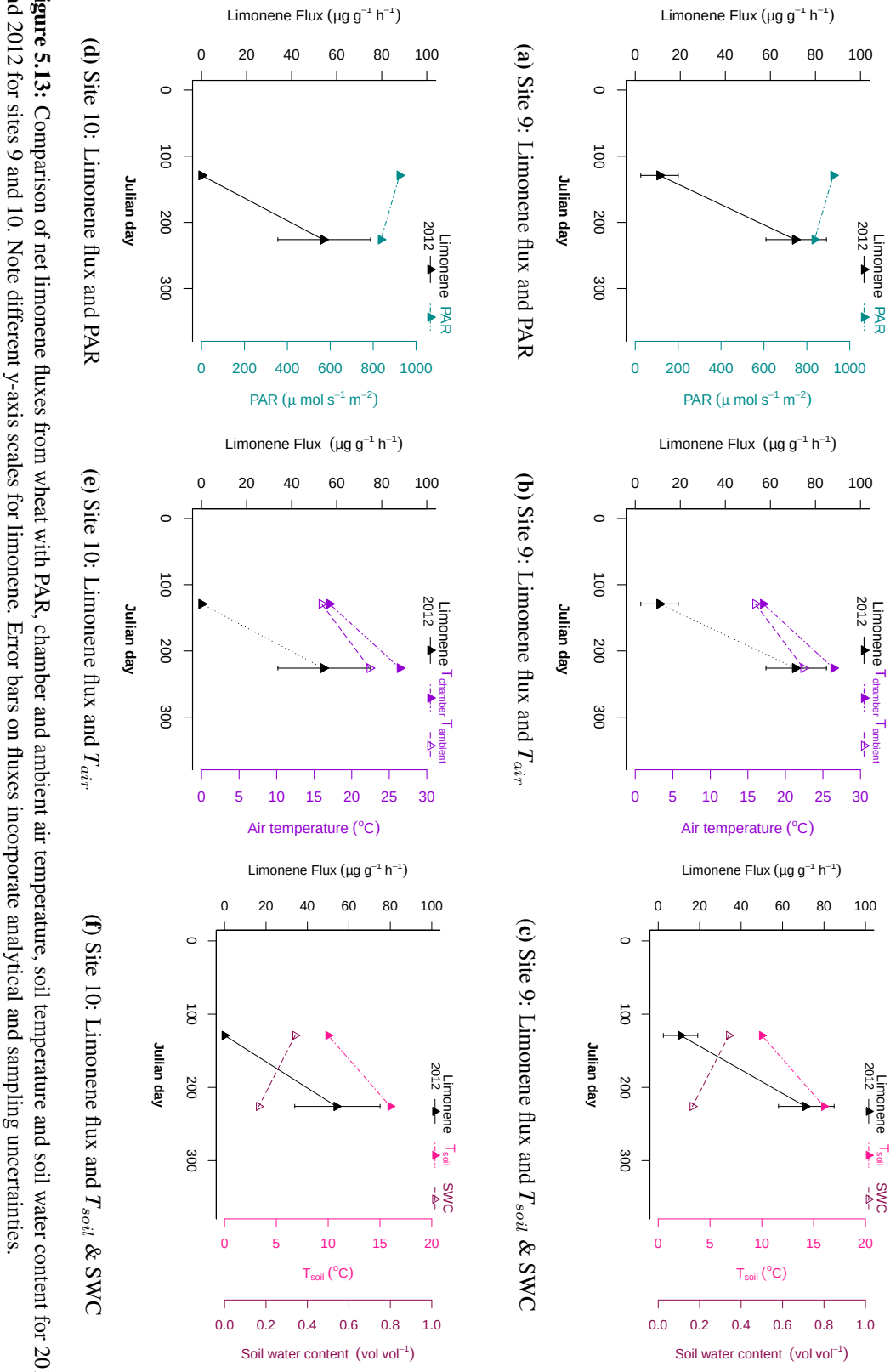
(c) Site 7: Limonene flux and T_{soil} & SWC

(d) Site 8: Limonene flux and PAR

(e) Site 8: Limonene flux and T_{air}

(f) Site 8: Limonene flux and T_{soil} & SWC

Figure 5.12: Comparison of net limonene fluxes from wheat with PAR, chamber and ambient air temperature, soil temperature and soil water content for 2010 and 2012 for sites 7 and 8. Note different y-axis scales for limonene. Error bars on fluxes incorporate analytical and sampling uncertainties.



(a) Site 9: Limonene flux and PAR

(b) Site 9: Limonene flux and T_{air}

(c) Site 9: Limonene flux and T_{soil} & SWC

(d) Site 10: Limonene flux and PAR

(e) Site 10: Limonene flux and T_{air}

(f) Site 10: Limonene flux and T_{soil} & SWC

Figure 5.13: Comparison of net limonene fluxes from wheat with PAR, chamber and ambient air temperature, soil temperature and soil water content for 2010 and 2012 for sites 9 and 10. Note different y-axis scales for limonene. Error bars on fluxes incorporate analytical and sampling uncertainties.

Other monoterpenes

β-pinene fluxes of between 47.8 and 125 $\mu g\, g^{-1}\, h^{-1}$ were measured at sites 1 to 3 in May 2010, but have large associated uncertainties. No β-pinene was detected again until May 2012, when a maximum flux of 0.1 $\mu g\, g^{-1}\, h^{-1}$ was measured. δ-3-carene fluxes of between 90.8 to 186 $\mu g\, g^{-1}\, h^{-1}$ were measured in May 2010, again with large associated uncertainties. No δ-3-carene was detected again until August 2012, when a maximum flux of 18.4 $\mu g\, g^{-1}\, h^{-1}$ was measured with a large associated uncertainty. Although fairly high fluxes of these two important monoterpene compounds were detected during 2010, the measurements have sufficiently large uncertainties that they are not likely to be important fluxes.

5.3.3 Statistical analysis of seasonal fluxes and potential drivers of BVOC fluxes from wheat

Three types of analyses were carried out on the long term BVOC time series:

- Variation in α-pinene and limonene fluxes between sites and between sampling dates were analysed for significance using the Kruskal-Wallis function (multi-variate ANOVA) within the R i386 2.15.1 software package
- α-pinene and limonene fluxes were also analysed for their association with measured environmental parameters

Analysis of variation according to site and sampling date

Using multivariate ANOVA, the amount of variation in α-pinene and limonene fluxes from wheat caused by location within the field (referred to as Site) and the sampling date (Date) was investigated. Variation in neither α-pinene nor limonene fluxes was found to be significantly associated with site (Table 5.3). The sampling date however did have a significant effect on fluxes with p values of < 0.001 for α-pinene and limonene. This result was anticipated as observation of the data suggests a greater variation in net fluxes between sampling dates than between sites within the field.

Table 5.3: Analysis of BVOC flux variation according to site and date derived using multivariate ANOVA. Degrees of freedom (d.f), χ^2 value and p value for the effect of site, date and site-date interaction terms on α-pinene and limonene fluxes are presented. At a significance level of 95% the null hypothesis is rejected if $p \leq 0.05$.

		α-pinene		limonene	
	d.f	χ^2	p	χ^2	p
Date	1	19.2	<0.001	24.2	<0.001
Site	9	3.42	0.946	2.56	0.979
Date*Site	9	28.0	0.464	28.0	0.464

Potential environmental drivers

Correlations of measured α-pinene and limonene fluxes with concurrent observations of PAR, internal chamber and external ambient air temperature, soil temperature and soil moisture were investigated. α-pinene and limonene fluxes were first normalised to the highest flux recorded over the measurement period.

Significant Spearman's Rank correlation coefficients were found between α-pinene flux and PAR (Table 5.4)). However, limonene fluxes were significantly correlated with all of the environmental variables except PAR, with ρ values of between -0.914 and 0.681 with corresponding p values ≤ 0.05). Statistical analysis of limonene fluxes in wheat showed significant correlations between limonene flux and internal chamber and external ambient air temperature, soil temperature and soil moisture. The correlation between higher limonene fluxes and higher air temperatures is consistent with the view that rate of production of monoterpenes is controlled by enzymatic activity and therefore by temperature (Lerdau et al., 1997; Monson et al., 1995). Higher soil temperatures and lower soil water contents were significantly correlated with higher limonene fluxes. This may be linked to the stresses on the plant as emissions of limonene have been found to decrease with increased moisture stress (Gilmore, 1977).

Table 5.4: Spearman's rank correlation coefficients between environmental variables and α-pinene and limonene fluxes from wheat. Significant correlations ($p \leq 0.05$) are highlighted in bold.

Factor	α-pinene	Limonene
PAR	**0.386**	-0.095
$\boldsymbol{T}_{chamber}$	0.296	**0.621**
$\boldsymbol{T}_{ambient\,air}$	0.325	**0.681**
$\boldsymbol{T}_{soil}$	-0.242	**0.923**
Soil moisture	0.253	**-0.914**

5.4 Outline of CH_3X and BVOC flux measurements in oilseed rape

CH_3X fluxes from oilseed rape were investigated, with 34 measurements made between November 2010 and July 2011. Seasonal and temporal trends in CH_3X fluxes from oilseed rape are examined using time series of CH_3Br and CH_3Cl fluxes from individual sampling sites plotted with the concurrent PAR, ambient and chamber air temperature, soil temperature and soil water content observations.

Statistical analysis of the CH_3X fluxes from oilseed rape is then presented. CH_3X fluxes were tested for significant correlations with monitored environmental parameters in order to investigate possible drivers of emissions. Correlations between CH_3Br and CH_3Cl fluxes were tested for significance as was the dependence of variation in CH_3X flux on season and sampling site.

The behaviour of CH_3X fluxes from oilseed rape throughout the day at different times of the year is examined in separate sub-diurnal studies carried out in June and July 2011.

The results of BVOC flux measurements from oilseed rape are also presented. A total of 34 BVOC flux measurements were made between November 2010 and July 2011.

5.4.1 CH_3X flux trends in oilseed rape

CH_3Br

A total of 34 CH_3Br flux measurements were taken from the oilseed rape crop between November 2010 and July 2011. Soil chambers were used for measurements made in November and January as the crop was not tall enough to enclose in a branch chamber. Therefore the measurements from these two months represent soil and vegetation fluxes.

The CH_3Br fluxes from all oilseed rape sampling sites combined between November 2010 to July 2011 and the mean of those values on each sampling occasion is illustrated in Figure 5.14. In November 2010 zero fluxes were measured at all sites. Zero fluxes were measured again in January 2011 with the exception of one emission flux of 81.2 ng g^{-1} h^{-1} recorded at site 2. High emission fluxes of between 48.8 and 152 ng g^{-1} h^{-1} were measured in April 2011. Zero fluxes were measured in June and fluxes of between 0 and 4.77 ng g^{-1} h^{-1} were recorded in July.

The CH_3Br fluxes from all sites followed a seasonal trend. The highest emissions occurred in April and the lowest in November/January and June/July. This corresponds to the growth stage of the plants and the weather they were experiencing during the measurements. The crops growing in November measured around 10 cm on average. The lowest PAR levels were observed during the measurements in November and air temperature was also low. In January, the plants

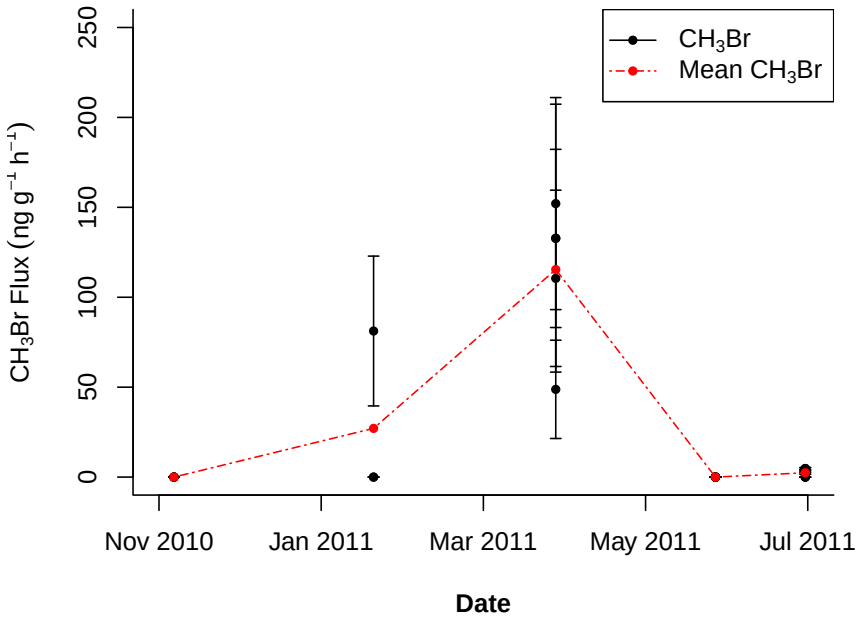


Figure 5.14: CH_3Br fluxes on oilseed rape at all ten sampling points and the mean of those values on each sampling occasion between November 2010 and July 2011. Error bars on fluxes incorporate analytical and sampling uncertainties (as described in Section 2.6.1).

had doubled in height to around 20 cm and a ground frost covered the plants, likely suppressing any activity or emissions. The plants had again doubled in height by April and this was also when the highest PAR levels were observed. Air temperatures were highest by June and July.

The oilseed rape was blossoming when flux measurements were taken in June and post-blossom flux measurements were made in July when the crop had senesced. No CH_3Br emissions were recorded during these last two months of measurements, suggesting that oilseed rape blossoms are not significant emitters of CH_3Br and that the crop does not continue to emit CH_3Br in senescence.

Time series of CH_3Br fluxes from each individual site between November 2010 to July 2011 together with concurrent PAR, ambient and chamber air temperature, soil temperature and soil water content observations are illustrated in Figures 5.15 to 5.19.

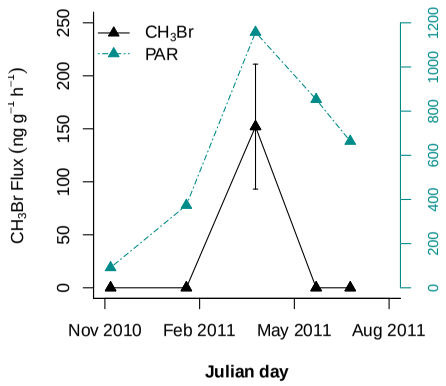
The highest emissions were detected at site 1 with a maximum recorded flux of 152 ng g^{-1} h^{-1} measured in April 2011 (Table 5.5). A minimum flux of zero was recorded at all sites. The highest mean emission fluxes were calculated for sites 1-5 (between 9.76 to 42.8 ng g^{-1} h^{-1}) and the lowest at sites 6-10 (0.78 to 2.38 ng g^{-1} h^{-1}). The highest maximum emissions also

followed the same trend, with the highest maximum emissions measured at sites 1-5 (48.8 to 152 ng g^{-1} h^{-1}) and the lowest at sites 6-10 (1.56 to 4.77 ng g^{-1} h^{-1}). The results indicate a high temporal variation of CH_3Br fluxes within the field. However, samples were only taken from sites 7 to 10 in June and July 2011 when fluxes were low across all sites, and not during months when fluxes were higher, therefore biasing the results for these sites. A mean flux of 20 ng g^{-1} h^{-1} was calculated from the measurements from all sites during the measurement period.

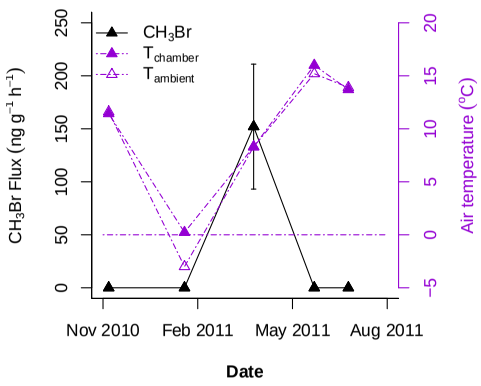
Trends in CH_3Br fluxes appear to follow trends in PAR levels closely, with increased PAR leading to higher fluxes. It is less clear whether any significant relationships exist between the other measured environmental variables and CH_3Br fluxes. The statistical significance of correlations between CH_3Br fluxes and environmental variables is described in Section 5.4.2.

Table 5.5: Mean, median, minimum and maximum net CH_3Br fluxes from oilseed rape for November 2010 to July 2011. All flux values are in ng g^{-1} h^{-1}. The final column gives the number of measurements made. The last row summarises all fluxes from all sites.

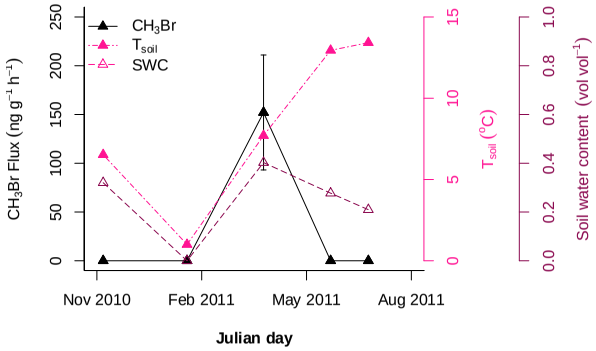
Site	Mean	Median	Min	Max	Number
O1	30.4	0.00	0.00	152	5
O2	42.8	0.00	0.00	133	5
O3	9.76	0.00	0.00	48.8	5
O4	28.8	2.33	0.00	111	4
O5	34.0	1.66	0.00	133	4
O6	1.57	0.00	0.00	4.70	3
O7	2.38	2.38	0.00	4.77	2
O8	1.52	1.52	0.00	3.04	2
O9	1.09	1.09	0.00	2.17	2
O10	0.78	0.78	0.00	1.56	2
All	20.1	0.00	0.00	152	34



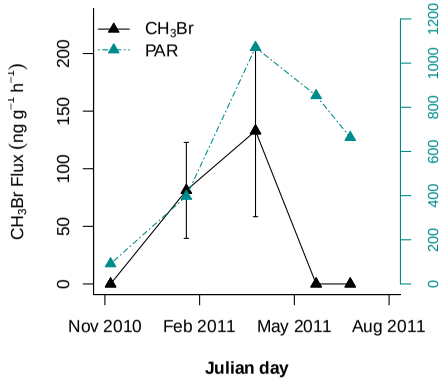
(a) Site 1: CH_3Br flux and PAR



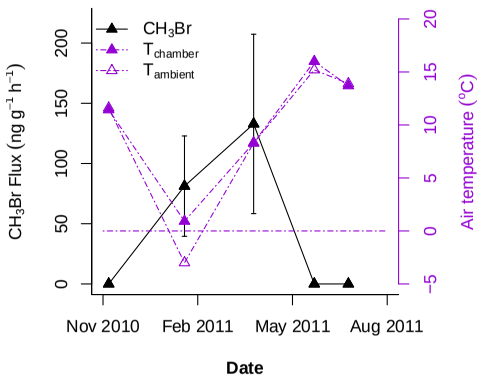
(b) Site 1: CH_3Br flux and T_{air}



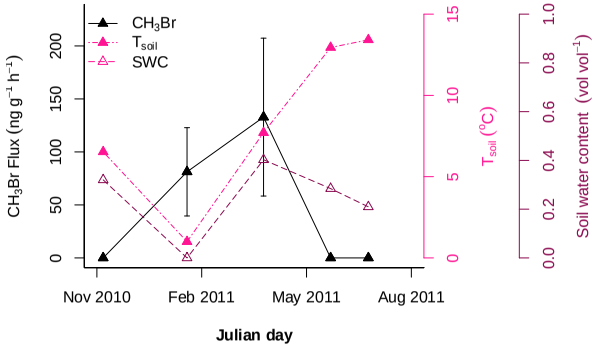
(c) Site 1: CH_3Br flux and T_{soil} & SWC



(d) Site 2: CH_3Br flux and PAR

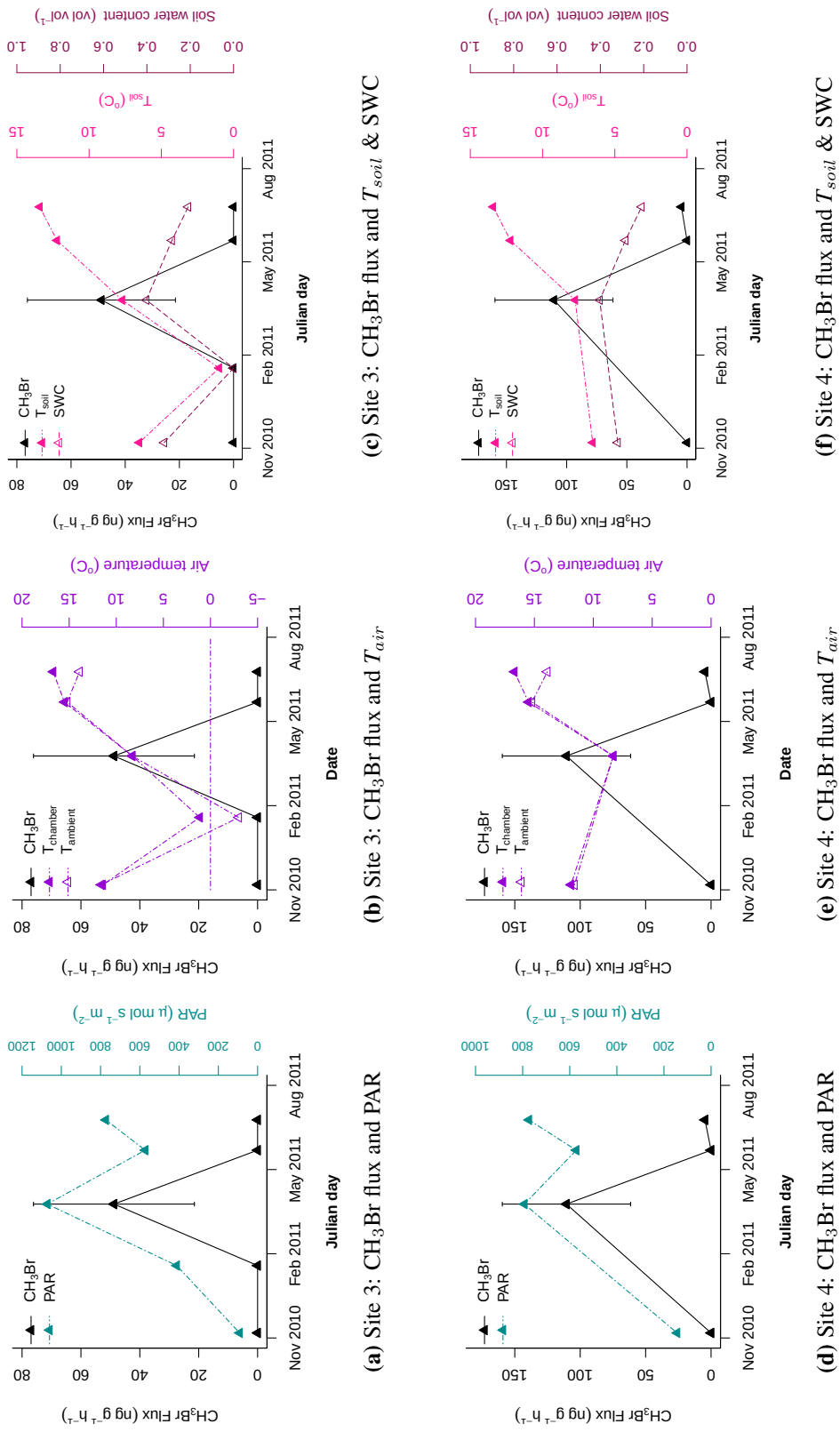


(e) Site 2: CH_3Br flux and T_{air}



(f) Site 2: CH_3Br flux and T_{soil} & SWC

Figure 5.15: Comparison of net CH_3Br fluxes from oilseed with PAR, chamber and ambient air temperature, soil temperature and soil water content for 2010 and 2012 for sites 1 and 2. Note different y-axis scales for CH_3Br . Error bars on fluxes incorporate analytical and sampling uncertainties. Colour-coded dashed lines denote zero on appropriate y-axis.



(a) Site 3: CH_3Br flux and PAR

(b) Site 3: CH_3Br flux and T_{air}

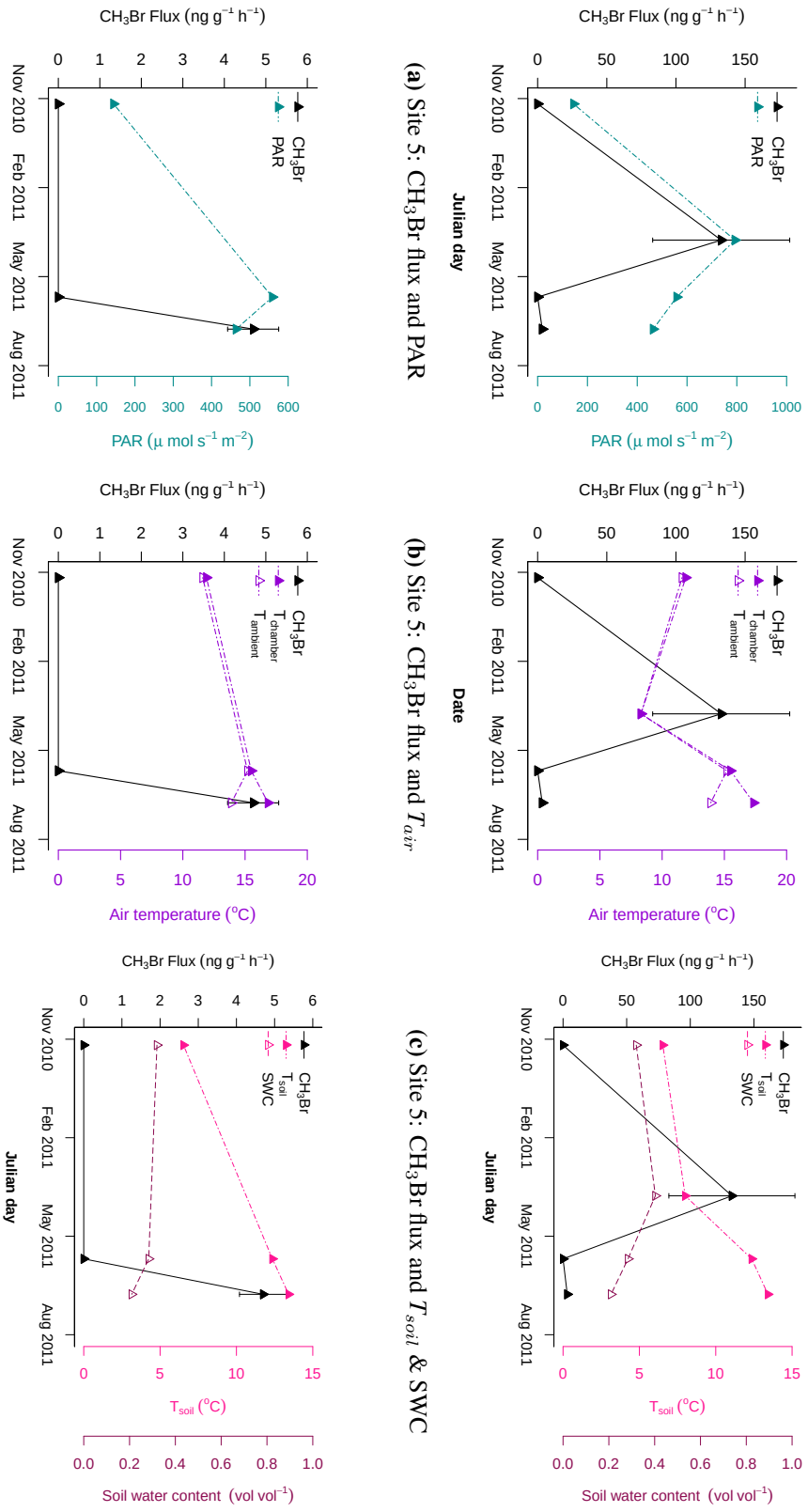
(c) Site 3: CH_3Br flux and T_{soil} & SWC

(d) Site 4: CH_3Br flux and PAR

(e) Site 4: CH_3Br flux and T_{air}

(f) Site 4: CH_3Br flux and T_{soil} & SWC

Figure 5.16: Comparison of net CH_3Br fluxes from oilseed with PAR, chamber and ambient air temperature, soil temperature and soil water content for 2010 and 2012 for sites 3 and 4. Note different y-axis scales for CH_3Br . Error bars on fluxes incorporate analytical and sampling uncertainties. Colour-coded dashed lines denote zero on appropriate y-axis.



(a) Site 5: CH_3Br flux and PAR

(b) Site 5: CH_3Br flux and T_{air}

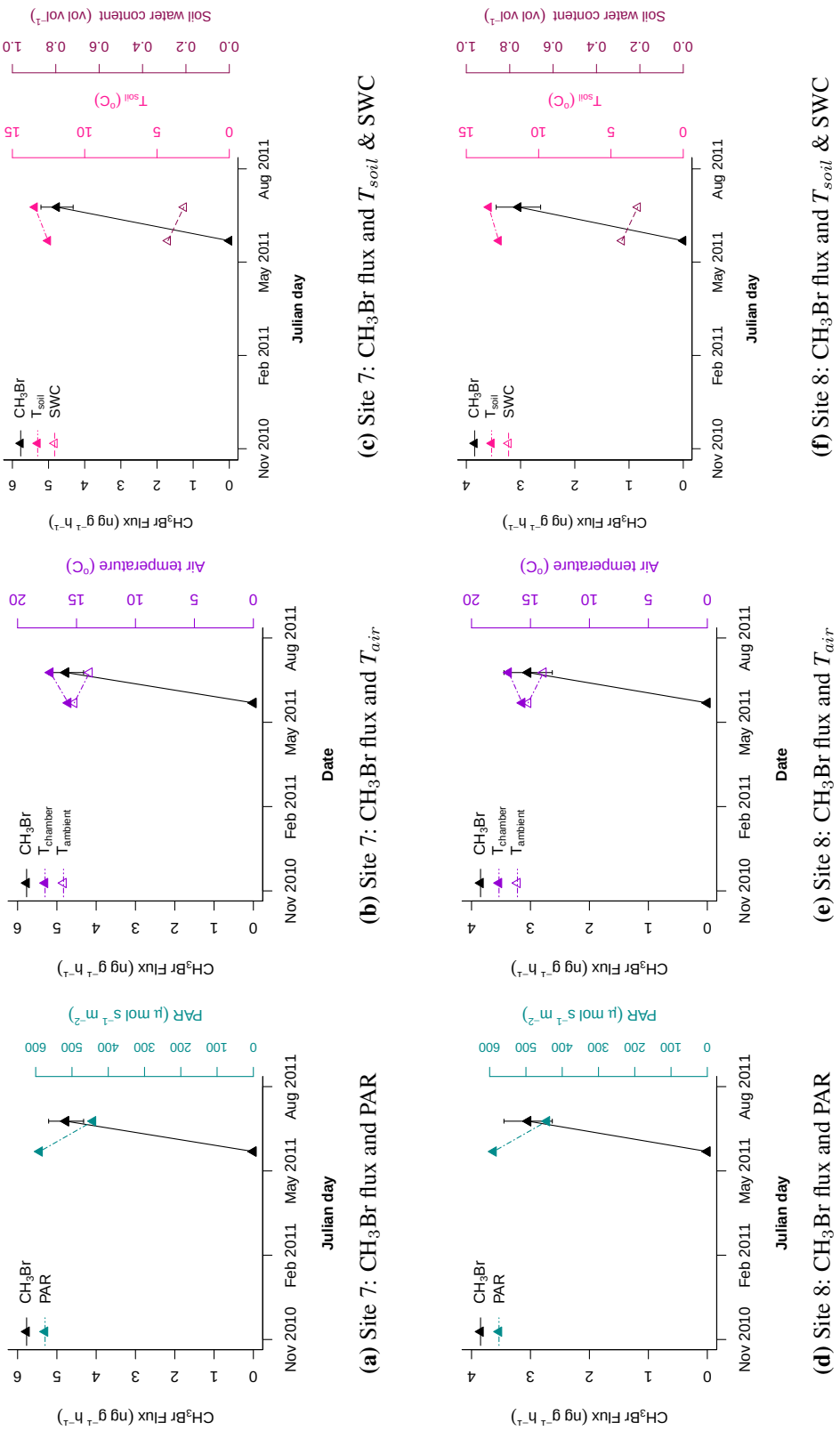
(c) Site 5: CH_3Br flux and T_{soil} & SWC

(d) Site 6: CH_3Br flux and PAR

(e) Site 6: CH_3Br flux and T_{air}

(f) Site 6: CH_3Br flux and T_{soil} & SWC

Figure 5.17: Comparison of net CH_3Br fluxes from oilseed with PAR, chamber and ambient air temperature, soil temperature and soil water content for 2010 and 2012 for sites 5 and 6. Note different y-axis scales for CH_3Br . Error bars on fluxes incorporate analytical and sampling uncertainties.



(a) Site 7: CH_3Br flux and PAR

(b) Site 7: CH_3Br flux and T_{air}

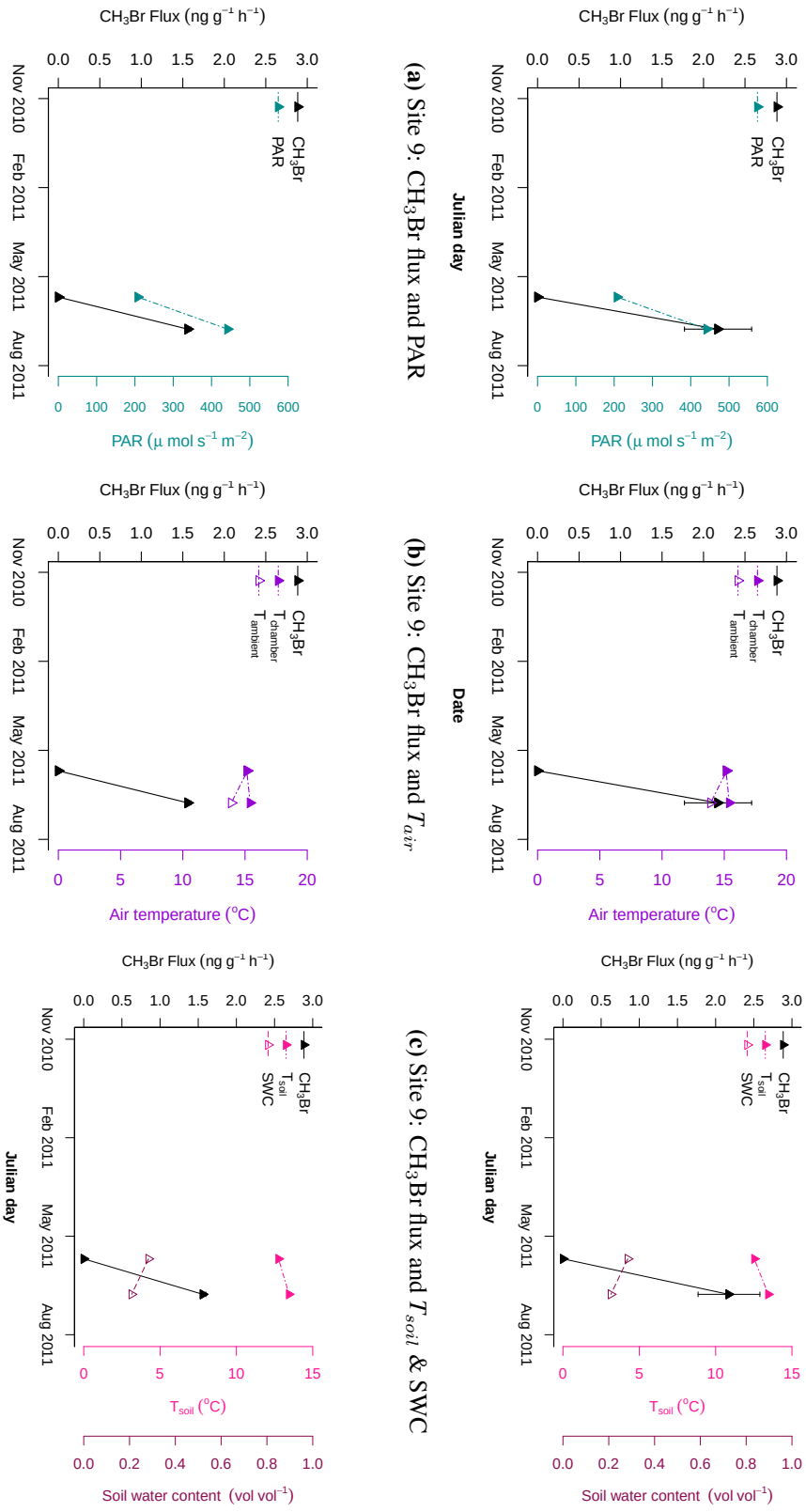
(c) Site 7: CH_3Br flux and T_{soil} & SWC

(d) Site 8: CH_3Br flux and PAR

(e) Site 8: CH_3Br flux and T_{air}

(f) Site 8: CH_3Br flux and T_{soil} & SWC

Figure 5.18: Comparison of net CH_3Br fluxes from oilseed with PAR, chamber and ambient air temperature, soil temperature and soil water content for 2010 and 2012 for sites 7 and 8. Note different y-axis scales for CH_3Br . Error bars on fluxes incorporate analytical and sampling uncertainties.



(a) Site 9: CH_3Br flux and PAR

(b) Site 9: CH_3Br flux and T_{air}

(c) Site 9: CH_3Br flux and T_{soil} & SWC

(d) Site 10: CH_3Br flux and PAR

(e) Site 10: CH_3Br flux and T_{air}

(f) Site 10: CH_3Br flux and T_{soil} & SWC

Figure 5.19: Comparison of net CH_3Br fluxes from oilseed with PAR, chamber and ambient air temperature, soil temperature and soil water content for 2010 and 2012 for sites 9 and 10. Note different y-axis scales for CH_3Br . Error bars on fluxes incorporate analytical and sampling uncertainties.

CH_3Cl

A total of 34 CH_3Cl flux measurements were taken in the oilseed rape crop between November 2010 and July 2011. Measurements were made using soil chambers in November and January so these results represent soil and vegetation fluxes. Time series of CH_3Cl fluxes from all oilseed rape sampling sites combined between November 2010 to July 2011 and the mean CH_3Cl flux on each sampling occasion are illustrated in Figure 5.20.

Emission fluxes of between 0 and 276 ng g^{-1} h^{-1} were measured in November 2010. The maximum emission flux was almost four times higher in January 2011 with measured fluxes of between 0 and 1070 ng g^{-1} h^{-1}. In April 2011 the maximum emission flux increased again with fluxes of between 0 and 1330 ng g^{-1} h^{-1}. Fluxes dropped in June and July 2011 with measured fluxes of between 0 to 22.3 ng g^{-1} h^{-1} and 0 to 15.4 ng g^{-1} h^{-1} respectively.

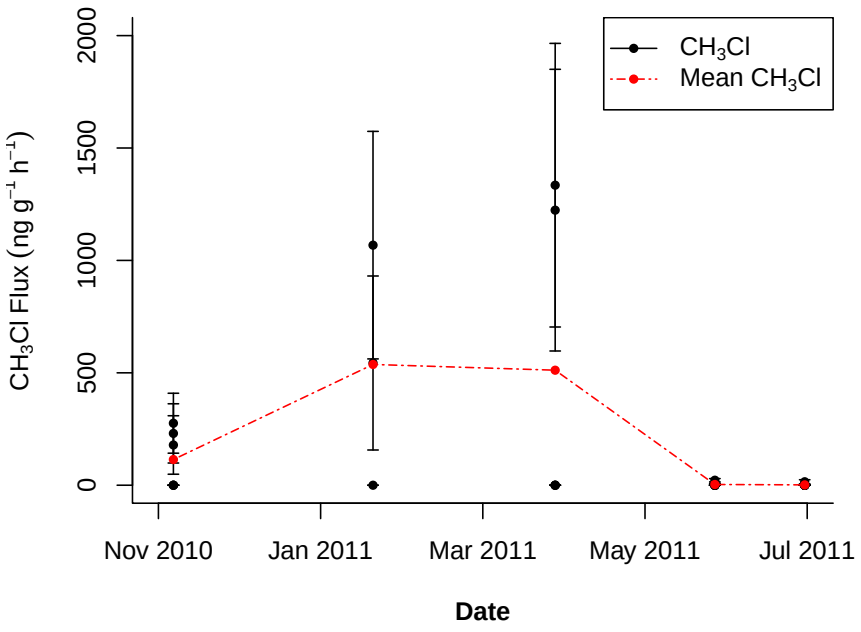


Figure 5.20: CH_3Cl fluxes from oilseed rape at all ten sampling points and the mean of those values on each sampling occasion between November 2010 and July 2011. Error bars on fluxes incorporate analytical and sampling uncertainties (as described in Chapter 2).

The results show that CH_3Cl fluxes followed a seasonal trend. The highest emissions occurred in January and April (mean emission around 500 ng g^{-1} h^{-1}) and the lowest in November and June/July (no emissions in June or July during blossoming and senescence). This is similar to the pattern found for CH_3Br fluxes, except that high CH_3Cl fluxes (544 to 1068 ng g^{-1} h^{-1})

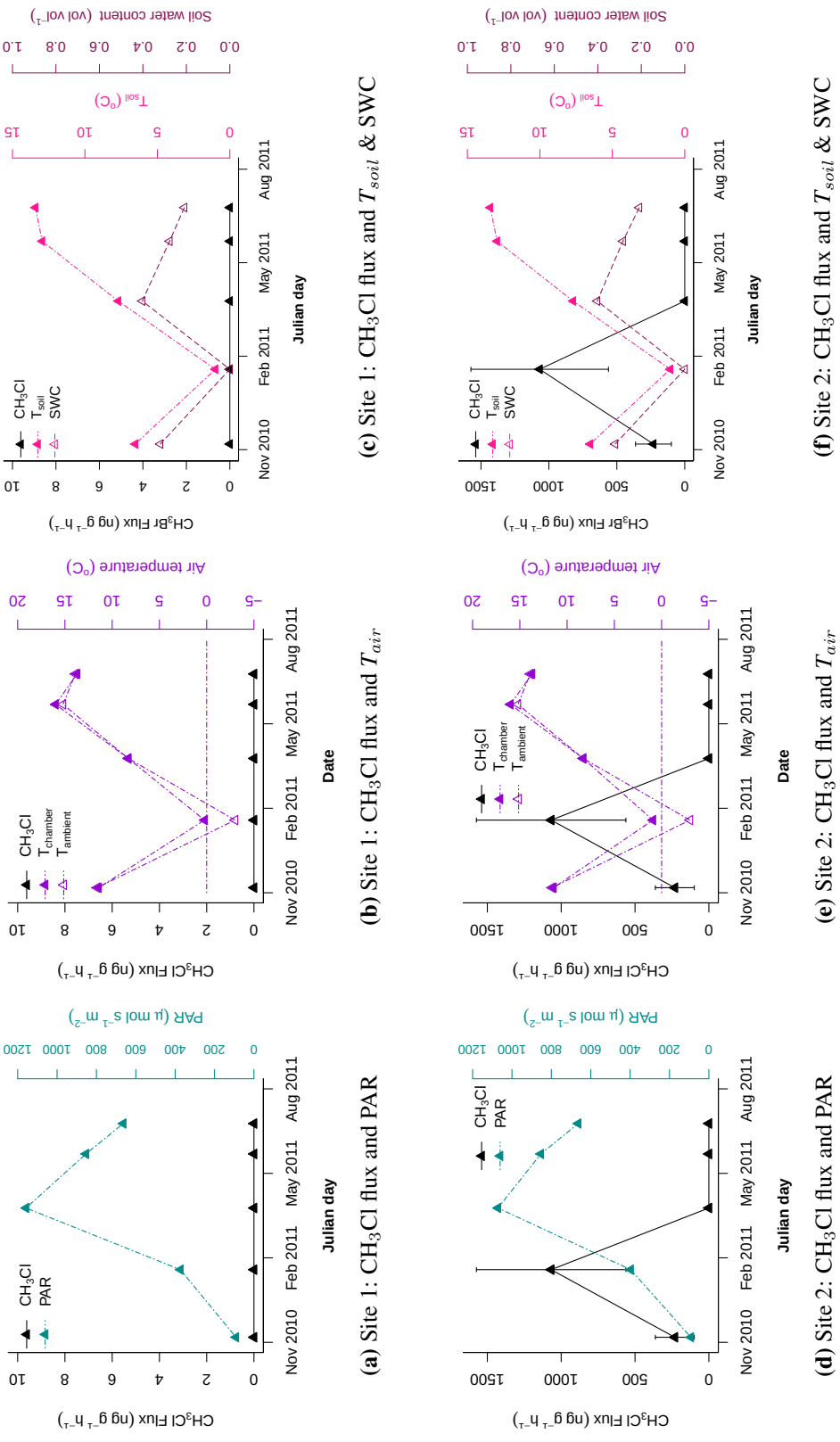
were measured in January but only one non-zero CH_3Br flux was measured (81 ng g^{-1} h^{-1}). This was not expected as the ground and plants were covered in frost during the measurements but may be due to emissions from the soil since soil chambers were used.

Time series of CH_3Cl fluxes from individual sites between November 2010 to July 2011 together with observed PAR, chamber and ambient air temperature, soil temperature and soil water content are illustrated in Figures 5.21 to 5.25. Observation of the data suggests that there are no clear relationships between CH_3Cl fluxes and the measured environmental variables, the statistical significance is described in Section 5.4.2.

A maximum CH_3Cl emission of 1330 ng g^{-1} h^{-1} was measured from site 5 (Table 5.6) in April. The minimum flux recorded at all sites was zero. High temporal variation was suggested with the highest emissions measured at sites 2 to 6 (mean fluxes between 61.3 and 334 ng g^{-1} h^{-1}) and the lowest at sites 1 and 7 to 10 (mean fluxes between 0 and 11.2 ng g^{-1} h^{-1}). The maximum emissions followed the same trend with the highest maximum emission fluxes measured at sites 2 to 6 (between 179 and 1330 ng g^{-1} h^{-1}) and the lowest at sites 1 and 7 to 10 (between 0 and 22.3 ng g^{-1} h^{-1}) However, sites 7 to 10 were only measured in June and July 2011 when CH_3Cl fluxes at all sites were low, and no measurements were taken during times of the year when fluxes were high, therefore biasing the results from these sites. A mean CH_3Cl flux of 144 ng g^{-1} h^{-1} was calculated from results for all sites for all measurement months.

Table 5.6: Mean, median, minimum and maximum net CH_3Cl fluxes from oilseed rape for November 2010 to July 2011. All flux values are given as ng g^{-1} h^{-1}. The final column gives the number of measurements made. The last row presents all fluxes from all sites.

Site	Mean	Median	Min	Max	Number
O1	0.00	0.00	0.00	0.00	5
O2	260	0.00	0.00	1070	5
O3	164	0.00	0.00	544	5
O4	306	0.00	0.00	1220	4
O5	334	0.00	0.00	1330	4
O6	61.3	4.96	0.00	179	3
O7	11.2	11.2	0.00	22.3	2
O8	7.70	7.70	0.00	15.4	2
O9	0.00	0.00	0.00	0.00	2
O10	2.65	2.65	0.00	5.30	2
All	144	0.00	0.00	1330	34



(a) Site 1: CH_3Cl flux and PAR

(b) Site 1: CH_3Cl flux and T_{air}

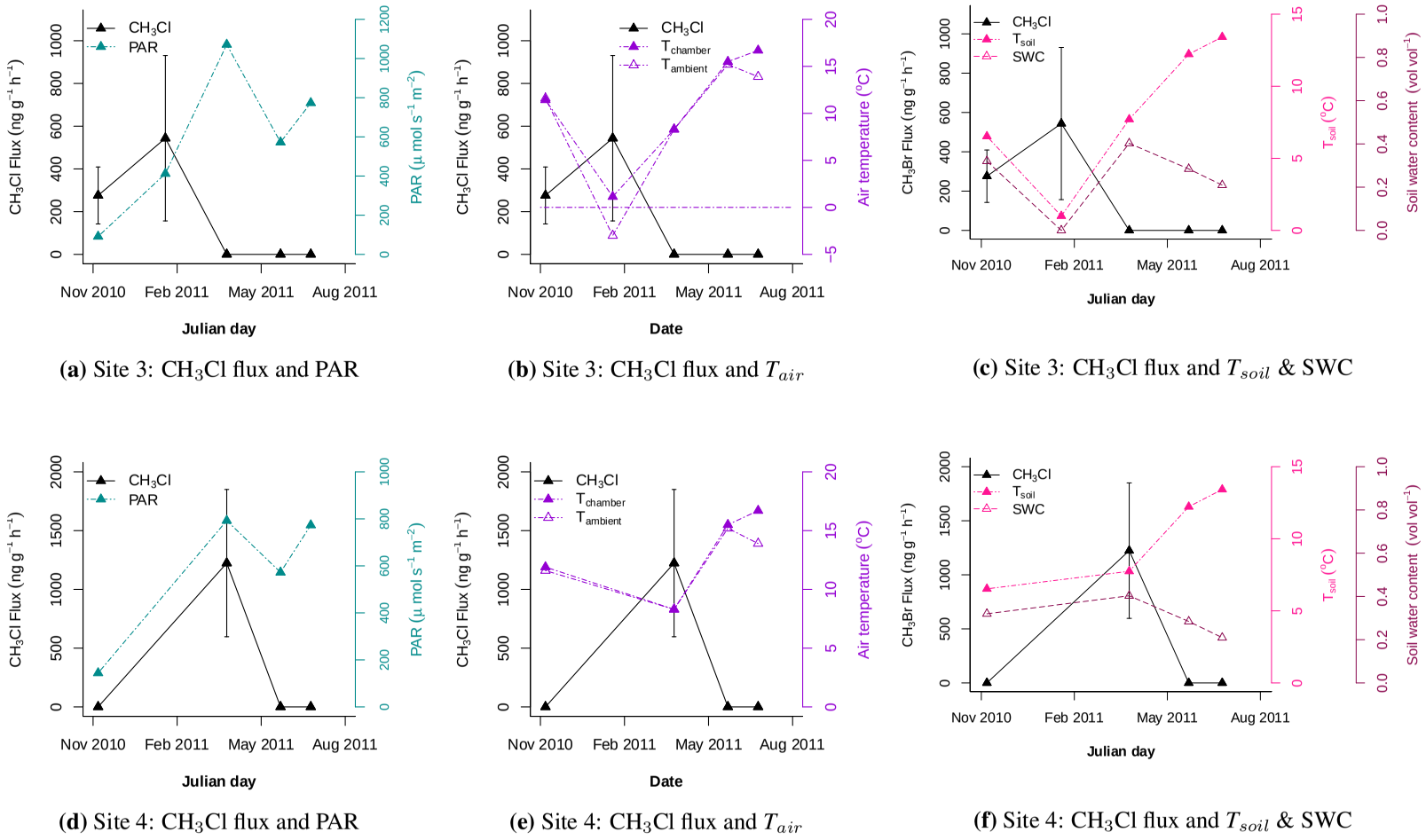
(c) Site 1: CH_3Cl flux and T_{soil} & SWC

(d) Site 2: CH_3Cl flux and PAR

(e) Site 2: CH_3Cl flux and T_{air}

(f) Site 2: CH_3Cl flux and T_{soil} & SWC

Figure 5.21: Comparison of net CH_3Cl fluxes from oilseed with PAR, chamber and ambient air temperature, soil temperature and soil water content for 2010 and 2012 for sites 1 and 2. Note different y-axis scales for CH_3Cl . Error bars on fluxes incorporate analytical and sampling uncertainties. Colour-coded dashed lines denote zero on appropriate y-axis.



(a) Site 3: CH_3Cl flux and PAR

(b) Site 3: CH_3Cl flux and T_{air}

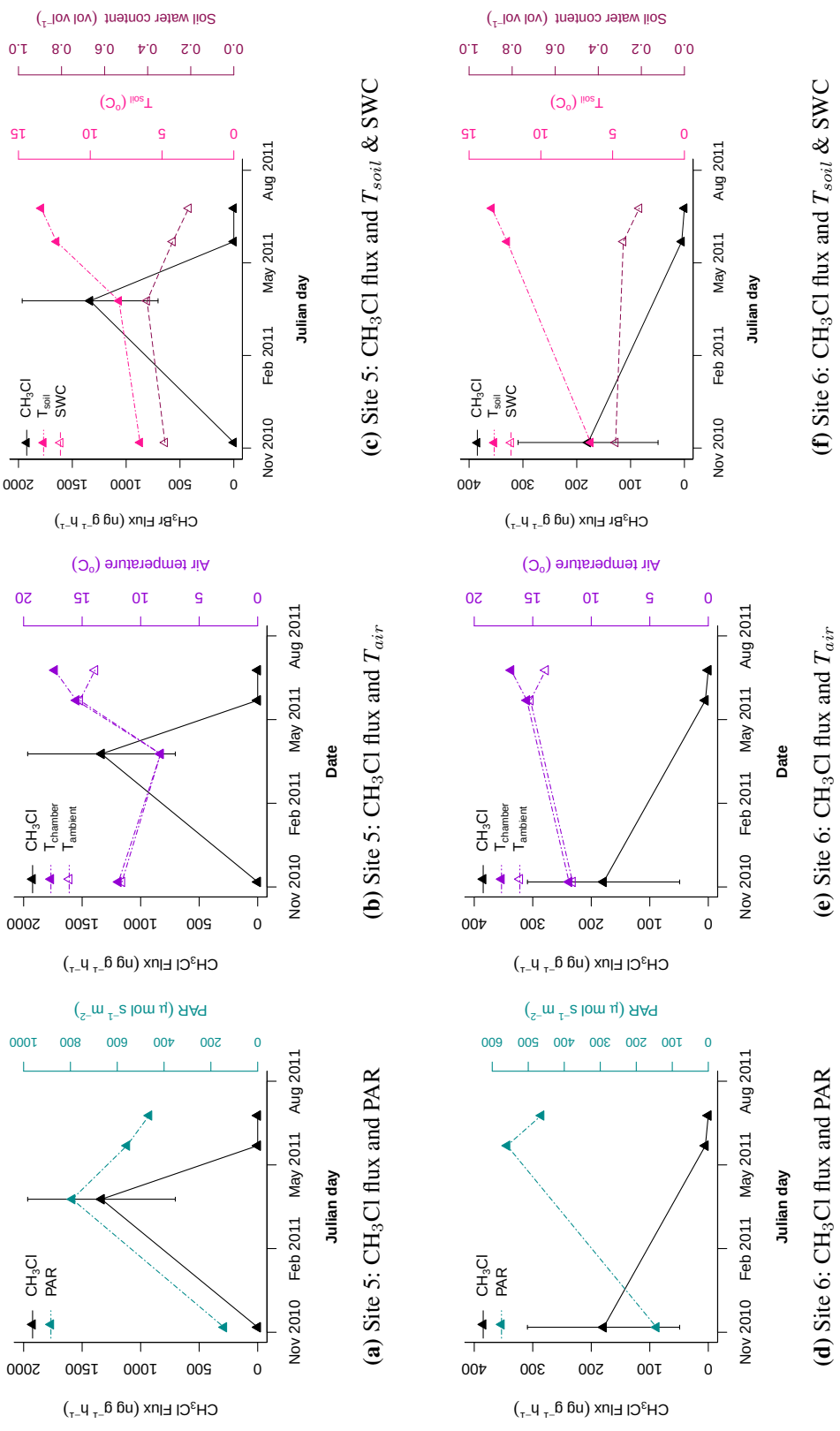
(c) Site 3: CH_3Cl flux and T_{soil} & SWC

(d) Site 4: CH_3Cl flux and PAR

(e) Site 4: CH_3Cl flux and T_{air}

(f) Site 4: CH_3Cl flux and T_{soil} & SWC

Figure 5.22: Comparison of net CH_3Cl fluxes from oilseed with PAR, chamber and ambient air temperature, soil temperature and soil water content for 2010 and 2012 for sites 3 and 4. Note different y-axis scales for CH_3Cl . Error bars on fluxes incorporate analytical and sampling uncertainties. Colour-coded dashed lines denote zero on appropriate y-axis.



(a) Site 5: CH_3Cl flux and PAR

(b) Site 5: CH_3Cl flux and T_{air}

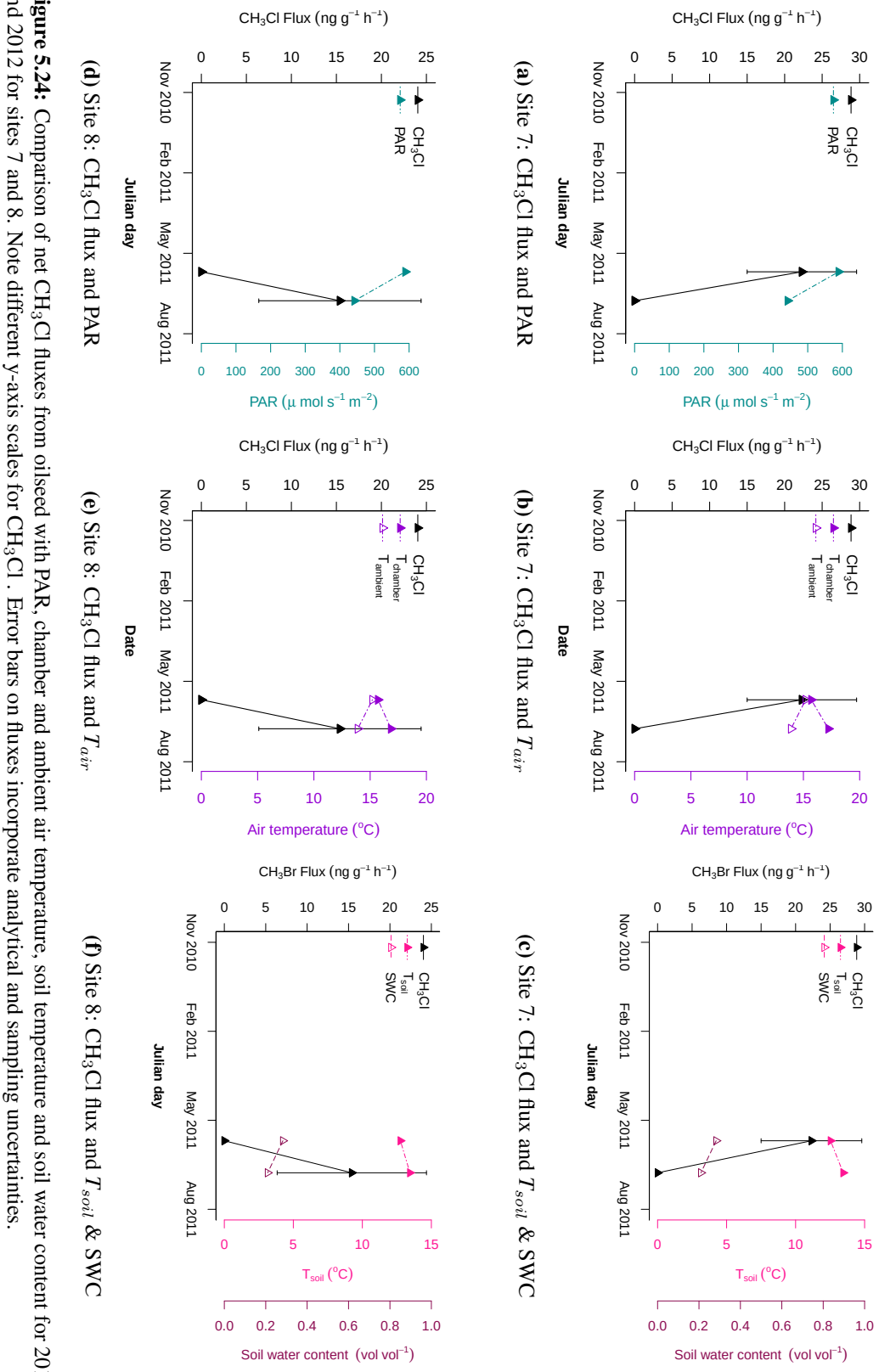
(c) Site 5: CH_3Cl flux and T_{soil} & SWC

(d) Site 6: CH_3Cl flux and PAR

(e) Site 6: CH_3Cl flux and T_{air}

(f) Site 6: CH_3Cl flux and T_{soil} & SWC

Figure 5.23: Comparison of net CH_3Cl fluxes from oilseed with PAR, chamber and ambient air temperature, soil temperature and soil water content for 2010 and 2012 for sites 5 and 6. Note different y-axis scales for CH_3Cl . Error bars on fluxes incorporate analytical and sampling uncertainties.



(a) Site 7: CH_3Cl flux and PAR

(b) Site 7: CH_3Cl flux and T_{air}

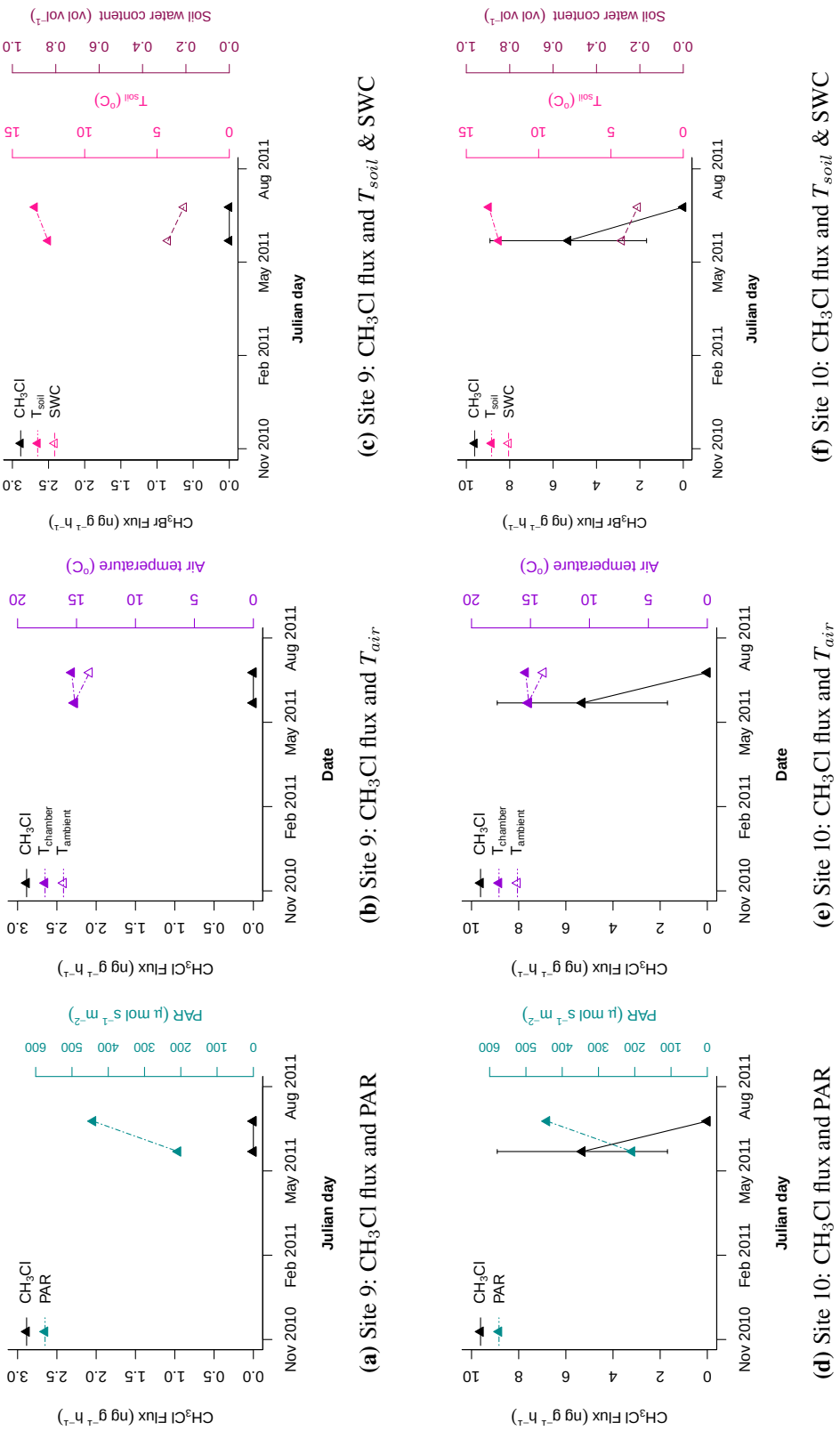
(c) Site 7: CH_3Cl flux and T_{soil} & SWC

(d) Site 8: CH_3Cl flux and PAR

(e) Site 8: CH_3Cl flux and T_{air}

(f) Site 8: CH_3Cl flux and T_{soil} & SWC

Figure 5.24: Comparison of net CH_3Cl fluxes from oilseed with PAR, chamber and ambient air temperature, soil temperature and soil water content for 2010 and 2012 for sites 7 and 8. Note different y-axis scales for CH_3Cl . Error bars on fluxes incorporate analytical and sampling uncertainties.



(a) Site 9: CH_3Cl flux and PAR

(b) Site 9: CH_3Cl flux and T_{air}

(c) Site 9: CH_3Cl flux and T_{soil} & SWC

(d) Site 10: CH_3Cl flux and PAR

(e) Site 10: CH_3Cl flux and T_{air}

(f) Site 10: CH_3Cl flux and T_{soil} & SWC

Figure 5.25: Comparison of net CH_3Cl fluxes from oilseed with PAR, chamber and ambient air temperature, soil temperature and soil water content for 2010 and 2012 for sites 9 and 10. Note different y-axis scales for CH_3Cl . Error bars on fluxes incorporate analytical and sampling uncertainties.

5.4.2 Statistical analysis of seasonal fluxes and potential drivers of CH_3X fluxes from oilseed rape

Three types of analyses were carried out on the long term CH_3X time series:

- Variation in CH_3X fluxes between sites and between growing and non-growing season were analysed for significance using the Kruskal-Wallis function (multi-variate ANOVA) within the R i386 2.15.1 software package
- CH_3X fluxes were also analysed for their association with measured environmental parameters

Analysis of variation according to site and season

Using multivariate ANOVA, the amount of variation in fluxes from oilseed rape caused by different factors was investigated. Variation in CH_3X fluxes due to location (different sites in the field), season (growing and non-growing), and from the interaction between these two factors were analysed. The data were divided into a growing season (November 2010 to April 2011) and a non-growing season (June and July 2011) based on observational evidence of plant growth.

Variation in both CH_3Cl but not CH_3Br fluxes was found to be significantly associated with season (Table 5.7). As expected, higher fluxes were associated with the growing season and low to zero fluxes with the non-growing season. Significant variation due to location within the field was not apparent from observation of the data and was not derived during statistical analysis.

Table 5.7: Analysis of CH_3X flux variation according to site and season derived using multivariate ANOVA. Degrees of freedom (d.f), χ^2 value and p value for the effect of site, season and season-site interaction terms on CH_3Br and CH_3Cl fluxes are presented. At a significance level of 95% the null hypothesis is rejected if $p \leq 0.05$.

		CH_3Br		**CH_3Cl**	
	d.f	χ^2	p	χ^2	p
Season	1	1.64	0.200	5.56	0.018
Site	9	1.71	0.995	4.48	0.877
Season*Site	9	6.97	0.958	14.20	0.514

Potential environmental drivers

Correlations of CH_3Br and CH_3Cl fluxes with PAR, chamber and ambient air temperature, soil temperature and soil moisture were investigated. CH_3Br and CH_3Cl fluxes were first normalised to the highest flux recorded over the measurement period.

Significant correlations between CH_3Br fluxes and observed PAR levels and ambient air temperature were identified (Table 5.8). Significant correlations were also found between CH_3Cl fluxes and chamber and ambient air temperature.

Table 5.8: Spearman's rank correlation coefficients between potential drivers and CH_3X fluxes from oilseed rape. Significant correlations ($p \leq 0.05$) are highlighted in bold.

Factor	CH_3Br	CH_3Cl
PAR	**0.339**	-0.244
$\boldsymbol{T}_{chamber}$	-0.022	**-0.298**
$\boldsymbol{T}_{ambient\,air}$	**-0.379**	-0.248
$\boldsymbol{T}_{soil}$	0.291	-0.307
Soil moisture	-0.014	0.077

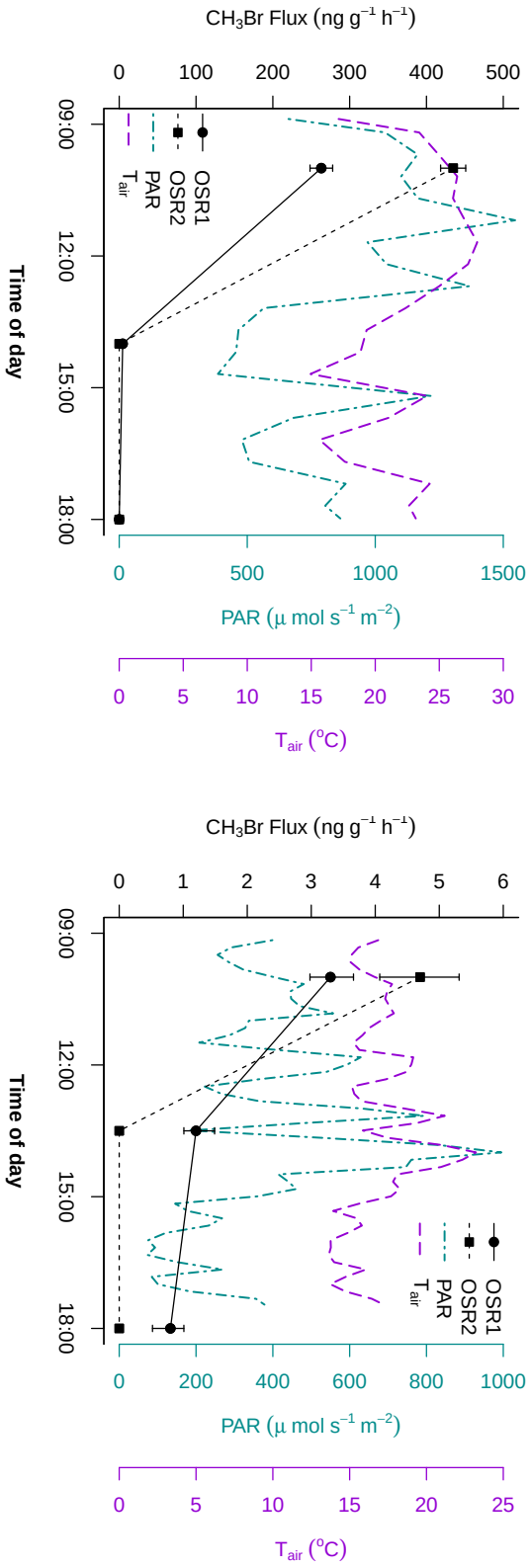
5.4.3 Sub-diurnal trends CH_3X fluxes in oilseed rape

CH_3Br

Two sub-diurnal measurement campaigns were conducted in June and July 2011 (Figure 5.26). The first of these was carried out at sites 1 and 2 on the 7th June 2011 (Figure 5.26a). CH_3Br fluxes from both site 1 and 2 were highest at the start of the day (260 and 430 ng g^{-1} h^{-1} for site 1 and 2 respectively) and low to zero at midday and at 6 pm. PAR and air temperature were also lower during the later part of the day.

It is noticeable that there were two high CH_3Br fluxes from oilseed rape during the diurnal measurements on June 7th but only zero fluxes were measured during the other time series measurements which were conducted on the following day. Although the high diurnal CH_3Br fluxes and the time series measurements were conducted at the same time in the morning on two consecutive days, when the time series measurements were conducted on the second day the air temperature was around 6 °C lower than on the first day and PAR levels were between 2 and 4 times lower. This supports evidence presented in the previous Section (5.3.3) that CH_3X production rates are significantly influenced by air temperature and PAR levels.

During the sub-diurnal measurements on 13th July, the weather was fairly sunny in the morning with cloudy intervals followed by showers in the afternoon, starting at around 4 pm. CH_3Br fluxes measured from site 1 and 2 were very low in comparison to those measured the month before. Again, fluxes were highest in the morning from both sites (around 5 ng g^{-1} h^{-1}) and lower in the afternoon (between 0 and 2 ng g^{-1} h^{-1}) (Figure 5.26b).



(a) 7th June 2011

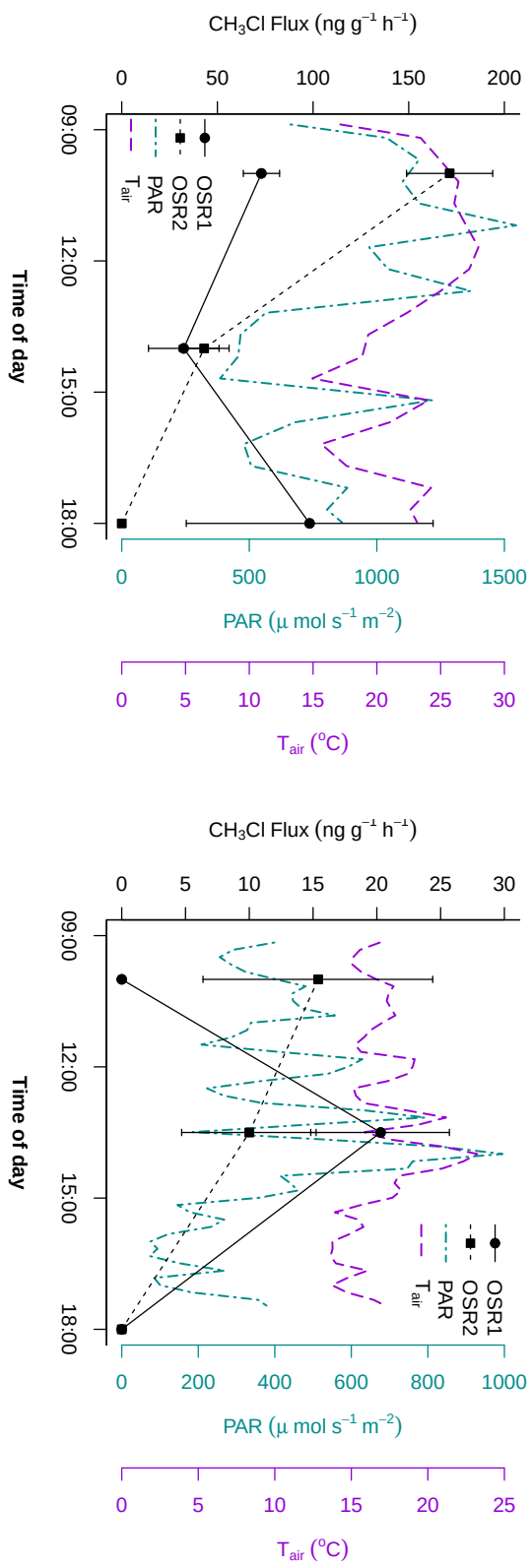
(b) 13th July 2011

Figure 5.26: Sub-diurnal CH_3Br fluxes in oilseed rape in June and July 2011 plotted with ambient air temperature and PAR. Error bars on fluxes incorporate analytical and sampling uncertainties. Note the different scales used in each figure.

CH_3Cl

The measured CH_3Cl fluxes from two sub-diurnal campaigns conducted in June and July 2011 are presented in Figure 5.27. The results from the measurements conducted at sites 1 and 2 on the 7th June 2011 show that the CH_3Cl flux was highest from both sites at 9 am (70 to 170 ng g^{-1} h^{-1}) which coincides with the high PAR and air temperatures observed during the morning (Figure 5.27a). CH_3Cl fluxes from both sites decreased to around 50 ng g^{-1} h^{-1} at 2 pm, corresponding to a drop in PAR and air temperature. At 6 pm, fluxes of CH_3Cl from site 1 increased again to around 100 ng g^{-1} h^{-1}, whereas at site 2 they decreased to zero.

Sub-diurnal fluxes from sites 1 and 2 were measured again on the 13th July 2011, with results showing a slightly different trend in CH_3Cl fluxes at each site (Figure 5.27b). At site 1 there was no detectable flux in the morning, a flux of 20 ng g^{-1} h^{-1}in the afternoon and a zero flux again at 6 pm. A peak emission flux of 15 ng g^{-1} h^{-1} from site 2 occurred in the morning, this decreased to 10 ng g^{-1} h^{-1}in the afternoon and, similarly to site 1, fell to zero at 6 pm.



(a) 7th June 2011

(b) 13th July 2011

Figure 5.27: Sub-diurnal CH_3Cl fluxes in oilseed rape in June and July 2011 plotted with ambient air temperature and PAR. Error bars on fluxes incorporate analytical and sampling uncertainties. Note the different scales used in each figure.

5.4.4 BVOC flux trends in oilseed rape

There were 34 BVOC measurements taken in oilseed rape between November 2010 and July 2011. Only two non-zero isoprene fluxes of 0.18 $\mu g\, g^{-1}\, h^{-1}$ from site 1 and 0.35 $\mu g\, g^{-1}\, h^{-1}$ from site 2 were measured on 13th July 2011. No other significant isoprene fluxes were measured. These results are in line with previous measurements of BVOCs from oilseed rape that did not find significant emissions of isoprene (König et al., 1995; Winer et al., 1992). However, no significant monoterpene fluxes were detected, unlike the findings of a previous study which described fluxes of around 35 $\mu g\, g^{-1}\, h^{-1}$ from oilseed rape crops (König et al., 1995).

5.5 Summary

Low annual net fluxes of CH_3Br and zero CH_3Cl fluxes were measured from the wheat crop during the sampling period. Wheat did not emit significant fluxes of isoprene but was found to emit small fluxes of various monoterpenes including α-pinene and limonene. Emissions of α-pinene were higher in 2010 than in 2012 with peak emissions occurring during spring. The opposite trend was found for limonene, with higher fluxes measured from wheat in summer during 2012 rather than in 2010.

The mean limonene flux from wheat (24.5 $\mu g\, g^{-1}\, h^{-1}$) calculated from results for all sites for all measurement months was less than half of the mean α-pinene flux (64.5 $\mu g\, g^{-1}\, h^{-1}$). The absolute maximum emission flux of limonene (104 $\mu g\, g^{-1}\, h^{-1}$) was less than a quarter than that for α-pinene (422 $\mu g\, g^{-1}\, h^{-1}$).

Assuming that around 30 plants were enclosed during measurements, and assuming a planting density of 200 plants per square meter (Shearman et al., 2005), the mean α-pinene flux was 430 $ng\, m^{-2}\, h^{-1}$ and the mean limonene flux was 160 $ng\, m^{-2}\, h^{-1}$.

The spatial trends were found to be fairly similar with sites 1-3, 5 and 9 high emitters of both α-pinene and limonene and other sites generally slightly lower emitters. The highest maximum limonene emission was measured at site 3 whereas the highest maximum α-pinene emission was measured at site 2.

Trends in temporal variation were found to be quite different. The highest fluxes of α-pinene occurred in springtime in both 2010 and 2012 but the corresponding limonene fluxes were fairly low. The highest limonene fluxes occurred in August 2012, when α-pinene fluxes were at their lowest.

The trend of high α-pinene and limonene emission fluxes in spring (May) and lower fluxes later in the year is likely to be strongly associated with the plant growth cycle. In contrast to

α-pinene fluxes, which were consistently highest in spring, limonene fluxes were fairly low in spring 2010 and low to zero in spring 2012. The highest emissions were measured much later in the year during August 2012. Significant correlations were derived between α-pinene and limonene fluxes and date. It is probable that this trend is also associated with plant growth cycle. In May 2010 and 2012, the wheat crop was around 20 cm, growing to 45 cm in June 2012 and 80 cm in August 2012. Although α-pinene emission fluxes decreased as the growing season progressed, in the case of limonene it appears that emission fluxes increased with increased leaf material. Accordingly, although it is common for monoterpenes to be emitted during the leaf development stage, it is also known that the composition of the monoterpene emissions changes throughout the plant growth cycle and the season as appears to be the situation here (Hakola et al., 1998; Kesselmeier and Staudt, 1999; Robertson et al., 1995; Staudt et al., 1997, 2000; Staudt and Bertin, 2002).

Oilseed rape was found to emit CH_3Br and CH_3Cl in large quantities. These fluxes varied significantly with season and growth stage but not with sampling site. The highest CH_3Br and CH_3Cl emissions occurred in April (maximum fluxes of 152 and 1330 ng g^{-1} h^{-1} respectively) and the lowest in winter. No CH_3X were emitted by oilseed rape during blossoming nor by the senescent crop in the summer months.

The mean CH_3Cl flux (144 ng g^{-1} h^{-1}) calculated from results for all sites for all measurement months was over seven times higher than the mean CH_3Br flux (20 ng g^{-1} h^{-1}). Maximum CH_3Cl fluxes reached almost nine times higher than the maximum CH_3Br fluxes.

Assuming that on average 3 oilseed plants were enclosed during measurements and that the average plant density was 100 plants per metre squared (Leach et al., 1999), the mean CH_3X fluxes measured were 130 ng m^{-2} h^{-1} and 960 ng m^{-2} h^{-1} for CH_3Br and CH_3Cl respectively.

The spatial and temporal trends were found to be very similar. The highest CH_3X fluxes occurred in April and the lowest in November and July. Sites 2-5 were consistently higher CH_3X emitters than sites 6-10, although as discussed previously, measurements taken at different sites at different times of year have biased these results somewhat. Some significant positive correlations between CH_3Br and CH_3Cl fluxes were derived at high emitting sites.

Some significant correlations were found between CH_3X fluxes from oilseed rape and the environmental variables measured including PAR, chamber temperature and ambient air temperature. This indicates a general relationship between fluxes and season and with the plant growth cycle. This suggests that CH_3X production from oilseed rape plants is controlled by two processes, one of which is dependent on photosynthesis and one which depends on enzymatic activity.

Sub-diurnal CH_3X measurements showed a clear pattern with CH_3X fluxes decreasing during

colder and darker periods and peaking when sunlight and air temperature are highest. No significant BVOC fluxes were measured during the sub-diurnal campaigns.

5.6 Discussion

This study presents measurements of CH_3X and BVOCs fluxes from the annual arable crops wheat and oilseed rape using enclosure methods. This is the first study to measure emissions of these species from plantations in the UK. Wheat does not emit significant quantities of CH_3X but small monoterpene fluxes were measured during this study, in contradiction to previous studies. Oilseed rape is an important source of both CH_3Br and CH_3Cl but should not be considered a significant source of the BVOCs considered in this study.

More wheat crops being planted than in previous years may lead to an increase in atmospheric concentrations of monoterpenes such as α-pinene, although these results are not conclusive. As discussed in Section 1.4, monoterpenes directly and indirectly affect the production of air pollutants and GHGs as well as the production of secondary organic aerosols.

Although oilseed rape is considered as an annual arable crop in this study, it is also becoming more popular for use in the production of biodiesel. An increase in planting of oilseed rape, for biodiesel or otherwise, would affect the regional atmospheric composition of CH_3Br and CH_3Cl and may have consequences for the recovery prospects of the ozone layer.

The fluxes estimated by Gan et al. (1998) were used by Mead et al. (2008c) to estimate the global CH_3Br fluxes from oilseed rape between 1961 and 2003. The study concluded that there been a 10-fold increase in emissions since 1961 and that the rise in emissions from Europe and North America had been the most extreme. Mead et al. (2008c) also anticipated that oilseed rape production would continue to expand due to various factors including the increasing interest in oilseed rape as a biofuel crop. This increase, coupled with increased emission rates due to increased plant activity due to increasing temperatures, may result in a further rise in CH_3Br emissions from oilseed rape in future.

Chapter 6

Comparison of perennial bioenergy crops and annual arable crops

This research characterises the magnitude of CH_3X and BVOC fluxes, and their trends, from both perennial bioenergy crops and annual arable crops and allows comparison of the fluxes from each crop type. A large number of measurements were made in both the perennial bioenergy crops *Miscanthus* and SRC willow and the annual arable crops oilseed rape and wheat in order to capture the seasonality of CH_3X and BVOC fluxes and investigate inter-annual trends. The observed heterogeneity in the CH_3X and BVOC fluxes between the seasons and between years highlight the need for long-term datasets, like those obtained here, in order to better scale-up fluxes. The scale-up of CH_3X and BVOC fluxes to UK-, Europe- and global-scale is addressed in Chapter 8.

A unique aspect of this work was that the different plant species were investigated simultaneously for a period of almost 3 years. No other studies have focused on several types of trace gases from several plants species at the same site, under the same soil and climate conditions, for such a long time period. Previous studies into CH_3X fluxes have investigated soil fluxes over several years but measurements were taken at different sites each year (Redeker and Cicerone, 2004). Other long-term studies on soil fluxes have focused on a particular ecosystem type rather than plant type (Drewer et al., 2006; White et al., 2005).

At present, there are no published measurements of CH_3X from *Miscanthus* and only one published study on BVOCs measured from *Miscanthus* during one month in summer using an EC PTR-MS technique (Copeland et al., 2012). Fluxes of BVOCs from various willow species are well documented, although again these studies focus on measurements made during one month in summer (Copeland et al., 2012; Isebrands et al., 1999; Niinemets et al., 2010) or for slightly longer periods of two to three months during the growing season (Hakola et al., 1998; Olofsson et al., 2005). This study has produced a comprehensive, long-term dataset covering several growing seasons as well as non-growing seasons.

Measurements of CH_3X activity in leaf disks of *Brassica* spp. (not including oilseed rape) have been reported (Attieh et al., 1995; Saini et al., 1995), as well as limited direct measurements of

the production of CH_3Br in oilseed rape (Gan et al., 1998). However no data exists on direct measurements of CH_3X from wheat and a more comprehensive investigation of CH_3X fluxes from oilseed rape crops has yet to be reported. Measurements of BVOCs from wheat (Buttery et al., 1985; König et al., 1995; Winer et al., 1992) and from oilseed rape (König et al., 1995) have been made previously but have focused on sampling for a a few days during summer rather than sampling over several months or years. Considerable uncertainties still exist regarding variations in fluxes in relation to plant growth stage and temperature dependence. Analysis of the long-term dataset compiled during this study addresses some of these issues.

6.1 Comparison of CH_3X fluxes in perennial bioenergy and annual arable crops

6.1.1 Comparison of CH_3X fluxes to other studies

There is a paucity of data on CH_3X fluxes from different crops. No comparable data exists on CH_3X fluxes from *Miscanthus* or wheat but fluxes measured from willow in this study are similar to fluxes from tropical rainforests (Blei et al., 2010a) (Table 6.1). Measurements of fluxes from oilseed rape also fall within the range of CH_3X fluxes measured in two previous studies (Gan et al., 1998; Harper et al., 1999).

Table 6.1: Mean CH_3Br and CH_3Cl fluxes in $\mathrm{ng\,g^{-1}\,h^{-1}}$ measured in this study in comparison to previous studies.

Species	Mean CH_3Br ($\mathrm{ng\,g^{-1}\,h^{-1}}$)	Mean CH_3Cl ($\mathrm{ng\,g^{-1}\,h^{-1}}$)	Measurement type	Reference
Miscanthus	2.03	12.4	Branch enclosure	(This study)
Willow (*Salix* spp.)	0.88	6.27	Branch enclosure	(This study)
Tropical rainforest	2.15	55.0	Branch enclosure	(Blei et al., 2010a)
Wheat	0.80	11.9	Branch enclosure	(This study)
Oilseed rape (*Brassica napus*)	19.0	93.9	Branch enclosure	(This study)
Oilseed rape	1.04	-	Field study	(Gan et al., 1998)
Other *Brassica* spp: Broccoli	9.87	-	Field study	(Gan et al., 1998)
Cabbage	0.75	-	Field study	(Gan et al., 1998))
Wild mustard	1.50	-	Field study	(Gan et al., 1998)
Potato crop	-	327	Field study	(Harper et al., 1999)

6.1.2 Annual CH_3X flux trends

Net fluxes of CH_3Br and CH_3Cl from both of the bioenergy crops (*Miscanthus* and SRC willow) followed a clear seasonal trend with the highest flux values in summer and lowest values in winter (see Sections 3.3.1 and 4.3.1). Oilseed rape was grown as a winter crop and the trend in CH_3X fluxes therefore followed a slightly different pattern, with the highest fluxes occurring around April during the peak growth of the crop (see Section 5.4.1). CH_3X fluxes from wheat were negligible (see Section 5.3.1). Trends in fluxes from the bioenergy crops and oilseed rape are both likely to be linked to plant growth and are also indirectly related to temperature and sunlight levels. Despite noticeable variation in CH_3X fluxes between sampling sites in a crop field, CH_3X fluxes did not differ significantly with sampling site in any of the crops measured.

A similar range of CH_3X fluxes was measured for both of the bioenergy crops *Miscanthus* and willow with CH_3Br fluxes between zero and 34 ng g^{-1} h^{-1} and CH_3Cl fluxes between zero and 120 to 190 ng g^{-1} h^{-1} (Figure 6.1). Fluxes of CH_3Br from oilseed rape were over four times higher than from the bioenergy crops (zero to 152 ng g^{-1} h^{-1}). Fluxes of CH_3Cl were almost seven times higher from oilseed rape than from the bioenergy crops (zero to 1330 ng g^{-1} h^{-1}). Fluxes of CH_3X from wheat were negligible.

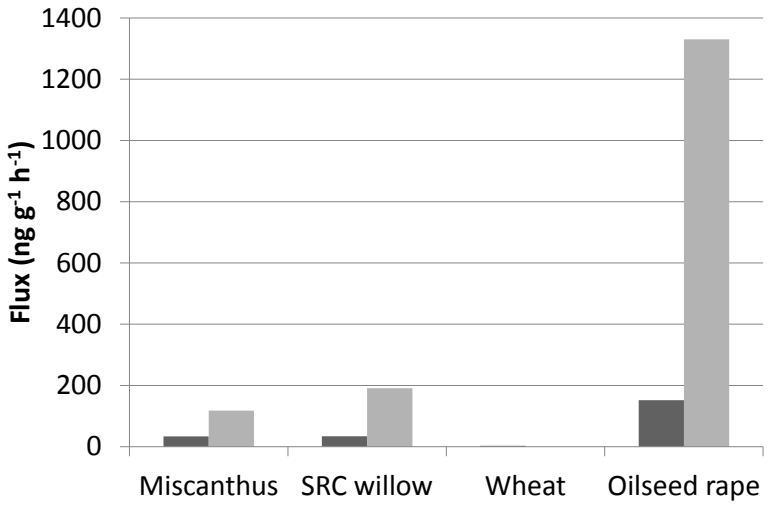


Figure 6.1: Range of fluxes (in ng g^{-1} h^{-1}) of CH_3Br (■) and CH_3Cl (■) from *Miscanthus*, SRC willow, wheat and oilseed rape.

6.1.3 Diurnal CH_3X flux trends

A clear diurnal pattern was observed during the diurnal sampling campaign carried out in the *Miscanthus* field in Brattleby in July 2010 but not during other diurnal or sub-diurnal campaigns. In the July diurnal sampling campaign CH_3Cl fluxes were too low to detect any flux trends,

however the highest CH_3Br fluxes were measured during daylight hours and low to zero fluxes were detected during the night (see Section 3.3.3). During other sub-diurnal measurements, low fluxes and changeable weather meant it was difficult to distinguish any trends in fluxes and peak fluxes did not always occur at midday (see Sections 4.2.5 and 5.4.3). Trends in both CH_3Br and CH_3Cl fluxes from all crop types generally tended to follow trends in observed PAR and air temperature which is indicative of a diurnal trend.

6.1.4 Behaviour of CH_3Br and CH_3Cl fluxes

The magnitudes of CH_3Br fluxes from *Miscanthus* were fairly similar in all years of measurement. CH_3Cl fluxes however were slightly higher in 2011. This may be due to the higher air and soil temperatures during 2011, as discussed in the following section. CH_3Cl fluxes in 2012 also appeared to be following the same trend as those in 2011, although sampling finished before the end of growing season so the magnitude of peak emissions from that year is not known.

Both CH_3Br and CH_3Cl fluxes from SRC willow were higher in 2011 than in 2010 and 2012. This may again be linked to higher air and soil temperatures during 2011. This may also be due to the growth stage of the plants as they were harvested in winter 2010. These observations suggest that young SRC willow plants emit relatively higher amounts of CH_3X than plants with one or two years growth.

Despite CH_3Br and CH_3Cl fluxes following the same seasonal trends, only a few significant correlations between CH_3Br and CH_3Cl fluxes were identified at a 95% confidence level. Inter-annual trends in CH_3Br and CH_3Cl fluxes from *Miscanthus* were different but very similar from SRC willow. It is therefore unclear whether production of CH_3Br and CH_3Cl were driven by the same molecular mechanism.

6.1.5 Influence of environmental variables on CH_3X fluxes

It was anticipated that by collecting a large amount of environmental observations, factors such as sunlight, temperature and soil water content might be identified as drivers for the trends observed in the CH_3X fluxes and their magnitude. Several significant correlations were found but no general rule could be applied to fluxes from all crop types.

Significant positive correlations between CH_3X fluxes and the temperature of the chamber, ambient air and soil were identified for both bioenergy crops (see Sections 3.3.2, 4.2.4 and 4.3.3). This is likely due to the general increase in plant activity in warmer temperatures. CH_3X fluxes from oilseed rape, however, were negatively correlated with air temperature (see Section 5.4.2). This is likely due to fewer data points and the fact that oilseed was grown as a winter crop with peak growth of the crop not occurring during the highest temperatures.

6.2 Comparison of BVOC fluxes in perennial bioenergy and annual arable crops

6.2.1 Comparison of BVOC fluxes to other studies

There is little data on BVOC fluxes from different crop types to compare the BVOC fluxes measured in this study. Most of the measurements carried out have focussed on isoprene, and the isoprene fluxes measured from different crop types in this study are presented along with any comparable fluxes from previous studies in Table 6.2.

There are no comparable BVOC fluxes for *Miscanthus* other than Copeland et al. (2012) who found no measurable BVOC fluxes above the *Miscanthus* crops at Brattleby using a PTR-MS technique. The same study also found fluxes of isoprene comparable to those measured in this study with a standard emission rate of 20 $\mu g\, g^{-1}\, h^{-1}$measured by Copeland et al. (2012) and 16.6 $\mu g\, g^{-1}\, h^{-1}$ measured in this study. This standard emission rate is broadly in line with other previous measurements of between 12 and 32 $\mu g\, g^{-1}\, h^{-1}$.

Fluxes of isoprene from wheat of around 0.2 $\mu g\, g^{-1}\, h^{-1}$measured were similar to the fluxes of between zero and 0.5 $\mu g\, g^{-1}\, h^{-1}$ measured by Karl et al. (2009); König et al. (1995). No isoprene was detected from oilseed rape in this study, similarly to previous studies by Karl et al. (2009); Kesselmeier and Staudt (1999).

Table 6.2: Standard isoprene emission rate in $\mu g\, g^{-1}\, h^{-1}$ measured in this study in comparison to other studies.

Species	Standard isoprene emission rate / $\mu g\, g^{-1}\, h^{-1}$	Measurement type	Reference
Miscanthus	0.48	Branch enclosure	This study
Miscanthus	0	Canopy-scale, PTR-MS	(Copeland et al., 2012)
SRC Willow (*Salix* spp.)	16.6	Branch enclosure	This study
Salix spp.	20	Canopy-scale, PTR-MS	(Copeland et al., 2012)
Salix spp.	28	Branch enclosure	(Owen and Hewitt, 2000)
Salix alba	18	Branch enclosure, lab conditions	(Pio et al., 1993)
Salix caprea	18.9	Branch enclosure	(Karl et al., 2009)
Salix caroliniana	12.5	Air-exchange branch enclosure	(Zimmerman, 1979)
Salix nigra	25.2	Whole plant, air-exchange chamber	(Evans et al., 1982)
Salix phylicifolia	32	Branch enclosure	(Hakola et al., 1998)
Salix viminalis	12	Canopy-scale, REA	(Olofsson et al., 2005)
Wheat	0.19	Branch enclosure	This study
Wheat	0 0.5	Branch enclosure	(Karl et al., 2009; König et al., 1995)
Oilseed rape	0	Branch enclosure	This study
Oilseed rape	0	-	(Karl et al., 2009; Kesselmeier and Staudt, 1999)

6.2.2 Annual BVOC flux trends

Net fluxes of BVOCs from both of the bioenergy crops *Miscanthus* and SRC willow followed a clear seasonal trend with the highest values in summer and lowest values in winter (see Sections 3.4.1, 4.2.7 and 4.3.4). This pattern is likely to be linked to plant growth and thus also to temperature and sunlight levels. No seasonal trend can be determined for BVOC fluxes from the annual arable crop wheat as they were only sampled during the summer. BVOC fluxes from

oilseed rape were negligible. Despite variation between sampling sites within a field, BVOC fluxes did not differ significantly at a 95% confidence level with sampling site in any of the crops measured.

The bioenergy crop *Miscanthus* had a much lower isoprene flux than SRC willow with fluxes of 0–42.5 $\mu g\, g^{-1}\, h^{-1}$ compared to 0–1960 $\mu g\, g^{-1}\, h^{-1}$ (Figure 6.2). However both bioenergy crops emitted more isoprene than the annual arable crops wheat (0–6 $\mu g\, g^{-1}\, h^{-1}$) and oilseed rape (0–0.35 $\mu g\, g^{-1}\, h^{-1}$).

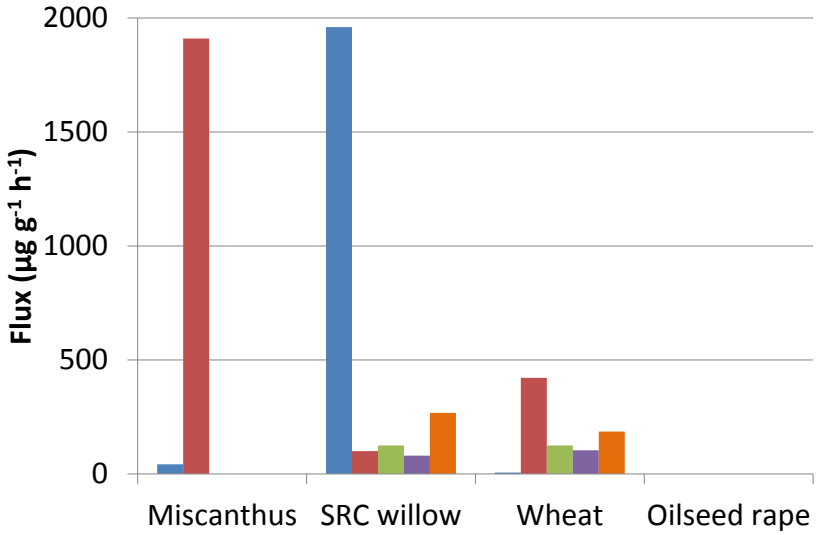


Figure 6.2: Range of fluxes (in $\mu g\, g^{-1}\, h^{-1}$) of isoprene (■), α-pinene (■), β-pinene (■), limonene (■) and δ-3-carene (■) from *Miscanthus*, SRC willow, oilseed rape and wheat.

Fluxes of α-pinene from wheat were the highest of all crop types, with a range of fluxes between zero and 1910 $\mu g\, g^{-1}\, h^{-1}$. However, fluxes of α-pinene were only detected from *Miscanthus* in 2010 (with large associated uncertainties) and were not detected the following two years. It is therefore not possible to state categorically whether or not *Miscanthus* is an important source of α-pinene.

High fluxes of α-pinene were also measured from wheat, with a range of fluxes between zero and 422 $\mu g\, g^{-1}\, h^{-1}$. Emissions from SRC willow were less than a quarter of those from wheat with a range between zero and 100 $\mu g\, g^{-1}\, h^{-1}$. Emissions of monoterpenes from oilseed rape were negligible. Emissions of other monoterpenes from *Miscanthus* were negligible.

The same range of β-pinene fluxes were measured from SRC willow and from wheat (0–125 $\mu g\, g^{-1}\, h^{-1}$). Emissions of limonene were slightly higher from wheat than from SRC willow, 0–104 $\mu g\, g^{-1}\, h^{-1}$ compared to 0–80.4 $\mu g\, g^{-1}\, h^{-1}$. However, emissions of δ-3-carene were 1.4 times higher from SRC willow than from wheat, 0–268 $\mu g\, g^{-1}\, h^{-1}$ compared to 0–186 $\mu g\, g^{-1}\, h^{-1}$.

6.2.3 Diurnal BVOC flux trends

Fluxes of BVOCs from *Miscanthus* were too low to detect any significant diurnal trends (see Section 3.4.2). Sub-diurnal measurements of isoprene from SRC willow also failed to establish whether a diurnal trend was present (see Section 4.2.9). This may be due to the changeable weather, where small fluctuations of temperature and PAR levels occurred frequently but were perhaps not extreme enough to provoke a response in isoprene fluxes. No BVOCs were detected during sub-diurnal measurements in wheat.

6.2.4 Behaviour of various BVOC fluxes

Fluxes of isoprene, α-pinene, β-pinene and δ-3-carene from SRC willow were highest in 2010. However, the limonene fluxes were higher in 2012 than in 2010. This may be due to variation in climate between years, as limonene fluxes were found to be correlated to different environmental variables than other BVOC fluxes, as discussed in the following section. This inter-annual variation might also be due to the age of the SRC willow plants. The rate of BVOC emissions has previously been shown to vary with plant age (Street et al., 1997). Studies on *Pinus* and *Camellia* species have also observed variation in the composition of BVOC emissions with plant age with younger plants emitting a wider range of monoterpenes (Kim et al., 2005; Nunes and Pio, 2001). However, another study of coniferous plants of different ages found no variation in BVOC composition with age (Lim et al., 2008).

Isoprene, α-pinene, β-pinene, limonene and δ-3-carene fluxes from wheat were not significantly correlated with each other (see Section 5.3.3). This is most likely due to the low fluxes measured from this crop. On the other hand, all BVOC fluxes from SRC willow were found to be significantly correlated with each other for all sites combined and for some sites individually (see Sections 4.2.8 and 4.3.5). A correlation between different BVOC compounds occurs because the production of both isoprene and monoterpenes is dependent on the availability of the isopentenyl pyrophosphate (IPP) precursor. The correlations between a variety of monoterpenes occurs because monoterpene synthases have the ability to produce more than one product. These enzymes use a common mechanism and variations on this simple mechanism, involving subsequent reactions of the α-terpinyl carbocation, are responsible for the enzymatic formation of most monoterpene skeletons (Croteau, 1987).

6.2.5 Influence of environmental variables on BVOC fluxes

BVOC fluxes are known to be influenced by environmental variables such as air temperature and PAR, so it was anticipated that significant correlations with these variables might explain some of the variation in fluxes. BVOC fluxes from *Miscanthus* were not significantly linked to any

environmental factors, likely due to the very low fluxes measured. In contrast, variation in the fluxes of the different BVOCs detected from SRC willow was linked to various environmental observations (see Sections 4.2.8 and 4.3.5). Fluxes of isoprene and α-pinene were significantly correlated with all of the environmental parameters, namely PAR, chamber temperature, ambient air temperature, soil temperature and soil moisture.

α-pinene fluxes from wheat were associated with PAR levels, although, interestingly, limonene fluxes were linked to all of the other environmental parameters except PAR (see Section 5.3.3). Limonene fluxes from wheat were strongly negatively correlated with soil moisture, as were isoprene fluxes from willow. This may be due to a stress-induced reduction in emissions caused by water-logged soil. Overall, several significant correlations were found but no general rule could be applied to BVOC fluxes from all crop types.

6.3 Summary

One similarity in fluxes between perennial bioenergy crops and annual arable crops was distinguished. Fluxes from all crop types were found to be strongly linked to growth stage. Some fluxes were also significantly correlated to the same observed environmental variables.

The highest fluxes of CH_3X were measured from oilseed rape. These were over four times higher than both perennial bioenergy crops, which had a similar range of CH_3X fluxes. The highest isoprene fluxes were measured from SRC willow and were orders of magnitude higher than fluxes from both annual arable crops. There were also interesting variations in BVOC fluxes from SRC willow between years, with higher isoprene and α-pinene, β-pinene and δ-3-carene fluxes from older plants in 2010 and higher limonene fluxes from younger plants in 2012.

The characterisation of α-pinene fluxes is somewhat unclear. Large fluxes of α-pinene were measured from *Miscanthus* in 2010 but were not detected the following years, therefore *Miscanthus* may or may not be an important source of α-pinene. High fluxes of α-pinene and limonene were measured from wheat but δ-3-carene fluxes were highest from SRC willow.

It is difficult to distinguish clear relationships between fluxes of CH_3X and BVOCs and environmental observations due to confounding between factors. However, fluxes from perennial bioenergy crops were linked to several environmental variables at a significance level of $p < 0.05$. Less measurements were made in the annual arable crops due to the nature of their growth pattern and it was therefore difficult to identify any correlations to environmental parameters.

Overall, given the differences in crop management regime, plant biology and hydrology, and many other variables, between perennial bioenergy crops and annual arable crops, the differences in CH_3X and BVOC fluxes are unequivocal. This study presents the first reported measurements

of the majority of these compounds from these crops. The flux magnitudes reported here are broadly in line with what little comparable data already exists.

Chapter 7

Controlled experiment

7.1 Introduction

The adoption of bioenergy crops in the UK is primarily for their perceived environmental benefits in comparison to fossil fuels. It is important to consider how their contribution to cleaner energy production may be affected by the use of fertiliser, both through the impact on CO_2 mitigation but also through the impact on budgets of other important trace gases. There have been several Life Cycle Analyses (LCAs) for bioenergy crops to assess properties such as soil organic carbon, energy use and greenhouse gas emissions (Brandão et al., 2011; Heller et al., 2003; Hillier et al., 2009). However there have been few measurement studies and data on the response of trace gas emissions to fertiliser is sparse.

Current guidelines for fertiliser application to SRC willow recommend the application of 40, 60 and 100 kg N ha^{-1} y^{-1} for the 1st, 2nd and 3rd years of the harvest cycle respectively (Johnson, 1999). The use of fertiliser has been proven to increase the biomass of the SRC willow crop. A field experiment in Syracuse, New York, found that the application of NH_4NO_3 fertilizer at a rate equivalent to 90 kg N ha^{-1} y^{-1} induced a 24% increase in total biomass of willow relative to the control over a period of 4 months (Arevalo et al., 2005).

However, the use of fertiliser may minimise the CO_2 mitigation that bioenergy crops are meant to provide by way of carbon uptake during their growth. An LCA of SRC willow in New York, USA, found that applying an inorganic nitrogen fertiliser ($(NH_4)_2SO_4$) at a rate of 100 kg N ha^{-1} y^{-1} (based on NY State regulations) had a strong influence on environmental performance of willow biomass crop production systems (Heller et al., 2003). Fertiliser inputs accounted for 37% of the non-renewable fossil energy input into the system. The manufacture of the fertiliser made up 75% of the greenhouse gas emissions included under the heading "agricultural inputs". N_2O emissions of 3.97 Mg CO_2 eq. ha^{-1} were estimated to originate from $(NH_4)_2SO_4$ fertiliser applied to SRC willow under the modelled scenario.

In order to determine the effects of nitrogen fertiliser on the greenhouse gas budget of *Miscanthus* (the other main bioenergy crop grown in the UK), ^{15}N-labelled fertiliser was

applied to *Miscanthus* during an experiment at the Brattleby fieldsite (Drewer et al., 2011). Application of $^{14}NH_4{}^{15}NO_3$ at a rate equivalent to 50 kg N ha^{-1} resulted in a fertiliser-induced increase in N_2O emission. Before the application of fertiliser, *Miscanthus* N_2O emissions were around zero but N_2O emissions increased within a day. A maximum N_2O emission of 320 μg m^{-2} h^{-1} was measured 36 hours after fertiliser application. Emissions decreased steadily and dropped to zero after 3 days.

The application of waste sewage sludge to SRC willow as a more environmentally friendly fertiliser than commercially produced compounds has also received attention in recent years. In the LCA analysis carried out by Heller et al. (2003), substituting inorganic nitrogen fertilizer with sewage sludge increased the net energy ratio of the willow biomass production system by more than 40%. The net energy ratio of bioenergy production is dependent on how the biomass source is grown, harvested and managed (e.g. application of fertiliser), and on the efficiency of the conversion to usable energy.

In one field experiment in Tully, New York, nitrogen-poor sludge was applied to a 10 year old SRC willow field and a young field regrowing after its first coppicing, with no discernible response in soil or foliar chemistry from either field (Quaye et al., 2011).

The effect of sewage sludge on plant growth and terpene emissions from three different tree species (*Quercus coccifera*, *Rosmarinus officinalis* and *Cistus albidus*) was investigated in a field experiment carried out in a Mediterranean shrubland over 3 consecutive summers (Olivier et al., 2011). Terpene content was not found to be affected by sludge treatment but leaf and stem growth were enhanced significantly. The long-term nature of the experiment allowed Olivier et al. (2011) to conclude that there was no direct effect on leaf terpene emissions due to application of sewage sludge but that it indirectly lead to their increase through enhanced leaf biomass.

The aim of the experiment described in this chapter was to assess the short-term effect of nitrogen fertiliser on CH_3X and BVOC fluxes from SRC willow. Other studies have examined the effect of fertiliser on the CO_2 mitigating capabilities of SRC willow as a bioenergy crop. The short term effect of nitrogen fertilisation on budgets of N_2O from the other main bioenergy crop *Miscanthus* has been studied and the emission rates of BVOCs from waste-treated tree species have also been observed but no previous work exists on the short term effect of fertiliser on fluxes of CH_3X and BVOCs from SRC willow.

7.2 Experimental design

In order to assess the short-term effect of nitrogen fertiliser on CH_3X and BVOC fluxes from SRC willow, several willow cuttings were taken from the Arnot and Brattleby field sites and

were grown in soil taken from the corresponding site. The fieldsites are described in Sections 2.7.2 and 2.7.1, respectively. The willow trees at the Arnot fieldsite were previously treated with 15 tonnes per hectare of lime stabilised sewage sludge cake during the establishment phase (June 2008). This is equivalent to around 338 kg N ha^{-1} if the N content is defined as 40.3 g kg^{-1} (Guo et al., 2012). This was the only treatment applied to these crops. At the Brattleby fieldsite, the bioenergy crops did not receive any nitrogen fertiliser during this research nor during the establishment phase.

Six willow cuttings were taken from the Brattleby fieldsite and six from the Arnot fieldsite in mid-March 2012 and planted immediately. The 30 cm cuttings were planted in buckets of 10 L capacity filled with soil taken from the corresponding fieldsite to a depth of around 10 cm. Although the intention had been to allow the plants to grow outside in order to mimic natural conditions as closely as possible, the cuttings were grown in the greenhouse as the inclement weather conditions (in 2012 the UK experienced the wettest April, May and June for over a century) made it impossible for the plants to survive outside.

After allowing 3 months for the plants to establish themselves, baseline flux measurements were taken 2 weeks before and the day before the application of fertiliser (see Table 7.1). Further samples were then taken immediately after the application of the fertiliser and at 24 hours, 72 hours and 168 hours after application.

During the experiment the photosynthetically-active radiation (PAR), total solar radiation and the inner chamber temperature were recorded every 2 seconds via a small weather station (H21-002 Hobo Micro Station Data Logger, Onset Computer Corporation, Bourne MA, USA). The PAR sensor (S-LIA-M003 Photosynthetic Light Smart Sensor, Onset Computer Corporation, Bourne MA, USA) and total solar radiation sensor (S-LIB-M003 Solar Radiation Sensor, Onset Computer Corporation, Bourne MA, USA) were mounted level on a tripod at the same height as the vegetation inside the enclosure. The ambient air temperature was recorded by a stainless steel temperature probe (S-TMB-M002 12-Bit Temp Smart Sensor, Onset Computer Corporation, Bourne MA, USA) which was placed at vegetation height.

Three plants from each field site were designated as controls and three received fertiliser treatment, giving 3 replicates of treated and non-treated plants for each field and a total of 6 treated plants and 6 controls. 1 g of NH_4NO_3 fertiliser dissolved in 0.5 L of deionised water (equivalent to 50 kg N ha^{-1}) was applied to the soil of each non-control plant. 0.5 L deionised water added to the soil of the control plants.

7.2.1 Vegetation enclosure design

Samples were taken using adapted commercially bought hemispherical plexiglass (poly(methyl methacrylate)) plant protection enclosure chambers with a 45 cm diameter and volume of

Table 7.1: Timetable of fertiliser experiment on SRC willow from Arnot and Brattleby.

Day	Date	Activity
	15th March	Cuttings planted
	30th March	Plants moved inside greenhouse
-14	19th June	Pre-treatment samples taken
-1	2nd July	Pre-treatment samples taken
0	3rd July	Treatment applied to pots
0	3rd July	Post-treatment samples taken
1	4th July	Post-treatment samples taken
3	6th July	Post-treatment samples taken
7	10th July	Post-treatment samples taken

23.86 L (Figure 7.1). These were previously fitted with sampling valves cut from Tedlar bags. Polyethylene sheets were attached round the open edge of the chamber to allow them to be tied around the plant pot to create an enclosure.

7.2.2 Sample collection

For CH_3X measurements, a background ambient sample was taken before the plant and soil in the bucket were enclosed for 10 minutes, in a similar manner to the long-term sampling technique described in Section 2.2.1. An air sample was extracted using an acrylic gas syringe (1000MAR-LL-GT, SGE Analytical Science Pty Ltd, Ringwood, VIC, Australia) with three-way tap and then stored in 1 L Tedlar bags (polyvinyl fluoride) with polypropylene valves (232-01, SKC Inc., PA, USA). Background samples of ambient air were collected and stored in the same manner. The sample volume typically ranged from 500 mL to 700 mL. Once filled the sample bags were stored in darkness until analysis. Samples were taken in sets of six, as six chambers were available, with three background samples for every six enclosure samples. It took around 30 minutes to take one whole set of samples. Due to problems with the analytical equipment at the time the CH_3X fluxes could not be determined.

Measurements of BVOCs were then taken, after allowing a gap of at least 15 minutes from the removal of the enclosure chambers for CH_3X measurements in order to flush the plants. Three plants were sampled at once, in a similar manner to the long-term sampling technique described in Section 2.3.1, with one background ambient sample taken concurrently for each set of three measurements. Samples were taken by pumping air from the enclosure through adsorbent-packed tubes at a rate of 200 ml min^{-1} for 10 minutes, to give a 2 L sample volume. Four mass-flow control Pocket Pumps (210-1000 Series, SKC Inc., PA, USA) were used to take the three enclosure samples and background sample almost concurrently. The pumps passed air through 6 mm OD stainless steel ATD tubes (L4270123, PerkinElmer, Waltham, MA,



Figure 7.1: Modified commercial plant protection chamber of around 24 L volume.

USA) packed with 200 mg poly(2,6-diphenylphenylene oxide) (Tenax® TA) (11982 SUPELCO, Sigma Aldrich, St Louis, MO, USA) and 100 mg Carbotrap® (20273 SUPELCO, Sigma Aldrich, St Louis, MO, USA). Prior to sampling, the packed tubes were conditioned at 300 °C for 15 minutes with a flow of helium (100 mL min^{-1}). Samples were then analysed for BVOCs using GC techniques as described in Section 2.3.4.

7.3 Results

Fluxes of BVOCs were measured during the 21 days of the experiment, with a range of net isoprene fluxes between 0.03 and 14.5 $\mu g\, g^{-1}\, h^{-1}$. Monoterpene fluxes (α-pinene, limonene and δ-3-carene) were smaller and ranged between zero and 0.68 $\mu g\, g^{-1}\, h^{-1}$. These flux ranges are consistent with the range of fluxes derived from the monthly measurements made at the Arnot and Brattleby fieldsites.

7.3.1 Arnot

Fluxes of isoprene and δ-3-carene measured from both treated and untreated plants followed the same general trend, seeming to vary more greatly with the conditions on the day of sampling

than with any treatment applied (see Figures 7.2a and 7.2d). The flux trends closely follow the trends in air temperature and PAR level and no clear response to the application of nitrogen fertiliser could be identified.

Temperatures and PAR levels were highest when measurements were taken on the day of treatment and again 24 hours later, making it difficult to distinguish the effects of the treatment and the effects of the conditions on the variation in fluxes. However, fluxes of isoprene and δ-3-carene from both treated and untreated plots were very similar, apart from one high isoprene flux (15 $\mu g\, g^{-1}\, h^{-1}$) from an untreated plot, making it unlikely that the treatment had a great effect on fluxes.

Measured fluxes of α-pinene and limonene followed a similar trend to isoprene and δ-3-carene fluxes but were lower or zero during pre-treatment and therefore appeared to respond more obviously to treatment rather than environmental conditions. The untreated plots emitted greater quantities of α-pinene than the treated plots, suggesting a possible suppression of α-pinene emissions by fertiliser treatment. Fluxes of limonene from treated and untreated plots followed an almost identical trend.

Before fertilizer application, isoprene fluxes were between and 0.06 and 5.4 $\mu g\, g^{-1}\, h^{-1}$, which ties in with the monthly measurements taken from the willow plants at Arnot (Figure 7.2a). Immediately after application of fertiliser to treated plots and deionised water to untreated plots, isoprene fluxes at the treated plots did not change dramatically (between 2 and 3.1 $\mu g\, g^{-1}\, h^{-1}$) but fluxes from untreated plots rose to between 1.6 and 15 $\mu g\, g^{-1}\, h^{-1}$.

24 hours after fertiliser application to treated plots, isoprene fluxes from the treated plots remained very similar to the measurements taken immediately after fertiliser application, ranging between 0.48 and 2.4 $\mu g\, g^{-1}\, h^{-1}$. Fluxes from untreated plots fell to between 1.1 - 2.1 $\mu g\, g^{-1}\, h^{-1}$. Isoprene fluxes of between 0.03 and 3.7 $\mu g\, g^{-1}\, h^{-1}$ from the treated plots were measured 3 days and 7 days after fertiliser application and fluxes from the untreated plots ranged between 0.07 and 1.5 $\mu g\, g^{-1}\, h^{-1}$.

The maximum isoprene fluxes measured from the treated plants occurred 2 weeks before the treatment began (a maximum of 3.9 $\mu g\, g^{-1}\, h^{-1}$) and then again immediately after fertiliser application (a maximum of 3.1 $\mu g\, g^{-1}\, h^{-1}$). The untreated plants reached their maximum isoprene fluxes immediately after the application of deionised water as a control for the addition of fertiliser to the treated plants (a maximum of 15 $\mu g\, g^{-1}\, h^{-1}$).

Before the application of any fertilizer to treated plots, α-pinene fluxes were between zero and 0.12 $\mu g\, g^{-1}\, h^{-1}$ (Figure 7.2b), which is in agreement with the monthly measurements taken from the willow plants at Arnot. Immediately after the application of fertiliser to treated plots and deionised water to untreated plots, α-pinene fluxes were unchanged, ranging between 0.04 and 0.07 $\mu g\, g^{-1}\, h^{-1}$ for treated plots and between 0.08 and 0.19 $\mu g\, g^{-1}\, h^{-1}$ for untreated

plots.

Fluxes of α-pinene were slightly higher from treated plots 24 hours after the application of fertiliser, with a range of fluxes between 0.05 and 0.12 $\mu g\, g^{-1}\, h^{-1}$. However, fluxes were also slightly higher from untreated plots after 24 hours, with a range of between 0.15 and 0.29 $\mu g\, g^{-1}\, h^{-1}$.

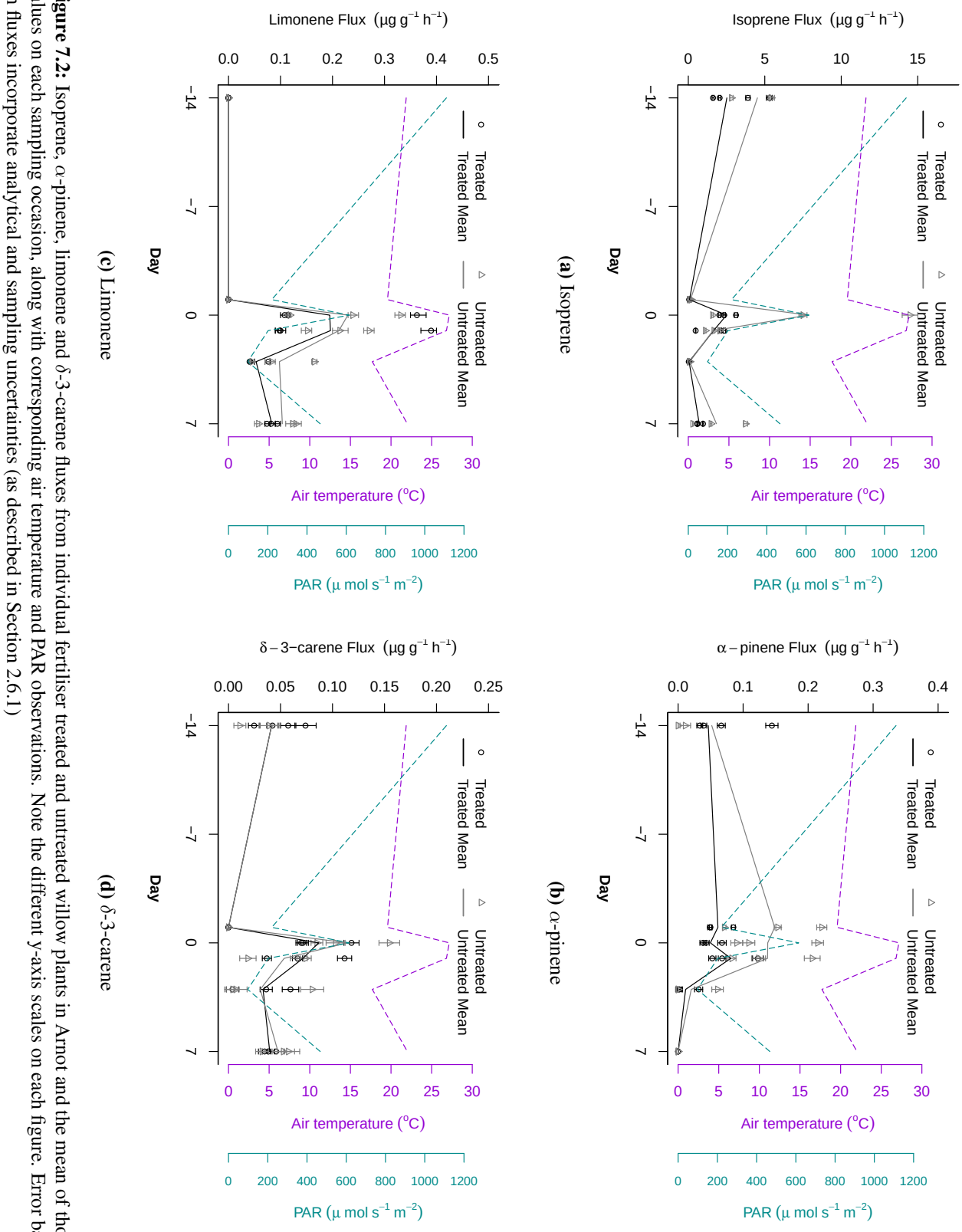
3 days after fertiliser application, α-pinene fluxes fell to between zero and 0.03 $\mu g\, g^{-1}\, h^{-1}$ from treated plots and between zero and 0.22 $\mu g\, g^{-1}\, h^{-1}$ from untreated plots. Zero fluxes were measured from all plots after 7 days.

No limonene fluxes were measured at any of the plots before the application of fertiliser or deionised water to the treated and untreated plots respectively (Figure 7.2c). Immediately after treatment, limonene fluxes rose to between 0.11 and 0.36 $\mu g\, g^{-1}\, h^{-1}$ for treated plots and fluxes of between 0.11 and 0.68 $\mu g\, g^{-1}\, h^{-1}$ were measured at untreated plots.

After 24 hours, fluxes of limonene remained unchanged. After 3 days and 7 days, fluxes fell to between 0.04 and 0.09 $\mu g\, g^{-1}\, h^{-1}$ from treated plots and between zero and 0.25 $\mu g\, g^{-1}\, h^{-1}$ from untreated plots.

Baseline flux measurements of δ-3-carene taken before treatment encompassed the range from zero to 0.07 $\mu g\, g^{-1}\, h^{-1}$ (Figure 7.2d). Fluxes increased after treatment, with a range of 0.07 to 0.12 $\mu g\, g^{-1}\, h^{-1}$ from treated plots and 0.07 to 0.21 $\mu g\, g^{-1}\, h^{-1}$ from untreated plots.

After 24 hours, fluxes from all plots decreased to between 0.04 and 0.11 $\mu g\, g^{-1}\, h^{-1}$ from treated and 0.09 and 0.15 $\mu g\, g^{-1}\, h^{-1}$ from untreated plots. After 3 days they decreased again to between zero and 0.06 $\mu g\, g^{-1}\, h^{-1}$ from treated and 0.01 and 0.06 $\mu g\, g^{-1}\, h^{-1}$ from untreated plots. After 7 days they decreased slightly to between 0.03 and 0.05 $\mu g\, g^{-1}\, h^{-1}$ from treated and 0.07 and 0.08 $\mu g\, g^{-1}\, h^{-1}$ from untreated plots.



(a) Isoprene **(b)** α-pinene **(c)** Limonene **(d)** δ-3-carene

Figure 7.2: Isoprene, α-pinene, limonene and δ-3-carene fluxes from individual fertiliser treated and untreated willow plants in Arnot and the mean of those values on each sampling occasion, along with corresponding air temperature and PAR observations. Note the different y-axis scales on each figure. Error bars on fluxes incorporate analytical and sampling uncertainties (as described in Section 2.6.1)

7.3.2 Brattleby

Similarly to the results from the Arnot plots, fluxes of isoprene measured from both treated and untreated plants from Brattleby followed the same general trend, varying more notably with sunshine and temperature levels than treatment applied (see Figures 7.3a and 7.3d). Fluxes of α-pinene, limonene and δ-3-carene appeared to be more responsive to treatment, with higher mean emissions from fertiliser treated plots than from untreated plots.

Fluxes of isoprene were at a maximum on the first day of measurement (two weeks before application of fertiliser) ranging between and 0.62 and 6.7 $\mu g\, g^{-1}\, h^{-1}$ (Figure 7.3a). Fluxes fell to between 0.06 to 0.32 $\mu g\, g^{-1}\, h^{-1}$ on the day before treatment. Fluxes from treated and untreated plots were larger immediately after application of fertiliser to treated plots and deionised water to untreated plots to between 0.19 and 4.4 $\mu g\, g^{-1}\, h^{-1}$. Fluxes from treated plots varied between 0.19 and 4.3 $\mu g\, g^{-1}\, h^{-1}$ and from untreated plots between 0.97 and 2.6 $\mu g\, g^{-1}\, h^{-1}$.

24 hours later, fluxes from all plots had decreased to between 0.26 and 0.97 $\mu g\, g^{-1}\, h^{-1}$. After 3 days, fluxes from all plots fell to between 0.04 and 0.12 $\mu g\, g^{-1}\, h^{-1}$ before rising again to between 0.08 and 1.9 $\mu g\, g^{-1}\, h^{-1}$ after 7 days.

Two weeks before treatment, fluxes of α-pinene were low, varying between zero and 0.12 $\mu g\, g^{-1}\, h^{-1}$ (Figure 7.3b). This increased slightly to between 0.06 and 0.13 $\mu g\, g^{-1}\, h^{-1}$ the day before treatment. Immediately after treatment fluxes from one treated plot increased to 0.19 $\mu g\, g^{-1}\, h^{-1}$ but the others remained within the same range as the day before.

Fluxes of α-pinene were slightly higher from treated plots 24 hours after the application of fertiliser, with a range of fluxes between 0.15 and 0.29 $\mu g\, g^{-1}\, h^{-1}$. However, fluxes were also slightly higher, though not as high, from untreated plots after 24 hours, with a range of between 0.08 and 0.13 $\mu g\, g^{-1}\, h^{-1}$.

3 days after fertiliser application, α-pinene fluxes fell slightly from all plots to between zero and 0.08 $\mu g\, g^{-1}\, h^{-1}$, with the exception of one treated plot where a flux of 0.22 $\mu g\, g^{-1}\, h^{-1}$ was measured. Zero fluxes were measured from all plots 7 days after treatment.

Zero limonene fluxes were measured before the application of fertiliser or deionised water to the treated and untreated plots respectively (Figure 7.3c). Immediately after treatment, limonene fluxes rose to between 0.11 and 0.68 $\mu g\, g^{-1}\, h^{-1}$ for treated plots and fluxes of between 0.13 and 0.33 $\mu g\, g^{-1}\, h^{-1}$ were measured at untreated plots.

After 24 hours, fluxes of limonene remained almost unchanged at both the treated plots and untreated plots . After 3 days fluxes fell to between zero and 0.25 $\mu g\, g^{-1}\, h^{-1}$ from treated plots and between zero and 0.14 $\mu g\, g^{-1}\, h^{-1}$ from untreated plots. A similar range was measured after 7 days.

Measurements of δ-3-carene taken before treatment found a range of fluxes between zero and 0.06 $\mu g\, g^{-1}\, h^{-1}$ (Figure 7.3d). Fluxes increased after treatment, with treated plots increasing the most to between 0.07 and 0.21 $\mu g\, g^{-1}\, h^{-1}$ untreated plots increasing slightly to between and 0.06 and 0.10 $\mu g\, g^{-1}\, h^{-1}$.

After 24 hours, fluxes at untreated plots remained similar but fluxes from treated plots decreased to between 0.09 and 0.15 $\mu g\, g^{-1}\, h^{-1}$. After 3 days fluxes from all plots decreased slightly to between 0.01 and 0.06 $\mu g\, g^{-1}\, h^{-1}$ from treated and 0.01 and 0.08 $\mu g\, g^{-1}\, h^{-1}$ from untreated plots. After 7 days fluxes at the treated plots stayed at the top end of the range measured after 3 days, with fluxes of between 0.07 and 0.08 $\mu g\, g^{-1}\, h^{-1}$. Fluxes from untreated plots were mid-range in comparison to those measured after 3 days, varying between 0.04 and 0.05 $\mu g\, g^{-1}\, h^{-1}$.

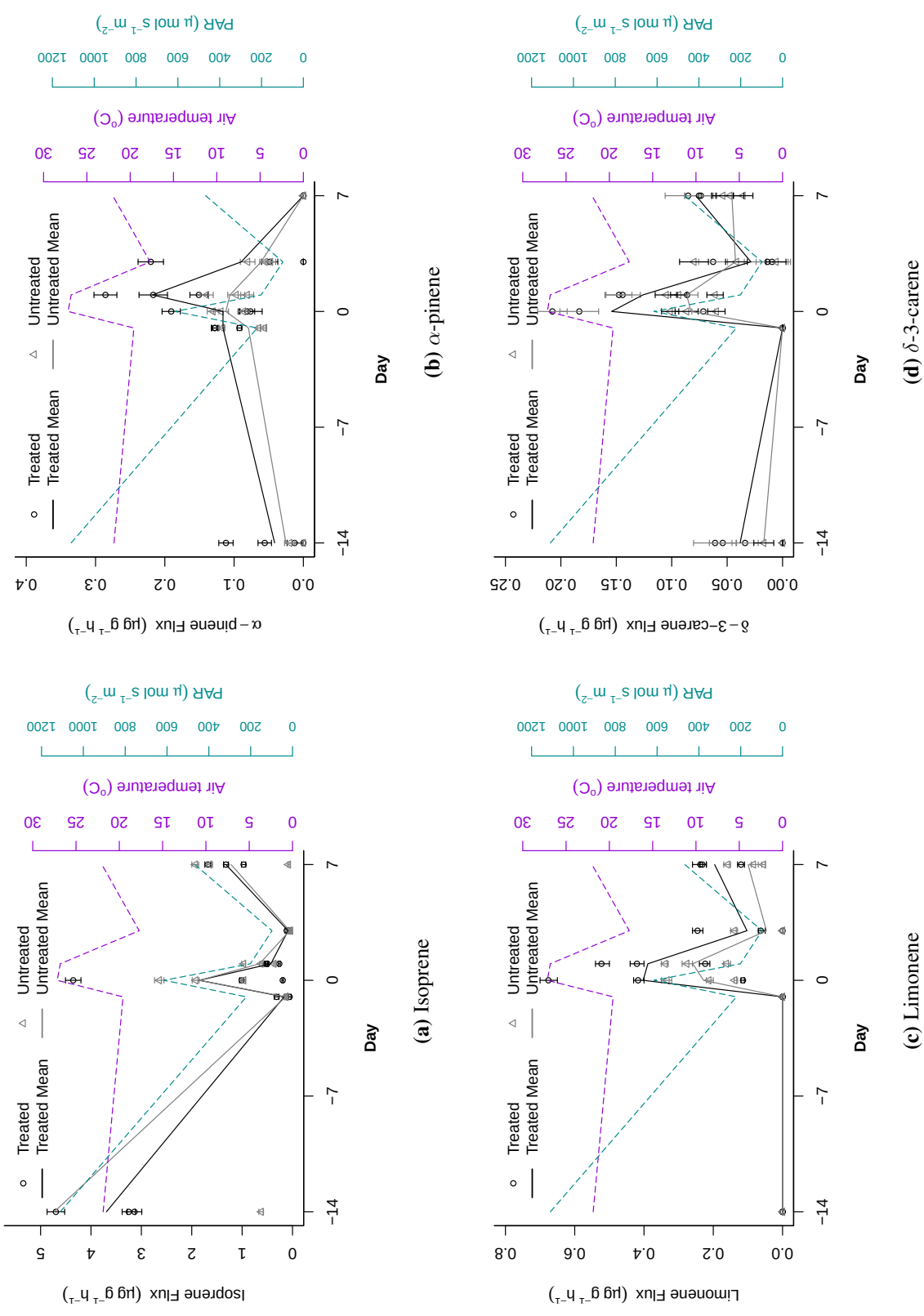


Figure 7.3: Isoprene, α-pinene, limonene and δ-3-carene fluxes from individual fertiliser treated and untreated willow plants from Brattleby and the mean of those values on each sampling occasion, along with corresponding air temperature and PAR observations. Note the different y-axis scales on each figure. Error bars on fluxes incorporate analytical and sampling uncertainties (as described in Section 2.6.1)

7.3.3 Statistical Analysis

Data were checked for normality and homogeneity by visual inspections of plots of residuals against fitted values. Using multivariate ANOVA (R Core Team, 2012), the amount of variation in fluxes associated with different factors was investigated. The associations of isoprene, α-pinene, limonene and δ-3-carene fluxes with sampling day, the plant sampled, the treatment regime and the fieldsite that the plant and soil came from were determined.

Fluxes of isoprene, α-pinene, limonene and δ-3-carene were found to vary significantly with sampling day with F values of 10.3, 11.2, 18.5 and 19.6, respectively and corresponding $p < 0.05$ (Table 7.2). However, no such significance was found with treatment however, nor with plant sampled or fieldsite that the plant and soil were taken from.

Table 7.2: Analysis using multivariate ANOVA of isoprene, α-pinene, limonene and δ-3-carene flux variation with sampling day, plant, treatment and fieldsite. Degrees of freedom (D.f), F and p values for these effects on BVOC fluxes from treated and untreated willow plants are presented. Significant variation in BVOC flux ($p \leq 0.05$) is highlighted in bold.

		Isoprene		α-pinene		Limonene		δ-3-carene	
	d.f	F	p	F	p	F	p	F	p
Day	5	**10.3**	< 0.001	**11.2**	< 0.001	**18.5**	< 0.001	**19.6**	< 0.001
Plant	11	0.873	0.57	0.89	0.55	0.92	0.53	0.83	0.61
Treatment	1	2.18	0.14	0.06	0.80	0.69	0.41	1.07	0.31
Fieldsite	1	0.92	0.34	1.28	0.26	1.85	0.18	1.12	0.29

A linear mixed effects model was fitted using the R packages "lme4" (Bates et al., 2012) and "languageR" (Baayen, 2011) in order to investigate changes in BVOC fluxes with nitrogen treatment as a fixed effect and day, plant and site as random effects. To assess the validity of the mixed effects analyses, likelihood ratio tests were performed by comparing the models with fixed effects to the null models with only the random effects. Results for all BVOC fluxes were rejected as the model including fixed effects did not differ significantly from the null model.

As it was apparent that all BVOC fluxes varied significantly with sampling day, and the only thing that changed between sampling days apart from treatment timing was the environmental conditions, correlations between fluxes and environmental variables were tested for significance. In order to test for any significant correlations between environmental parameters and fluxes measured, all fluxes for a particular plant pot were first normalised to the maximum flux measured for that pot during the entire experiment. This dataset was used to assess the influences of air temperature and PAR levels on BVOC fluxes by dividing the data into two sets, treated and untreated plants, and then testing for significant correlations with the two environmental variables using multi-variate ANOVA.

The temperature range in the greenhouse during measurements varied between 17 and 28 °C and the PAR levels varied between 83 and 1230 μmol m^{-2} s^{-1}. Very similar significant correlations were found for both treated and untreated plants (Table 7.3). Significant correlations were found between isoprene and PAR for both treated and untreated plants with *r* values of 0.79 and 0.73 respectively. A significant negative correlation was found between limonene and PAR in the treated plants but was not significant for the untreated plants, although the correlation coefficients were quite similar (*r* values of -0.36 and -0.28 for treated and untreated respectively). Fluxes of isoprene, α-pinene and limonene from both treated and untreated plants were significantly correlated with ambient air temperature (*r* values between 0.37 and 0.63).

Table 7.3: Pearson product-moment correlation coefficients between PAR, air temperature and normalised BVOC fluxes (isoprene, α-pinene, limonene and δ-3-carene) from fertiliser treated and untreated willow plants. Significant correlations ($p \leq 0.05$) are highlighted in bold.

	Treated		Unreated	
	PAR	$T_{ambient\ air}$	PAR	$T_{ambient\ air}$
Isoprene	**0.789**	**0.418**	**0.728**	**0.367**
α-pinene	-0.015	**0.463**	-0.024	**0.445**
Limonene	**-0.360**	**0.518**	-0.276	**0.633**
δ-3-carene	0.126	0.147	0.207	0.198

7.4 Summary

The results presented in this chapter describe the short-term effects of nitrogen fertiliser on BVOC fluxes from SRC willow. There was no clear increase or decrease in fluxes of BVOCs in response to fertiliser treatment, instead fluxes were found to vary significantly with some of the environmental parameters observed. There was no evidence that strong correlations of fluxes to PAR and air temperature masked response to fertiliser treatment effects. The trends in fluxes found from SRC willow cuttings taken from the Arnot fieldsite were very similar to those found at the Brattleby fieldsite.

Although no short-term effects on BVOC emissions were observed in this experiment, it is likely that application of fertiliser to willow trees will result in long-term effects on emissions. Willow trees are known to respond to N inputs and it has been shown that N fertiliser increases total willow biomass significantly (Arevalo et al., 2005). One long-term experiment has shown that greater leaf biomass due to fertilisation leads to increased BVOC emissions (Olivier et al., 2011). The long-term measurements carried out at the Arnot and Brattleby fieldsites (from which the cuttings for this experiment were taken from) show that willow trees are an important source of isoprene emissions (see Section 4.2.7). An increase in leaf biomass due to fertiliser

treatment would most likely lead to even greater isoprene emissions, although this would need to be investigated.

If fertiliser is to be used then using some form of treated sewage sludge rather than commercial treatments, for example the lime stabilised sewage sludge cake employed at the Arnot fieldsite during the establishment phase, would improve the environmental performance of willow biomass crop production systems, as previously calculated in a Life Cycle Analysis (LCA) by Heller et al. (2003). Increased total willow biomass would also presumably mean that more energy could be generated from the crops which might improve the net energy ratio calculated in a LCA, depending on the amount of energy required to produce and apply the treatment.

The use of fertiliser on bioenergy crops such as SRC willow is important because it also affects their associated greenhouse gas budgets. In comparison to annual arable crops, willow bioenergy crops are less nitrogen demanding with much lower nitrogen to dry matter ratios (Tilman et al., 2006) resulting in smaller N_2O emissions (Crutzen et al., 2007). Measurements taken at the Brattleby fieldsite by Drewer et al. (2011) have shown that N_2O emissions from the soil under willow are significantly lower than those from fields planted with wheat and oilseed rape rotations (8 kg CO_2 eq. ha^{-1} y^{-1} from willow and 339 and 1326 kg CO_2 eq. ha^{-1} y^{-1} from fields planted with wheat and oilseed rape rotations). However, a fertilisation experiment carried out on *Miscanthus* plants at the same site has shown that application of N fertiliser to bioenergy crops will probably significantly increase N_2O emissions (Drewer et al., 2011).

The perceived environmental benefits of bioenergy crops, such as CO_2 mitigation, may be reduced by the use of fertiliser. Unfertilised bioenergy crops emit significantly less N_2O than annual arable crops. However, if fertiliser is used on bioenergy crops, as is common in countries such as Ireland, their environmental benefits in comparison to annual arable crops are reduced. A significant increase in N_2O emissions is predicted and the possibility of long-term increases in isoprene emissions must also be considered.

Chapter 8

Scale up of CH_3X and BVOC fluxes

8.1 Introduction

In order to improve our knowledge of atmospheric composition at different spatial and temporal resolutions, two techniques are employed. The first of these is the top-down approach which uses data from satellites or air sampling networks combined with knowledge of atmospheric processes. This aids the study of the strength and location of global scale sources and sinks. The other is the bottom-up approach, which utilises measurements made at smaller spatial scales and often includes comparative and process studies such as manipulation experiments to provide information on mechanisms. These measurements allow the development and validation of atmosphere-biosphere models. Both techniques have their benefits and drawbacks and a combination of both approaches is necessary to better understand atmospheric composition at different scales.

Estimates of CH_3X and BVOC fluxes have been calculated using modelling methods (Anastasi et al., 1991; Ashworth et al., 2013; Guenther et al., 1995, 2000; Helmig et al., 1999; Karl et al., 2009; Lee-Taylor et al., 2001; Lee-Taylor and Redeker, 2005; Warwick et al., 2006a; Yoshida et al., 2006). However, there is a lack of data on these fluxes from terrestrial vegetation with which to develop modelling systems. There is also great spatial and temporal variability in fluxes which hinders the estimation of current and future budgets.

Difficulties have previously been encountered when scaling up fluxes from limited temporal and spatial measurements. For example, whilst there was good agreement between Dimmer et al. (2001) and Varner et al. (1999a) on estimated global emissions of CH_3Br from peatlands based on measurements in different parts of the world, their estimated emissions of CH_3Cl differed by an order of magnitude. Three studies on isoprene emissions from *Salix alba* at various locations worldwide found three different standard emission rates (Karl et al., 2009; Niinemets et al., 2010; Pio et al., 1993), therefore estimating global emissions with these individual results would give three different outcomes. It is important to use representative data collected from different sites in order to reduce uncertainties in estimating budgets.

Previously, CH_3Br fluxes from litter decomposition (Lee-Taylor et al., 2001), temperate woodlands (Drewer, 2007) and rice paddies (Lee-Taylor and Redeker, 2005) have been estimated. Blei (2010) also used measurements from temperate forest leaf litter to scale up to global estimates of CH_3Br and CH_3Cl from leaf litter. Global models of CH_3Br (Warwick et al., 2006a) and CH_3Cl (Yoshida et al., 2006) have endeavoured to balance atmospheric budgets of CH_3X by refining current estimates of sources and sinks and ascertaining whether there are unidentified sources (see Section 1.3.1).

There are a multitude of BVOC emission estimates, beginning half a century ago with an estimated total BVOC emission of 175 $Tg\,C\,y^{-1}$ calculated by Went (1960). Twenty years later the estimate had more than doubled to 480 $Tg\,C\,y^{-1}$ (Zimmerman, 1979) and more than doubled again after a further 15 years, with current estimates of 1150 $Tg\,C\,y^{-1}$ (Guenther et al., 1995) (see Table 8.1). More recently, region-specific BVOC emission inventories have been produced for the USA (Guenther et al., 2000; Helmig et al., 1999), the UK (Anastasi et al., 1991) and Europe (Karl et al., 2009).

Table 8.1: Global BVOC emission rate estimates ($Tg\,C\,y^{-1}$) for isoprene, monoterpenes and total BVOCs from the literature.

	Isoprene	Monoterpenes	Total
Went (1960)			175
Rasmussen and Went (1965)			432
Robinson and Robbins (1968)			480
Zimmerman (1979)	350	480	
Rasmussen and Khalil (1988)	452		
Warneck (1988)			>800
Dignon and Logan (1990)	450		
Turner et al. (1991)	285		
Müller (1992)	250	147	
Guenther et al. (1995)	503	127	1150

Many of the BVOC emission estimates are based on canopy-scale measurements. However, extrapolating branch-level emission measurements to give emission rates, as is done here, provides information on compound speciation and source strength. These estimates can also provide emission inputs for atmospheric chemistry models for vegetation types where canopy-scale measurements have not been made.

The scaling-up of fluxes measured in this work using vegetation enclosures is intrinsically challenging. The flux datasets are limited to three sites and are not temporally and spatially resolved for all manifestations of all types of bioenergy plantation. Uncertainties arise in extrapolating spatial and temporal point measurements to all such vegetation and times. However, the long-term nature of these studies and the large number of measurements over spatial area

and range of field sites should contribute to estimates of CH_3X and BVOC budgets based on a more accurate characterisation of underpinning fluxes.

Currently, total UK plantings of *Miscanthus* and SRC willow are minor in comparison to annual arable crops such as oilseed rape and wheat (DEFRA, 2009). However, due to concerns about climate change and energy security, the government is seeking to increase the amount of perennial energy crops produced in the UK, with the potential to use up to around 6% of UK total arable land by 2020 (DEFRA, 2007). In Europe, it is anticipated that crop yields will continue to increase, releasing substantial areas of agricultural land for the expansion of bioenergy plantations (Ewert et al., 2005). However, estimations of future land requirements are fairly speculative due to the limited information on the anticipated supply and spatial yield data of these crops and how this will develop in the future (Aylott et al., 2008).

Taking into account the results reported in this thesis, a tentative estimate of UK- and Europe-wide net methyl halide and BVOC emissions from the perennial bioenergy crops *Miscanthus* and SRC willow are made for current land cover area and potential future land cover area.

8.2 Method

Initially, mean CH_3X and BVOC fluxes from each bioenergy crop type were determined. Important considerations in this step were:

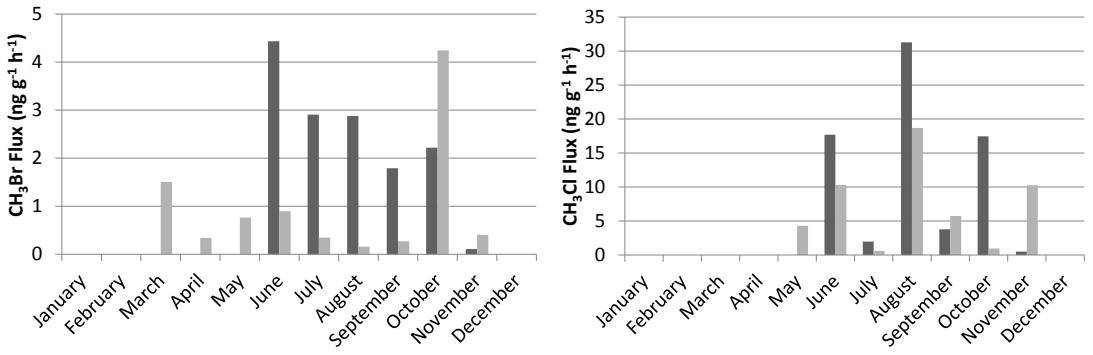
- temporal variation in fluxes on seasonal timescales
- temporal variation in fluxes on diurnal timescales

Accounting for seasonal variation was straightforward as emissions from the bioenergy crops only occurred during the growing season and no emission or uptake was measured during the non-growing season. The mean emissions were individually calculated at each sampling point and field site for each month of the year using measurements for that month from 2010, 2011 and 2012 for CH_3X (Figure 8.1) and BVOCs (Figure 8.2). A mean annual net flux, which included the growing and the non-growing season, was then calculated for CH_3X and BVOCs.

It should be noted however that the data does not show a perfect seasonal pattern. There was a larger than expected mean CH_3Br flux from SRC willow in October (due to one very high flux, as discussed in Section 4.2.3). There were smaller than expected mean CH_3Cl fluxes from both *Miscanthus* and SRC willow in July (probably due to the weather conditions on the day of measurement, as discussed in Sections 3.3.1 and 4.2.3).

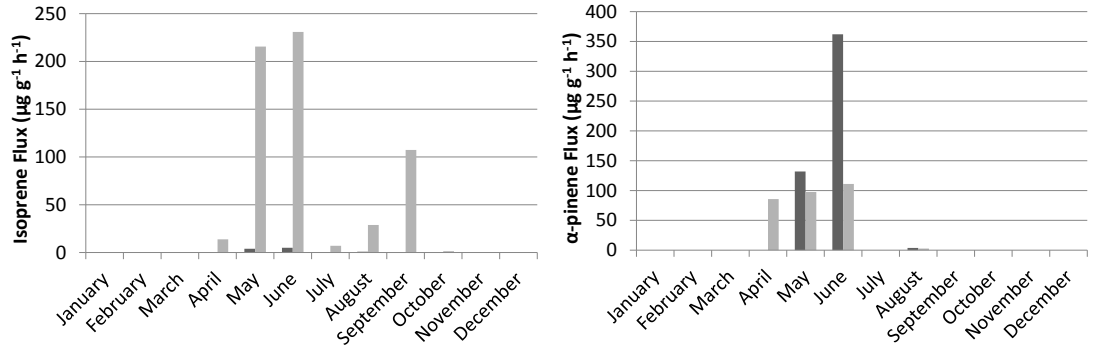
Mean fluxes of isoprene from SRC willow were also lower than expected in July and August. This is probably due to the lower emissions from the recently harvest plants in 2011 (as discussed in Section 4.2.7). It is also important to note that for the purposes of this scale-up it was assumed

that the mean α-pinene fluxes calculated for *Miscanthus* were representative and relevant despite the uncertainty surrounding the large fluxes measured in 2010 and the detection of very low fluxes in 2011 and 2012 (as discussed in Section 3.4.1).



(a) CH_3Br **(b)** CH_3Cl

Figure 8.1: Monthly mean CH_3Br and CH_3Cl emissions from all *Miscanthus* (■) and SRC willow (■) sampling points and fieldsites from January to December.



(a) Isoprene **(b)** α-pinene

Figure 8.2: Monthly mean isoprene and α-pinene emissions from all *Miscanthus* (■) and SRC willow (■) sampling points and fieldsites from January to December.

It was more difficult to account for diurnal variation in the scale up calculations. Evaluation of the full and sub-diurnal studies (discussed in detail in the relevant bioenergy crop chapter) demonstrated that the majority of the fluxes measured at night-time were zero. However, during the sub-diurnal measurements it was often found that fluxes did not conform to a standard diurnal cycle i.e. fluxes were not always at a maximum at midday. It was therefore assumed for the purposes of scaling up that the measurements were made at some intermediate point between the maximum and minimum flux and that the value would suffice as a mean value for that 24 hour period.

The annual mean net fluxes ($\pm$ the standard error of the mean) of CH_3Br and CH_3Cl were calculated as 1.2 ± 0.6 ng g^{-1} h^{-1} and 6.1 ± 3.5 ng g^{-1} h^{-1} respectively, from *Miscanthus* and

0.74 ± 0.3 ng g^{-1} h^{-1} and 4.2 ± 3 ng g^{-1} h^{-1} respectively, from SRC willow. The annual mean net fluxes of isoprene and α-pinene were calculated to be 0.85 ± 0.5 µg g^{-1} h^{-1} and 41 ± 37 µg g^{-1} h^{-1} from *Miscanthus* and 33 ± 25 µg g^{-1} h^{-1} and 17 ± 13 µg g^{-1} h^{-1} from SRC willow, respectively. No standard deviation values are given since it is felt that they would imply an unrealistic level of precision. However the standard error of the mean (SEM) was calculated for the annual mean net fluxes employed as this establishes a reasonable estimate of the error in this value. The large SEM values calculated demonstrate the inherent uncertainty associated with extrapolating spatial and temporal point measurements of fluxes.

The annual mean net fluxes were then converted from units per $g_{(dry\,weight)}$ to units per m^2 using a foliar biomass density of 150 $g_{(dry\,weight)}$ m^{-2} for SRC willow (Karl et al., 2009) and a planting density of 4 plants per m^2 for *Miscanthus* (Bullard and Nixon, 1999). For *Miscanthus* it was assumed that around half of the *Miscanthus* plant biomass was enclosed during measurements so the annual mean net flux calculated was doubled before it was used for scaling up of fluxes. The annual mean net fluxes per m^2 were then converted into g ha^{-1} y^{-1} and scaled up via multiplication by estimates of current and future land cover of perennial bioenergy crops in the UK and Europe as in Equation 8.2.1.

$$UK/Europe\,Regional\,Flux = local\,flux \times land\,area \tag{8.2.1}$$

Some assumptions were made; that all sites in the UK and Europe exhibit similar flux trends to the sites studied, that planting densities are the same at all crop sites, that fluxes from unenclosed vegetation are the same as the enclosed vegetation, and that the influence of variations in light and temperature with changing latitude is negligible. The latter assumption is reasonable for CH_3X as they are relatively long-lived and therefore seasonality does not affect their overall impact on global atmospheric chemistry. However, seasonality is important for BVOCs in terms of their impact on SOA and O_3 photochemical formation as both emissions and light levels and temperatures are higher in summer, enhancing the atmospheric processes by which BVOCs impact on global atmospheric budgets (as discussed in Chapter 9).

Also, soil fluxes and fluxes from leaf litter were not included as no data was available. Inclusion of soil and leaf litter fluxes may have increased or decreased the total CH_3X fluxes calculated as leaf litter degradation has been found to be a source of CH_3X (e.g. Blei et al. (2010a)) and soil has previously been found to be both a source (e.g. Drewer et al. (2008)) and a sink (e.g. Rhew et al. (2010)) for CH_3X fluxes.

In the UK, the most recent available land-use data stated that there were 12 700 ha of *Miscanthus* and 6 400 ha of SRC willow at the end of 2009 (DEFRA, 2009). The total area planted with bioenergy crops is projected to increase to up to 350 000 ha in the next 10 years. In Europe in 2009/2010, the land cover area for *Miscanthus* was around 25 756 ha and for SRC

willow was around 24 185 ha (giving a total of 49 941 ha) (Don et al., 2011). Up to 72 Mha could be planted with bioenergy crops in the future (Ashworth et al., 2013).

Emissions from current land cover for *Miscanthus* and SRC willow individually and combined in the UK and in Europe were calculated. As there are no figures available for how many hectares will be planted with a specific type of perennial bioenergy crop in the future, three hypothetical scenarios were considered for the UK and for Europe:

- Full area available for bioenergy crops planted only with *Miscanthus*
- Full area planted only with SRC willow
- 50% of the area planted with *Miscanthus* and 50% with SRC willow

8.3 Results

8.3.1 CH_3X emission estimates

Estimates of both CH_3Br and CH_3Cl emissions from *Miscanthus* are relatively low at UK and Europe level for current UK and European land cover and potential future land cover (Table 8.2). Estimates for emissions under current land cover areas are 0.01 Mg y^{-1} and 0.02 Mg y^{-1} respectively for CH_3Br, and 0.05 Mg y^{-1} and 0.11 Mg y^{-1} respectively for CH_3Cl. If all of the land potentially available for perennial bioenergy crops is planted with *Miscanthus* only, the emissions for the UK and Europe are projected to increase to 0.29 Mg y^{-1} and 60 Mg y^{-1} respectively for CH_3Br, and to 1.5 Mg y^{-1} and 310 Mg y^{-1} respectively for CH_3Cl.

Emissions of CH_3Br and CH_3Cl from SRC willow are estimated to be slightly higher than for *Miscanthus* for both current and potential future land cover (Table 8.2). The estimated emissions from the current land cover in the UK and in Europe are 0.06 Mg y^{-1} and 0.24 Mg y^{-1} for CH_3Br and 0.36 Mg y^{-1} and 1.4 Mg y^{-1} for CH_3Cl, respectively. The estimates for emissions of CH_3Br and CH_3Cl from SRC willow are are around an order of magnitude higher than those from *Miscanthus*.

In future, if the potential land area available for perennial bioenergy crops in the UK and in Europe was planted only with SRC willow, emissions of CH_3Br are estimated to be around 3.4 Mg y^{-1} and 700 Mg y^{-1}, respectively. Emissions of CH_3Cl are estimated to be up to 19 Mg y^{-1} and 4000 Mg y^{-1}, respectively. Estimates for both CH_3Br and CH_3Cl from SRC willow are around an order of magnitude higher than those for *Miscanthus*.

If the 50/50 scenario is considered, where 50% of the potential bioenergy crop land is planted with *Miscanthus* and 50% with SRC willow, then CH_3X emissions are estimated to be lower than those from 100% SRC willow cover but higher than those from 100% *Miscanthus* cover as SRC willow makes the largest contribution.

Table 8.2: CH_3Br and CH_3Cl emission estimates in $Mg\,y^{-1}$ from *Miscanthus* and SRC willow individually and combined for current land area coverages in the UK and in Europe. Also given are emission estimates for potential future bioenergy crop land cover area for 3 scenarios; the first is that all potential bioenergy crop land is planted only with *Miscanthus* , the second that it is only planted with SRC willow and the third that it is planted with both, with 50% planted with *Miscanthus* and 50% with SRC willow. Standard errors of the mean are given in brackets.

		CH_3Br		CH_3Cl	
		Current	Future	Current	Future
UK	*Miscanthus*	0.01 ($\pm$ 0.006)	0.29 ($\pm$ 0.16)	0.05 ($\pm$ 0.03)	1.5 ($\pm$ 0.87)
	SRC willow	0.06 ($\pm$ 0.0002)	3.4 ($\pm$ 0.009)	0.36 ($\pm$ 0.002)	19 ($\pm$ 0.09)
	Both	0.07 ($\pm$ 0.006)	1.9 ($\pm$ 0.08)	0.41 ($\pm$ 0.03)	10 ($\pm$ 0.48)
Europe	*Miscanthus*	0.02 ($\pm$ 0.001)	60 ($\pm$ 32)	0.11 ($\pm$ 0.06)	310 ($\pm$ 180)
	SRC willow	0.24 ($\pm$ 0.001)	700 ($\pm$ 1.8)	1.4 ($\pm$ 0.006)	4000 ($\pm$ 19)
	Both	0.26 ($\pm$ 0.01)	380 ($\pm$ 17)	1.5 ($\pm$ 0.07)	2200 ($\pm$ 98)

8.3.2 Implications for CH_3X budgets

Using the estimated annual global turnover of $200\,Gg\,y^{-1}$ for CH_3Br and $4400\,Gg\,y^{-1}$ for CH_3Cl (WMO, 2006), the contribution of the estimated emissions from *Miscanthus* and SRC willow to global CH_3X budgets was calculated.

As a percentage of global turnover, the estimated contribution of CH_3X emissions from both *Miscanthus* and SRC willow are low (Table 8.3). Emissions from *Miscanthus* under current land cover in the UK and in Europe account for only 5×10^{-6}% and 1×10^{-5}% of global CH_3Br respectively. Emissions for the UK and Europe for a 100% *Miscanthus* land cover scenario are estimated to account for 2×10^{-4} % and 0.03 % of global CH_3Br respectively. Contributions to global CH_3Cl budgets are slightly smaller, with emissions from current land cover in the UK and Europe estimated to account for 1×10^{-6} % and 3×10^{-6} %, respectively. Under a 100% *Miscanthus* future land cover scenario, this is projected to increase to 3×10^{-5} % and 7×10^{-3} % respectively.

SRC willow is a slightly higher emitter of CH_3X in comparison to *Miscanthus* and therefore contributes slightly more to the global turnover (Table 8.3). Emissions of CH_3Br from current land cover in the UK and Europe account for 3×10^{-5} % and 1×10^{-4} % respectively of global CH_3Br. In future, this could rise to 0.002 % and 0.4 % of global CH_3Br respectively, if all potentially available land is planted with SRC willow. The contribution to global CH_3Cl turnover is again slightly less, with current UK and Europe land cover areas accounting for 8×10^{-6} % and 3×10^{-5} % of global CH_3Cl respectively. This could potentially rise to 4×10^{-4} % and 0.09 % of global CH_3Cl respectively, under the 100% SRC willow scenario.

Under the 50/50 scenario, there is estimated to be a contribution of 9×10^{-5}% to the global

CH_3Br budget and $2\times10^{-5}\%$ to the global CH_3Cl budget from land cover in the UK. In Europe, an estimated contribution of 0.2% to the global CH_3Br budget and 0.05% to the global CH_3Cl budget was calculated.

Table 8.3: CH_3Br and CH_3Cl emissions for current land cover area and for the three scenarios of potential future bioenergy crop land cover area for *Miscanthus* and SRC willow as a percentage$\times10^{-3}$ of their respective global annual turnovers.

		CH_3Br		CH_3Cl	
		Current	Future	Current	Future
UK	*Miscanthus*	0.005	0.1	0.001	0.03
	SRC willow	0.03	2	0.008	0.4
	Both	0.04	0.09	0.009	0.2
Europe	*Miscanthus*	0.01	30	0.003	7
	SRC willow	0.1	350	0.03	90
	Both	0.1	200	0.03	50

To put this study in context with other CH_3X sources, CH_3X measurements made in a tropical rainforest were scaled up to estimate global annual emissions of 18 Gg y^{-1} CH_3Br and 1.1 Tg y^{-1} CH_3Cl weighted by species (Blei et al., 2010a). These values corresponded to 9% and 25% of current estimated total global annual fluxes. Here emissions from *Miscanthus* under the largest planting area scenario (100% of the 72 Mha in Europe) were estimated to be 0.06 Gg y^{-1} CH_3Br and 3×10^{-4} Tg y^{-1} CH_3Cl which correspond to 0.03% and 0.007% of total annual global fluxes. Emissions from SRC willow under the same scenario were estimated to be 0.7 Gg y^{-1} CH_3Br and 0.004 Tg y^{-1} CH_3Cl which correspond to 0.3% and 0.09% of total annual global fluxes.

In comparison to the two annual arable crops studied in this work, *Miscanthus* and SRC willow emit slightly higher amounts of CH_3X than wheat but much lower amounts than oilseed rape (Gan et al., 1998; Mead et al., 2008c). Replacing arable land with these perennial bioenergy crops will not have a great effect on CH_3X budgets, unless they replace oilseed rape in which case a reduction in emissions of CH_3Br and CH_3Cl would be expected.

8.3.3 BVOC emission estimates

Isoprene emissions from *Miscanthus* are estimated to be very low for current and potential future land cover in the UK and Europe (Table 8.4). Estimates for current emissions for the UK and Europe are around 1×10^{-5} Tg y^{-1} and 2×10^{-5} Tg y^{-1}, respectively. Estimates of α-pinene are higher, with an estimated 4×10^{-4} Tg y^{-1} for the UK and 8×10^{-4} Tg y^{-1} for Europe. If all of the land potentially available for perennial bioenergy crops is planted with *Miscanthus* only,

the isoprene emissions for the UK and Europe are projected to increase to 2×10^{-4} Tg y^{-1} and 0.04 Tg y^{-1}, respectively, and for α-pinene to 0.01 Tg y^{-1} and 2 Tg y^{-1}, respectively.

The largest estimated BVOC emissions were calculated for SRC willow (Table 8.4). Emissions of isoprene and α-pinene at current land cover in the UK are estimated to be 0.003 Tg y^{-1} and 0.001 Tg y^{-1}, respectively. This may increase to 0.15 Tg y^{-1} and 0.08 Tg y^{-1} if all potential bioenergy crop land resources are planted with SRC willow in the future.

In Europe, estimates for isoprene and α-pinene emissions under current land cover are 0.01 Tg y^{-1} and 0.005 Tg y^{-1}, respectively. This may increase to 30 Tg y^{-1} and 16 Tg y^{-1}, respectively, if all land available for perennial bioenergy crops is planted with SRC willow in the future.

Table 8.4: Isoprene and α-pinene emissions in Gg y^{-1} from *Miscanthus* and SRC willow individually and combined for current land area coverages in the UK and in Europe. Also given are emission estimates for potential future bioenergy crop land cover area for 3 scenarios; the first is that all potential bioenergy crop land is planted only with *Miscanthus* , the second that it is only planted with SRC willow and the third that it is planted with both, with 50% planted with *Miscanthus* and 50% with SRC willow. Standard errors of the mean are given in brackets.

		Isoprene		α-pinene	
		Current	Future	Current	Future
UK	*Miscanthus*	0.01 ($\pm$ 0.005)	0.2 ($\pm$ 0.1)	0.4 ($\pm$ 0.3)	10 ($\pm$ 9)
	SRC willow	3 ($\pm$ 0.01)	150 ($\pm$ 0.8)	1 ($\pm$ 0.01)	80 ($\pm$ 3)
	Both	3 ($\pm$ 0.02)	80 ($\pm$ 0.4)	2 ($\pm$ 0.3)	40 ($\pm$ 5)
Europe	*Miscanthus*	0.02 ($\pm$ 0.01)	40 ($\pm$ 30)	0.8 ($\pm$ 0.7)	2000 ($\pm$ 1900)
	SRC willow	10 ($\pm$ 0.05)	30000 ($\pm$ 200)	5 ($\pm$ 0.03)	16 000 ($\pm$ 80)
	Both	10 ($\pm$ 0.06)	16 000 ($\pm$ 90)	6 ($\pm$ 0.7)	9000 ($\pm$ 1000)

8.3.4 Implications for BVOC budgets

Using the estimated annual global turnover of around 500 Tg y^{-1} for isoprene and 120 Tg y^{-1} for α-pinene (Guenther et al., 1995), the contribution of these estimated emissions from *Miscanthus* and SRC willow to global BVOC budgets was calculated. Considering the much larger global turnover of BVOCs in comparison to CH_3X, a discernible contribution is made to the isoprene budget by estimated current and projected SRC willow emissions but the contribution from *Miscanthus* is negligible (see Table 8.5).

Emissions from *Miscanthus* under current land cover in the UK and in Europe account for only 2×10^{-6} % and 3×10^{-6} % of global isoprene respectively (Table 8.5). Future emissions for the UK and Europe are estimated to account for 4×10^{-4} % and 0.009 % of global isoprene respectively. Contributions to the global α-pinene budget are higher, with emissions from

current land cover in the UK and Europe estimated to account for 3×10^{-4} % and 6×10^{-4} %, respectively. Under a 100% *Miscanthus* future land cover scenario, this is projected to increase to 0.009 % and 2 % respectively. However, this assumes that *Miscanthus* emits α-pinene, which was not conclusively proven by the measurements described in this thesis.

SRC willow is a much higher emitter of isoprene in comparison to *Miscanthus* and therefore contributes more to the global turnover (Table 8.5). Emissions from current land cover in the UK and Europe account for 6×10^{-4} % and 0.002 % of global isoprene respectively. In future, this could rise to 0.03 % and 6 % of global isoprene respectively, if all potentially available land is planted with SRC willow. The contribution to global α-pinene turnover is similar, with current UK and Europe land cover areas accounting for 0.001 % and 0.005 % of global α-pinene, respectively. This could potentially rise to 0.07 % and 13 % of global α-pinene respectively, under the 100% SRC willow scenario.

Table 8.5: Isoprene and α-pinene emissions for current land cover area and for the three scenarios of potential future bioenergy crop land cover area for *Miscanthus* and SRC willow as a percentage$\times10^{-3}$ of their respective global annual turnovers.

		Isoprene		α-pinene	
		Current	Future	Current	Future
UK	*Miscanthus*	0.002	0.04	0.3	9
	SRC willow	0.6	30	1	70
	Both	0.6	20	2	40
Europe	*Miscanthus*	0.003	9	0.6	2000
	SRC willow	2	6000	5	13 000
	Both	2	3000	5	8000

Using literature values for the standard emission rate of isoprene from various willow species (described in detail in Section 4.1), scaled-up annual emissions calculated using this method were estimated to be between 0.06 and 0.5 Tg y^{-1} in the UK and between 11.4 and 110 Tg y^{-1} in Europe for the 100% SRC willow future planting scenario. As the standard emission rates in the literature are based on peak summer fluxes, they are slightly higher than the estimates calculated here which used annual net mean fluxes to estimate comparable emissions of 0.15 Tg y^{-1} for the UK and 31 Tg y^{-1} for Europe.

SRC willow emits much greater quantities of isoprene than the annual arable crops wheat and oilseed rape, as discussed in Section 4.5. Conversion from low BVOC-emitting annual arable crops to SRC willow will result in an increase of the global budget of isoprene. A study by Ashworth et al. (2013) estimated this increase to be around 5.5 Tg C y^{-1} in Europe if all of the potential 72 Mha available are planted with SRC willow. However, replacing annual arable crops with *Miscanthus* is not likely to have a big impact on BVOC budgets as it does not emit

significant amounts of isoprene and emissions of α-pinene were not definitively proven to be important.

8.4 Conclusion

Due to the rudimentary nature of the scale-up method, the estimates presented in this chapter should be considered as semi-quantitative and preliminary in nature. A more thorough assessment of the impact on CH_3X and BVOC budgets would take greater account of seasonal and diurnal variation and would require PAR and temperature data across the likely planting sites in the UK and Europe to be incorporated into a whole-canopy model. However, the use of several large long-term datasets provide a reasonable representation of fluxes from both perennial bioenergy crops *Miscanthus* and SRC willow from which to extrapolate to wider areas.

These estimates also give an indication of what impact continued expansion of bioenergy crops might have on atmospheric budgets of CH_3X and BVOCs. SRC willow in particular emits more isoprene than the low BVOC emitting annual arable crops that it is replacing. This has the potential to impact local and regional air quality by contributing to tropospheric ozone production and SOA formation. A recent study estimated that cultivation of 72 Mha of SRC willow in Europe would lead to a 2 ppbv increase in summertime mean ground-level ozone, impacting on human mortality and crop yields (Ashworth et al., 2013). These findings reinforce the importance of considering more than just the carbon budget when assessing bioenergy crops for climate change mitigation.

Chapter 9

Final conclusions

Methyl halide (CH_3Br and CH_3Cl) and BVOC fluxes were successfully measured from perennial bioenergy crops and annual arable crops. Factors influencing flux magnitudes and flux patterns were investigated and estimates of potential global flux magnitudes were calculated. The following results were obtained:

Plant species determined net flux magnitudes

The main factor in determining net flux magnitudes of both CH_3X and BVOCs was plant species. Oilseed rape was found to emit large quantities of methyl halides, in line with previous measurements of oilseed rape and other *Brassica* species (Attieh et al., 1995; Gan et al., 1998; Saini et al., 1995). Fluxes of CH_3X from bioenergy crops were much lower than those from oilseed rape and fluxes from both bioenergy crops fell within a similar range.

Higher net emissions of one methyl halide from a plant species were indicative of high net emissions of the other. However, no significant correlations were derived between CH_3Br and CH_3Cl fluxes. Where CH_3X were emitted, the magnitude of CH_3Cl fluxes was consistently higher than CH_3Br fluxes. This is likely due in part to the comparative availability of Cl^- in the soil. However, variation in the expression of the halogenating methyl transferase enzyme present in many vascular plants is also likely to drive part of the variation in CH_3X fluxes (Manley, 2002).

Fluxes of isoprene were highest from SRC willow, in line with previous measurements of willow species (Copeland et al., 2012; Evans et al., 1982; Hakola et al., 1998; Isebrands et al., 1999; Karl et al., 2009; Niinemets et al., 2010; Olofsson et al., 2005; Owen and Hewitt, 2000; Owen et al., 2003; Pio et al., 1993; Winer et al., 1992; Zimmerman, 1979). Isoprene fluxes from all other crops were much lower. It was not conclusively established whether *Miscanthus* was a significant emitter of α-pinene. Fluxes of the other monoterpenes detected (β-pinene, limonene and δ-3-carene) were emitted in similar quantities from wheat and SRC willow.

High emissions of one BVOC did not always imply higher emissions of others. Significant

correlations between BVOC fluxes were identified where emissions were high and enough data was available.

Temporal and spatial resolution of CH_3X and BVOC fluxes

Fluxes from bioenergy crops were strongly associated with season and followed distinct seasonal cycles. Diurnal trends in fluxes were less obvious. Whilst there was some variation in fluxes between sampling sites within crop types, this was not found to be significant. This is likely due to the homogeneity of the soil and climate conditions and plant physiology within the fieldsites.

CH_3X are relatively long-lived species and therefore seasonality in emissions does not have a great effect on their overall impact on global atmospheric chemistry. However, seasonality in emissions is important for BVOC emissions in terms of their impact on SOA and O_3 photochemical formation. Light levels and temperatures are higher in summer, enhancing the atmospheric processes by which BVOCs impact on global atmospheric budgets.

It is therefore important to note that the highest BVOC emissions from bioenergy crops measured here, in particular the emission of isoprene from SRC willow, occurred during the summer growing season. The atmospheric oxidation of isoprene and other VOCs is dependent on the availability of the OH radical, ozone and the NO_3 radical and the presence of light (Atkinson, 2000). In Europe, high background levels of NOx typically lead to a low VOC:NOx ratio therefore photochemical production of ozone is sensitive to VOC concentration (Finlayson-Pitts and Pitts, 2000). High isoprene emissions tend to lead to increased ozone formation. The response of ozone and SOA budgets to greatly increased planting of SRC willow in Europe was simulated in a recent study (Ashworth et al., 2013). In the model simulation, the highest monthly increase in ozone was found to occur in July (+2.5 ppbv).

High isoprene emissions are also likely to result in increased SOA formation (Tsigaridis and Kanakidou, 2007). Isoprene is not the dominant source of SOA (on a per-molecule basis) but higher isoprene emission rates result in higher SOA yields. Increased competition for OH has been hypothesised to both increase SOA yields from monoterpenes and to inhibit them (Kiendler-Scharr et al., 2009).

The influence of environmental parameters and future trends in fluxes

Neither temperature nor sunlight were proven to account directly for the observed flux variations from plants. However, many significant correlations were made between environmental observations and plant emissions. Other factors, such as general plant growth patterns and physiological changes, are themselves also likely to be strongly dependent on temperature and/or

sunlight. Variation in fluxes during the year and between years are therefore likely to be directly and indirectly influenced by temperature and sunlight.

Significant positive correlations between CH_3X fluxes and the temperature of the chamber, the ambient air and the soil were identified for both bioenergy crops. Fluxes of BVOCs were correlated with all environmental observations where fluxes were relatively high and a large number of data points were available. Although BVOC fluxes have been successfully modelled (Guenther et al., 1995), methyl halide fluxes are rather more difficult to predict or to model using a simple causal response model. It is unlikely that a reliable forecast of CH_3X fluxes for future scenarios can be made based on the direct effect of changes in climate. However, as CH_3X and BVOC emissions were found to be highly dependant on the growing season, greater emissions may occur over a longer period of time due to a warmer climate and the corresponding increase in growing season length predicted to occur with climate change.

A tentative scale-up using measurements from this study found that replacing annual arable crops with perennial bioenergy crops will have an impact on global CH_3X and BVOC budgets, depending on the crop type being replaced and the type of bioenergy crop employed. Replacing high CH_3X emitting oilseed rape with lower CH_3X emitting bioenergy crops may actually decrease the stratospheric ozone depletion caused by Br and Cl atoms from naturally-emitted halogen carriers. However, replacing large areas of annual arable crops with SRC willow may cause other problems. SRC willow emits large quantities of isoprene in comparison to low-emitting annual arable crops. Isoprene emissions are of particular concern as they are strongly correlated with temperature and sunlight. Coupled with a warming climate, the potential exists for even higher emissions to occur in future, with the associated effects on tropospheric ozone and SOA.

Although not modelled in this study, the planting of wheat and oilseed rape for biofuel production is also likely to increase in the future. So rather than replacing these crop types with bioenergy crops, all four crop types investigated here may be planted more extensively. Therefore the most negative outcome in terms of atmospheric chemistry could be an increase in both stratospheric ozone depletion, due to increased emissions of CH_3X from oilseed rape, and an increase in tropospheric ozone production related to increased emissions of isoprene from SRC willow.

Remaining uncertainties and future work

This work would have benefited from more diurnal studies to clarify whether BVOC fluxes followed diurnal trends and to confirm the diurnal trend identified in one CH_3X measurement campaign. The other main issues were quality control issues. More rigorous testing of the effects of enclosure time and disturbance on plant stress and linearity of flux may have been beneficial. In addition, more measurements from the individual sampling points over several

consecutive days would have enabled short-term variation in fluxes to be assessed. However, the long analysis time required for determination of CH_3X mixing ratios limited the number of samples that could reasonably be analysed. The fixed term of the project also limited the amount of fieldwork that could be conducted.

It would also have been interesting to conduct further controlled greenhouse studies on nitrogen fertiliser addition to willow trees. Taking measurements over a longer time period, months or years instead of weeks, would have allowed a long-term assessment of the effects of fertiliser on emissions.

An investigation into the wider impact of the fluxes measured in this study, such as the effect on human health and crop yields as simulated by Ashworth et al. (2013), would also be very interesting. Ashworth et al. (2013) found that increased planting of bioenergy crops led to a projected increase in human mortality of around 6% of the deaths attributed at present to ozone in Europe, with an associated cost of 7 billion USD. Wheat is known to be very ozone-sensitive (Mills et al., 2007). Under the scenario simulated by Ashworth et al. (2013), wheat crops were damaged and yields reduced.

More widely, measurements of these fluxes from bioenergy crops at other latitudes would also enable comparison of flux magnitudes and patterns in different climate zones. Until measurements are made in such areas, source strengths will be uncertain. Most importantly however, is a greater understanding of how and why plants emit more or less CH_3X and BVOCs.

The importance of this work

This study has addressed the previously highlighted lack of data on CH_3X fluxes from terrestrial ecosystems in general (Warwick et al., 2006b), as well as from annual arable and perennial bioenergy crops in particular. A large temporally and spatially resolved dataset for CH_3X and BVOC fluxes from both crop types is provided which should assist future modelling studies. The comparison between fluxes from perennial bioenergy and annual arable crops should also be useful when considering government policy on bioenergy crops.

The planting of all of the crop types studied here for bioenergy and biofuel production is likely to increase in the future. The information provided by this study contributes to our knowledge of the possible impacts on atmospheric budgets caused by this increase.

Bibliography

Adler, P. R., Grosso, S. J. D., and Parton, W. J. (2007). Life-cycle assessment of net greenhouse-gas flux for bioenergy cropping systems. *Ecological Applications*, 17(3):675–691.

Anastasi, C., Hopkinson, L., and Simpson, V. J. (1991). Natural hydrocarbon emissions in the United Kingdom. *Atmospheric Environment*, 25(7):1403–1408.

Andersen, R. S., Towers, W., and Smith, P. (2005). Assessing the potential for biomass energy to contribute to Scotland's renewable energy needs. *Biomass & Bioenergy*, 29(2):73–82.

Andreae, M. O. and Merlet, P. (2001). Emission of trace gases and aerosols from biomass burning. *Global Biogeochemical Cycles*, 15(4):955–966.

Arevalo, C. B. M., Drew, A. P., and Volk, T. A. (2005). The effect of common dutch white clover (*Trifolium repens L.*), as a green manure, on biomass production, allometric growth and foliar nitrogen of two willow clones. *Biomass and Bioenergy*, 29(1):22 – 31.

Arneth, A., Miller, P. A., Scholze, M., Hickler, T., Schurgers, G., Smith, B., and Prentice, I. C. (2007). CO_2 inhibition of global terrestrial isoprene emissions: Potential implications for atmospheric chemistry. *Geophysical Research Letters*, 34(18). doi:10.1029/2007GL030615.

Ashworth, K., Wild, O., and Hewitt, C. (2013). Impacts of biofuel cultivation on mortality and crop yields. *Nature Climate Change*, 3:492–496.

Atkinson, R. (2000). Atmospheric chemistry of VOCs and NOx. *Atmospheric Environment*, 34:12–14.

Attieh, J. M., Hanson, A. D., and Saini, H. S. (1995). Purification and characterization of a novel methyltransferase responsible for biosynthesis of halomethanes and methanethiol in *Brassica oleracea*. *Journal of Biological Chemistry*, 270(16):9250–9257.

Aylott, M. J., Casella, E., Tubby, I., Street, N. R., Smith, P., and Taylor, G. (2008). Yield and spatial supply of bioenergy poplar and willow short-rotation coppice in the UK. *New Phytologist*, 178(2):358–370.

Baayen, R. H. (2011). *languageR: Data sets and functions with "Analyzing Linguistic Data: A practical introduction to statistics"*. R package version 1.4.

Bates, D., Maechler, M., and Bolker, B. (2012). *lme4: Linear mixed-effects models using S4 classes*. R package version 0.999999-0.

Bauen, A. W., Dunnett, A. J., Richter, G. M., Dailey, A. G., Aylott, M., Casella, E., and Taylor, G. (2010). Modelling supply and demand of bioenergy from short rotation coppice and Miscanthus in the UK. *Bioresource Technology*, 101(21):8132–8143.

Beale, C. and Long, S. (1997). Seasonal dynamics of nutrient accumulation and partitioning in the perennial C_4-grasses *Miscanthus X giganteus* and *Spartina cynosuroides*. *Biomass and Bioenergy*, 12(6):419 – 428.

Blei, E. (2010). *Methyl halide emissions from temperate and tropical ecosystems*. PhD thesis, University of Edinburgh.

Blei, E., Hardacre, C. J., Mills, G. P., Heal, K. V., and Heal, M. R. (2010a). Identification and quantification of methyl halide sources in a lowland tropical rainforest. *Atmospheric Environment*, 44:1005–1010.

Blei, E. and Heal, M. R. (2011). Methyl bromide and methyl chloride fluxes from temperate forest litter. *Atmospheric Environment*, 45(8):1543–1547.

Blei, E., Heal, M. R., and Heal, K. V. (2010b). Long-term CH_3Br and CH_3Cl flux measurements in temperate salt marshes.

Bocquého, G. and Jacquet, F. (2010). The adoption of switchgrass and miscanthus by farmers: Impact of liquidity constraints and risk preferences. *Energy Policy*, 38(5):2598–2607.

Boman, U. R. and Turnbull, J. H. (1997). Integrated biomass energy systems and emissions of carbon dioxide. *Biomass and Bioenergy*, 13(6):333–343.

Bonn, B. and Moortgat, G. K. (2003). Sesquiterpene ozonolysis: Origin of atmospheric new particle formation from biogenic hydrocarbons. *Geophysical Research Letters*, 30(11):1585.

Bonn, B., von Kuhlmann, R., and Lawrence, M. G. (2004). High contribution of biogenic hydroperoxides to secondary organic aerosol formation. *Geophysical Research Letters*, 31(10):L10108.

Boyle, G. (2004). *Renewable Energy*. Oxford University Press.

Brandão, M., Milá i Canals, L., and Clift, R. (2011). Soil organic carbon changes in the cultivation of energy crops: Implications for GHG balances and soil quality for use in LCA. *Biomass and Bioenergy*, 35(6):2323 – 2336.

Bullard, M. and Nixon, P. (1999). *Miscanthus x giganteus* agronomy for fuel and industrial uses. Technical report, Project Report (NF0403) for MAFF.

Butler, J. H. (2000). Atmospheric chemistry: Better budgets for methyl halides? *Nature*, 403:260–261.

Buttery, R. G., Xu, C., and Ling, L. C. (1985). Volatile components of wheat leaves (and stems): possible insect attractants. *Journal of Agricultural and Food Chemistry*, 33(1):115–117.

Camargo, J. L. C. and Kapos, V. (1995). Complex edge effects on soil moisture and microclimate in central amazonian forest. *Journal of Tropical Ecology*, 11(2):205–221.

Cannell, M. G. (2003). Carbon sequestration and biomass energy offset: theoretical, potential and achievable capacities globally, in Europe and the UK. *Biomass and Bioenergy*, 24(2):97 – 116.

Christian, D., Riche, A., and Yates, N. (2008). Growth, yield and mineral content of *Miscanthus giganteus* grown as a biofuel for 14 successive harvests. *Industrial Crops and Products*, 28(3):320 – 327.

Ciccioli, P., Brancaleoni, E., Cecinato, A., Sparapani, R., and Frattoni, M. (1993). Identification and determination of biogenic and anthropogenic volatile organic compounds in forest areas of northern and southern europe and a remote site of the himalaya region by high-resolution gas chromatography mass spectrometry. *Journal of Chromatography A*, 643(12):55 – 69.

Claeys, M., Wang, W., Ion, A. C., Kourtchev, I., Gelencsér, A., and Maenhaut, W. (2004). Formation of secondary organic aerosols from isoprene and its gas-phase oxidation products through reaction with hydrogen peroxide. *Atmospheric Environment*, 38(25):4093–4098.

Clifton-Brown, J. C., Breuer, J., and Jones, M. B. (2007). Carbon mitigation by the energy crop, *Miscanthus*. *Global Change Biology*, 13(11):2296–2307.

Clifton-Brown, J. C. and Jones, M. B. (1997). The thermal response of leaf extension rate in genotypes of the c4-grass miscanthus: An important factor in determining the potential productivity of different genotypes. *Journal of experimental botany*, 48(313):1573–1581.

Clifton-Brown, J. C., Stampfl, P. F., and Jones, M. B. (2004). *Miscanthus* biomass production for energy in Europe and its potential contribution to decreasing fossil fuel carbon emissions. *Global Change Biology*, 10(4):509–518.

Copeland, N., Cape, J. N., and Heal, M. R. (2012). Volatile organic compound emissions from *Miscanthus* and short rotation coppice willow bioenergy crops. *Atmospheric Environment*, 60:327 – 335.

Cox, M. L., Fraser, P. J., Sturrock, G. A., Siems, S. T., and Porter, L. W. (2004). Terrestrial sources and sinks of halomethanes near Cape Grim, Tasmania. *Atmospheric Environment*, 38:3839–3852.

Croteau, R. (1987). Biosynthesis and catabolism of monoterpenoids. *Chemical Reviews*, 87(5):929–954.

Crutzen, P. J., Mosier, A. R., Smith, K. A., and Winiwarter, W. (2007). N_2O release from agro-biofuel production negates global warming reduction by replacing fossil fuels. *Atmospheric Chemistry and Physics Discussions*, 7(4):11191–11205.

Danalatos, N. G., Archontoulis, S. V., and Mitsios, I. (2007). Potential growth and biomass productivity of *Miscanthus X giganteus* as affected by plant density and N-fertilization in central Greece. *Biomass & Bioenergy*, 31:145–152.

Davis, S., Parton, W., Dohleman, F., Smith, C., Grosso, S., Kent, A., and DeLucia, E. (2010). Comparative biogeochemical cycles of bioenergy crops reveal nitrogen-fixation and low greenhouse gas emissions in a *Miscanthus X giganteus* agro-ecosystem. *Ecosystems*, 13(1):144–156.

Davison, B., Brunner, A., Ammann, C., Spirig, C., Jocher, M., and Neftel, A. (2008). Cut-induced VOC emissions from agricultural grasslands. *Plant Biology*, 10(1):76–85.

De Moraes, C. M., Mescher, M. C., and Tumlinson, J. H. (2001). Caterpillar-induced nocturnal plant volatiles repel conspecific females. *Nature*, 410(6828):577–580.

DEFRA (2004). Best Practice Guidelines For Applicants to Defras Energy Crops Scheme. Technical report, Department for Environment, Food and Rural Affairs.

DEFRA (2007). UK Biomass Strategy. Technical report, Department for Environment, Food and Rural Affairs.

DEFRA (2009). Experimental statistics. Non-food crop areas: United Kingdom. Technical report, Department for Environment, Food and Rural Affairs.

DEFRA (2012). Agriculture in the United Kingdom, 2011. Technical report, Department for Environment, Food and Rural Affairs.

Dignon, J. and Logan, J. (1990). Biogenic emissions of isoprene: A global inventory. *EOS Transactions American Geophysical Union*, 71:1260.

Dimmer, C. H., Simmonds, P. G., Nickless, G., and Bassford, M. R. (2001). Biogenic fluxes of halomethanes from Irish peatland ecosystems. *Atmospheric Environment*, 35(2):321–330.

Don, A., Osborne, B., Hastings, A., Skiba, U., Carter, M. S., Drewer, J., Flessa, H., Freibauer, A., Hyvnen, N., Jones, M. B., Lanigan, G. J., Mander, l., Monti, A., Djomo, S. N., Valentine, J., Walter, K., Zegada-Lizarazu, W., and Zenone, T. (2011). Land-use change to bioenergy production in Europe: implications for the greenhouse gas balance and soil carbon. *Global Change Biology - Bioenergy*, pages 1757–1707.

Dondini, M., Hastings, A., Saiz, G., Jones, M. B., and Smith, P. (2009). The potential of *Miscanthus* to sequester carbon in soils: comparing field measurements in Carlow, Ireland to model predictions. *Global Change Biology - Bioenergy*, 1(6):413–425.

Drewer, J. (2007). *Investigation of natural methyl bromide (CH_3Br) fluxes from terrestrial salt marsh and woodland ecosystems*. PhD thesis, University of Edinburgh.

Drewer, J., Finch, J. W., Lloyd, C. R., Baggs, E. M., and Skiba, U. (2011). How do soil emissions of N_2O, CH_4 and CO_2 from perennial bioenergy crops differ from arable annual crops? *Global Change Biology - Bioenergy*, pages 1757–1707.

Drewer, J., Heal, K. V., Smith, K. A., and Heal, M. R. (2008). Methyl bromide emissions to the atmosphere from temperate woodland ecosystems. *Global Change Biology*, 14(11):2539–2547.

Drewer, J., Heal, M. R., Heal, K. V., and Smith, K. A. (2006). Temporal and spatial variation in methyl bromide flux from a salt marsh. *Geophysical Research Letters*, 33(16). doi:10.1029/2006GL026814.

DTI (2007). Meeting the Energy Challenge - A White Paper on Energy. Technical report, Department for Trade and Industry.

Edenhofer, O., Pichs-Madruga, R., Sokona, Y., Seyboth, K., Kadner, S., Zwickel, T., Eickemeier, P., Hansen, G., Schlömer, S., von Stechow, C., et al. (2011). *Renewable energy sources and climate change mitigation: special report of the intergovernmental panel on climate change*. Cambridge University Press.

EEA (2006). How much bioenergy can Europe produce without harming the environment? Technical report, European Environment Agency.

Eller, A., Sekimoto, K., Gilman, J., Kuster, W., de Gouw, J., Monson, R., Graus, M., Crespo, E., Warneke, C., and Fall, R. (2011). Volatile organic compound emissions from switchgrass cultivars used as biofuel crops. *Atmospheric Environment*, 45(19):3333 – 3337.

Evans, R., Tingey, D., Gumpertz, M., and Burns, W. (1982). Estimates of isoprene and monoterpene emission rates in plants. *Botanical Gazette*, 143:304–310.

Ewert, F., Rounsevell, M., Reginster, I., Metzger, M., and Leemans, R. (2005). Future scenarios of european agricultural land use: I. estimating changes in crop productivity. *Agriculture, Ecosystems & Environment*, 107(2):101–116.

Fahey, D. (2007). *Scientific Assessment of Ozone Depletion: 2006, chap. Twenty questions and answers about the ozone layer: 2006 update*. World Meteorological Organization, Geneva, Switzerland.

Fall, R. (1999). *Biogenic emissions of volatile organic compounds from higher plants*. Reactive Hydrocarbons in the Atmosphere. Academic Press, San Diego.

Fall, R. and Wildermuth, M. C. (1998). Isoprene synthase: From biochemical mechanism to emission algorithm. *Journal of Geophysical Research*, 103:25599–25609.

Fehsenfeld, F., Calvert, J., Fall, R., Goldan, P., Guenther, A. B., Hewitt, C. N., Lamb, B., Liu, S., Trainer, M., Westberg, H., and Zimmerman, P. (1992). Emissions of volatile organic compounds from vegetation and the implications for atmospheric chemistry. *Global Biogeochemical Cycles*, 6(4):389–430.

Fernandes, S. D., Trautmann, N. M., Streets, D. G., Roden, C. A., and Bond, T. C. (2007). Global biofuel use, 1850 - 2000. *Global Biogeochemical Cycles*, 21(2):GB2019.

Finlayson-Pitts, B. J. and Pitts, J. N. J. (2000). *Chemistry of the Upper and Lower Atmosphere*. Harcourt Science and Technology, London.

Foereid, B., de Neergaard, A., and Høgh-Jensen, H. (2004). Turnover of organic matter in a *Miscanthus* field: effect of time in *Miscanthus* cultivation and inorganic nitrogen supply. *Soil Biology and Biochemistry*, 36(7):1075–1085.

Fukui, Y. and Doskey, P. V. (1998). Air-surface exchange of nonmethane organic compounds at a grassland site: Seasonal variations and stressed emissions. *Journal of Geophysical Research-Atmospheres*, 103(D11):13153–13168.

Gan, J., Yates, S. R., Ohr, H. D., and Sims, J. J. (1998). Production of methyl bromide by terrestrial higher plants. *Geophysical Research Letters*, 25(19):3595–3598.

Gatehouse, J. A. (2002). Plant resistance towards insect herbivores: a dynamic interaction. *New phytologist*, 156(2):145–169.

Gebhardt, S., Colomb, A., Hofmann, R., Williams, J., and Lelieveld, J. (2008). Halogenated organic species over the tropical south american rainforest. *Atmospheric Chemistry and Physics*, 8:3185–3197.

Geron, C., Guenther, A., Sharkey, T., and Arnts, R. R. (2000). Temporal variability in basal isoprene emission factor. *Tree Physiology*, 20(12):799–805.

Gilmore, A. (1977). Effects of soil moisture stress on monoterpenes in Loblolly pine. *Journal of Chemical Ecology*, 3:667–676.

Glowacka, K. (2011). A review of the genetic study of the energy crop miscanthus. *Biomass and Bioenergy*, 35:2445–2454.

Goldan, P. D., Kuster, W. C., Fehsenfeld, F. C., and Montzka, S. A. (1993). The observation of a C5 alcohol emission in a North American pine forest. *Geophysical Research Letters*, 20(11):1039–1042.

Grogan, P. and Matthews, R. (2002). A modelling analysis of the potential for soil carbon sequestration under short rotation coppice willow bioenergy plantations. *Soil Use and Management*, 18(3):175–183.

Groszko, W. and Moore, R. M. (1998). Ocean-atmosphere exchange of methyl bromide: NW Atlantic and Pacific Ocean studies. *Journal of Geophysical Research*, 103:16737–16741.

Guenther, A., Geron, C., Pierce, T., Lamb, B., Harley, P., and Fall, R. (2000). Natural emissions of non-methane volatile organic compounds, carbon monoxide, and oxides of nitrogen from North America. *Atmospheric Environment*, 34(1214):2205 – 2230.

Guenther, A., Hewitt, C. N., Erickson, D., Fall, R., Geron, C., Graedel, T., Harley, P., Klinger, L., Lerdau, M., Mckay, W. A., Pierce, T., Scholes, B., Steinbrecher, R., Tallamraju, R., Taylor, J., and Zimmerman, P. (1995). A global model of natural volatile organic compound emissions. *Journal of Geophysical Research*, 100:8873–8892.

Guenther, A., Karl, T., Harley, P., Wiedinmyer, C., Palmer, P. I., and Geron, C. (2006). Estimates of global terrestrial isoprene emissions using MEGAN (Model of Emissions of Gases and Aerosols from Nature). *Atmospheric Chemistry and Physics*, 6:107–173.

Guenther, A., Zimmerman, P., Harley, P., Monson, R., and Fall, R. (1993). Isoprene and Monoterpene Emission Rate Variability: Model Evaluations and Sensitivity Analyses. *Journal of Geophysical Research*, 98:609–617.

Guenther, A. B., Monson, R. K., and Fall, R. (1991). Isoprene and monoterpene emission rate variability: Observations with eucalyptus and emission rate algorithm development. *Journal of Geophysical Research*, 96:10799–10808.

Guo, M., Song, W., and Kazda, R. (2012). Fertilizer value of lime-stabilized biosolids as a soil amendment. *Agronomy Journal*, 104:1679–1686.

Hakola, H., Rinne, J., and Laurila, T. (1998). The hydrocarbon emission rates of Tea-leafed willow (*Salix phylicifolia*), Silver birch (*Betula pendula*) and European aspen (*Populus tremula*). *Atmospheric Environment*, 32(10):1825 – 1833.

Hakola, H., Rinne, J., and Laurila, T. (1999). VOC emission rates of boreal deciduous trees. Technical report, Commission of the European Communities, Luxembourg.

Hamilton, J. T., McRoberts, W. C., Keppler, F., Kalin, R. M., and Harper, D. B. (2003). Chloride methylation by plant pectin: an efficient environmentally significant process. *Science*, 301(5630):206–209.

Hansen, E. M., Christensen, B. T., Jensen, L., and Kristensen, K. (2004). le *Miscanthus* plantations as determined by ^{13}C abundance. *Biomass and Bioenergy*, 26(2):97–105.

Hardacre, C. (2010). *Characterisation of CH_3X fluxes from Scottish and high latitude wetlands*. PhD thesis, The University of Edinburgh.

Hardacre, C. J., Blei, E., and Heal, M. R. (2009). Growing season methyl bromide and methyl chloride fluxes at a sub-arctic wetland in sweden. *Geophysical Research Letters*, 36.

Hardacre, C. J. and Heal, M. R. (2013). Characterization of methyl bromide and methyl chloride fluxes at temperate freshwater wetlands. *Journal of Geophysical Research*, 118:977–991.

Harper, D. B. (1985). Halomethane from halide ion - a highly efficient fungal conversion of environmental significance. *Nature*, 315:55–57.

Harper, D. B., Buswell, J. A., Kennedy, J. T., and Hamilton, J. T. (1990). Chloromethane, methyl donor in veratryl alcohol biosynthesis in phanerochaete chrysosporium and other lignin-degrading fungi. *Applied and Environmental Microbiology*, 56(11):3450–3457.

Harper, D. B., Hamilton, J. T. G., Kennedy, J. T., and McNally, K. J. (1989). Chloromethane, a novel methyl donor for biosynthesis of esters and anisoles in *Phellinus pomaceus*. *Applied and Environmental Microbiology*, 55(8):1981–1989.

Harper, D. B., Harvey, B. M. R., Jeffers, M. R., and Kennedy, J. T. (1999). Emissions, biogenesis and metabolic utilization of chloromethane by tubers of the potato (solanum tuberosum). *New Phytologist*, 142(1):5–17. 1469-8137.

Hastings, A., Clifton-Brown, J., Wattenbach, M., Mitchell, C. P., and Smith, P. (2009). The development of MISCANFOR, a new Miscanthus crop growth model: towards more robust yield predictions under different climatic and soil conditions. *GCB Bioenergy*, 1(2):154–170.

Heaton, E. A., Dohleman, F. G., Fernando Miguez, A., Juvik, J. A., Lozovaya, V., Widholm, J., Zabotina, O. A., McIsaac, G. F., David, M. B., and Voigt, T. B. (2010). Miscanthus: a promising biomass crop. *Advances in Botanical Research*, 56(10).

Heller, M. C., Keoleian, G. A., and Volk, T. A. (2003). Life cycle assessment of a willow bioenergy cropping system. *Biomass and Bioenergy*, 25(2):147 – 165.

Helmig, D., Klinger, L. F., Guenther, A., Vierling, L., Geron, C., and Zimmerman, P. (1999). Biogenic volatile organic compound emissions (BVOCs) I. Identifications from three continental sites in the U.S. *Chemosphere*, 38(9):2163 – 2187.

Hillier, J., Whittaker, C., Dailey, G., Aylott, M., Casella, E., Richter, G. M., Riche, A., Murphy, R., Taylor, G., and Smith, P. (2009). Greenhouse gas emissions from four bioenergy crops in England and Wales: Integrating spatial estimates of yield and soil carbon balance in life cycle analyses. *Global Change Biology - Bioenergy*, 1(4):267–281.

Himken, M., Lammel, J., Neukirchen, D., Czypionka-Krause, U., and Olfs, H.-W. (1997). Cultivation of *Miscanthus* under West European conditions: Seasonal changes in dry matter production, nutrient uptake and remobilization. *Plant and Soil*, 189:117–126.

HSE (1992). Methods for the Determination of Hazardous Substances (MDHS). MDHS 72. Volatile organic compounds in air. Laboratory method using pumped solid sorbent tubes, thermal desorption and gas chromatography. Technical report, UK Health and Safety Executive.

Huang, W. L., Bu, X., Nguyen, L., Gammon, R. H., and Bullister, J. L. (2000). Production and consumption of methyl halides in a freshwater lake. *Limnology and Oceanography*, 45(7):1537–1545.

Hyatt, D. C., Youn, B., Zhao, Y., Santhamma, B., Coates, R. M., Croteau, R. B., and Kang, C. (2007). Structure of limonene synthase, a simple model for terpenoid cyclase catalysis. *Proceedings of the National Academy of Sciences*, 104(13):5360–5365.

IPCC (2007). Climate change 2007: the physical science basis. Technical report, International Panel on Climate Change.

Isebrands, J., Guenther, A., Harley, P., Helmig, D., Klinger, L., Vierling, L., Zimmerman, P., and Geron, C. (1999). Volatile organic compound emission rates from mixed deciduous and coniferous forests in Northern Wisconsin, USA. *Atmospheric Environment*, 33(16):2527 – 2536.

Itoh, N., Toda, H., Matsuda, M., Negishi, T., Taniguchi, T., and Ohsawa, N. (2009). Involvement of S-adenosylmethionine-dependent halide/thiol methyltransferase (HTMT) in methyl halide emissions from agricultural plants: isolation and characterization of an HTMT-coding gene from *Raphanus sativus* (Daikon radish). *BMC Plant Biology*, 9:116.

Janson, R.; Kristensson, J. (1991). Sampling and analysis of atmospheric monoterpenes, Report CM-79. Technical report, Dept. of Meteorology, Stockholm University.

Johnson, P. (1999). Fertiliser requirements for short rotation coppice. Technical report, Energy Technology Support Unit (ETSU).

Jørgensen, U., Dalgaard, T., and Kristensen, E. S. (2005). Biomass energy in organic farming - the potential role of short rotation coppice. *Biomass and Bioenergy*, 28(2):237–248.

Jug, A., Makeschin, F., Rehfuess, K., and Hofmann-Schielle, C. (1999). Short-rotation plantations of balsam poplars, aspen and willows on former arable land in the Federal Republic of Germany. III. Soil ecological effects. *Forest Ecology and Management*, 121(12):85 – 99.

Kahle, P., Beuch, S., Boelcke, B., Leinweber, P., and Schulten, H.-R. (2001). Cropping of *Miscanthus* in Central Europe: biomass production and influence on nutrients and soil organic matter. *European Journal of Agronomy*, 15(3):171–184.

Karl, M., Guenther, A., Köble, R., Leip, A., and Seufert, G. (2009). A new European plant-specific emission inventory of biogenic volatile organic compounds for use in atmospheric transport models. *Biogeosciences*, 6:1059–1087.

Keene, W. C., Khalil, M. A. K., Erickson, D. J., McCulloch, A., Graedel, T. E., Lobert, J. M., Aucott, M. L., Gong, S. L., Harper, D. B., Kleiman, G., Midgley, P., Moore, R. M., Seuzaret, C., Sturges, W. T., Benkovitz, C. M., Koropalov, V., Barrie, L. A., and Li, Y. F. (1999). Composite global emissions of reactive chlorine from anthropogenic and natural sources: Reactive chlorine emissions inventory. *Journal of Geophysical Research-Atmospheres*, 104(D7):8429–8440.

Kerwin, R. A., Crill, P. M., Talbot, R. W., Hines, M. E., Shorter, J. H., Kolb, C. E., and Harriss, R. C. (1996). Determination of atmospheric methyl bromide by cryotrapping gas chromatography and application to soil kinetic studies using a dynamic dilution system. *Analytical Chemistry*, 68:899–903.

Kesselmeier, J. and Staudt, M. (1999). Biogenic volatile organic compounds (VOCs): an overview on emission, physiology and ecology. *Journal of Atmospheric Chemistry*, 33:23–88.

Khalil, M. A. K. and Rasmussen, R. A. (1999). Atmospheric methyl chloride. *Atmospheric Environment*, 33(8):1305–1321.

Kiendler-Scharr, A., Wildt, J., Dal Maso, M., Hohaus, T., Kleist, E., Mentel, T. F., Tillmann, R., Uerlings, R., Schurr, U., and Wahner, A. (2009). New particle formation in forests inhibited by isoprene emissions. *Nature*, 461(7262):381–384.

Kim, J.-C., Kim, K.-J., Kim, D.-S., and Han, J.-S. (2005). Seasonal variations of monoterpene emissions from coniferous trees of different ages in korea. *Chemosphere*, 59:1685 – 1696.

King, D. B., Butler, J. H., Yvon-Lewis, S. A., and Cotton, S. A. (2002). Predicting oceanic methyl bromide saturation from SST. *Geophysical Research Letters*, 29:52–1–52–4.

King, J., Bradley, R., Harrison, R., and Carter, A. (2004). Carbon sequestration and saving potential associated with changes to the management of agricultural soils in England. *Soil Use and Management*, 20(4):394–402.

Kirstine, W., Galbally, I., Ye, Y., and Hooper, M. (1998). Emissions of volatile organic compounds (primarily oxygenated species) from pasture. *Journal of Geophysical Research*, 103(D9):10605–10619.

Komenda, M., Parusel, E., Wedel, A., and Koppmann, R. (2001). Measurements of biogenic VOC emissions: sampling, analysis and calibration. *Atmospheric Environment*, 35(12):2069–2080.

König, G., Brunda, M., Puxbaum, H., Hewitt, C., Duckham, S., and Rudolph, J. (1995). Relative contribution of oxygenated hydrocarbons to the total biogenic VOC emissions of selected mid-European agricultural and natural plant species. *Atmospheric Environment*, 29(8):861 – 874.

Lamb, B., Gay, D., Westberg, H., and Pierce, T. (1993). A biogenic hydrocarbon emission inventory for the U.S.A. using a simple forest canopy model. *Atmospheric Environment*, 27(11):1673 – 1690.

Laothawornkitkul, J., Taylor, J. E., Paul, N. D., and Hewitt, C. N. (2009). Biogenic volatile organic compounds in the earth system. *New Phytologist*, 183(1):27–51.

Lathiere, J., Hauglustaine, D., Friend, A., De Noblet-Ducoudré, N., Viovy, N., and Folberth, G. (2006). Impact of climate variability and land use changes on global biogenic volatile organic compound emissions. *Atmospheric Chemistry and Physics*, 6(8):2129–2146.

Laurance, W. F., Laurance, S. G., and Delamonica, P. (1998). Tropical forest fragmentation and greenhouse gas emissions. *Forest Ecology and Management*, 110(13):173 – 180.

Leach, J., Stevenson, H., Rainbow, A., and Mullen, L. (1999). Effects of high plant populations on the growth and yield of winter oilseed rape(*Brassica napus*). *The Journal of Agricultural Science*, 132(2):173–180.

Lee-Taylor, J. and Redeker, K. R. (2005). Reevaluation of global emissions from rice paddies of methyl iodide and other species. *Geophysical Research Letters*, 32(15):L15801.

Lee-Taylor, J. M., Brasseur, G. P., and Yokouchi, Y. (2001). A preliminary three-dimensional global model study of atmospheric methyl chloride distributions. *Journal of Geophysical Research*, 106(D24):34221–34233.

Lee-Taylor, J. M. and Holland, E. A. (2000). Litter decomposition as a potential natural source of methyl bromide. *Journal of Geophysical Research*, 105(D7):8857–8864.

Lemus, R. and Lal, R. (2005). Bioenergy crops and carbon sequestration. *Critical Reviews in Plant Sciences*, 24(1):1–21.

Lerdau, M., Guenther, A., and Monson, R. (1997). Plant production and emission of volatile organic compounds. *BioScience*, 47(6):373–383.

Lerdau, M., Matson, P., Fall, R., and Monson, R. (1995). Ecological controls over monoterpene emissions from Douglas Fir (*Pseudotsuga Menziesii*). *Ecology*, 76(8):2640–2647.

Lewandowski, I., Clifton-Brown, J., Scurlock, J., and Huisman, W. (2000). *Miscanthus*: European experience with a novel energy crop. *Biomass and Bioenergy*, 19(4):209–227.

Lewandowski, I. and Kicherer, A. (1997). Combustion quality of biomass: practical relevance and experiments to modify the biomass quality of *Miscanthus x giganteus*. *European Journal of Agronomy*, 6(3):163–177.

Lewandowski, I., Kicherer, A., and Vonier, P. (1995). CO_2-balance for the cultivation and combustion of *Miscanthus*. *Biomass and Bioenergy*, 8(2):81 – 90.

Lewandowski, I. and Schmidt, U. (2006). Nitrogen, energy and land use efficiencies of *Miscanthus*, reed canary grass and triticale as determined by the boundary line approach. *Agriculture, Ecosystems & Environment*, 112(4):335–346.

Liebig, M., Johnson, H., Hanson, J., and Frank, A. (2005). Soil carbon under switchgrass stands and cultivated cropland. *Biomass & Bioenergy*, 28:347–354.

Lim, H.-J., Carlton, A. G., and Turpin, B. J. (2005). Isoprene forms secondary organic aerosol through cloud processing: Model simulations. *Environmental Science & Technology*, 39(12):4441–4446.

Lim, J.-H., Kim, J.-C., Kim, K.-J., Son, Y.-S., Sunwoo, Y., and Han, J.-S. (2008). Seasonal variations of monoterpene emissions from pinus densiflora in east asia. *Chemosphere*, 73:470 – 478.

Lindquist, F.; Balkeren, H. (1990). Stability of chlorinated hydrocarbons on Tenax, Report No. R90/268. Technical report, Commission of European Communities commissioned report from TNO, the Netherlands.

Loreto, F., Barta, C., Brilli, F., and Nogues, I. (2006). On the induction of volatile organic compound emissions by plants as consequence of wounding or fluctuations of light and temperature. *Plant, cell & environment*, 29(9):1820–1828.

Loreto, F. and Velikova, V. (2001). Isoprene produced by leaves protects the photosynthetic apparatus against ozone damage, quenches ozone products, and reduces lipid peroxidation of cellular membranes. *Plant Physiology*, 127(4):1781–1787.

Lovelock, J. (1958). A sensitive detector for gas chromatography. *Journal of Chromatography*, 1:35 – 46.

Lovelock, J. (1971). Atmospheric fluorine compounds as indicators of air movements. *Nature*, 230:379.

Lovelock, J. E., Maggs, R. J., and Wade, R. J. (1973). Halogenated hydrocarbons in and over the atlantic. *Nature*, 241(5386):194–196.

Maier, J. (2009). *Bioenergy: Neither Golden Solution nor Prescription for Disaster*. Earthscan/James & James.

Manley, S. L. (2002). Phytogenesis of Halomethanes: A Product of Selection or a Metabolic Accident? *Biogeochemistry*, 60:16–180.

Manley, S. L., Wang, N. Y., Walser, M. L., and Cicerone, R. J. (2006). Coastal salt marshes as global methyl halide sources from determinations of intrinsic production by marsh plants. *Global Biogeochemical Cycles*, 20(3):GB3015.

Manley, S. L., Wang, N. Y., Walser, M. L., and Cicerone, R. J. (2007). Methyl halide emissions from greenhouse-grown mangroves. *Geophysical Research Letters*, 34(1).

Martin, D. M., Gershenzon, J., and Bohlmann, J. (2003). Induction of volatile terpene biosynthesis and diurnal emission by methyl jasmonate in foliage of norway spruce. *Plant physiology*, 132(3):1586–1599.

Matson, P. A. and Harris, R. C. (1995). *Biogenic Trace Gases: Measuring Emissions from Soil and Water*. Methods in Ecology. Blackwell, Oxford.

Matthews, R. (2001). Modelling of energy and carbon budgets of wood fuel coppice systems. *Biomass and Bioenergy*, 21(1):1–19.

McAnulla, C., McDonald, I. R., and Murrell, J. C. (2001). Methyl chloride utilising bacteria are ubiquitous in the natural environment. *FEMS Microbiology Letters*, 201(2):151–155.

McGarvey, D. J. and Croteau, R. (1995). Terpenoid metabolism. *The Plant Cell Online*, 7(7):1015–26.

McKay, H. (2006). Environmental, economic, social and political drivers for increasing use of woodfuel as a renewable resource in Britain. *Biomass and Bioenergy*, 30(4):308–315.

Mead, M. I., Khan, M. A. H., Nickless, G., Greally, B. R., Tainton, D., Pitman, T., and Shallcross, D. E. (2008a). Leaf cutter ants: a possible missing source of biogenic halocarbons. *Environmental Chemistry*, 5(1):5–10.

Mead, M. I., Khan, M. A. H., White, I. R., Nickless, G., and Shallcross, D. E. (2008b). Methyl halide emission estimates from domestic biomass burning in africa. *Atmospheric Environment*, 42(21):5241–5250.

Mead, M. I., White, L. R., Nickless, G., Wang, K. Y., and Shallcross, D. E. (2008c). An estimation of the global emission of methyl bromide from rapeseed (brassica napus) from 1961 to 2003. *Atmospheric Environment*, 42(2):337–345.

Miller, P., Fitz, D., and Winer, A. (1983). *Investigation of the role of natural hydrocarbons in photochemical smog formation in California*. University of California, Riverside. Statewide Air Pollution Research Center.

Mills, G., Buse, A., Gimeno, B., Bermejo, V., Holland, M., Emberson, L., and Pleijel, H. (2007). A synthesis of AOT40-based response functions and critical levels of ozone for agricultural and horticultural crops. *Atmospheric Environment*, 41(12):2630 – 2643.

Monks, P. S. (2003). Tropospheric photochemistry. In Hewitt, C. N. and Jackson, A., editors, *Handbook of Atmospheric Science*. Blackwell Science Ltd, Oxford.

Monson, R. K. (2002). Volatile organic compound emissions from terrestrial ecosystems: a primary biological control over atmospheric chemistry. *Israel Journal of Chemistry*, 42(1):29–42.

Monson, R. K., Harley, P. C., Litvak, M. E., Wildermuth, M., Guenther, A. B., Zimmerman, P. R., and Fall, R. (1994). Environmental and developmental controls over the seasonal pattern of isoprene emission from aspen leaves. *Oecologia*, 99(3):260–270.

Monson, R. K. and Holland, E. A. (2001). Biospheric trace gas fluxes and their control over tropospheric chemistry. *Annual Review of Ecology and Systematics*, pages 547–576.

Monson, R. K., Jaeger, C. H., Adams, W. W., Driggers, E. M., Silver, G. M., and Fall, R. (1992). Relationships among isoprene emission rate, photosynthesis, and isoprene synthase activity as influenced by temperature. *Plant Physiology*, 98(3):1175–1180.

Monson, R. K., Lerdau, M. T., Sharkey, T. D., Schimel, D. S., and Fall, R. (1995). Biological aspects of constructing volatile organic compound emission inventories. *Atmospheric Environment*, 29(21):2989 – 3002.

Montzka, S. A., Butler, J. H., Hall, B. D., Mondeel, D. J., and Elkins, J. W. (2003). A decline in tropospheric organic bromine. *Geophysical Research Letters*, 30(15).

Moore, R. (2000). The solubility of a suite of low molecular weight organochlorine compounds in seawater and implications for estimating the marine source of methyl chloride to the atmosphere. *Chemosphere-Global Change Science*, 2(1):95–99.

Moore, R. M., Groszko, W., and Niven, S. J. (1996). Ocean-atmosphere exchange of methyl chloride: Results from NW Atlantic and Pacific ocean studies. *Journal of Geophysical Research*, 101:529–538.

Müller, J.-F. (1992). Geographical distribution and seasonal variation of surface emissions and deposition velocities of atmospheric trace gases. *Journal of Geophysical Research*, 97(D4):3787–3804.

Naidu, S. L., Moose, S. P., Al-Shoaibi, A. K., Raines, C. A., and Long, S. P. (2003). Cold tolerance of C_4 photosynthesis in *Miscanthus x giganteus*: Adaptation in amounts and sequence of C_4 photosynthetic enzymes. *Plant Physiology*, 132:1688–1697.

Neeb, P., Bode, K., Beck, J., Schäfer, L., Kesselmeier, J., and Moortgat, G. (1997). Influence of gas-phase oxidation on estimated emission rates of biogenic hydrocarbons. In *Proceedings of the 7th European Symposium on Physico-Chemical Behaviour of Atmospheric Pollutants: The Oxidizing Capacity of the Troposphere*, pages 295–299.

Ni, X. and Hager, L. P. (1999). Expression of *Batis maritima* methyl chloride transferase in *Escherichia coli*. *Proceedings of the National Academy of Sciences*, 96(7):3611–3615.

Niinemets, U., Copolovici, L., and Hüve, K. (2010). High within-canopy variation in isoprene emission potentials in temperate trees: Implications for predicting canopy-scale isoprene fluxes. *Journal of Geophysical Research*, 115(G4). doi:10.1029/2010JG001436.

Nunes, T. and Pio, C. (2001). Emission of volatile organic compounds from portuguese eucalyptus forests. *Chemosphere - Global Change Science*, 3:239 – 248.

Olivier, R., Lavoir, A.-V., Ormeo, E., Mouillot, F., Greff, S., Lecareux, C., Staudt, M., and Fernandez, C. (2011). Compost spreading in Mediterranean shrubland indirectly increases biogenic emissions by promoting growth of VOC-emitting plant parts. *Atmospheric Environment*, 45(21):3631 – 3639.

Olofsson, M., Ek-Olausson, B., Jensen, N., Langer, S., and Ljungström, E. (2005). The flux of isoprene from a willow coppice plantation and the effect on local air quality. *Atmospheric Environment*, 39(11):2061 – 2070.

Owen, S. M., Boissard, C., and Hewitt, C. N. (2001). Volatile organic compounds (VOCs) emitted from 40 Mediterranean plant species: VOC speciation and extrapolation to habitat scale. *Atmospheric Environment*, 35(32):5393 – 5409.

Owen, S. M. and Hewitt, C. (2000). Extrapolating branch enclosure measurements to estimates of regional scale biogenic VOC fluxes in the northwestern Mediterranean basin. *Journal of Geophysical Research*, 105 (D9):11573–11583.

Owen, S. M., Mackenzie, A. R., Stewart, H., Donovan, R., and Hewitt, C. N. (2003). Biogenic volatile organic compound flux from the UK West Midlands urban tree canopy. *Ecological Applications*, 13(4):927–938.

Pierce, T., Geron, C., Bender, L., Dennis, R., Tonnesen, G., and Guenther, A. (1998). Influence

of increased isoprene emissions on regional ozone modeling. *Journal of Geophysical Research*, 103(D19):25611–25629.

Pio, C., Nunes, T., and Brito, S. (1993). Volatile hydrocarbon emissions from common and native species of vegetation in portugal. In *Proceedings of the Joint Workshop of CEC/BIATEX of EUROTRAC, General assessment of biogenic emissions and deposition of nitrogen compounds, sulphur compounds and oxidants in Europe. Air Pollution Research Report*, volume 47, pages 251–257.

Pressley, S., Lamb, B., Westberg, H., Flaherty, J., Chen, J., and Vogel, C. (2005). Long-term isoprene flux measurements above a northern hardwood forest. *Journal of Geophysical Research*, 110. doi:10.1029/2004JD005523.

Price, L., Bullard, M., Lyons, H., Anthony, S., and Nixon, P. (2004). Identifying the yield potential of *Miscanthus X giganteus*: an assessment of the spatial and temporal variability of *Miscanthus X giganteus*biomass productivity across England and Wales. *Biomass and Bioenergy*, 26(1):3–13.

Prinn, R. G., Weiss, R. F., Fraser, P. J., Simmonds, P. G., Cunnold, D. M., Alyea, F. N., O'Doherty, S., Salameh, P., Miller, B. R., Huang, J., Wang, R. H. J., Hartley, D. E., Harth, C., Steele, L. P., Sturrock, G., Midgley, P. M., and McCulloch, A. (2000). A history of chemically and radiatively important gases in air deduced from ALE/GAGE/AGAGE. *Journal of Geophysical Research*, 105:17751–17792.

Quaye, A. K., Volk, T. A., Hafner, S., Leopold, D. J., and Schirmer, C. (2011). Impacts of paper sludge and manure on soil and biomass production of willow. *Biomass and Bioenergy*, 35(7):2796 – 2806.

R Core Team (2012). *R: A Language and Environment for Statistical Computing*. R Foundation for Statistical Computing, Vienna, Austria. ISBN 3-900051-07-0.

Rasmussen, R. A. and Khalil, M. A. K. (1988). Isoprene over the amazon basin. *Journal of Geophysical Research: Atmospheres*, 93(D2):1417–1421.

Rasmussen, R. A. and Went, F. W. (1965). Volatile organic material of plant origin in the atmosphere. *Proceedings of the National Academy of Sciences USA*, 53:215–220.

Redeker, K. R. and Cicerone, R. J. (2004). Environmental controls over methyl halide emissions from rice paddies. *Global Biogeochemical Cycles*, 18(1). doi:10.1029/2003GB002092.

Redeker, K. R., Manley, S. L., Walser, M., and Cicerone, R. J. (2004). Physiological and biochemical controls over methyl halide emissions from rice plants. *Global Biogeochemical Cycles*, 18(1).

Redeker, K. R., Meinardi, S., Blake, D., and Sass, R. (2003). Gaseous emissions from flooded rice paddy agriculture. *Journal of Geophysical Research*, 108(D13). doi:10.1029/2002JD002814.

Redeker, K. R., Wang, N. Y., Low, J. C., McMillan, A., Tyler, S. C., and Cicerone, R. J. (2000). Emissions of methyl halides and methane from rice paddies. *Science*, 290:966–969.

Rhew, R. C. (2011). Sources and sinks of methyl bromide and methyl chloride in the tallgrass prairie: Applying a stable isotope tracer technique over highly variable gross fluxes. *Journal of Geophysical Research*, 116(G3):G03026.

Rhew, R. C. and Abel, T. (2007). Measuring simultaneous production and consumption fluxes of methyl chloride and methyl bromide in annual temperate grasslands. *Environmental Science & Technology*, 41(22):7837–7843.

Rhew, R. C., Aydin, M., and Saltzman, E. S. (2003a). Measuring terrestrial fluxes of methyl chloride and methyl bromide using a stable isotope tracer technique. *Geophysical Research Letters*, 30(21):2103.

Rhew, R. C., Chen, C., Teh, Y. A., and Baldocchi, D. (2010). Gross fluxes of methyl chloride and methyl bromide in a California oak-savanna woodland. *Atmospheric Environment*, 44(16):2054–2061.

Rhew, R. C., Miller, B. R., Bill, M., Goldstein, A. H., and Weiss, R. F. (2002). Environmental and biological controls on methyl halide emissions from southern California coastal salt marshes. *Biogeochemistry*, 60(2):141–161.

Rhew, R. C., Miller, B. R., Vollmer, M. K., and Weiss, R. F. (2001). Shrubland fluxes of methyl bromide and methyl chloride. *Journal of Geophysical Research*, 106(D18):20875–20882.

Rhew, R. C., Miller, B. R., and Weiss, R. F. (2000). Natural methyl bromide and methyl chloride emissions from coastal salt marshes. *Nature*, 403:292–295.

Rhew, R. C., Ostergaard, L., Saltzman, E. S., and Yanofsky, M. F. (2003b). Genetic control of methyl halide production in arabidopsis. *Current Biology*, 13(20):1809–1813.

Rhew, R. C., Teh, Y. A., and Abel, T. (2007). Methyl halide and methane fluxes in the northern Alaskan coastal tundra. *Journal of Geophysical Research*, 112(G2). doi:10.1029/2006JG000314.

Richter, G. M., Riche, A. B., Dailey, A. G., Gezan, S. A., and Powlson, D. S. (2008). Is uk biofuel supply from miscanthus water-limited? *Soil Use and Management*, 24(3):235–245.

Robertson, G., Griffiths, D., Woodford, J., and Birch, A. (1995). Changes in the chemical composition of volatiles released by the flowers and fruits of the red raspberry (*Rubus idaeus*) cultivar glen prosen. *Phytochemistry*, 38(5):1175–1179.

Robinson, E. and Robbins, R. (1968). *Sources, Abundance, and Fate of Gaseous Atmospheric Pollutants: Final Report Prepared for the American Petroleum Institute*. Stanford Research Institute.

Roselle, S. J. (1994). Effects of biogenic emission uncertainties on regional photochemical modeling of control strategies. *Atmospheric Environment*, 28(10):1757–1772.

Rosenstiel, T., Ebbets, A., Khatri, W., Fall, R., and Monson, R. (2004). Induction of poplar leaf nitrate reductase: a test of extrachloroplastic control of isoprene emission rate. *Plant Biology*, 6(1):12–21.

Rowe, R. L., Street, N. R., and Taylor, G. (2009). Identifying potential environmental impacts of large-scale deployment of dedicated bioenergy crops in the UK. *Renewable & Sustainable Energy Reviews*, 13(1):260–279.

Sage, R. and Monson, R. (1998). *C_4 Plant Biology*. Physiological Ecology. Elsevier Science.

Saini, H. S., Attieh, J. M., and Hanson, A. D. (1995). Biosynthesis of halomethanes and methanethiol by higher plants via a novel methyltransferase reaction. *Plant, Cell & Environment*, 18(9):1027–1033.

Saito, T. and Yokouchi, Y. (2006). Diurnal variation in methyl halide emission rates from tropical ferns. *Atmospheric Environment*, 40:2806–2811.

Saito, T., Yokouchi, Y., Kosugi, Y., Tani, M., Philip, E., and Okuda, T. (2008). Methyl chloride and isoprene emissions from tropical rain forest in southeast asia. *Geophysical Research Letters*, 35(19):L19812.

Schnitzler, J. P., Bauknecht, N., Bruggemann, N., Einig, W., Forkel, R., Hampp, R., Heiden, A. C., Heizmann, U., Hoffmann, T., Holzke, C., Jaeger, L., Klauer, M., Komenda, M., Koppmann, R., Kreuzwieser, J., Mayer, H., Rennenberg, H., Smiatek, G., Steinbrecher, R., Wildt, J., and Zimmer, W. (2002). Emission of biogenic volatile organic compounds: An overview of field, laboratory and modelling studies performed during the Tropospheric Research Program (TFS) 1997-2000. *Journal of Atmospheric Chemistry*, 42(1):159–177.

Schuh, G., Heiden, A. C., Hoffmann, T., Kahl, J., Rockel, P., Rudolph, J., and Wildt, J. (1997). Emissions of volatile organic compounds from sunflower and beech: Dependence on temperature and light intensity. *Journal of Atmospheric Chemistry*, 27:291–318.

SEERAD (2006). Review of Greenhouse Gas Life Cycle Emissions, Air Pollution Impacts and Economics of Biomass Production and Consumption in Scotland. Technical Report 2100, Scottish Executive, Edinburgh.

Seinfeld, J. H. and Spyros, N. P. (2006). *Atmospheric Chemistry and Physics*. John Wiley & Sons, Hoboken, second edition.

Serça, D., Guenther, A., Klinger, L., Helmig, D., Hereid, D., and Zimmerman, P. (1998). Methyl bromide deposition to soils. *Atmosperic Environment*, 32:1581–1586.

Shallcross, D. E., Wang, K.-Y., and Dimmer, C. H. (2003). Biogeochemical cycles and residence times. In Hewitt, C. N. and Jackson, A., editors, *Handbook of Atmospheric Science*. Blackwell Science Ltd, Oxford.

Sharkey, T. D. and Yeh, S. (2001). Isoprene emission from plants. *Annual review of plant biology*, 52(1):407–436.

Shearman, V., Sylvester-Bradley, R., Scott, R., and Foulkes, M. (2005). Physiological processes associated with wheat yield progress in the uk. *Crop Science*, 45(1):175–185.

Shorter, J. H., Kolb, C. E., Crill, P. M., Kerwin, R. A., Talbot, R. W., Hines, M. E., and Harriss, R. C. (1995). Rapid degradation of atmospheric methyl-bromide in soils. *Nature*, 377(6551):717–719.

Simpson, D., Winiwarter, W., Börjesson, G., Cinderby, S., Ferreiro, A., Guenther, A., Hewitt, C. N., Janson, R., Khalil, M. A. K., Owen, S., Pierce, T. E., Puxbaum, H., Shearer, M., Skiba, U., Steinbrecher, R., Tarrasón, L., and Öquist, M. G. (1999). Inventorying emissions from nature in Europe. *Journal of Geophysical Research*, 104 (D7):81138152.

Singh, H., O'Hara, D., Herlth, D., Sachse, W., Blake, D., Bradshaw, J., Kanakidou, M., and Crutzen, P. (1994). Acetone in the atmosphere: Distribution, sources, and sinks. *Journal of Geophysical Research*, 99(D1):1805–1819.

Singh, H. B., Kanakidou, M., Crutzen, P., and Jacob, D. (1995). High concentrations and photochemical fate of oxygenated hydrocarbons in the global troposphere. *Nature*, 378:50 – 54.

Smith, R. and Slater, F. M. (2010). The effects of organic and inorganic fertilizer applications to *Miscanthus X giganteus*, *Arundo donax* and *Phalaris arundinacea*, when grown as energy crops in Wales, UK. *Global Change Biology - Bioenergy*, 2(4):169–179.

Staudt, M. and Bertin, N. (2002). Light and temperature dependence of the emission of cyclic and acyclic monoterpenes from Holm oak (Q*uercus ilex*) leaves. *Plant, Cell and Environment*, 21:385–395.

Staudt, M., Bertin, N., Frenzel, B., and Seufert, G. (2000). Seasonal variation in amount and composition of monoterpenes emitted by young *Pinus pinea* trees: implications for emission modeling. *Journal of Atmospheric Chemistry*, 35:77–99.

Staudt, M., Bertin, N., Hansen, U., Seufert, G., Cicciolij, P., Foster, P., Frenzel, B., and Fugit, J.-L. (1997). Seasonal and diurnal patterns of monoterpene emissions from *Pinus pinea* (L.) under field conditions. *Atmospheric Environment*, 31, Supplement 1(0):145 – 156.

Street, R., Owen, S., Duckham, S., Boissard, C., and Hewitt, C. (1997). Effect of habitat and age on variations in volatile organic compound (voc) emissions from quercus ilex and pinus pinea. *Atmospheric Environment*, 31:89 – 100.

Tanaka, K., Kim, H.-J., Saito, K., Takahashi, H. G., Watanabe, M., Yokohata, T., Kimoto, M., Takata, K., and Yasunari, T. (2012). How have both cultivation and warming influenced annual global isoprene and monoterpene emissions since the pre-industrial era? *Atmospheric Chemistry and Physics Discussions*, 12(7):16515–16555.

Teh, Y. A., Rhew, R. C., Atwood, A., and Abel, T. (2008). Water, temperature, and vegetation regulation of methyl chloride and methyl bromide fluxes from a shortgrass steppe ecosystem. *Global Change Biology*, 14(1):77–91.

Thomas, V., Bedford, J., and Cicerone, R. (1997). Bromine emissions from leaded gasoline. *Geophysical Research Letters*, 24(11):1371–1374.

Tilman, D., Hill, J., and Lehman, C. (2006). Carbon-negative biofuels from low-input high-diversity grassland biomass. *Science*, 314(5805):1598–1600.

Tirado, M., Cohen, M., Aberman, N., Meerman, J., and Thompson, B. (2010). Addressing the challenges of climate change and biofuel production for food and nutrition security. *Food Research International*, 43(7):1729–1744.

Tolbert, V., Todd Jr, D., Mann, L., Jawdy, C., Mays, D., Malik, R., Bandaranayake, W., Houston, A., Tyler, D., and Pettry, D. (2002). Changes in soil quality and below-ground carbon storage with conversion of traditional agricultural crop lands to bioenergy crop production. *Environmental Pollution*, 116:S97–S106.

Toome, M., Randjärv, P., Copolovici, L., Niinemets, U., Heinsoo, K., Luik, A., and Noe, S. (2010). Leaf rust induced volatile organic compounds signalling in willow during the infection. *Planta*, 232:235–243.

Tsigaridis, K. and Kanakidou, M. (2007). Secondary organic aerosol importance in the future atmosphere. *Atmospheric Environment*, 41(22):4682–4692.

Tuck, G., Glendining, M. J., Smith, P., House, J. I., and Wattenbach, M. (2006). The potential distribution of bioenergy crops in europe under present and future climate. *Biomass & Bioenergy*, 30(3):183–197.

Turlings, T., Loughrin, J. H., Mccall, P. J., Röse, U., Lewis, W. J., and Tumlinson, J. H. (1995). How caterpillar-damaged plants protect themselves by attracting parasitic wasps. *Proceedings of the National Academy of Sciences*, 92(10):4169–4174.

Turner, D. P., Baglio, J. V., Wones, A. G., Pross, D., Vong, R., McVeety, B. D., and Phillips, D. L. (1991). Climate change and isoprene emissions from vegetation. *Chemosphere*, 23(1):37–56.

UNEP (2007). 2006 Report of the Methyl Bromide Technical Options Committee 2006 Assessment, coordinated by M. Pizano, I. Porter, M. Marcotte, M. Besri, and J. Banks, Nariobi, Kenya. Technical report, United Nations Environment Programme.

UNEP/TEAP (2010). Report of the Technology and Economic Assessment Panel (TEAP), Progress report, Volume 2, coordinated by L. Kuipers and M. Seki, Nairobi, Kenya. Technical report, United Nations Environment Programme/ Technology and Economic Assessment Panel.

Upreti, B. R. (2004). Conflict over biomass energy development in the United Kingdom: some observations and lessons from England and Wales. *Energy Policy*, 32(6):785–800.

Vandendriessche, S.; Griepink, B. (1989). The certification of benzene, toluene and m-xylene sorbed on Tenax TA in tubes: CRM-112. Technical report, Commission of European Communities, Bureau Communit de Reference, EUR12308 EN.

VanReken, T., Greenberg, J., Harley, P., Guenther, A., and Smith, J. (2006). Direct measurement of particle formation and growth from the oxidation of biogenic emissions. *Atmospheric Chemistry and Physics*, 6(12):4403–4413.

Varner, R. K., Crill, P. M., and Talbot, R. W. (1999a). Wetlands: a potentially significant source of atmospheric methyl bromide and methyl chloride. *Geophysical Research Letters*, 26(16):2433–2435.

Varner, R. K., Crill, P. M., Talbot, R. W., and Shorter, J. H. (1999b). An estimate of the uptake of atmospheric methyl bromide by agricultural soils. *Geophysical Research Letters*, 26(6):727–730.

Varner, R. K., White, M. L., Mosedale, C. H., and Crill, P. M. (2003). Production of methyl bromide in a temperate forest soil. *Geophysical Research Letters*, 30(10):1521.

Volkamer, R., Jimenez, J. L., San Martini, F., Dzepina, K., Zhang, Q., Salcedo, D., Molina, L. T., Worsnop, D. R., and Molina, M. J. (2006). Secondary organic aerosol formation from anthropogenic air pollution: Rapid and higher than expected. *Geophysical Research Letters*, 33(17):L17811.

Von Fircks, H. A. (1994). *Frost resistance in Salix*. PhD thesis, Swedish University of Agricultural Sciences, Department of Ecology and Environmental Research.

Warneck, P. (1988). *Chemistry of the Natural Atmosphere*, volume 41. Academic Press.

Warwick, N. J., Pyle, J. A., Carver, G. D., Yang, X., Savage, N. H., O'Connor, F. M., and Cox, R. A. (2006a). Global modeling of biogenic bromocarbons. *Journal of Geophysical Research-Atmospheres*, 111(D24).

Warwick, N. J., Pyle, J. A., and Shallcross, D. E. (2006b). Global modelling of the atmospheric methyl bromide budget. *Journal of Atmospheric Chemistry*, 54:133–159.

Watling, R. and Harper, D. B. (1998). Chloromethane production by wood-rotting fungi and an estimate of the global flux to the atmosphere. *Mycological Research*, 102:769–787.

Went, F. (1955). *Global aspects of air pollution as checked by damage to vegetation*. California Institute of Technology, Pasadena, CA, USA.

Went, F. W. (1960). Organic matter in the atmosphere, and its possible relation to petroleum formation. *Proceedings of the National Academy of Sciences of the United States of America*, 46:212–221.

White, M. L., Varner, R. K., Crill, P. M., and Mosedale, C. H. (2005). Controls on the seasonal exchange of CH_3Br in temperate peatlands. *Global Biogeochemical Cycles*, 19(4). doi:10.1029/2004GB002343.

Wiedinmyer, C., Tie, X., Guenther, A., Neilson, R., and Granier, C. (2006). Future changes in biogenic isoprene emissions: how might they affect regional and global atmospheric chemistry? *Earth Interactions*, 10(3):1–19.

Wikberg, J. and Ögren, E. (2004). Interrelationships between water use and growth traits in biomass-producing willows. *Trees*, 18(1):70–76.

Winer, A. M., Arey, J., Atkinson, R., Aschmann, S. M., Long, W. D., Morrison, C. L., and Olszyk, D. M. (1992). Emission rates of organics from vegetation in California's Central Valley. *Atmosperic Environment*, 26:2647–2659.

Wishkerman, A., Gebhardt, S., McRoberts, C. W., Hamilton, J. T. G., Williams, J., and Keppler, F. (2008). Abiotic methyl bromide formation from vegetation, and its strong dependence on temperature. *Environmental Science & Technology*, 42:6837–6842.

WMO (2003). Scientific Assessment of Ozone Depletion: 2002, Global Ozone Research and Monitoring Project-Report No. 47. Technical report, World Meteorological Organization, Geneva, Switzerland.

WMO (2006). Scientific Assessment of Ozone Depletion: 2006, Global Ozone Research and Monitoring Project - Report No. 50. Technical report, World Meteorological Organization, Geneve, Switzerland.

WMO (2011). Scientific Assessment of Ozone Depletion: 2010, Global Ozone Research and Monitoring Project-Report No. 52. Technical report, World Meteorological Organization, Geneva, Switzerland.

Woods, J., Tipper, R., Brown, G., Diaz-Chavez, R., Lovell, J., and de Groot, P. (2006). Evaluating the Sustainability of Co-firing in the UK. *Report URN 06/1960*.

Worton, D. R., Mills, G. P., Oram, D. E., and Sturges, W. T. (2008). Gas chromatography negative ion chemical ionization mass spectrometry: Application to the detection of alkyl nitrates and halocarbons in the atmosphere. *Journal of Chromatography A*, 1201:112–119.

Wuosmaa, A. M. and Hager, L. P. (1990). Methyl chloride transferase: a carbocation route for biosynthesis of halometabolites. *Science*, 249:160–162.

Yokouchi, Y. and Ambe, Y. (1984). Factors affecting the emission of monoterpenes from red pine (*Pinus densiflora*). *Plant Physiology*, 75(4):1009–1012.

Yokouchi, Y., Ikeda, M., Inuzuka, Y., and Yukawa, T. (2002). Strong emission of methyl chloride from tropical plants. *Nature*, 416(6877):163–165.

Yokouchi, Y., Noijiri, Y., Barrie, L. A., Toom-Sauntry, D., Machida, T., Inuzuka, Y., Akimoto, H., Li, H. J., Fujinuma, Y., and Aoki, S. (2000). A strong source of methyl chloride to the atmosphere from tropical coastal land. *Nature*, 403:295–298.

Yoshida, Y., Wang, Y., Zeng, T., and Yantosca, R. (2004). A three-dimensional global model study of atmospheric methyl chloride budget and distributions. *Journal of Geophysical Research*, 109(D24):D24309.

Yoshida, Y., Wang, Y. H., Shim, C., Cunnold, D., Blake, D. R., and Dutton, G. S. (2006). Inverse modeling of the global methyl chloride sources. *Journal of Geophysical Research-Atmospheres*, 111(D16).

Young, A. and Mitchell, N. (1994). Microclimate and vegetation edge effects in a fragmented podocarp-broadleaf forest in new zealand. *Biological Conservation*, 67(1):63 – 72.

Yvon-Lewis, S. A., Saltzman, E. S., and Montzka, S. A. (2009). Recent trends in atmospheric methyl bromide: analysis of post-Montreal Protocol variability. *Atmospheric Chemistry and Physics*, 9(16):5963–5974.

Zimmerman, P. R. (1979). Testing of hydrocarbon emissions from vegetation, leaf litter, and aquatic surfaces, and development of a methodology for compiling biogenic emission inventories. Technical Report EPA-450-4-70-004, U.S. Environmental Protection Agency, Research Triangle Park, NC.

Zlatkis, A. and Poole, C. (1981). *The design and operation of the electron-capture detector*, volume 20 of *Journal of Chromatography Library*. Elsevier, Amsterdam-Oxford-New York.

